AD NUMBER

AD037467

NEW LIMITATION CHANGE

TO

Approved for public release, distribution unlimited

FROM

Distribution authorized to U.S. Gov't. agencies and their contractors; Administrative/Operational Use; 1950. Other requests shall be referred to Office of Naval Research, Arlington, VA 22217.

AUTHORITY

ONR ltr, 4 Sep 2003

Reproduced From
Best Available Copy

37 467

Reproduced

Armed Services Tech, ical Information Agency

ARLINGTON HALL STATI N; ARLINGTON 12 VIRGINIA

1950

volume III

The Damage Process

OFFICE OF NAVAL RESEARCH ★ DEPARTMENT OF THE NAVY

Bibliography

Most of the papers in this volume contain references to further work, some of which may be included within this Compendium. Properly qualified persons may obtain additional references or material on application to the following establishments:

1. Secretary, Undex Sub-Panel
   Naval Construction Research Establishment
   Rosyth
   Fife
   Scotland

2. Chief of Naval Research
   c/o Navy Research Section
   Library of Congress
   Washington 25, D. C.

3. The Director
   David W. Taylor Model Basin
   Carderock, Maryland

4. The Commander
   U.S. Naval Ordnance Laboratory
   White Oak, Maryland

PREFACE

During the recent war there arose on both sides of the Atlantic among research workers in the field of underwater explosions the feeling that some of the problems posed by the conditions of undersea warfare had already presented themselves in the past and that various attempts had been made to solve them. Many of the records, however, had been lost or effectively hidden except for what had crept into open publications and consequently a whole new literature had to be developed at considerable cost in both time and money, encompassing both old and new problems. A corollary of this experience has been the firm conviction that this new literature should not suffer a similar fate. The idea of the joint publication of American and British research in the field of underwater explosions took form in the latter part of 1946 and the idea was further explored with the Bureau of Ordnance and the Bureau of Ships, United States Navy Department and with the British Admiralty. The Office of Naval Research, Navy Department, in its capacity of disseminator of scientific information undertook to sponsor the publication and has eventually seen the project through to its present form.

The Compendium has three major purposes: first, to give a greater availability to many papers which otherwise would exist in a very small number of copies, and to preserve and revive certain rare items, the scarcity of which was due to wartime shortages rather than to any deficiencies in the papers themselves; second, to present a representative summary of original source material and then to display the scope of this material in a manner which might make it of more unity and interest to schools and colleges as a branch of applied science; and third, to stimulate interest in this field for the general benefit of the sciences of Naval Architecture and Naval Ordnance and to provide those working in these fields with ready reference material on many of the important problems which they must face in their work.

The scheme of the Compendium is as follows: All of the papers selected, which represent between 10 and 20 percent of the total quantity of material known to exist, have been divided into three volumes. The first volume is devoted to the primary underwater shock wave, the second to the hydrodynamical effects falling under incompressible theory including the oscillations and behaviour of the gas globe formed by the explosion products, and the third to the effects of all of these phenomena on structures and to the measurement and calculation of the resulting damage. Three papers have been selected with the object of summarizing the knowledge of the field within the scope of the Compendium; these papers, which are placed in the first one, serve to introduce the subject both in general terms, and also with some mathematical detail.

The allocation of the original papers to the different volumes has, in a few cases, not been obvious and the editors must assume full responsibility for any arbitrary assignments. A far greater responsibility of the editors has lain in the selection of the papers and in this, various considerations have had a voice.

Many of the older papers have been included for their historical interest. Some papers have been used to provide suitable introductory or background material. Most of the other papers have been included intact and represent the opinions of the authors at the time of writing. A few of the papers have been reworked and consist of new material incorporated into the older original papers, or consist of a summary of several progress reports which were too repetitive for economical inclusion without condensation. Papers which have been rewritten are so marked with the new date affixed. In general, selections have been made in an effort to give the best review of the entire subject in order to convey the most, and the best information within the space limitations imposed by the exigencies of publication, and within the scope permitted by considerations of security. Both these features prevent this compilation from being exhaustive, and the latter feature prevents many successful workers in this field from receiving recognition here.

The editors believe that this Compendium is a new venture in international co-operation and hope that this effort may prove useful in pointing the way for other similar joint enterprises which may be considered desirable.

It is our desire to acknowledge the continued interest of Dr. A. T. Waterman, Deputy Chief, Office of Naval Research, Navy Department, without whose help these volumes could not

vi

TABLE OF CONTENTS

VOLUME III

THE DAMAGE PROCESS

* (A) American Contribution
  (B) British Contribution

* (A) American Contribution
* (B) British Contribution

viii

* (B) British Contribution

DAMAGE TO SHIP'S PLATES BY UNDERWATER EXPLOSIONS

S. Butterworth
Admiralty Research Laboratory

British Contribution

July 1924

DAMAGE TO SHIP'S PLATES BY UNDERWATER EXPLOSIONS

S. Butterworth.

July 1924

* * * * * * * * *

Summary.

This paper deals with the effect of an explosive wave upon a circular plate in an otherwise rigid wall separating water from air. It is assumed as a first approximation that the period of free vibration of the plate is large compared either with the duration of the wave or the time required for the wave to travel a distance equal to the diameter of the plate. In these circumstances the effect of the wave is to impart kinetic energy to the material of the plate and to the surrounding water. It is considered that this energy by being partially converted to strain energy is the factor producing distortion and (if large enough) rupture of the plate. A formula for calculating this energy (equation 29) is given. The formula indicates that the energy is proportional to the power 4/3 of the weight of the charge and to the inverse square of the distance from the charge. These results are in agreement with those obtained in sea-trials. An attempt is made to estimate the effect of the period of the plate in relation to the duration of the wave. The result expected is that the $w^{4/3}$ law becomes w^x where x is somewhat less than 4/3 but must be greater than 2/3. A comparison with the results obtained with copper-diaphragm gauges shows that the available energy so estimated is about double that absorbed by the gauges.

Nature of explosive wave.

The experiments carried out by means of the piezo-electric gauge show that the pressure wave transmitted through water due to the detonation of a high explosive charge consists of a very rapid increase of pressure followed by a much slower rate of decay and may roughly be imitated by an equation of the type

$$p = p_0 e^{-mt} \tag{1}$$

in which p is the instantaneous pressure, p_0 the maximum pressure, t the time and m a constant for a charge of given weight and nature. For a point at distance D from a charge of given explosive having weight w the records indicate that

$$P_0 = kw^{1/3}/D, \quad m = a/w^{1/3} \tag{2}$$

For T.N.T. if we put

$$k = 14,000, \quad a = 7,400 \tag{3}$$

this pressure being measured in lbs. per square inch, w in lbs. and D in feet; equation (1) will fit the records as regards momenta ($\int_0^\infty p dt$) and energy ($\int_0^\infty p^2 dt$) but will give maximum pressures about 20% higher than the observed values. Since in the following notes we are concerned mainly with momenta, the above constants will be taken and if I is the momentum in lb. seconds crossing one square inch

$$I = \int_0^\infty p dt = \frac{p_0}{m} = \frac{k}{a} \frac{w^{2/3}}{D} = 1.9 \frac{w^{2/3}}{D} \tag{4}$$

According to equation (1) this momentum requires an infinite time to be delivered but actually the major portion is delivered in a very short time. Thus 99% of the momentum will pass in a time

$$\tau = 4.6 \, w^{1/3}/a$$

so that if w = 1000 lbs., a = 7400, τ = 0.006 second.

for .....

for smaller charges the time is less so that it may be stated that the blow delivered by the direct
wave to any structure is wholly spent in a time which is less than 0.01 second.

Behaviour of thin plate in path of explosion wave.

Let the water in which the explosion wave is generated be separated from air by a rigid wall.
Suppose a circular hole of radius a to be cut in this wall, the aperture being rendered water-tight
by a thin plate.   Suppose the natural period of oscillation of the plate to be long compared with
the duration of the wave and with the time taken by an explosion wave to travel across its diameter.
When the pressure wave impinges upon this plate each element will begin to move inwards but in so
doing will send out a secondary wavelet causing relief of pressure on the surrounding elements so
that in determining the motion of the plate we must take into account not only the force required to
accelerate the plate elements but also the force required to balance the relief pressure due to motion.

If u is the velocity of an element ds of the plate at an instant t then the wavelet thrown
out by this element exerts a relief pressure $\frac{\rho}{2\pi} \frac{ds}{r} \frac{\partial u}{\partial t}$ at distance r from ds and at a time r/c
later than t.   In this relation ρ is the density of the water and c the velocity of propagation in
water.   Hence if v is the ultimate velocity of the element ds after the passage of the wave the
whole relief must   contributed at a distance r is $\frac{\rho v}{2\pi} \frac{ds}{r}$ the only effect of finite velocity of
propagation being a retardation of delivery of this momentum by a time r/c.   Thus the momentum I
delivered to any element of the plate is partially neutralized by the relief momentum contributed by
all elements of the plate and the residue is spent in increasing the momentum of the plate element.
It is here assumed that forces depending on displacement have not had time to come into play.

If the plate is very thin the momentum required for the plate elements may be neglected so
that we have in this case

$$I = \frac{\rho}{2\pi} \iint v \frac{ds}{r} \tag{5}$$

and this must hold for all elements.   Now the right hand side of (5) is the same as the expression
for the electrical potential at a point on a plate which has a charge of surface density v and in
this case the condition implied in (5) is that the charge must be such that the plate is at constant
potential.   Now for a circular disc it is known that an electric charge distribution must be of the
form $v = v_0\, a/\sqrt{a^2 - x^2}$ where v_0 is the charge density at the centre v the charge density at x
from the centre and a the radius of the plate.   Inserting this in (5) we find using the central
element $v_0 = \frac{2}{\pi} \frac{I}{\rho a}$ so that

$$v = \frac{2 \cdot I}{\pi \rho \sqrt{a^2 - x^2}} \tag{6}$$

Equation (6) indicates that the velocity is least at the centre and increases indefinitely at the
edges.   The result is a consequence of neglecting all forces due to relative displacement and
indicates how water would flow into a circular aperture previously closed by a very weak diaphragm.
It also shows that when the diaphragm offers resistance to distortion the greatest stresses will be
at the edges.   This is to be expected as the relief momentum cannot then act as effectively at the
edges as at the centre.

We may, however, pursue this case further and determine the kinetic energy of the inflowing
water immediately after the blow.

Thus if a pressure p is applied for a short time τ to the plate, the work done on an element
ds of the plate is $pv\tau ds = v\delta I ds$, since $p\tau$ represents an increment δI is the corresponding increase
of kinetic energy of the water associated with the plate

$$\frac{dE}{dI} = \iint v\,ds = \frac{4I}{\rho} \int_0^a \frac{x\,dx}{\sqrt{a^2 - x^2}} = \frac{4Ia}{\rho}$$

by equation (6)

Hence $E = 2 I^2 a/\rho$ (7)

The .....

The results of this section show that the effect of an explosive wave upon a circular aperture in a rigid wall initially closed by a very weak diaphragm is to produce an inflow of water into the aperture whose velocity distribution is given by (6) and whose total energy is given by (7). The result holds whether the water is regarded as incompressible or not so long as the time taken by a wave to cross the the aperture is so short that forces depending upon displacement have no time to be developed.

Aperture blocked by a piston.

Suppose next that the inflow is forced to assume a uniform velocity throughout the aperture say by the introduction of a piston. The relief momentum is now given by

$$\frac{E}{2\pi} \; v \iint \frac{ds}{r} = \frac{2\rho\, va}{\pi} \; E\left(\frac{x}{a}\right)$$

where v is the final piston velocity, a the radius of the aperture and the expression holds at a point distance x from the centre. $E\left(\frac{x}{a}\right)$ is the elliptic integral of the second kind and has the value $\frac{\pi}{2}$ when x = 0 and the value 1 when x = a. The relief momentum therefore diminishes from 1.57 to 1 as we proceed from the centre outwards. This non-uniformity of distribution need not, however, prevent us from equating the whole relief momentum over the piston to the applied momentum as the translational momentum must be balanced. Thus neglecting the mass of the piston

$$\pi a^2 I = 4\rho\, vs \int_0^a x\, E\left(\frac{x}{a}\right) dx = \frac{2}{3}\rho\, va^3$$

so that the final velocity v is given by

$$v = \frac{3\pi}{8} \frac{I}{\rho a} \tag{8}$$

The energy E of the inflowing water is such that

$$\frac{dE}{dT} = v \iint ds = \pi a^2 v$$

so that by (8)

$$E = \frac{3\pi^2}{15} \frac{I^2}{\rho} = 1.851\, I^2\, a/\rho \tag{9}$$

Miscellaneous forms of restriction.

If more generally we assume that v is restricted to the form

$$v = v_0\left[1 + a_2\frac{x^2}{a^2} + a_4\frac{x^4}{a^4} + a_6\frac{x^6}{a^6} + \dots\right] \tag{10}$$

It is shown in the appendix that

$$I = \frac{4}{\pi}\rho a v_0\left[\frac{2}{3} + \frac{14}{45} a_2 + \frac{314}{1575} a_4 + \frac{4676}{11025} a_6 + \right] \tag{11}$$

$$E = \pi\rho a^3 v_0^2 \sum_{n=0}\left[a_{2n} R_n \sum_{m=0} \frac{a_{2m}}{2(m+n+3)}\right] \tag{12}$$

in which .....

- 4 -

In which

$$R_0 = 1, \quad R_1 = \frac{5}{5}, \quad R_2 = \frac{89}{225}, \quad R_3 = \frac{381}{1225} \text{ etc.}$$

Thus if we take a form intermediate between those dealt with in Sections (2) and (3) viz:—

$$v = v_0 \left[1 + \frac{x^2}{a^2} \right] \text{ we find}$$

$$i = \frac{175}{75\,\pi} \rho a\, v_0, \quad \varepsilon = \frac{508}{105} \rho a^3 v_0^2 \tag{13}$$

or on eliminating the central velocity v_0

$$\varepsilon = 1.868 \, i^2 \, a/\rho \tag{14}$$

The form

$$v = v_0 \left[1 - \frac{6}{5} \frac{x^2}{a^2} + \frac{1}{5} \frac{x^4}{a^4} \right] \tag{15}$$

which is such that v and $\frac{d^2 v}{dx^2} = 0$ at $x = a$ gives

$$i = \frac{1.3724}{\pi} \rho a\, v_0, \quad \varepsilon = 0.21015 \rho a^3 v_0^2 \tag{16}$$

that is

$$\varepsilon = 1.891 \, i^2 \, a/\rho \tag{17}$$

Finally, the form

$$v = v_0 \left(1 - \frac{x^2}{a^2} \right)^2 \tag{18}$$

which is such that v and $\frac{dv}{dx} = 0$ at $x = a$ gives

$$i = \frac{512}{525\,\pi} \rho a\, v_0, \quad \varepsilon = 0.21015 \rho a^3 v_0^2 \tag{19}$$

or

$$\varepsilon = 2.181 \, i^2 \, a/\rho \tag{20}$$

A comparison of equations (9), (14), (17), (20) shows that the form assumed by the plate under the action of a blow of given momentum is not of great consequence in regard to the energy of the inflowing water after the blow and we may therefore take for this energy

$$\varepsilon = 2 \, i^2 \, a/\rho \tag{21}$$

The formula assumes the plate so light that its own momentum and kinetic energy are negligible in comparison with the momentum and kinetic energy of the associated water.

We now proceed to determine the effect of the mass of the plate.

Modification due to inertia of plate.

Let the plate have density σ and thickness t. Then assuming first piston motion the momentum of the plate is $\pi a^2 \sigma t v$ so that equation (6) must be replaced by

$$i = \left(\frac{8}{3\,\pi} \rho a + \sigma t \right) v \tag{22}$$

The ......

The kinetic energy of the plate is $\frac{1}{2}\pi a^2 \sigma t\, v^2$ and the equation of energy gives

$$E = \frac{1}{2}\pi a^2 \left[\frac{a}{3} \rho a + \sigma t \right] v^2 \tag{23}$$

the first term corresponding to the energy of the inflowing water and the second to that of the plate. In terms of the applied momentum

$$E = 1.851\, I^2\, a/\rho \left(1 + 1.174\frac{\sigma t}{\rho a} \right) \tag{24}$$

The ratio $\frac{1.179\,\sigma t}{\rho a}$ gives the relative proportion of energy or momentum residing in the plate and associated water respectively.

Thus in the case of steel for which $\frac{\sigma}{\rho} = 7.7$ if $t = 0.5$ inch $a = 2$ feet this ratio is 0.189 so that of the whole energy communicated by the blow only 16% resides in the material of the plate.

If we take the form $v = v_0 \left(1 + \frac{x^2}{a^2} \right)$ the plate momentum is

$$2\pi v_0 \sigma t \int_0^a x \left(1 + \frac{x^2}{a^2} \right) dx = \frac{3}{2}\pi a^2 \sigma t\, v_0$$

while the plate energy is

$$\pi v_0^2 \sigma t \int_0^a x \left(1 + \frac{x^2}{a^2} \right)^2 dx = \frac{7}{6}\pi a^2 \sigma t\, v_0^2$$

These give in place of (13)

$$I = \left[\frac{173}{15\pi} \rho a + \frac{3}{2}\sigma \right] v_0, \quad E = \pi a^2 \left[\frac{304}{105\pi} \rho a + \frac{7}{6}\sigma t \right] v_0^2 \tag{25}$$

and in place of (14)

$$E = 1.368\, \frac{I^2 a}{\rho}\, \frac{1 + 1.266\frac{\sigma t}{\rho a}}{(1 + 1.205\frac{\sigma t}{\rho a})^2} \tag{26}$$

The formula corresponding to (26) for the motion

$$v = v_0 \left[1 - \frac{6}{5}\frac{x^2}{a^2} + \frac{1}{5}\frac{x^4}{a^4} \right] \quad \text{is}$$

$$E = 1.891\, \frac{I^2 a}{\rho}\, \frac{1 + 1.311\frac{\sigma t}{\rho a}}{(1 + 1.068\frac{\sigma t}{\rho a})^2} \tag{27}$$

and for motion

$$v = v_0 \left(1 - \frac{x^2}{a^2} \right)^2, \quad E = 2.181\, \frac{I^2 a}{\rho}\, \frac{1 + 1.895\frac{\sigma t}{\rho a}}{(1 + 1.074\frac{\sigma t}{\rho a})^2} \tag{28}$$

If we take what is probably an extreme case viz:- $\frac{\sigma t}{\rho a} = 1$ equations (24), (26), (27), (28), give $\frac{\rho E}{I^2 a} = 0.850, 0.870, 1.022, 1.265$ respectively.

These .....

These differences are not very considerable, and considering the tendency of the plate to present a convex surface to the blow (see section 2) in the absence of forces of restitution it is considered that the 'piston' equation may be taken as fairly representing the energy produced by the blow.

Using equations (24) and (4), and inserting the values of ρ for water and σ for steel viz. ρ = 62.3 lbs. per cubic foot σ/ρ = 7.7 we find for the kinetic energy produced by the explosion of a weight W lb. of T.N.T. when acting on a steel plate of radius a feet and thickness t inches fixed in a rigid wall at distance D feet from the charge

$$E \text{ (in foot lbs.)} = \frac{7.16 \, W^{4/3} \, a}{D^2 (1 + 0.78 \, t/a)} \tag{29}$$

This energy is the kinetic energy residing partly in the plate but mainly in the surrounding water just after the pressure wave has died away. The energy in the water is due to the water following up the plate in its inward motion and is derived not merely from that portion of the wave which impinges on the plate area but also from surrounding portions. The fact that the establishment of this flow produces a relief pressure over the whole of the wall is sufficient to show that this is the case. We need not therefore be alarmed if it turns out that equation (29) gives greater energy than that calculated from the energy content of the charge radiating outwards in all directions.

Modification due to finite duration of blow.

It has been shown previously that if a wave of the form e^{-mt} is to act upon a vibrating system of natural period τ the maximum deflection obtained depends upon the value of $m\tau$. For a wave of given momentum the greatest deflection is obtained when $m\tau$ is very large. For finite values of $m\tau$ the relative values of the deflection are given by the following table

$2\pi/m\tau$ =	0	0.5	1.0	1.5	2.0	2.5	
Maximum deflection =	1.000	0.896	0.757	0.640	0.554	0.485	
$2\pi/m\tau$ =	3.0	3.5	4.0	5.0	6.0	8.0	10.0
Maximum deflection =	0.435	0.395	0.358	0.310	0.270	0.210	0.172

Since the strain energy developed in the system is proportional to the square of the maximum deflection this table may be used to find the proportion of the energy given by (29) which it is possible to convert to strain energy in the absence of dissipative forces. Thus if the natural period of the plate is 0.011 second and the weight of the shot is 300 lbs.,

$$m = \frac{7400}{(300)^{1/3}} = 1100$$

so that $2\pi/m\tau$ = 0.5. Hence from the table the modifying factor is $(0.896)^2$ = 0.8 or 80% of the energy given by (29) will be converted to strain energy in the plate if dissipative forces are absent. The real difficulty in applying this correction is in estimating the natural period of the plate. If the plate is to be ultimately stretched beyond its elastic limit then initially the plate behaves as a clamped plate having no slope at its edges. This condition alone imposes the maximum stress at the edge and in addition the loss of relief pressure at the edges will cause a further stress to be developed there. It is probable that under a heavy blow the elastic limit at the edges is reached at an early stage and thereafter the plate will more probably behave as a stretched membrane the tension of this membrane being of the order of the mean tension load between elastic limit and breaking point. If the plate had no water load the period would then be given by

$$\tau = 2.6 \, a \sqrt{\sigma/t} \tag{29}$$

where σ is the tension load and for steel is of the order 22 tons per square inch.

With .....

With the water load (air assuming membrane motion of the type of equation 15) σ must be replaced by $\sigma + 0.7625 \rho \frac{a}{T}$. Applying the formula to a plate of steel, $\frac{1}{2}$ inch in thickness and 2 feet in radius we find that $T = 0.019$ second and for larger plates the time is still greater. We may safely conclude that for moderately large plates the influence of the duration of the explosive wave is only slight.

Appendix .....

APPENDIX

Motion of Circular Plates with Air-Water
backings.

Let the plate be of radius a and let it be situated in a rigid wall. Then if v is the inward velocity of any element ds of the plate the velocity potential at any point at distance r from ds due to the motion of the plate is

$$\phi = \frac{1}{2\pi} \int\int v \, ds/r \qquad (1)$$

where the integration is carried out over the surface of the plate. If water is compressible and c is the velocity of propagation in the water the value of v which determines ϕ at a time t should be that which holds at a time $t - \frac{r}{c}$. It will be assumed, however, that the water is incompressible.

The pressure p at r is $-\rho\dot\phi$ so that

$$p = -\frac{\rho}{2\pi} \int\int \dot{v} \, \frac{ds}{r} \qquad (2)$$

Suppose the motion symmetrical about the centre and therefore at radius x write

$$v = v_0 \left[1 + a_2 \frac{x^2}{a^2} + a_4 \frac{x^4}{a^4} + \cdots \right] \qquad (3)$$

The pressure is now

$$p = -\frac{\rho \dot{v}_0}{2\pi} \sum_{n=0} \frac{a_{2n}}{a^{2n}} \int\int \frac{x^{2n} ds}{r} \qquad (4)$$

The determination of the pressure distribution over the surface of the plate due to its own motion is now reduced to the determination of the integral $\int\int \frac{x^{2n} ds}{r}$ where r is the distance of a point on the plate at radius x to another point (at radius ξ say) where the pressure is required. This integral is equivalent to determining the potential due to a distribution of matter whose density varies as x^{2n}.

For a ring of unit linear density and of radius x the potential at radius ξ in the plane of the ring is $4 \frac{x}{\xi} \cdot K\left(\frac{x}{\xi}\right)$ if $\xi > x$ and $4K\left(\frac{\xi}{x}\right)$ if $\xi < x$ where $K(\mu)$ is the elliptic integral of the first kind to modulus μ. Hence if the density is proportional to x^{2n} the potential at ξ is

$$4\left[\int_0^{\xi} \frac{x^{2n+1}}{\xi} K\left(\frac{x}{\xi}\right) dx + \int_{\xi}^{a} x^{2n} K\left(\frac{\xi}{x}\right) dx \right] \qquad (5)$$

$$= 4\xi^{2n+1} \left[\int_0^1 \mu^{2n+1} K(\mu) d\mu + \int_{\xi/a}^{1} K(\mu) d\mu/\mu^{2n+1} \right]$$

$$= 4 \xi^{2n+1} \, q_n \, (\xi/a) \quad \text{say}$$

and $p = \frac{-2\rho \dot{v}_0 \xi}{\pi} \sum_0 a_{2n} \left(\frac{\xi}{a}\right)^{2n} q_n\left(\frac{\xi}{a}\right) \qquad (6)$

The .....

The whole reaction force over the plate is

$$F = -2\pi \int_0^a \xi \, p \, d\xi = 4\rho \, \dot{v}_0 \, \varepsilon^3 \sum_0 a_{2n} \int_0^1 \mu^{2n+2} \, \phi_n(\mu) \, d\mu \qquad (7)$$

Calling the integral in (7) I_n we have

$$
\begin{aligned}
I_n &= \int_0^1 \mu^{2n+2} \, \phi_n(\mu) \, d\mu \\
&= \left[\frac{\phi_n \mu^{2n+3}}{2n+3} - \int \frac{\mu^{2n+3}}{2n+3} \, \frac{d\phi_n}{d\mu} \right]_0^1 \\
&= \frac{1}{2n+3} \left[\int_0^1 \mu^{2n+1} \, K d\mu + \int_0^1 \mu \, K d\mu \right]
\end{aligned} \qquad (8)
$$

Since $\dfrac{d\phi}{d\mu} = -K/\mu^{2n+2}$

To determine the definite integrals we have the reduction formula

$$(2n+1)^2 \int_0^1 \mu^{2n+1} \, K d\mu = 1 + (2n)^2 \int_0^1 \mu^{2n-1} \, K d\mu \qquad (9)$$

while $\displaystyle \int_0^1 \mu \, K d\mu = 1 \qquad (10)$

Using (9) and (10) to evaluate (8) we obtain

$$I_0 = \frac{2}{3}, \quad I_1 = \frac{14}{45}, \quad I_2 = \frac{314}{1575}, \quad I_3 = \frac{1606}{11025} \qquad (11)$$

so that the whole reaction force opposing depression is

$$F = 4\rho \, \dot{v}_0 \, a^3 \left\{ \frac{2}{3} + \frac{14}{45} a_2 + \frac{1606}{11025} a_6 + \cdots \right\} \qquad (12)$$

In the case of a sudden blow of momentum I per unit area

$$\pi a^2 I = \int F \, dt$$

If the plate is very light, so that

$$I = \frac{4}{\pi} \rho v_0 a \left[\frac{2}{3} + \frac{14}{45} a_2 + \frac{314}{1575} a_4 + \frac{1606}{11025} a_6 + \cdots \right] \qquad (13)$$

Energy of following water.

The velocity v of any element is assisted by the pressure p so that the work done by the water on the plate is $2\pi \int_0^a \xi \, p \, v d\xi$ or the work done on the water by the plate is $-2\pi \int_0^a \xi \, p v \, d\xi$.

The ......

The last expression gives the rate of increase of the water energy (E)

$$\text{now} \quad v = v_0 \sum_0 a_{2n} \left\{ \frac{\xi}{a} \right\}^{2n}$$

$$\text{and} \quad p = \frac{-\rho}{2\pi} \dot{v}_0 = \sum_0 a_{2m} \left\{ \frac{\xi}{a} \right\}^{2m+1} \Phi_m \left\{ \frac{\xi}{a} \right\}$$

$$\text{so that} \quad \frac{dE}{dt} = 4\rho v_0 \dot{v}_0 a^3 \sum\sum a_{2n} a_{2m} \int_0^1 \phi_m (\mu) \, \mu^{2m+2n+2} \, d\mu$$

Using the value of ϕ_m in (5) we find

$$E = 4\rho v_0^2 a^3 \sum_{n=0} a_{2n} R_n \sum_{m=0} \frac{a_{2m}}{2(m+n)+3} \tag{14}$$

in which $R_n = \int_0^1 \mu^{2n+1} \, \kappa d\mu$

Evaluating this integral

$$R_0 = 1, \quad R_1 = \frac{5}{9}, \quad R_2 = \frac{89}{225}, \quad R_3 = \frac{381}{1225} \quad \text{etc.}$$

THE EFFECT OF A PRESSURE WAVE ON A PLATE OR DIAPHRAGM

E. H. Kennard
David W. Taylor Model Basin

American Contribution

March 1944

NOTATION

A An inertia coefficient defined by Equation [52]

a Radius of a circular plate

B An inertia coefficient defined by Equation [34a]

c Speed of sound in a liquid

E Energy delivered to the plate

E_w Total energy transmitted across unit area in a shock wave

e Naplerian base, 2.718

F_1 Effective force on the plate, Equation [51a]

h Thickness of the plate

I $\int p\,dt$ or impulse per unit area

M Effective mass of the plate, Equation [30]

M_b Effective mass for action of a baffle, Equation [34b]

M_l Effective mass of liquid following the plate in non-compressive motion, Equation [36]

m Mass per unit area of the plate

N Dynamic response factor or load factor, Equation [89]

p Pressure; especially, pressure at the surface of the liquid

p_i Pressure in an incident pressure wave, in open water

p_m Maximum value of p_i

P_l Excess of pressure above p_0 in the liquid

p_0 Total hydrostatic pressure, including atmospheric pressure, on the face of the plate

p_0 Total hydrostatic pressure, including atmospheric pressure, on the back of the plate

p_s Net force per unit area on the plate due to stresses

q Equals α/μ or $2T_s/\pi T_w$, Equation [91]

R Distance from center of a detonated charge

r Distance along a circular plate measured from its center

s Distance between two elements of area

T_d Diffraction time or average time for a sound wave to travel from the edge to the center

T_m Compliance time or time for an element or a structure to acquire maximum velocity

T_p Damping time of a plane plate acted on by plane waves, equal to $m/\omega c$

T_s Swing time or time for a plate or other structure to swing out to a maximum deflection

t Time

U Velocity of propagation of a cavitation edge

v Velocity

v_c Velocity of the center

v_{cm} Maximum value of v_c

v_m Maximum value of v

x Equal to $\rho c / \alpha m$

z Deflection of the plate normal to its initial plane; z refers in analytical work to an element, but in deflection formulas to the center, where it replaces z_c

z_b Displacement of a plane baffle

z_c Value of z at the center

z_{co} Value of z due to static pressure

z_e Central z at the elastic limit

z_l Normal velocity of a liquid surface

z_m Maximum of z at the center, before unloading

z_1 Value of z_c calculated with disregard of the elastic range

z_p Normal velocity of a point on the plate

α A constant in the formula for an exponential pressure wave, $p_1 = p_m e^{-\alpha t}$

μ 2π times frequency

ρ or ρ_l Density of a liquid

ρ_d Density of material composing the plate

σ Yield stress

ϕ Net force per unit area on the plate due to stresses in it and to hydrostatic pressure on its two faces

Φ Effective force due to ϕ, Equation [31b]

Note:- In all cases, the word "diaphragm" may be substituted for the word "plate."

TABLE OF CONTENTS

THE EFFECT OF A PRESSURE WAVE ON A PLATE OR DIAPHRAGM

ABSTRACT

A systematic study of the phenomena attending the impact of a pressure wave upon a plate, usually a shock wave, is introduced by a discussion of the commonest case, followed by the treatment of a number of special topics: the various characteristic times that are involved; cavitation at the interface; the transition to non-compressive action; the effect of a baffle; formulas for the swing time and the deflection of a diaphragm; the factors determining damage; and the departure from Hooke's law in water.

The formulas are applied with fair success to some test data from experiments conducted by the Bureau of Ships and the David Taylor Model Basin.

Most of the mathematical treatment is set down in an appendix to the report.

INTRODUCTION

In ship design it would be a great advantage if effects of underwater explosions on the structure could be calculated analytically. However, the problem thus presented is one of considerable difficulty, especially for contact explosions. Even in the case of the shock wave from a distant explosion, and when the structure is idealized in simple form, complications arise because the motion of the structure reacts back upon the water and thereby modifies the pressure field. The treatment of this effect involves the solution of problems in the diffraction of waves. Further complications may arise from the occurrence of cavitation. Only one case is easily treated analytically; this is the case of a plane plate or diaphragm of infinite lateral extent.

The problem of a diaphragm loaded by a shock wave has been treated several times by more or less approximate methods (1) (2) (3) (4) * In his second report on the subject, Kirkwood gave a general treatment in which adequate allowance was made for diffraction (5) (6) (7) (8), and in a later report the effect of cavitation was discussed (9).

It is the purpose of this report to collect the material that has been assembled at the David Taylor Model Basin for attacking problems of this kind and to consider its application to a few of the available data. The material to be presented consists in part of analytical formulas and in part of conceptions which are useful in thinking about the action of shock waves.

---

* Numbers in parentheses indicate references on page 62 of this report.

The target will usually be idealized in the form of a plate or diaphragm, initially plane, backed by air at a pressure equal to the hydrostatic pressure. Only non-contact explosions are considered in this report.

In view of the complexity of the phenomena, the analytical results will first be described in general terms for the case that is most common in practice. Some of the ideas developed in this discussion will be made the basis for the classification of other cases that may arise. After a few remarks on the role of the Bernoulli effect, the analytical methods will then be described. This will be followed by the discussion of other cases and a more detailed treatment of certain phases of the damaging process. The closing sections of the report will give some formulas for the deflection of a diaphragm, a discussion of the features of the pressure wave that determine damage, and an application of the formulas to some of the available data.

Many of the appropriate analytical methods for dealing with these problems have already been published in other reports, a number of which are listed in pages 62 to 64, but for convenience a rather complete and systematic mathematical treatment is included as an appendix to this report.

PART 1.   DESCRIPTION OF A COMMON CASE PRESENTED FOR ORIENTATION
THE WAVES OF PRESSURE PRODUCED BY A NON-CONTACT UNDERWATER EXPLOSION

When a charge is detonated under water, it produces effects upon structures submerged in the water only by producing pressures in the water. The distribution of this pressure will be influenced by the associated motion of the water - indeed, it is transmitted by such motion - and motion of the structure itself will in turn modify the pressure in the water. A complete description of the action by the water on the structure can be given, however, in terms of the pressures acting upon the surfaces of that structure.

In the primary pulse of pressure produced by the detonation, the pressure rises almost instantly to a high value and then decreases. The rate of decrease diminishes, however, so that the time graph of the pressure pulse has a long "tail." This is illustrated in Figure 1, which has reference to a 300-pound charge of TNT 50 feet away, and in Figure 2, which is reproduced from an oscillogram given by a pressure gage at a distance of 17 inches from a charge of 1 ounce of tetryl.

The high-pressure part, sometimes called the A-phase or the shock wave, is of such short duration that it takes the form of a distinct wave of pressure traveling through the water at finite speed. In the tail or B-phase, on the other hand, the relative rate of change of pressure is much slower, and the pressure in the water soon comes to stand in a definite relation to the simultaneous motion of the expanding gas globe. The appearance of wave propagation thus disappears in this phase, and the pressure and the motion
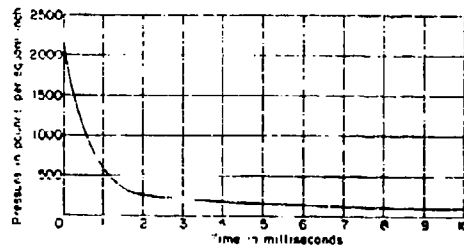
Figure 1 - Approximate Shock-Wave
Pressure in the Water at 50 Feet
from 300 Pounds of TNT

The ordinate represents the pressure in open water
as it would be recorded by a gage so small as to cause
no appreciable modification of the pressure field.
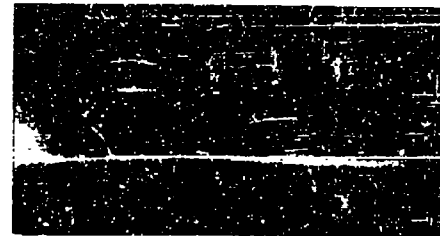
Figure 2 - Oscillogram Showing the
Pressure in the Water at 17 Inches
from a Charge of 1 Ounce of Tetryl

The pressure rises almost instantaneously to
a peak value of 3400 pounds per square inch.

come to be related almost in the way in which they would be related if the
water were incompressible. Any effects that may be produced by the tail of
the pressure wave constitute those effects which are sometimes ascribed, not
to the pressure wave, but to the expansion of the gas globe.

During subsequent recompressions of the gas globe, secondary pulses
of pressure are emitted. The character of these is not yet certain. The
theory of an oscillating spherical gas globe indicates that the time graph of
the pressure in the secondary pulses should be roughly symmetrical about the
point of peak pressure, without any shock front, and should be weaker and
much broader than the initial shock wave. See Reference (10).

PRIMARY SHOCK WAVE AND AN AIR-BACKED PLATE:
A TYPICAL SEQUENCE OF EVENTS

The analytical results will now be described for the case of a
shock wave falling upon one of the plates of a ship's shell, or for a corre-
sponding test on model scale. The wave will be assumed to fall normally upon
the plate, and both wave and plate will be assumed to be sensibly plane. The
action can be divided into two distinct phases, which will be discussed in
order.

Primary Shock Phase

In the cases considered here, the time required for an elastic wave
to traverse the thickness of the plate is so short that it may be neglected;
the plate can be treated, therefore, as a two-dimensional structure with a
certain mass m per unit area.

Before the beginning of the explosive action, the elastic stresses
in the plate will be in equilibrium with the difference between the hydro-
static pressure in front of the plate and the pressure on the back face.
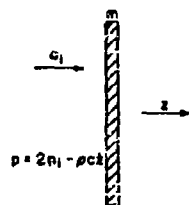
Figure 3 - Illustration of a Plane Wave
Incident Normally upon a Plane Plate
of Infinite Lateral Extent

p_i is the incident wave pressure, m is the mass per
unit area of the plate, and z is the displacement of
the plate. The pressure p on the plate is the dif-
ference between the incident pressure, doubled by
reflection, and a relief term proportional to the
velocity z of the plate.

When the shock wave arrives, there-
fore, each element of the plate will
start moving as if it were part of
an infinite plate acted upon by a
plane wave of infinite lateral ex-
tent, as is suggested by Figure 3,
and for a short time the simple the-
ory of the one-dimensional case will
be applicable.

At first the increment of
pressure p_i due to the incident wave
is doubled by reflection; then, as
the plate accelerates, a relief ef-
fect occurs and the pressure rapidly
falls.

Let it be assumed that hydrostatic pressure on the face of the
plate is balanced by an equal pressure on its back surface. Then the approx-
imate equation of motion for each element of the plate during the initial
phase is

$$m \frac{d^2z}{dt^2} = 2p_i - \rho c \frac{dz}{dt}$$ [1]

where z is the displacement of the element in a direction perpendicular to
the face of the plate, ρ is the density of water in dynamical units, c the
speed of sound in it, and their product is the specific impedance of the wa-
ter. The incident pressure p_i is a function of the time t. See Equation
[107] in the Appendix, in which ϕ is here equal to 0. The right-hand member
of Equation [1] represents the load pressure on the plate; the term in dz/dt
represents the relief effect due to the motion of the plate.

The A-phase of the primary pulse can be represented approximately
by

$$p_i = p_m e^{-\alpha t}$$ [2]

where p_m and α are constants and the time t is measured from the instant of
onset of the wave. If p_i varies in this manner and the plate starts with $z =$
0, $dz/dt = 0$ at time $t = 0$, it is found from Equation [1] that

$$\frac{dz}{dt} = \frac{2p_m}{\rho c - \alpha m} \left(e^{-\alpha t} - e^{-\frac{\rho c t}{m}} \right)$$ [3]

so that the load pressure on the plate is
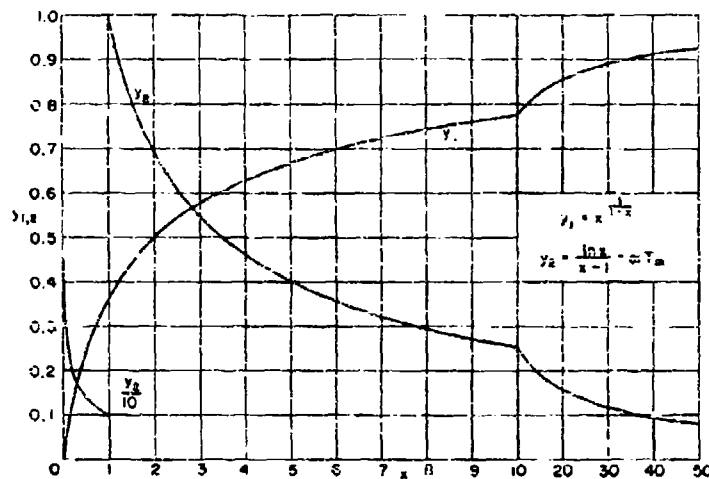
Figure 4 - Parameters Relating to the Incidence
of an Exponential Wave on a Plate

$$m \frac{d^2 z}{dt^2} = \frac{2 m p_m}{\rho c - \alpha m} \left(-\alpha e^{-\alpha t} + \frac{\rho c}{m} e^{-\frac{\rho c t}{m}} \right) \qquad [4]$$

where e is the Naplerian base; see TMB Report 480 (10), page 25.

From this equation it is found that the load pressure vanishes at the time

$$t = T_m = \frac{1}{\alpha} \frac{\ln z}{z - 1}, \quad z = \frac{\rho c}{\alpha m} \qquad [5a, b]$$

where ln denotes the natural logarithm. At this time the incident pressure as given by Equation [2], which would be the actual pressure in the water if the plate were not present, has decreased to

$$p_1 = p_m z^{\frac{1}{1-z}} \qquad [6]$$

and the velocity of the plate has attained its maximum value of magnitude

$$v_m = 2 \frac{p_m}{\rho c} z^{\frac{1}{1-z}} \qquad [7]$$

See TMB Report 489 (11), page 7.

In Figure 4 there are shown plots of αT_m or $\ln z/(z - 1)$, and of the factor $x^{\frac{1}{1-x}}$ or $\rho c v_m / 2 p_m$, as functions of z.

The parameter z defined by Equation [5b] can be interpreted as the ratio of two time constants, as follows:

$$x = \frac{T_u}{T_p}, \quad T_w = \frac{1}{\alpha}, \quad T_p = \frac{m}{\rho c} \qquad [8a,\ b,\ c]$$

Here T_u is the time constant of the incident wave. T_p is called by Kirkwood the *damping time* of the plate; if the plate, in contact with the water, is given an impulsive velocity and then left to itself, its velocity decreases in the ratio $1/e = 1/2.718$ in the time T_p, provided no forces act other than those called into existence by the motion of the plate against the water. T_p may be visualized as the time required for a sound wave to traverse a thickness of water having the same mass as the plate.

The time T_m might be defined more generally, for any type of pressure wave, as the time required for the plate to attain its maximum forward velocity. It may be called the *compliance time* for the plate under the action of the wave.

In the case of the exponential wave, if $T_w = T_p$, $x = 1$ and $T_m = T_w = T_p$. Thus the compliance time is the same as the damping time for a wave of equal time constant. If $T_w \neq T_p$, the compliance time T_m lies between the damping time T_p and the time constant of the wave T_w. Thus for a very light plate, $T_p < T_m < T_w$: in this case the positive action of the wave on the plate ceases while the wave is still strong. If T_p is much smaller than T_w, so that x is much larger than unity, the maximum velocity v_m approaches $2p_m/\rho c$ or twice the particle velocity in the incident wave. For a relatively heavy plate, on the other hand, $T_p > T_m > T_w$. As the plate is made still heavier, both T_p and T_m increase without limit.

As an example, for the shock wave at 50 feet from 300 pounds of TNT exploded in sea water, p_m and α are of the order of 2100 pounds per square inch and 1300 second^{-1}, respectively. Thus $T_w = 1/1300$ second. The values of the compliance time T_m for such a wave falling on steel plates of several thicknesses are shown in Table 1, together with the values of x and of the damping time T_p of the plates against sea water.

TABLE 1

Thickness of plate inches	x	T_p milliseconds	T_m milliseconds	$e^{-\alpha T_m} = x^{\frac{1}{1-x}}$
10	0.6	1.29	0.96	0.28
3	2.0	0.39	0.55	0.50
1	6.0	0.129	0.28	0.70
0.3	20	0.039	0.121	0.85
0.1	60	0.0129	0.052	0.93
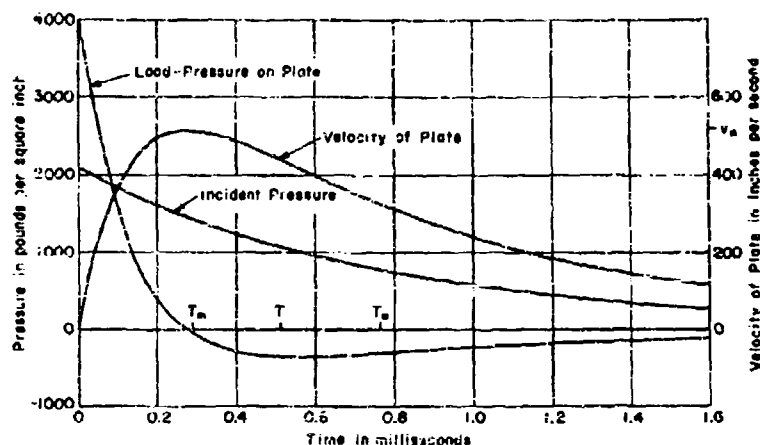
Figure 5 - Curves Illustrating the Incidence of a Shock Wave
on a Plate when Cavitation Does Not Occur

The curves are drawn for the wave from 300 pounds of TNT falling upon an air-backed 1-inch steel
plate 50 feet away. T_m is the compliance time, at which the plate has acquired maximum
velocity; T_w is the time constant of the wave or $1/a$ in the formula, $p_i = p_m e^{-at}$.

In the last column of Table 1 is shown the value of e^{-aT_m}, or the
ratio of the incident pressure at the time $t = T_m$ to the maximum incident
pressure.

In many model tests conditions occur that are comparable in terms
of similitude to the wave from 300 pounds falling on a 1-inch plate. Curves
for this case, with the plate at 50 feet from the charge, as calculated from
the one-dimensional theory, are shown in Figure 5.

The use of the one-dimensional formulas implies the tacit assump-
tion that during the time T_m diffraction effects may be neglected. This is
justified provided the plate is sufficiently large in lateral dimensions.
Consideration of this condition leads to the introduction of a third charac-
teristic time, which may be called the *diffraction time*, T_d. This can be de-
fined with sufficient precision for practical purposes as the time required
for a sound wave in the water to travel from the center of the plate to the
edge. Thus for a circular plate of radius a, $T_d = a/c$, where c is the speed
of sound in water.

Diffraction can be regarded as a process acting to equalize the
pressure laterally, or in directions perpendicular to the direction of prop-
agation of a wave. Because of this process, a wave that has passed through
an opening in a screen spreads laterally, contrary to the laws of the recti-
linear propagation of waves. Similarly, when a wave of pressure falls on a

High
Pressure
E

Direction of
Incident
Pressure Wave

Low
Pressure

σ

E
High
Pressure
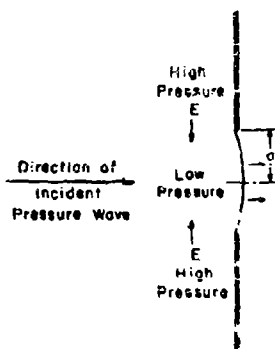
Figure 6 - Diagram to Illustrate
Diffraction of a Pressure Wave

By moving forward, the diaphragm relieves the
pressure, and equalization of the pressure by
diffraction then occurs in the direction of
the arrows F.

diaphragm mounted in a heavy ring, be-
cause the forward motion of the dia-
phragm relieves the pressure over the
diaphragm, a process of equalization of
pressure in the water sets in and acts
to lower the pressure in front of the
ring and to raise it in front of the
diaphragm, as illustrated in Figure 6.

Since, however, effects of
moderate magnitude are propagated
through water only at the speed of
sound, the equalization requires time
for its completion. Thus, during an
interval much shorter than the diffrac-
tion time, after a shock wave has
struck a plate, lateral equalization
of pressure between the water in front
of the plate and that beyond its edge, or even between different parts of the
plate, will not have had time to progress very far. During this short time
each part of the plate will respond to the incident wave more or less inde-
pendently, according to the laws that hold for the one-dimensional action of
shock waves on plates.

In the example just described, if the plate is 10 feet across, the
diffraction time T_d is one millisecond. This exceeds the compliance time T_m
by a good margin for plates up to a thickness of 1 or 2 inches, as is evident
from Table 1, so that the one-dimensional formulas should give good results.
On a plate 10 inches thick, however, diffraction from the edge would produce
a large effect.

It has been assumed in the foregoing discussion that appreciable
stress forces are not called into play by the small displacement of the plate
that occurs during the time T_m. This is usually true in practical cases. In
the example just described, for instance, the maximum velocity acquired by a
1-inch plate is, from Equation [7],

$$v_m = 2 \frac{2100}{5.68} 5.5^{-\frac{1}{4.6}} = 510 \text{ in/sec}$$

Even in a millisecond, therefore, the plate will have become displaced by
less than half of its thickness. Stress forces, if appreciable, would have
the effect of reducing the maximum velocity.

Phenomena in the second phase of the action, now to be discussed,
will depend upon whether cavitation does or does not occur.

No Cavitation: The Tension Phase

If the water remains in contact with the plate, as in Figure 7, tension develops in it, and this tension tends to arrest the motion of the plate.

In the one-dimensional case, the plate is thus brought to rest in the end, and its total displacement is just twice the displacement produced in free water by the passage of the incident wave; see TMB Report 480 (10), page 25. This case is illustrated in Figure 5. If the plate is limited in extent, however, forming part of a larger structure of some sort, the influence of diffraction

Figure 7 - Schematic Illustration of the Deflection of a Plate without Cavitation

will usually be such that the plate retains part of the velocity that it acquired during the primary shock phase. If the shock wave is of very brief duration, the plate may come almost to rest and then be accelerated again as the diffracted pressure is propagated in from the edge.

The analysis indicates that the residual velocity left in the plate should be of the order of the velocity that would be calculated by non-compressive theory with allowance for loading of the plate by the water: this is verified in a special case in the Appendix. If there is open water beyond the edge of the plate, the calculation should be made for a pressure equal to the incident pressure; in this case, although the pressure is doubled at first by reflection, the doubling quickly fades away as diffracted waves arrive from beyond the edge of the plate. If the plate is mounted in a large rigid baffle, however, the doubling persists and the non-compressive calculation should be made with twice the incident pressure.

The plate will then continue moving until it is arrested by forces due to other parts of the structure. During the process of arrest, the kinetic energy in the plate and in the adjacent water becomes converted into other forms, perhaps partly or wholly into plastic work. The time required for the final arrest of the plate constitutes a fourth characteristic time, which may be called the *swing time* of the plate, denoted by T_s. Here the swing time under water-loading is involved. In the case of ships or comparable models the swing time is usually many times longer than the duration of the A-phase of the pressure wave.

Some formulas that may be used in making rough estimates of swing times will be found as Formulas [65] to [66] on pages 43 and 44.
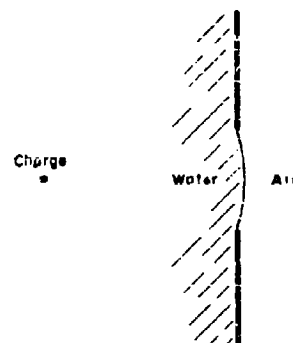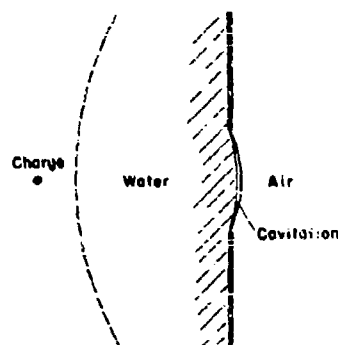
Figure 8 - Schematic Illustration of
Deflection of a Plate with Cavitation
Only at the Plate

The broken curve represents the front of the
reflected shock wave.

Cavitation at the Plate.
The Free-Flight Phase

It has repeatedly been ob-
served that cavitation occurs near the
interface between water and a solid,
when tension develops in the water be-
hind a reflected shock wave. See, for
example, Figure 13. If cavitation
were to occur at the interface and
there only, as in Figure 8, just as
the increment of pressure due to the
wave sank to zero, the plate would
leave the water at the time T_m with
the velocity v_m given by Equation [7];
see Figure 5. In reality, cavitation
cannot occur until the pressure sinks
at least to the vapor pressure of the
liquid, and it may not begin until a lower pressure is reached. Hence in
practice a short phase of negative acceleration would intervene and the plate
would leave the water, with a velocity somewhat less than v_m; for example, at
the time T' in Figure 5. Many initial velocities agreeing with this deduc-
tion from theory have been observed at the Taylor Model Basin. A streak pho-
tograph illustrating the sudden acquisition of velocity by a plate is repro-
duced in Figure 9.
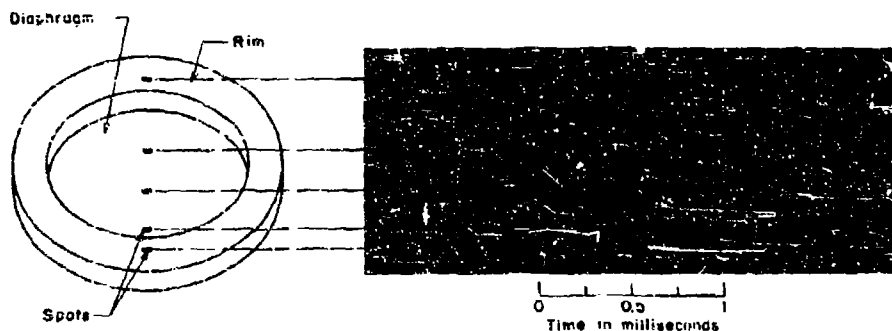
Figure 9 - A Streak Photograph Showing Impulsive Acceleration
of a Diaphragm by a Shock Wave

The streaks were made by light from 5 spots, one on the center of the diaphragm, two others half way
to the edge, and two on the supporting rim. The line of view was at 30 degrees to the plane of the
diaphragm. The streaks were made from left to right. The sudden bend terminating the straight portion
of each streak indicates an impulsive acquisition of velocity by the diaphragm.

The plate will then swing away from the water; see Figure 8. It may swing freely until it is arrested by the combined action of the elastic or plastic stresses in the plate and of any difference in pressure that may exist between its two sides. The kinetic energy to be absorbed in this process will be only that of the plate itself; and the swing time will be that of the plate without water-loading.

The motion of the water surface during this time must also be considered. According to the results of analysis, the velocity of the surface should decrease, but it should not entirely disappear, because of diffraction effects; see the discussion in the Appendix. Furthermore, if a considerable part of the shock wave arrives after the departure of the plate, this will cause further acceleration of the water. It is possible, therefore, that the plate may be overtaken by spray projected from the water surface, and it will certainly be overtaken eventually by the water surface itself; the motion of the plate may thus be prolonged, with a corresponding increase in the plastic work (3).

If the plate is held at its edges, the outer parts of the plate must be jerked to rest by the support almost immediately, while the central part continues moving. Such motion has been observed in 10-inch diaphragms at the Taylor Model Basin. Cavitation occurring over the outer parts of the diaphragm must, therefore, be short-lived; here the water must overtake the plate almost immediately.

As an alternative to the simple process just described, the cavitation might begin in the water itself, in the form of bubbles, so that for a time there would continue to be a layer of unbroken water next to the plate, as in Figure 10a. Or, as a special case, it might begin at the plate and proceed at once to spread out into the water, as in Figure 10b. This possibility has been explored in general terms (12), and its practical application has been discussed in TMB Report 511 (13) and independently by Kirkwood (9).

If the cavitation process is of this character, the motion of
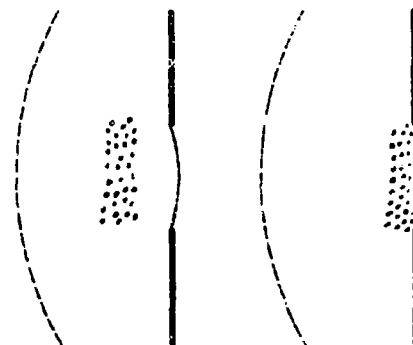
Figure 10a – With Bulk Cavitation at Some Distance in Front of the Plate

Figure 10b – With Bulk Cavitation Extending Outward from the Plate

Figure 10 – Illustration of Deflection of a Plate

The broken curve represents the front of the reflected shock wave.

the diaphragm will be influenced continually by the presence of water in contact with it. Analytical treatment is easy in the one-dimensional case, provided the artificial assumption is made that cavitation occurs at a fixed and known breaking-pressure; but the three-dimensional case presents considerable difficulty. For this reason, only cavitation at the face of the plate will be dealt with in the present report. The final deflection of the plate may not be greatly influenced by the exact mode in which cavitation occurs.

PART 2. THE VARIOUS TYPES OF ACTION BY A SHOCK WAVE

THE FOUR CHARACTERISTIC TIMES

In the foregoing discussion of a typical sequence of events, the relative magnitudes of four characteristic times have played a determining role. These times may be listed together as follows:

1. The time constant or approximate time of duration of the shock wave, T_w; this is equal to $1/\alpha$, for an exponential wave characterized by the expression $p = p_m e^{-\alpha t}$;

2. The compliance time T_m of the structure, or the time required for the shock wave to set the structure in motion at maximum velocity;

3. The diffraction time T_d, or the time required for a wave to travel from the center of the structure to its edge;

4. The swing time T_s of the structure, or the time required for it to undergo maximum deflection and come to rest.

An attempt to picture the significance of these four times in a typical case is made in Figure 11.
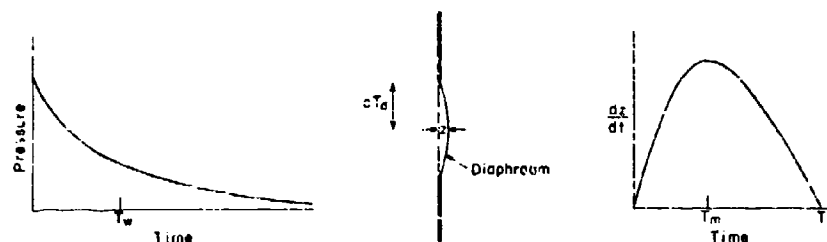
Figure 11 – Illustration of the Significance
of Time Factors for a Diaphragm

T_w is the time constant of a shock wave,
T_d is the diffraction time,
T_m is the compliance time,
T_s is the swing time, and
c is the speed of sound in water.

In the case of a complicated structure such as the side of a ship, several different diffraction times and swing times may be distinguished, according to the dimensions of the part of the structure that is under consideration. Thus there will be a diffraction time and a swing time for the motion of the segment of a plate between two adjacent stiffeners, and longer times for the motion of the stiffened plate as restrained by bulkheads or belt frames.

The characteristic times are useful in classifying the various cases that may arise. There are two simple cases which are particularly useful to bear in mind as a background in considering more complicated situations. These two cases will be discussed in some detail.

THE CASE OF LOCAL ACTION

The typical situation contemplated in the preceding discussion was distinguished by the condition that

$$T_m \ll T_d, \quad T_m \ll T_s \qquad [9a, b]$$

where the symbol $\ll$ means "is much less than." In other words, the compliance time is several times shorter than either the diffraction time or the swing time. The diaphragm acquires maximum velocity and cavitation sets in before diffraction from the edge has had time to influence the motion appreciably, and also before the stresses in the diaphragm have produced appreciable effects. The action in such cases is essentially a local one, since, in large measure, each element of the target is set in motion by the wave independently of other elements.

This case can occur only provided the time constant of the wave, T_w, is not too long. It is sufficient, for example, if $T_w \ll T_d$ and $T_w \ll T_s$, that is, if the action of the wave is completed in a time much shorter than either the diffraction time or the swing time.

An especially important feature of the case of local action is that in this case the conception of conveyance by waves is valid for both energy and momentum. Any part of the target can receive at most only so much energy as is brought up to that part by the incident wave; and part of this incident energy will usually be reflected back into the water. The momentum brought up to each part of the target, also, must be either taken up by the target or reflected. Since momentum is a vector quantity, however, the laws of its reflection are more complicated than are those for the reflection of energy; the momentum delivered to the target may be greater than that brought up by the incident wave, up to a maximum of twice as much if the target is rigid.

NON-COMPRESSIVE ACTION ON A TARGET

At the opposite extreme from local action lies the case of approximately non-compressive action.* The condition for this is that no great change shall occur in the incident pressure during an interval comparable with the diffraction time, that is, that

$$T_w \gg T_d$$

where the symbol $\gg$ means "is much greater than." When this condition holds, the pressures become readjusted by diffraction with such relative rapidity over the face of the target that local effects due to compressibility of the water are largely ironed out and the action on the target becomes essentially the same as it would be if the water were incompressible. Viewed in the large, the pressure field results from a compressional wave propagated up to the target, but its local effects are about the same as those due to an equal pressure field at the target resulting from ordinary hydraulic action.

An important feature of non-compressive action, and one that distinguishes it sharply from the typical local action of waves, is that the energy given to the target may greatly exceed the energy that would fall upon it according to the laws of wave propagation. In non-compressive action energy is propagated through moving water by the pressure just as it is in a hydraulic press.

An excellent example is presented by a Hilliar pressure gage (14) subjected to the shock wave from a charge of several hundred pounds. The face of the gage, H-H in Figure 12, is perhaps 4 inches across, so that the diffraction time T_d may be 1/30 millisecond, whereas the time constant of the wave is of the order of a millisecond. Thus non-compressive theory should give a good account of the effect of a shock wave on a Hilliar gage. The energy acquired by the piston of the gage may greatly exceed that which is propagated in the shock wave across an area equal to that of the face of the piston. The motion of the piston sets
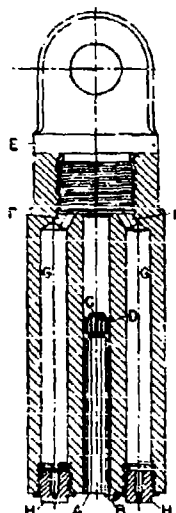
Figure 12 - Illustration of a Hilliar Pressure Gage

The steel piston A is projected upwards by the pressure due to the shock wave, thereby hammering the copper cylinder C against the top of the gage. This diagram is copied from Figure 34 in Reference (14).

* This is action conditioned by flow, as of an incompressible fluid.

up a local flow in the adjacent water which, in co.   tion with the pressure,
acts like a funnel to collect energy from a broad area of the incident wave.

The non-compressive case also possesses a still wider significance.
There exists a continual tendency for the effects of any pressure wave to
undergo changes in the direction of non-compressive action. Any sudden im-
pulse of pressure produces an increment of motion in the structure according
to the laws of local action; but within a time of the order of the diffrac-
tion time. diffracted waves act so as to convert this motion at least roughly
into the motion that would have been produced by the same pressure impulse
acting in incompressible water, except, of course, as the motion may have
been further altered by forces arising within the structure. This drift to-
ward the non-compressive type of motion has already been mentioned in the
discussion of the tension phase on page 9.

A variety of other cases can be imagined, characterized by various
relations among the four time constants. In considering such cases, the fol-
lowing general rules, already illustrated in the discussion, will often en-
able a step to be taken toward a solution:

1.   During an initial interval much shorter than the diffraction time
T_d, the formulas pertaining to plane waves will be applicable. In special
cases, when $T_s \ll T_d$, this interval may cover the whole of the action on the
target.

2.   During an initial interval much shorter than the swing time T_s, the
elements of the target will be accelerated independently.

3.   For a plate or diaphragm, the equation of motion will be approxi-
mately as given in Equation [1] during an initial interval that is much
shorter than either the diffraction time T_d or the swing time T_s.

CONDITIONS UNDER WHICH CAVITATION MAY OCCUR

In the consideration of cavitation it may be conducive to clarity
if a distinction is made between cavitation due to elastic overshoot and cav-
itation due to fluid inertia.

Cavitation due to inertia is a familiar phenomenon in the non-
compressive motion of water. On the back of a propeller blade, for example,
cavitation occurs because the inertia of the water prevents it from following
the blade.

Cavitation between a shock wave and a plate, as discussed in a pre-
vious section, arises in a different manner and is closely associated with
the elasticity of the water. The plate, together with the water in contact
with it, is accelerated so rapidly that the water farther away is unable to

16
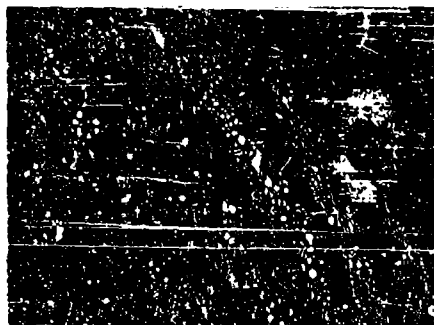
Figure 13 - Photograph Showing Cavitation
Bubbles Produced by a Shock Wave
in Water near a Lucite Window

The gas globe produced by the explosion
is visible at the left.

share fully in the motion. The water thus becomes expanded and its energy of compression is converted into the kinetic energy of the plate; the process of expansion progresses to the point where tension begins to develop in the water, and cavitation results. The water and plate behave much like a spring loaded with a mass. If the spring is compressed and then released, the motion overshoots the position of equilibrium, and the initial state of compression thereby comes to be replaced momentarily by one of tension. A picture of what appears to be cavitation due to elastic overshoot, in front of a lucite window struck by the shock wave from a small charge, is shown in Figure 13.

Under ordinary circumstances, a necessary condition for the occurrence of cavitation due to elastic overshoot appears to be that the compliance time of the structure, or time required for it to attain a maximum velocity under the action of the wave, shall be less than the diffraction time:

$$T_m < T_d$$

If this condition is not satisfied, inflow of water from regions beyond the edge of the structure is likely to equalize the pressures and so to prevent the occurrence of tension in the water.

The occurrence of cavitation should be the same on the usual model scale as on full scale, at least if the hydrostatic pressure is the same in the two cases. For, if all linear dimensions including those of the charge are altered in a given ratio, all characteristic times will be changed in the same ratio; in Equation [5a, b], for example, $1/\alpha$ and m will be changed in the ratio of the linear dimensions and x is unchanged. Thus the ratio of T_m to T_d is not altered by the change of scale.

Large hydrostatic pressure, however, may act to prevent the occurrence of cavitation. The pressure due to the incident wave, as modified by reflection and the motion of the target, is superposed upon the hydrostatic pressure p_0, and, if p_0 is sufficiently great, the resultant pressure may never sink to the pressure at which cavitation occurs.

Since it is the excess of pressure above p_0 that accelerates the plate, the total pressure in the water at the plate will be

$$p = p_0 + m \frac{d^2 z}{d t^2}$$

In the case of the exponential wave represented by Equation [2], $m\, d^2 z/dt^2$ is given by Equation [4]. In this case, by equating dp/dt to zero, the minimum value of p is found to occur at the time $t = 2T_m$, where T_m is given by Equation [5a], and to have the magnitude

$$p_{min} = p_0 - 2p_m x^{\frac{1+x}{1-x}} \tag{10}$$

Thus, if cavitation occurs when the pressure sinks to a certain breaking-pressure p_b, which cannot exceed the vapor pressure and may be negative, then cavitation can occur only if $p_{min} < p_b$ or

$$2 p_m x^{\frac{1+x}{1-x}} > p_0 - p_b$$

Here it can be shown that the factor $2x^{\frac{1+x}{1-x}}$ has a maximum value of $2/e^2 = 0.27$ at $x = 1$ and decreases toward zero as $x \to 0$ or $x \to \infty$.

The maximum depths at which cavitation can occur, as calculated from this formula, come out too large to be of interest. The shock wave from 300 pounds of TNT, for example, falling on an air-backed steel plate 1 inch thick at a distance of 50 feet, could cause cavitation at zero pressure down to a depth of 700 feet below the surface.

Both in the action of shock waves on ships and in comparable model tests the necessary conditions for the occurrence of cavitation due to elastic overshoot at a pressure not far from zero appear to be met, and observations on the initial velocities of diaphragms at the Taylor Model Basin indicate that it does occur.

For a Hilliar gage, on the other hand, the compliance time, or the time in which the piston would attain maximum velocity if it were not stopped by anything, is much longer than the diffraction time. Thus cavitation is not to be expected on the face of the piston.

A more detailed discussion of the phenomena accompanying cavitation near a plate or diaphragm will be given later in this report, on pages 38 to 42.

THE BERNOULLI PRESSURE AND THE DEVIATION FROM HOOKE'S LAW

At this point it may be worth while to digress slightly for a moment and consider one or two minor matters. The question is often asked, whether the expression for the pressure caused by the impact of a plane wave

upon a rigid wall ought not to include a term of magnitude ρv^2 or $\rho v^2/2$. The answer furnished by analysis is in the negative.

Even the exact theory of Riemann for the propagation of plane waves of finite amplitude leads to no direct contribution from the particle velocity v to the pressure on a rigid wall. The pressure should be a little more than twice the incident pressure, but the excess is due entirely to departures from Hooke's law of elasticity; see the Appendix. It can be said that the entire increase in pressure arises from the arrest of the particle motion by the wall. No further increase corresponding to ρv^2 should, therefore, be expected.

As an example, when water is compressed adiabatically from zero pressure and a temperature of 20 degrees Centigrade, its pressure, up to 10,000 pounds per square inch, is approximately given by the formula

$$p = 309000\,s\,\left(1 + \frac{p}{75000}\right)\,\text{lb/in}^2 \qquad [11]$$

where s is the fractional compression or the decrease in volume divided by the original volume; see the Appendix, Equation [184]. The term $p/75000$ represents the departure from Hooke's law. Because of this term, the pressure on a rigid wall due to the incidence of a wave of pressure of magnitude p_i pounds per square inch is raised from $2p_i$ to

$$2p_i\,\left(1 + \frac{p_i}{150000}\right) \qquad [12]$$

See the Appendix, Equation [185]. For an incident wave having a pressure of 5000 pounds per square inch, the increase is 3 per cent.

In the reflection of spherical waves, also, the usual *linear* theory leads to the conclusion that the pressure against a rigid wall is simply doubled; the afterflow velocity* gives rise to no additional term in the pressure.

The familiar Bernoulli term in the pressure formula thus puts in its appearance only when (a) the pressure field is two- or three-dimensional, and (b) terms of the second order in the velocity are included. A small pitot tube, for example, turned with its mouth toward the oncoming wave, will register a pressure equal to $p + \rho v^2/2$ where p is the pressure and v is the particle velocity caused by the wave in unbroken water, whereas with its mouth turned at right angles to the direction of propagation it registers just the pressure p. The motion around the tube is three-dimensional; and the increase in pressure is of order v^2. Similarly, the pressure at the

---

* See TMB Report 480 (10), page 39.

front stagnation point, or point of zero velocity, on any small rigid obstacle in the path of the waves should be $p + \rho v^2/2$; likewise, the pressure on the piston of a Hilliar gage (14) should be approximately $p - \rho v_p^2/2$, where v_p is the velocity of the piston.

The Bernoulli effect as represented by the term ρv^2 in such expressions will thus in some cases play a part in modifying the pressure field in front of a target. Analysis furnishes no reason, however, to expect additional effects on the target from a "kinetic wave" following the shock wave. The pressure field in the water constitutes the mechanism by which the water is set moving outward and then presently arrested; the pressure field is physically inseparable from the motion, and its effects on the target include all effects that might be ascribed to the action of the moving water.

At any fixed distance from the center of the explosion, the pressure in open water should fall continually as the gas globe expands, and it appears from analytical results that the same should be true of the pressure on the target. Thus no upward surge of pressure is to be expected "as the moving water reaches the target"; the idea of a water projectile propelled by the gas globe and subsequently impinging upon the target is inappropriate and misleading.

PART 3. THEORY OF A PLANE TARGET

The discussion has been kept in general terms up to this point, and few exact formulas have been given. General analytical results are difficult to obtain, and numerical integration has scarcely seemed worth while hitherto because of incomplete knowledge of the relevant fundamental data.

There is one three-dimensional case, however, in which exact analytical formulas are readily written down. This is the case in which everything of interest happens in the neighborhood of a plane surface, which may be supposed to extend laterally to infinity. This case will now be taken up for discussion in some detail. For generality, the fluid present will not be restricted to water.

PRESSURE ON AN INFINITE PLANE

When waves fall upon the initially plane face of a target of effectively infinite lateral extent, an expression is easily obtained for the resulting pressure at any point on the face. The waves may be plane, spherical or of any other type. It must be assumed, however, that they are of sufficiently small amplitude so that the ordinary linear theory of acoustics is applicable, and that the displacement of the water or other fluid at points on the plane is small. The first condition should be sufficiently well satisfied at pressures up to 10,000 pounds per square inch in water.

The expression for the pressure can be constructed by using the principle of superposition.

The waves are first imagined to be reflected from the surface of the target as if it were rigid. This gives a resultant wave field in which, at the surface, the incident pressure is doubled, while the particle velocity has no component normal to the surface.

A correction is then added to allow for the motion of the surface. This correction is obtained by assuming the existence on the surface of a suitable distribution of simple point sources emitting waves of pressure. Because the surface is plane, each of these waves affects the normal component of the particle velocity only at the element that emits the wave. For this reason the strength of the point sources is easily adjusted so as to satisfy the necessary boundary condition, which is that the surface and the adjacent fluid must have a common component of velocity normal to the surface. It is found that the pressure emitted by each element of the surface must be proportional to its normal component of acceleration.

The contributions made by the emitted waves to the pressure at any given point in the fluid will be retarded in time because of the time required for the waves to travel from their point of origin. The following expression is obtained for the pressure at any point Q on the surface at time

$$p = 2p_i - \frac{\rho}{2\pi} \int \frac{1}{s} \ddot{z}_{t-\frac{s}{c}}\, dS + p_0 \qquad [13]$$

where p_0 is the total hydrostatic pressure, including atmospheric pressure,

p_i is the incident pressure at the point Q and at the time t,

ρ is the density of the fluid,

c is the speed of sound in the fluid,

dS is an element of area on the face of the target,

z is the component of displacement of dS in a direction perpendicular to the initial position of the target, measured positively away from the fluid, and

s is the distance of dS from Q.

$\ddot{z}$ denotes d^2z/dt^2, and the subscript $t - s/c$ means that each element dS is to be multiplied by the value of its acceleration $\ddot{z}$ not at the time t but at the time $t - s/c$.

The integration extends over the entire face. See the Appendix, Equation [100], and Figure 14.

The factor 2 in Equation [13] may be regarded as a reflection effect arising from the mere presence of the target. The term containing the integral represents a relief of pressure, as explained by Butterworth [1], or

an emission of negative pressure caused
by acceleration of the face of the tar-
get. Positive pressure is emitted, how-
ever, by any element at which $\ddot{z}$ is nega-
tive. The release or emission effect is
propagated from one point to another in
the fluid at the speed of sound.

     The surface on which the pres-
sure is calculated has been supposed to
be the surface of a solid body. Nothing
would be altered, however, if the sur-
face were, wholly or in part, merely a
geometrical plane drawn in the fluid; in
Equation [13] z will then be merely the
displacement of the fluid itself perpen-
dicular to the surface. This extension
of the interpretation will be useful
later.

Figure 14 - Diagram Illustrating
the Theory of the Incidence of a
Wave of Pressure upon a Nearly
Plane Moving Surface

The pressure p_i due to incident waves causes
a net pressure p on the surface; s denotes
the distance of an element of area dS from a
point Q on the surface, at which the displace-
ment of the surface is s.

    The theory of the relief pressure as described here constitutes the
mathematical theory, for a plane surface, of the process of diffraction or
equalization of pressure which was described in general terms on page 7.

MOTION OF AN INITIALLY PLANE PLATE OR DIAPHRAGM
OF UNLIMITED LATERAL EXTENT

    So long as the plate or diaphragm remains approximately plane, its
equation of motion can now be written in the form

$$m \frac{d^2 z}{dt^2} = p_w + \phi \qquad [14]$$

where m is its mass per unit area, z is its displacement at any point perpen-
dicular to the plane occupied initially by its face, p_w is the total incre-
ment of pressure caused, directly or indirectly, by incident waves, and

$$\phi = p_0 - p_0' + p_e \qquad [15]$$

where p_0 is the total hydrostatic pressure, p_0' is the pressure on the back of
the plate and p_e is the net force per unit area in the direction of z due to
stresses in the plate. Motion parallel to the initial plane is assumed to be
negligible so far as inertial effects are concerned. Here m, z, p, and ϕ may
all vary over the plate. Inserting the value of $p_w = p - p_0$ from Equation
[13]

$$m\frac{d^2z}{dt^2} = 2p_i + \phi - \frac{\rho}{2\pi}\int\left(\frac{d^2z}{dt^2}\right)_{t-\frac{r}{c}}\frac{dS}{s} \qquad [16]$$

It is readily shown that, if the plate remains accurately plane, this equation reduces to the familiar one-dimensional equation; see the Appendix. The relief term, or the term containing the integral in Equation [16], becomes the last or damping term in Equation [1]. Or, if plane waves are incident at an angle θ, and if $\phi = 0$, so that the elements of the plate move independently, Equation [16] becomes, as shown by Taylor (4),

$$m\frac{d^2z}{dt^2} + \frac{\rho c}{\cos\theta}\frac{dz}{dt} = 2p_i \qquad [17]$$

The general equation is thus seen to be consistent with others that can be obtained more simply. The case of spherical waves has been considered by Fox (15).
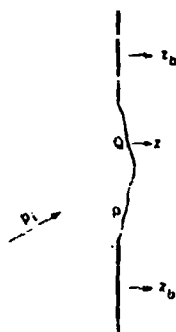
Figure 15 - Diagram Illustrating
Incidence of a Wave on a Plate
Mounted in a Movable Baffle

The displacement of the baffle, assumed
plane, is z_b; the displacement of any
point of the plate is z.

PLATE OR DIAPHRAGM OF FINITE EXTENT SURROUNDED BY A PLANE BAFFLE

In tests, a plate or diaphragm is commonly mounted in a support that approximates a rigid baffle; such a mounting constitutes a first approximation to the mounting of a plate in the side of a ship. In some cases it may be necessary to allow for motion of the support.

If only part of the structure just considered consists of a movable plate or diaphragm, while the remainder forms a fixed plane baffle, the integral in Equations [13] or [16] need be extended only over the movable part. Or, more generally, as is illustrated in Figure 15, if the baffle is itself movable as a whole but remains plane, the equation for the motion of any point of the plate can be put into the form,

$$m\frac{d^2z}{dt^2} = 2p_i + \phi - \rho c\frac{dz_b}{dt} - \frac{\rho}{2\pi}\int_{plate}\frac{1}{s}\left(\frac{d^2z}{dt^2} - \frac{d^2z_b}{dt^2}\right)_{t-\frac{r}{c}} dS \qquad [18]$$

where z_b is the displacement of the baffle, all quantities are taken at time t except the values of the integrand, and the integral extends only over the plate; see the Appendix, Equation [109].

Comparison of the last equation with Equation [16] shows that the principal effect of motion of the baffle is to relieve the load pressure on

the diaphragm to the extent of ρc times the velocity of the baffle, or to increase the pressure to this extent if the baffle is moving toward the side of incidence. The factor ρc is the same as the ratio of the pressure to the particle velocity in a plane wave, or about 70 pounds per square inch for each foot per second of velocity. If the velocity of the baffle is variable, however, the release effect is modified by the presence of the term in $d^2 z_b/dt^2$.

Other useful forms of the equation are possible. In the case of a circular plate of radius a, for example, with everything symmetrical about the axis of the circle, Equation [16] as applied to the central element of the plate can be written in the alternative form

$$ m\ddot{z} = 2p_i + \phi - \rho c\left[\dot{z}_b\left(t - \frac{r_1}{c}\right) - \dot{z}_b\left(t - \frac{r_2}{c}\right)\right] - \rho\int_0^a \ddot{z}_{t-\frac{r}{c}}\, dr \qquad [19] $$

Here the first three terms refer to quantities at the center and at time t, and in the integral s has been replaced by r, the distance from the center of the plate; also, because of the symmetry, it is possible to write $dS = 2\pi r\, dr$. The part of the release integral that contains $d^2 z_b/dt^2$ has been transformed as in Equation [105] of the Appendix. For generality, it has been assumed here that only the part of the baffle lying between $r = r_1$ and $r = r_2$ is movable, while the remainder is at rest; $\dot{z}_b(t)$ is the velocity of the movable part at time t.

If the entire baffle is movable, the equation becomes

$$ m\ddot{z} = 2p_i + \phi - \rho c\,\dot{z}_b\left(t - \frac{a}{c}\right) - \rho\int_0^a \ddot{z}_{t-\frac{r}{c}}\, dr \qquad [20] $$

FINITE PLATE OR DIAPHRAGM WITH NO BAFFLE

For a plate or diaphragm forming one side of an air-filled box, an approximate equation of motion may be obtained from the last equation by the following argument. Equation [16] should hold even if part of the "plate" is reduced to a mere imaginary plane drawn through the fluid; see Figure 16. Then, in the integral, at elements dS located on the imaginary plane, $d^2 z/dt^2$ refers to the acceleration of the fluid. These values of $d^2 z/dt^2$ are not known accurately because the pressure in the fluid is modified in an unknown manner by the presence of the plate. For an approximate result, however, we may resort to the assumption that is commonly employed with success in phenomena of optical diffraction.

Let it be assumed that the disturbance in the fluid beyond the edge of the plate is the same as it would be if the plate were not there. Then, if the incident wave is plane and falls normally on the plate, $d^2 z/dt^2$ is
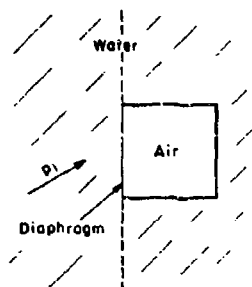
Figure 16 - An Air-Backed
Diaphragm Forming One
Side of a Box

The pressure due to incident waves
is p_i. The broken lines represent
a continuation of the plane of the
diaphragm into the water.

uniform over the plane beyond the edge, as it
would be if a plane baffle were present, hence
Equation [18] can be used in place of Equation
[16]. Here dz_o/dt is now merely the particle ve-
locity in the incident wave or $p_i/\rho c$, so that the
term containing this velocity becomes $-p_i$. Thus
Equation [18] becomes, for the motion of any ele-
ment of the plate,

$$m\frac{d^2z}{dt^2} = p_i + \phi - \frac{\rho}{2\pi}\int_{plate}\left(\frac{d^2z}{dt^2} - \frac{1}{\rho c}\frac{\partial p_i}{\partial t}\right)_{t-\frac{s}{c}}\frac{dS}{s} \quad [21]$$

or, if the incident wave varies slowly enough,
approximately,

$$m\frac{d^2z}{dt^2} = p_i + \phi - \frac{\rho}{2\pi}\int_{plate}\left(\frac{d^2z}{dt^2}\right)_{t-\frac{s}{c}}\frac{dS}{s} \quad [22]$$

In the special case of axial symmetry, again, a simpler alternative
equation is useful. If the plate is a circle of radius a and if everything
is symmetrical about its axis, then similar changes in Equation [109] of the
Appendix give, for the motion of the central element only, the approximate
equation

$$m\frac{d^2z}{dt^2} = 2p_i(t) - p_i\left(t - \frac{a}{c}\right) + \phi - \rho\int_0^a\left(\frac{d^2z}{dt^2}\right)_{t-\frac{r}{c}}dr \quad [23]$$

in which d^2z/dt^2 on the left and $p_i(t)$ and ϕ refer to time t, while $p_i(t-a/c)$
is the value of p_i at time $t - a/c$, r denotes distance from the center of the
plate, and dS has been replaced by $2\pi r dr$.

Thus the diffractive release of pressure around the edge of the
plate has the effect of diminishing or even eliminating the doubling of the
incident pressure that results from reflection.

If the plate is mounted in a supporting ring with a plane face,
this ring can be treated in the equations as if it formed part of the plate.

MOTION OF THE FREE SURFACE OF A LIQUID

Equation [16] can be applied also to the motion of the free surface
of a liquid. This can be done by setting $m = 0$, replacing ϕ by $p_0 - p$, where
p_0 is the hydrostatic pressure at the level of the surface and p is the ex-
ternal pressure on the surface itself, and interpreting z as the displacement
of the surface. Atmospheric pressure is included here in p_0, which may dif-
fer from p because of an accelerating pressure-gradient in the liquid.

The resulting equation can be written in the form

$$\frac{\rho}{2\pi} \int \left(\frac{d^2 z}{d t^2}\right)_{t-\frac{r}{c}} \frac{dS}{s} = 2p_i + p_0 - p \qquad [24]$$

In this form the equation holds, indeed, quite generally, for any liquid surface that is nearly plane and effectively unlimited in lateral extent, even when the surface is partly or wholly in contact with a solid body. See Appendix, Equation [103]. The equation fixes the acceleration of the surface at each point in terms of previous accelerations at all points and the various pressures.

Furthermore, with similar changes, Equation [18] can be applied to the motion of the liquid surface as exposed in a hole in a movable plane baffle lying on the surface.

It may be noted that the liquid surface does not exhibit the same kind of resilience that is characteristic of ordinary elastic bodies. Thus a rubber ball dropped onto the floor bounces back. If the surface of a liquid similarly impinges upon a rigid obstacle, however, there is no rebound. During the impact the surface undergoes momentary negative accelerations of large magnitude, and Equation [24] shows that these accelerations must be accompanied by a positive pressure acting on the surface, and also, therefore, on the obstacle. However, on the assumption that only a limited part of the surface was in motion, the integral in Equation [24] ultimately fades out without changing sign, and the corresponding part of p must, therefore, do the same. Since negative values of p do not occur, there is no tendency for the liquid surface to leave the obstacle.

Elastic rebound such as that of the rubber ball is exhibited only by bodies, solid or liquid, whose dimension perpendicular to the surface of contact is effectively finite.

IMPULSE PER UNIT AREA DUE TO THE WAVES

Before considering solutions of the equations of motion, the following interesting conclusion concerning the impulse may be noted.

Suppose that the plate, after having been at rest until a certain instant, moves in any manner and then comes permanently to rest again. If it is surrounded by a baffle that also moves, let the baffle likewise come to rest. Let I denote the total impulse per unit area caused by the incident waves or $\int p_w \, dt$, where p_w is the excess of pressure above hydrostatic pressure and the integral extends over all time. Then, for a plate in a wide plane baffle, it turns out that

$$I = 2 \int p \, dt \qquad [25]$$

where p_i is the incident excess of pressure above hydrostatic pressure, or, if there is no baffle, approximately

$$I = \int p_i\, dt \qquad [26]$$

here $\int p_i\, dt$ represents the incident impulse per unit area.

To obtain this result, it is only necessary to multiply the equation of motion of the plate by dt and integrate. From Equation [14]

$$I = \int p_w\, dt = \int \left(m\frac{d^2 z}{dt^2} - \phi \right) dt$$

When the value of d^2z/dt^2 is substituted here from the equation of motion, the double integral in dt and dS vanishes, as is seen at once upon inverting the order of integration. For example

$$\int dt \int \left(\frac{d^2 z}{dt^2}\right)_{t-\frac{s}{c}} \frac{dS}{s} = \int \frac{dS}{s} \int \left(\frac{d^2 z}{dt^2}\right)_{t-\frac{s}{c}} dt = \int \frac{dS}{s}\left[\Delta\left(\frac{dz}{dt}\right)_{t-\frac{s}{c}}\right] = 0$$

since every point on the plate begins and eventually ends in a state of rest. Thus, from Equation [16] or [18], $I = 2\int p_i\, dt$, as stated. Or, if Equation [21] is used, since $\int (\partial p_i/\partial t)dt = \Delta p_i = 0$, $I = \int p_i\, dt$, at least approximately, in the absence of a baffle.

Similar treatment of Equation [24] gives for the surface of the liquid, whether free or not,

$$\int (p - p_0)dt = 2\int p_i\, dt \qquad [27]$$

for the total impulse in excess of hydrostatic pressure due to external forces, on unit area of the surface, provided the surface is at rest except during a certain finite interval of time.

The effect of the relief pressure, and hence the effect of diffraction, thus vanishes in the end if the motion of the surface is limited in time.

It must be assumed also, however, that the motion is such as to make the integrals containing dS converge.

THE PROPORTIONALLY CONSTRAINED PLATE OR DIAPHRAGM

Equations [16], [18], and [21] to [24] are of the integrodifferential type, and they are difficult to solve because z is a function both of the time and of position on the plate. For this reason interest attaches to the solutions of the following artificially simplified problem, which can be handled more readily.

Let it be assumed that all parts of the plate execute proportional motions. Then z can be written in the form

$$z = z_c(t) f(x, y) \qquad [28]$$

where z_c is the deflection of a certain point on the plate, which may be thought of as its center, and is a function of the time t alone, while $f(x, y)$ is a shape factor represented by a fixed function of the cartesian coordinates x, y specifying position on the plate; see Figure 17. The natural small oscillations of a plate are actual examples of proportional motion.

After introducing this assumption into Equation [16], the equation can be reduced to an ordinary integrodifferential equation in z and t by integrating over the plate. The most useful result is obtained if the equation is multiplied through by $f(x, y)$ before integrating, namely;

Figure 17 - Illustration of Proportional Motion of a Plate or Diaphragm

The deflection z is at every point proportional to the displacement z_c of a chosen base point or center.

$$M \frac{d^2 z_c}{dt^2} = 2F_i + \phi - \frac{\rho}{2\pi} \int f(x, y) \, dS \int \left(\frac{d^2 z_c}{dt^2} \right)_{t - \frac{s}{c}} f(x', y') \frac{dS'}{s} \qquad [29]$$

where

$$M = \int m \left[f(x, y) \right]^2 dS \qquad [30]$$

$$F_i = \int p_i f(x, y) \, dS, \quad \phi = \int \phi f(x, y) \, dS \qquad [31a, b]$$

In the first integral s is the distance between the elements of area dS and dS', which could be replaced by $dx\,dy$ and $dx'dy'$, respectively. It must be assumed that $f(x, y)$ vanishes fast enough toward infinity to make the integrals converge.

The quantity M represents an effective mass of the plate, while F_i and ϕ represent effective forces; the last term in Equation [29] represents an effective force due to release of pressure by the motion. The center of the plate moves as would a mass M under a force equal to the right-hand member of Equation [29]. Furthermore, the kinetic energy of the plate is actually equal to $M(dz_c/dt)^2/2$; see Equation [115] in the Appendix.

The proportional motion of the plate may be supposed to be guaranteed through the action of suitable internal constraints which do no work on the whole, so that the energy balance is not affected. These constraints contribute nothing to ϕ, as is shown in the Appendix.

Equation [29] is applicable either to an infinite plate or to a plate mounted in an infinite fixed plane baffle; in the latter case the

integrals extend only over ... plate. The equation should also hold roughly when there is no baffle at all provided $2F_i$ is replaced by F_i.

If the baffle is movable, it is more convenient to replace Equation [28] by

$$z = z_b + z_c(t) f(x,y) \tag{32}$$

where z_b is the displacement of the baffle. Thus z_c refers, as before, to the relative displacement between plate and baffle. If this expression for z is introduced into Equation [18], and if the equation is then multiplied through by $f(x,y)$ and integrated over the plate, the result is

$$M \frac{d^2 z_c}{dt^2} = 2F_i + \Phi - \rho c B \frac{dz_b}{dt} - M_b \frac{d^2 z_b}{dt^2}$$

$$- \frac{\rho}{2\pi} \int_{plate} f(x,y) \, dS \int_{plate} \left(\frac{d^2 z_c}{dt^2} \right)_{t - \frac{s}{c}} f(x',y') \frac{dS'}{s} \tag{33}$$

where

$$B = \int f(x,y) \, dS, \quad M_b = \int m \, f(x,y) \, dS \tag{34a, b}$$

Here B represents an equivalent area of the plate and M_b an equivalent mass, both defined with respect to interaction with the baffle.

Comparison of Equations [33] and [29] shows that the relative motion of plate and baffle is affected by the motion of the baffle in the same way as if, with the baffle fixed, the effective driving force $2F_i + \Phi$ were replaced by

$$2F_i + \Phi - \rho c B \frac{dz_b}{dt} - M_b \frac{d^2 z_b}{dt^2}$$

Thus forward velocity of the baffle effectively decreases the load pressure. If the motion of the baffle is accelerated, the relative acceleration of the plate is further decreased in proportion to the acceleration of the baffle.

The absolute motion of the plate is then the sum of its relative motion and the motion of the baffle.

A more convenient form of the integral in Equations [29] and [33] is given in Equation [116] of the Appendix.

Unfortunately, the actual motions of plates or diaphragms under the action of shock waves probably show little resemblance to any type of proportional motion. This is brought out clearly by many observations which have been made at the Taylor Model Basin; these will be described in other reports. The study of proportional motion must find its justification in its mathematical simplicity and in the hope that certain of its features as

revealed by analysis will find their counterpart in the behavior of actual
structures.

The Non-Compressive Case

For a proportionally constrained plate, in a rigid plane baffle, a
definite treatment can be given of the non-compressive case that was dis-
cussed previously in general terms. In the Appendix, Equations [126] and
[127], the following statement is proved:

At any time when the acceleration has been sensibly uniform, at
least during the immediately preceding interval of length D/c, where D is the
maximum diameter of the plate, Equation [29] reduces temporarily to the ordi-
nary differential equation,

$$(M + M_l)\frac{d^2 z_c}{d t^2} = 2F_i + \phi \qquad [35]$$

where

$$M_l = \frac{\rho}{2\pi} \int f(x, y)\, dS \int f(x', y')\frac{dS'}{s} \qquad [36]$$

Here M_l may be regarded as the effective mass of the liquid that
is following the plate; it represents the same loading of the plate by the
liquid that would occur if the liquid were incompressible. The kinetic en-
ergy of the liquid that follows the plate is $M_l(dz_c/dt)^2/2$; see the Appendix.
Thus, when the acceleration varies sufficiently slowly, the release effect
produces the loading by the liquid as calculated from non-compressive theory.

An analogous result for an unconstrained plate is difficult to ob-
tain, but it may be inferred that even in this case there will be some degree
of approach to the motion as calculated for incompressible liquid whenever
the acceleration of the plate satisfies the condition just stated. A rough
estimate of the accelerations to be expected in such cases can probably be
made by assuming some plausible type of proportional constraint and using
Equations [35] and [36].

Some Simple Types of Proportional Constraint

Several forms of proportionally constrained motion were, in effect,
treated by Butterworth (1). His formulas do not contain the factor 2 that
arises from the reflection of the wave, and the retardation in time is omitted
after a brief mention of it; hence his results are in reality those that would
be produced in incompressible water by a pulse of pressure having the same
form as the incident wave.

If the plate moves like a piston, the shape factor in Equation [28] becomes $f(x,y) = 1$. If the plate is circular and of radius a, it is found, as in Equation [128b] in the Appendix, that

$$M_i = \frac{8}{3} \rho a^3 \qquad [37]$$

Furthermore, if m or p_i, respectively, is uniform over the plate, it is obvious from Equations [30], [31a], and [34a, b] that

$$M = \pi m a^2, \quad F_i = \pi a^2 \bar{p}_i \qquad [38a, b]$$

$$M_b = M, \quad B = \pi a^2 \qquad [39a, b]$$

Piston-like motion involves, however, a discontinuity at the edge.

A simple type in which there is no discontinuity is the paraboloidal form,

$$f(x,y) = 1 - \frac{r^2}{a^2}, \quad z = z_c\left(1 - \frac{r^2}{a^2}\right) \qquad [40a, b]$$

where r denotes distance from the center and $r = a$ represents the fixed rim. A spherical shape is scarcely different so long as the curvature remains small. In this case, as in Equation [128a] of the Appendix,

$$M_i = 0.813 \, \rho a^3 \qquad [41]$$

and if m or p_i, respectively, is uniform, Equations [30], [31a] and [34a, b] give

$$M = \frac{\pi}{3} m a^2, \quad F_i = \frac{\pi}{2} a^2 p_i \qquad [42a, b]$$

$$M_b = \frac{3}{2} M, \quad B = \frac{1}{2} \pi a^2 \qquad [43a, b]$$

see Appendix, Equations [120] and [121].

Approximately spherical or paraboloidal shapes are produced by static pressure, but under explosive loading more pointed shapes appear to be commoner; see Figure 18.

The results just cited suggest that in general the formula

$$M_i = 0.8 \frac{\rho a}{m} M \qquad [44]$$
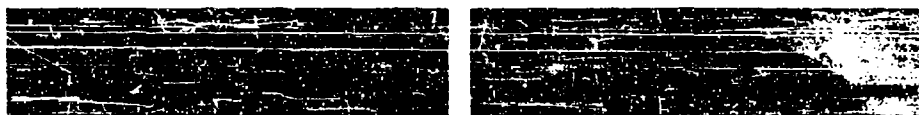
Figure 18 - Typical Profiles of a Diaphragm Deflected by a Non-Contact Underwater Explosion (Left) or by Static Pressure (Right)

may be a good approximation; for the paraboloidal motion, 0.8 is replaced by 0.78, and for the piston motion, by 0.84.

A third type of some interest is

$$f(x,y) = \left(1 - \frac{r^2}{a^2}\right)^{-\frac{1}{2}}, \quad z = z_c\left(1 - \frac{r^2}{a^2}\right)^{-\frac{1}{2}} \qquad [45a, b]$$

for which, as in Equation [132] of the Appendix.

$$M_l = \pi^2 \rho a^3 \qquad [46]$$

and, if p_i is uniform, Equation [31a] gives

$$F_i = 2\pi p_i \int_0^a \left(1 - \frac{r^2}{a^2}\right)^{-\frac{1}{2}} r\, dr = 2\pi a^2 p_i \qquad [47]$$

This form of $f(x,y)$ represents the distribution of velocities with which, according to non-compressive theory, liquid should begin to issue from a circular hole because of a sudden application of pressure; see the Appendix, and Reference (1). Here the liquid surface is assumed to be plane initially. The average velocity is $2dz_c/dt$. As the motion continues, however, second-order effects become appreciable and the usual vena contracta develops; at the edge it will begin forming immediately.

The distribution of velocity over the plate is illustrated for the three types of motion in Figure 19.

In all three cases a rigid baffle beyond the plate or hole has been assumed. If the plate merely forms one side of an air-filled caisson or box, the estimation of M_l is more difficult. From the consideration of a solvable case in the Appendix it appears that the absence of a baffle might reduce M_l for the paraboloidal diaphragm by a factor of about 2, and for a diaphragm moving like a piston by a factor nearer 3.
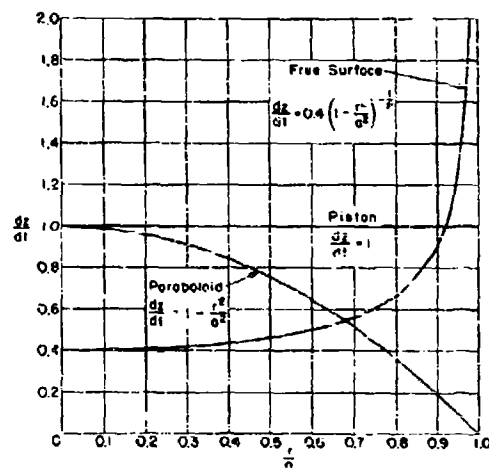
Figure 19 - Distribution of Velocities in Three Types of Proportional Motion, for a Circular Diaphragm

dz/dt is the velocity perpendicular to the initial plane at a distance r from the center of the diaphragm whose radius is a. The velocity is shown in each case on an arbitrary scale.

It may be noted that for the circular piston and for the parabo-
loidal form the intagrodifferential equation can be replaced without great
error by a more easily handled difference-differential equation; for example,
Equation [29] is replaced by

$$\frac{d^2 z_c}{dt^2} + k \frac{dz_c}{dt} - b\left[z_c - z_{c,t-T}\right] = \frac{2F_1 + \phi}{M} \tag{48}$$

or Equation [33] by

$$\mu \frac{d^2 z_c}{dt^2} + k \frac{dz_c}{dt} + \rho c B \frac{dz_b}{dt} + M_b \frac{d^2 z_b}{dt^2}$$

$$- b\left[z_c - z_{c,t-T}\right] = \frac{2F_1 + \phi}{M} \tag{49}$$

Here $z_{c,t-T}$ denotes the value of z_c at time $t - T$, where T is a retardation
time of the order of the diffraction time T_d, while all other quantities re-
fer to time t. If thinning of the diaphragm is neglected, k and b are con-
stants; see Equation [125] in the Appendix.

An equation rather similar to Equation [48] but containing an in-
tegral was used by Kirkwood in developing a theory of damage in the absence
of cavitation (6) (7) (8). His equation was obtained for the central ele-
ment of the diaphragm on the assumption of a paraboloidal form, without the
provision of any mechanism for the maintenance of this form. In the theory
as developed in the present report, the form is assumed to be maintained by
suitable constraints and an equation of motion for the entire diaphragm is
obtained. The results in practical cases differ little, however, and it is
doubtful whether either type of theory represents the motion of an actual
diaphragm very closely.

THE REDUCTION PRINCIPLE

It has already been noted that under suitable circumstances suf-
ficiently accurate results can be obtained from non-compressive theory, in
which the compressibility of the liquid is ignored. This is in reality a
special case of a more general principle. The action of a wave tends con-
tinually to change into or reduce to the type of action that is characteris-
tic of incompressible liquid. For convenience, this principle is called in
this report the reduction principle.

Consider, for example, a flat-topped wave form in which the pres-
sure rises discontinuously to a value p_1 and then remains at this value for
a considerable time. The discontinuous wave front is propagated past an ob-
stacle in strictly rectilinear fashion, leaving a perfect shadow behind the

obstacle. After the front has passed, however, lateral equalization of
pressure sets in and produces the phenomena known collectively as diffrac-
tion. Pressure builds up in the shadow; and all modifications of the pres-
sure field that may have been caused by reflection in front of the obstacle
fade out. The final result is a uniform pressure of magnitude p_1 all around
the obstacle, such as would be inferred from the ordinary hydrostatic, non-
compressive theory. The time required for approximate equalization of the
pressure is roughly equal to the diffraction time for the obstacle, or to
its radius divided by the speed of sound in the liquid.

Any sudden increment of pressure, positive or negative, behaves in
a similar manner. At first, its effects exhibit the characteristics of wave
action; then the effect changes in continuous fashion until it reduces to the
effect that would have been produced in incompressible liquid by the same in-
crement of pressure.

Furthermore, any pressure wave can be regarded as a succession of
small increments. Thus the usual conclusion is reached that waves much
shorter than the diameter of an obstacle will behave in a manner strongly
resembling rectilinear propagation, whereas waves that are much longer will
act more nearly like a static pressure. The non-compressive case previously
noted is one in which changes of pressure occur so slowly that reduction is
practically complete all of the time.

The reduction principle is difficult to formulate mathematically in
the general case, but an exact expression of it is easily obtained for a
proportionally constrained plate. In this case the chief content of the
principle, as deduced in the Appendix, is the following. Suppose that the
plate has been at rest for a time exceeding D/c where D is its greatest di-
ameter. Suppose also that thinning of the plate may be neglected, so that M
and M_l may be treated as constants. Then, during any subsequent interval of
time equal to D/c, both acceleration and velocity take on at least once the
non-compressive values as calculated for the time i at the end of that in-
terval, namely, from Equation [35],

$$\frac{d^2 z}{dt^2} = \frac{2F_1 + \varphi}{M + M_l}, \quad \frac{dz_c}{dt} = \frac{\int(2F_1 + \phi)dt}{M + M_l} \qquad [50a, b]$$

Here M_l is the mass due to loading by the liquid as given by Equation [36],
F_1 and the derivatives of z_c stand for values at time i, and $\int F_1 dt$ extends
from the beginning of the action up to that time.

From this statement it is fairly clear, after a little reflection,
that, if $2F_1 + \phi$ is constant, $d^2 z_c/dt^2$ must oscillate about the non-
compressive value as given by Equation [50a] and gradually settle down

to this value; whereas, if $2F_i + \phi$ continually increases with the time, $d^2 z_c/dt^2$ must exceed the non-compressive value, while if $2F_i + \phi$ decreases, $d^2 z_c/dt^2$ must be somewhat smaller than the non-compressive value. Analogous statements hold for dz_c/dt.

IMPULSIVE EFFECTS

The following two special cases are of interest, partly because of the light they throw upon the qualitative aspects of the action.

Steady Pressure Suddenly Applied

After a plate or diaphragm has been at rest and free from wave action for a long time, let a wave of constant pressure suddenly begin to fall upon it. During the quiescent period, $\phi = 0$ in Equation [16] in order to keep $d^2 z/dt^2 = 0$, and for a short time thereafter ϕ will be small. In the neighborhood of any point of the plate, furthermore, the incident wave will approximate to a plane wave incident at a certain angle. For a short time after its arrival, therefore, the equation appropriate to plane waves, Equation [17], can be used. Each element will begin moving according to this equation independently of all others, and every element will execute the same motion, but with a certain displacement in time if the incidence is oblique.

The plane-wave equation will hold until waves of relief pressure arrive, coming from elements of the plate whose motion differs in other ways than merely by a time difference due to oblique incidence. Thereafter the action becomes more complicated and Equation [16] must be used. In many practical cases, however, the action of a shock wave is almost entirely completed before the simpler Equation [17] begins to fail noticeably.

If the plate is *proportionally constrained*, further light can be thrown upon its later motion. In this case, for a plate mounted in a rigid baffle, if $\phi = 0$, Equation [29] becomes initially

$$M \frac{d^2 z_c}{dt^2} = 2F_i - \rho c A \frac{dz_c}{dt} \qquad [51]$$

where

$$A = \int \left[f(x,y) \right]^2 dS \qquad [52]$$

and represents an effective area; see the Appendix, Equations [140] and [141]. This is the analog for the plate as a whole of Equation [17] for the individual elements. If the mass per unit area m is uniform, $A = M/m$, where M is the effective mass as defined in Equation [30]. If the plate also moves paraboloidally, as represented by Equations [40a, b], $A = \pi a^2/3$, or a third of the actual area.

As the elapsed time approaches the diffraction time, Equation [51] fails and the complete Equation [29] must be used. As soon as the time considerably exceeds the diffraction time, however, a simple description of the motion again becomes possible. The motion then approximates rapidly to the motion that would have occurred if the water had been incompressible. This conclusion may be inferred with sufficient cogency from the reduction principle just described.

From this principle, and, in particular, from Equation [50a], it is sufficiently clear that the acceleration of the plate will take on the non-compressive value as stated in Equation [35] within a time less than D/c, and will oscillate thereafter about this value with a rapidly diminishing amplitude of oscillation. The initial acceleration, which is $2F_i/M$ from Equation [51], is relatively high because the effective mass is at first that of the diaphragm alone, but as the loading by the liquid takes effect the acceleration decreases toward the non-compressive value. Because of the high initial acceleration, however, the velocity remains permanently somewhat in excess of the non-compressive velocity.

The transition from one type of motion to the other is easily followed in detail if the accurate integrodifferential equation is replaced by the approximately equivalent difference-differential equation, Equation [48]. This equation is readily solved in simple cases, provided thinning of the diaphragm is neglected, so that k and o are constants.

In the case under discussion, $z_c = 0$ and $\dot{z}_c = 0$ up to a certain instant, which may be taken as $t = 0$, and thereafter $\phi = 0$ and $2F_i/M$ is equal to a constant. An example of the results obtained from Equation [48] for this case is shown in Figure 20. The curves represent the central acceleration $\ddot{z}_c$ and velocity $\dot{z}_c$ of the diaphragm as functions of the time t; the noncompressive values as given by Equations [50a] and [50b] are shown by straight lines. The unit of time is taken to be the diffraction time, or $T_d = a/c$, where c is the speed of sound in the adjacent liquid and a is the radius of the diaphragm, assumed circular; and the incident pressure is assumed to have such a value that the initial acceleration, $2F_i/M$, is unity. With a constant incident pressure of different magnitude, all ordinates would be changed in proportion to the pressure. The figure refers to the special case in which $pa/m = 12.5$ and hence $M_i = 9.7 M$; then $k = 13.4$ and $b = 9.34$.

The figure would be applicable, for example, to a 10-inch steel diaphragm of thickness 0.05 inch, acted on by a steep-fronted wave in which the pressure behind the front is uniformly 1700 pounds per square inch. Then z_c is in inches, and the unit of time is $T_d = 5/59 = 0.085$ millisecond.

The figure confirms the statements just made as to the approach to non-compressive values, which is very rapid in the case represented. The
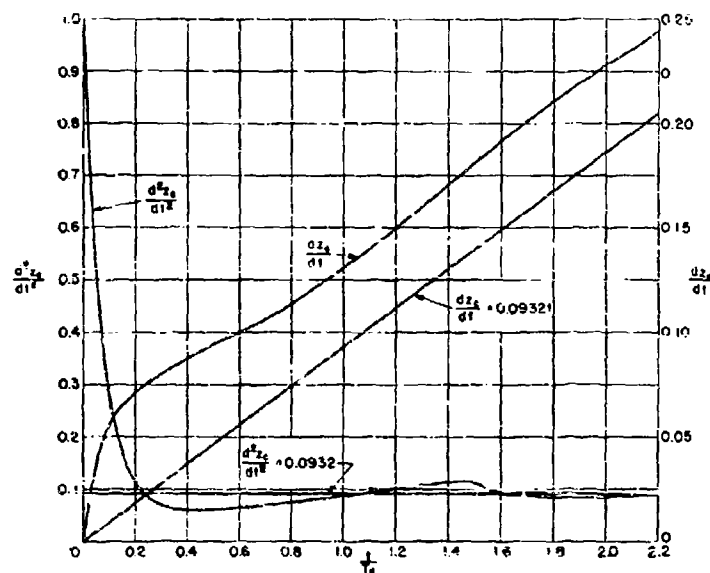
Figure 20 - Curves for a Diaphragm under Uniform Pressure Suddenly Applied

The diaphragm is constrained to move paraboloidally; z_c is the deflection of its center, t is the time, and T_d is the diffraction time, equal to the radius of the diaphragm divided by the speed of sound. The curves represent actual values of acceleration and velocity, the lines represent the non-compressive values. The plot is drawn for a particular case, as explained in the text, and is only approximate.

figure would not be greatly changed if the more correct integrodifferential equation were employed, instead of the approximate difference-differential equation.

    Impulsive Pressure
        The second special case that is of particular interest is the following. After the plate has been at rest for a time exceeding D/c, let it be given by impulsive action a velocity $\dot{z}_c = v_0$ and then left to itself, with $F_i = \phi = 0$. In this case it is evident, by integration of Equation [48] during the time of impulsive action, that

$$v_0 = \frac{dz_c}{dt} = \frac{2}{M} \int F_i \, dt$$

whereas according to the reduction principle the velocity dz_c/dt will approximate within the diffraction time to the non-compressive value as given by Equation [50b] or
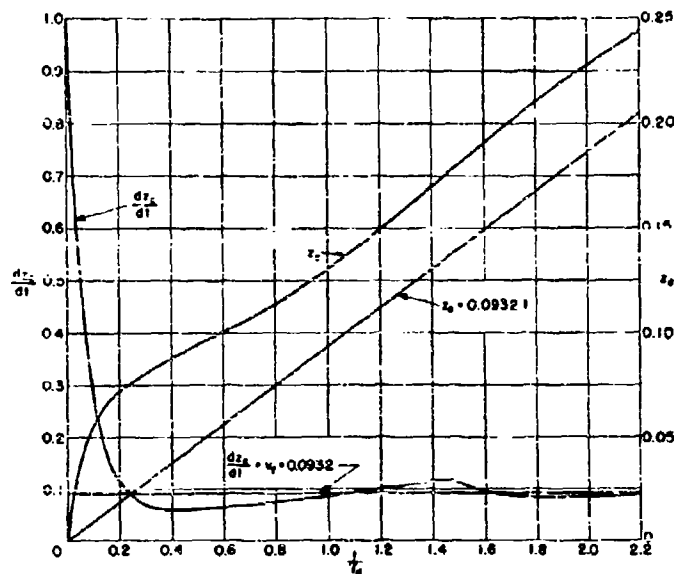
Figure 21 - Curves for a Diaphragm Loaded Impulsively

For further explanation, see the text and the note under Figure 20.

$$v_f = \frac{2}{M + M_l} \int F_i\, dt = \frac{M}{M + M_l}\, v_0 \qquad [53]$$

Thus the initial velocity soon becomes reduced in the ratio $M/(M + M_l)$ as the loading by the liquid comes into play.

The corresponding curves for the velocity dz_c/dt and for z_c as obtained from the approximate difference-differential equation, for $v_0 = 1$ and $\rho a/m = 12.5$, are shown in Figure 21; the horizontal line represents v_f. The curves and lines happen to be exact copies of those in Figure 20. The rapid approach to the non-compressive velocity is again evident.

Solutions for either of these two simple cases could be utilized to construct by addition the general solution of Equation [48], provided Φ is known as well as F_i. The case first discussed corresponds to Heaviside's unit function.

MOTION OF A PLATE OR DIAPHRAGM CONSTRAINED ONLY AT THE EDGE

The accurate treatment of a plate that is not constrained as to shape presents a very difficult problem even on the hydrodynamic side, apart from all the difficulties that arise from the varying elastic and plastic

behavior of the material of the plate. All complications due to the material of the plate have been hidden in the present treatment under the symbol ϕ or Φ and no detailed consideration of them will be attempted in this report.

In the absence of exact solutions, semiquantitative results of some utility may be obtained by assuming a convenient or plausible type of proportional constraint and applying the corresponding results of analysis. A principle equivalent to the reduction principle may be expected to hold, although ., as has been stated, it is not easy to prove or even to formulate in the general case. The velocities generated by a short impulse of pressure, for example, should be relatively large at first, but they should decrease, within a time less than the diffraction time, approximately to the velocities that would have been generated if the water had been incompressible.

CAVITATION AT A PLATE OR DIAPHRAGM

The analysis is readily extended to cover the occurrence of cavitation at the interface between a liquid and a plate or diaphragm that remains

approximately plane, provided sufficiently simple assumptions are made concerning the laws of cavitation. Let it be assumed that cavitation sets in wherever the pressure at the interface sinks below a fixed breaking-pressure p_b, and let all complications due to surface tension or to the projection of spray from the free surface of the liquid be ignored. The cavitated region will thus be assumed to have a sharp bounding edge on the diaphragm, as illustrated in Figure 22. The results obtained on these assumptions will be described here, with reference for further details to the Appendix; they should find at least qualitative application to actual cavitation at an interface, unaccompanied by cavitation in the midst of the liquid.

Figure 22 - Illustration of the Edge of a Cavitated Area

In the left-hand figure the edge is advancing at speed U over the face of the diaphragm. In the right-hand figure it is receding; at the edge, the tangent to the liquid surface makes an angle ϕ with the tangent to the diaphragm, and, as the edge passes, each point of the liquid surface changes its normal velocity from $\dot{z}_1$ to the normal velocity $\dot{z}_2$ of the plate.

In practical cases the cavitation should usually begin, if at all, during the initial phase of the motion, and at a central point where the incidence of the waves is nearly normal. For this phase, therefore, the formulas for the free plate should hold approximately, as discussed on page 4.

There remain then, for discussion, the process by which the region of cavitation spreads over the plate, the subsequent motion of the free liquid surface, and the final process by which the cavitation is destroyed.

After cavitation has begun, the edge of the cavitated region will advance over the plate for a time as a breaking-edge, enlarging the area of cavitation; then it will halt and eventually return as a closing-edge; see Figure 22. It must begin its advance from the initial point at infinite speed; and it may happen that the cavitation spreads instantaneously over a finite area. Similarly the cavitation may disappear simultaneously over a certain area, in which case the closing-edge may be supposed to move at an infinite speed. In other cases the edge will move at a finite speed.

The process at the edge turns out to be distinctly different according as U, the velocity of its propagation in a direction perpendicular to itself, is less or greater than c, the speed of sound in the liquid.

If $U < c$, it appears that no discontinuities of pressure or particle velocity can occur at the edge of the cavitated region, and U is merely the velocity with which the liquid next to the edge is streaming over the plate. This velocity, in turn, is determined jointly by the incident wave and by all of the diffracted waves emitted by various parts of the plate, and no simple statement in regard to its value can be made.

If $U \geq c$, on the other hand, the propagation of the edge is essentially a local phenomenon, and mathematical treatment is easy. For effects can be propagated through the liquid only at the speed c, and no such effects coming from points behind the moving edge can overtake it; thus its behavior must be determined solely by conditions just ahead of it, and these in turn cannot be affected by the approach of the edge. For the same reason, the analytical results are not limited now to small displacements of the plate. Impulsive effects also become possible.

For a breaking-edge moving in this manner:

$$U = -\frac{\dfrac{\partial p}{\partial t}}{\dfrac{\partial p}{\partial n}} \qquad [54]$$

where $\partial p/\partial t$ is the rate of change of the pressure in the liquid ahead of the edge, as determined by the incident pressure wave and the motion of the plate, and $\partial p/\partial n$ is the gradient of this pressure over the plate in a direction normal to the edge, see Equation [147] in the Appendix. Here, necessarily, $\partial p/\partial t < 0$. Thus the edge of the cavitated area will advance toward the unbroken side at the speed $U \geq c$ provided $-\partial p/\partial t \geq c\,\partial p/\partial n$.

As the edge advances, the particle velocity of the liquid in a direction normal to the plate changes impulsively by

$$\Delta \dot{z} = \frac{p_b - p_c}{\rho c}\left(1 - \frac{c^2}{U^2}\right)^{\frac{1}{2}} \tag{55}$$

where p_c is the pressure in the cavitated region, assumed uniform; see Equation [149] in the Appendix. Or, if U is infinite, as in the instantaneous occurrence of cavitation over a finite area,

$$\Delta \dot{z} = \frac{p_b - p_c}{\rho c} \tag{56}$$

as in one-dimensional motion. If $p_b = p_c$, or if $U = c$, $\Delta \dot{z} = 0$. Otherwise $\Delta \dot{z} \leq 0$, since the liquid cannot penetrate the plate; this agrees with the fact that $p_b \leq p_c$.

The analogous formula for a closing-edge is

$$U = \frac{\dot{z}_l - \dot{z}_p}{\tan \theta} \tag{57}$$

where $\dot{z}_l$ and $\dot{z}_p$ are normal velocities of liquid surface and plate just ahead of the edge in the cavitated area, and θ is the angle at which the edge meets the plate; see Equation [152] in the Appendix, and Figure 22. Thus $U \geq c$ only if $\dot{z}_l - \dot{z}_p \geq c \tan \theta$. As an exceptional case, it appears that the liquid surface might roll onto the surface like a rug being rolled onto the floor, with $\dot{z}_l = \dot{z}_p$, and $\theta = 0$ at the edge of contact. If $\dot{z}_l > \dot{z}_p$, the pressure in the liquid adjacent to the plate rises impulsively, as the edge passes, from p_c to $p_c + \Delta p$ where

$$\Delta p = \rho c \left(\dot{z}_l - \dot{z}_p\right)\left(1 - \frac{c^2}{U^2}\right)^{-\frac{1}{2}} \tag{58}$$

or, if $U = \infty$, as where closure of cavitation occurs simultaneously over a certain area,

$$\Delta p \qquad \left(\dot{z}_l - \dot{z}_p\right) \tag{59}$$

See Equation [151] in the Appendix. Equation [59] is familiar in one-dimensional water-hammer theory.

Before and after the passage of the edge, each element of the liquid surface will follow one of the differential equations already written down. In the cavitated region this will be Equation [24] or

$$\frac{\rho}{2\pi} \int \left(\frac{d^2 z}{dt^2}\right)_{t-\frac{s}{c}} \frac{dS}{s} = 2p_i + p_0 - p_c \tag{60}$$

in which p_e represents the actual pressure p on the surface. At the same
time, elements in contact with the plate will be moving according to some
other equation such as Equation [16]. The symbol (d^2z/dt^2), e in any equa-
tion may be taken to refer always to the acceleration of an element of the
liquid surface, whether free or in contact with the plate.

The impulse

It is noteworthy that the total impulse on any point of the plate
should not be affected by the occurrence of cavitation. For the pressure on
the plate is always the same as that on the liquid surface, according to the
assumptions that have been made. Hence, from Equation [24], the total im-
pulse per unit area on the plate due to the waves, up to a time at which the
plate has come to rest and all effects of diffraction have ceased, is

$$I = \int (p - p_0) \, dt = 2\int p_i \, dt \qquad [61]$$

where p_i is the pressure in the incident wave. The integral of the left-hand
member of Equation [24] with respect to the time vanishes in the end, since
dz/dt begins and ends at zero. The intervention of cavitation has no effect
upon Equation [61].

A Proportionally Constrained Plate

The problem becomes much simplified and can be treated completely
if the very arbitrary mathematical assumption is made that both plate and
liquid surface move proportionally and in the same manner, so that their dis-
placements are both represented by equations of the type of Equation [28] but
with different values of $z_c(t)$ during the cavitation phase. Cavitation then
appears and disappears simultaneously at all points of the plate. Successive
phases of such motion are illustrated in Figure 23.

Figure 23 - Illustration of Cavitation
According to the Assumption of
Proportional Constraint

The left-hand figure shows the initially flat dia-
phragm; in the middle, cavitation has occurred, but
both diaphragm and liquid surface are assumed to be
deformed in the same proportional manner; right, the
cavitation has disappeared simultaneously over the
entire diaphragm.
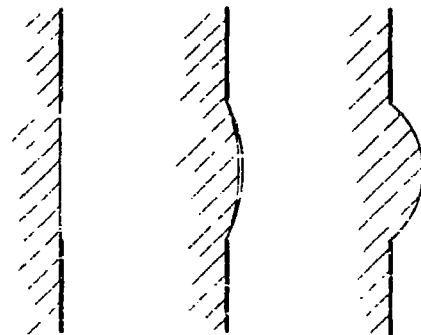
With this assumption, the tendency for the motion to approximate ultimately to the non-compressive type can be formulated mathematically. At the instant of cavitation, an impulsive decrease may occur in the velocity of the liquid surface, but this is not of much significance. For it may be inferred from the reduction principle as developed in the Appendix that, within a time of the order of the diffraction time T_i after the onset of cavitation at a certain time t_1, the velocity of the center of the liquid surface will approximate to the value

$$\dot{z}_c = \dot{z}_c' + \frac{1}{M_i} \int_{t_1}^t (2F_i + \phi_s)\, dt \qquad [62]$$

Here F_i and M_i are given by Equations [31a] and [36], respectively;

$$\phi_s = \iint (p_0 - p_c)\, f\,(x, y)\, dx\, dy \qquad [63]$$

where p_0 is the total hydrostatic pressure in the liquid at the level of the point x, y on the cavitated surface, p_c is the pressure in the cavity, and the integral extends over the entire surface of the liquid under the place; and, finally, $\dot{z}_c'$ stands for the velocity of the combined plate-liquid surface at a time that precedes the onset of cavitation by an interval of the order of the diffraction time; see Equation [158] in the Appendix.

The value of $\dot{z}_c$ given by Equation [62] differs from the value given by non-compressive theory only in that the initial velocity $\dot{z}_c'$ is not taken at the instant of cavitation. If cavitation occurs very soon after the arrival of the pressure wave, $\dot{z}_c'$ is practically the same as the value of $\dot{z}_c$ just before the arrival of the wave.

Similarly, after closure of the cavitation at a time t_2, the velocity of the combined liquid-plate surface soon becomes

$$\dot{z}_c = \frac{M_i}{M + M_i} \dot{z}_{cl}' + \frac{M}{M + M_i} \dot{z}_{cp} + \frac{1}{M + M_i} \int_{t_2}^t (2F_i + \phi)\, dt \qquad [64]$$

where M, ϕ and F_i are as in Equation [29], $\dot{z}_{cp}$ is the velocity of the plate just before impact, and $\dot{z}_{cl}'$ is the velocity of the liquid surface at a time that precedes t_2 by an interval of the order of the diffraction time. See the Appendix, Equations [161] and [162], where an explicit expression for $\dot{z}_{cl}'$ is given.

This is again nearly the non-compressive result. The last term in Equation [64] represents the change in velocity of the liquid-loaded plate that is caused by the applied forces. If $\dot{z}_{cl}'$ were replaced by the velocity of the liquid surface at the moment of impact, the first two terms would

represent the resultant velocity as given by the usual formula for an inelastic impact between masses M and M_l.

If the liquid surface is not constrained in shape, as in reality it is not, expressions comparable to these are hard to obtain. It appears, however, that at least the order of magnitude of the effects to be expected may be ascertained in a given case by assuming a reasonable form of proportional constraint for both plate and liquid surface and employing Equations [62] and [64]. The equations will hold so long as no further short-lived pressure waves arrive to cause temporary departures from the non-compressive motion.

In using the equations it may be possible to fix the value of $\dot{z}_o'$ or $\dot{z}_{ol}$ only within certain limits, but this may be sufficient for practical purposes.

PART 4.   DAMAGE TO A DIAPHRAGM
A FEW SWING TIMES

It is often desired to estimate the swing time of a plate or diaphragm. A rough estimate can be based upon the formula for the following special case; see the Appendix, Equation [173].

Consider a circular diaphragm of radius a and uniform thickness, held rigidly at the edge, and thin enough so that bending resistance can be neglected. Assume that the elastic range is negligible, that the yield stress has the constant value σ, that the diaphragm, initially flat, remains symmetrical and paraboloidal in form during its motion, and that thinning may be neglected. Then the swing time, or time for the diaphragm to swing freely through a short distance from the flat position and come to rest at its maximum deflection, if there is gas at equal pressure on both sides, is

$$T_s = \frac{\pi a}{2\sqrt{6}}\sqrt{\frac{\rho_d}{\sigma}} \qquad [65]$$

where ρ_d is the density of the material. If the density is 0.283 pounds per cubic inch, as for steel, so that in dynamical units $\rho_d = 0.283/386$, if $\sigma = 60,000$ pounds per square inch, which may be a reasonable nominal estimate for mild steel under high strain rate, and if a is in inches and T_s in milliseconds,

$$T_s = \frac{17.4\,a}{\sqrt{\sigma}} = 0.061\,a \qquad [66]$$

If the diaphragm is mounted in a rigid baffle with liquid of density ρ_l on one side, the hydrostatic pressure in the liquid being the same as the pressure of the gas on the opposite face, then the swing time is increased, as a result of loading by the liquid, to

$$T_s = \frac{\pi a}{2\sqrt{C}} \sqrt{\frac{\rho_d}{\sigma}\left(1 + 0.78 \frac{\rho_l}{\rho_d}\frac{a}{h}\right)} \qquad [67]$$

where h is the thickness of the diaphragm. For the same steel and for water this becomes

$$T_s = 0.061\, a \sqrt{1 + 0.100\frac{a}{h}} \text{ milliseconds} \qquad [68]$$

provided a and h are expressed in the same unit. If there is liquid on both sides of the diaphragm and of the baffle, having a density ρ_1 on one side and ρ_2 on the other, ρ_l is to be replaced in Equation [67] by $\rho_1 + \rho_2$.

If the diaphragm is mounted in one side of a gas-filled box only slightly larger in diameter, the coefficient 0.78 in Equation [67] is changed to something like 0.4, and 0.100 in Equation [68] to roughly 0.05.

The effect of the elastic range is discussed in the Appendix.

DEFLECTION FORMULAS FOR A DIAPHRAGM

From a survey of the preceding analytical results it appears that only limited progress has been made as yet toward an exact treatment of the hydrodynamical side of the problem that is presented by the impact of a shock wave upon a diaphragm. The situation is somewhat better as regards the behavior of the diaphragm itself, although even here complexities and uncertainties are encountered because of work hardening, increase of stress at high strain rate and thinning of the diaphragm. It is not the purpose of this report to attempt an accurate theory of the plastic deformation of a diaphragm. Simplified assumptions as to its behavior will be adopted in order to obtain a few approximate formulas possessing a limited usefulness.

Let the yield stress σ be constant. For steel this is more nearly true at high strain rates than at low rates. Let both the elastic range and the thinning be neglected. Actually, the thinning may extend to 1/3 or even 2/5, but its effect is at least in the opposite direction to that of work hardening. With these assumptions the fundamental equation for plastic deflection can be written in the simple form,

$$E = \sigma h \Delta A \qquad [69]$$

where E is the net energy delivered to the diaphragm, h is its thickness and ΔA is its increase in area due to plastic flow.

For a circular diaphragm deflected into a spherical form, $\Delta A = \pi z^2$ in terms of the central deflection z; this formula is almost correct also for the paraboloidal form. For a circular cone,* $\Delta A = \pi z^2/2$. Profiles for these

---

* Shapes between spherical and conical are often produced by underwater explosion; they are nearly hyperboloidal, as illustrated in Figure 24. Certain observations indicate that in the course of the damaging process nearly conical shapes may occur momentarily.

shapes are compared in Figure
24. For a rectangle w_1 and w_2
on a side, deflected into the
shape characteristic of mem-
brane vibration in the lowest
mode, so that the deflection
at any point is $z \sin\frac{\pi x}{w_1} \sin\frac{\pi y}{w_2}$
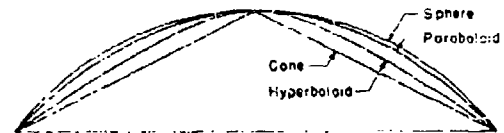
Figure 24 – Curves Illustrating Four Types
of Diametrical Profiles for a Diaphragm

$$\Delta A = \left(\frac{\pi^2}{8}\right)\left(\frac{w_1}{w_2} + \frac{w_2}{w_1}\right)z^2$$

for small z. Thus for circle, cone and rectangle, respectively, for small z,

$$E = \pi \sigma h z^2, \quad E = \frac{1}{2}\pi \sigma h z^2, \quad E = \frac{1}{8}\pi^2 \sigma h \left(\frac{w_1}{w_2} + \frac{w_2}{w_1}\right)z^2 \quad [70a, b, c]$$

For a square or $w_1 = w_2$, E is $\pi/4$ times as great as for a circle at the same
central deflection.

A correction for the elastic range is easily made, if required,
provided it is assumed that the elastic constants are unaltered by plastic
flow and provided resistance to bending may be neglected. During deformation
up to the elastic limit the area will increase by a definite amount ΔA_e.
Since the stresses are at each instant proportional to the increase in area
up to that instant, the average stress will be $\sigma/2$ and the energy absorbed
up to the elastic limit will be

$$E_e = \frac{\sigma}{2} h \Delta A_e$$

or half what it would be if the stress were constant. Thus, if E denotes the
total energy absorbed by the diaphragm, initially flat, up to a maximum in-
crease of area ΔA_m,

$$E = \frac{1}{2}\sigma h \Delta A_e + \sigma h (\Delta A_m - \Delta A_e)$$

If ΔA is the residual increase in area after removal of the load, $\Delta A =$
$\Delta A_m - \Delta A_e$. Hence

$$E = \sigma h \left(\Delta A_m - \frac{1}{2}\Delta A_e\right) = \sigma h \left(\Delta A + \frac{1}{2}\Delta A_e\right) \qquad [71]$$

In general, the increase in area is proportional to the square of
the central deflection, for small deflections. Hence, if the central deflec-
tion is z_e to the elastic limit, z_m to the maximum under full load and z for
the permanent set, from Equation [71]

$$z^2 = z_1^2 - \frac{1}{2}z_3^2, \quad z_m^2 = z^2 + z_e^2 \qquad [72a, b]$$
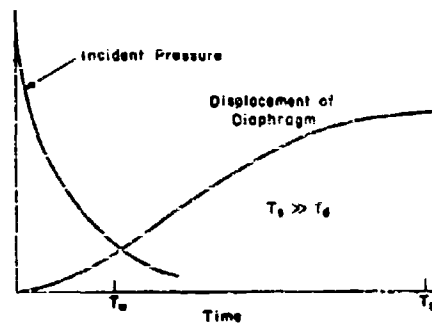
Figure 25 - Illustration of Case 1,
Relatively Long Swing Time

The swing time of the diaphragm, T_s, is much longer
than either the time constant T_w of the incident
pressure wave or the diffraction time T_d.

where z_1 is the deflection calcu-
lated from E with neglect of the
elastic range, that is, from $E =$
$\sigma h \Delta A_1$ where ΔA_1 corresponds to z_1,
or by putting $z = z_1$ in Equation
[70a, b, c]. It is assumed here
that the same shape occurs at all
deflections mentioned.

In a few special cases,
formulas for the deflection pro-
duced in a diaphragm by a shock
wave can now be obtained by bring-
ing forward suitable formulas for
E.

CASE 1: Relatively Long Swing Time, No Cavitation; i.e., $T_s \gg T_d$ and $T_s \gg T_w$,
or the swing time of the diaphragm several times longer than either the dif-
fraction time or the time constant of the wave, as illustrated in Figure 25.
These conditions as to the times are usually satisfied in practical test as-
semblies because of the thinness of the diaphragms.

Let the diaphragm be mounted in a fixed plane baffle. Then, if it
is assumed to be proportionally constrained in its motion, in the sense de-
fined on page 26, its center will acquire a velocity

$$v_{cm} = \frac{2 \int F_i \, dt}{M + M_i} \qquad [73]$$

This equation results from integration of Equation [35] in case $T_d \ll T_w$, so
that non-compressive theory holds; otherwise it follows from the reduction
principle as expressed in Equation [50b]. It is only necessary that stresses
in the structure have little effect on the diaphragm until the hydrodynamic
action is completed.

The combined kinetic energy of diaphragm and water will then be
converted into plastic work, so that

$$E = \frac{1}{2} (M + M_i) v_{cm}^2 = \frac{2 \left[\int F_i \, dt \right]^2}{M + M_i} \qquad [74]$$

For a circular diaphragm of radius a deflected paraboloidally,

$$F_i = \pi a^2 \frac{p_i}{2}, \quad M = \pi \rho_d h \frac{a^2}{5}, \quad M_i = 0.813 \rho a^3$$

in terms of the incident pressure p_i, thickness h, density of diaphragm material ρ_d and of water ρ; see Equations [42b], [42a], and [44]. Hence, from Equation [72a], for a small central set deflection z,

$$z^2 = z_1^2 - \tfrac{1}{2}\, z_e^2 \qquad [75]$$

where z_e is the deflection at the elastic limit and z_1 is found from Equations [70a] and [74] to be

$$z_1 = v_{cm}\sqrt{\frac{M + M_i}{2\pi\sigma h}} \qquad [76]$$

or

$$z_1 = \frac{a}{h}\left(\int p_i\, dt\right)\left(\frac{3}{2}\,\frac{1}{\sigma\rho_d}\,\frac{1}{1 + 0.776\,\frac{\rho}{\rho_d}\,\frac{a}{h}}\right)^{\tfrac{1}{2}} \qquad [77]$$

If the incident wave is of exponential form, so that $p_i = p_m e^{-\alpha t}$, $\int p_i\, dt$ may be replaced by p_m/α.

Equation [77] implies a variation of z as $\int p_i\, dt$ and hence roughly as $W^{\tfrac{2}{3}}/R$, where W is the weight of the charge and R is the distance from the charge to the diaphragm. This latter statement is based on similitude combined with the assumption that p varies simply as $1/R$ for a given charge.

According to similitude, the same pressures occur at distances and at times proportional to $W^{\tfrac{1}{3}}$; hence, if $f(R', t')$ denotes the pressure as a function of the distance R' and of the elapsed time t' since detonation for a unit charge or $W = 1$, the pressure due to any other charge at distance R and time t is

$$p_i = f\!\left(\frac{R}{W^{\tfrac{1}{3}}},\frac{t}{W^{\tfrac{1}{3}}}\right)$$

hence

$$\int p_i\, dt = \int f\!\left(\frac{R}{W^{\tfrac{1}{3}}},\frac{t}{W^{\tfrac{1}{3}}}\right) dt = W^{\tfrac{1}{3}}\int f\!\left(\frac{R}{W^{\tfrac{1}{3}}},t'\right) dt'$$

where $t' = t/W^{\tfrac{1}{3}}$. But the value of $\int p_i\, dt$ for $W = 1$ is a function of R' given by

$$I_1(R') = \int f(R', t')\, dt'$$

Thus at a distance from any charge

$$I = \int p_i\, dt = W^{\tfrac{1}{3}}\, I_1\!\left(\frac{R}{W^{\tfrac{1}{3}}}\right) \qquad [78]$$

Roughly, $I_1(R') \propto W^{\tfrac{1}{3}}/R'$ and hence $I \propto W^{\tfrac{2}{3}}/R$. Actually, according to theoretical estimates partially confirmed by observation, the maximum pressure

should vary more rapidly than as $1/R$. Furthermore, the duration of the pressure wave at a given point should increase somewhat with an increase in R; for an exponential wave this is represented by a slow decrease in α. These two changes have opposite effects upon I, but the first should predominate. Thus $I_1(R')$ should vary somewhat more rapidly than as $1/R'$.

A further complication arises in practical cases from the spherical form of the wave. This further decreases the deflection somewhat; and the decrease should be greater at small distances. Work hardening and increased strain-rate effects in the diaphragm will also have the effect of decreasing the larger deflections as compared with the smaller.

The final result seems to be that Equation [77] implies a variation of z as $W^{\frac{1}{3}}F(W^{\frac{1}{3}}/R)$ where $F(W^{\frac{1}{3}}/R)$ equals $I_1(R/W^{\frac{1}{3}})$ multiplied by a factor to correct for sphericity and other minor factors; and $F(W^{\frac{1}{3}}/R)$ might vary either more rapidly or less rapidly than as $W^{\frac{1}{3}}/R$. The variation of z might happen to be nearly as $W^{\frac{n+1}{3}}/R^n$ where n is a constant either a little greater or a little less than unity.

Other cases in which cavitation does not occur may be treated by integrating one of the other equations of motion. Kirkwood solved his equation for the paraboloidal diaphragm, which was mentioned in connection with Equation [48], with the help of Fourier Analysis; the results may be found in his reports, References (6) (7) and (8).

CASE 2: Prompt and Lasting Cavitation at the Diaphragm Only; $T_m \ll T_d$, $T_m \ll T_s$, or the compliance time is much less than either the diffraction time or the swing time, as illustrated in Figure 26. It is assumed here that cavitation sets in so quickly that the diaphragm acquires maximum velocity before the pressure field has been appreciably modified by diffraction, and also before the diaphragm has moved far enough to call appreciable stress forces into play. It is also assumed that no further deflection is produced when the cavitation disappears. These conditions as to times are commonly satisfied in test assemblies; if cavitation occurs at all, it should usually occur relatively early in the damaging process.

Under the conditions stated, all parts of the diaphragm will be
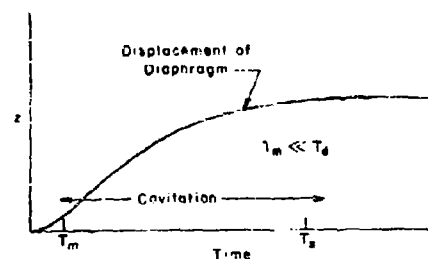
Figure 26 - Illustration of Case 2, Prompt and Lasting Cavitation at the Diaphragm

At the compliance time T_m the diaphragm has reached maximum velocity; cavitation is then assumed to occur and to last at least until the diaphragm has completed its outward swing.

projected with a common velocity v_m, and the entire diaphragm will acquire kinetic energy of magnitude

$$E = \frac{1}{2} h \rho_d A v_m^2 \tag{79}$$

where A is its area. This energy will then be converted into elastic and plastic work, and if the relation between this work and the deflection is known, the deflection can be calculated.

Equation [72a], with z_1 calculated from [70a] and [79], thus gives, for a circular diaphragm of radius a, deflected into a spherical shape,

$$z^2 = z_1^2 - \frac{1}{2} z_i^2, \quad z_1 = a v_m \sqrt{\frac{\rho_d}{2\sigma}} \tag{80a, b}$$

For a shock wave of exponential form, $p_i = \bar{p}_m e^{-\alpha t}$, the maximum velocity is given by Equation [7], and

$$z_1 = \frac{a p_m}{\rho c} \sqrt{\frac{2\rho_d}{\sigma}} \; x^{\frac{1}{1-z}} \tag{81}$$

where $x = \rho c/\alpha \rho_d h$, in which ρ is the density of water in dynamical units and c the speed of sound in it.

If the diaphragm is deformed into a more pointed shape, as commonly happens, z will be somewhat greater; for a conical form, z_1 would be greater in the ratio $\sqrt{2}$. On the other hand, the actual maximum velocity will probably be somewhat less than v_m as given by Equation [7], because cavitation will probably not occur until the pressure has sunk more or less below the hydrostatic value; z will be correspondingly reduced.

These equations predict nearly the same variation of z with distance R from the charge as was inferred for Case 1, but, for ordinary thin diaphragms, a somewhat slower variation with charge weight W. The difference arises from a decreased influence of the duration of the wave. This influence is represented, for an exponential wave, by the factor $x^{\frac{1}{1-z}}$ in Equation [81]. Since $x = \rho c/\alpha m$, x increases in proportion to $1/\alpha$ and hence in the same ratio as does the factor $\int p_i \, dt$ in Equation [77]; but in practical cases x lies between some such limits as 2 to 10, and a glance at Figure 4 on page 5 shows that in this range $x^{\frac{1}{1-z}}$ increases much less rapidly than does x.

The deflection z and the projection velocity v_m may vary, therefore, in this case, either a little more rapidly or a little less rapidly than as $1/R$; they should vary more rapidly than as $W^{\frac{1}{3}}$, but not so rapidly as $W^{\frac{2}{3}}$. Both z_1 and v_m might happen to be nearly proportional to $W^{\frac{1}{2}}$.

CASE 2a: Same as Case 2 with Reloading after Cavitation at the Diaphragm; Figure 27. After the occurrence of cavitation the remainder of the shock wave should act on the water surface and accelerate it toward the diaphragm,

unless the shock wave is so short that its duration does not exceed the compliance time T_m. The effect on the water should be especially strong near the edge of the diaphragm; and here, also, the motion of the diaphragm is soon checked by the support. At the edge, therefore, the cavitation must begin to disappear immediately, and it should then disappear progressively toward the center. The boundary of the cavitated area may move at supersonic velocity and will then be accompanied by an impulsive increment of pressure.

Figure 27 - Illustration of Case 2a, Cavitation at the Diaphragm with Reloading

This differs from Figure 26 in that the cavitation closes again and the water gives the diaphragm a fresh impetus outward.

Such an action is hard to follow analytically. The only easy case is the rather different ideal one in which both diaphragm and water surface are assumed to move in the same proportional manner, as on page 41. Then the cavitation closes impulsively on all parts of the diaphragm at once.

If the duration of the cavitation is considerably longer than the diffraction time, Equation [62] gives for the velocity acquired by the center of the water surface while free

$$\dot{z}_c = \frac{2}{M_1} \int_{T_m} F_i \, dt$$

where T_m is the time of the beginning of cavitation; this time is assumed to follow the arrival of the wave so closely that $\dot{z}_c'$ in Equation [62] can be dropped, and ϕ_s is assumed to be equal to zero.

When the water subsequently overtakes the diaphragm, an impulsive equalization of their velocities will occur, resulting in a partial reflection of the kinetic energy back into the water. If the diaphragm has already been brought to rest by the action of internal stresses, their common velocity soon after the impact of the water should be $M_1 \dot{z}_c / (M + M_1)$, according to the first term on the right in Equation [64], and their combined kinetic energy should then be

$$\frac{1}{2}(M + M_i)\left(\frac{M_i \dot{z}_c}{M + M_i}\right)^2 = \frac{2\left[\int_{T_m} F_i \, dt\right]^2}{M + M_i} \qquad [82]$$

This energy represents a fraction $M/(M + M_i)$ of the energy of the moving water, whose total magnitude is

$$\frac{1}{2} M_i \dot{z}_c^2 = \frac{2\left[\int_{T_m} F_i \, dt\right]^2}{M_i} \qquad [83]$$

The fraction $M_i/(M + M_i)$ will, however, be close to unity in practical cases; and if the diaphragm is moving at the time of impact, it will take on a still larger fraction of the kinetic energy of the water.

The kinetic energy of water and diaphragm will then be converted into additional plastic work. The total work should thus be at least as large as

$$E = \frac{1}{2} h \rho_d \, A v_m^2 + \frac{2\left[\int_{T_m} F_i \, dt\right]^2}{M + M_i}$$

Inserting again the values for the paraboloidal circular diaphragm and v_m from Equation [7], noting that, if $p_i = p_m e^{-\alpha t}$

$$\int_{T_m} F_i \, dt = \frac{1}{2} \pi a^2 \int_{T_m}^{\infty} p_m e^{-\alpha t} dt = \frac{\pi a^2 p_m}{2\alpha} \, x^{\frac{1}{1-x}}$$

by Equation [5a], and equating the value found for E to $\pi \sigma h z_i^2$, it is found that Equation [81] is replaced by

$$z_1 = \frac{a p_m}{\rho c} \sqrt{\frac{2 \rho_d}{\sigma}} \, x^{\frac{1}{1-x}} \left(1 + \frac{3}{4} \frac{x^2}{1 + 0.776 \frac{\rho}{\rho_d} \frac{a}{h}}\right)^{\frac{1}{2}} \qquad [84]$$

for an incident wave of exponential form. In these formulas it might be more nearly correct to omit M, or the 1 in the denominator under x^2 in the last equation.

Comparison of Equation [84] with Equation [81] shows that the reloading increases the deflection in the ratio

$$\left(1 + \frac{3}{4} \frac{x^2}{1 + 0.776 \frac{\rho}{\rho_d} \frac{a}{h}}\right)^{\frac{1}{2}}$$

Since x increases with $1/\alpha$, or with the duration of the wave, it appears from the considerations advanced in the discussion of Case 1 that the deflection

should probably be more nearly proportional to $1/R$ in this case than in either of the other two cases, but should increase with W more rapidly than in Case 2.

The applicability of Equation [84] in actual cases is doubtful, however, because of the artificial assumption that has been made as to the motion of the water. If closure of the cavitation in reality progresses from the edge inward, it is possible that support of the water by the outer part of the diaphragm may greatly decrease the development of kinetic energy in the water. Furthermore, a fixed baffle has been assumed. If there is no baffle, or if it yields, the kinetic energy acquired by the water and the resulting increase in the plastic work will be less.

CASE 3: Negligible Diffraction Time T_d but Wave Not Short; $T_d \ll T_w$ and $T_d \ll T_s$. Under these circumstances non-compressive theory can be used. If also $T_w \ll T_s$, or the time constant of the wave is much less than the swing time, the situation is that of Case 1. Otherwise the action of the wave overlaps on that of the stress forces, and the motion of the diaphragm is more complicated.

For a proportionally moving diaphragm mounted in a large plane fixed baffle, quantitative results are easily obtained. According to the simple assumptions that were made in the beginning, the net stress-force resisting its motion will be proportional to its deflection; hence it is possible to write $\Phi = -kz_c$ where k is a constant. Then Equation [35] becomes

$$(M + M_l)\frac{d^2 z_c}{dt^2} + kz_c = 2F_i \qquad [85]$$

which is of the same form as for a forced harmonic oscillator. For the exponential wave or $p_i = p_m e^{-at}$, F_i can be written $F_i = F_0 e^{-at}$ where F_0 is a constant. The appropriate solution of Equation [85], when $z_c = z_c = 0$ at $t = 0$, is then

$$z_c = \frac{2F_0}{(M + M_l)(\alpha^2 + \mu^2)}\left(e^{-at} + \frac{\alpha}{\mu}\sin\mu t - \cos\mu t\right) \qquad [86]$$

where

$$\mu = \sqrt{\frac{k}{M + M_l}} \qquad [87]$$

The final deflection z_{cm} will be the first maximum value of z_c; find it requires the solution of a transcendental equation. It may conveniently be expressed in terms of the deflection under a static load of magnitude F_0, that is, under a static pressure equal to the maximum incident

pressure p_m. The corresponding static deflection, obtained from Equation [85] with $2F_i$ replaced by F_0 is

$$z_{co} = \frac{F_0}{k} \qquad [88]$$

From Equations [86] and [87]

$$z_{cm} = 2Nz_{co} \qquad [89]$$

where the dynamic response factor or load factor N is the first maximum value of

$$\frac{\mu^2}{\alpha^2 + \mu^2}\left(e^{-\alpha t} + \frac{\alpha}{\mu}\sin\mu t - \cos\mu t\right)$$

Or, N is the first maximum value for $x > 0$ of

$$\frac{1}{1 + q^2}(e^{-qx} + q\sin x - \cos x)$$

which is the solution for $y = dy/dx = 0$ at $x = 0$ of the type equation

$$\frac{d^2 y}{dx^2} + y = e^{-qx} \qquad [90]$$

A plot of N is given in Figure 28; the abscissa represents q from 0 to 1, then $1/q$ from $q = 1$ to $q = \infty$. In the present connection,

$$q = \frac{\alpha}{\mu} = \frac{2\alpha}{\pi}T_s = \frac{2}{\pi}\frac{T_s}{T_w} \qquad [91]$$

where $T_w = 1/\alpha$ and represents the time constant of the wave, while $T_s = \pi/2\mu$ and represents the swing time or the time required for a maximum deflection when the diaphragm is started moving from its flat position and then left to itself.

The greatest possible value of z_{cm} for a wave of positive pressure is $4z_{co}$; this is attained when the pressure remains sensibly constant during the entire swing time. The factor 4 arises from a doubling by reflection of the incident wave, and a second doubling by dynamical overshoot.[*]

If no baffle is present, so that even the diffraction time for the entire target is small as compared with the time constant of the wave, the factor 2 is to be omitted from Equations [85] and [86], and Equation [89] becomes

$$z_{cm} = 2Nz_{co} \qquad [92]$$

In this case, for a very long wave, only the doubling by dynamical overshoot remains.

---

[*] See also Reference (25).
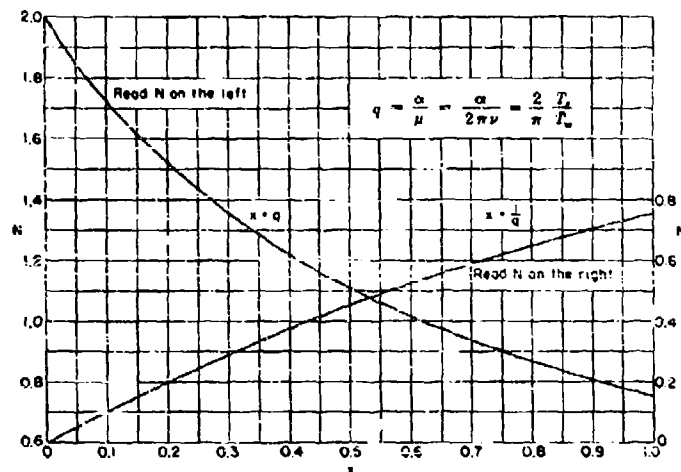
Figure 28 - Plot of the Dynamic Response Factor or Load Factor N
for a Harmonic System under Exponential Forcing

N represents the ratio of the maximum deflection of a harmonic system of natural frequency ν, when acted on by a suddenly applied force $F_0 e^{-\alpha t}$, to its static deflection under a steady force F_0. Here t is the time and α and F_0 are constants. The plot serves also for a proportionally constrained diaphragm whose swing time is T_s, when acted on by an exponential pressure wave of time constant $T_w = 1/\alpha$; that is, the incident pressure is $p_i = p_m e^{-\alpha t}$ where t is the time and p_m and α are constants.

For the circular diaphragm already considered, z_{co} can be calculated either from formulas already given for M, M_1, F_i, and T_s, or directly. For a pressure equal to p_m, $F_0 = \pi a^2 p_m/2$ by Equation [42b]. The curvature of the diaphragm is given nearly enough by the approximate formula for a sphere, $2z_c/a^2$ for small z_c; hence the stress force per unit area normal to the plane of the diaphragm is $\phi = -4\sigma h z_c/a^2$, on the assumption of equal hydrostatic pressures on the front and back. Thus by Equations [31b] and [40b],

$$\phi = -\frac{4\sigma h z_c}{a^2} \int_0^a \left(1 - \frac{r^2}{a^2}\right) 2r\, dr = -2\pi\sigma h z_c$$

and $k = 2\pi\sigma h$. Hence, for small z_{co},

$$z_{co} = \frac{a^2 p_m}{4\sigma h} \qquad\qquad [93]$$

If the accurate formula for the curvature is used, or $C = \frac{2z_c}{a^2 + z_c^2}$ a quadratic equation must be solved for z_{co}.

Detailed formulas have been given here for only one type of wave, the idealized shock wave of exponential form. The waves emitted during recompression of the gas globe can be approximated roughly by superposing several exponential terms, but simple final formulas are not obtainable; see Reference (16).

THE FACTORS DETERMINING DAMAGE

The question is often asked, upon what feature of the shock wave does the damage to a plate or diaphragm depend? Is it the maximum pressure, the impulse or the energy? A related question is the law according to which damage varies with size of charge and with distance.

The results of this and other analyses indicate clearly that no simple and general answers to these questions are to be expected, but that in special cases a few approximate rules can be given.

1. *Maximum pressure* should be the chief factor determining damage to *relatively small structures*, namely, whenever the time of action of the pressure greatly exceeds both the swing time and the diffraction time for the structure, or $T_w \gg T_s$, $T_w \gg T_d$. The rapidity with which the pressure is applied, however, will also be of significance.

For a diaphragm of radius a inches, this condition should hold at least for shock waves from charges in excess of 50 a^3 pounds. This estimate is based on $T_w = 1/a = (W/300)^{\frac{1}{3}}/1300$ and $T_s < 0.1a \times 10^{-3}$ from Equation [68]. The condition should be satisfied for Modugno gages in the presence of charges of 10 pounds or over.

If the diffraction time is also much less than the swing time, so that $T_w \gg T \gg T_d$, non-compressive theory can be used, as on page 52. If, furthermore, the application of pressure is gradual, the action is essentially a static one and the damage corresponds in the static manner to the maximum pressure. On the other hand, if the pressure is applied rapidly, the damage will be increased in proportion to an appropriate dynamic response factor or "load factor." If the application is effectively instantaneous as in loading by a shock wave, and if the resistance varies linearly with deflection, as is more or less true for a plate or diaphragm in the plastic range, the deflection should be almost twice the static value.

Since the pressure due either to shock waves or to gas globe oscillations, except near the globe, varies roughly as the cube root of the charge and inversely as the distance, the resulting deflection of a plate should vary in the same way, under the conditions assumed, except that at great distances a large correction for the elastic range will be required; for the pressure p required to give a diaphragm of radius a and negligible thickness a small deflection z is proportional to z; see Equation [8] in TMB Report 490 (17). Thus the maximum deflection will be approximately, $bW^{\frac{1}{3}}/r$, where b is a constant, and, from Equation [72a],

$$z = \sqrt{\frac{b^2 W^{\frac{2}{3}}}{r^2} - z_e^2} = \frac{bW^{\frac{1}{3}}}{r}\sqrt{1 - \frac{r^2 z_e^2}{b^2 W^{\frac{2}{3}}}} \qquad [94]$$

where z_e is the deflection at the elastic limit.

The pressure to be used in calculating the deflection will be the maximum pressure in the incident wave when the dimensions of the entire target are small as compared with the length of the wave in the water, or twice the maximum pressure if the diaphragm is surrounded by a large rigid baffle.

2. *The impulse* $\int p\,dt$ should determine damage when (a) cavitation does not occur and (b) the time of action of the pressure is much less than the swing time of the structure, or $T_w \ll T_s$. For a diaphragm of radius a inches this should hold for a charge of $a^3/100$ pounds or less.

This case is exemplified by Case 1 as previously described, and in particular in Equation [77]. In Case 1 the diffraction time was also assumed to be relatively short; but the statement just made concerning the impulse should hold independently of the diffraction time. For the influence of diffraction is confined to the relief pressure, as represented by the integral in Equation [16], and the relief pressure in turn is determined by the motion of the diaphragm itself. Thus the whole motion depends upon the initial velocities given to the structure by the incident wave; and since the wave, by assumption, acts only during a small part of the swing time of the structure, the initial velocities produced by it are proportional to the impulse, independently of the maximum pressure or the duration of the wave.

The variation with W and R should be as described for Case 1 in the last section. To a first approximation, the set deflection z should be given by

$$z = B\frac{W^{\frac{2}{3}}}{R} \qquad [95]$$

where B is almost constant for a given structure, provided the elastic range can be neglected.

This case will probably not arise often, however, because of the common intervention of cavitation.

3. The *energy* carried by the wave, $\int p^2 dt/\rho c$, does not appear in any simple damage formula obtained from the present dynamical analysis. The energy should be significant whenever circumstances are such that little reflection of the wave occurs; but such cases are not easy to define precisely. More generally, the energy will be the significant quantity if, for any reason, the plastic work stands in a fixed ratio to the energy brought up by the wave. Since the incident energy varies in proportion to the charge weight W and roughly as $1/R^2$, the deflection, which is nearly proportional to the square root of the plastic work, will then vary as $W^{\frac{1}{2}}/R$, or

$$z = C\frac{W^{\frac{1}{2}}}{R} \qquad [96]$$

where C is a nearly constant coefficient, so long as elastic effects can be neglected. The factor $W^{\frac{1}{2}}$ in this expression represents a variation intermediate between the $W^{\frac{1}{3}}$ for the pressure and the $W^{\frac{2}{3}}$ for the impulse, or a variation as the square root of the product of maximum pressure and impulse.

Observations generally show a variation of the deflection more or less as in Equation [96]. The plastic work commonly differs, in fact, by less than a factor of 2 from the energy brought up by the wave. A discussion of the data is contained in TMB Report 492 (18).

From the analytical standpoint, however, correlation of damage with the energy in the wave appears to be somewhat of an accident, contingent upon the range of magnitude of various factors as they occur in practice, rather than a direct consequence of the conservation of energy. There exists no general necessity for the plastic work done on a structure to equal the energy that is directly incident upon it according to the laws of the rectilinear propagation of waves. Part of the incident energy may be reflected; or, on the other hand, if the motion approximates to the non-compressive type, it is possible for the energy absorbed by the structure greatly to exceed that which is brought up by the wave.

In TMB Report 489 (11) it was inferred, nevertheless, from the example of the free plate, that damage to a diaphragm should probably correlate better with the incident energy than with the incident momentum. The argument is substantially that by which it was concluded in Case 2 that the set deflection z might vary about as $W^{\frac{1}{2}}$. Or, it might be that the more rapid variation introduced by reloading, as in Case 2a, would assist in bringing about rough proportionality of z to $W^{\frac{1}{2}}$.

The analytical formulas indicate, furthermore, that in most tests on diaphragms the plastic work should not differ greatly from actual equality with the energy that is brought up to the diaphragm by the incident wave. For an exponential wave, Equation [2], and a circular diaphragm of radius a, this energy will be

$$E_w = \pi a^2 \int \frac{p_\perp^2}{\rho c}\, dt = \frac{\pi a^2 p_m^2}{2 a \rho c} \qquad (97)$$

Thus the ratio of the energy absorbed by the diaphragm, estimated as $\pi J A z_i^2$, to that brought up by the incident wave will be, for three cases treated in the last section, from Equation [77], [81], or [84], respectively,

(1) non-compressive: $\dfrac{E}{E_w} = \dfrac{2z}{1 + 0.776\,\dfrac{p}{\rho_d}\,\dfrac{a}{h}}$

(2) lasting cavitation: $\dfrac{E}{E_w} = 4\,z^{\frac{1+z}{1-z}}$

(2a) cavitation and reloading: $\dfrac{E}{E_w} = 4 z^{\frac{1+z}{1-z}} \left(1 + \dfrac{3}{4} \dfrac{z^2}{1 + 0.776 \dfrac{\rho}{\rho_d} \dfrac{a}{h}} \right)$

In tests on steel diaphragms $\rho/\rho_d = 1/7.83$, while a/h is of the order of 100 and z lies between 5 and 10. For such values, in the absence of cavitation, E somewhat exceeds E_w. In the case of cavitation without reloading, the factor $z^{\frac{1+z}{1-z}}$ ranges from 1/11 to 1/17, so that E is only a third or a quarter of E_w; the reloading by the water will then probably increase E to something between $E_w/2$ and $2E_w$. In some cases it may happen that $E = E_w$.

Thus, although exact formulas are not easy to obtain, it can at least be said that the observed rough proportionality of the deflections of many diaphragms or similar structures to $W^{\frac{1}{2}}/R$, or at least to the square root of the energy in the incident wave, and the approximate equality of the plastic work to the incident energy, stand in fair harmony with analytical expectations.

To sum up, the analytical results suggest that the major factor controlling damage

1.   should be the maximum pressure for relatively small structures, whose swing time and diffraction time are both small as compared with the time constant of the incident wave;

2.   should be the incident impulse when the swing time of the target is much greater than the time of action of the pressure, provided cavitation does not occur;

3.   may be something nearly proportional or even equal to the incident energy in some intermediate cases, or when cavitation occurs.

PART 5. ANALYSIS OF A FEW DATA ON DIAPHRAGMS

The application of the preceding formulas to recent observations made at the Taylor Model Basin will be discussed in the report on those observations. Two other sets of test data, reported by the Bureau of Ships, will be discussed here.

MODUGNO GAGES

The data published by the Bureau of Ships on Modugno gages (19) are in partial agreement with the theoretical expectations set forth here.

The diameter of the gages was 1 inch for the diaphragm itself and 2.6 inches overall. Thus the diffraction time T_d would be 0.008 millisecond for the diaphragm or $1.3/59 = 0.022$ millisecond for the entire gage.

The time constant T_w of the shock wave would be perhaps 0.05 millisecond for a charge of 0.2 pound and more than 0.1 millisecond for charges of a pound or larger.

Thus, at least for the larger charges, T_d is relatively small, and Case 3 as described on page 52 is present. Compressibility of the water can be neglected; cavitation should not occur. Furthermore, there should be no appreciable increase in the pressure by reflection, except during the first few microseconds.

The swing time of the diaphragm with water loading may be estimated from Equation [67] as

$$T_s = \frac{0.5\,\pi}{2\sqrt{6}}\left[\frac{0.000832}{35000}\left(1 + \frac{0.32}{8.89\,h}\right)\right]^{\frac{1}{2}}$$

Here 8.89 is the specific gravity of copper and 0.000832 its density in inch dynamical units, and the yield stress has been taken as 35.000. According to this formula T_s varies from 0.078 for a thickness $h = 0.03$ inch to 0.060 millisecond for $h = 0.1$ inch. This is of the same order as the duration of the wave. Hence some increase of deflection by dynamical overshoot is to be expected.

For charges of 1 to 300 pounds of TNT, the static pressure P required to produce the same deflection as does the explosion was found experimentally to vary nearly as $R^{-1.14}$ where R is the distance in feet from the charge to the gage; see Figure 18 in Reference (19). The exponent 1.14 might arise chiefly from the variation with distance of the pressure due to a charge of TNT. A variation with distance of this order was found at Woods Hole for tetryl (20). Similitude would then imply a general variation of P as $(W^{\frac{1}{3}}/R)^{1.14}$ or as $W^{0.38}/R^{1.14}$; whereas the data indicate a variation more nearly as $W^{0.5}/R^{1.14}$

The more rapid increase with W may be partly the result of increased dynamical overshoot. For 1 pound, $q = 2T_s/(\pi T_w) = 2 \times 0.07/(0.11\pi) = 0.40$, roughly, at which, in Figure 28, $N = 1.22$. For 200 pounds, $q = 2 \times 0.07/(0.64\pi) = 0.07$, at which $N = 1$. Thus Equation [92] implies an increase in the deflection due to increased overshoot, as the charge is increased from 1 pound to 200 pounds in the ratio 1.80/1.22, or in the ratio $W^{0.07}$ On the assumption that deflection and equivalent static pressure are nearly proportional to each other, therefore, the total variation of the equivalent static pressure would be about as $W^{0.38+0.07} = W^{0.45}$, which is not too different from the observed $W^{0.5}$.

In absolute magnitude, however, the equivalent static pressures are considerably below the estimated peak pressures in the explosion wave. For

example, the wave from 1 pound of TNT at 7.5 feet, corresponding to that from 300 pounds at 50 feet, should have a peak pressure of about 2100 pounds per square inch, but it produces only the same deflection as a static pressure of 1650 pounds. The occurrence of dynamical overshoot should make the wave equivalent perhaps to 2100 × 1.22 = 2560 pounds. An increase of 55 per cent in the yield stress of the copper diaphragm above the static value, due to high strain rate, would remove the discrepancy, but such an increase seems excessive.

Other features of the data cannot be interpreted with certainty.

21-INCH DIAPHRAGMS

Data pertaining to tests on 21-inch steel diaphragms have recently been reported by Lt. Comdr. R.W. Goranson, USNR, for the Bureau of Ships (22). The diaphragms were securely fastened to the equivalent of a heavy steel ring 1 foot wide mounted on the front of a heavy caisson and were attacked by charges of 1 pound of TNT. Perhaps the ring can be regarded as roughly equivalent to an infinite baffle.

In Table 2 there are shown, for seven shots, the kind of steel, the thickness h, the distance R of the charge, the average dynamic yield stress σ as estimated in the original report, the observed final set deflections z, and several computed values of z.

TABLE 2

21-Inch Steel Diaphragms of Special Treatment Steel, High Tensile Steel, Medium Steel and Furniture Steel

Kind of Steel	h inches	R feet	σ lb/in²	$z_{obs.}$ inches	$z_{calc.}$ inches	z_{free} inches	$z_{no\,rev.}$ inches	z_e inches	v_m feet per second
STS	0.125	4	125000	1.22	1.13	0	1.46	0.82	83
HTS	0.125	3	85000	2.04	2.00	0.77	2.52	0.67	111
MS	0.125	3	85000	2.00	2.00	0.77	2.52	0.67	111
FS	0.109	2.5	45000	3.30 4.15	3.69	1.50	4.52	0.49	136
FS	0.063	4.5	45000	2.70	2.39	0.88	3.36	0.49	83
FS	0.032	10.0	45000	1.35	1.92	0.33	2.14	0.49	47
MS	0.125	1.75	65000	3.95 (avg)	4.01	1.74	4.91	0.59	190

h is the thickness, σ the assumed average dynamic yield stress, R is the distance to the charge. $z_{obs.}$ is the observed central set deflection, z_e the calculated value at the elastic limit; for other values of z and for z_m, see the text.

A fair approximate estimate of the high-pressure part of the shock wave at a distance of R feet from 1 pound of TNT, according to measurements by Hilliar (14) or with piezoelectric gages (22) seems to be

$$p = \frac{15600}{R}\ e^{-8700t}\ \ \mathrm{lb/in^2}$$

The time constant of the wave is thus about $T_w = 0.115$ millisecond. This is comparable with the diffraction time for the diaphragm or $T_d = 10.5/59 = 0.18$ millisecond, but it is much less than the swing time, which is given by Equation [66] as 0.64 millisecond. The swing time will be longer if water loading is included.

Thus, if cavitation does not occur, Case 1 as described on page 46 of the present report is present. Deflections calculated on this assumption, from Equation [77], are shown in Table 2 as $z_{no\ cav}$. They are decidedly larger* than the observed values. The discrepancy is probably great enough to outweigh possible sources of error in the necessarily simplified mode of calculation that is employed here. It may be concluded, therefore, that the diaphragms were protected in some way, probably by the occurrence of cavitation.

The pressure on the diaphragm should sink very quickly from its initial peak value. The value of x in Equation [5b] is $5.7/(8700 \times 0.000733h)$ or $0.89/h$, where h is the thickness of the diaphragm in inches. Hence, for $h = 0.125$ inch, $x = 7.1$, and the compliance time, at which the pressure has become hydrostatic and the diaphragm is moving at maximum velocity, is, from Equation [5a], $T_m = \ln 7.1/(8700 \times 6.1)$ second $= 0.037$ millisecond. This is a small fraction of the swing time. For thinner diaphragms T_m will be even less. The pressure will then become negative, and cavitation is to be expected.

On the assumption that cavitation occurs at the surface of the diaphragm as soon as the pressure on it sinks below the hydrostatic value, the maximum velocity of the diaphragm is v_m as given by Equation [7]. Velocities calculated from this equation, with $p_m = 15600/R$, $\rho c = 5.7$, $x = 0.89/h$, are given as a matter of interest as v_m in Table 2. If no further energy is delivered to the diaphragm by the water, and if it takes on a nearly spherical shape, its central net deflection z will be given approximately by Equations [80a] and [81]. Values calculated from these equations, using $a = 10.5$ inches and the values of v given in the table, are shown in Table 2 as z_{free}. They are much smaller than the observed values. Even smaller calculated

---

* In the original report (27) much smaller calculated values are given owing to the use of a different method of calculation. The method employed in this report is believed to be preferable.

values of z, and also smaller values of v_m, are obtained if cavitation is assumed to set in at a pressure below hydrostatic pressure.

Hence, as was pointed out in the original report (21), an additional source of energy must be found. The water will in fact, overtake the diaphragm and may do additional plastic work upon it. According to the analytical results, the water should acquire considerable velocity even if the incident wave has entirely ceased; but, actually, at $t = T_m = 0.037$ millisecond, the incident pressure has decreased only to a fraction $e^{-8700 \times 37 \times 10^{-6}}$ or 0.73 of its initial value. An attempt to allow for the additional plastic work was made in Equation [84], and values of z calculated from this equation and [80a] are shown in Table 2 as z_{calc}. These values are in good agreement with the observed deflections.

The assumptions underlying Equation [84] are certainly wide of the mark in certain details, but it may be that in their broad outlines these assumptions reproduce roughly the process that actually occurred. If this is so, about three-fourths of the plastic energy was delivered to the diaphragms by the water as it impinged upon them after closure of the cavitation.

The final result will presumably not be very different if cavitation occurs first in the water, or if, beginning at the diaphragm, it then spreads back into the water.

REFERENCES

(1) "Damage to Ship's Plates by Underwater Explosions," by S. Butterworth, Admiralty Research Laboratory Report ARL/S/10, July 1924.

(2) "Note on the Motion of a Finite Plate Due to an Underwater Explosion," by S. Butterworth, Admiralty Research Laboratory Report ARL/N1/H4, August 1942.

(3) "The Distortion under Pressure of a Diaphragm Which Is Clamped along Its Edge and Stressed beyond the Elastic Limit," by Professor G. I. Taylor, F.R.S., Ministry of Home Security, S.W. 24 September 1942.

(4) Professor G. I. Taylor, F.R.S., Ministry of Home Security, R.C. 240, July 1941.

(5) "Memorandum on the Plastic Deformation of Marine Structures by an Underwater Explosion to August 1, 1942," by John G. Kirkwood, NDRC 305, OSRD 793, August 1942.

(6) "The Plastic Deformation of Marine Structures by an Underwater Explosion. II, to November 15, 1942," by John G. Kirkwood, NDRC, 450, OSRD 1115, December 1942.

(7) John G. Kirkwood, NDRC, OSRD, Division 8, Woods Hole Oceanographic Institute, Interim Report UE-7, February 15 to March 15, 1943.

(8) John G. Kirkwood, NDRC, OSRD, Division 8, Woods Hole Oceanographic Institute, Interim Report UE-12, July 15 to August 15, 1943.

(9) John G. Kirkwood, NDRC, OSRD, Division 8, Woods Hole Oceanographic Institute, Interim Report UE-10, May 15 to June 15, 1943.

(10) "Report on Underwater Explosions" by Professor E.H. Kennard, TMB Report 480, October 1941.

(11) "Effects of Underwater Explosions - General Considerations," by Professor E.H. Kennard, TMB Report 489, September 1942.

(12) "Cavitation in an Elastic Liquid," by E.H. Kennard, The Physical Review, Vol. 63, Nos. 5 and 6, pp. 172-181, March 1 and March 15, 1943.

(13) "Explosive Load on Underwater Structures as Modified by Bulk Cavitation," by Professor E. H. Kennard, TMB Report 511, May 1943.

(14) "Experiments on the Pressure Wave Thrown out by Submarine Explosions," by H.W. Hilliar, Research Experiment 142/19, 1919.

(15) Dr. E.N. Fox, Ministry of Home Security, S.W. 18, December 1942.

(16) Road Research Laboratory, Department of Scientific and Industrial Research, UNDEX 14, Note No. ADM/95/GC.ARB, February 1943.

(17) "Protection against Underwater Explosion - Plastic Deformation of a Circular Plate," by A.N. Gleyzal, Ph.D., TMB Report 490, September 1942.

(18) "The Design of Ship Structure to Resist Underwater Explosion - Nominal Theory," by Captain W.P. Roop, USN, TMB Report 492, August 1943.

(19) Navy Department, Bureau of Ships, Underwater Explosion Report 1942-3, October 1942.

(20) NDRC, OSRD, Division 8, Woods Hole Oceanographic Institute, Interim Report UE-6.

(21) Lt. Comdr. R.W. Goranson, USNR, Navy Department, Bureau of Ships, Underwater Explosion Report 1942-4, August 1943.

(22) "Nature of the Pressure Impulse Produced by the Detonation of Explosives Under Water. An Investigation by the Piezo-Electric Cathode-Ray Oscillograph Method," Admiralty Research Laboratory Report ARL/S/12, November 1924.

(23) "Hydrodynamics," by Horace Lamb, M.A., LLD., Sc.D., F.R.S., University Press, Cambridge, 1924.

(24) "Pressure-Time Curves for Submarine Explosions," by Dr. W.G. Penney and Dr. H.K. Dasgupta, Ministry of Home Security, R.C. 333, July 1942.

(25) G.K. Hartmann, BuOrd Memo for file Re6b, 25 September 1942, TMB file C-S87-6-(1).

MATHEMATICAL APPENDIX

WAVES INCIDENT UPON THE INFINITE PLANE FACE OF A TARGET

The only case of wave reflection that can be handled easily is the incidence of waves upon a plane reflecting surface of infinite lateral extent. The waves may be of any type and incident at any angle, but it must be assumed that they are weak enough to make the linear theory of wave propagation applicable. Furthermore, if movement of the surface occurs, its displacement must be small. The surface will be called a target, but it may be wholly or in part merely the free surface of the water. The case thus characterized will be under discussion except as otherwise stated.

Under these conditions, an expression for the pressure field in the fluid in front of the target can be built up by the method of superposition. Let p_i denote the pressure that is added to the hydrostatic pressure p_0 at any point in the fluid by the incident wave or waves; that is, $p_0 + p_i$ is the pressure that would exist there if the target were replaced by fluid. Let a set of reflected waves be added such as would occur if the target were rigid. These waves are simply the mirror image of the incident waves in the face of the target; together with the incident waves, they give a pressure field in which, at any point on the target, the excess of pressure is $2p_i$, while the component of the particle velocity perpendicular to the face is zero.

The target and the fluid must, however, have the same normal component of velocity. This may be secured by adding further waves such as would be emitted by a suitable distribution of point sources located on the face of the target. In the waves emitted by a point source, the pressure p and the particle velocity v at a distance s from the element may be written

$$p_1 = \frac{1}{s} f'\left(t - \frac{s}{c}\right), \quad v_1 = \frac{1}{\rho c s} f'\left(t - \frac{s}{c}\right) + \frac{1}{\rho s^2} f\left(t - \frac{s}{c}\right) \qquad [98]$$

where t is the time, ρ is the density of the fluid, c is the speed of sound in it, and where $f(t - s/c)$ stands for some function of the variable $t - s/c$, and f' for the derivative of this function. The fluid emitted by the source will be that which crosses a small hemisphere drawn about the source as a center; see Figure 29. The volume V_1 emitted per second will be, therefore, $2\pi s^2 v_1$. Or, since the first term in Equation [98] becomes negligible in comparison with the second as $s \to 0$,

$$V_1 = \lim_{s \to 0}\left[2\pi s^2 \frac{1}{\rho s^2} f\left(t - \frac{s}{c}\right)\right] = \frac{2\pi}{\rho} f(t)$$

If there are N sources per unit area, the volume emitted per second from an element δS of the surface will be $N V_1 \delta S$.

Figure 29

In the resultant motion of the fluid as a whole, this volum⋯ ⋯rried outward from the surface by the normal component of the resul⋯ ⋯t ⋯article velocity v_n. Hence

$$v_n \, \delta S = NV_i \, \delta S = \frac{2\pi N}{\rho} f(t) \, \delta S$$

The velocity v_n, however, must be the same as the normal component of velocity of the target. Hence, if z is a coordinate of position for the element δS, measured perpendicularly to the initial plane and, for convenience, in the direction away from the fluid,

$$v_n = -\frac{dz}{dt} = -\dot{z}$$

The proper particle velocity will exist, therefore, at the target if $f(t)$ is such a function that

$$\frac{2\pi N}{\rho} f(t) = v_n = -\dot{z}$$

Then

$$f'(t) = \frac{d}{dt} f(t) = -\frac{\rho}{2\pi N} \ddot{z}$$

where $\ddot{z} = d^2 z / dt^2$; and

$$f'\left(t - \frac{s}{c}\right) = -\frac{\rho}{2\pi N} \ddot{z}_{t-\frac{s}{c}}$$

where $\ddot{z}_{t-\frac{s}{c}}$ denotes the value that the acceleration $\ddot{z}$ has, not at time t, but at the earlier time $t - s/c$.

The pressure at a distance s from the element δS, due to all sources on it, is, therefore, by [98]

$$(N \delta S)p_1 = \frac{N \delta S}{s} f'\left(t - \frac{s}{c}\right) = -\frac{\rho \delta S}{2\pi s} \ddot{z}_{t-\frac{s}{c}}$$

and at any point on the face of the target the pressure due to all sources is

$$p_z = -\frac{\rho}{2\pi} \int \frac{1}{s} \ddot{z}_{t-\frac{s}{c}} \, dS \tag{99}$$

where s denotes distance from the point to the element dS. Here p_z refers to a particular point on the target and to time t, $\ddot{z}_{t-\frac{s}{c}}$ is the value of $\ddot{z}$ at dS but at a time $t - s/c$, and the integration extends over the face of the target.

The pressure at any point on the target due to all causes is then

$$p = 2p_1 + p_z + p_0 = 2p_1 + p_0 - \frac{\rho}{2\pi} \int \frac{1}{s} \ddot{z}_{t-\frac{s}{c}} \, dS \tag{100}$$

Here even p_0 may vary from one point of the target to another.

THE MOTION OF A PLATE, DIAPHRAGM OR LIQUID SURFACE

Suppose that, in the case just considered, the target consists of a plate or diaphragm, initially plane. Then its equation of motion will be

$$m\ddot{z} = p + \phi - p_0 \qquad [101]$$

where m is its mass per unit area, and ϕ stands for the difference between the hydrostatic pressure p_0 on the front face and the pressure p_0 on the back face, plus the net force per unit area due to stresses, if any. Or, by [100],

$$m\ddot{z} = 2p_1 + \phi - \frac{\rho}{2\pi} \int \frac{1}{s} \ddot{z}_{t-\frac{s}{c}} \, dS \qquad [102]$$

The displacement is assumed here to remain small enough so that its component parallel to the initial plane can be ignored. Equation [102] is an integro-differential equation for z, which is a function both of time and of position on the plate.

The "target" may actually consist wholly or in part of the free surface of the liquid, for nothing in the calculation of the pressure rests upon the assumption of a solid target. At any point where the surface is free, or, for that matter, at any other point as well, z will represent the normal displacement of the liquid surface.

At a point on the free surface, [100] may conveniently be written

$$\frac{\rho}{2\pi} \int \frac{1}{s} \ddot{z}_{t-\frac{s}{c}} \, dS = 2p_1 + p_0 - p \qquad [103]$$

where p is the external pressure on the surface. The integral extends as usual over the entire plane. This equation, when needed, can be formed from [102] by setting $m = 0$ and $\phi = p_0 - p$. Here p_0 includes atmospheric pressure and may differ from p because of an accelerational pressure gradient in the liquid. At any point where the surface of the liquid is in contact with a plate or diaphragm, [102] will continue to hold.

THE CASE OF PLANE WAVES

If the plate remains accurately plane, and if p_1 is uniform over it, then $\ddot{z}$ is also uniform and hence is a function of t only. Thus in the integral in [102] the quantity $\ddot{z}_{t-\frac{s}{c}}$ is a function of t and s only. Hence in this integral dS may be replaced by $2\pi s \, ds$, representing a ring-shaped element of area on the plane, and

$$\int \frac{1}{s} \ddot{z}_{t-\frac{s}{c}} \, dS = 2\pi \int \ddot{z}_{t-\frac{s}{c}} \, ds$$

Now a dot over $z_{t-\frac{s}{c}}$ is equivalent to differentiation with respect to the argument $t - s/c$, so that

$$\ddot{z}_{t-\frac{s}{c}} = \frac{d}{d\left(t-\frac{s}{c}\right)}\dot{z}_{t-\frac{s}{c}} = -c\frac{d}{ds}\dot{z}_{t-\frac{s}{c}} \qquad [104]$$

where $\dot{z}_{t-\frac{s}{c}}$ is the velocity at time $t - s/c$.

Hence, if the integration is restricted to a ring-shaped area between $s = s_1$ and $s = s_2$:

$$\int_{s=s_1}^{s=s_2}\ddot{z}_{t-\frac{s}{c}}\,\frac{dS}{s} = -2\pi c\int_{s_1}^{s_2}\frac{d}{ds}\dot{z}_{t-\frac{s}{c}}\,ds = -2\pi c\,\dot{z}_{t-\frac{s}{c}}\Big|_{s_1}^{s_2}$$

$$= 2\pi c\left[\dot{z}\left(t - \frac{s_1}{c}\right) - \dot{z}\left(t - \frac{s_2}{c}\right)\right] \qquad [105]$$

whereas if the integration covers the entire plane, and if the plate started from rest so that $\dot{z}(-\infty) = 0$,

$$\int\ddot{z}_{t-\frac{s}{c}}\,\frac{dS}{s} = 2\pi c\,\dot{z}(t) \qquad [106]$$

Thus [102] becomes

$$m\ddot{z} + \rho c\dot{z} = 2p_i + \phi \qquad [107]$$

where all quantities refer to time t. This is an obvious generalization of the one-dimensional equation; see Equations [10] and [11] on pages 24 and 26 of TMB Report 480 (10).
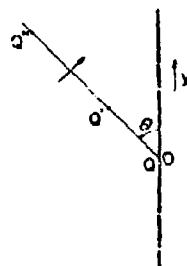
Equation [107] has reference to plane waves at normal incidence. It was pointed out by Taylor (4) that the case of plane waves incident at any angle θ can easily be treated provided it is assumed that $\phi = 0$, so that the elements of the diaphragm move independently.

Let y denote distance measured along the diaphragm in the plane of incidence. In Figure 30 there is shown an incident wave $QQ'Q''$, at all points of which the incident pressure has the same value. If Q strikes the origin for y at time t, Q' will not strike the diaphragm until a time $\frac{y\sin\theta}{c}$ later, where c is the speed of sound in the liquid. Thus if $p_i(t)$ denotes the incident pressure at $y = 0$, its value elsewhere on the diaphragm is $p_i\left(t - \frac{y\sin\theta}{c}\right)$.

Figure 30

It is a natural surmise now, to be verified in the sequel, that the displacement z will also be a function of the same argument or $z\left(t - \frac{y\sin\theta}{c}\right)$. Then all elements execute the same motion but in different phase; and

$$\int z_{t-\frac{s}{c}}\,\frac{dS}{s} = \int z\left(t - \frac{s + y\sin\theta}{c}\right)\frac{dS}{s}$$

Introducing polars s, ψ on the diaphragm so that $y = s \cos \psi$ and $dS = s \, ds \, d\psi$, changing from s to $s' = s + s \cos \psi \sin \theta$, so that $ds' = (1 + \sin \theta \cos \psi) ds$, and proceeding as in obtaining [105],

$$\int \ddot{z}_{t - \frac{s}{c}} \frac{dS}{s} = \int_0^{\frac{z}{r}} \int_0^{\bar{\pi}} \ddot{z}\left(t - \frac{s'}{c}\right) \frac{ds' \, d\psi}{1 + \sin \theta \cos \psi} = \frac{2\pi c}{\cos \theta} \dot{z}(t)$$

provided $\dot{z}(-\infty) = 0$. Hence [102] becomes, as a generalization of [107],

$$m\ddot{z} + \frac{\rho c \dot{z}}{\cos \theta} = 2p_1 + \phi \tag{108}$$

This equation is also obtained easily from a simple consideration of the process of reflection.

EFFECT OF AN INFINITE BAFFLE

Let part of the target consist of a plane baffle extending laterally to an infinite distance from the edge of the plate.

If the baffle is fixed in position, its only effect upon [102] is that the range of integration for the integral need be extended only over the face of the plate, since elsewhere $\ddot{z} = 0$.

If the baffle is movable, let z_b denote its displacement. Then over the baffle z_b is uniform and is a function only of the time t or $z_b(t)$. Let the integral in [102] be divided as follows:

$$\int \frac{1}{s} \ddot{z}_{t - \frac{s}{c}} \, dS = \int \frac{1}{s} \ddot{z}_b\left(t - \frac{s}{c}\right) dS + \int_{\text{plate}} \frac{1}{s}\left[\ddot{z}_{t - \frac{s}{c}} - \ddot{z}_b\left(t - \frac{s}{c}\right)\right] dS$$

in which the first integral on the right is arbitrarily extended over the plate as well as over the baffle, and the error thus introduced is compensated for by the second term in the second integral, which extends only over the plate. The first integral on the right can then be transformed as in [105], since $\ddot{z}_b(t - s/c)$ is a function only of $t - s/c$, giving

$$\int \frac{1}{s} \ddot{z}_b\left(t - \frac{s}{c}\right) dS = 2\pi c \, \dot{z}_b(t)$$

in terms of the velocity $\dot{z}_b$ of the baffle at time t. Hence [102] may be written

$$m\ddot{z} = 2p_1 + \phi - \rho c \dot{z}_b - \frac{\rho}{2\pi} \int_{\text{plate}} \frac{1}{s} \left[\ddot{z} - \ddot{z}_b\right]_{t - \frac{s}{c}} dS \tag{109}$$

where all quantities except $\ddot{z} - \ddot{z}_b$ in the integrand are taken at time t. Another form for a special case is given in Equation [19] or [20].

PLATE OR DIAPHRAGM PROPORTIONALLY CONSTRAINED AND MOUNTED
IN AN INFINITE PLANE BAFFLE

Let it be assumed that in the displacement of the plate from its initial plane position all elements move in fixed proportion, so that it is possible to write

$$z = z_c(t)\, f(x,y) \qquad [110]$$

where z_c is a function of the time whereas $f(x,y)$ is a fixed function of position on the initial plane; z_c may represent the displacement of some point on the plate, such as the center, at which then $f(x,y) = 1$. Let the baffle be immovable.

Then [102] becomes, with dS replaced by $dx'dy'$,

$$m\ddot{z}_c(t)\, f(x,y) = 2p_i + \phi - \frac{\rho}{2\pi} \iint \frac{1}{s}\, \ddot{z}_c\!\left(t - \frac{s}{c}\right) f(x',y')\, dx'\, dy'$$

Here z_c, in contrast with z in [102], is a function of time alone, and $\ddot{z}_c(t - s/c)$ denotes the value of d^2z_c/dt^2 at a time $t - s/c$. By multiplying through by $f(x,y)$ and integrating again over the whole area of the plate, a convenient ordinary integrodifferential equation is obtained for z_c:

$$M\ddot{z}_c = 2F_i + \phi - \frac{\rho}{2\pi} \iint f(x,y)\, dx\, dy \iint \frac{1}{s}\, \ddot{z}_c\!\left(t - \frac{s}{c}\right) f(x',y')\, dx'\, dy' \qquad [111]$$

where

$$M = \iint m\big[f(x,y)\big]^2 dx\, dy \qquad [112]$$

$$F_i = \iint p_i\, f(x,y)\, dx\, dy, \quad \phi = \iint \phi\, f(x,y)\, dx\, dy \qquad [113a,\ b]$$

Since, from [110],

$$\dot{z} = \dot{z}_c\, f(x,y) \qquad [114]$$

the kinetic energy of the plate is

$$K = \iint \frac{1}{2} m \dot{z}^2\, dx\, dy = \frac{1}{2} \dot{z}_c^2 \iint m\big[f(x,y)\big]^2 dx\, dy = \frac{1}{2} M \dot{z}_c^2 \qquad [115]$$

A more useful form for the integral in [111] is obtained if x',y' are replaced by polars s, θ, with origin at the movable point x, y, but with the axis in a fixed direction, so that $dx'dy'$ is replaced by $s\,d\theta\,ds$. Here s and θ may be defined by the equations

$$x' - x = s\cos\theta, \quad y' - y = s\sin\theta$$

see Figure 31. Then, after changing the order of integration, [111] can be written

$$MF_r = 2F_r + \phi - \rho \int_\delta^D z.\left(z - \frac{s}{c}\right) \eta(s)\,ds \qquad [116]$$

where D is the maximum diameter of the plate and

$$\eta(s) = \frac{1}{2\pi} \int_0^{2\pi} d\theta \iint f(z,y)f(z,y)\,dz\,dy \qquad [117]$$

in which $f(z,y)$ is to be understood as expressed in terms of x, y, s, θ. If s is too large, the integral in x and y will vanish for certain values of θ; and the entire integral vanishes for $s > D$.

Motion of the elements parallel to the initial plane of the plate is ignored here, as usual. An equation containing corrections for motion of the baffle is obtained on page 28 of the text as Equation [33].

The proportional shape may be supposed to be maintained by suitable internal constraint forces which on the whole do no work in any displacement of the plate. These forces are in addition to those due to stresses; they might be supplied, for example, by a suitable linkwork mounted on the diaphragm.

Figure 31

If ϕ' denotes the net force on unit area due to the constraints, the element of work done by them is $dW' = \int(\phi'\,dz)dS = 0$, or, if $x = z_0 + z_c f(x,y)$ as in [32], to allow for motion of the baffle.

$$dW' = dz_0 \int \phi'\,dS + dz_c \int \phi' f(z,y)dS = 0$$

But $\int \phi'\,dS$ is the total force due to the constraints and must vanish. Hence $\int \phi' f(x,y)dS = 0$. The vanishing of this integral prevents ϕ' from contributing to ϕ.

As a special case, if a circular diaphragm of radius a is assumed to remain symmetric about it's axis but to become paraboloidal in form, and if z_c is taken to represent the displacement of the center, then

$$f(x,y) = 1 - \frac{r^2}{a^2} \qquad [118]$$

where r denotes distance from the center, and it is found that, whereas $\eta(s) = 0$ for $s \geq 2a$, for $0 \leq s < 2a$
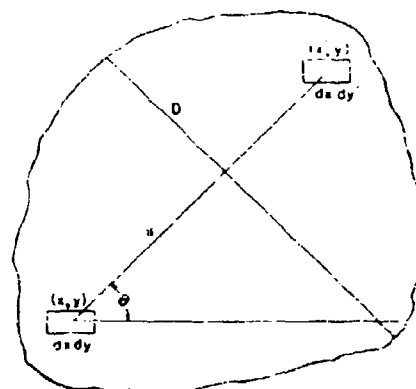
$$\eta(s) \approx \frac{1}{3} a^2\left[(2 - 3R^2)\cos^{-1}\frac{R}{2} + \left(\frac{1}{2}R + \frac{2}{3}R^3 - \frac{1}{24}R^5\right)\sqrt{4 - R^2}\right] \quad [119]$$

where $R = s/a$. Furthermore, from [112], if m is uniform over the plate,

$$M = \frac{\pi}{3} ma^2 \tag{120}$$

and, if the incident pressure p_i is also uniform, from [113a],

$$F_i = \frac{1}{2}\pi a^2 p_i \tag{121}$$

Or, if the diaphragm moves like a piston, except for a negligible ring at the edge, $f(x,y) = 1$ and

$$\eta(s) = a^2\left(2\cos^{-1}\frac{R}{2} - \frac{R}{2}\sqrt{4 - R^2}\right) \tag{122}$$

$$M = \pi ma^2, \quad F = \pi a^2 p_i \tag{123a, b}$$

The curves for $\eta(s)$ corresponding to these two formulas do not vary much from straight lines of the form

$$\eta(s) = \pi a^2\left(A' - B'\frac{s}{a}\right) \tag{124}$$

If the constants A' and B' are determined so as to give correct values to the two integrals

$$\int_0^{2a} \eta(s)\, ds, \quad \int_0^{2a} s\,\eta(s)\, ds$$

then, for paraboloidal constraint, $A' = 0.357$, $B' = 0.246$; for the piston-like constraint, $A' = 0.961$, $B' = 0.544$. The curves for $\eta/\pi a^2$ and the corresponding lines are shown in Figure 32.

If an expression for η of the form of [124] is substituted in [116], the integral can be evaluated. For the upper limit, however, $2a$ must be replaced by $s = A'a/B'$, at which η as given by [124] vanishes. A dot over $z_c(t - s/c)$ is equivalent to differentiation with respect to the argument $(t - s/c)$, hence, at fixed t, in analogy with [104],

$$\frac{d^2}{ds^2}\left[z_c\left(t - \frac{s}{c}\right)\right] = -\frac{1}{c}\frac{d}{ds}\left[\dot{z}_c\left(t - \frac{s}{c}\right)\right] = \frac{1}{c^2}\ddot{z}_c\left(t - \frac{s}{c}\right)$$

Hence, integrating by parts,

$$\int_0^{\frac{A'a}{B'}}\left(A' - B'\frac{s}{a}\right)\ddot{z}_c\left(t - \frac{s}{c}\right)ds = \left[-c\left(A' - B'\frac{s}{a}\right)\dot{z}_c\left(t - \frac{s}{c}\right) + \frac{c^2}{a}B'z_c\left(t - \frac{s}{c}\right)\right]\Big|_{s=0}^{s=\frac{A'a}{B'}}$$

$$= cA'\dot{z}_c(t) + \frac{c^2}{a}B'\left[z_c\left(t - \frac{A'a}{B'c}\right) - z_c(t)\right]$$
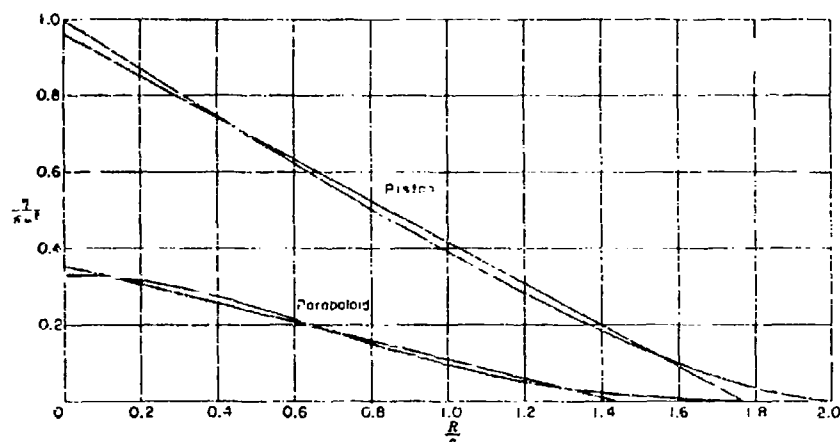
Figure 32 - Plot to Represent the Function η

For a piston η is defined in Equation [122]: for a paraboloidal diaphragm, in Equation [119]. The radius of the diaphragm is a, and the distance from its center is R. The curves represent $\eta/\pi a^2$; the straight lines represent linear approximations having the same area under them as the curves and also the same moment about the axis, $R = 0$.

If this expression multiplied by πa^2 is substituted for the integral in [116], and also

$$\frac{\pi \rho c a^2 A'}{M} = k, \quad \frac{\pi o c^2 a B'}{M} = b, \quad \frac{A'a}{B'c} = T$$

Equation [116] becomes the difference-differential equation

$$\ddot{z}_c(t) + k \dot{z}_c(t) - b\left[z_c(t) - z_c(t - T)\right] = \frac{2F_1 + \phi}{M} \tag{125}$$

This equation is more easily handled than the more accurate integrodifferential equation; in simple cases it can be solved completely.

THE NON-COMPRESSIVE CASE WITH PROPORTIONAL CONSTRAINT

Let $\ddot{z}_c$ change so slowly with time that it changes only by a negligible amount during a time D/c. Then in Equation [111] or [116] $\ddot{z}_c$ can be treated as independent of s and can be taken out from under the integral sign, with the result that

$$(M + M_l)\ddot{z}_c = 2F_1 + \phi \tag{126}$$

$$M_l = \frac{\rho}{2\pi} \iint f(x,y)\,dx\,dy \iint \frac{1}{s} f(x',y')\,dx'\,dy' = \rho \int_0^D \eta(s)\,ds \tag{127}$$

in which s denotes the distance between the elements $dx\,dy$ and $dx'\,dy'$.

For a circular diaphragm of radius a, substitution of [119] or [122] for η in [127] and evaluation of the integral gives, for the paraboloidal and the piston-like motions, respectively,

$$M_i = 0.813\,\rho a^3, \quad M_i = \frac{8}{3}\rho a^3 \tag{128a, b}$$

A third type of motion that is of some interest is described by

$$z = z_c(t)f(x,y) = z_c(t)\left(1 - \frac{r^2}{a^2}\right)^{-\frac{1}{2}} \quad \text{for } r < a \tag{129}$$

The integral in [102] becomes in this case, when $\ddot{z}$ varies slowly enough with the time,

$$\int \frac{1}{s}\ddot{z}_{c-s}\,dS = \ddot{z}_c\int \frac{1}{s}\left(1 - \frac{r^2}{a^2}\right)^{-\frac{1}{2}}dS \tag{130}$$

Now this last integral represents the electrical potential at any point of a disk due to a density of charge on it equal to $(1 - r^2/a^2)^{-\frac{1}{2}}$; and it is a known theorem in electrostatics that a surface density varying in this manner produces a constant potential over the disk. The constant value of the integral is easily found by evaluating it for a point at the center, where $s = r$ and dS may be replaced by $2\pi r\,dr$, so that

$$\int \frac{1}{s}\left(1 - \frac{r^2}{a^2}\right)^{-\frac{1}{2}}dS = \int_0^a\left(1 - \frac{r^2}{a^2}\right)^{-\frac{1}{2}}2\pi\,dr = \pi^2 a \tag{131}$$

With the use of this result, the integral for M_i in [127] is easily evaluated, thus:

$$M_i = \frac{\rho}{2\pi}\int_0^a\left(1 - \frac{r^2}{a^2}\right)^{-\frac{1}{2}}2\pi r\,dr\int_0^a\left(1 - \frac{r'^2}{a^2}\right)^{-\frac{1}{2}}2\pi\,dr'$$

$$= \pi^2\rho a\int_0^a\left(1 - \frac{r^2}{a^2}\right)^{-\frac{1}{2}}r\,dr = \pi^2\rho a^3 \tag{132}$$

Furthermore, substitution from [130] and [131] for the integral in [103] gives

$$\frac{\pi}{2}\rho a\ddot{z}_c = 2p_i + p_0 - p \tag{133}$$

This result will hold for the water surface exposed in a circular opening of radius a in a plate lying against the water, when, with the exposed surface initially plane and stationary, a comparatively steady pressure equal to $2p_i + p_0$ is generated in the water back of the hole while the pressure on the exposed surface is p. Then [129] represents the displacement of the water

surface provided z_c is such a function of the time that $\ddot{z}_c$ has the value given by [133].

The electrostatic analogy can be utilized in all cases to show that $M_i \dot{z}_c^2/2$ represents the kinetic energy in the water. This may also be shown from [126] as follows. Let the mass of the diaphragm be negligible, so that M can be set equal to 0 and stress forces can be neglected in ϕ, and let $F_i = 0$. Then Equation [126], multiplied through by $\dot{z}_c$, can be written, using [113b],

$$M_i \dot{z}_c \ddot{z}_c = \iint \phi \, \dot{z}_c \, f(z,y) \, dz \, dy$$

Here ϕ is now the difference between hydrostatic pressure and the pressure on the back face of the plate, and $\dot{z}_c f(z,y)$ is the velocity; hence the integral represents the rate at which the net pressure is doing work. This must equal the rate at which the kinetic energy of the water is increasing, and the left-hand member of the equation is in fact equal to

$$\frac{d}{dt}\left(\frac{1}{2} M_i \dot{z}_c^2\right)$$

Up to this point it has been assumed that the diaphragm is surrounded by a fixed plane baffle of infinite extent. If there is no baffle, and the diaphragm forms one side of an air-filled box, the determination of M_i is much more difficult. In order to estimate the order of magnitude of the difference, the value of M_i was calculated for a sphere whose surface over one hemisphere moves radially outward while the other hemisphere remains at rest. The motion of potential flow is easily written out for this case in terms of spherical harmonics; summation of the resulting series gives $M_i = 0.832\pi\rho a^3$ where a is the radius of the sphere and ρ the density of the surrounding fluid. Had the fluid been confined by a plane baffle continuing the plane of the base of the expanding hemisphere, M_i would have been $2\pi\rho a^3$. Thus removal of the baffle decreases M_i in the ratio 0.416. It is a plausible surmise that the decrease in M_i would be somewhat less for a paraboloidal diaphragm and somewhat more for a piston.

THE REDUCTION PRINCIPLE, IN THE CASE OF PROPORTIONAL CONSTRAINT

Suppose again that only part of the target is movable, the rest constituting an infinite rigid baffle; as before, let the maximum diameter of the movable plate be D. Let M and M_i be constants. Then the following statements are true:

1. Within any time interval of length D/c, at least once

$$\frac{d^2 z_c}{dt^2} = \frac{(2F_i + \phi)_i}{M + M_i} \tag{134}$$

where a subscript f means that values are to be taken at the end of the interval, while $d^2 z_c/dt^2$ is the acceleration at some unknown instant during the interval. Alternatively, $d^2 z_c/dt^2$ may merely change discontinuously from a value on one side of that stated to a value on the other side.

2.   Within any time interval of length D/c, at least at one instant t

$$\dot{z}_c(t) = \dot{z}_c(t_1) + \frac{1}{M + M_i}\left\{\rho\int_0^D\left[\dot{z}_c\left(t_1 - \frac{s}{c}\right) - \dot{z}_c(t_1)\right]\eta(s)\,ds + \int_{t_1}^{t_f}(2F_i + \phi)\,dt\right\} \quad [135]$$

or

$$\dot{z}_c(t) = \dot{z}_c(t_1') + \frac{1}{M + M_i}\int_{t_1}^{t_f}(2F_i + \phi)\,dt \quad\quad\quad [136]$$

where t_f is the time at the end of the interval and t_1 is any chosen time not later than its beginning, while t_j' is some unknown instant lying between $t_1 - D/c$ and t_1. Thus

$$t_1 - \frac{D}{c} < t_1' < t_1 < t < t_f$$

and t_f and t_1 are arbitrary except that

$$t_f - t_1 \geqq \frac{D}{c}$$

To prove the first of these statements, multiply [116] through by $M_i(M + M_i)$:

$$(M + M_i)M_i M\ddot{z}_c(t) = M_i(M + M_i)\left[2F_i + \phi - \rho\int_0^D \ddot{z}_c\left(t - \frac{s}{c}\right)\eta(s)\,ds\right] \quad [137]$$

Now, if Q is any quantity independent of s, by [127]

$$M_i Q = \rho\int_0^D Q\,\eta(s)\,ds \quad\quad\quad [138]$$

By applying this transformation to $\ddot{z}_c(t)$, F_i and ϕ, it is easily seen that [137] can be written

$$\rho\int_0^D\left\{M\left[(M + M_i)\ddot{z}_c(t) - 2F_i - \phi\right] + M_i\left[(M + M_i)\ddot{z}_c\left(t - \frac{s}{c}\right) - 2F_i - \phi\right]\right\}\eta(s)\,ds = 0$$

Now if the second expression in brackets does not vanish for any value of s in the range of integration, and nowhere jumps from positive to negative or vice versa, then it has everywhere the same sign, and the same sign as the first bracket, which is its own value for $s = 0$; the entire integrand has,

therefore, the same sign throughout, and the integral cannot vanish. Hence for at least one value s' between 0 and D the second bracket must either vanish or change sign discontinuously. At the corresponding time, $t - s'/c$, $\ddot{z}_c$ or $\ddot{z}_c(t - s'/c)$ has the value stated in [134].

To prove [135], Equation [116] is first integrated with respect to the time from t_1 to t_f:

$$M\left[\dot{z}_c(t_f) - \dot{z}_c(t_1)\right] = \int_{t_1}^{t_f} (2F_i + \Phi)\,dt - \rho \int_0^D \left[\dot{z}_c\left(t_f - \frac{s}{c}\right) - \dot{z}_c\left(t_1 - \frac{s}{c}\right)\right] \eta(s)\,ds$$

Multiplying by $M_l(M + M_l)$ and applying [138] to all terms except

$$\rho \int_0^D \dot{z}_c\left(t_f - \frac{s}{c}\right) \eta(s)\,ds$$

there results

$$\rho \int_0^D \left\{ M\left[(M + M_l)\dot{z}_c(t_f) - M\dot{z}_c(t_1) - \int_{t_1}^{t_f}(2F_i + \Phi)\,dt - \rho\int_0^D \dot{z}_c\left(t_1 - \frac{s'}{c}\right)ds'\right] \right.$$

$$+ M_l\left[(M + M_l)\dot{z}_c\left(t_f - \frac{s}{c}\right) - M\dot{z}_c(t_1) - \int_{t_1}^{t_f}(2F_i + \Phi)\,dt\right.$$

$$\left.\left. - \rho\int_0^D \dot{z}_c\left(t_1 - \frac{s'}{c}\right)\eta(s')\,ds'\right]\right\}\eta(s)\,ds = 0$$

and by reasoning as before and then using [127], Equation [135] is obtained. To convert this equation into [136], note that, since η is positive and $z_c(t)$ is continuous, there exists a value s'' between 0 and D such that

$$\rho \int_0^D \left[\dot{z}_c\left(t_1 - \frac{s}{c}\right) - \dot{z}_c(t_1)\right]\eta(s)\,ds = \left[\dot{z}_c\left(t_1 - \frac{s''}{c}\right) - \dot{z}_c(t_1)\right]\rho\int_0^D \eta(s)\,ds$$

$$= M_l\left[\dot{z}_c\left(t_1 - \frac{s''}{c}\right) - \dot{z}_c(t_1)\right]$$

by [127]. The terms containing t_1 in [135] can thus be written

$$\dot{z}_c(t_1) + \frac{M_l}{M + M_l}\left[\dot{z}_c\left(t_1 - \frac{s''}{c}\right) - \dot{z}_c(t_1)\right]$$

This expression lies between $\dot{z}_c(t_1)$ and $\dot{z}_c(t_1 - s''/c)$; it is, therefore, the value of $\dot{z}_c(t_1 - s/c)$ at some other value s' between 0 and s'', or the value of $\dot{z}_c(t)$ at some time t_1' between $t_1 - D/c$ and t_1.

Comparison with [126] and with the result of integrating this equation from t_1 to t_f. respectively, shows that the values of z_c and $\dot{z}_c$ given by [134] and [135] or [136] are equal to the values obtained from non-compressive theory except for the initial correction due to the first integral in [135] or the substitution of t_1' for t_1 in [136].

INITIAL MOTION OF A PROPORTIONALLY CONSTRAINED PLATE

After a proportionally constrained plate has been either at rest or moving uniformly for a time greater than D/c, let a wave of pressure p_i suddenly begin to fall upon it, at time $t = 0$. Then, in [111], $\ddot{z}_c(t - s/c)$ will at first differ from zero only for small s, for which $f(x', y')$ may be replaced by $f(x, y)$ and taken out from under the integral sign. The integration with respect to $dx'dy'$ or dS' can then be carried out in analogy with [106]:

$$\int \ddot{z}_c\left(t - \frac{s}{c}\right)\frac{dS'}{s} = 2\pi c\, \dot{z}_c(t) \tag{139}$$

provided $\dot{z}_c(-\infty) = 0$. Thus [111], becomes, approximately, for a short time,

$$M\ddot{z}_c + \rho c A \dot{z}_c = 2F_i + \Phi \tag{140}$$

where

$$A = \iint \left[f(x,y)\right]^2 dx\,dy \tag{141}$$

EFFECT OF FLUID ON BOTH SIDES OF THE PLATE

If there is fluid of appreciable density behind the plate as well as in front of it, a release pressure will be developed on both sides. That in front will be, from [99],

$$p_{s1} = -\frac{\rho_1}{2\pi}\int \frac{1}{s}\ddot{z}_{t-\frac{s}{c_1}}\,dS$$

where ρ_1 is the density of the fluid in front and c_1 is the speed of sound in this fluid. The release pressure behind the plate will be similarly,

$$p_{s2} = \frac{\rho_2}{2\pi}\int \frac{1}{s}\ddot{z}_{t-\frac{s}{c_2}}\,dS \tag{142}$$

where ρ_2 and c_2 refer to the fluid behind the plate. The reversal of sign here arises from the fact that in obtaining the formula for the release pressure $\ddot{z}$ was assumed to be measured positively away from the fluid, whereas here the positive direction for $\ddot{z}$ is taken always toward the back side of the plate. The total pressure on the back face is then

$$p_2 = p_{02} + p_{s2}$$

where p_{02} is the hydrostatic pressure on that face.

The second release pressure p_{s2} is automatically allowed for in the quantities ϕ and Φ as originally defined. Hence, if desired, all of the preceding formulas, Equations [100] to [141], will still hold provided ρ and c in those formulas are replaced by ρ_1 and c_1.

As an alternative, ϕ may be defined as

$$\phi = \phi_0 - p_{s2} = \phi_0 - \frac{\rho_2}{2\pi} \int \frac{1}{s} \ddot{z}_{t - \frac{s}{c_2}} dS \qquad [143]$$

where ϕ_0 denotes the difference between hydrostatic pressure on the front and on the back, plus the net force on the plate per unit area due to stresses. Then by [113b] and the transformation leading to [116]

$$\Phi = \Phi_0 - \frac{\rho_2}{2\pi} \iint f(x,y)\, dx\, dy \iint \frac{1}{s} \ddot{z}_c\left(t - \frac{s}{c_2}\right) f(x', y')\, dx'\, dy'$$

$$= \Phi_0 - \rho_2 \int_0^D \ddot{z}_c\left(t - \frac{s}{c_2}\right) \eta(s)\, ds \qquad [144]$$

where

$$\Phi_0 = \int \phi_0 f(x,y) dS \qquad [145]$$

If this is done, it is readily seen that, besides the substitution of ϕ_0 for ϕ in all equations, every term containing an integral with $\ddot{z}_{t-\frac{s}{c}}$ or $\ddot{z}(t - s/c)$ in the integrand is replaced by the sum of two similar terms with ρ and c changed to ρ_1 and c_1 or to ρ_2 and c_2, respectively; furthermore, in such equations for M, as [127], [128a, b] and [132], ρ is replaced by $\rho_1 + \rho_2$, and where the acoustic impedance ρc occurs, as in [107], [108], [109], and [140], it is replaced by the sum of the two impedances, $\rho_1 c_1 + \rho_2 c_2$.

In particular, for a uniform plane plate between two fluids, with plane waves incident normally upon it on one side, [107] becomes

$$m\ddot{z} + (\rho_1 c_1 + \rho_2 c_2)\dot{z} = 2p_i + \phi_0 \qquad [146]$$

CAVITATION AT A PLATE OR DIAPHRAGM

The analytical theory of cavitation at the interface between a plate and a liquid will be developed here on the two assumptions that cavitation occurs whenever the pressure sinks to a fixed breaking-pressure p_b, and that the pressure in the cavitated region has a definite value p_c, not less than p_b. The assumptions hitherto made concerning the plate will be retained.

On these assumptions, cavitation will begin in an area on the plate in which the pressure is decreasing and at a point at which a local minimum

of pressure occurs. Since in the neighborhood of such a point the pressure differs only by a quantity of the second order, cavitation will then at once occur at neighboring points as well. Thus the edge of the cavitated region, advancing over the plate as a *breaking-edge*, will move at first at infinite speed. Eventually it will halt and return toward the cavitated area as a *closing-edge*, leaving the liquid behind it in contact with the plate.

Let U denote the speed of propagation of the edge in a direction perpendicular to itself, and let c denote the speed of sound in the liquid.

If $U \geq c$, the phenomena at the edge are essentially local in character and the analytical treatment is easy. For effects can be propagated through the liquid only at speed c; hence no effects propagated from points behind the edge can overtake it, so that its behavior is determined entirely by conditions ahead of it, and these conditions, in turn, are entirely uninfluenced by the approach of the edge.

Consider, first, a breaking-edge. Let dn denote the perpendicular distance from the edge to a point P ahead of it.

Then the pressure, which is p_b at the edge, is

$$\bar{p}_b + \frac{\partial p}{\partial n} dn$$

at P, where $\partial p/\partial n$ denotes the gradient of the pressure P in a direction perpendicular to the edge. The pressure at P will sink to p_b, and the edge will, therefore, move up to P, in a time

$$dt = \frac{\frac{\partial p}{\partial n} dn}{-\frac{\partial p}{\partial t}}$$

where $\partial p/\partial t$ is the time derivative of the pressure in the liquid just ahead of the edge. Hence

$$U = \frac{dn}{dt} = -\frac{\frac{\partial p}{\partial t}}{\frac{\partial p}{\partial n}} \qquad [147]$$

Thus $U \geq c$ only if $-\partial p/\partial t \geq c\,\partial p/\partial n$.

As the edge passes P, the pressure on the liquid surface, previously p_b, becomes p_c. If $p_c > p_b$, the sudden increase in the value of p in [105] requires a compensating negative increment of the integral in that equation. This increment can arise only from high momentary accelerations of the liquid surface. Hence, as the edge passes P, there occurs an impulsive change in the velocity of the liquid surface perpendicular to the plate. This change is easily calculated.

The high values of the acceleration associated with the passage of the edge travel along with it. Hence, if x is the coordinate of any point on the plate measured from P perpendicularly to the edge and in its direction of motion, and if $\ddot{z}_1(t)$ is the special, high acceleration due to the edge at P at a certain time t, the simultaneous value of this acceleration at any other point will be the same as the value that was at P at the earlier time $t - x/U$, or $\ddot{z}_1(t - x/U)$. Thus the total contribution of the edge to the integral in [103] can be written

$$\Delta \int \ddot{z}_{t-\frac{s}{c}} \frac{dS}{s} = \int \ddot{z}_1\left(t - \frac{s}{c} - \frac{x}{U}\right) \frac{dS}{s}$$

Just after the edge has passed P, the integrand in the last integral is easily seen to differ from zero only for elements dS lying near a small ellipse surrounding P.

Let polars r, ϑ be introduced such that $s = r$, $x = r \cos \vartheta$. Then $dS = 2\pi r\, dr\, d\theta$ and the last equation becomes

$$\Delta \int \ddot{z}_{t-\frac{s}{c}} \frac{dS}{s} = \int_0^{2\pi} d\theta \int_0^{\infty} \ddot{z}_1\left(t - \frac{r}{c} - \frac{r\cos\theta}{U}\right) dr$$

$$= -\int_0^{2\pi} d\theta \int_0^{\infty} \frac{c}{1 + \frac{c}{U}\cos\theta} \frac{d}{dr}\, \dot{z}_1\left(t - \frac{r}{c} - \frac{r\cos\theta}{U}\right) dr$$

$$= c(\Delta \dot{z}) \int_0^{2\pi} \frac{d\theta}{1 + \frac{c}{U}\cos\theta} = 2\pi c(\Delta \dot{z})\left(1 - \frac{c^2}{U^2}\right)^{-\frac{1}{2}}$$

where $\Delta \dot{z}$ is the jump in the velocity $\dot{z}$ at the edge taken in the direction of decreasing r.

Thus, according to [103],

$$\frac{\rho}{2\pi}\left[2\pi c(\Delta \dot{z})\left(1 - \frac{c^2}{U^2}\right)^{-\frac{1}{2}}\right] = -\Delta p = -(p_c - p_b) \qquad [148]$$

$$\Delta \dot{z} = -\frac{p_c - p_b}{\rho c}\left(1 - \frac{c^2}{U^2}\right)^{\frac{1}{2}} \qquad [149]$$

Or, since according to [101] the pressure just before the edge arrived was connected with conditions in the plate by the equation

$$p = p_b = m\ddot{z} - \phi + p_0$$

$$\Delta \dot{z} = -\frac{1}{\rho c}\left(1 - \frac{c^2}{U^2}\right)^{\frac{1}{2}}(p_c - m\ddot{z} + \phi - p_0) \qquad [150]$$

For a closing-edge, the same calculation applies except that here $\Delta \dot{z}$ is fixed by conditions in the cavitated region ahead of the advancing edge, and the impulsive change Δp in the pressure at the surface of the liquid is to be found. As closing occurs, the velocity of the liquid surface suddenly changes from some value z_l to the velocity $\dot{z}_p$ of the plate. The liquid surface behaves like a plate of zero mass, hence it alone changes velocity in the impact. Hence, from the first part of [148],

$$\Delta p = \rho c \left(1 - \frac{c^2}{U^2}\right)^{\frac{1}{2}} (\dot{z}_l - \dot{z}_w) \qquad [151]$$

If $\dot{z}_l$ exceeds $\dot{z}_p$ ahead of the edge, the liquid surface will usually meet the plate at a finite angle θ. Then in time dt the edge will advance a distance $U\,dt$ over the plate of such magnitude that $U\,dt \tan \theta = (\dot{z}_l - \dot{z}_p)dt$. Hence for a closing-edge of the type under consideration

$$U = \frac{\dot{z}_l - \dot{z}_p}{\tan \theta} \qquad [152]$$

and an edge can advance as a closing-edge moving at speed $U \gtrless c$ only if $\dot{z}_l - \dot{z}_p \gtrless c \tan \theta$. Exceptionally, it might happen momentarily that $\theta = 0$ and $\dot{z}_l = \dot{z}_p$.

If conditions are not such as to cause the edge of the cavitated area to travel at a speed equal to or greater than c, it seems clear that the edge will usually stand still, except as it may be carried along by flow of the liquid parallel to the plate. For, propagation of pressure waves from or to the free surface of the liquid should prevent the occurrence of large differences of pressure in the liquid near the edge. Hence, if $p_b < p_c$, pressures so low as p_b cannot occur at the edge, and further cavitation cannot occur. Impulsive changes of velocity are likewise impossible; if such impulsive action begins, but the edge moves at a speed less than c, the impulsive pressure developed will produce such a redistribution of velocities in the liquid as to equalize $\dot{z}_l$ and $\dot{z}_p$ on the cavitated side of the edge. As an exceptional case, the liquid surface might perhaps roll onto the plate like a rug being laid down on a floor.

Otherwise, under the assumed conditions, the edge will move only as it is carried along by the liquid in its particle motion. In a strict linear theory, therefore, in which all particle velocities are assumed to be negligibly small, the edge of the cavitated area must stand still except when it can move at least at the speed of sound.

CAVITATION WITH DOUBLE PROPORTIONAL CONSTRAINT

Something more can be inferred, including useful relations with non-compressive theory, if the surface of the liquid is arbitrarily assumed

to move under the same type of proportional constraint as the plate. Let the plate be mounted in a fixed plane baffle. Then the reduction principle stated on page 75 can be utilized by the following trick.

While the liquid is in contact with the plate, [116] holds; this equation can be written

$$0 = 2F_i + \phi - M\ddot{z}_c - \rho\int_0^U \ddot{z}_c\left(t - \frac{s}{c}\right)\eta(s)\,ds \qquad [153]$$

When free, the surface is equivalent to a plate containing neither mass nor stress forces; its equation can be formed from [153] by putting $M = 0$ and $\phi = \phi_s$ where

$$\phi_s = \iint(p_0 - p_c)f(x,y)\,dx\,dy \qquad [154]$$

and represents the effect of the difference between the hydrostatic pressure p_0 and the pressure p_c on the surface. The equation for the surface when free is thus

$$0 = 2F_i + \phi_s - \rho\int_0^U \ddot{z}_c\left(t - \frac{s}{c}\right)\eta(s)\,ds \qquad [155]$$

Finally, to avoid discontinuous change, the pressure on the surface may be supposed to change rapidly but continuously from the pressure exerted on it by the plate just before cavitation to the value p_c. During this transition process the equation for motion of the surface of the liquid may be written

$$0 = 2F_i + \phi' - \rho\int_0^U \ddot{z}_c\left(t - \frac{s}{c}\right)\eta(s)\,ds \qquad [156]$$

where ϕ' changes rapidly from $\phi - M\ddot{z}_c$ to ϕ_s; here $\ddot{z}_c$ stands for the acceleration just before the transition begins.

During the transition, high accelerations may occur, with the result that the velocity $\dot{z}_{cl}$ of the liquid surface changes by $\Delta\dot{z}_{cl}$ where, in analogy with [150] when $U = \infty$,

$$\Delta\dot{z}_{cl} = \frac{1}{\rho c\eta(0)}(M\ddot{z}_c - \phi + \phi_s) \qquad [157]$$

The reduction principle on page 75, which was based on [116], can now be applied by noting that [153], [156], and [155] can be regarded as successive forms of [116] in which the constant M is first replaced by 0, and $2F_i + \phi$ is then replaced by an appropriate expression. In [156], let t_1 be taken as the instant at which the transition to cavitation begins. Then, in the integral in [136], during the transition $2F_i + \phi$ is replaced by $2F_i + \phi'$,

as in [156], but the resulting contribution to the integral is negligible be-
cause of the extreme shortness of the time interval. Hence, the integral may
be written simply as

$$\int_{t_{cv}}^{t_f} (2F_i + \phi_s)\, dt$$

from [155], where t_{cv} is the time at which cavitation occurs.

Hence, putting $M = 0$ in [156], it may be concluded that, after the
onset of cavitation, within any time interval of length D/c the velocity of
the surface of the liquid will take on at least once the value

$$\dot{z}_{cl} = \dot{z}_c(t'_{cv}) + \frac{1}{M_l}\int_{t_{cr}}^{t_f}(2F_i + \phi_s)\, dt \tag{158}$$

Here t_f is the time at the end of the chosen interval and $z_c(t'_{cv})$ is the com-
mon velocity of liquid surface and plate at some instant that precedes the
onset of cavitation by an interval less than D/c. A specific expression for
$\dot{z}_c(t'_{cv})$ can be obtained by using [135] instead of [136]. From this expres-
sion it is easily seen that, if cavitation follows the incidence of a pres-
sure wave within an interval much less than D/c, then $\dot{z}_c(t'_{cv})$ is approximately
equal to the velocity of the plate just prior to the incidence of the wave.

It will be noted that the value of $\dot{z}_{cl}$ given by [158] represents
the value of $\dot{z}_{cl}$ at time t_f as calculated from non-compressive theory, ex-
cept for the substitution of $\dot{z}_c(t'_{cv})$ for $\dot{z}_c(t_{cv})$ as the initial velocity.
For the non-compressive value can be obtained by integrating the analog of
[126] for a free surface or

$$M_l\ddot{z}_{cl} = 2F_i + \phi_s \tag{159}$$

In [158] the initial impulsive change of velocity has disappeared.

During the reverse process that occurs when the cavitation closes,
the velocity of the liquid surface changes impulsively from some value $\dot{z}_{cl}$ to
the velocity $\dot{z}_{cp}$ which the plate happens to have at that instant. Thereafter
[153] holds again; but in this equation some of those values of $\ddot{z}_c(t - s/c)$
that have reference to times before the closure of the cavitation are now
values of the acceleration of the free liquid surface.

During a time after the closure that is short relatively to the
diffraction time, [153] can be written approximately as

$$M\ddot{z}_c = 2F_i + \phi + \rho c A(\dot{z}_{cl} - \dot{z}_c) - \rho\int_{s_l}^{F}\ddot{z}_c\left(t - \frac{s}{c}\right)\eta(s)\, ds \tag{160}$$

where s_1 is such a value of s that $t - s_1/c$ represents the time at which closure occurred and A is given by [141]. Here z_{oi} is a constant, and the part of the integral for $0 < s < s_1$ has been transformed into the term containing A in the same way in which the similar term in [140] was obtained.

The reduction principle can again be invoked in order to obtain an expression for the final value of $\dot{z}_c$, the common velocity of liquid and plate. If, in [136], t_1 is taken at the beginning of the transition process, the transition itself again contributes nothing appreciable to the integral in [136], which becomes here, from [153] used as a form of [116],

$$\int_{t_{11}}^{t_f}(2F_i + \phi - M\ddot{z}_c)dt = M\Big[\dot{z}_c(t_{11}) - \dot{z}_c(t_f)\Big] + \int_{t_{11}}^{t_f}(2F_i + \phi)dt$$

where t_{11} is the instant just after the completion of the transition. In the last integral t_{11} becomes replaced, as the time of transition is shortened to zero, by the time t_1 or t_{cl} at which the cavitation disappears; but $\dot{z}_c(t_{11})$ becomes $\dot{z}_{cp}(t_{cl})$ or the velocity of the plate, not that of the liquid or $\dot{z}_{cl}(t_{cl})$.

Hence it follows from [136], with the M in that equation replaced by 0, that, after the closure of cavitation at time t_{cl}, at some instant within any interval of length D/c the common velocity of liquid surface and plate takes on momentarily the value

$$\dot{z}_c = \frac{1}{M + M_i}\Big[M_i\dot{z}_{cl}(t_{cl}') + M\dot{z}_{cp}(t_{cl}) + \int_{t_{cl}}^{t_f}(2F_i + \phi)dt\Big] \qquad [161]$$

where $\dot{z}_{cp}(t_{cl})$ is the velocity of the plate at the instant t_{cl}, whereas $\dot{z}_{cl}(t_{cl}')$ is the velocity of the liquid surface at an instant t_{cl}' that precedes t_{cl} by less than D/c and usually by less than the diffraction time, T_d. Here in [136] t_1 has been replaced by t_{cl} and $\dot{z}_c(t_1')$ by $\dot{z}_{cl}(t_{cl}')$. Actually, the value of $\dot{z}_c$ that is obtained from [136] in the manner described is somewhat different; if it is denoted by $\dot{z}_c'$, its relation to $\dot{z}_c$, as defined by [161], can be written in the form

$$\dot{z}_c = \dot{z}_c' + \frac{M}{M + M_i}\Big[\dot{z}_c(t_f) - \dot{z}_c'\Big]$$

hence, since $M/(M + M_i) < 1$, $\dot{z}_c$ lies between $\dot{z}_c'$ and $\dot{z}_c(t_f)$, and, since the velocity eventually traverses the entire range from $\dot{z}_c'$ to $\dot{z}_c(t_f)$, the value $\dot{z}_c$ occurs also. The explicit expression for $\dot{z}_{cl}(t_{cl}')$, obtained by using [135] instead of [136], is

$$\dot{z}_{cl}(t_{cl}') = \dot{z}_{cl}(t_{cl}) + \frac{\rho}{M_i}\int_0^D\Big[\dot{z}_{cl}\Big(t_{cl} - \frac{s}{c}\Big) - \dot{z}_{cl}(t_{cl})\Big]\eta(s)ds \qquad [162]$$

The value of $\dot{z}_c$ given by [161] represents the velocity as calculated for the time t_f from non-compressive theory, except that in the equalization of velocities by impact as represented by the first two terms on the right the velocity of the liquid surface is taken, not at the time of impact t_{ci}, but at a somewhat earlier time t'_{ci}.

So far nothing has been said as to fluid back of the plate. If the plate, or plate and baffle, lie between fluids in which the density and speed of sound are, respectively, ρ_1, c_1, and ρ_2, c_2, then all of the results in this section will hold good provided ρ and c are replaced by ρ_1 and c_1, with the understanding that ϕ or Φ includes an allowance for the release pressure in the second fluid. More explicit formulas can be obtained by substituting for ϕ or Φ (but not Φ_s) from [143] or [144].

SOME SWING TIMES

Suppose that a plate, mounted in a fixed plane baffle and constrained to move proportionally, is free from incident pressure, and that the motion is slow enough so that the water or whatever liquid is in contact with its faces can be treated as incompressible. Furthermore, let the motion be small enough so that its component parallel to the plane of the diaphragm can be ignored. Then [126] becomes

$$(M + M_l)\ddot{z}_c = \phi \qquad [163]$$

This can be integrated after multiplication by $\dot{z}_c\,dt$:

$$(M + M_l)\ddot{z}_c\dot{z}_c\,dt = \phi\dot{z}_c\,dt = \phi\,dz_c$$

whence

$$\frac{1}{2}(M + M_l)\dot{z}_c^{\,2} = \int \phi\,dz_c \qquad [164]$$

From a knowledge of $\dot{z}_c$ as a function of z_c the swing time can be found as

$$T_s = \int dt = \int\left(\frac{dz_c}{dt}\right)^{-1}dz_c = \int \dot{z}_c^{-1}\,dz_c \qquad [165]$$

taken between the limits $z_c = 0$ and the first value of z_c at which $\dot{z}_c = 0$.

The most important case is that of a circular diaphragm of radius a and uniform thickness h, constrained to move in symmetrical paraboloidal form or according to [118]. For the small motions considered here, the difference between a paraboloid and a sphere can also be ignored; the diaphragm can be assumed, therefore, to behave as a spherical membrane under uniform tension. Elementary theory then gives, as in the deduction of [95], for the contribution of the stresses to Φ,

$$\phi_z = -2\pi\sigma h z_c \qquad [166]$$

If the hydrostatic pressures on the two sides of the diaphragm are equal, $\phi = \phi_o$ in [164].

If the diaphragm, flat initially, remains within the elastic range it is readily shown that

$$\bar{\sigma} = \frac{E}{1-\mu}\ \frac{z_c^2}{2a^2} \qquad [167]$$

approximately, where E is Young's modulus and μ is Poisson's ratio; see TMB Report 490, Equations [11], [17]. In this case, after evaluation of the integral with $\phi = \phi_o$ as given in [166], Equation [164] gives

$$\dot{z}_c^2 = \frac{1}{M + M_l}\ \frac{\pi E h}{2(1-\mu)a^2}(z_{cm}^4 - z_c^4) \qquad [168]$$

where z_{cm} is the value of z_c at which $\dot{z}_c = 0$. The swing time then involves the integral

$$\int_0^{z_{cm}} \frac{dz_c}{\sqrt{z_{cm}^4 - z_c^4}} = \frac{1}{z_{cm}} \int_0^1 \frac{dx}{\sqrt{1-x^4}} = \frac{1.311}{z_{cm}} \qquad [169]$$

The values of M and M_l may also be inserted from [120] and [128a], in which $m = \rho_d h$ and $\rho = \rho_l$ in terms of the density ρ_d of the diaphragm and the density ρ_l of the adjacent liquid, or

$$M = \frac{\pi}{3}\rho_d h a^2, \quad M_l = 0.813\,\rho_l a^3 \qquad [170a,\ b]$$

With these values, [165] and [168] give for the elastic swing time

$$T_d = \frac{1.07a^2}{z_{cm}} \sqrt{\frac{1-\mu}{E}\left(\rho_d + 0.776\,\frac{a}{h}\,\rho_l\right)} \qquad [171]$$

Thus in the elastic range the swing time varies with the amplitude z_{cm}. If the initial velocity $\dot{z}_{co}$ is known, the amplitude z_{cm} can be found by setting $\dot{z}_c = \dot{z}_{co}$ and $z_c = 0$ in [168] and solving for z_{cm}.

As an alternative, if the diaphragm stretches plastically under a constant yield stress σ and if the initial elastic range of the motion can be neglected, from [164] and [166]

$$\dot{z}_c^2 = \frac{2\pi\sigma h}{M + M_l}(z_{cm}^2 - z_c^2) \qquad [172]$$

and the integral that is needed is

$$\int_0^{z_{cm}} \frac{dz_c}{\sqrt{z_{cm}^2 - z_c^2}} = \int_0^1 \frac{dx}{\sqrt{1-x^2}} = \frac{\pi}{2}$$

Then

$$T_s = \frac{\pi}{2\sqrt{6}} \, a \sqrt{\frac{1}{\sigma}\left(\rho_d + 0.776 \, \frac{a}{h} \, \rho_l\right)} \qquad [173]$$

Inclusion of both the elastic and the plastic ranges leads to very complicated formulas. The error is not large, however, if the plastic formula [173] is used for all motions that extend into the plastic range. The error is greatest when the maximum displacement z_{cm} just attains the elastic limit z_{ce}, which is found by substituting z_{ce} for z_c in [167] and interpreting σ as the yield stress:

$$z_{ce} = a \sqrt{\frac{2(1-\mu)\sigma}{E}} \qquad [174]$$

When $z_{cm} = z_{ce}$, the correct elastic formula, [171], gives

$$T_s = 0.76 \, a \sqrt{\frac{1}{\sigma}\left(\rho_d + 0.776 \, \frac{a}{h} \, \rho_l\right)} \qquad [175]$$

whereas the plastic formula [173] would change the coefficient from 0.76 to 0.64.

Swing times for a similar diaphragm not loaded by liquid on either side and with equal pressures on the two faces can be obtained by setting $\rho_l = 0$ in [171] and [173]. Or, if there is liquid on both sides of the diaphragm, with densities ρ_1 and ρ_2 on the two sides, respectively, ρ_l is to be replaced by $\rho_1 + \rho_2$ for the reason explained on page 79.

SECOND-ORDER EFFECTS IN REFLECTION

In linear or first-order acoustic theory, when either plane or spherical waves fall upon a rigid wall, the boundary condition can be satisfied by assuming reflected waves which are the mirror image in the surface of the incident waves. Thus even the afterflow part* of the particle velocity in a spherical wave has equal and opposite components perpendicular to the surface in the two waves, so that the resultant component in this direction vanishes. The pressure on the surface due to the waves is exactly doubled by reflection.

The case of large amplitudes can easily be investigated, for plane waves at normal incidence, by the method of Riemann, which is explained in Section 282 of Lamb's "Hydrodynamics" (23). It can be imagined that, in the medium carrying the waves, values of the quantity $Q = \mu + \rho_0 c_0 v$ are propagated forward without change, while values of $S = \mu - \rho_0 c_0 v$ are at the same

* For the terminology, see TMB Report 480, page 39 (10).

time propagated backward, where

$$\mu = \rho_0 c_0 \int_{\rho_0}^{\rho} \sqrt{\frac{dp}{d\rho}}\; \frac{d\rho}{\rho} \qquad [176]$$

in terms of the pressure p and the density ρ of the fluid; ρ_0 is the density and c_0 the speed of sound for the undisturbed fluid, v is the particle velocity, and $dp/d\rho$ is to be taken along an appropriate adiabatic. The velocities of propagation of Q and S differ somewhat from c_0, but that is of no present interest. Thus in the medium there exists a continuous array of values of Q which are advancing toward the reflecting surface, and another array of values of S which are moving backward. The local values of μ and v at any point are related to Q and S by the equations

$$\mu = \frac{1}{2}(Q + S), \quad \rho_0 c_0 v = \frac{1}{2}(Q - S) \qquad [177a, \; b]$$

As the incident wave advances, it meets zero values of S coming from the undisturbed region ahead; hence in this wave, by [177a, b], $\mu = \rho_0 c_0 v$. Similarly, in the reflected wave, as soon as it becomes distinct from the incident wave, $Q = 0$ and $\mu = -\rho_0 c_0 v$. Thus, if subscripts i and r denote values in the separate incident and reflected waves, respectively,

$$\mu_i = \rho_0 c_0 v_i = \frac{1}{2} Q_i, \quad \mu_r = -\rho_0 c_0 v_r = \frac{1}{2} S_r, \qquad [178a, \; b]$$

At the reflecting surface, $v = 0$; hence by [177b]

$$S = Q$$

which means that the arriving values of Q are continually being converted into equal values of S, which are then propagated backward. Consequently, at corresponding points on the reflected and incident waves $S_r = Q_i$, and, by [178a, b], $\mu_r = \mu_i$, and also, since μ and p vary together,

$$p_r = p_i$$

This is the usual law of reflection.

At the wall itself, however,

$$\mu = \frac{1}{2}(Q + S) = Q = Q_i = 2\mu_i \qquad [179]$$

where Q_i is the arriving value of Q and μ_i is the value of μ at the corresponding point in the incident wave. This equation represents the appropriate generalization of the law that holds at the wall for infinitesimal waves, namely, $p = 2p_i$.

Now if the fluid obeyed Hooke's law, the pressure p would be

$$p = p_0 + \rho_0 c_0^2 s, \quad s = \frac{V_0 - V}{V_0} \qquad [180a, b]$$

where V is the volume of unit mass and ρ_0, V_0 denote values when $\rho = \rho_0$; s represents the strain and $\rho_0 c_0^2$ the elasticity, since $c_0 = $ (elasticity/density)$^{\frac{1}{2}}$. More generally, p can be written as a series in powers of s:

$$p = p_0 + \rho_0 c_0^2 s + b_2 s^2 + \cdots \qquad [181]$$

Since $V = 1/\rho$, $V_0 = 1/\rho_0$

$$s = 1 - \frac{\rho_0}{\rho}, \quad ds = \frac{\rho_0}{\rho^2} d\rho, \quad \frac{dp}{ds} = \frac{\rho^2}{\rho_0} \frac{dp}{d\rho}$$

Hence from [176]

$$\mu = c_0 \sqrt{\rho_0} \int_0^s \left(\frac{dp}{ds}\right)^{\frac{1}{2}} ds = c_0 \sqrt{\rho_0} \int_0^s (\rho_0 c_0^2 + 2b_2 s \cdots)^{\frac{1}{2}} ds$$

or, after expanding in powers of s and integrating,

$$\mu = \rho_0 c_0^2 s + \frac{1}{2} b_2 s^2 \cdots$$

Subtraction of [181] from this equation gives

$$\mu = p - p_0 - \frac{1}{2} b_2 s^2 \cdots$$

Thus, if Hooke's law holds so that b_2 and all higher coefficients vanish, as in [180a], $\mu = p - p_0$, and [179] gives for the pressure on the wall due to waves of any amplitude, $p - p_0 = 2(p_i - p_0)$, as for small waves.

If only terms through s^2 are to be kept, s^2 may conveniently be replaced by its value as found from the first three terms of [181]; then, as far as terms in s^2,

$$\mu = p - p_0 - \frac{b_2}{2\rho_0^2 c_0^4} (p - p_0)^2 \qquad [182]$$

At the wall, [179] then gives, with [182],

$$p - p_0 - \frac{b_2}{2\rho_0^2 c_0^4} (p - p_0)^2 = 2(p_i - p_0) - \frac{b_2}{\rho_0^2 c_0^4} (p_i - p_0)^2$$

or, since in the small quadratic term it is sufficiently accurate to write $p - p_0 = 2(p_i - p_0)$,

$$p - p_0 = 2(p_i - p_0) + \frac{b_2}{\rho_0^2 c_0^4} (p_i - p_0)^2 \qquad [183]$$

In dealing with water it is convenient to choose $p_0 = 0$. The adiabatic for water that passes through a pressure of one atmosphere and a temperature of 20 degrees centigrade is given by Penney and Dasgupta (24) as $v(p + 3)^{0.138} = 1.666$, where v is in cubic centimeters per gram and the unit for p is 10^3 kilograms per square centimeter. With the help of the binomial expansion and Equation [181] it is easily found that the equivalent series in s, when p is in pounds per square inch, is

$$p = 309000\, s\, (1 + 4.12\, s + 23.6\, s^2 \cdots)$$

or, approximately, if s is replaced by $p/309000$ in the s^2 term,

$$p = 309000\, s\, \left(1 + \frac{p}{75000}\right) \text{ pounds per square inch} \qquad [184]$$

Comparison with [181], in which p_0 is now 0, shows that $\rho_0 c_0^2 = 309,000$, $b_2 = 4.12\, \rho_0 c_0^2 = 1.273 \times 10^6$.

Hence [183] for the pressure on the wall may be written, for water, when the incident pressure p_i is in pounds per square inch, if $p_0 = 0$,

$$p = 2p_i\left(1 + \frac{p_i}{150000}\right) \qquad [185]$$

106

INDEX

THE DISTORTION UNDER PRESSURE OF A DIAPHRAGM WHICH IS CLAMPED ALONG ITS EDGE AND STRESSED BEYOND THE ELASTIC LIMIT

G. I. Taylor
Cambridge University

British Contribution

September 1942

THE DISTORTION UNDER PRESSURE OF A DIAPHRAGM WHICH IS CLAMPED ALONG ITS EDGE AND STRESSED BEYOND THE ELASTIC LIMIT

G. I. Taylor

September 1942

*   ■   *   ■   *   ■   *   ■

PART 1.   *Theoretical considerations.*

It will be assumed that the plastic material has the ideal property that it deforms by a negligible amount until the yield point is reached and that it subsequently flows plastically without further increase in stress. In other words, it will be assumed that no strain hardening occurs.

In general the criterion for plastic flow is that some function of the stress components shall exceed a certain limit. Two such criteria have been extensively used, namely (i) that of Mohr, according to which the material flows when the maximum stress difference exceeds a certain limit, (ii) that of von Mises, according to which flow occurs when the sum of the squares of the principal stress differences exceeds a certain limit. If σ_1 and σ_2 are the principal stress components parallel to the surface of the diaphragm and both are positive (i.e. tensions), and if both are large compared with the stress perpendicular to the diaphragm, then the two criteria for plastic flow are:-

$$\left.\begin{array}{l} \sigma_1 = P \quad \text{when} \quad \sigma_1 > \sigma_2 \\ \sigma_2 = P \quad \text{when} \quad \sigma_2 > \sigma_1 \end{array}\right\} \tag{1}$$

Mohr.

von Mises. $$\sigma_1^2 + \sigma_2^2 - \sigma_1 \sigma_2 = P^2 \tag{2}$$

where P is the tensile strength as measured in a testing machine.

Circular diaphragm.

If σ_1 is the radial stress and σ_2 the tangential stress, the equation of equilibrium of an element in the radial direction is

$$r \frac{d\sigma_1}{dr} + \sigma_1 - \sigma_2 = 0 \tag{3}$$

where r is the radial co-ordinate. In the centre of the diaphragm symmetry alone requires that $\sigma_1 = \sigma_2 = P$. If Mohr's criterion is accepted three alternatives are possible, either

(i) $\sigma_2 = P$, $\sigma_1 < P$. This must be rejected because it is inconsistent with (3).

(ii) $\sigma_2 < P$, $\sigma_1 = P$. In this case (3) gives $\sigma_1 = \sigma_2$

(iii) $\sigma_1 = \sigma_2 = P$.

Thus only the third alternative is possible. Similar reasoning gives the same result if von Mises' criterion is accepted so that in either case $\sigma_1 = \sigma_2$ and the stress distribution is like that of a soap film or stretched membrane. The sheet therefore assumes a spherical form under the action of a uniform pressure p. If h_0 is the displacement of the centre the displacement perpendicular to the plane of the edge at radius r is

$$z = h_0 \left(1 - r^2/r_1^2\right) \tag{4}$$

where .....

where r_1 is the radius of the diaphragm. The pressure necessary to produce the displacement is

$$p = 4Pth_0/r_1^2 \tag{5}$$

where t is the thickness of the sheet.

The work δW done on the material by the pressure during the displacement of the centre from h_0 to $h_0 + \delta h_0$ is

$$\delta W = \int_0^r 2\pi \, pr \left[\frac{dz}{dh} \, \delta h_0 \right] dr \tag{6}$$

Substituting for p and z from (4) and (5) and integrating with respect to r and h_0 the total work done is

$$W = \pi Pt \, h_0^2 \tag{7}$$

Since πr_1^2 is the area of the diaphragm the average work done per c.c. of the material of the plate is

$$\xi_p = Ph_0^2/r_1^2 \tag{8}$$

Distribution of plastic strain in the diaphragm.

Though (8) represents the average amount of work done over the whole area of the diaphragm the distribution of strain, and therefore the work done per c.c., is far from uniform. If ζ is the radial component of displacement parallel to the initial plane of the diaphragm the two components of strain are

$$\left. \begin{array}{l} \text{radial,} \quad \epsilon_1 = \dfrac{d\zeta}{dr} + \dfrac{1}{2}\left(\dfrac{dz}{dr}\right)^2 \\[3mm] \text{tangential,} \quad \epsilon_2 = \zeta/r \end{array} \right\} \tag{9}$$

Since $\sigma_1 = \sigma_2$ symmetry ensures that $\epsilon_1 = \epsilon_2$. The equation for ζ is therefore

$$\frac{d\zeta}{dr} + \frac{1}{2}\left(\frac{dz}{dr}\right)^2 = \zeta/r \tag{10}$$

and substituting for z from (4) this becomes

$$\frac{d\zeta}{dr} - \frac{\zeta}{r} + \frac{2h_0^2 r^2}{r_1^4} = 0 \tag{11}$$

The solution of (11) which corresponds with $\zeta = 0$ at $r = r_1$ is

$$\zeta = h_0^2 \left[\frac{r}{r_1^2} - \frac{r^3}{r_1^4} \right] \tag{12}$$

The principal strains ϵ_1 and ϵ_2 are each equal to

$$\zeta/r = \frac{h_0^2}{r_1^2} \left(1 - \frac{r^2}{r_1^2} \right) \tag{13}$$

It appears therefore that the strain is zero at the edge and equal to h_0^2/r_1^2 at the centre. The strain at any point in the surface of the sheet is proportional to the displacement of that

point .....

point from its initial position in a direction perpendicular to the sheet, at any rate so far as any one state of the diaphragm is concerned. When the strains at a given point in the diaphragm are compared at various stages of displacement they are proportional to h_o^2.

The mean displacement is

$$\bar{z} = \frac{\text{Volume, V, between initial and final positions of diaphragm}}{\text{Area, A, of diaphragm}}$$

For a circular diaphragm and small displacement

$$\bar{z} = \tfrac{1}{2} h_o \tag{14}$$

Elliptical and other non-circular diaphragms.

Though the distortion of a non-circular diaphragm cannot be treated so simply as that of a circular one, an approximation to the displacement might be made by assuming that the diaphragm assumes the same form as a flat membrane or soap film when displaced by a uniform pressure perpendicular to its plane. There is, however, one non-circular shape for which the complete calculation of stress, strain and displacement can be made, namely for elliptical diaphragms. This calculation is here carried through in order to estimate the error that may be expected if the assumption is made that the diaphragm is displaced into the same form as a membrane with uniform tension in all directions.

Taking the equation for the edge of the elliptic diaphragm or plate as

$$\frac{x^2}{a^2} + \frac{y^2}{b^2} = 1 \tag{15}$$

where $2a$ is the major axis, it will be assumed that the equation for the displaced sheet is

$$\frac{z}{h_o} = 1 - \frac{x^2}{a^2} - \frac{y^2}{b^2} \tag{16}$$

and it will be shown that this assumption is consistent with the satisfaction of all the required plastic stress, strain and equilibrium conditions. It will be assumed provisionally that the stress is uniform at all points but not isotropic, thus σ_x and σ_y will be taken as the components of stress parallel to the surface of the plate. The condition of equilibrium in direction normal to the surface is

$$p = t \left(\frac{\sigma_x}{\rho_x} + \frac{\sigma_y}{\rho_y} \right) \tag{17}$$

where t is the thickness of the plate and ρ_x, ρ_y are the principal radii of curvature. For a sheet of the form (16) $1/\rho_x = 2h_o/a^2$, $1/\rho_y = 2h_o/b^2$ so that

$$p = h_o t \left(\frac{\sigma_x}{a^2} + \frac{\sigma_y}{b^2} \right) \tag{18}$$

Since (18) does not contain x or y it can be satisfied if, as has been assumed, σ_x and σ_y are independent of x and y. It will be noticed that (16) shows that the displaced plastic sheet is in fact of the same shape as a displaced soap film. The fact that $\sigma_x = \sigma_y$ in the soap film, but not in the present case, makes no difference to the form of (16).

It now remains to find out whether a distribution of displacements and strains in the surface of the sheet can be found which is consistent with the normal displacement (16) and at the same time allows the plastic stress-strain relations to be satisfied.

Plastic stress-strain relationships.

Assuming that σ_x/σ_y is constant over the ellipse and equal to α, it seems clear that, whatever the stress-strain relationships may be, the ratio of the strain components in the surface

of the .....

of the plate, namely ϵ_x and ϵ_y, must also be constant. Taking $\epsilon_x/\epsilon_y = \beta$ the experimental law of plasticity will define the relationship between α and β. Investigations by Lode[1] and by Taylor and Quinney[2] by different experimental methods give results which are in good agreement. They have been expressed in terms of Lode's variables

$$\left.\begin{array}{c} \mu = 2\left[\dfrac{\sigma_2 - \sigma_3}{\sigma_1 - \sigma_3}\right] - 1 \\[3mm] \nu = 2\left[\dfrac{\epsilon_2 - \epsilon_3}{\epsilon_1 - \epsilon_3}\right] - 1 \end{array}\right\} \tag{19}$$

where σ_1, σ_2, σ_3, ϵ_1, ϵ_2, ϵ_3 are the principal stresses and strains and $\sigma_1 > \sigma_2 > \sigma_3$. The experimental relationship between μ and ν is shown in Figure 10 of Taylor and Quinney's paper.

In the present case where the strains σ_1 and σ_2 are in the plane of the sheet we may take $\sigma_3 = 0$. Since it will be found that $\sigma_y > \sigma_x$ it is necessary to take σ_x as σ_2 and σ_y as σ_1. In this case therefore

$$\mu = 2\alpha - 1 \tag{20}$$

Since the material may be taken as incompressible to the degree of approximation here required

$$\epsilon_1 + \epsilon_2 + \epsilon_3 = 0 \tag{21}$$

and substituting this in Lode's variable ν

$$\nu = 3\beta/(\beta + 2) \tag{22}$$

Some values of μ and the corresponding experimental values of ν taken from Figure 10 of Taylor and Quinney's paper are given in columns 1 and 3 of Table 1. The values of α from (20) are given in column 2. Values of β, found by using the values of ν given in column 3 in (22), are given in column 4. This experimental relationship between α and β is shown in Figure 1.

TABLE 1.

1	2	3	4
μ	α	ν (obs.)	β (from column 3 using (22))
+ 1.0	1.00	+ 1.00	+ 1.000
+ 0.9	0.95	+ 0.770	+ 0.691
+ 0.8	0.90	+ 0.635	+ 0.536
+ 0.7	0.85	+ 0.535	+ 0.438
+ 0.6	0.80	+ 0.440	+ 0.343
+ 0.5	0.75	+ 0.360	+ 0.273
+ 0.4	0.70	+ 0.280	+ 0.206
+ 0.3	0.65	+ 0.195	+ 0.139
+ 0.2	0.60	+ 0.120	+ 0.083
+ 0.1	0.55	+ 0.050	+ 0.034
0	0.50	0	0
− 0.1	0.45	− 0.050	− 0.033
− 0.2	0.40	− 0.120	− 0.077
− 0.3	0.35	− 0.195	− 0.172
− 0.4	0.30	− 0.280	− 0.171
− 0.5	0.25	− 0.360	− 0.214
− 0.6	0.20	− 0.440	− 0.256
− 0.7	0.15	− 0.535	− 0.302
− 0.8	0.10	− 0.635	− 0.347
− 0.9	0.05	− 0.770	− 0.408
− 1.0	0.00	− 1.000	− 0.500

The .....

The only relevant a priori theory on this subject is that the ratios of the stress components in a plastic body are related to the ratios of strain components by the same relationship that applies to viscous fluids, namely $\mu = \nu$. From (20) and (22) it will be seen that, in terms of α and β, this would give

$$\beta = (2\alpha - 1)/(2 - \alpha) \qquad (23)$$

This relationship is also shown in Figure 1. It has been used by von Mises and others in deriving theoretical solutions of problems in plasticity.

Strain and displacement of particles.

The form of the expression (12) for the radial displacement of particles in a circular diaphragm suggests the possibility that a solution may be found by assuming for the two components of displacement ξ, η parallel to the axes x and y the form

$$\left. \begin{array}{l} \xi = Ax \ (1 - x^2/a^2 - y^2/b^2) \\[2mm] \eta = By \ (1 - x^2/a^2 - y^2/b^2) \end{array} \right\} \qquad (24)$$

This assumption satisfied the condition that $\xi = \eta = 0$ at the edge of the plate. The components of strain in the surface of the distorted plate are then

$$\left. \begin{array}{l} \epsilon_x = \dfrac{\partial \xi}{\partial x} + \dfrac{1}{2}\left(\dfrac{\partial z}{\partial x}\right)^2 = A\left(1 - \dfrac{3x^2}{a^2} - \dfrac{y^2}{b^2}\right) + \dfrac{2h_0^2 x^2}{a^4} \\[4mm] \epsilon_y = \dfrac{\partial \eta}{\partial y} + \dfrac{1}{2}\left(\dfrac{\partial z}{\partial y}\right)^2 = B\left(1 - \dfrac{x^2}{a^2} - \dfrac{3y^2}{b^2}\right) + \dfrac{2h_0^2 y^2}{b^4} \end{array} \right\} \qquad (25)$$

Since it has been assumed that $\sigma_x / \sigma_y = \alpha$ is independent of x and y, the unique experimental relationship between α and β ensures that $\beta = \epsilon_x/\epsilon_y$ shall be independent of x and y. Substituting for ϵ_x and ϵ_y from (25) in the equation $\epsilon_x = \beta \epsilon_y$ the condition that β may be independent of x and y is found by equating the constant terms and the coefficients of x^2 and y^2. Hence

$$\left. \begin{array}{l} A = \beta B \\[2mm] B(-3/a^2 + 1/a^2) + 2h_0^2/\beta\, a^4 = 0 \\[2mm] B(-1/b^2 + 3/b^2) - 2h_0^2/b^4 = 0 \end{array} \right\} \qquad (26)$$

and therefore

$$\left. \begin{array}{l} B = h_0^2/b^2 \\[2mm] A = h_0^2/a^2 \\[2mm] \beta = b^2/a^2 \end{array} \right\} \qquad (27)$$

Having determined β from (27) and hence α from the curve Figure 1, σ_x and σ_y can be connected with P, the testing machine measured yield stress, by the formulae

$$\sigma_x = P\alpha, \ \sigma_y = P \qquad \text{if Mohr's theory is used} \qquad (28)$$

$$\text{or} \quad \sigma_x = P\alpha\sqrt{1 - \alpha + \alpha^2}, \ \sigma_y = P\sqrt{1 - \alpha + \alpha^2} \quad \text{according to} \qquad (29)$$
$$\text{von Mises' theory.}$$

This completes the solution of the problem, all the necessary conditions being satisfied. Substituting from (28) or (29) in (18) the following expressions are derived connecting the pressure, the maximum displacement h_0 and the yield stress:-

$$\nu = \ldots\ldots$$

$$p = \frac{h_0 t P}{a^2} \ (\alpha + 1/\beta) \qquad \text{according t Mohr's theory} \tag{30}$$

$$\text{or} \quad p = \frac{h_0 t P}{a^2} \ (\alpha + 1/\beta)(1 - \alpha + \alpha^2)^{-\frac{1}{2}} \quad \text{according to von Mises' theory} \tag{31}$$

If the stress is assumed uniform, as in a soap film, $\sigma_x = \sigma_y = P$ so that

$$p = \frac{h_0 t P}{a^2} \ (1 + 1/\beta) \tag{32}$$

For the case when $b/a = 2/3$, $\beta = a/b$ and the curve of Figure 1 gives $\alpha = 0.86$.   In this case the factors multiplying $h_0 t P/a^2$ in (30), (31) and (32) are 3.11, 3.31 and 3.25 respectively. The assumption that the plate behaves like a membrane with uniform tension equal to P in all directions therefore overestimates the work which is necessary to produce a given displacement by 4.5% if Mohr's criterion is accepted.   On the other hand this assumption underestimates the work by 1.9% if von Mises' strain energy criterion is used.

As the length of the ellipse increases the error increases if von Mises' criterion is used.   It is 6% when $a/b = 2$, 10% when $a/b = 3$ and 15% when a becomes infinite.

Rectangular Plate dished by uniform pressure.

Though the exact analysis which can be completed for the elliptic plate is very difficult for other shapes, the approximate calculation assuming equal tensions in all directions can be carried out for rectangular plates.   For plates 6 feet x 4 feet, such as are used in the box model trials, the error involved in making this approximate assumption is likely to be of the same order as the error in making the same assumption for elliptic plates with axes in the ratio 3 : 2.   This error has been seen to be about 2%.

If $2a$ and $2b$ are now the lengths of the sides of a rectangular plate, the volume V enclosed between the distorted plate and the original plane is, on the above assumption,

$$V = \frac{p}{Pt} \left\{ \frac{4}{3} ab^3 \right\} \left\{ 1 - \frac{192}{\pi^5} \left(\frac{b}{a} \right) \left[\tanh \frac{\pi a}{2b} + \frac{1}{3^5} \tanh \frac{3\pi a}{2b} + \dots \right] \right\} \tag{33}$$

when $b/a = 2/3$ this becomes

$$V = 0.232 \ pa^4/Pt \tag{34}$$

The maximum displacement in the middle of the plate is

$$h_0 = \frac{p}{Pt} \left(\frac{16b^2}{\pi^3} \right) \left[\sec \frac{\pi a}{2b} - 3^{-3} \sec \frac{3\pi a}{2b} + 5^{-3} \sec \frac{5\pi a}{2b} - \dots \right] \tag{35}$$

and for $b/a = 2/3$, (35) gives

$$h_0 = 0.179 \ pa^2/Pt \tag{36}$$

The mean value of displacement of the plate is

$$\bar{z} = V/4ab = 0.0870 \ pa^2/Pt \quad \text{when } b/a = 2/3$$

so that

$$\bar{z}/h_0 = 0.087/0.179 = 0.485$$

$$\text{or} \quad h_0/\bar{z} = 2.06 \tag{37}$$

This may be compared with $\bar{z}/h_0 = 0.5$ for a circular plate.   Since V is proportional to p, the work done on the plate ($b/a = 2/3$) is

$$E_p = \frac{1}{2}pV = 2.16 \ PtV^2/a^4 = 5.76 \ aPt(\bar{z})^2/a^2 \tag{38}$$

where .....

where $A = 8a^2/3$ is the area of the plate.   The mean work done per unit volume of the material is

$$w_0 = \text{...}.10 \; F(\bar{z})^2/a^2 \tag{39}$$

Rectangular plate dished by a non-uniform distribution of pressure.

The only simple case in which the displacement of a rectangular membrane by non-uniform pressure can be calculated is when the pressure is proportional to $\cos \frac{\pi x}{2a} \cos \frac{\pi y}{2b}$.   The equation of equilibrium is

$$p = p_0 \cos \frac{\pi x}{2a} \cos \frac{\pi y}{2b} = P_t \left(\frac{\partial^2 z}{\partial x^2} + \frac{\partial^2 z}{\partial y^2} \right) \tag{40}$$

This is satisfied by taking $z = h_0 \cos \frac{\pi x}{2a} \cos \frac{\pi y}{2b}$ \tag{41}

and $$p_0 = P_t \left(\frac{\pi^2}{4} \right) \left(\frac{1}{a^2} + \frac{1}{b^2} \right) \tag{42}$$

The mean value of $\cos \frac{\pi x}{2a} \cos \frac{\pi y}{2b}$ over the rectangle is $\frac{4}{\pi^2} = 0.406$, so that for this distribution of pressure

$$\bar{z}/h_0 = 0.406 \quad \text{or} \quad h_0/\bar{z} = 2.46 \tag{43}$$

Contours of the displacements are shown in Figure 2.

Dishing of thin plastic plates under suddenly applied pressures.

Normal modes.

The foregoing study of the dishing of a plastic plate under static pressure leads to the conclusion that it may, without much error, be treated as a membrane with uniform tension in all directions.   If this approximation is made to a plastic plate distorted by a very large load applied for a very short time, the motion of the plate can be identical with that of a membrane during the first quarter of its period.   The condition that this particular solution will apply is that the plate is given initially a distribution of velocity corresponding with the velocity of a membrane which is executing simple harmonic oscillations.   If this condition is satisfied, the time τ required for the dishing of the plate is $\frac{1}{4}$ of the period of the vibration of the corresponding membrane.   The membrane of course would return towards its equilibrium position after the first $\frac{1}{4}$ period but the plastic plate stays in the position of maximum distortion.   The longest period of a circular membrane of radius c is $2.613a/c$ where $c^2 = P/\rho$, ρ is its density and Pt the stress per unit length; t is the thickness.   The period of a rectangular membrane of sides $2a$ and $2b$ is $4ab/c\sqrt{a^2 + b^2}$.

$$\left. \begin{array}{ll} \text{Thus} \quad \tau = 0.65 \; a/c & \text{for a circular plate} \\ \\ \text{and} \quad \tau = ab/c\sqrt{a^2 + b^2} & \text{for a rectangular plate} \end{array} \right\} \tag{44}$$

It will be noticed that c depends only on the stress per unit thickness of the membrane. Thus τ is the same for all thicknesses of plate.   For steel plates of density 7.8 with 20 tons/square inch yield, $c^2 = 20 \times 1.54 \times 10^8/7.8$, so that

$$\left. \begin{array}{ll} c = 1.99 \times 10^4 \; \text{cm./second} = 654 \; \text{feet/second for 20 ton steel} \\ \\ \text{and} \quad c = 2.48 \times 10^4 \; \text{cm./second} = 800 \; \text{feet/second for 30 ton steel} \end{array} \right\} \tag{45}$$

For the 6 feet x 4 feet plates used in the investigation .

$$\left. \begin{array}{ll} \tau = 3 \times 2/654 \sqrt{3^2 + 2^2} = 2.55 \times 10^{-3} \; \text{seconds for 20 ton yield} \\ \\ \text{or} \quad \tau = 2.08 \times 10^{-3} \; \text{seconds} \quad \text{for 30 ton yield} \end{array} \right\} \tag{46}$$

Uniform .....

Uniform distribution of impulsive load.

The foregoing discussion assumes that the velocity given to the plate is that which would apply in a normal vibration of a membrane. For the rectangular plate this implies a distribution of initial impulsive velocity proportional to $\cos \frac{\pi x}{2A} \cos \frac{\pi y}{2B}$, i.e. it is greatest in the middle and falls gradually to zero at the edges. If a plastic plate is subjected to a uniformly distributed impulse such as would be given by a very large pressure acting for a time which is small compared with T the central part of the plate will go on moving with uniform velocity till the transverse wave of material which has stopped moving reaches it. The velocity with which this wave is propagated from the edge is c. For a circular elastic membrane the motion is complicated because the outer part comes to rest before the inner part and begins to return to the equilibrium position while the centre is still moving away from it. With a circular plastic diaphragm, however, this complication will not arise. If the ideal plastic stress-strain relationship is assumed (i.e. no strain till the elastic limit is reached and then constant stress with increasing strain) a circular diaphragm dishes into a circular cone. The angle which the generators of this cone make with the plane of the undistorted diaphragm is $\theta = v/c$, where v is the initial velocity given to the diaphragm by the impulse. A similar simple solution might perhaps apply when the plate is rectangular. If such a solution is possible the central flat area will remain flat and parallel to the original position of the sheet while its area diminishes with time owing to the fact that the sloping sides are propagated into it with velocity c. The final "dished" shape of the rectangle is like the roof of a house whose plan form is rectangular. Contours are shown in Figure 3.

The contours of the dished plate for constant values of $\bar{z}/h_0$ are the same as those shown in Figure 2 for the displacement which results from that distribution of impulse which corresponds with the slowest normal mode or vibration of a membrane (i.e. $\bar{z}/h_0 = \cos \frac{\pi x}{2A} \cos \frac{\pi y}{2B}$). It is not suggested that a real plate would actually be displaced into such a shape, the properties of steel are not those of the ideal plastic sheet contemplated, but it might be interesting to measure some "dished" steel plates to see how near they are to one or other of these shapes.

The ratio $\bar{z}/h_0$ for the shape shown in Figure 3 is

$$\frac{\bar{z}}{h_0} = \frac{1}{3}\left(\frac{2}{4}\right) + \frac{1}{2}\left(\frac{4}{8}\right) = 0.39 \quad \text{or} \quad \frac{h_0}{\bar{z}} = 2.57 \tag{47}$$

PART 2.   *Comparison of box model experiments with theoretical discussion.*

In the box model experiments steel plates approximately 6 feet $\times$ 4 feet were bolted round the edge of a heavy iron box so that they formed one side of the box. The plate was thus air-backed and supported round its edges. The box was lowered to the required depth in water and explosives fired at various distances. In general they were situated on the normal to the plate through its mid point and at distance X from it. The principal measurements made in cases where the plate did not burst were the volume V contained between the dished plate and its original position and the maximum displacement h_0. The mean displacement $\bar{z}$ is evidently (if the plates are 6 feet $\times$ 4 feet)

$$\bar{z} = \frac{V}{4ab} = \frac{\text{Volume in cubic inches}}{4 \times 6 \times 144} = \frac{V}{3456} \text{ inches} \tag{48}$$

The mean displacement or deflection of the plates, z', was also estimated by measurement and tabulated. On comparison with the value obtained using (48) it was found that in all cases $z'/\bar{z} = 1.07$. This discrepancy can be accounted for if the area of the plate is 7% less than assumed. This error can be explained if the plate is really 5 feet 10 inches x 3 feet 10 inches instead of 6 feet x 4 feet. If a 1 inch border is rendered immobile by the arrangements for gripping the edge, this discrepancy is removed. Assuming this to be the case we may now write

$$\bar{z} = \frac{V}{70 \times 46} = \frac{V}{3220} \text{ inches} \tag{48a}$$

Value .....

Value of $h_0/\bar{z}$

It has been pointed out that the ratio of the maximum deflection h_0 of the plate to its mean deflection $\bar{z}$ may be expected to bear some relationship either to the degree of concentration of loading towards the centre of the plate or to the suddenness of its application. The maximum value to be expected with uniform pressure is 2.57(5). The minimum for uniform pressure is 2.06(6). Of the 19 shots analysed in Table 2 (overleaf) only shot 6/1 gives a higher value than this range and then is only 1% above it. Two shots 107 and 109 give values of $h_0/\bar{z}$ below 2.06.

The values of $h_0/\bar{z}$ are given in column 6 of Table 2, and are shown in Figure 5. In this figure they are plotted with X, the distance of the charge from the plate, as ordinate because the concentration of loading near the middle of the plate must increase as X decreases.

If the deflection were due entirely to the impulse supplied by the shockwave during the small fraction of a millisecond when the water is in contact with the plate and acting on it with a positive pressure, the values of $h_0/\bar{z}$ might perhaps be expected to be in the neighbourhood of 2.4. If, however, the plate is bombarded with spray after losing contact with the water or if the duration of the pressure is prolonged by the pressure of a kinetic wave following the pressure pulse $h_0/\bar{z}$ may be expected to approach the value 2.06, appropriate to a uniform static loading, for large values of X.

It will be seen in Figure 5 that as X increases $h_0/\bar{z}$ does in fact decrease towards the value 2.06 and that it increases with decreasing value of X down to X = 3½ feet. For nearer explosions at 1½ and 2 feet $h_0/\bar{z}$ again decreases towards the value corresponding with uniform steady pressure.

Energy used in doing work against plastic stress in the plate.

The distribution of plastic strain energy absorption in the plate does not necessarily bear any definite relationship to the distribution of pressure. On the other hand, if the edges of the plate may be regarded as fixed, all the energy put into the plate by the pressure over its surface is used in doing work against the plastic stresses. The total energy given to the plate by the pressure distribution is therefore equal to W_p x (area of the plate), see equation (39), and the mean energy given to unit volume of the plate is equal to W_p. The accurate value of W_p would only be calculated by taking a complete set of distortion measurements. The value given by (39) is the minimum value consistent with a given value of $\bar{z}$. Using a = 2 feet 11 inches, P = 20 tons/square inch = 3.09 x 10^9 dynes/sq.cm., (39) gives

$$W_p = 5.76 \times 3.09 \times 10^9 \ (\bar{z}/95)^2 = 1.95 \times 10^7 \times \bar{z}^2 \tag{49}$$

where W_p is expressed in ergs/c.c. of steel and $\bar{z}$ is expressed in inches, as measured. Values of $\bar{z}$ are given in column 5, Table 2, and of W_p in column 8.

Comparison with energy given to the plate by the pressure pulse.

The velocity with which the plate is discharged from the surface of the water by the pressure pulse has been calculated(5) on the assumption that a plane compression pulse of form $p = p_0 e^{-nt}$ strikes the plate. Values of p_0 and n are known for certain explosives, notably T.N.T. The motion of the plate rapidly gives rise to a negative pressure and the motion subsequent to the attainment of zero pressure depends on whether water can sustain tension either internally or at the surface of the plate. The velocity of the plate at the moment when zero pressure is attained is(6)

$$\dot{\xi} = \frac{2p_0}{m} \ \epsilon^{-\epsilon/\epsilon-1} \tag{50}$$

where $\epsilon = pc/mn \sin\theta$, c is the velocity of sound in water, $m = t(\rho$ steel$) = 7.81$ is the mass per unit area of the plate, ρ is the density of water, θ is the angle of incidence of the wave on the plate. We may use this first to calculate the velocity with which the central portion of the plate is discharged. Here $\theta = 90°$ so that (50) may be written

$$\dot{\xi} = \frac{2p_0}{\mu} \ e^{-1/\epsilon-1} \tag{51}$$

Measurements with the piezo-electric and other gauges give the following mean values for T.N.T.

$$p_0 = 4.6 \times 10^9 \ (M^{1/3}/r) \ \text{dynes/cm}^2$$

$$n = 7.5 \times 10^4 \ M^{-1/3} \ \text{sec}^{-1}$$

(52)

where M is the mass of the charge in grammes and r is the distance from the charge in centimetres. The value of r at the centre of the plate is X. Values of e and $M^{1/3}/x(?)$ appropriate to the middle of the plate were calculated from (52) and are tabulated in columns 9 and 10 of Table 2. Values of ξ at the moment the pressure on the plate becomes zero (or strictly the hydrostatic pressure at the depth considered) are given in column 11. The kinetic energy of the middle part of the plate is $\frac{1}{2}$ (ρ steel) $\dot{\xi}^2$ per c.c.

When X is larger than a, i.e. than 3 feet, the velocity $\dot{\xi}$ of the plate might be expected to be nearly constant over the surface because $\sin\theta$ is not very different from 1.0 and r is nearly equal to X. At closer distances, however, the outer parts of the plate will receive from the pressure wave less energy than the middle. This effect has been discussed by Fox in the report "The reflection of a spherical wave from an infinite plate" who finds that the formulae (50) and (51) are sufficiently accurate for many purposes if applied to elements of the spherical wave. To calculate the mean value of ξ^2 over the plate using the expressions (50) and (51) at all points of the plate using the appropriate values of r and θ would be extremely laborious. An approximation can be calculated in the form of a factor F by which the value of $\dot{\xi}^2$ at the centre must be reduced to get the mean value over the plate.

Consider a circular plate of radius R_0 and suppose that σ_v is proportional to $1/r = 1/\sqrt{R^2 + x^2}$. It can be shown that it is a fairly good approximation to take the effect of obliquity on $\dot{\xi}$ as reducing it in the ratio $\sin\theta : 1$ below its value for normal incidence. The factor F which expresses the ratio of the mean value of $\dot{\xi}^2$ to the value $\dot{\xi}_0^2$ at the centre of the plate may therefore be taken as

$$F = \frac{\int_0^{R_0} \dot{\xi}^2 \ 2\pi R \ dR}{\pi R_0^2 \dot{\xi}_0^2} = \int_0^{R_0} \sin^2\theta \left\{ \frac{x^2}{x^2 + R^2} \right\} \left(\frac{2RdR}{R_0^2} \right)$$

(53)

Since $\sin\theta = x/\sqrt{x^2 + a^2}$ (53) gives

$$F = x^2/(R^2 + x^2)$$

(53a)

To apply (53a) to the rectangular plate we may take R_0 as the mean of a and b. Thus $R_0 = \bar{a}$ feet. The mean value of the kinetic energy given by the shockwave to the plate may now be taken approximately as

$$T = \frac{1}{2} (\rho \text{ steel}) \ F \dot{\xi}^2$$

(54)

The values of T, using ρ steel = 7.8, F from (53a) and the values of $\dot{\xi}_0$ from column 11, Table 2, are given in column 12. If the whole of the energy of the plate were communicated during the early part of the pulse when the pressure is positive it would be expected that W_p would be equal to T. Values of W_p/T are given in column 13. It will be seen that only in shots 107 and 108 can the energy be attributed mainly to this cause. Shots 107 and 109 give values of W_p/T less than 1 but in these two cases the permanent dishing was very small. It seems certain that elastic recovery would be comparable with the small values of $\bar{Z}$, namely 0.41 inches and 0.50 inches, obtained in these cases. In all other cases the work done by the pressure is considerably greater than T.

At least three possible explanations of this divergence from the theory of the report "The pressure and impulse of submarine explosion waves on plates" can be investigated.

(1)   The duration of the actual pressure on the plate before it falls to zero may be greater than the calculated value because the plate is fixed at the edges so that the rapid cutting off of the pressure by motion of the plate does not happen close to the edge. This effect is likely to extend only a short way inwards from the edge because the duration of the positive pressure is calculated in most of the trials to be less than $\frac{1}{10}$th of a millisecond. In this time sound only travels 5 inches, so that diffraction from the edge would only have time to affect the pressure over a small part of the total area of the plate.

(2) .....

(2)   The pressure due to the pressure wave may rise again after falling to zero, either by cavitation in the water some way away from the surface of the plate (an effect which would allow the water between the cavitation zone and the plate to move forward and exert a pressure on the plate as if is decelerated by the stresses in the plate) or by drops shooting forward towards the plate after it has parted from the water at the instant of zero pressure.

(3)   The long continued pressure due to the expansion of the bubble or pressure effects accompanying its first re-compression.

It is not, in general, possible to distinguish between these alternatives, using only the measurements of the dishing of the plates.   On the other hand (2) may be dismissed as inadequate in cases where the energy used in distorting the plate is considerably greater than the whole energy of the part of the pressure wave which falls on the plate.   For this reason this energy has been calculated.

Total energy of pressure wave falling on the plate.

To calculate the total energy which falls on the plate it is necessary to find an expression for the solid angle ω subtended at the charge position by the plate.   Integration gives the formula

$$\omega \;=\; 4 \tan^{-1} \left[\frac{ab}{x\sqrt{x^2 + a^2 + b^2}} \right] \tag{55}$$

when the charge is situated on the normal through the mid-point of the plate.   The total energy of the pressure wave is

$$E_w \;=\; 4\pi \int_0^\infty (\tfrac{1}{2}\rho\, cu^2 + \tfrac{c}{2}\, \rho u)\, r^2 dt \tag{56}$$

and at some distance from the centre, i.e. when the extent of the disturbance along a radius is small compared with the radius, $p = \rho\, cu$ so that the total energy is

$$E_w \;=\; 4\pi/\rho\, c \int_0^\infty p^2 r^2 dt \tag{57}$$

Assuming that the pressure may be represented by the expression $p = p_0 e^{-nt}$ and that p_0 and n have the values given in (52)

$$E_w \;=\; \frac{2\pi}{\rho\, c} \left\{ \frac{(4.6 \times 10^9)^2}{7.5 \times 10^4} \right\} \quad M \;=\; 1.21 \times 10^{10}\, M \text{ ergs} \tag{58}$$

This may be compared with the amount of kinetic energy which is left behind in the kinetic wave(8) surrounding the bubble, namely

$$w \;=\; 1.85 \times 10^{10}\, M \tag{59}$$

The total energy falling on the plate is, therefore, from (55)

$$\left[E_w \right]_{plate} \;=\; \frac{\omega\, E_w}{4\pi} \;=\; 1.21 \times 10^{10}\; \frac{M}{\pi} \tan^{-1} \left(\frac{ab}{x\sqrt{x^2 + a^2 + b^2}} \right) \tag{60}$$

Using a = 35 inches, b = 23 inches, some values of $\frac{1}{\pi}\tan^{-1}\left[\dfrac{ab}{x\sqrt{x^2 + a^2 + b^2}} \right]$ are given Table 3.

TABLE 3.

x (ft.)	1.5	2	3.5	4	5	6	7	8	14
$\frac{1}{\pi}\tan^{-1}\left(\frac{ab}{x\sqrt{x^2 + a^2 + b^2}} \right)$	0.4303	0.1974	0.1045	0.0620	0.0578	0.0426	0.0348	0.0255	0.0058

For .....

118   — 12 —

For comparison with the amount of energy used up in stretching the plate, the mean energy of the
pressure wave per unit volume of the material of the plate has been calculated. This is $\bar{E}_{wp} =$
$(1/4abt)\,[E_w]_{plate}$ and the values of $\bar{E}_{wp}$ are tabulated in column 14 of Table 2. Comparing these
with the corresponding figures of column 8 for wave energy used in stretching the plate, it is
seen that in 14 of the 19 cases analysed more energy was given to the plate than there was in the
part of the original pressure wave which fell on the plate. The ratio $w_p/\bar{E}_{wp}$ is given in column 15.
Though some error is likely in estimating both w_p and $\bar{E}_{wp}$ it does not seem possible that it could
give rise to values of $w_p/\bar{E}_{wp}$ as much in excess of 1.0 as many of those tabulated in column 15.

Possible errors in w_p.

Errors in w_p might arise from three causes.

(1)   The yield point of the mild steel might be different from 20 tons/square inch. Since
w_p is proportional to the yield stress the figures for $w_p/\bar{E}_{wp}$ could only be reduced by assuming
a yield stress lower than 20 tons/square inch. This is a very unlikely explanation of such
large values as those given in column 15.

(2)   The type of dishing is not quite the same as that assumed in calculating w_p. The values
of $h_o/\bar{t}$ are in almost all cases greater than 2.06, the value corresponding with the distortion
of a soap film by uniform pressure. Since the latter is the distortion corresponding with the
minimum work for a given value of $\bar{t}$, any error due to this cause would lead to an underestimate
of w_p and a more accurate analysis of distortion would therefore give rise to an increase in the
figures in columns 8 and 15.

(3)   The plate might not be held sufficiently firmly at the edges to justify the use of the
fixed edge condition. Errors due to this cause would give rise to a decrease in the figures of
columns 8 and 15. It does not seem likely that any very considerable error could arise from
this cause.

Errors in E_w.

Apart from the question whether some energy might not be drawn by diffraction from the
part of the shockwave outside the plate (and this is likely to be small for reasons already given)
the energy in the shockwave may be less than that given by (58). Errors of this kind, however,
cannot be large because the figures in (58) are derived directly from piezo-gauge measurements
which are remarkably consistent. In this connection it is worth noticing that the energy of the
flow round the bubble is, according to (58) and (59),

$$(1.85 + 1.21) \times 10^{10} = 3.06 \times 10^{10}\ \text{ergs/gm. of T.N.T.}$$

Expressed in calories this is 730 calories/gm. Penney has calculated that about 30% of the
available energy is wasted in irreversible heating of the water near the bubble by the very
intense shockwave.

The energy which T.N.T. is capable of giving up by adiabatic expansion of the products of
detonation is, according to Robertson(9), 926 calories/gm. H.Jones' theoretical calculation makes
it 980 calories/gm. Both these values are greater than 880 calories/gm. which is the figure taken
by Conyers Herring. Taking Jones' value the wastage, according to Penney, is 30% of 980 = 294
calories, so that the total work done by the explosive is 730 + 294 = 1024 calories. This is 4%
greater than Jones' calculations. It will be seen, therefore, that any appreciable increase in
the estimated energy of the pressure wave would be inconsistent with the known thermo-chemical data
of the energy available on combustion of T.N.T.

Comments on results given in Table 2.

It is shown that only a fraction of the energy which is communicated to the plate is due
to the pressure in the pressure wave before this pressure falls to zero. The empirical hypothesis
that the whole of the energy of the wave striking the plate is given up to it would enable a more
accurate prediction of damage in the cases analysed to be made than the assumption that no further
energy is given to the plate after the pressure on it falls to zero. Even this hypothesis, however,
underestimates the energy which the water gives to the plate in most cases. It seems necessary

to .....

to consider the effect of the long continued, low pressure, kinetic wave as well as the pressure
wave.

It is worth noticing that shot 107 was made at depth 3 feet and horizontal distance 14 feet,
so that the positive pressure wave would be cut off 0.5 milliseconds after the explosion. This
would prevent water from the back surface of the cavitation formed behind the plate when the pressure
falls to zero from being discharged and exerting further pressure on the plate, so that in this
case a theory which assumes that no further pressure is exerted after the plate has become detached
from the water may be applicable.

Cases 44, 45 and 59 in which small charges were placed close to the plate are interesting
because the effect of the kinetic wave might be expected to be greater relative to the pressure
wave than in the other cases. The way in which the value of $h_o/\bar{z}$ is much more nearly that which
corresponds with a static pressure than the higher values associated with impulsive pressures is
a striking feature of Figure 4. This seems to be an indication that in this case the main cause
of damage may be the kinetic wave rather than the pressure wave.

References.

(1)   Lode, Zeits. f. Physik. 36, page 913, 1926.

(2)   Taylor and Quinney, "The plastic distortion of metals," Phil. Trans., A, 230.

(3)   See equation (47).

(4)   See equation (37).

(5)   "The pressure and impulse of submarine explosion waves on plates".

(6)   See equation (27) of the above mentioned report.

(7)   X is here expressed in centimetres so that $W^{1/3}/X$ shall be in C.G.S. units.

(8)   Equation (10) of report "Vertical motion of a spherical bubble and the pressure
       surrounding it".

(9)   Sir R. Roberton and W.E. Garner, Proc. Roy. Soc., A, 103, 1923.

TABLE 2.

Shot No.	μ grammes	x ft.	H ft.	z in.	h₀/z	t in.	u_p ×10⁻⁶	ε	μ^(1/3)/x	ξ cm/sec ×10⁻³	t ×10⁻⁶	u_y/z	ξ_mp ×10⁻⁶	u_p/T_mp
1/1	964	5	7	2.35	2.30	.242	80	4.02	0.045	2.58	21	3.8	55	1.51
2/1	960	4	4.6	1.75	2.34	.245	44	3.97	0.061	3.21	28	1.6	74	0.60
4/1	963	5	7	2.65	2.25	.251	50	3.87	0.044	2.55	20	4.5	51	1.76
5/1	972	4	7	2.88	2.44	.250	120	3.90	0.031	3.19	28	4.3	88	1.65
6/1	920	3.5	7	3.11	2.60	.245	140	3.91	0.091	3.61	34	4.1	40	1.59
8/1	501	6	7	1.84	2.22	.238	43	4.10	0.034	2.16	16	3.1	30	1.22
9/1	953	7	7	1.50	2.10	.236	33	4.10	0.040	1.85	12	2.7	81	1.10
11/1	2060	6	7	2.70	2.26	.248	106	5.09	0.370	2.95	29	3.6	99	1.31
12/1	2030	5.5	7	3.62	2.26	.234	190	5.31	0.076	3.22	34	5.6	66	1.92
13/1	2080	7	7	2.32	2.20	.236	78	5.32	0.050	2.54	22	3.5	42	1.16
14/1	2020	8	7	1.43	2.10	.248	30	5.02	0.050	2.18	17	1.8	25	0.62
106	2110	14	6	2.07	1.98	.173	12	7.30	0.000	1.38	7.3	8.5	25	2.8
107	21.0	14	6	0.58	1.83	.173	1.9	7.28	0.030	1.38	7.2	0.7	11	0.20
108	599	8	6	0.64	2.13	.312	5.9	2.66	0.035	1.21	5.2	1.1	9	0.51
109	599	8	6	0.41	2.32	.375	2.5	2.21	0.035	1.13	4.6	0.5	75	0.28
44	420	2	7	2.70	2.16	.248	106	2.97	0.123	4.45	53	3.5	93	1.41
45	923	1.5	7	3.09	2.47	.246	139	2.99	0.164	5.89	34	4.1	55	1.40
49	913	7	7	2.55	2.47	.124	94	7.72	0.046	2.11	15	6.3	55	1.71
59		2	7	3.28	2.24	.357	156	2.67	0.159	5.55	47	3.3	11+	1.37

/ Charge vertically below the box model which was hung horizontally.

Explanation of symbols – Table 2.

μ = mass of charge in grammes.

x = distance from charge (feet).

H = depth of centre of target (feet).

z = mean depth of dish (inches)

h₀ = maximum depth of disk (inches)

t = thickness of plate (inches)

u_p = work zone on material of plate per c.c. in ergs.

ε = ρc/mn (see report "The pressure and impulse of submarine explosion waves on plates"

$\mu^{1/3}/x$ = expressed in C.G.S. units, i.e. t in cm., M in grammes.

ξ = velocity of plate when pressure on plate falls to hydrostatic pressure at the depth H.

$\bar{t}$ = mean energy of plate in ergs/c.c. of steel when velocity is ξ

T_{mp} = mean energy in ergs/c.c. which is given to the plate if the whole energy of the pressure wave falling on the area of the plate is absorbed by it.
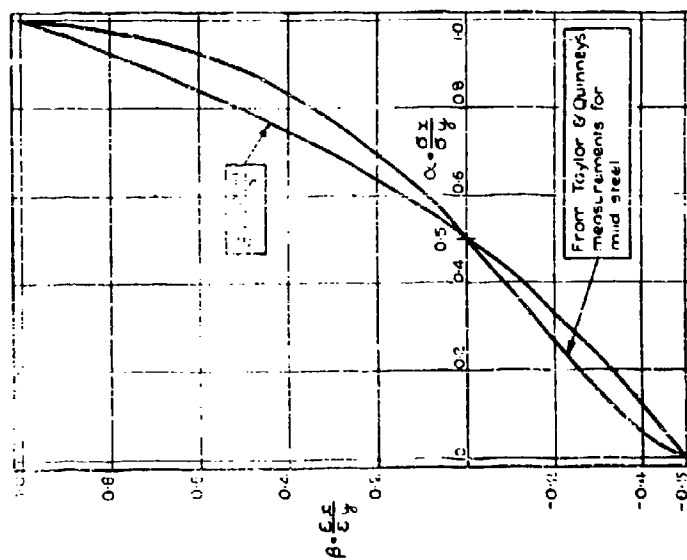
Fig 2
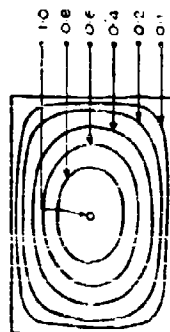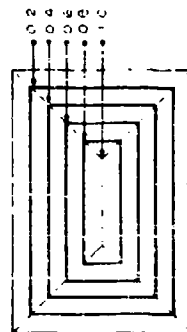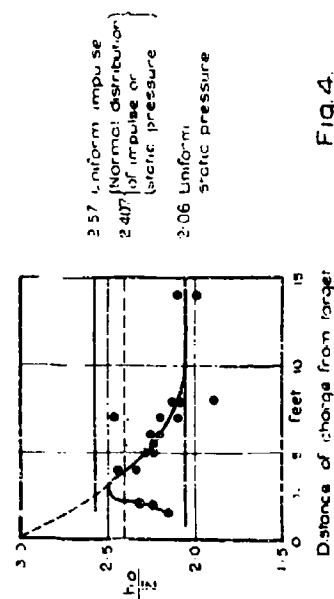
Fig 3

1·0
0·8
0·6
0·4
0·2
0·1

0·2
0·4
0·6
0·8
1·0

2·57 Uniform impulse
2·407 {Normal distribution of impulse or static pressure}
2·06 Uniform static pressure

Fig. 4

3·0

2·5

$\frac{h_0}{h_2}$

2·0

1·5

0   5   10   15
Feet
Distance of charge from target

$\beta = \frac{\varepsilon_x}{\varepsilon_y}$

1·0

0·8

0·6

0·4

0·2

-0·2

-0·4

-0·5

0   0·2   0·4 0·5 0·6   0·8   1·0

$\alpha = \frac{\sigma_x}{\sigma_y}$

From Taylor & Quinneys measurements for mild steel

Fig. 1

NOTE ON AN APPROXIMATE METHOD
FOR THE SOLUTION OF DYNAMICAL PROBLEMS

E. N. Fox
Admiralty Undex Works, Rosyth, Scotland

British Contribution

September 1943

NOTE ON AN APPROXIMATE METHOD FOR THE
SOLUTION OF DYNAMICAL PROBLEMS

E. N. Fox

Admiralty Undex Works

September 1943

*   *   *   *   *   *   *   *

Summary.

An approximate method, analogous to the energy method used in statical problems, is suggested for the solution of dynamical problems, in particular problems of impulsive loading on structures such as a ship's hull composed of plates supported on frames. The method is illustrated by application to the problem of impulsive loading on a plate clamped in an elastically-supported rigid frame.

Proposed method.

For the solution of problems relating to structures or structural units under static loading, a widely used approximate method is that in which the shape of the deflections in the structure are assumed and their magnitudes then determined by making the total energy a minimum. This method derives from the fact that the true solution is that which makes the total energy a minimum for all possible shapes and magnitudes of deflections. A corresponding theorem in dynamics is furnished by Hamilton's principle which for a conservative system may be written

$$\int_{t_1}^{t_2} \delta L \; dt = 0 \tag{1}$$

where, $L = T - V$
T = kinetic energy of system
V = Potential energy of system

and δ denotes any arbitrary small variation of the co-ordinates of particles forming the system provided δ does not affect time or the initial and final co-ordinates at t_1 and t_2.

In general the problem is to determine dependent variables q_1, q_2 ... in terms of independent variables, time t and space co-ordinates x, y, z. The integrand L will usually be expressible as a function of the q's, their partial derivatives with respect to t, x, y, z and of time t.

The proposed approximate method is to assume space distributions for q_1, q_2 ... which satisfy the boundary conditions and to determine the time variations of the q's by use of equation (1). In general L will then become a function of time t, q_1, q_2 ... and the velocities $\dot{q}_1$, $\dot{q}_2$ ... and the solution of equation (1) will be given as in particle dynamics by Lagrange's equations

$$\frac{d}{dt}\left(\frac{\partial L}{\partial \dot{q}}\right) = \frac{\partial L}{\partial q}, \quad q = q_1, q_2 \ldots \tag{2}$$

This system of ordinary differential equations will usually be more amenable to solution than the corresponding system of partial differential equations for the exact solution.

The chief merit of the approximate method lies in its application to problems where the exact equations are either intractable or necessitate very lengthy numerical computation to give a solution which is of practical use.

The value of the approximate solution depends of course on the extent to which the assumed space distributions approximate to those of the exact solution and in this particular connection one

the product of a simply supported elastic beam subjected to bending by an impulsive load. The exact solution for the deflection y in this case can be expressed as an infinite series of the following form

$$y = \Sigma \; \phi_n (t) \; \psi_n (x) \qquad\qquad (3)$$

each term of which is the product of a time function and a space function the latter corresponding to the shape of the beam when vibrating in a normal mode. If we apply the approximate method to this problem by assuming the solution to be the sum of two terms only of the form

$$y = f_r (t) \; \psi_r (x) \; + \; f_s (t) \; \psi_s (x) \qquad\qquad (4)$$

then the application of the method would give

$$\left.\begin{array}{l} f_r (t) = \phi_r (t) \\[2mm] f_s (t) = \phi_s (t) \end{array}\right\} \qquad\qquad (5)$$

Thus in this example the approximate method would give the exact contribution for the two terms assumed but would give no information regarding the remaining terms in the exact solution. The accuracy of the approximate solution thus depends on whether the assumed terms are those giving the major contribution to deflection, stress or whatever quantity it is desired to estimate.

For application to practical problems the above limitation is not so drastic as at first sight might appear since appeal can usually be made to experimental results, such as final deflected shape, when deciding what space distributions to assume. Similar recourse may sometimes be had to known exact solutions for simpler problems, for example the solution for a beam problem may suggest the deflection form for a plate problem.

Possible applications.

The method is of general application to the behaviour under impulsive loading of structures such as a ship's hull composed of plates supported on frameworks. The example given in the Appendix is a simple problem of this type for elastic deflections. An important practical problem to which the method is to be applied is that of a ribbed circular cylinder, simulating the pressure hull of a submarine, under impulsive loading with particular reference to the relative amounts of plastic distortion given to the ribs and the plating under different systems of loading.

A plastic problem to which the method has already been applied is that of the relative amounts of energy absorbed respectively in plate stretching and in pulling-in at edges for the target plates in Box Model trials.

A general problem to which the method might also be usefully applied is that of the effect of bodily motion of a target in reducing damage sustained by the target when subjected to an underwater explosion. In general the method is not expected to be of great applicability to hydrodynamical problems due to the difficulty of assuming the space distribution of velocity, etc. In this particular problem, however, use can possibly be made of the known solutions for bodily motion of a rigid sphere.

In general the method is expected to be more useful for problems in which the deformation is essentially of vibrational type than to problems in which the essential feature is the propagation of waves. Certain features of wave motion can, however, be incorporated when applying the method, for example the deflection of a beam under impulsive loading could be assumed as given by two different space functions in different parts of the beam, the boundary between these being taken as moving along the beam with a certain velocity; this velocity would then appear as one of the dependent variables in the resulting equations. As a tentative suggestion it may also be possible to generalise the method somewhat by leaving in certain arbitrary functions of a wave type and, after substitution in the integrand of equation (3), obtaining the equations by use of the calculus of variations.

In conclusion, it must be emphasized that the method is proposed not as a substitute for exact methods but as a supplementary method which can be applied in cases where either the exact solution is unobtainable or a formal solution is possible but presents excessive computational difficulties.

APPENDIX

To illustrate the application of the proposed approximate method consider the motion under uniformly distributed impulsive pressure of a rectangular plate which is clamped in a rigid frame mounted on elastic supports as depicted sectionally in Figure 1.   The plate and frame are assumed initially at rest and of uniform mass so that all deflections are symmetrical about the centre of the plate.   The deflection of the plate relative to the frame is assumed small enough for the usual theory of elastic bending of thin plates to apply.

The following notation will be used:-

t	=	time
2a	=	length of plate.
2b	=	width of plate.
M	=	total mass of plate.
D	=	flexual rigidity of plate.
ν	=	Poisson's ratio for plate.
x,y,	=	rectangular co-ordinates in plane of plate referred to centre as origin.
v	=	deflection of frame.
v + z =		deflection of point (x, y) of plate.
v + w =		deflection of centre of plate.
M_1	=	total mass of frame.
k_1	=	total stiffness of elastic supports to frame.
F(t)	=	total force at time t due to applied pressure.
T	=	total kinetic energy of system.
V	=	total potential energy of system including applied pressure
L	=	T-V

Using dots to denote differentiation with respect to time the kinetic energy of the frame is

$$\tfrac{1}{2}\, M_1\, \dot{v}^2 \tag{6}$$

while the kinetic energy of the plate is

$$\frac{M}{2\,ab} \int_0^a \int_0^b (\dot{u} + \dot{z})^2 \cdot dx\, dy. \tag{7}$$

The potential energy in the elastic supports to the frame is

$$\tfrac{1}{2}\, k_1\, v^2 \tag{8}$$

while the potential energy of bending in the plate is

$$2D \int_0^a \int_0^b \left[\left(\frac{\partial^2 z}{\partial x^2} + \frac{\partial^2 z}{\partial y^2} \right)^2 + 2(1-\nu) \left\{ \left(\frac{\partial^2 z}{\partial x\, \partial y} \right)^2 - \frac{\partial^2 z}{\partial x^2} \frac{\partial^2 z}{\partial y^2} \right\} \right] dx\, dy \tag{9}$$

where it may be noted that the second term in the integral vanishes on integration in view of the boundary conditions.

Finally the potential energy of the applied pressure is

$$\frac{F(t)}{a\, b} \int_0^a \int_0^b (u + z)\, dx\, dy \tag{10}$$

As the first step in the approximate solution we now assume for the deflection z of the plate relative to the frame,

$$z = w \left\{ 1 - \frac{x^2}{a^2} \right\}^2 \left\{ 1 - \frac{y^2}{b^2} \right\}^2 \tag{11}$$

which satisfies conditions that the plate is clamped round its edge to the frame.

Substituting .....

— 4 —

Substituting from equation (11) in equation (7) we find after integration that the total kinetic energy T is given by

$$T = \tfrac{1}{2} M_1 \dot{u}^2 + \tfrac{1}{2} M \left[\dot{u}^2 + \frac{128}{225} \dot{u}\dot{w} + \left(\frac{128}{315} \right)^2 \dot{w}^2 \right] \tag{12}$$

We find similarly, by substituting from equation (11) in equation (10), that the total potential energy V is given by

$$V = \tfrac{1}{2} k_1 u^2 + \tfrac{1}{2} k w^2 - \left(u + \frac{64w}{225} \right) F(t) \tag{13}$$

where

$$k = \frac{640}{ab} \left[\frac{512}{1575} \left(\frac{a^2}{b^2} + \frac{b^2}{a^2} \right) + \frac{2048}{11025} \right] \tag{14}$$

By definition $L = T - V$ and applying equation (2) by taking $q = u$ and $q = w$ we obtain the equations

$$\left. \begin{array}{l} (M + M_1) \ddot{u} + \dfrac{64}{225} M \ddot{w} + k_1 u = F(t) \\[2mm] \dfrac{64}{225} M \ddot{u} + \left(\dfrac{128}{315} \right)^2 M \ddot{w} + k w = \dfrac{64}{225} F(t) \end{array} \right\} \tag{15}$$

which together with the initial conditions

$$\left. \begin{array}{l} u = \dot{u} = 0 \\[2mm] w = \dot{w} = c \end{array} \right\} \quad t = 0$$

suffice to determine u and w as functions of t.

The solution of equations (15) is elementary and needs no comments, but it is instructive to compare this solution with that for a double system composed of a mass on a spring supported on a second mass on a spring as shown in Figure 2.
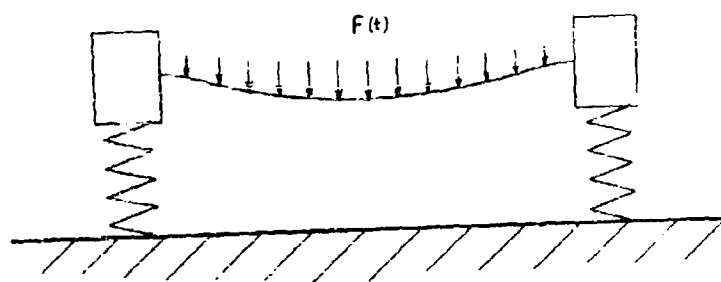
FIGURE 1.
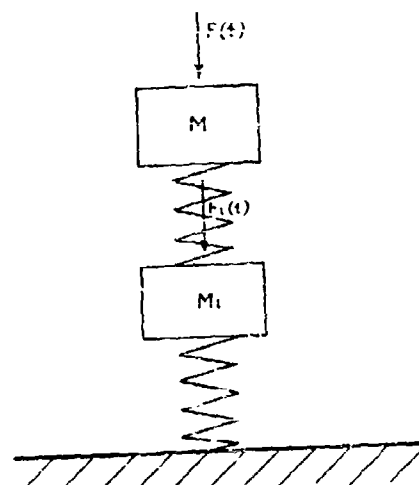
FIGURE 2.

PLASTIC DEFORMATION OF AND ABSORPTION OF ENERGY
BY THIN CIRCULAR PLATES UNDER NORMAL LOADING

A. N. Gleyzal
David W. Taylor Model Basin

American Contribution

May 1944

PLASTIC DEFORMATION OF AND ABSORPTION OF ENERGY
BY THIN CIRCULAR PLATES UNDER NORMAL LOADING

By A.N. Gleyzal

INTRODUCTION

The deformation of thin circular plates by static and by explosive
pressures has been the subject of intensive investigation at the David Taylor
Model Basin (13) (10) (14)* In this connection tests have been made on metal
diaphragms rigidly supported at the rim and subjected to static pressures on
one face. Two quantities derivable from the test results are of particular
interest. These are the deflection of a diaphragm at its center and the en-
ergy required to deform a diaphragm as it distends under static pressure.

It was believed that unification of the test results on the basis
of these two quantities for diaphragms of different dimensions and material
could be accomplished by plotting the quantities in terms of non-dimensional
coordinates involving the dimensions, and perhaps the yield stress or the ul-
timate tensile strength of the material as obtained from tensile tests. Rea-
sonably good predictions of deflection and of energy absorbed for any thin
circular plate under pressure might be possible from curves based on these
selected coordinates, provided the material of the plate had a plastic be-
havior similar to that of the plates used in the tests. Predictions of high
accuracy would be expected for plates of materials similar to those tested.
With these considerations in mind data on diaphragms of different materials
are reported here and analyzed.

THEORETICAL CONSIDERATIONS

Deflection measurements on the circular plates show that, for stat-
ic pressures of sufficient magnitude to cause *plastic flow*, the plates form
very nearly spherical caps. Thus, for a particular pressure, the tension is
nearly constant throughout the plate. Moreover, calculations show that this
tension tends to be constant as the pressure is increased; this constancy may
be ascribed to the balancing of two effects; i.e., the strain-hardening of
the material and the decrease of thickness as the pressure is increased. Thus
under sufficiently large pressures the thin plates act somewhat as membranes
with constant tension.

Suppose pressure is applied, as in Figure 36, to one face of a cir-
cular membrane with tension τ.** It may readily be shown (13) that the pres-
sure p and the center deflection z are related by the equation

---

* Numbers in parenthesis indicate references at the end of this paper.

** In a thin plate the tension at a point is the product of the thickness
and the stress at the point

$$p = \frac{4\tau z}{a^2 + z^2} \qquad [14]$$

where a is the radius of the boundary of the membrane.

A membrane deflected under pressure forms a spherical cap. The volume enclosed by such a cap and the plane of its boundary is

$$V = \frac{1}{2} \pi a^2 z + \frac{1}{6} \pi z^3 \qquad [15]$$

The energy W absorbed by the membrane as its central deflection increases from zero to z is

$$W = \int p\, dV = \int \frac{4\tau z}{a^2 + z^2} \frac{1}{2} \pi (a^2 + z^2)\, dz = \pi \tau z^2 \qquad [16]$$

For a thin plate deformed plastically under pressure the tension τ is given by $\tau = \sigma' h'$, where h' is the thickness and σ' is the stress in the plate, assumed to be of equal magnitude in all directions parallel to the tangent plane of the surface at a given point. As stated in the foregoing, τ remains approximately constant as the pressure is increased. The value of the constant for different plates may be approximated in several ways. In this report it is supposed that the constant is determined by the ultimate tensile strength σ_u of the material, and the initial thickness h of the plate according to the formula

Figure 36 - Diagram Showing Notation

$$\tau = \alpha \sigma_u h \qquad [17]$$

where α is a constant for all diaphragms made of the material.

Equation [17] may be based on a notion of affine* materials (16) introduced later in this report.

We may write, using Equations [14], [16], and [17]

$$p = \frac{4\alpha \sigma_u h z}{a^2 + z^2}$$

---

* Dr Osgood in References (16) and (17) discusses stress-strain curves which are affinely related. The concept is suggested here by the phrase "affine materials" by which is meant materials whose plastic behavior, when referred to a given property of each material, reduces to the same form in all of them. The property chosen in the present case is ultimate strength.

and

$$W - \pi \cup \sigma_u h z^2$$

These formulas relate the pressure applied, the deflection at the center, and the energy absorbed by a thin plate with constant tension $a\sigma_u h$.

They may be rewritten in the following form to secure non-dimensionality

$$\frac{pa}{\sigma_u h} = \alpha \; \frac{4\frac{z}{a}}{1 + \left(\frac{z}{a}\right)^2} \tag{18}$$

$$\frac{W}{\pi a^2 h \sigma_u} = \alpha \; \frac{z^2}{a^2} \tag{19}$$

Equations [18] and [19] suggest the use of $p' = pa/\sigma_u h$ as the non-dimensional coordinate corresponding to pressure, $W' = W/\pi a^2 h \sigma_u$ as the non-dimensional coordinate corresponding to energy, and z/a as the non-dimensional coordinate corresponding to center deflection. We term p' the proportionate pressure and W' the proportionate energy. W is the energy per cubic inch of plate material per unit ultimate stress.

Although Equations [18] and [19] were based on membrane formulas it is profitable again to dissociate mentally the diaphragm from a membrane and treat $W' = W/\pi a^2 h \sigma_u$ and z/a as important intrinsic quantities associated with a thin plate regardless of whether the plate behaves as a membrane or not. If we then plot experimentally determined values of W' against z/a, we obtain an accurate and assumptionless curve showing the behavior of a particular plate. The assumption that this curve will be valid for all thin plates is less exacting than the assumption that the plate is a membrane, and therefore more likely to be valid than Equations [18] and [19].

It is readily shown, moreover, by similitude considerations that when $pa/\sigma_u h$ is plotted against z/a for a thin plate of a given material, the curve for any other thin plate of identical composition should be the same except for secondary variations caused by bending effects. These will vary with relative thickness and their influence is less in the plastic range than in the elastic range. Another effect which may be of importance with thin plates of different thicknesses is surface hardening. Thinner plates would be affected to a greater degree by such hardening.

Of course it is not enough just to use non-dimensional quantities to bring the data from different cases into agreement. Thus Young's modulus of *elasticity* could not be used in place of the *plastic* quantity, ultimate stress. An elastic quantity, even though of the dimensions of stress, would certainly not serve for the desired unification of the data.

The existence of unique pressure-deflection or energy-deflection curves for infinitesimally thin plates may be rigorously based on a concept of affine materials (16) defined as follows: Two materials A and B are said to be affine if for any pair of strain states ϵ and ϵ' the ratio of corresponding stresses is the same for both materials.

This is expressed by

$$\frac{\sigma_A(\epsilon_1, \epsilon_2, \epsilon_3)}{\sigma_A(\epsilon_1', \epsilon_2', \epsilon_3')} = \frac{\sigma_B(\epsilon_1, \epsilon_2, \epsilon_3)}{\sigma_B(\epsilon_1', \epsilon_2', \epsilon_3')}$$

where ϵ_1, ϵ_2, ϵ_3 are the principal strains in the first state ϵ,

ϵ_1', ϵ_2', ϵ_3' are the principal strains in the second state ϵ', and

σ_A and σ_B are the corresponding stresses in materials A and B respectively.

In the case of uniaxial stresses for example, if $L(\epsilon)$ is the load-strain curve for material A, then the load-strain curve for material B must be $\rho L(\epsilon)$, where ρ is a constant.

With the help of this notion of affine materials, a logical basis for the identity of the pressure-deflection and energy-deflection curves may be established for thin circular plates of different radius, thickness, and material. This notion can also serve as a basis for predicting the *plastic* behavior of other types of structures from the action of a model of different material. When models of the same material are used in a static test quite accurate predictions can be expected for plastic action even from models far removed in scale. The choice of a set of plasticity laws is not required in such an analysis.

TEST RESULTS

The quantities of interest to be introduced as observed values are the dimensions of the plate, the ultimate tensile strength of the material, and the central deflection of the plate as a function of the applied pressure. The apparatus for deforming the diaphragms has been described elsewhere (14) (15). The tensile strength was measured for a specimen cut from the same stock used to make the diaphragm. The ultimate stresses are given in Table 6, with other information on the diaphragms.

In Figure 37, for purposes of comparison of different metals, the quantity L/L_u, load divided by ultimate load in a tensile test, is plotted on a basis of strain. Values were obtained from tests on specimens taken from the same stock as the plates.

To unify the pressure-deflection data for the different specimens the non-dimensional quantities derived in the foregoing have been used.

TABLE 6

Data on Circular Plates

Material	Number of Plates Tested	a = Radius inches	h = Thickness inches	σ_u = Ultimate Stress* lb/in^2
Copper	2	2.56	0.016	39,625
Furniture Steel	2	2.56	0.030	49,825
Furniture Steel	2	10.25	0.109	49,825
Medium Steel	2	10.25	0.125 and 0.063	73,500
High Tensile Steel	2	10.25	0.125 and 0.063	87,500
Special Treatment Steel	2	10.25	0.125 and 0.063	125,000

* The ultimate stress is taken as the maximum load divided by the original area.
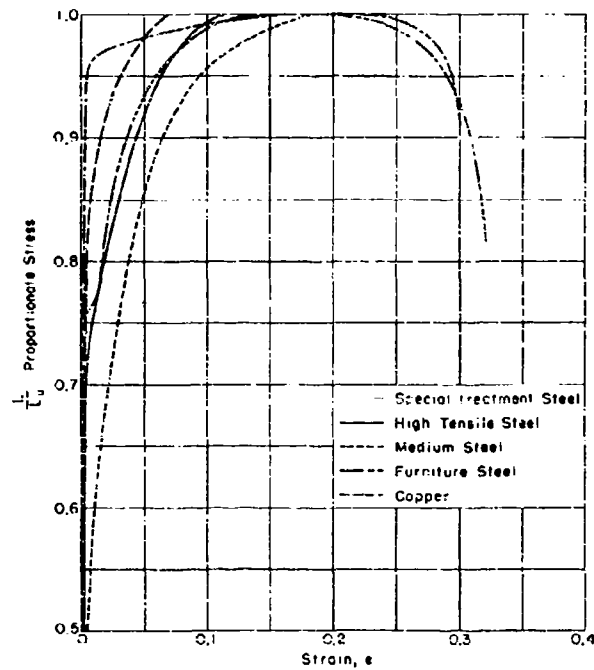
Figure 37 - Stress-Strain Curves for Various Metals
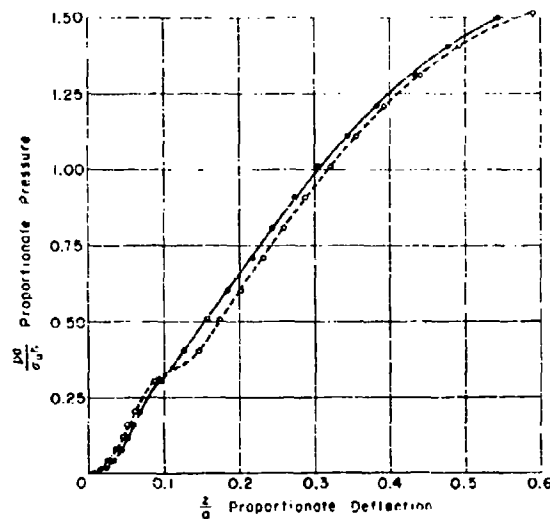
Figure 38 — Pressure-Deflection Curves for Two Copper Plates

a = 2.56 inches   h = 0.016 inch σ_u = 39,625 pounds per square inch

In Figures 38, 39, 40, 41, and 42, p' has been plotted against z/a for different specimens of each of the five materials used. Figure 43 shows, for each of the five metals, average values of p' plotted against z/a. In this and the following figures the plots extend only over the range of the weakest specimens. Thus the highest values for furniture steel are excluded.

The energy W required to deform the diaphragms was estimated from the pressures deforming the diaphragms and the change in the volume V enclosed between the deformed diaphragm and its initial plane. The measurements indicated that the distended diaphragms closely approximated spherical caps in configuration. Therefore, with good accuracy, by Equation [15]

$$V = \frac{1}{2}\pi a^2 z + \frac{1}{6}\pi z^3$$

and

$$dV = \frac{1}{2}\pi(a^2 - z^2)\,dz$$

Accordingly, the change in volume was estimated from the central deflection, and the energy $W = \int p\,dV$ calculated by numerical integration. Figure 44 shows for each of the five metals, average values of W' plotted against z/a. As in Figure 43 the curves fall closely together.
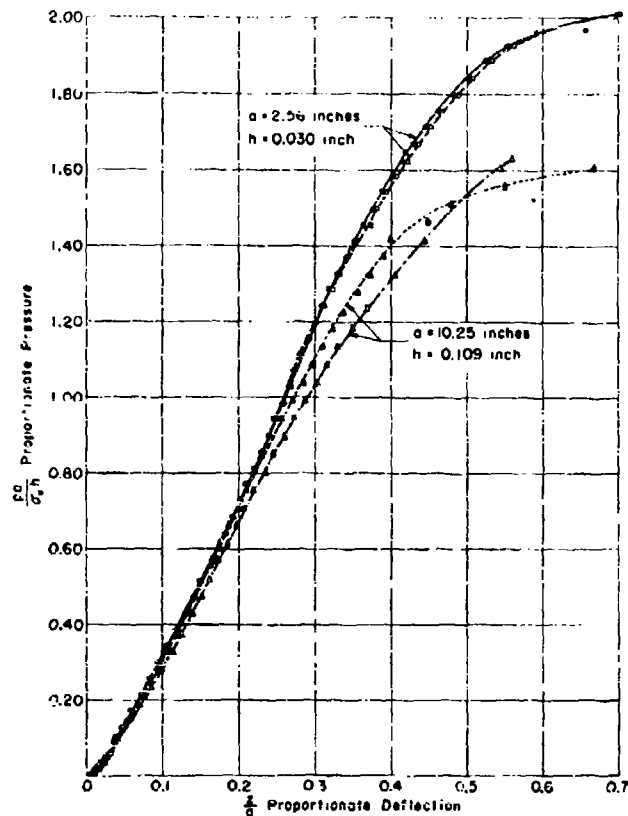
Figure 39 - Pressure-Deflection Curves for Two Sets of Furniture Steel Plates
$\sigma_u = 49,825$ pounds per square inch

Equations [18] and [19] suggest plotting $p' = pa/\sigma_u h$ against $4(z/a) \div [1 + (z/a)^2]$ and $W' = W/\pi a^2 \sigma_u h$ against $(z/a)^2$. This has been done in Figures 45 and 46, respectively, for each of the five metals, using average values. The proportionality factor α may be read from these figures and is seen to be between 0.88 and 1.02 in Figure 45, and between 0.80 and 0.95 in Figure 46.

DISCUSSION OF RESULTS

Inspection of Figures 38, 39, 40, 41, and 42 shows that there is some deviation in the pressure-deflection curves for different plates of a given material. From Figures 38 and 39 it appears that plates, even of the same size and material, exhibit differences. From Figures 39, 41, and 42 it
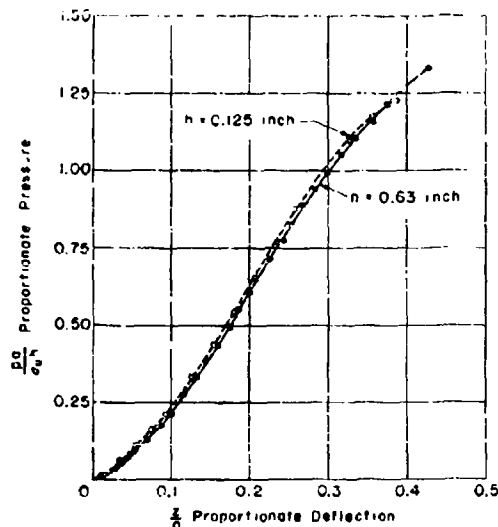
Figure 40 - Pressure-Deflection Curves for Two MS Plates

a = 10.25 inches $\quad$ σ_u = 73,500 pounds per square inch
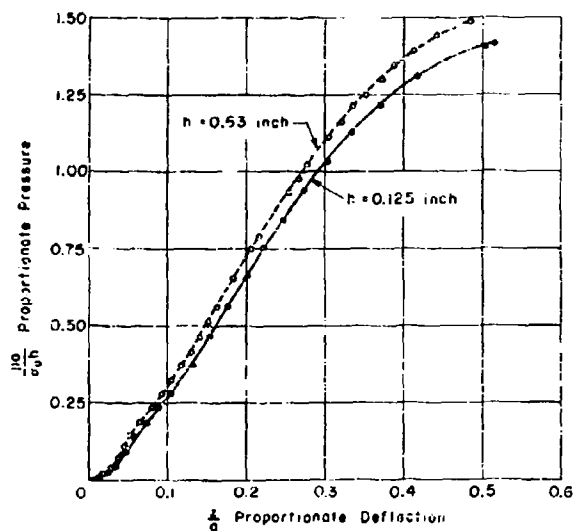
Figure 41 - Pressure-Deflection Curves for Two HTS Plates

a = 10.25 inches $\quad$ σ_u = 87,500 pounds per square inch
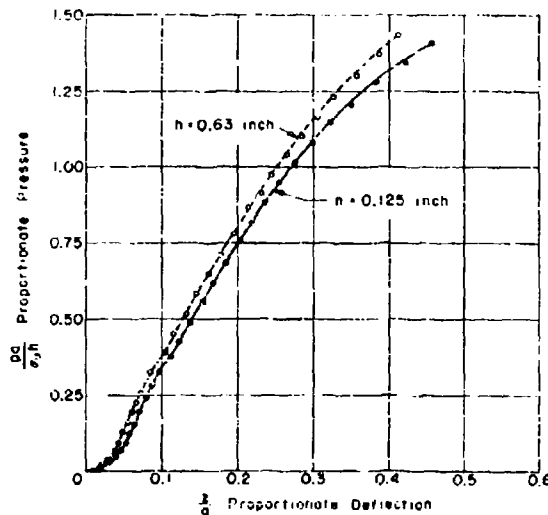
Figure 42 - Pressure-Deflection Curves for Two STS Plates

a = 10.25 inches σ_u = 125,000 pounds per square inch

appears that there is also a possibility of size effects; thinner materials require proportionately more pressure. However, with the exception of the curves for furniture steel in Figure 39, the differences are relatively small; the deviations from the average are generally less than 5 per cent. For a given material, accordingly, it may be concluded that for approximate analyses variations caused by differences in relative thickness or manufacture can frequently be ignored.

The deviations in the composite curves of Figure 43 are larger, 10 per cent or more from the average in some instances. In this case the differences in the *plastic* stress-strain properties of the materials are an important factor. The biaxial stress-strain characteristics of the materials are not directly given, but it is of some interest to examine the curves in the light of the uniaxial stress-strain curves of Figure 37. If proportionate deflection is taken to be related to strain, and proportionate pressure is related to stress, then the sequence from top to bottom of the two sets of curves might be expected to be the same. In this respect Figure 43 partially agrees with Figure 37. Special treatment steel is highest and medium steel lowest over much of the range. Copper starts at high values in Figure 43 but ultimately assumes the lowest values plotted. High tensile and furniture steels occupy an intermediate position in agreement with Figure 37. However,
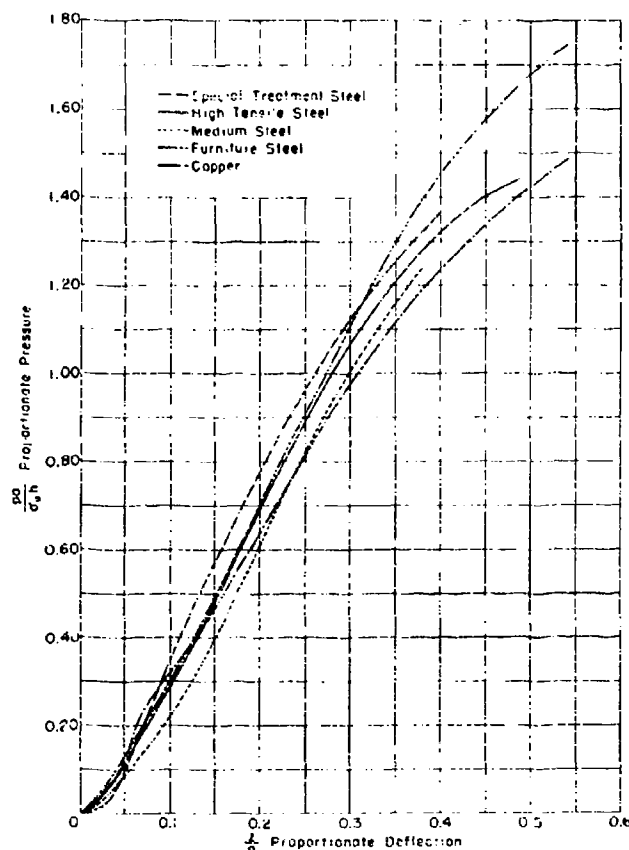
Figure 43 - Pressure-Deflection Curves

Those curves are averages of the curves shown in Figures 38 to 42. This graph may be used to predict
pressure or deflection for any thin circular plate of any of the five materials.

the curve for furniture steel assumes excessively high values as a result of
the data for the plates of diameter 2.56 inches of Figure 39.

A more refined analysis than the membrane analysis considered ear-
lier in this report would attempt to correct for variations in stress-strain
characteristics by estimating the strains at various values of z/a and using
the corresponding stresses in place of σ_u for evaluating the proportionate
pressure.

The energy-deflection curves of Figure 44 exhibit deviations of
somewhat lower magnitudes than do the pressures. Comparison may be made of
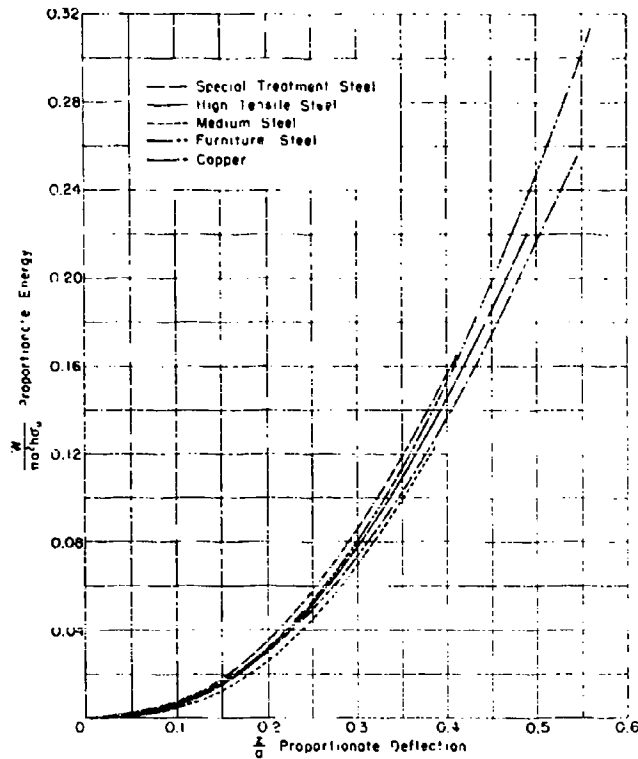
Figure 44 - Energy-Deflection Curves

The curves plotted are averages of the data obtained on the plates tested.

This graph may be used to predict the variation of absorbed energy with deflection for any thin circular plate of any of the five materials.

the energy curves with areas under the tensile curves of Figure 37, which are also proportional to energy absorption with deformation. The correspondence is about as good as that of Figures 37 and 43. It should be noted that the ordinates of Figure 44 do not represent directly total energy absorption. To obtain a quantity proportional to total energy absorption the plotted values must be multiplied by σ_u. If this be done, it will be seen that furniture steel absorbs less energy than special treatment steel but more than medium steel before rupture. The greater ductility of the furniture steel and the fact that energy absorption varies approximately as the square of the deflection are the underlying reasons.

$$\frac{ca}{\sigma_i h} = \alpha \frac{4\frac{z}{a}}{1+\frac{z^2}{a^2}}$$

with $\alpha = 0.96$
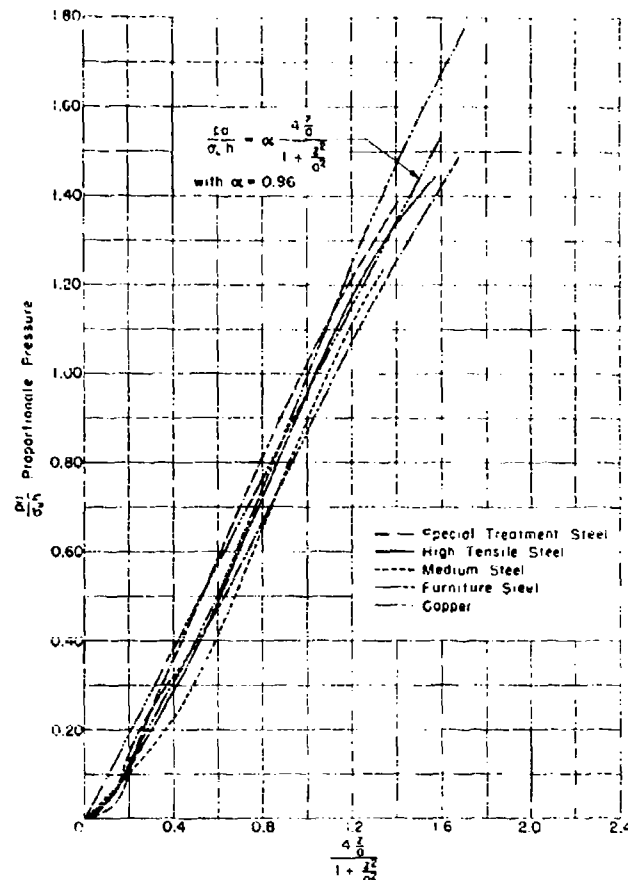
Figure 45 - Pressure-Deflection Curves

The curves plotted are averages of the data obtained on the plates tested. This graph indicates that pressure and deflection can be calculated with rough approximation by Equation [19] when $z/a > 0.2$ and $\alpha = 0.96$.

If the plates tested behaved as ideal membranes, the curves of Figures 45 and 46 would be straight lines. Pronounced deviations are apparent near the origin, where z/a is small. In this region the actual stresses are far below the ultimate values and the condition of approximately constant tension mentioned on page 42 has not been attained. Consequently relatively less pressure is required to produce a given deflection than is required at higher values of z/a. Beyond this initial region the curves do approximate straight lines. If straight lines are fitted to the curves through the origin, the slopes vary between 0.80 and 1.02; those of the energy curves are generally
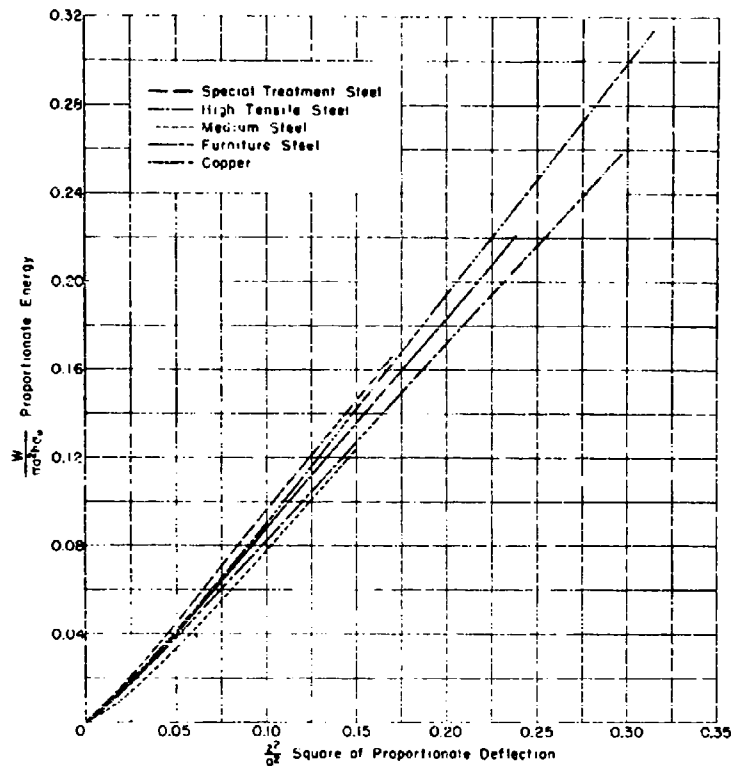
Figure 46 - Energy Plotted against Square of Deflection

The curves plotted are averages of the data obtained on the plates tested. This graph indicates that energy absorbed by a thin circular plate may be approximately computed from Equation [19] when $s/c > 0.2$. The appropriate values of α for the different materials are as follows:

Special Treatment Steel 0.97	High Tensile Steel 0.86
Furniture Steel 0.93	Copper 0.84
Medium Steel 0.81	

less than those of the pressure curves. Since the energy curves represent integrations of the pressure curves, the lower values of α in Figure 46 can be ascribed to the relatively low values of pressure in Figure 45.

CONCLUSIONS

Thin metal plates deformed by static pressure approximate membranes in their behavior. From a knowledge of the ultimate strength of the material and the dimensions of a plate, estimates of the deflection and of the energy absorbed in the plastic range can be made on the basis of membrane theory if the tension is taken to be $\alpha\sigma_u h$, where α can vary between about 0.8 and 1.02.

At values of deflection below about 0.2a the energy values thus estimated are definitely too large. More exact graphical determinations can be made if the pressure-deflection curve for a single thin circular plate of the material is known as in Figures 43 and 44.

REFERENCES

(10) "Early and Ultimate Damage due to Underwater Explosions against 10-inch Diaphragms," by G.E. Hudson, Ph.D., TMB CONFIDENTIAL Report 509, August 1943.

(13) "Protection against Underwater Explosion, Plastic Deformation of a Circular Plate," by A.N. Gleyzal, Ph.D., TMB Report 490, September 1942.

(14) "Plastic Strain and Deflection Tests on Clamped Circular Steel Plates 20 Inches in Diameter," by A.N. Gleyzal, Ph.D., TMB Report R-142, in preparation.

(15) "Normal Pressure Tests of Circular Plates with Clamped Edges," by Albert E. McPherson, Walter Ramberg, and Samuel Levy, NACA Technical Notes 848, June 1942.

(16) "Description of Stress-Strain Curves by Three Parameters," by Walter Ramberg and William R. Osgood, NACA Technical Notes 902, July 1943.

(17) "A Rational Definition of Yield Strength," by William R. Osgood, Journal of Applied Mechanics, Vol. 7, Number 2, June 1940.

A METHOD FOR DETERMINING THE ENERGY ABSORPTION
OF THIN STEEL DIAPHRAGMS UNDER HYDROSTATIC PRESSURE

M. A. Greenfield
David W. Taylor Model Basin

American Contribution

May 1944

A METHOD FOR DETERMINING THE ENERGY ABSORPTION
OF THIN STEEL DIAPHRAGMS UNDER HYDROSTATIC PRESSURE

By M.A. Greenfield

In Part I of the Progress Report (1)* for TMB Research Project E139, dated February 1944, it was stated that two independent methods are used at the David Taylor Model Basin to calculate the energy absorbed by a thin steel diaphragm which has been deformed into a plastic state. The first method expresses the energy in terms of the forces acting on the diaphragm. If p is the pressure on the diaphragm and v is the volume bounded by the initial and final positions of the diaphragm, then the work done on the diaphragm is $\int p\,dv$.

The second method expresses the energy in terms of the physical properties of the steel and the measured strains corresponding to a given deformation.

Each method can be used either for statically or dynamically deformed diaphragms.

The present report describes the second method in some detail. It also gives a comparison of both methods as applied to a diaphragm which was deformed by hydrostatic pressure. This diaphragm was 1/8 inch thick and had a diameter of 20 inches.

Since the diaphragm is deformed plastically the following laws (2) of plastic flow will be adopted in making the analysis.

    a. The directions of the principal extensions coincide with those of the principal stresses at all times.

    b. The volume of the material remains constant.

    c. The principal shearing stresses remain proportional to the corresponding principal shearing strains.

Let σ_1, σ_2, σ_3 be the true stresses and ϵ_1, ϵ_2, ϵ_3 be the natural strains. The natural strain is related to the conventional strain $\bar{\epsilon}$ by the relation

$$\epsilon = \ln(1 + \bar{\epsilon}) \tag{1}$$

Rule (b) may be expressed as

$$\epsilon_1 + \epsilon_2 + \epsilon_3 = 0 \tag{2}$$

and Rule (c) as

$$\frac{\sigma_1 - \sigma_2}{\epsilon_1 - \epsilon_2} = \frac{\sigma_2 - \sigma_3}{\epsilon_2 - \epsilon_3} \tag{3}$$

---

* Numbers in parenthesis indicate references at the end of this paper.

Consider a small element of the stressed body in the shape of a cube oriented so that the faces are perpendicular to the principal stresses. Consider the plane whose normal makes equal angles with the directions of the principal stresses. The normal stresses on this plane do no work because of the constancy of volume. The shearing stress and the corresponding shearing strain are called the octahedral shearing stress and octahedral shearing strain. They are designated hereafter by the symbols τ and γ respectively and are related to the principal stresses and strains as follows:

$$\tau = \frac{1}{3}\sqrt{(\sigma_1 - \sigma_2)^2 + (\sigma_2 - \sigma_3)^2 + (\sigma_3 - \sigma_1)^2} \qquad [4]$$

$$\gamma = \frac{2}{3}\sqrt{(\epsilon_1 - \epsilon_2)^2 + (\epsilon_2 - \epsilon_3)^2 + (\epsilon_3 - \epsilon_1)^2} \qquad [5]$$

If Equations [2] and [5] are combined to eliminate ϵ_3 then

$$\gamma = \frac{2}{3}\sqrt{6}\sqrt{\epsilon_1^2 + \epsilon_1\epsilon_2 + \epsilon_2^2} \qquad [6]$$

There is some experimental evidence (3) (4) that in ductile materials the quantity τ, thought of as a single variable, can be used to define the state of stress in the material. It is considered also that the quantity γ can be used to define the state of strain.

The fundamental assumption (3) is now made that

$$\tau = \tau(\gamma) \qquad [7]$$

for the case of static loading. Thus τ is completely specified for a given value of γ. It is assumed that the stress-strain relation, regardless of the particular type of loading that produced it, will yield points that lie on this curve, which describes a physical property of the material. This means in particular that simple tensile tests and complicated tests producing biaxial and triaxial stress conditions can be described in terms of a single generalized stress-strain curve.

Some evidence for this assumption is found in unpublished work done by Dr. A. Nadai at the Westinghouse Research Laboratories in Pittsburgh. Biaxial tests were performed on very carefully machined, hollow, tubular test specimens of annealed medium steel in which axial loading and internal pressure were used. The ratio of tangential to longitudinal stress was maintained as a constant for a given specimen but a different value of this ratio was taken for each of the ten specimens tested. The measured stresses and strains were used to compute the octahedral shearing stresses and strains. These values were then all plotted with τ as the ordinate and γ as the abscissa, as shown in Figure 1. All the points fall remarkably well on a single curve. For a given value of γ the maximum deviation of τ is about 7 per cent. Generally the deviation is considerably less.
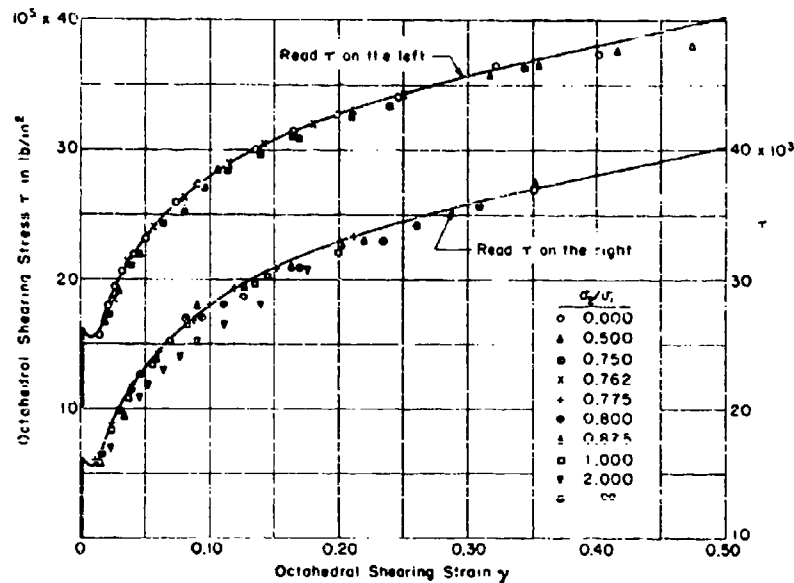
Figure 1 - Octahedral Shearing Stress-Strain Curve Based on Combined-Stress Tests of Ten Hollow Tubular Specimens

σ_2/σ_1 is the ratio of the tangential to longitudinal stress and is a constant during the testing of a given specimen.

The two curves are identical and are separated to avoid overcrowding the plotted points.

Since all of these data, including those for a tube under pure tension, fall on this curve, it follows that the curve can be established from a simple tensile test of a conventional test specimen. Once the τ-γ curve has been established from such a coupon test, calculations can be made of the energy absorption for some other type of stress distribution, as for example that resulting from the loading of a steel diaphragm under hydrostatic pressure. A description of such energy calculations in terms of the octahedral variables is now given.

For the general case of triaxial stress the energy ΔE absorbed per unit volume (5) is given in terms of the true principal stresses and the natural principal strains as follows:

$$\Delta E = \int (\sigma_1 \, d\epsilon_1 + \sigma_2 \, d\epsilon_2 + \sigma_3 \, d\epsilon_3) \qquad [8]$$

Rules (b) and (c) for plastic flow state that

$$\epsilon_1 + \epsilon_2 + \epsilon_3 = 0 \qquad [2]$$

4

$$\frac{\sigma_1 - \sigma_2}{\epsilon_1 - \epsilon_2} = \frac{\sigma_2 - \sigma_3}{\epsilon_2 - \epsilon_3} \qquad [3]$$

By combining Equations [2], [3], [4], [5], and [8], it has been shown by a number of writers (5) that ΔE may be expressed entirely in terms of τ and γ as follows:

$$\Delta E = \frac{3}{2} \int \tau \, d\gamma \qquad [9]$$

If a τ-γ curve is available from any source, as for example from a simple tensile test, the curve relating ΔE and γ can be obtained by mechanical integration. It is then relatively easy to calculate the energy absorbed during the deformation of a structure fabricated from the same material provided the distribution of the principal strains is known. The distribution of the octahedral shearing strains can then be obtained by using Equation [5].

The method will be illustrated in detail for the case of a circular diaphragm of medium steel clamped rigidly along its rim and deformed by hydrostatic pressure. A τ-γ curve is obtained from a tensile test coupon, and a ΔE-γ curve is obtained by mechanical integration. The distribution of the octahedral shearing strains in the deformed diaphragm is represented by the function $\gamma(r_0)$, where r_0 is the distance of a particle from the center of the diaphragm before distortion. The corresponding value of ΔE is then obtained from the ΔE-γ curve. The total energy absorbed by the diaphragm is given by

$$E = \int_0^a \Delta E \times h_0 \times 2\pi r_0 \, dr_0 \qquad [10]$$

where a is the radius and h_0 the original thickness of the undeformed diaphragm.

This method will now be applied to an actual case.

A medium-steel circular diaphragm was deformed hydrostatically by applying pressures in increments up to 1125 pounds per square inch. The diaphragm had a radius of 10 inches and a thickness of 0.125 inch. The profile of the deformed diaphragm was measured at each successive pressure. The energy required to produce the deformation corresponding to the maximum pressure was obtained by evaluating

$$\int p \, dv$$

This energy was found to be 385,000 inch-pounds.

A 1-inch grid was drawn on the diaphragm in its original condition. The final grid measurements are as represented in Figure 2.
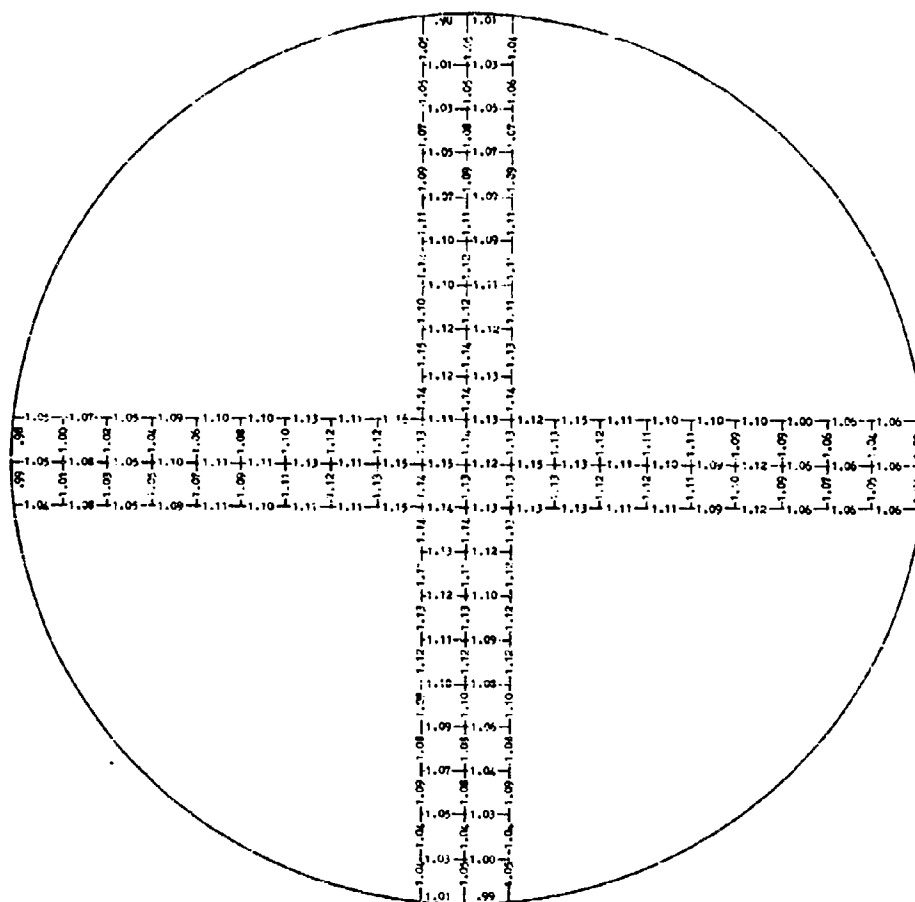
Figure 2 - Drawing Representing Diaphragm in Original Condition
with Final Strain Grid Measurements Superimposed

Several quantities are required for the calculation. The arc length
s is measured along the deformed diaphragm from the center as shown in Figure
3. Values of s are computed from the
grid data shown in Figure 2; r_0 is the
distance from the center of a particle
F in the undistorted form. Then ϵ_r,
the conventional radial strain, is

$$\epsilon_r = \frac{d}{dr_0}(s - r_0)$$
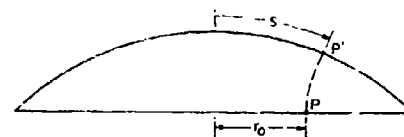
Figure 3 - Schematic Cross Section
of Deformed Diaphragm

6
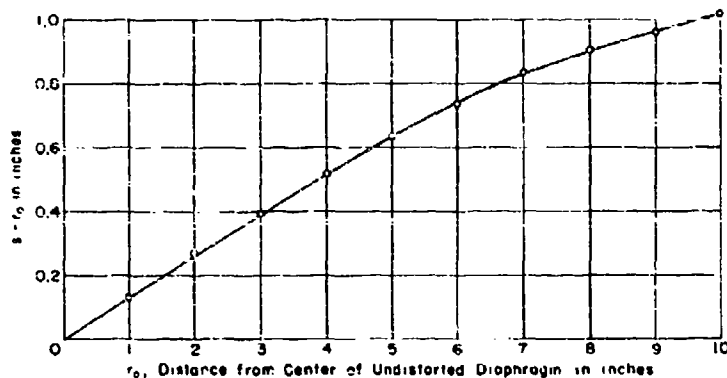
Figure 4 - Integrated Radial Strain Corresponding to a Station
on the Undistorted Diaphragm

The slope of this curve is the radial strain ϵ_r.

and ϵ_h, the conventional thickness strain, is

$$\epsilon_h = \frac{h - h_0}{h_0} \quad \text{or} \quad 1 + \epsilon_h = \frac{h}{h_0}$$

Since the density of the material remains constant, the convention-
al tangential strain ϵ_θ can be found from the equation expressing that fact

$$(1 + \epsilon_r)(1 + \epsilon_\theta)(1 + \epsilon_h) = 1 \tag{11}$$

or

$$\epsilon_\theta = \frac{h_0}{h} \; \frac{1}{1 + \epsilon_r} - 1 \tag{12}$$

The values of these strains were found from the experimental data
as follows. A graph was drawn with $(s - r_0)$ as ordinate and r_0 as abscissa
as shown in Figure 4. The radial strain ϵ_r is obtained by measuring the
slope of the curve graphically.

Since the volume remains constant,

$$h_0 \times 1 \times 1 = h \times l_i \times l_j$$

where l_i and l_j are the final lengths of the sides of the grid and h_0 and h
are the original and final thicknesses of the material within the grid.
Then

$$\frac{h_0}{h} = l_i \times l_j$$

Thus h_0/h is calculated directly from the grid data given in Figure
2. ϵ_θ can then be calculated with the use of Equation [12].

In Figure 5 ϵ_r and ϵ_θ are plotted as ordinates and r_0 is plotted as
abscissa. It is interesting to note that the tangential strain ϵ_θ is very
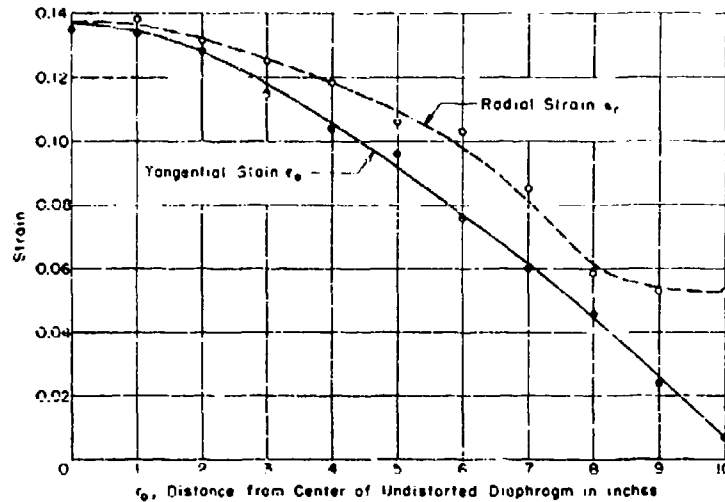
Figure 5 - Observed Radial and Tangential Strain on a
Circular Diaphragm under Hydrostatic Pressure

small at the clamped boundary of the diaphragm. It should be zero if the boundary is perfectly clamped.

The natural strains are now computed from Equation [1] as $\epsilon_1 = \ln(1 + \epsilon_r)$ and $\epsilon_2 = \ln(1 + \epsilon_\theta)$. The octahedral shearing strain is finally obtained from the relation

$$\gamma = \frac{2}{3}\sqrt{6}\ \sqrt{\epsilon_1^2 + \epsilon_1\epsilon_2 + \epsilon_2^2} \qquad [6]$$

A tabulation of r_0, $(s - r_0)$, ϵ_r, ϵ_θ, h_0/h and γ is given in Table 1. The values of ϵ_r and ϵ_θ were taken from the faired curve of Figure 5.

A specimen cut from the same plate as the diaphragm was subjected to a standard tensile test. A true stress-strain curve was obtained for this coupon. The $\tau - \gamma$ curve of Figure 6 is based on this true stress-strain curve. Figure 7 is the integrated curve with $\frac{3}{4}\int \tau\,d\gamma$ plotted as the ordinate and γ as the abscissa. The ordinate gives the energy absorbed per unit volume corresponding to a given value of γ.

The area of the diaphragm before distortion is divided into eleven annular regions bounded by concentric circles whose diameters are 0 inch, 1 inch, 3 inches, and so on. The values of r_0 at the points midway between two consecutive circles are 1/4 inch, 1 inch, 2 inches, ... It is assumed that the values of γ at the stations $r_0 = 1/4$ inch, 1 inch, 2 inches, ... are the average for the corresponding annular rings.

TABLE 1

Observed Changes in the Dimensions of the Diaphragm and the Calculated Strains

r_0 inches	$(s - r_0)$ inches	$\frac{\lambda_0}{\lambda}$	ϵ_r	ϵ_θ	γ
0	0	1.288	0.138	0.138	0.363
1	0.135	1.291	0.136	0.134	0.359
2	0.280	1.276	0.133	0.128	0.347
3	0.402	1.254	0.127	0.1175	0.327
4	0.525	1.236	0.119	0.105	0.300
5	0.638	1.212	0.110	0.0915	0.272
6	0.740	1.187	0.097	0.077	0.235
7	0.838	1.150	0.0815	0.062	0.196
8	0.905	1.108	0.062	0.046	0.149
9	0.962	1.078	0.0545	0.0275	0.115
10	1.015	1.062	0.0535	0.006	0.0895
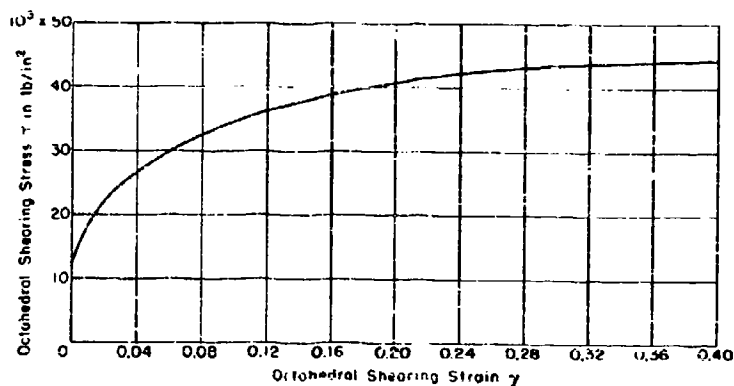
Figure 6 - Octahedral Shearing Stress-Strain Curve
Based on a Tensile Test of a Standard Specimen

The volume of material in each of these eleven regions and the corresponding values of γ and $\frac{3}{2}\int \tau d\gamma$, the energy per unit volume, are listed in Table 2, together with the product of volume and energy per unit volume. The summation of this product gives the total energy absorbed by the diaphragm. This summation yields a value of 392,000 inch-pounds as compared to 385,000 inch-pounds as calculated from the observed pressures and measured changes in volume.

TABLE 2

Calculated Energies Absorbed Per Unit Volume

The calculated total energy (sum of Column 4) is compared with the measured
total energy absorbed by the diaphragm, Column 5.

1	2	3	4	5
Volume inches^3	$\frac{3}{2}\int \tau\, d\gamma$ inch-pounds/in^3	γ	Col. 2 x Col. 1 inch-pounds	$\int p\, dv$ inch-pounds
0.0982	20,000	0.363	1,960	
1.080	19,800	0.359	21,400	
1.376	19,020	0.347	24,300	
2.356	17,700	0.327	41,700	
3.142	15,940	0.300	50,100	
3.927	14,140	0.272	55,500	
4.712	11,820	0.235	55,700	
5.498	9,450	0.196	51,600	
6.283	6,690	0.149	42,000	
7.069	4,840	0.115	34,200	
3.829	3,560	0.0895	13,600	
			392,000	385,000
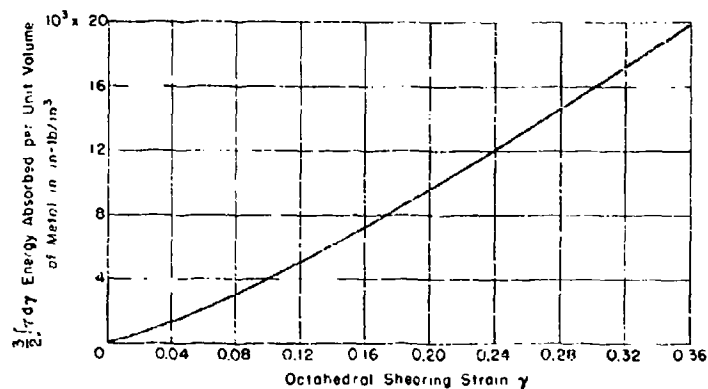
Figure 7 - Energies Absorbed per Unit Volume of Metal, Corresponding to
Values of the Octahedral Shearing Strain

Thus it will be observed that measurement of the final strains on the diaphragm, coupled with the use of the octahedral shearing stress-strain relations as obtained from a simple tensile test on a conventional coupon, suffices to permit a calculation of the energy absorbed by the diaphragm. The good agreement, in this case within 2 per cent, is further verification of the utility of the octahedral shearing stress-strain relations as applied to energy calculations.

REFERENCES

(1) "Progress Report on Underwater Explosion Research - Bureau of Ships Symbol E139 - Part 1 - A Method for Determining Energy Absorption of Steel at High Rates of Loading," by M.A. Greenfield, TMB ████████ Report R-202, February 1944.

(2) "Plasticity," by A. Nadai, McGraw-Hill Book Company, 1931, p. 75.

(3) "Plastic Behaviour of Metals in the Strain-Hardening Range, Part I," by A. Nadai, Journal of Applied Physics, Vol. 8, 1937, p. 205.

(4) "Increase of Stress with Permanent Strain and Stress-Strain Relations in the Plastic State for Copper Under Combined Stresses," by E.A. Davis, Journal of Applied Mechanics, 1943, p. A-187.

(5) "On the Determination of the Energy of Plastic Deformation Absorbed in a Diaphragm," by G.H. Handelman and W. Prager, Applied Mathematics Group, Brown University, for the Applied Mathematics Panel of the National Defense Research Committee, July 1943, pp. 3 and 9.

DIMENSIONAL ANALYSIS: AN APPROACH FROM
TRANSFORMATION THEORY AND A CRITERION
FOR SCALING MODEL EXPERIMENTS

J. C. Decius
Underwater Explosives Research Laboratory
Woods Hole Oceanographic Institution

American Contribution

May 1948

DIMENSIONAL ANALYSIS: AN APPROACH FROM TRANSFORMATION THEORY AND A CRITERION FOR SCALING MODEL EXPERIMENTS.[1]

BY

J. C. DECIUS.[2]

1. THE INVARIANTS OF CONTINUOUS TRANSFORMATION GROUPS.

In a recent article in this journal, Langhaar (1)[3] has drawn attention to a method of dimensional analysis in which the kinds of physical quantities are explicitly given a vector representation. The crucial theorem of this subject was proved by Langhaar in terms of theorems on homogeneous functions.

The author of the present paper has formalized the subject matter of dimensional analysis from a slightly different mathematical point of view, in which, however, as is natural, the material receives a practically identical representation. Because of the relationship of the following method to a very general method of discussing problems in mathematical physics, it seems worth-while to set it forth here. In addition, since the development is aimed at the treatment of scaling laws for model experiments, a new criterion is given for the possibility of satisfying the scaling laws when certain restrictions are imposed upon the variables.

A fruitful approach to the problems of dimensional analysis may be made by regarding any physical equation as the expression of an invariant under the transformations of some group. Frequently the knowledge of some form of spatial symmetry, the requirement of invariance under permutation of indistinguishable particles, or the necessity of special invariant properties which must obtain under transformations simultaneously involving temporal and spatial coordinates has been used to simplify or actually to advance the mathematical description of the physical world. Although the results of the following application of invariant theory are all rather well known, the method itself is rather elucidating, particularly with regard to the derivation of the laws of similitude which govern the scaling of model experiments.

It will be shown below that all of the results of dimensional analysis follow from the single postulate that all physical relations must be expressible in a form which does not depend upon the "magnitude" of the various physical units of measurement requisite for the description of a given physical situation.

---

[3] The boldface numbers in parentheses refer to the list of references appended to this paper.

Such changes of unit magnitude form the representation of a group
of continuous transformations. A group of continuous transformations
may be represented by the equations:

$$\bar{x}^i = \quad x^2, \cdots x^n; \quad \lambda^1, \lambda^2, \cdots \lambda^m), \qquad (1.1)$$
$$i \quad 1 \ldots \cdots n$$

in which the barred quantities are the new values of the variables, which
were originally $x^1, x^2, \cdots x^n$, after the transformation induced by the set
of continuously variable, independent parameters, $\lambda^j (j = 1, 2, \cdots m)$.
The usual postulates for a group require that the λ^j can assume such
values as will:

1. Induce the identity transformation

$$x^i = \xi^i(x^1 \cdots x^n; \quad \lambda_0{}^1 \cdots \lambda_0{}^m).$$

2. Induce the resultant of two or more successive transformations in
one step, that is, if

$$\bar{x}^i = \xi^i(x^1 \cdots x^n; \quad \lambda_1{}^i \cdots \lambda_1{}^m),$$
$$\bar{\bar{x}}^i = \xi^i(\bar{x}^1 \cdots \bar{x}^n; \quad \lambda_2{}^1 \cdots \lambda_2{}^m),$$

then

$$\bar{\bar{x}}^i = \xi^i(x^1 \cdots x^n; \quad \lambda_{12}{}^1 \cdots \lambda_{12}{}^m).$$

3. Induce a transformation "inverse" to every given transformation,
that is, if

$$\bar{x}^i = \xi^i(x^1 \cdots x^n; \quad \lambda_1{}^1 \cdots \lambda_1{}^m),$$
$$x^i = \xi^i(\bar{x}^1 \cdots \bar{x}^n; \quad \lambda_{-1}{}^1 \cdots \lambda_{-1}{}^m).$$

It may then be shown that the equations of transformation (1.1)
determine a set of linear partial differential operators

$$U_j = \left(\frac{\partial \xi^i}{\partial \lambda^j}\right)_0 \frac{\partial}{\partial x^i} \qquad (1.2)^4$$

which represent the independent infinitesimal transformations of the
group (the subscript zero for $\partial \xi^i / \partial \lambda^j$ implies that the derivative is to be
evaluated for those values of the parameters, λ^j, which induce the
identity transformation; without loss of generality these values may
henceforth be assumed to be zero). The most general infinitesimal
transformation is represented by

$$U = \alpha^j U_j \qquad (1.3)$$

in which the α^j are arbitrary constants; any finite transformation is

---

[4] The summation convention of tensor notation is used throughout. Thus $\left(\frac{\partial \xi^i}{\partial \lambda^j}\right)_0 \frac{\partial}{\partial x^i}$
implies $\sum_{i=1}^{n} \left(\frac{\partial \xi^i}{\partial \lambda^j}\right)_0 \frac{\partial}{\partial x^i}$; this is true only if the index appears in one place as a superscript, in
another place as a subscript.

generated by an integration of the differential operation signified by (1.3).

The important consequence for the present purposes is that if any function of the variables x^i, say

$$F(x^1, \cdots x^n) = 0, \tag{1.4}$$

is known to be invariant under the group represented by (1.1), then it is always possible to express (1.4) in terms of a complete set of fundamental invariants $y^1, y^2, \cdots y^{n-r}$, which are determined by

$$Uy = 0 \tag{1.5}$$

as functions of the x^i. Thus

$$F(x^1, \cdots x^n) = \Phi(y^1, \cdots y^{n-r}) = 0 \tag{1.6}$$

and the number of independent variables has been reduced by r, which is equal to the rank of the matrix $\left\| \left(\dfrac{\partial \xi^i}{\partial \lambda^j} \right)_0 \right\|$.

2. DETERMINATION OF THE INVARIANTS OF A GENERAL PHYSICAL EQUATION UNDER TRANSFORMATIONS OF THE UNITS.

The nature of the number, x^i, resulting from a physical measurement of the jth kind of physical quantity is such that it is determined only within a transformation of the type:

$$\bar{x}^j = \exp[\lambda^j]x^j, \tag{2.1}[a]$$
$$-\infty < \lambda^j < +\infty.$$

If it is desired to deduce the possible kinds of functions of the *magnitudes* of a basic set of physical quantities, which give the *magnitude* of a resultant physical quantity derivable from the basic ones, it is possible to apply the principles of Section 1 in the following manner. The resultant magnitude itself must obey a transformation law of the same form as (2.1)

$$\bar{x} = \exp[f(\lambda^j)]x \tag{2.2}$$

in which the value of f may be taken as zero when $\lambda^j = 0$, all j. Then Eq. 1.3 requires that the relation between x and x^j be expressible in terms of a function y determined by

$$\alpha^k \left[\delta_k{}^j x^k \frac{\partial y}{\partial x^j} + \left(\frac{\partial f}{\partial \lambda^k} \right)_0 x \frac{\partial y}{\partial x} \right] = 0. \tag{2.3}$$

The α^k being arbitrary constants, (2.3) is equivalent to the m relations

$$\frac{\partial y}{\partial \ln x^k} = - \left(\frac{\partial f}{\partial \lambda^k} \right)_0 \frac{\partial y}{\partial \ln x}, \tag{2.4}$$

$$k = 1, 2, \cdots m.$$

---

[a] It is clear that the range of the λ^j indicated will contain values satisfying all the group postulates of Section 1.

An acceptable solution of this system is

$$y = \prod_{k=1}^{m} \frac{(x^k)^{a_k}}{x},$$ (2.5)

where $a_k = \left(\frac{\partial f}{\partial \lambda^k}\right)_0$ is a constant, so that, y being actually an invariant, which can be assumed to have the numerical value of unity, the acceptable form for the combination of magnitudes is

$$x = \prod_{k=1}^{m} (x^k)^{a_k}$$ (2.6)

with the transformation law:

$$\bar{x} = \exp\left[a_k \lambda^k\right] x.$$ (2.7)

It is immediately perceived that the numbers a_k characterize the *kind* of the derived quantity and that they may be regarded as the components of an m-dimensional vector in the basis in which the lth component of the kth fundamental quantity is the Kronecker symbol, δ_l^k. In other words, the general symbol, a_j^i, is the ordinary exponent occurring in the conventional dimensional formula for the ith *kind* of variable relative to the jth fundamental *kind* of quantity; for example, let $i = 1$ designate energy; $j = 1, 2, 3$ correspond to mass, length, and time, respectively, then $a_1^1 = 1$, $a_2^1 = 2$, $a_3^1 = -2$.

Now let x^i be a set of derived magnitudes expressible in terms of the basic set, x^j. Then the transformation laws are:

$$\bar{x}^i = \exp\left[a_j^i \lambda^j\right] x^i,$$
$$i = 1, 2, \cdots n; \quad j = 1, 2, \cdots m.$$ (2.8)

Now let

$$F(x^i) = 0$$

be the expression of an unknown physical relation in terms of the magnitudes, x^i. Equations 1.2, 1.3, and 1.5 require that the relation be expressible in terms of y^a, the solutions of

$$a^j a_j^i x^i \frac{\partial y^k}{\partial x^i} = 0$$

or

$$a_j^i \frac{\partial y^k}{\partial \ln x^i} = 0$$ (2.9)

for $j = 1, 2, \cdots m$.

Solution of Eq. 2.9 gives

$$y^k = \prod_{i=1}^{n} (x^i)^{b_i^k},$$ (2.10)

$$k = 1, 2, \cdots n - r,$$

where the b_i^k are constants determined by

$$- {}_ib_i^k = 0 \tag{2.11}$$

and where r is the rank of the matrix $\|a_j^i\|$.

This result is, of course, the well-known "π-theorem" as described by Buckingham (2) or Bridgman (3). The virtue of having used the transformation theory lies chiefly in the following two points:

1. The "alias-alibi" duality of any transformation immediately allows the conclusion that although the deductions were based on the assumption that the "absolute" magnitude of the physical quantities were unchanged during the transformation, the invariants, y^k, will certainly satisfy the equation

$$\Psi(y^k) = 0$$

throughout a transformation in which the fundamental magnitudes are fixed and the magnitudes of the x^i are "actually" changed but in such a way as to keep the y^k constant. In other words, empirical physical information satisfying

$$F(x^i) = 0$$

on a given *scale* may be used to predict a physical relation on any other scale, provided only that the x^i are varied in such a way as to maintain the constancy of the y^k.

2. The simplification of a physical problem brought about by the reduction of the degrees of freedom, n, by the number r, is not mathematically different in kind from the complete solution of the problem (the determination of the form of the unknown function, F) which is obtained when $(n-1)$ independent transformation parameters are obtained.

3. A FORMAL SOLUTION FOR b_i^k.

Equations 2.11 are equivalent to the matrix equation

$$AB = 0, \tag{3.1}$$

where $A = \|a_j^i\|$, $B = \|b_i^k\|$. The rank of A is r; by mere rearrangement of rows and columns, the non-vanishing determinant can be made to appear in the upper right-hand corner of A (under the last r columns and the first r rows; it will be supposed that the subscript is the row index, the superscript the column index). Call this portion of the matrix A_1, call the first $(n-r)$ columns and first r rows A_2; let the last $(m-r)$ rows be called A_0 (if $r = m$, A_0 does not exist).

Make a corresponding partition of B, calling the first $(n-r)$ rows

B_2, the remaining rows B_1. Then Eq. 3.1 is equivalent to

$$\left\| \begin{array}{c} A_2B_2 + A_1B_1 \\ \hline A_0 \left\| \begin{array}{c} B_2 \\ \hline B_1 \end{array} \right\| \end{array} \right\| = 0. \tag{3.2}$$

But since the rows of A_0 are linearly dependent upon the rows of $\|A_2 \vdots A_1\|$, any solution of

$$A_1B_1 = - A_2B_2 \tag{3.3}$$

automatically makes $A_0 \left\| \begin{array}{c} B_2 \\ \hline B_1 \end{array} \right\|$ vanish. Since $|A_1| \neq 0$, A_1^{-1} exists and

$$B_1 = - A_1^{-1}A_2B_2. \tag{3.4}$$

The elements of B_2 are now completely arbitrary, and it is convenient, as will be shown below, to let B_2 equal the negative unit matrix, whence

$$B_1 = A_1^{-1}A_2. \tag{3.5}$$

Combination with Eqs. 2.10 and 2.11 gives the result that the invariants are:

$$y^k = \prod_{p=1}^{r} \frac{(x^{n-r+p})^{b_p^k}_{A-r+p}}{x^k}, \tag{3.6}$$

that is, since the y^k are to be held constant, the first $(n - r)$ variables must be individually proportional to a set of products involving only the last r variables which may be changed arbitrarily.

4. THE SCALING CRITERION.

In the application of these results to the design of model experiments certain difficulties arise which have not previously been considered in the general case. It frequently occurs that some of the variables essential to a given problem may not be readily changed with scale. As examples, the acceleration of gravity, or, in certain cases, even the properties of liquid and solid media cannot be readily altered in general so as to satisfy Eqs. 3.6 and must therefore be regarded as fixed. In order to set up a general criterion for determining whether scaling is possible, it will be useful to classify the variables in three types: those which are fixed, those which are to be arbitrarily (and independently) scaled, and those which are unrestricted. We shall use the subscripts f and s to designate the first two types respectively; r_s, r_f, r_{sf} will stand for the rank of the sub-matrix of A corresponding to all the variables of types s, f, and both s and f, respectively; t_s, t_f, t_{sf} will stand for the number of y^k which involve variables of type s, f, s and/or f, respectively; and n_s, n_f are the numbers of variables of type s and of type f. A neces-

saiy and sufficient condition that scaling be possible is that

$$n_i + r_j = r_{ij}. \tag{4.1}$$

To prove the necessity of the condition, suppose $n_i + r_j \neq r_{ij}$. Since r_{ij} cannot exceed $n_i + r_j$, we must suppose $n_i + r_j > r_{ij}$ or $n_i + n_j - r_{ij} > n_j - r_j$, but since

$$i_{ij} = n_i + n_j - r_{ij}$$

and

$$l_j = n_j - r_j$$

we should have

$$l_{ij} > l_j$$

so that there would be either or both of the following types of y^k:

1. those containing arbitrarily scaled variables oniy,
2. those containing arbitrarily scaled and fixed, but not unrestricted variables,

neither of which types can be allowed.

To prove that the condition is sufficient, distinguish the two possible cases:

1. $r_{ij} = r$
2. $r_{ij} < r$.

In case (1), that part of A_{ij} with the $r_{ij} \times r_{ij}$ non-vanishing determinant can be taken as A_1; consequently (since such a determinant can be found which contains columns from all the arbitrarily scaled variables) all the arbitrarily scaled variables will appear in the set x^{n-r+r}, the fixed variables (if any) not contained in A_1 will be expressible in terms of fixed variables in A_1 only, and there will be just enough restricted variables to complete the set of $(n - r)y^k$'s with one such variable to each y^k involving arbitrarily scaled variables.

If, on the other hand, case (2) obtains, the same proof will hold (with the modification that some unrestricted variables will appear in the set x^{n-r+r}) provided only that the $r_{ij} \times r_{ij}$ non-vanishing determinant contained in A_{ij} is contained in some $r \times r$ non-vanishing determinant of A.

That this latter requirement is always satisfied follows, for example, from the definition of rank in terms of linear independence as shown by Birkhoff and MacLane (4). This completes the proof of the scaling criterion.

In concluding this section it should be remarked that the criterion furnished by Eq. 4.1 is independent of the basis of fundamental units adopted, since the only quantities appearing are numbers of variables and the rank of various sub-matrices, taken by columns, which are, of course, all invariant under the group of homogeneous linear transformations on the $a_i{}^k$, $A \to \bar{A} = TA$, $|T| \neq 0$, which corresponds to all conceivable choices of a basic set of fundamental units.

5. APPLICATION TO HYDRODYNAMICS.

Consider the dimensional composition of the variables appearing in the analytical description of fluid flow. The Navier-Stokes equation and the equation of continuity contain variables of the following dimensional types: v = velocity, p = pressure, R = any length, t = time, ρ = density, μ = viscosity. If the external forces are due to gravity, the acceleration of gravity, g, is included. In addition, there exists an equation of state which expresses ρ as a function of p alone in case the flow is assumed to be isothermal or adiabatic. The implication of this last condition is important in the consideration of possible scaling solutions: although the specific form of the equation of state is unknown, it must be expressible in terms of variables, such as the bulk modulus, whose columns in A are linear combinations of the columns in A representing ρ and p. In order to maintain, temporarily, the generality of the discussion, it will be supposed that the density is given by the series:

$$\rho = \sum_{i=\alpha}^{\omega} \rho_i(p)^i \tag{5.1}$$

with $\alpha \leq \omega$.

The A matrix is then as follows:

A	v	p	t	ρ_i	μ	g	R
M	0	1	0	$1-i$	1	0	0
L	1	-1	0	$-3+i$	-1	1	1
T	-1	-2	1	$2i$	-1	-2	0

A model experiment will now be considered in which R plays the role of the deliberately scaled variables: $n_s = 1$. Then the criterion of Eq. 4.1 requires $r_{sf} = r_f + 1$. If the medium is unchanged with scale, in the general case the rank of (ρ_i, μ) is 3 so that, since r_{sf} also equals 3, scaling is impossible. Even for an incompressible fluid ($\rho_i = 0$ except for $i = 0$) a scaling solution with fixed g is impossible if μ is fixed. The idealizations which lead to the familiar scaling approximations in terms of the Froude, Reynolds, and Mach numbers are described in Table I. In each case the set of variables designated as "ignored" are shown to be

TABLE I.

Scaling Laws for Hydrodynamics.

Typical Invariant	Ignorable Variables	v	p	t	ρ_i	μ	g	Fixed Variables
Froude Number	$\rho_i(i \neq 0), \mu$	$\frac{1}{2}$	1	$\frac{1}{2}$	$(-i)$	$(\frac{1}{2})$	0	v, g
Reynolds Number	$\rho_i(i \neq 0), g$	-1	-2	$\frac{1}{2}$	$(2i)$	0	(-3)	ρ_0, μ
Mach Number	μ, g	0	0	1	0	(1)	(-1)	ρ_i
—	$\rho_i(i \neq 0, 1), \mu$	$\frac{1}{2}$	0	$\frac{1}{2}$	$[-1]$	$(\frac{1}{2})$	0	$\frac{\rho_i}{\rho_j}, v$

required to follow rather impractical scaling laws, but by assuming that their influence on the flow is unimportant in a certain range of velocities, a solution is obtained by omitting them from further consideration. The dependence of the variables is expressed in terms of the exponent $b_i{}^R$ in the expression

$$x^i = x^{io} \left(\frac{R}{R^o}\right)^{b_i{}^R},\qquad (5.2)$$

where x^i is the appropriate value of the ith variable on any scale with a typical length R related to the model scale with corresponding values x^{io} and R^o. The computation of the $b_i{}^R$ requires only the determination of that row of $A_1{}^{-1}$ which corresponds to the column of A_1 in which R appears.

REFERENCES.

(1) H. L. LANGHAAR, JOURNAL FRANKLIN INST., Vol. 242. p. 459 (1946).
(2) E. BUCKINGHAM, *Phys. Rev.*, Vol. 4, o. 345 (1914).
(3) P. BRIDGMAN, "Dimensional Analysis," Yale University Press, 1922.
(4) G. BIRKHOFF AND S. MACLANE, "A Survey of Modern Algebra," Macmillan, 1944.

A THEORY OF THE DYNAMIC PLASTIC DEFORMATION OF A THIN DIAPHRAGM

G. E. Hudson
New York University

American Contribution

1950

TABLE OF CONTENTS

164

Historical Background

In connection with the torpedo-protection program which was conducted at the Taylor Model Basin, U. S. Navy, during the War, detailed studies were made of the damage done by underwater explosions to thin metal circular diaphragms, air-backed, and held rigidly at their peripheries. The idea was, that if an adequate description and explanation of the phenomena attendant on the damage to such an apparently simple structure could be obtained, some progress toward an understanding of damage produced similarly in more complex structures might be made. At the same time smaller metal diaphragms were used by several other research groups as underwater gauges for estimating from their deformations the relative strengths of underwater explosions. These investigations led to certain theoretical developments along this line but from a point of view different from that taken in this article.* On a later occasion, the necessity arose for the development of a simple mechanical gauge to measure the velocities acquired impulsively by large structures when they are subjected to a very great force of very brief duration. For this purpose, a small thin lead diaphragm was mounted in a rigid closed container which was then attached to a given structure. When an impulsive velocity was imparted to the structure, normal to the plane of the diaphragm, the diaphragm container moved and the diaphragm material tended to remain behind. The resulting deformation was of course the same as if the diaphragm itself had suddenly had impressed on it an equal but opposite uniform velocity normal to its plane while the container remained fixed. The theory presented in this article was developed in an attempt to describe the observed motion and deforma   tal diaphragms under some of the conditions encountered in these experiments   th these instruments.

Observations of Deformation of Diaphragms

When a thin metal diaphragm is held rigidly at its periphery, and a sufficiently large uniform velocity is suddenly imparted to it perpendicular to its initial plane, the following phenomena have been observed.   As soon as

*See , for example, J.G. Kirkwood and J.M. Richardson, "The plastic deformation of circular diaphragms under dynamic loading by an underwater explosion wave", OSRD 4200 (1944). This unclassified report is a summary of most of the work presented in two earlier reports by Kirkwood, OSRD 793, and 1115, also unclassified.

the diaphragm begins to move, the material at the outer edge is jerked to rest by the rigid constraint there. The news of this retardation is carried radially inwards by a rather sharply defined bending wave, shown in Figure 1, which travels at a nearly constant velocity until it reaches the vicinity of the center of the diaphragm, where it appears to speed up. The material in the flat central region of the diaphragm, ahead of the bending wave, continues to move with almost its initial velocity until the wave reaches it. Then, as the bending wave sweeps over it, the material is brought quickly to rest. Finally the bending wave reaches the center, leaving the diaphragm deformed into a characteristic shape, generally a surface of revolution, nearly conical, with, however, a somewhat rounded apex.*

Thickness measurements along a generator of the surface of revolution show at the outer edge a relatively large and very localized thinning, as if the diaphragm has a strong tendency to shear loose from the restraining rim. Indeed, it is found necessary to round off the sharp rim somewhat at its inner edge to inhibit this shearing and to obtain the type of motion of interest here. As one proceeds inward, toward the center, the thickness decreases, gradually at first, from approximately the original thickness close to the diaphragm periphery. Near the center, the thinning becomes greater and greater and finally, right at the center there is usually observed a kind of dimple. The thickness at this dimple decreases with the total amount of deformation.

Measurements have also been made of the radial and tangential strains along a radius for a great many diaphragms. These measurements show that the two strains are nearly equal at each point.

* In some of the experiments with underwater explosions, further deformation of the diaphragm takes place which, however, is attributed to causes other than the initial impulse, and is therefore irrelevant to the present discussion.

-2-

Surmises Concerning the Motion

We may now draw certain inferences from the previously described observations and make certain surmises as to the details of the motions and as to the mechanisms involved. These surmises themselves have not yet been verified experimentally, but they seem physically reasonable in the light of present knowledge and in the light of the conclusions to which they lead.

At the initial instant the diaphragm material has a uniform normal velocity component v; the radial velocity component is certainly zero. However, the restraining effect of the rim must be felt quickly by the diaphragm material adjacent to it. This is considered to have two effects. First, the presence of the rigid edge constraint is quickly made known to the interior portion of the diaphragm. The news is no doubt transmitted by an elastic stress wave traveling inward at a high "sonic" velocity. We may surmise that this wave leaves the interior of the diaphragm in a state of plastic flow so that a non-zero radial velocity distribution may be superimposed on the uniform normal velocity, which itself remains practically unaffected. Elementary estimates indicate that this presumably takes place in a time which is very short compared to the time taken for the complete deformation of the diaphragm. Second, a plastic bending wave is generated near the edge and is propagated inward more slowly. It is believed that one function of this wave is to inhibit the tendency, as evidenced by the thinning at the edge, of the diaphragm to fail in shear.

As the bending wave sweeps inward over material flowing outward in a radial direction, the material loses most of its velocity, both its radial component and the original component, v, normal to the initial plane. It is surmised that little or no impulsive thinning or other form of plastic working is associated with this action; that is, the bending wave in effect simply

-3-

tilts each annular element as it sweeps over it, removing its kinetic energy. This is then transmitted to the central region where it is ultimately converted to plastic work of stretching and thinning. In this region, the diaphragm is still nearly flat, and therefore, in the absence of any normal force components it retains its uniform normal velocity; its initial radial velocity distribution, however, may be altered, both by dissipation of energy in plastic work, and by the probably non-uniform distribution of tension resulting from non-uniform radial flow, thinning, and work-hardening.

Because no motion is observed in the diaphragm material behind the bending wave, it is surmised that this material has been unloaded and returned to the elastic state. Indeed the somewhat conical shape assumed by the diaphragm suggests that the stresses in a particle momentarily behind the bending wave, although possibly near "the yield point" of the material, quickly subside.

As the bending wave sweeps inward, it speeds up. This is possibly due to a rise in the stress ahead of the wave because of work-hardening effects in the plastic material in the flat central region. This speeding up accounts at least partially for the rounding off of the diaphragm profile at the apex; in addition it is probable that the bending wave has a finite radius of curvature, that is, it may have a finite "length" in the radial direction, which would also help account for this rounding off.

Basic Suppositions

The exact non-linear partial differential equations of motion describing the dynamic plastic deformation of the metal in a diaphragm such as we have been considering are extremely complex. Even if it were possible to solve these with existing mathematical techniques the solution would

-4-

without doubt be so unwieldy as to necessitate the introduction of radical simplifying approximations. Hence it seems desirable to attack the theoretical problem of analysis of this motion by the artifice of replacing the actual mechanical system by a fictitious one in which are incorporated certain constraints which do no work and which operate to simplify the equations of motion. At the same time this idealized model must be so chosen that most of the main qualitative features of the actual diaphragm motion, as described or surmised in the foregoing, are preserved. In this way it is hoped that the motion of the model when found agrees closely enough with that of the real system so that certain quantities, such as thickness distribution, central deflection, total strain, and time of deformation do not differ too much in magnitude from their actually observed values.

Consider, therefore, an ideal thin metal circular diaphragm of uniform thickness h, and radius a, held rigidly at its periphery. Initially, suppose that the diaphragm material has a uniform velocity component v normal to its initial plane. Because in the actual diaphragm, an elastic wave may then quickly set the material in motion radially, we shall suppose in addition that in the ideal diaphragm, there may be an initial linear radial velocity distribution superimposed on the uniform normal velocity v.* Estimates of the magnitude of this effect will be made in a later section.

At any later instant, the situation is considered to be as follows. A plastic bending wave has traveled inward some distance from the edge. In connection with this wave, we shall suppose that its shape is as shown in Figure 2; that is, the bending wave represents a true discontinuity in the

_____

*This initial elastic stress phase has been investigated, but not published to the writer's knowledge, by H. Bohnenblust. He indicated orally some years ago to the writer that the circumferential stress component rises very quickly behind the elastic-stress wave in which the only non-vanishing stress component is the principal radial stress.

slope of the instantaneous profile of the diaphragm. As the wave sweeps over each annular material element in the flat central region, in effect it tilts it into the shape of an annular truncated conical element behind the wave. During this process, it is assumed that, because of the thinness of the diaphragm, no significant amount of work is done in bending. Moreover, no impulsive thinning is supposed to take place in the bend of the wave. We further suppose that the only stresses of importance at the bending wave are radial and circumferential principal stresses just ahead of the wave, and behind the wave in the tilted region, a normal stress component along the generator of the tilted element, a shear stress component, and a circumferential normal stress component.

Now the material passed over by the wave shall be supposed to have come to rest. The stresses which exist in this region are supposed to be such as to just hold the material in equilibrium – although their tendency to cause further plastic flow or not is a subject for further investigation, and might constitute a partial theoretical test of the model.

Within the central region which is as yet unaffected by the plastic bending wave, the diaphragm is still supposed to be flat, and therefore in the absence of normal force components it retains its uniform normal velocity v. At the same time, the material in the flat central region is supposed to be flowing radially outward and thinning. To avoid the extreme complexities of considering the probably non-uniform distributions of tension and thinning in an actual diaphragm, we introduce in this region a distribution of constraint forces which do no work and which produce a uniform thinning over the region during the motion. These constraints must be considered to yield a non-uniform stress system which is superimposed on the stresses arising from the uniform plastic deformation of this region.* Their

*Henceforth these latter are denoted as "plastic stresses" to distinguish them from the stresses arising from the constraints.

- 6 -

170

total effect is simply to bring about a simple radial velocity distribution
and to afford a means of transferring the kinetic energy lost at the bending
wave into kinetic energy of radial motion in the flat central region.
Kinetic energy of thinning is supposedly very tiny and is neglected.

As regards the properties of the metal of which the diaphragm is
composed, we shall suppose the following. Because we are here dealing with
finite deformations and strains, all purely elastic effects, other than those
of the initial stress wave which have already been mentioned, would seem to
be negligible. Consequently we shall suppose that except for the initial
elastic action, we are dealing with an ideal incompressible plastic material,
with a zero elastic strain range. This is consistent of course with the
surmise of the initial very high speed elastic stress wave and the "freezing"
of the material when it unloads as the bending wave passes by. Furthermore,
we shall suppose that there are no strain rate effects affecting the plastic
flow. We shall suppose, therefore, that the data obtained from a tensile
test of the diaphragm material in which the tensile stress is exhibited as
a definite function of the natural elongational strain, are, in combination
with general laws of plastic flow, sufficient to specify the plastic properties
of the material.

Naturally the mathematical statement of the problem depends to a
certain extent upon the choice of the type of plasticity theory, although
in any case an apparently consistent formulation may result. As a matter
of fact, for the type of motion herein investigated, no differences arise
whether one applies the plastic deformation type of theory, or the plastic
flow theory of plasticity.* The point of view of the latter is taken in this article.

*For a discussion of these basically different theories see W. Prager,
"Theory of Plastic Flow vs. Theory of Plastic Deformation", J. App. Phys., 19
540 (June, 1948).

- 7 -

With the ... g.ng picture in m..., it is f... .... develop a consiste... ...hematical formulation of the u... / of the main motion so as to s... ..., the fundamental laws of mechanic... **This is done in the following se... ...s.**

Mathematical for... ...on of the Theory

The ... ... suppositions and assumptions introduced the preceding section lead t... ...ain quantitative relations between the pa... ters which describe the c... ...rations and state of the diaphragm material. The developmont o... ...se relations can be divided into four main pa... **Part 1** has to do w... ...nservation of momentum, energy, and mass (volume) the neighborho... ...the bending wave. In Part 2, the equations of motion the mate... the central flat plastic portion are derived, and in Pa... plasticity ... ...y is introduced and applied. Part 4 is concerned with the specific ... ...of the initial state of the motion.

Part 1. ...po...itions in the Neighborhood of the Bending Wave.

...ppose that, at any time t, after the start of the motion, the dist... ... the bending wave from the center of the diaphragm is R, as sho... ...: ...igure 3. Let dL be the width of an elementar... ring of thickness H j... ...w of t... be.ding wave. During the time interval dt, this ring is ...pt ...r and, in effect, tilted by the bending wave as it is propagated inwa... ... ...stence traveled by the wave in this time is $-\dot{R}$ dt, the negative sign ... ...ause $\dot{R}$, the velocity of the bending wave, is negative. Let the material a... ... ... d... ahead of the bending wave

---

* The treatment of the initial elastic action is perhaps not qu... satisfactory, except when the hypothesis of a zero elastic strain ra... is rigidly maintained. This appears to be a subject for further investigati...

172

have a radial velocity U outward, so that it moves a distance Udt in time dt. Hence, as is evident from Figure 3, the rate at which material is swept over by the wave is

$$\frac{dL}{dt} = -\dot{R} + U \tag{1}$$

As the wave travels by, the material ring of width dL in effect is tilted impulsively into a curved conical ring of width dL and thickness H. In deforming, the inner edge of this ring undergoes a displacement v dt normal to the original plane of the diaphragm and the outer edge remains fixed. Actually, then, the bending wave travels a distance along the generator of the conical element while it is traveling inward along the radius a distance $-\dot{R}dt$. Hence, the rate at which the wave travels along the profile of the deformed diaphragm is given by

$$\frac{dL}{dt} = \sqrt{\dot{R}^2 + v^2} \tag{2}$$

It is clear, from this and Figure 3, that the generator of the conical element makes an angle α with the outward pointing radius, defined by the relations

$$\frac{dL}{dt} \cos \alpha = \dot{R} \tag{3}$$

$$\frac{dL}{dt} \sin \alpha = v \tag{4}$$

which together are equivalent to (2).

Let S'_{RR} be the total normal stress component parallel to a generator in the diaphragm at a point just behind the bending wave, and let S'_{RH} be the total shear stress component parallel to a plane element normal to the generator at this point as in Figure 4. By total stress is meant here the sum of the plastic and the constraint stresses. These components exert forces of magnitude $S'_{RR} H R d\theta$ and $S'_{RH} H R d\theta$ respectively on the outer edge of a segment of width dL and thickness H which subtends an angle $d\theta$ at the center of the diaphragm.

-9-

In time dt, this segment loses all its momentum component, $\rho HRd\Theta dLv$, normal to the original plane of the diaphragm. If the change in momentum is equated to the impulse $[-S'_{RR}HRd\Theta \sin \propto + S'_{RH}HRd\Theta \cos \propto]$ dt delivered in this direction in time dt, there results the relation

$$\rho \frac{dL}{dt} v = S'_{RR} \sin \propto - S'_{RH} \cos \propto \qquad (5)$$

Similarly, if S_R is the total principal radial stress component in the diaphragm material just ahead of the bending wave, as in Figure 4, the net radial force component on the same segment of the annular element while it is being tilted is $-S'_{RR}HRd\Theta \cos \propto - S_R HRd\Theta - S'_{RH}HRd\Theta \sin \propto$. In time dt this effects the removal of the radial momentum $\rho HRd\Theta$ dLU from the segment. Again if the change in the radial momentum component is equated to the impulse, we obtain the relation

$$\rho \frac{dL}{dt} U = S_R + S'_{RR} \cos \propto + S'_{RH} \sin \propto \qquad (6)$$

As the bending wave sweeps inward over the element depicted in Figure 4, S_R does work of amount $-S_R HRd\Theta$ Udt on it, while the stresses S'_{RR} and S_{RH} .... of constraint forces in the rigid stationary material behind the wave, . . . The work which is done in the time dt equals the increase in kinetic energy, ...

$$\frac{1}{2} \rho \frac{dL}{dt} (U^2 + v^2) = S_R U \qquad (7)$$

Several consequences of interest can be deduced quickly from equations through (7) inclusive. Recognizing from (1) and (2) that

$$U^2 + v^2 = 2U(U - \mathring{R})$$

and incorporating this in (7), and combining the result with (6), we find that

$$\rho \frac{dL}{dt} \mathring{R} = S'_{RR} \cos \propto + S'_{RH} \sin \propto \qquad (8)$$

174

Substituting for $\dot{R}$ in (8) and for v in (5) from (3) and (4), we find, since the determinant

$$\begin{vmatrix} \sin \alpha , & -\cos \alpha \\ \cos \alpha , & \sin \alpha \end{vmatrix} \neq 0$$

that the speed of the bending wave with respect to the material on either side of it is

$$\frac{dL}{dt} = \sqrt{\frac{S'_{RR}}{\rho}} \tag{9}$$

and that the shear stress behind the bending wave is

$$S'_{RH} = 0 \tag{10}$$

Substituting the value of U obtained from (1) into (6) and utilizing (6) and (9), we find that

$$S'_{RR} = S_R \tag{11}$$

so that there is no stress discontinuity and no shock in this sense at the bending wave. In addition (3) and (4) may be combined to give

$$\tan \alpha = \frac{v}{\dot{R}} \tag{12}$$

Similarly (1) and (2) yield

$$U^2 - 2U\dot{R} - v^2 = 0 \tag{13}$$

while utilization of $U^2 + v^2 = 2U(U - \dot{R})$, obtained previously from (1) and (2), in (7), and then substituting for $(U - \dot{R})$ from (1) and for $(\frac{dL}{dt})$ from (2), yields

$$\rho (\dot{R}^2 + v^2) = S_R \tag{14}$$

Equations (9) through (14) inclusive are entirely equivalent to the original six independent relations described by (1) through (7) inclusive. Clearly we may regard these equations as defining the six quantities $\frac{dL}{dt}$, S'_{RH}, $\dot{R}$, α, $\dot{R}$, and U in terms of v and ρ, and S_R.

-11-

Part 2. Equations of Motion in the Flat Central Region

The component velocity of any particle in the flat central region, perpendicular to the original diaphragm plane, is supposed to have the constant value v until the bending wave sweeps inward over it. This normal motion is quite independent of the radial motion, which in general might conceivably be much more complicated. The radial motion is of importance, for upon it depends, in part, the distribution of thinning in the diaphragm. Let us now consider this radial motion.

As mentioned previously, in order to avoid the mathematical complication of non uniform thinning in the flat central region and the necessity of attempting to solve non-linear partial differential equations of motion, we introduce a system of constraints which serve to maintain a uniform thickness H throughout this region. Consequently, at time t + dt, a disc which was of radius R – dL, and uniform thickness H at time t, has stretched into one of radius R – dL + Udt and uniform thickness H + Ḣdt. Since its volume is conserved we are led to the equation

$$\frac{\dot{H}}{H} + 2\frac{U}{R} = 0 \tag{15}$$

A similar consideration of an interior disc of momentary radius r < R, at time t, and initial radius r_o, shows that

$$\frac{r}{r_o} = \frac{\partial r}{\partial r_o} = \sqrt{\frac{h}{H}} \tag{16}$$

so that $\frac{r}{r_o}$ is a function of time only. Equations (16) will be termed the "constraint equations" for the flat central region.

Now the forces exerted on each material particle in the central region are due to the constraints and to the plastic stresses. We are supposing that the only normal plastic stresses in the central region are radial and circumferential stress components σ_r and σ_θ respectively. On

an elementary segment, of width dr and thickness H, which is a distance r from the center of the diaphragm where it subtends an angle dθ, these stresses exert a net force:

$$\left[-\frac{\partial}{\partial r} \cdot (r\,\sigma_r) - \sigma_\bullet\right] H d\theta dr \ .$$

But from the constraint expressed by (16), it is clear that the radial and tangential strains, and hence the radial and tangential strain velocities are equal and functions of the time only. It follows from plasticity theory that the radial and tangential plastic stress components are equal and are functions of the time only. (vide Part 3). Hence the plastic stresses exert no net accelerating force on the particles in the flat central region interior to the bending wave. The only possible accelerating forces in this region are the constraint forces, that is, we may define the outward accelerating force on the element of mass ρHr dr dθ by a differential quantity dΓdθ = $=\frac{\partial \Gamma}{\partial r}$ dr dθ, except for elements just ahead of the bending wave. Combining (16) with the equation of motion of this element, we find that

$$\rho H \frac{1}{4} r^2 \cdot \frac{d^2}{dt^2}\left(\frac{1}{\sqrt{n}}\right) = \frac{\partial \Gamma}{\partial r} \tag{17}$$

At the bending wave itself we must have

$$RH\,S_R = RH\,\sigma_r + \Gamma_R \tag{18}$$

where Γ_R is the value of Γ when r = R, and is to be so chosen that the constraint forces do no work. This means that the rate of working by the whole set of constraint forces is zero, viz.,

$$\int\int_0^R \frac{\partial r}{\partial t}\, d\Gamma d\theta - 2\pi\,\Gamma_R\, U = 0 \ ;$$

if this integration is carried out, using (15), (16), and (17), we see that

$$\Gamma_R = \rho\,H^{\frac{1}{4}}\frac{R^3}{4}\frac{d^2}{dt^2}\left(\frac{1}{\sqrt{n}}\right) \tag{19}$$

Equation (17) may now be integrated to yield

$$\Gamma = \frac{1}{12}\, \rho \, H^{\frac{1}{2}} (4r^3 - R^3)\, \frac{d^2}{dt^2}\left(\frac{1}{\sqrt{H}}\right) \tag{20}$$

as the quantity defining the distribution of constraint forces in the flat central region.

It is interesting to note (and a check on the work) that if one now equates the total rate of decrease of kinetic energy for the whole diaphragm to the rate at which energy is being absorbed in plastic working of the material, viz. $-\sigma_r H \pi R^2$, the resulting relation, after a bit of manipulation, is identical with (7), as it should be.

Part 3. The Application of Plasticity Theory

To complete the discussion in the previous section it is necessary now to introduce certain stress and strain relationships in the flat central region. Because the rates of change of the principal strains are proportional to the principal strains themselves, as a result of the constraint relation (16), it is not important to formulate the plastic flow relationships in a completely general fashion.* It suffices to write these laws in terms of the principal stresses σ_1, σ_2, σ_3 and principal natural strains ε_1, ε_2, ε_3 in the form

$$\varepsilon_1 + \varepsilon_2 + \varepsilon_3 = 0$$

and

$$\frac{\sigma_1 - \sigma_3}{\varepsilon_1 - \varepsilon_3} = \frac{\sigma_2 - \sigma_3}{\varepsilon_2 - \varepsilon_3} = \frac{\tau(\varepsilon)}{\gamma} \ .$$

The first states the law of conservation of volume, while the second, as a consequence of the first, states that the principle strains (more generally the strain rates) are proportional to the deviations of the stresses from

---

* For such formulations, see for example: G.H. Handelman, C.C.Lin, W. Prager, "On the mechanical behaviour of metals in the strain-hardening range", Quart. Appl. Math. $\underline{4}$ 397-407 (1947). In the present report, the plastic flow laws reduce to a form identical with that of the deformation theory of plasticity.

178

an isotropic stress state. The factor of proportionality, $\frac{\tau}{\gamma}$, is the ratio of the octahedral shear stress

$$\tau = \frac{1}{3}\sqrt{(\sigma_1 - \sigma_2)^2 + (\sigma_2 - \sigma_3)^2 + (\sigma_3 - \sigma_1)^2}$$

to the octahedral shear strain

$$\gamma = \sqrt{\frac{1}{3}(\varepsilon_1^2 + \varepsilon_2^2 + \varepsilon_3^2)}$$

and, when the material is yielding plastically, the ratio is a function of γ, having a form determined empirically from a tensile test for example. According to our previous supposition, in a tensile test, the tensile stress σ_T, is related to the natural longitudinal strain, ε_L, by

$$\sigma_T = \sigma(\varepsilon_L).$$

In a tensile test $\tau = \frac{\sqrt{2}}{3}\sigma_T$, while $\gamma = \frac{\sqrt{2}}{2}\varepsilon_L$. Hence, we may rewrite the above relation as

$$\tau(\gamma) = \frac{\sqrt{2}}{3}\sigma(\sqrt{2}\,\gamma)$$

which is now applicable to a more general stress state than that occurring in a tensile test.

Let us now apply these laws to the central flat region of the diaphragm. In this case

$$\sigma_1 = \sigma_r \qquad , \qquad \sigma_2 = \sigma_\theta \qquad , \qquad \sigma_3 = \sigma_H = 0$$

$$\varepsilon_1 = \varepsilon_r = \log\frac{\partial r}{\partial r_0}, \quad \varepsilon_2 = \varepsilon_\theta = \log\frac{r}{r_0}, \quad \varepsilon_3 = \varepsilon_H = \log\frac{H}{h},$$

where σ_H is the principal stress in the thickness direction, and ε_r, ε_θ, and ε_H are the natural (logarithmic) strains in the directions indicated by the subscripts. As a consequence of (16), $\varepsilon_1 = \varepsilon_2 = -\frac{1}{2}\varepsilon_3$, so we find that

$$\sigma_r = \sigma_\theta \tag{21}$$

and

$$\sigma_r = \sigma(\log\frac{h}{H}) \tag{22}$$

Equality (21) has already been used in the previous section in obtaining (17).

-15-

Part A. The Specification of the Initial State

As the initial elastic stress wave front sweeps inward from the edge it may accelerate the material particles, leaving any real diaphragm in a state of plastic flow with the material flowing radially outwards. However, for the ideal material with which we have been dealing, with a zero elastic strain range, the elastic stress wave would travel at an infinite speed from the periphery to the center. Consequently, although the discontinuity in stress across the front of such a wave is quite high, jumping from zero to the yield stress $\sigma = \sigma(0)$, the actual impulse delivered to any material particle swept over by the front would be zero. This seems to be possibly a rather extreme case, however, and since the theory does permit the assumption of an initial radial velocity distribution of a certain kind, a rough estimate of the possible magnitude of this effect will be made as follows.

In accordance with the constraints placed on the diaphragm material, we shall assume that the motion, generated in the elastic deformation, can be approximated by one of a normal type with a linear radial velocity distribution which is zero at the center and greatest at the periphery. Then the radial coordinate r of a particle, initially at r_o, is

$$r = r_o(1 + \frac{q(t)}{a})$$

where q is the normal coordinate of the constrained motion, and "a" is the radius of the diaphragm. The elastic stresses for such a motion are

$$\sigma_r = \sigma_\theta = \frac{E}{1-\nu} \cdot \frac{q}{a}$$

where E is Young's modulus and ν is Poisson's ratio. The motion begins at a time t = 0, when the stress at the edge rises suddenly to the yield stress σ. Hence the equation of motion is, after calculating the equivalent mass from the kinetic energy,

$$\frac{\rho a}{4} \ddot{q} + \frac{E}{1-\nu} \frac{q}{a} = \sigma$$

-16-

180

to be solved subject to $\dot{q}(0) = 0$, $q(0) = 0$. We find that

$$\dot{q}(t) = 2\sigma\sqrt{\frac{1-\nu}{\rho E}}\ \sin\frac{2}{a}\sqrt{\frac{E}{\rho(1-\nu)}}\ t$$

$$q(t) = \frac{a\ \sigma\ (1-\nu)}{E}\left[1 - \cos\frac{2}{a}\sqrt{\frac{E}{\rho(1-\nu)}}\ t\right]$$

When $\dot{q}$ is a maximum, the stresses in the diaphragm reach the yield point,
and from that time on, plastic flow takes over. This happens at a time

$$t_E = \frac{\pi a}{4}\sqrt{\frac{\rho(1-\nu)}{E}}\ ;$$

the velocity distribution may be written

$$\frac{\partial r}{\partial t} = \frac{r_0}{a}\ \dot{q}(t_E) = v\frac{r_0}{a}\sqrt{\frac{4\sigma}{\rho v^2}\cdot\frac{\sigma(1-\nu)}{E}}\tag{23}$$

The time for complete plastic deformation of a diaphragm may be estimated
roughly, considering the bending wave to travel along a radius with a

speed $\dot{R} = -\sqrt{\frac{\sigma}{\rho}}$.

It reaches the center at a time

$$t_S \cong a\sqrt{\frac{\rho}{\sigma}}\ ;$$

the ratio of t_E to t_S is thus

$$\frac{t_E}{t_S} \cong \frac{\pi}{4}\sqrt{\frac{\sigma(1-\nu)}{E}} \cong 3\ \%$$

for some steels.* Similarly, elastic considerations give the radial velocity
at the periphery,

$$\frac{\partial r}{\partial t}\bigg]_{Elastic} = v\sqrt{\frac{(1-\nu)\sigma}{E}}\ \sqrt{\frac{4\sigma}{\rho v^2}} \cong .675\ v$$

---

* Typical values of parameters for obtaining these quick estimates are:

$\sigma = 6 \times 10^4\ \text{lb/in}^2$ $\rho = .75 \times 10^{-3}\ \text{lb.sec}^2/\text{in.}^4$ $h = .05\ \text{in}$

$E = 3 \times 10^7\ \text{lb/in}^2$ $v = 10^3\ \text{in/sec}$ $a = 5\ \text{in}$

$\nu = .3$

-17-

while a rough order of magnitude of a typical plastic radial flow rate U may be obtained from (13):

$$U \cong \frac{v^2}{-2R} \cong v\sqrt{\frac{\rho v^2}{4\sigma}} \cong .055 \, v \quad ,$$

so that

$$\left. U \middle/ \frac{\partial r}{\partial t} \right]_{\text{elastic}} \cong \frac{55}{675} \cong 8 \, \%$$

From these results we see that although the initial elastic effects occur very rapidly, they may result in a radial velocity distribution of significantly large order of magnitude. Because of this, it is a bit unfortunate that the estimate (23) is not based on a firmer foundation; this appears to be a subject for further investigation.

The remaining initial conditions, other than (23) (which we now take to hold at $t = 0$) may be listed. The initial radius of the bending wave is

$$R(0) = a \, ; \tag{24}$$

the initial thickness is

$$H(0) = h \, ; \tag{25}$$

the initial radial velocity at the bending wave is

$$U(0) = v\sqrt{\frac{4\sigma}{\rho v^2} \cdot \frac{\sigma(1-\nu)}{E}} \tag{26}$$

where $L = 2L$, for a material of zero elastic strain range.

Finally in order to define the final shape of the diaphragm profile we introduce the distance $Z(t)$ of the central flat region from the initial plane of the diaphragm. Clearly,

$$Z = v \, t \tag{27}$$

so that once R is found as a function of t, elimination of t between R and Z will yield $Z = Z(R)$, the equation of the diaphragm profile. This concludes the mathematical formulation of the theory.

182

Summary of the Equations of Motion

For convenience, the relevant defining relations are collected here:

$$\text{(A)} \quad \begin{cases} \frac{dL}{dt} = \sqrt{\frac{S_R}{\rho}} \\[2mm] \tan \alpha = \frac{v}{R} \\[2mm] S'_{RR} = S_R \\[2mm] S'_{HH} = 0 \end{cases} \qquad \begin{aligned} &\Gamma_R = \rho\, H^{\frac{1}{4}} \frac{R^3}{4} \frac{d^2}{dt^2}\left(\frac{1}{\sqrt{H}}\right) \\[2mm] &S_R = \sigma_r + \frac{\Gamma_R}{RH} \\[2mm] &\sigma_r = \sigma_\theta = \sigma\left(\log \frac{h}{H}\right) \\[2mm] &z = v\,t \end{aligned}$$

$$\text{(B)} \quad \begin{cases} U^2 - 2HR - v^2 = 0 \\[2mm] \rho(\dot{R}^2 + v^2) = \sigma\left(\log \frac{h}{H}\right) + \frac{1}{4}\rho R^2 \sqrt{H}\, \frac{d^2}{dt^2}\left(\frac{1}{\sqrt{H}}\right) \\[2mm] \frac{\dot{H}}{H} + 2\frac{U}{R} = 0 \end{cases}$$

$$\text{(C)} \quad \begin{cases} R(0) = a \\[2mm] H(0) = h \\[2mm] U(0) = v\sqrt{\frac{4\sigma}{\rho v^2} + \frac{\sigma(1-\nu)}{E}} \end{cases}$$

In (A) the quantities on the left of the equations are defined in terms of ρ, h, v, $\sigma(\log \frac{h}{H})$, t, R, and H. The relations (B) constitute a differential system of third order in H, U, and R, so that (C) furnishes the necessary three initial conditions. In order to solve (B) it is necessary, in addition, to have an explicit functional form for $\sigma(\log \frac{h}{H})$. For example, if the ideal material is one which does not work harden, then we have simply

$$\sigma\left(\log \frac{h}{H}\right) = \sigma \tag{28}$$

where σ is a constant.

An Elementary Approximation to the Solution

In case the effect of the constraint forces, that is, acceleration of the material in the central flat region, is small throughout most of the motion, so that it may be neglected, the equations (B) take on a particularly simple form, especially if the material is one which does not work harden. Then the order of the set of differential relations becomes two, so that only two initial conditions, those on R and on H, can be applied. Although it is not necessary, it is also convenient to suppose that $\frac{\sigma}{\rho v^2}$ is a very large number. compared to unity, which is certainly true for many cases of interest. For the typical values listed in a previous section $\frac{\sigma}{\rho v^2} = 80$.

Let us denote the constant $\frac{\sigma}{\rho}$ by c^2. Then, neglecting high powers of $\frac{v}{c}$, the solution of the equations may be written

$$U = \frac{v^2}{2c} \qquad (a)$$

$$R = a - ct \qquad (b)$$

$$H = h \left(\frac{R}{a}\right)^{\frac{v^2}{c^2}} \qquad (c) \qquad\qquad (29)$$

so that

$$Z = \frac{v}{c}(a - R) \qquad (d)$$

These equations tell us that the radial speed U is a small constant at the bending wave, and that the speed of the bending wave from the edge to the center of the diaphragm is a constant, independent of the initially imposed normal velocity v. The thickness distribution in the deformed diaphragm given by equation (29)(c), shows a dimpling tendency at the center; in fact at the last moment the thickness becomes zero at the very center — no doubt a consequence of the idealizations and approximations.

-20-

184

In any event, the variation with R is so rapid near R = 0, the tiny pinhole would not actually be experimentally very apparent. Furthermore, this rapid variation of thickness indicates that at the last moment, when R/a << 1, the neglect of the constraint effects might be more serious than otherwise; however, this does not turn out to be the case in general, as shown in the next section. Equation (29)(d) shows that the diaphragm assumes a conical shape, as indicated by experiment, whose center deflection is proportional to the initial velocity v. This last is the basis for the use of such diaphragms as impulsive velocity indicators, as described earlier. Quantitatively there is also fair agreement between these results and experimental observations. Indeed, even the total time for deflection, which has been called the swing time t_S , of the diaphragm, and is given by

$$t_S = \frac{a}{c} ,$$

is seen to be independent of v, to this order of approximation; computed values where higher powers of $\frac{v}{c}$ are included agree rather well with the experimentally observed ones.

The results of this section on the elementary theory were implicit in the writer's first report on the diaphragm theory. In that report, as in this section, no serious attempt was made to estimate the effect of the motion in the central flat region on the explicit solution of the problem; that is, the non-linear partial differential equations of motion for this region were not taken into account by the introduction of constraints.

The present article is a generalization of the former one, as will be seen in the next section; there the exact solution of the equations (B) and (C) are obtained and inform us as to the effect of radial motion and thinning.

-21-

The Exact Solution of the Equations of Motion for a Material
with no Work-Hardening.

     Although the differential equations (B) are non-linear, still
they may be solved explicitly in a finite form involving a single quadrature,
at least in the case for which there is no work-hardening. Let us introduce
the non-dimensional parameters

$$\beta = \frac{R}{a} \qquad\qquad \zeta = \frac{vt}{a} = \frac{z}{a}$$

$$\mu = \frac{U}{v} \qquad\qquad \delta = \frac{4\sigma}{\rho v^2}$$

$$\eta = \frac{H}{h} \qquad\qquad \varkappa = \sqrt{\frac{4\sigma}{\rho v^2} \cdot \frac{\sigma(1-\nu)}{E}}$$

where, for the values suggested in a previous section $\delta = 320$, and
$\varkappa = 0$ or $.675$.

     After a certain amount of algebra, equations (B), reduce to

$$\frac{\eta'}{\eta} = -2\frac{\mu}{\beta} \qquad\qquad (a)$$

$$2\mu\beta' = \mu^2 - 1 \qquad\qquad (b) \qquad\qquad (30)$$

$$(2 - \mu^2)\beta' + \beta\mu\mu' = (3 - \delta)\mu \qquad (c)$$

where a prime means differentiation with respect to ζ. These equations are
to be solved subject to the initial conditions (C) which may be rewritten:

$$\beta = \eta = 1, \quad \mu = \varkappa, \quad \text{when } \zeta = 0. \qquad (d) \qquad\qquad (30)$$

By dividing the sides of (30)(c) by the corresponding sides of (30)(b), the
variable ζ is eliminated, and we are left with an integrable equation whose
variables are separated, relating β, and μ. Similarly by multiplying the
right side of (30)(a) by the left side of (30)(b) and conversely, and
employing the previous integrable expression to eliminate β, we find an
integrable relation involving η and μ. Finally ζ is found in quadrature
form in terms of μ, and $\beta(\mu)$ from (30)(b). This explicit solution may be
exhibited as

-22-

$$\frac{R}{a} = \rho(\mu) = \left(\frac{\mu^2 - x_1}{\chi^2 - x_1}\right)^{\frac{1}{4}\frac{x-1}{x_1 - x_2}} \left(\frac{\mu^2 - x_2}{\chi^2 - x_2}\right)^{\frac{1}{4}\frac{x_2 - 1}{x_2 - x_1}} \tag{a}$$

$$\frac{H}{h} = \eta(\mu) = \left(\frac{\mu^2 - x_1}{\chi^2 - x_1}\right)^{-\frac{1}{2}\frac{x_1}{x_1 - x_2}} \left(\frac{\mu^2 - x_2}{\chi^2 - x_2}\right)^{-\frac{1}{2}\frac{x_2}{x_2 - x_1}} \tag{b}$$

(31)

$$\frac{Z}{a} = \zeta(\mu) = \int_\chi^\mu \frac{2\mu^2}{(\mu^2 - x_1)(\mu^2 - x_2)} \rho(\mu) \, d\mu \tag{c}$$

where x_1, x_2, are the smaller and larger (positive) roots respectively of the quadratic equation

$$x^2 - (2\delta - 3)x + 2 = 0 \tag{32}$$

and $\mu = \frac{U}{v}$. Unfortunately (31)(c) is not integrable in terms of elementary functions, in general; still a great deal of information can be gained from an analysis of (30, (31) and (32), and from a consideration of special cases.

For positive values of δ, which are the only ones of physical interest, the roots of (32) occur in pairs of positive values. for $\frac{3}{2} + \sqrt{2} \leq \delta \leq \infty$, and as pairs of negative values for $0 \leq \delta \leq \frac{3}{2} - \sqrt{2}$ (a very small range). For intermediate values of δ, the roots are complex. We shall be interested only in values of $\delta \geq \frac{3}{2} + \sqrt{2}$. At the lower limit of this range, corresponding to very large v, or small σ values, we have $x_1 = x_2 = \sqrt{2}$. As δ becomes very large, $\sqrt{2} > x_1 \rightarrow 0$ and $\sqrt{2} < x_2 \rightarrow \infty$.

Special Cases

A.   A case of considerable interest arises when χ^2 coincides with one of the roots of (32). Now from (31) we see that the only possibility is for μ^2 itself to be constant and equal to χ^2. From (30) we then find that either $0 \leq \mu = \chi \leq 1$ or $\mu = -\chi \leq -1$, in order for β' to be negative. The first case only is admissible, since the second precludes $\mu = \chi$ initially. Thus we have

$$0 \leq \mu^2 = \chi^2 = x_1 = (\delta - \tfrac{3}{2}) - \sqrt{(\delta - \tfrac{3}{2})^2 - 2} \leq 1$$

and $\delta \geq 3$.

The solution of (30) may now be written as

$$R = a - \frac{1 - \chi^2}{2\chi} v t = a - \frac{1 - \chi^2}{2\chi} z \qquad \text{(a)}$$

$$H = h\left(\frac{R}{r}\right)^{\frac{\gamma \chi^2}{1 - \chi^2}} \qquad \text{(b)}$$

$$U = \chi v \qquad \text{(c)}$$

and

$$\delta = 4\frac{c^2}{v^2} = \frac{\chi^4 + 3\chi^2 + 2}{2\chi^2} \geq 3 \qquad \text{(d)}$$

$$(33)$$

where, it will be remembered, $C = \sqrt{\frac{\sigma}{\rho}}$

For $\chi = 1$, $\delta = 3$, and $v = \frac{2}{\sqrt{3}} c$, and the deformed diaphragm is cylindrical, i.e., it ruptures completely. (Possibly in practice, rupture would occur before this, due to excessive thinning at the center, or shearing at the edge; experiments indicated the central failure to occur first with properly designed edge restraints. The above value of v might be regarded as an upper limit.)

For other allowed values of $\chi (= \mu)$, this solution is quite similar to the elementary approximation presented earlier, even quantitatively so, for large δ values. For then

$$\chi \cong \frac{1}{\sqrt{\delta}} = \frac{v}{2c} \ll 1, \quad (\delta \gg 3)$$

and (33) reduces to (29).

B. Still another case, perhaps even the most important one for purposes of this paper, arises if we suppose that χ may have any desired positive value, within reason, and that δ is very large, so that x_1 is small and x_2 is large. We shall assume further that $\frac{\chi^2}{x_2} \ll 1$, as is $\frac{\mu^2}{x_2}$ (since μ^2 varies from χ to x_1). Under these simplifying conditions it is possible to derive an approximation to the integral (31)(c) but in a somewhat indirect way, much too long to reproduce here in detail. We find that:

- 21 -

$$x_1 \simeq \frac{1}{\delta} , \quad x_2 \simeq 2\delta \gg 1,$$

where δ, it will be remembered is $4\frac{c^2}{v^2}$. Then, provided δ is large enough

$$\frac{Z}{a} \simeq \frac{vt}{a} - \frac{2U_v}{v^t - U^t}\left(1 - \frac{R}{a}\right) \tag{a}$$

$$\frac{H}{h} = \left(\frac{R}{a}\right)^{\frac{v^t}{c^t}} \tag{b} \tag{34}$$

$$\frac{U}{v} = \frac{v}{2c}\left\{1 + \left(4\chi^2 \frac{c^2}{v^2} - 1\right)\left(\frac{R}{a}\right)^{16\frac{c^t}{v^t}}\right\}^{\frac{1}{2}} \tag{c}$$

It can be shown that this approximation is uniform over the range of $\frac{U}{v}$ from χ to $\frac{v}{2c}$, and the range of $\frac{R}{a}$ from 1 to 0 ; but the nearer χ is to 1, the larger δ must be . Now we may distinguish several possibilities. If $\chi = 0$, which is the case of a material which has strictly no elastic strain range, we find that the shape of the deformed profile, described by (34)(a) , is conical near the center, with a center deflection identical with that given by the elementary theory. At the edge, the slope is zero (as required by (30)(b). The thickness distribution is identical with that given by the elementary approximation, while from (34)(c), the radial velocity increases very rapidly from zero to $\frac{v^2}{2c}$. As χ increases the solution approaches the elementary approximation, the slope at the edge increasing, until when $\chi = \frac{v}{2c}$, the shape is exactly conical as in (29). As χ increases further, the slope at the edge becomes greater, the center deflection remaining the same, however, as does the thickness distribution. The radial velocity U, at the bending wave, decreases, again very rapidly, from χv to $\frac{v^2}{2c}$. These results all seem physically quite reasonable and might have been expected on such grounds. A calculation indicates that there is actually very little other effect of different χ values on the profile, as long as δ is very large.

Apparently, then, we may conclude that the elementary approximation is even more reliable than could have been hoped for, as long as there is no work hardening ; indeed, under the conditions noted, the entire discussion concerning equations (29) is applicable. In the next section we consider some effects of work hardening.

Considerations of Work Hardening

In line with the results of the last section, it seems apropos, when introducing the complication of work hardening, to neglect the radial motion, insofar as its inertial effects are concerned. This was done in the development of the elementary approximation in the previous section, as it is in the following.

Now the stress function of a material which work hardens may be written

$$\sigma \left(\log \frac{h}{H}\right) = \sigma + \omega \log \frac{h}{H} \tag{35}$$

where as before σ is the yield stress and ω is the work hardening stress per unit natural strain in a tensile test, and has a value of approximately 400×10^3 lb/in^2 for some medium steels. Such a stress-strain relation is not at all inconsistent with many empirical data.

After introducing (35) into the general equations (3), with the constraint forces deleted, the differential equations of motion can be written in terms of the previous non-dimensional notation with the addition of

$$\varepsilon = \frac{\omega}{\rho v^2}$$

If, furthermore, we let

$$\xi = \sqrt{\frac{\sigma}{4} - 1 + \varepsilon \log \frac{1}{\eta}}$$

the equations take the simple form

$$\mu^2 + 2\mu\xi - 1 = 0 \tag{a}$$

$$\frac{d\beta}{\beta} = -\frac{1}{\varepsilon}\frac{\zeta^2}{\mu}d\xi \tag{b}$$

$$\tag{36}$$

$$d\zeta = -\frac{d\beta}{\xi} \tag{c}$$

where for the time being ξ, not ζ, may be considered to be the independent variable. Although these equations can be solved explicitly with but one indicated quadrature remaining (from (36)(c)), the solutions are so complicated that it is more instructive to consider a special case in which the approximation

190

$\xi \gg 1$ may be made. It is clear that for the typical values we have been
utilizing this is the case (e.g., $\frac{\delta}{4} \cong 80$). Thus (36)(a) immediately yields

$$\mu = -\xi + \sqrt{\xi^2 + 1} \cong \frac{1}{2\xi} . \tag{37}$$

After some manipulation, the solutions, to this order of approximation, can
be rewritten with β, or $\frac{R}{a}$, as the independent variable. Thus, with $c^2 = \frac{\sigma}{\rho}$,
as before, and $d^2 = \frac{\omega}{\rho}$, we have

$$U = \frac{v^2}{2c} \left\{ 1 - \phi \right\}^{-\frac{1}{4}} \tag{a}$$

$$H = h\, e^{-\frac{\xi}{2}\left\{\sqrt{1-\phi} - 1\right\}} \tag{b} \tag{38}$$

$$Z = vt = -\frac{v}{c} \int_a^R \left\{ 1 - \phi \right\}^{-\frac{1}{4}} dR \tag{c}$$

where $\phi = 2\frac{v^2 d^2}{c^4} \log \frac{R}{a}$. It is interesting to note that as $d \to 0$, that is,
the work-hardening stress becomes small, the above solution reverts to the
elementary approximation (29), since ϕ vanishes like d^2 in the limit. One
major difference stands out between the above and the previous solutions — at
the center of the deformed diaphragm, $\left(\frac{dZ}{dR}\right)$ vanishes. That is, the apex of
the conical shape is rounded off, in complete qualitative agreement with the
observations, and with the surmise made in an earlier section. It is also
of interest to observe that the center deflection of the deformed diaphragm
is somewhat less than that of a diaphragm whose material does not work-harden,
but which has the same yield limit and initial conditions. These observations
are illustrated by the diagrams of Figure 5, in which are compared the deformed
diaphragm profiles for two materials, one of which does not work-harden. The
profiles of the diaphragms whose material work-hardens were calculated by
integrating numerically (38)(c) (which, incidentally, may be put in the form
of an incomplete Γ-function). It is probable, that by taking account of

strain-rate effects, which have not yet been incorporated into plasticity theory, an even more marked rounding off would occur at the center than is evident from Figure 5.

One should note that, as a result of neglecting the constraint forces in the approximate solution for a work-hardening material the initial value of U is completely determined, and equal to $\frac{v^2}{2c}$, as in the elementary theory. A more general solution including the constraint terms would of course allow this initial value to be given arbitrarily. Although such a solution has not been investigated, it is likely that U would quickly approach the value given by (38)(a), after performing its initial task of increasing or decreasing the slope of the diaphragm profile near the edge.

Conclusions

In partial conclusion, before summing up the accomplishments of this theory, it might be well to point out some of its shortcomings. First, the constraint forces imposed on the center flat portion are seen actually to yield an infinite constraint tension or stress just at the center of the diaphragm. However, other idealized theories have frequently led to similar paradoxes; e.g., the pressure (which is actually a constraint stress) imposed by the assumption of incompressibility is infinite at a sharp corner in the theory of potential flow of a liquid. Second, the imposition of rigidity on the material behind the bending wave is an obvious artificiality; finally, the assumption that the bending wave is an actual discontinuity in slope is

192

not strictly in accord with the facts. It would indeed be pleasant to be able to relax some or all of these idealizations; however, it is clear that, having recognized the artificialities for what they are, it has been quite necessary to invoke them in this paper in the name of mathematical simplicity.

Equations (A) (B) (C), together with an empirically determined stress-strain relation (analogous to (28) or (35)), specify completely the motion and plastic deformation of any diaphragm of radius a, thickness h, and initial velocity v. For instance, one may calculate the following:

1. The radius R of the bending wave as a function of the time.
2. The diaphragm profile at each instant.
3. The thickness distribution.
4. Displacement - time curves of particles in the diaphragm.
5. Stress and strain distributions.
6. The center deflection as a function of v.
7. The total time for the deformation to take place.

The viewpoint presented here admittedly has led to a kind of short-cut procedure which is designed to circumvent certain mathematical difficulties inherent in a more rigorous theory. Because of this method of attack, it may be necessary in the future, in order to make the results more generally applicable, to reexamine some of the basic assumptions made herein. Outstanding among these is the question of the initial radial velocity and stress distribution (although the results seem to indicate that this has only a slight effect on the final answer). Other investigations might consider such effects as the magnitude of the energy absorbed at the bending wave, equilibrium of the region behind the bending wave, and the possibility (which seems small) of plastic flow in it, and the possible non-uniform radial flow and tension in the central flat region.

-29-

To conclude, the theory presented herein describes a dynamically possible mode of motion, and one which can be handled simply, in a mathematical sense. Because the theory is based, for the most part, on experimentally observed facts, there is a strong possibility that the motion derived from it approximates closely that of a diaphragm deforming plastically after having been given an initial uniform velocity normal to its original plane.

194

Figure 1 -

(A) The diaphragm receives an initial impulsive velocity v, denoted by vertical arrows.

(B) The material has a radial velocity distribution, denoted by horizontal arrows, and is restrained from moving at the periphery.

(C) The bending wave, shown by the sharp corners in the profile has progressed inward from the edge.

(D) As the diaphragm deforms further, the central region remains flat and moves with its initial velocity v. The bending wave is traveling into the central region and progressively deforming it.

(E) As the bending wave nears the center it speeds up slightly.

(F) The speeding up of the bending wave results in rounding off the apex of the conically deformed diaphragm.
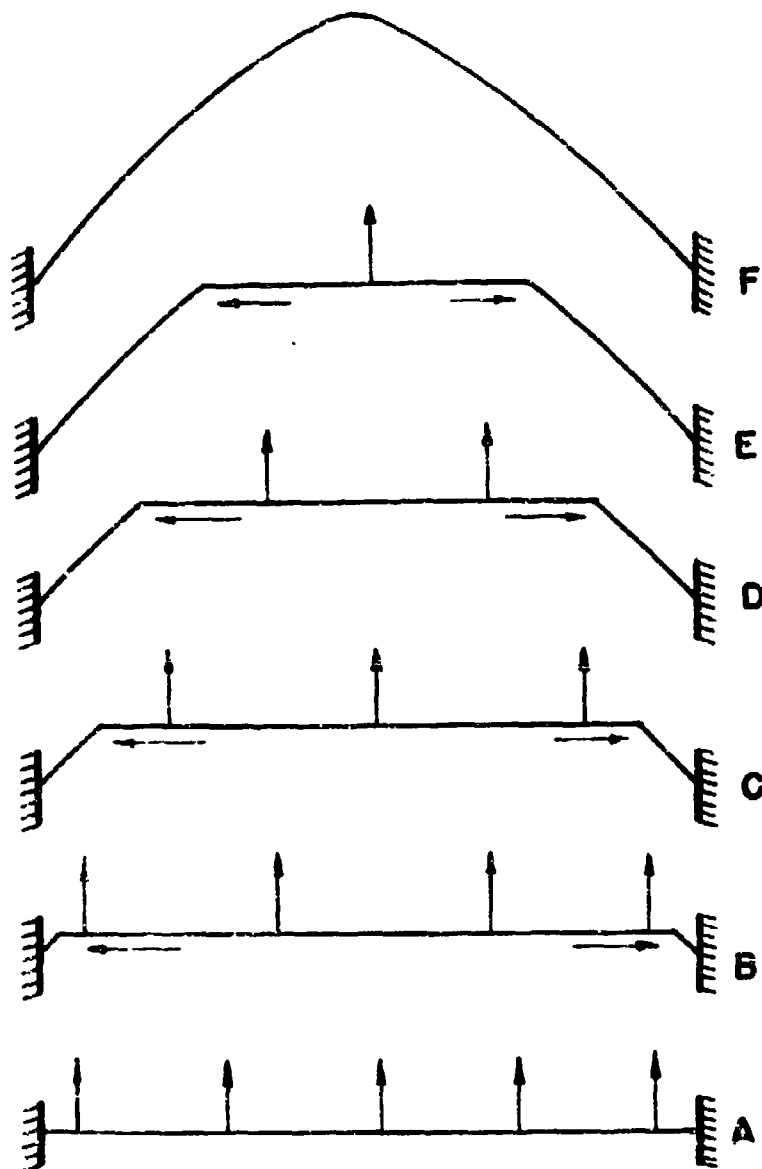
FIGURE i STAGES IN DYNAMIC
DEFORMATION OF DIAPHRAGM

196

FLAT CENTRAL REGION

BENDING WAVE

RIGID MATERIAL

RIGID RESTRAINING RING
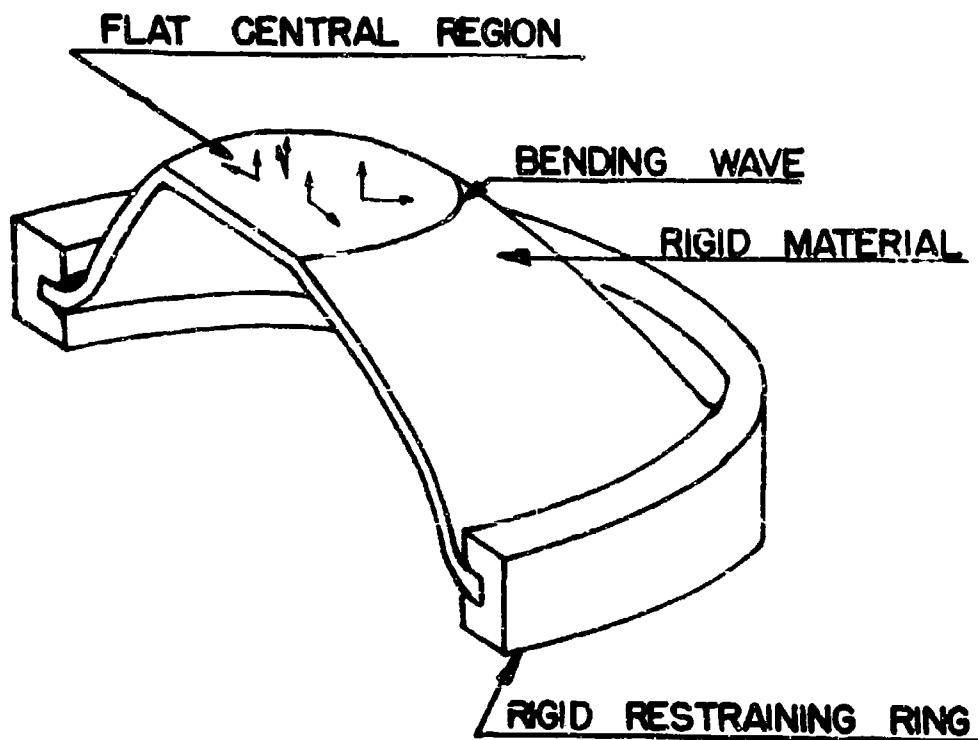
FIGURE 2

Cut-away Sketch of the Diaphragm at Some Instant After the Motion Has Begun.

The flat central plastic flow region ahead of the bending wave, the wave itself, and the deformed region behind the bending wave, in which the material is supposed to be rigid and at rest, are clearly shown.

197
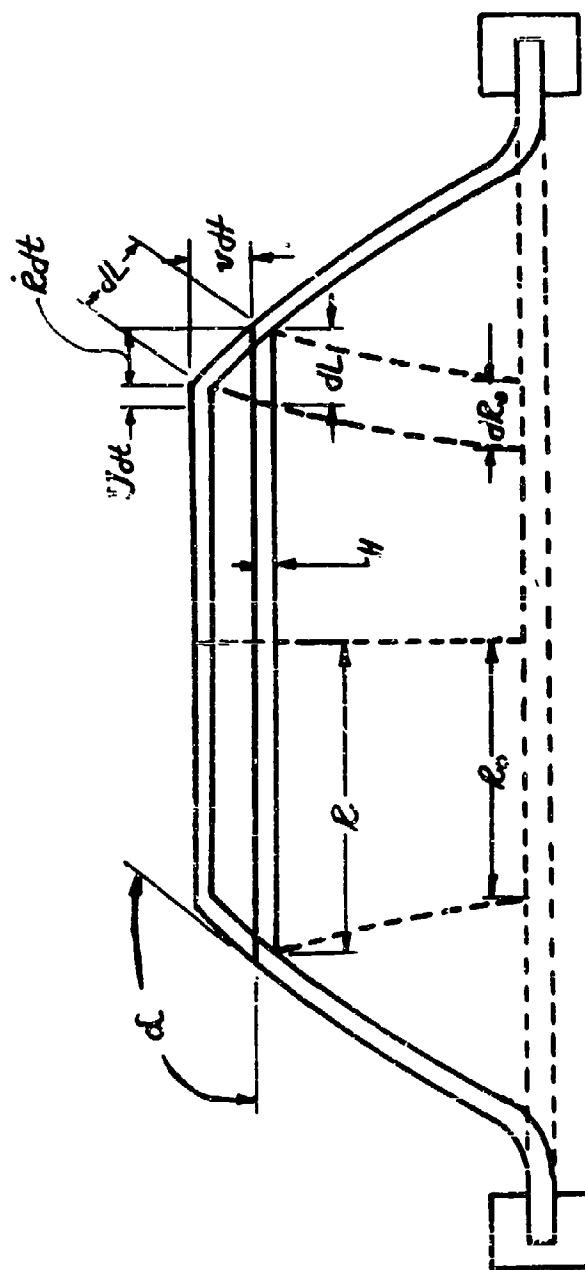
A Sketch of the Diaphragm Configurations at Two Successive Instants, t and t + dt.

The various quantities which enter into the several geometric and kinematic relations are portrayed here.

FIGURE 3

198
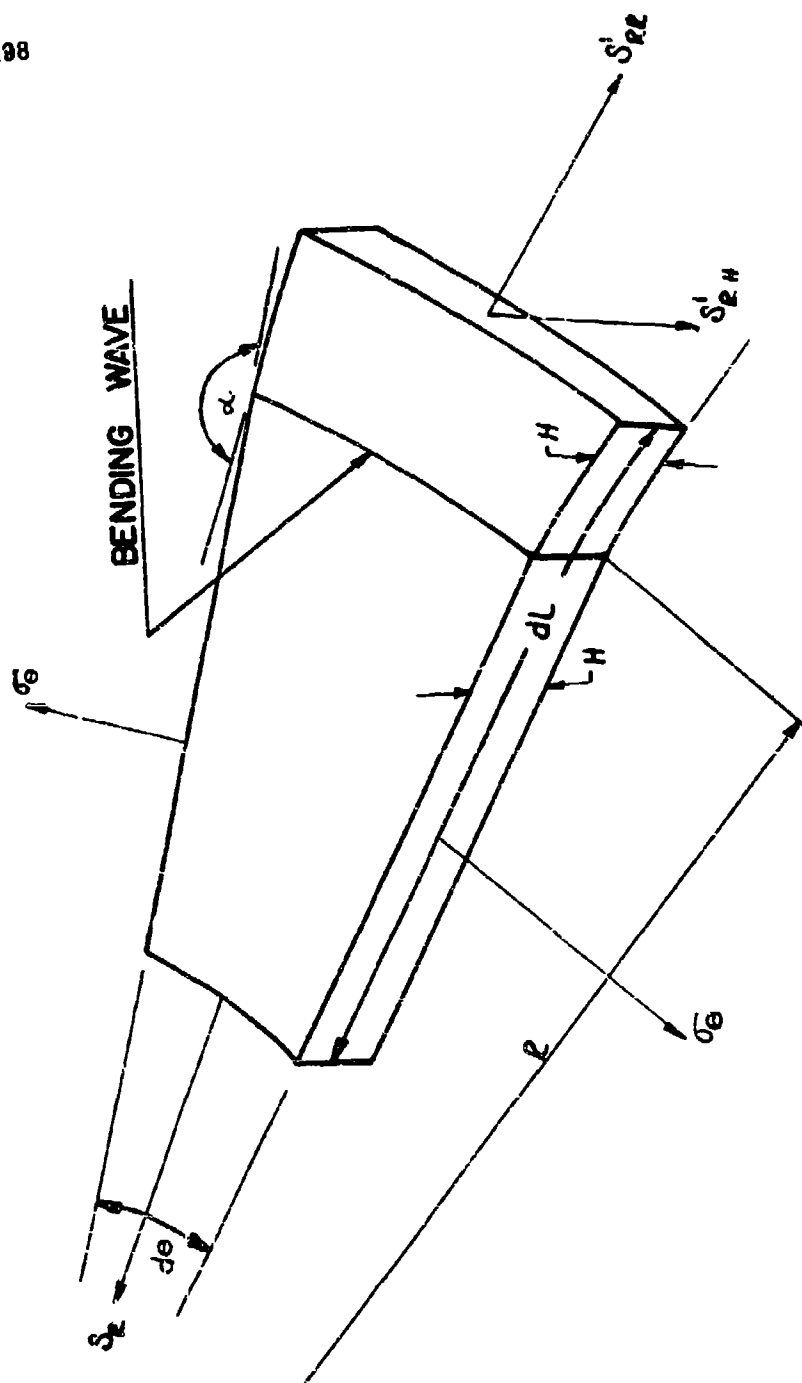
Plastic and Constraint Stresses at the Bending Wave.
The bending wave has traveled partly through a
segment of an annular element, and the various stresses
which serve to remove the momentum from this segment are
shown.

FIGURE 4

199

Curves a denote diaphragms whose material does not work-harden while b refers to diaphragms whose material work-hardens. The subscripts 1 and 2 refer to different initial conditions in which the initial velocity v was taken as 10^3 in/sec and 2×10^3 in/sec respectively. The effect of work-hardening in decreasing the center deflection is shown, and in rounding off the apex of the conical shape.
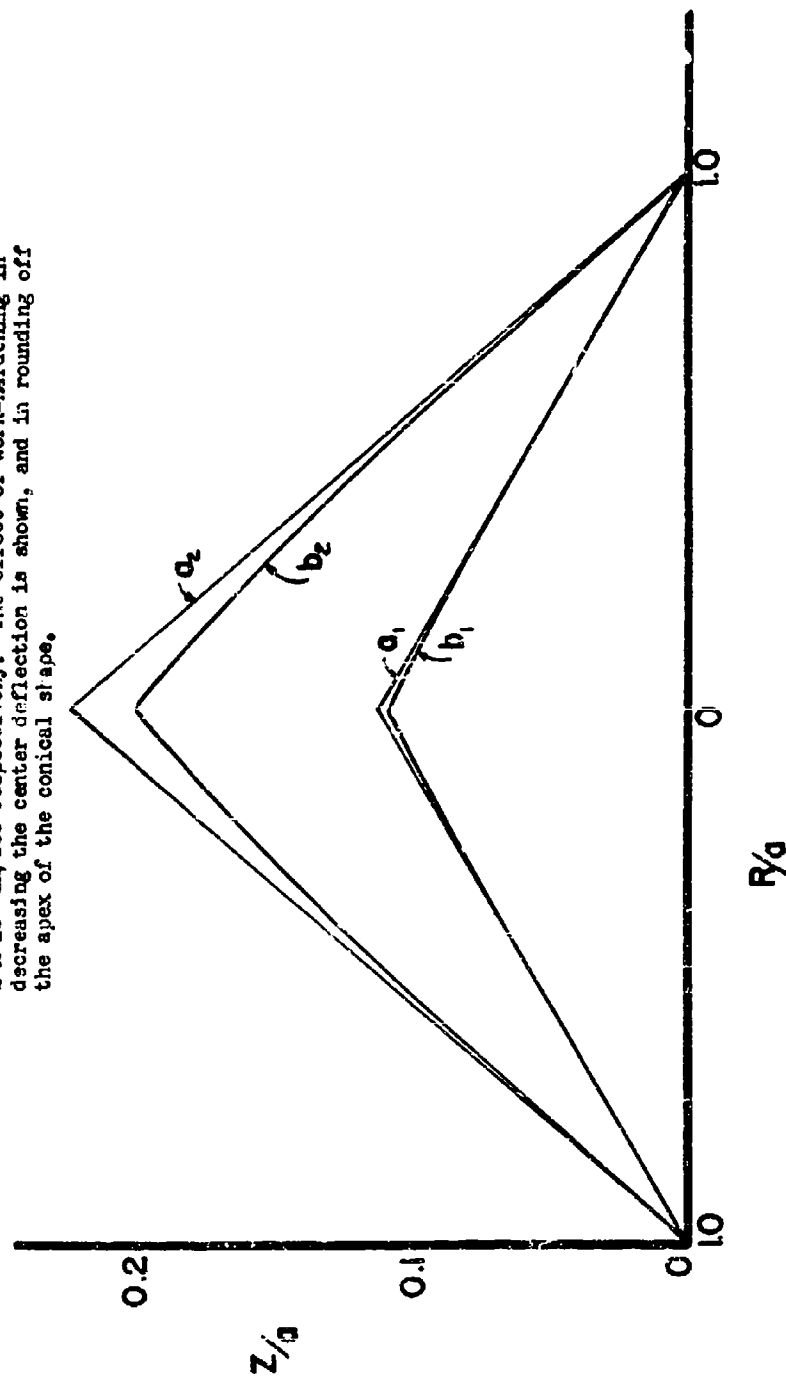
FIGURE 5   Profiles of Completely Deformed Diaphragms.

NOTE ON THE MOTION OF A FINITE PLATE DUE TO AN UNDERWATER EXPLOSION

S. Butterworth
Admiralty Research Laboratory

British Contribution

August 1942

NOTE ON THE MOTION OF A FINITE PLATE DUE
TO AN UNDERWATER EXPLOSION

S. Butterworth

August 1942

*　　*　　*　　*　　*　　*　　*

In the report "Damage to ship's plates by underwater explosions" a theory of the motion of an air backed circular plate in an otherwise rigid wall under the action of a submarine explosive wave was developed assuming that water could be regarded as incompressible.

Recently G.I. Taylor in the report "The pressure and impulse of submarine explosion waves on plates" has put forward a theory of the motion of an infinite plate under the action of an explosive wave propagated at the velocity of sound in water. This theory gives results which are totally different from those of the report "Damage to ship's plates by underwater explosions". In particular it leads to the conclusion that if water could be made incompressible the plate would suffer no motion at all under the action of an explosive wave. Although in the Appendix to the report "Damage to ship's plates by underwater explosions" qualitative reasons were given for preferring the theory there advanced, it seems now important to examine the differences more closely in view of the revival of the old theory.

Regard the plate as a piston of mass m per unit area and let it be moving inwards with velocity U at time t.

Each element of the plate sends out wavelets into the water which give reaction pressures on the rest of the plate. According to orthodox acoustic theory the reaction pressure at a distance r from an element of area ds is $-\frac{\rho}{2\pi} \frac{ds}{r} \frac{du}{dt}$ occurring at a time r/c later than t where ρ is the density of water and c the velocity of sound in water.

Thus the reaction pressure at the centre of the plate (assumed circular and of radius R) is:-

$$-\rho \int_0^{ct} \frac{d}{dt} \left\{ u(t - \tfrac{r}{c}) \right\} \, dr = \rho c \left\{ u(t) - u(o) \right\} \tag{1}$$

so long as t < R/c. When t > R/c the integration stops at R and the reaction pressure is:-

$$-\rho \int_0^{R} \frac{d}{dt} \left\{ u(t - \tfrac{r}{c}) \right\} \, dr = -\rho c \left\{ u(t) - u(\tfrac{R}{c}) \right\} \tag{2}$$

If the applied pressure is $P_0 e^{-nt}$ and if we approximate by assuming that the reaction pressure at the centre is that for the whole plate, the equation of motion is:-

$$m \frac{du}{dt} = P_0 e^{-nt} - \rho c \, u \tag{3}$$

so long as t < R/c and U = 0 when t = 0 and

$$m \frac{du}{dt} = P_0 e^{-nt} - \rho c \left\{ u(t) - u(t - T) \right\} \tag{4}$$

when t > R/c (= T).

Equation (3) is that used in the report "The pressure and impulse of submarine explosion waves on plates" and holds for all time for an infinite plate.

Equation .....

Equation (3) and (4) give straightforward solutions which change form at intervals T. By measuring time in each case from the beginning of each of those intervals we have:-

$$m \frac{du_1}{dt} = P_0 e^{-nt} - \rho c \, u \qquad\qquad t < T$$

$$m \frac{du_2}{dt} = P_0 e^{-nT} e^{-nt} - \rho c \, (u_2 - u_1) \qquad T < t < 2T \qquad (5)$$

$$m \frac{du_3}{dt} = P_0 e^{-2nT} e^{-nt} - \rho c \, (u_3 - u_2) \qquad 2T < t < 3T$$

Integrating and adding, we get

$$m \, u_\infty = \frac{P_0 \int_0^T e^{-nt} \, dt}{1 - e^{-nT}} - \rho c T \, u_\infty$$

or the final velocity is:-

$$u_\infty = \frac{P_0}{n \, (m + \rho c T)} = \frac{P_0}{n \, (m + \rho R)} \qquad\qquad (6)$$

This result is independent of c and (to the approximation made above) should agree with the solution given in the report "Damage to ship's plates by underwater explosions". According to equation (22) of that paper the value of u_L is $P_0/n \, (m + \frac{8}{3\pi} \rho R)$.

The factor $\frac{8}{3\pi}$ arises through taking into account the differences in reaction pressures over the plate area.

The way in which the final velocity is reached is illustrated in Figure 1 which holds for the case

$$m = 20.27 \text{ gms/sq.cm. (1.023 inches iron plate),}$$
$$n = 624.5 \text{ seconds,}$$
$$c = 5000 \text{ f.p.s.,}$$
$$R = 3.19 \text{ feet.}$$

The value of n is approximately that occurring on the detonation of 750 lb. torpex. The remaining figures are chosen so as to give the round values $\rho c/mn = 12$ and $nT = 0.80$ thus simplifying the calculations.

In Figure 1 the velocity curve up to $nt = 0.4$ is that of Taylor's theory. If water will not stand tension then the plate acquires the maximum velocity shown in this stage of the curve, and the rest of the curve is irrelevant, but if water will stand tension then the effect of reduction of relief pressure becomes apparent after $t = T$ and the velocity shows a further increase, tending by a series of oscillations to the value given by (6).

Figure 2 shows the nett pressure accelerating the plate. For the theory to hold, the tensions shown on that curve must not exceed those which water can stand.

The theory given is only approximate and depends on whether the centre point can be taken as typical in representing the whole reaction pressure over the plate. It does, however, show in what way the infinite plate theory is linked with that of a finite plate in an incompressible fluid.

APPENDIX

Removal of Approximation.

Consider an element of the plate situated at Q distant x from the centre of the plate
(Figure 3). The reaction pressure at Q may be regarded as the aggregate of a series of elementary
pressures generated in time intervals $\delta t'$. The elementary pressure at time t due to wavelets
generated between times $t - t' - \frac{1}{2} \delta t'$ and $t - t' + \frac{1}{2} \delta t'$ comes from the arc AB of radius
$r = ct'$ subtending an angle 2β at Q. From the orthodox formula, the pressure due to this set
of wavelets is:—

$$- \rho \dot{u} (t - t') \theta \, \delta r / \pi$$

The mean pressure over the plate due to all wavelets generated in the specified interval
$\delta t'$ is therefore:—

$$- \rho \frac{\dot{u}(t - t')}{\pi} \delta r \int_{x = 0}^{x = R} 2\pi \, dx \frac{2x}{\pi R^2}$$

$$= - \rho \dot{u}(t - t') \delta r \, F(r/R)$$

in which $F\left(\frac{r}{R}\right) = \frac{2}{\pi R^2} \int_{x = 0}^{x = R} \theta x \, dx$

Using $R^2 = x^2 + r^2 - 2 xr \cos\theta$, we find $F\left(\frac{r}{R}\right) = 1 - \frac{1}{\pi}(\sin 2\beta + 2\beta)$ in which
$\sin \beta = r/2R$ so long as $r < 2R$. When $r > 2R$, $F\left(\frac{r}{R}\right) = 0$.

Integrating again with respect to t' the total mean reaction pressure over the plate is:—

$$\bar{p} = - \rho c \int_0^t F\left(\frac{ct'}{R}\right) \dot{u}(t - t') \, dt'$$

or by integration by parts and taking $u(o) = 0$

$$\bar{p} = - \rho c \left[u(t) - \frac{2c}{\pi R} \int_0^t \sqrt{1 - \frac{c^2 t'^2}{4R^2}} \, u(t - t') \, dt' \right] \tag{1}$$

Hence if the applied pressure is $P_0 e^{-nt}$ the equation of motion of the plate (mass m per unit
area) is:—

$$m \frac{du}{dt} = P_0 e^{-nt} + \bar{p} \tag{2}$$

Equation (2) can be solved by step by step methods. Also the initial motion can be found
approximately by direct integration using:—

$$\bar{p} = - \rho c \left[u - \frac{2c}{\pi R} \int_0^t u(t) \, dt \right] \tag{3}$$

which is the approximate form of (1) when t is small. Identifying $\int_0^t u(t) \, dt$ with displacement S,
this gives:—

$$m \frac{d^2 S}{dt^2} + \rho c \frac{dS}{dt} - \frac{2 \rho c^2}{\pi R} S = P_0 e^{-nt} \tag{4}$$

the initial conditions being $S = \frac{dS}{dt} = 0$.

For the dimensions given in the example of the main report the solution of (4) is:—

$$\frac{dS}{dt} = \frac{P_0 (e^{-nt} + 1.191 e^{1.442nt} - 2.191 e^{-13.42nt})}{2.50 R \, \rho c}$$

Using .....

Using this up to nt = 0.2 and then using (1) and (2) step by step, the curve shown in Figure 3 is obtained.

Comparing with the approximate curve (Figure 1) it is seen that the regions of falling velocity (i.e. tension on surface of plate) have disappeared. Also the curve is tending reasonably satisfactorily to the ultimate value of U viz:-

$$U_{\infty} = P_0/n \ (m + \frac{8}{3\pi}\rho R) = 0.1971 \ P_0/mn.$$

The absence of regions of tension in the example calculated is due to the choice of a pressure wave in which n is not too large. If n had been made large so as to suit small charges, the ripple shown in the approximate theory would again appear.

LIMITED CIRCULAR PLATE IN RIGID WALL.

206

FIG 3
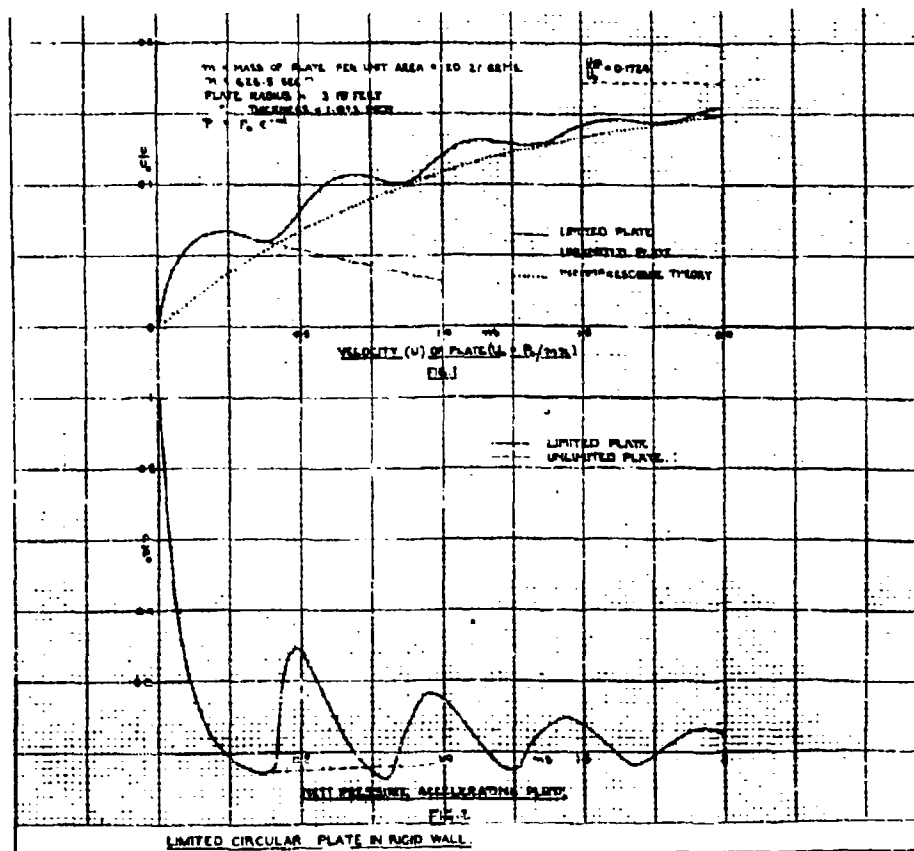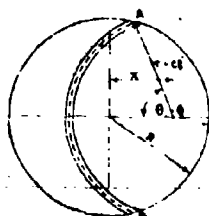
CONSTANTS OF PLATE AS IN FIG I

$\frac{U \cdot \alpha}{U_0}$ .97:

$\frac{U}{U_0}$

VELOCITY TIME CURVE AS CALCULATED BY STEP BY STEP METHOD
FROM EQUATIONS (I) AND (B) OF APPENDIX.

FIG 4

THE BODILY MOTION OF A SPHERE SUBJECTED TO THE PRESSURE PULSE FROM AN UNDERWATER EXPLOSION

E. N. Fox
Admiralty Undex Works, Rosyth, Scotland

THE BODILY MOTION OF A SPHERE SUBJECTED TO THE
PRESSURE PULSE FROM AN UNDERWATER EXPLOSION

E. N. Fox

February 1943

* c * * * * * * *

Summary.

(a)   The exact solution is given for the bodily motion of a rigid sphere subjected to an underwater pressure pulse on the assumptions that the pressure pulse can be treated as of small amplitude and that the bodily motion is small compared with the radius of the sphere.

(b)   The conclusion given by G.I. Taylor, that a sphere which is just buoyant does not reverse in motion if given an initial velocity, is not necessarily true for the motion produced by a pressure pulse in the water.   Quintitatively, however, the reverse motion in the latter case is of very small velocity compared to the forward motion.

(c)   Results of the analysis illustrate the equalisation of long pulses round the sphere and show that the impulsive effect of a positive pulse, even of short duration, can be subject eventually to appreciable diffraction.

(d)   In the cases of a large explosion (long pulse) at a large distance and of a small explosion (short pulse) at a near distance it is concluded that the major damage caused by the pressure pulse will in general be reasonably independent of whether the target is fixed or not.

Introduction.

In connection with the use of suspended targets or gauges in underwater explosion experiments it is sometimes desirable to obtain an estimate of the bodily motion due to the pressure pulse and for this purpose the solution for the case of a spherical target, which can be simply obtained theoretically, is of value.

The diffraction problem of a spherical wave striking a sphere, not necessarily fixed but of unyielding surface, is one capable of formal mathematical solution by assuming in addition to the incident wave an infinite series of wave-solutions of the form.

$$\sum_{j=0}^{\infty} r^j \left(\frac{\partial}{r\,\partial r}\right)^j \left\{\frac{f_j\,(ct-r)}{r}\right\} P_j\,(\cos\theta) \qquad\qquad (1)$$

where r, θ, are spherical-polar co-ordinates with centre of sphere as origin, t is time, c is wave velocity, j is integral, and P_j is Legendre's function of order j.

For the special case of a plane wave striking a fixed rigid sphere such formal mathematical solution was considered by the writer and A.J. Harris in connection with the diffraction of blast-waves in air.   It was then found that, while excessive algebra and numerical calculation would be necessary to evaluate the pressure at various points, the net force acting on the sphere could be simply obtained since it depended on only one term ($j = 1$) in the infinite series.

Since the only knowledge of pressure required to determine the bodily motion of the sphere when not fixed is the total net force on the sphere, the solution for such motion also depends only on the one term in the complete series solution and can be derived directly in the manner given below without recourse to the complete solution.

General solution.

Consider a sphere of radius a subjected to a pressure pulse from a point source distance x_0 from the centre of the sphere.   The pressure pulse will be assumed of small amplitude at the sphere so that the usual wave equation holds and it will also be assumed that the movement of the sphere is small compared with its radius.

The ......

The problem is one of axial symmetry and we take $r, \theta,$ to be the usual spherical-polar co-ordinates referred to the centre of the sphere as origin, the lines joining this origin to the point source being $\theta = 0$.

The pressure pulse diverging from the point source is taken to be

$$p = \frac{p_0 \, x_0}{r'} \; f\left\{ \frac{ct - r' + (x - 1) a}{a} \right\} \tag{2}$$

where r' is distance from the point source, c is wave velocity, p_0 is maximum pressure in pulse at the distance xa corresponding to centre of sphere, and t is time measured from the arrival of the incident wave at the nearest point of the sphere; the non-dimensional function f will thus be zero for negative values of its argument.

In Appendix A it is shown that the following relation holds at time t_1 for any solution p of the wave-equation,

$$\Sigma \iint \left[\begin{array}{c} \dfrac{1}{r} \dfrac{\partial r}{\partial n} \dfrac{\partial^2 p}{c^2 \partial t^2} + \dfrac{1}{r^2} \dfrac{\partial r}{\partial n} \dfrac{\partial p}{\partial t} \\[2mm] + \dfrac{1}{r} \dfrac{\partial^2 p}{c \partial n \partial t} + \dfrac{2p}{r^3} \dfrac{\partial r}{\partial n} + \dfrac{1}{r^2} \dfrac{\partial p}{\partial n} \end{array} \right]_{t=t_1 - r/c} \cos\theta \; dS$$

$$+ \; \Sigma \iint \left[\dfrac{1}{r} \dfrac{\partial p}{c \partial t} + \dfrac{p}{r^2} \right]_{t=t_1 - r/c} \sin\theta \dfrac{\partial \theta}{\partial n} \; dS = 0 \tag{3}$$

where the summation extends over all surfaces bounding the region within which the wave equation holds and n is the normal to the surface drawn into this region.

We apply equation (3) to the present problem by considering the region bounded externally by a sphere of very large radius $R \to \infty$ and internally by the sphere $r = a$ and a sphere of very small radius $\varepsilon \to 0$ surrounding the point source. The contribution to equation (3) from the large sphere becomes zero as $R \to \infty$ since for finite t_1 the integrand is then to be evaluated for negative time $(t_1 - R/c)$ prior to the setting up of the pressure pulse from the point source.

The contribution to equation (3) from the sphere $r = a$ comes solely from the first term, since $\partial\theta/\partial n = 0$, and is:-

$$2\pi a \int_0^\pi \left[\dfrac{\partial^2 p}{c^2 \partial t^2} + \dfrac{2}{a} \dfrac{\partial p}{c \partial t} + \dfrac{\partial^2 p}{c \partial n \partial t} + \dfrac{2p}{a^2} + \dfrac{1}{a} \dfrac{\partial p}{\partial r} \right]_{t=t_1 - a/c} \cos\theta \sin\theta \; d\theta \tag{4}$$

The contribution to equation (3) from the small sphere surrounding the point source will, as $\varepsilon \to 0$, arise solely from the terms in $1/\varepsilon^2$ due to the incident pressure pulse. Hence substituting from equation (2) in equation (3) and letting $\varepsilon \to 0$ we find for this final contribution,

$$- \frac{4\pi p_0}{a} \left[f'\left(\frac{ct_1 - a}{a} \right) + \frac{1}{x} \, f\left(\frac{ct_1 - a}{a} \right) \right] \tag{5}$$

Introducing the non-dimensional time T defined by

$$T = \frac{ct}{a} = \frac{ct_1 - a}{a}. \tag{6}$$

then from equations (3) (4) and (5) we obtain

$$\frac{2\pi}{a} \int_0^\pi \left[\dfrac{\partial^2 p}{\partial T^2} + 2 \dfrac{\partial p}{\partial T} + \dfrac{a}{c} \dfrac{\partial^2 p}{\partial T \partial r} + 2p + a \dfrac{\partial p}{\partial r} \right]_{r=a} \cos\theta \sin\theta \; d\theta$$

$$= \frac{4\pi p_0}{a} \left[f'(T) + \frac{1}{x} \, f(T) \right] \tag{7}$$

Now .....

Now if ϕ is the velocity potential and V is the velocity of the sphere away from the point source then, assuming movement of the sphere small with respect to its radius, we have as boundary condition at the surface of the sphere,

$$\frac{\partial \phi}{\partial r} = -V \cos \theta, \quad r = a \tag{8}$$

whence it follows that

$$\frac{\partial p}{\partial r} = -\rho \frac{\partial^2 \phi}{\partial r \partial t} = \rho \frac{c}{a} \frac{dV}{dT} \cos \theta, \quad r = a \tag{9}$$

Also if the total net force on the sphere in the direction away from the point source be denoted by P, then

$$P = 2 \pi a^2 \int_0^{\pi} p \cos \theta \sin \theta \, d\theta \tag{10}$$

Hence substituting from (9) and (10) in equation (7) we have after performing the integrations,

$$\frac{d^2 P}{dT^2} + 2 \frac{dP}{dT} + 2P + \frac{4 \pi \rho \, ca^2}{3} \left\{ \frac{d^2 V}{dT^2} + \frac{dV}{dT} \right\}$$

$$= 4 \pi \rho_0 a^2 \left\{ f'(T) + \frac{1}{\chi} f(T) \right\} \tag{11}$$

If the mass of the sphere be M then the equation of motion of the sphere is

$$M \frac{dV}{dt} = P \tag{12}$$

whence

$$\frac{dV}{dT} = \frac{Pa}{Mc} \tag{13}$$

From equations (11) and (13) the final equation determining P is thus,

$$\frac{d^2 P}{dT^2} + 2k \frac{dP}{dT} + 2K P = 4 \pi \rho_0 a^2 \left\{ f'(T) + \frac{1}{\chi} f(T) \right\} \tag{14}$$

where

$$2K = 2 + \frac{4 \pi a^3 \rho}{3 M} \tag{15}$$

For a given form of incident wave, equation (14) is a simple linear differential equation to determine P, whence the velocity V can be obtained from equation (13). The displacement s is then given by

$$s = \int_0^t V \, dt = \frac{a}{c} \int_0^T V \, dT \tag{16}$$

The initial conditions for P are given by

$$\left. \begin{array}{l} P = 0 \\[2mm] \frac{dP}{dT} = 4 \pi \rho_0 a^2 f(0) \end{array} \right\} \quad T \to 0 \tag{17}.$$

The first of these is an obvious physical requirement while the second corresponds to the physical condition of initial complete reflection at the element of the sphere's surface nearest the source.

It .....

It may be noted that the second term in the expression for $2k$ given in equation (15) is the ratio of the weight of displaced water to the weight of the sphere. In most underwater explosion experiments with submerged targets this ratio will be less than or equal to unity so that $2k$ will lie between the values 2 and 3 corresponding to the physical conditions.

$$2k = 2, \text{ infinitely heavy or fixed sphere}$$
$$2k = 3, \text{ buoyant sphere just waterborne}^{*} \qquad (18)$$

(* For brevity this case will be referred to as "buoyant sphere" in the remainder of the paper).

For $k \leqslant 2$, which includes the above range, the complementary function of the differential equation (16) is periodic and the formal solution of this equation subject to the initial conditions (17) is

$$\frac{p}{4 \pi a^2 \rho_0} = \frac{f(0)}{m} e^{-kT} \sin mT$$

$$+ \frac{1}{m} \int_0^T e^{-k(T-\lambda)} \sin m (T-\lambda) \left\{ f'(\lambda) + \frac{f(\lambda)}{k} \right\} d\lambda \qquad (19)$$

where

$$m = \sqrt{2k - k^2} \qquad (20)$$

For the particular cases of fixed and buoyant sphere the values of k and m are thus

$$\left. \begin{array}{l} k = 1, \quad m = 1, \quad \text{fixed sphere} \\ k = 3/2, \quad m = \sqrt{3}/2 \quad \text{buoyant sphere} \end{array} \right\} \qquad (21)$$

Solution for exponential pressure pulse.

When the incident pressure pulse is exponential in form we have

$$f(T) = e^{-qT} \qquad (22)$$

and the general solution (19) is easily integrated to give

$$\frac{p}{4 \pi a^2 \rho_0} = \frac{1 - \theta (q - k)}{m} e^{-kT} \sin mT$$

$$+ \theta (e^{-kT} \cos mT - e^{-qT}) \qquad (23)$$

where

$$\theta = \frac{qk - 1}{k (q^2 - 2kq + 2k)} \qquad (24)$$

From equation (13) the velocity of the sphere is then given by

$$\frac{V}{6 (k-1) v_0} = \frac{\theta (2 + q - 2k) - 1}{2m} e^{-kT} \sin mT$$

$$+ \frac{\theta}{q} (e^{-qT} - e^{-kT} \cos mT)$$

$$+ \frac{1}{2 kq k} (1 - e^{-kT} \cos mT) \qquad (25)$$

where, if ρ denotes the mass density of the medium,

$$v_0 = \frac{p_0}{\rho c} \qquad (26)$$

The ......

The displacement of the sphere is then, from equation (14), given by,

$$\frac{s}{6\,(k-1)\,s_0} = \frac{8\,k\,X\,(2k-2-q)+k-1}{2\,k\,m\,X}\;e^{-kT}\;\sin m\,T$$

$$+\;\frac{8}{q}\;(e^{-kT}\cos m\,T - e^{-qT})$$

$$+\;\frac{q\,X-1-q}{2k\,qX}\;(1 - e^{-kT}\cos m\,T)$$

$$+\;\frac{T}{2\,k\,X} \tag{27}$$

where

$$s_0 = \frac{a\,v_0}{qc} = \frac{a\,p_0}{\rho\,qc^2} \tag{28}$$

The unbalanced impulse A, defined by

$$A = \int_0^t P\,dt \tag{29}$$

can be simply obtained from equation (29) by virtue of the relation

$$\frac{A}{A_1} = \frac{2q\,V}{3\,(k-1)\,v_0} \tag{30}$$

where

$$A_1 = \frac{\pi\,p_0\,a^3}{cq} \tag{31}$$

The total impulse A_1 directly incident on the sphere can be obtained from equations (4), (10) and (29) which give,

$$\frac{A_1}{A_1} = \frac{2}{3X}\left\{1 - X^3 + (X^2+2)\sqrt{X^2-1}\;\right\} \tag{32}$$

For a plane incident wave $(X \to \infty)$ we note that $A_1 = A_1$, while p_0, v_0 and s_0 are the maximum pressure, velocity and displacement in the incident wave.

The preceding equations enable the motion of the sphere to be calculated for any special case. For the purpose of obtaining qualitative conclusions the solutions for the limiting cases of incident pulses long and short relative to the diameter of the sphere will now be given.

(1) Short pulses.

For short pulses, i.e. pulses in which the pressure becomes negligible in a time small compared with the time taken by the pulse to travel past the sphere, the value of q is large and retaining only the predominant items the preceding equations become,

$$\frac{P}{4\pi a^2 p_0} = \frac{1-k\,X}{m\,k\,q}\;e^{-kT}\;\sin m\,T + \frac{e^{-kT}\cos m\,T - e^{-qT}}{q} \tag{33}$$

$$\frac{A}{4\,q\,A_1} = \frac{V}{6\,(k-1)\,v_0} = \frac{2\,X-1}{2\,X\,mq}\;e^{-kT}\;\sin m\,T + \frac{1-e^{-kT}\cos m\,T}{2\,X\,kq} \tag{34}$$

$$\frac{s}{6\,(k-1)\,s_0} = \frac{k-1-kX}{2mkX}\;e^{-kT}\;\sin m\,T + \frac{(k-1)(1-e^{-kT}\cos m\,T)}{2\,k\,X} + \frac{T}{2kX} \tag{35}$$

(2) long pulses.

For long pulses where q is small we shall give the simplified asymptotic forms on the additional assumption that X is large since, as discussed later, the present analysis is not of practical application to underwater explosions when qX is smaller than order unity. On these

assumptions ......

assumptions we find for the predominant terms,

$$\frac{P}{4 \pi a^2 p_0} = \frac{1}{m} e^{-kT} \sin m T \tag{56}$$

$$\frac{A}{a q A_1} = \frac{v}{6 (k-1) v_0} = \frac{1 - e^{-qT}}{2 X kq} - \frac{1}{2m} e^{-kT} \cos m T$$

$$+ \frac{1}{2k} (e^{-qT} - e^{-kT} \cos m T) \tag{57}$$

$$\frac{s}{6 (k-1) s_0} = \frac{q (k-1)}{2mk} e^{-kT} \sin m T + \frac{(q X-1)(1 - e^{-qT})}{2X kq}$$

$$- \frac{q}{2k} (1 - e^{-kT} \cos m T) + \frac{T}{2kX} \tag{58}$$

Discussion of results.

(1)   Applicability of underwater explosions.

Considering the first fundamental assumption of the analysis that the incident pulse can be treated as of small amplitude it was shown in Appendix 1 of the report "The reflection of a spherical wave from an infinite plate" that this is reasonably accurate for distances D such that q D's ≥ 4 about. Thus the pulse can be regarded as of small amplitude even at the nearest point of the sphere if q (X — 1) ≥ 4, and beyond such a distance, corresponding to about 13 charge diameters, the analysis might be expected to give reasonably accurate predictions.   At somewhat closer distances the analysis begins to lose in accuracy but as a first approximation it may still be able to give the order of magnitude of bodily velocity in so far as this is due to the pressure pulse.   Thus from the results given by Penney, we see that at a radius of three charge diameters the maximum pressure is some 80% greater than would be expected if the pressure had continued to increase inversely as the distance when approaching the explosion.   Thus at three charge diameters corresponding to about q (X — 1) = 1.8 the present analysis is likely to be accurate within a factor of two and it can thus be used for these closer distances in cases where it is only desired to know order of magnitude, e.g. whether the bodily velocity is small or large.

The second fundamental assumption of the analysis is that the movement of the sphere is small with respect to its radius and for any particular case this is most easily checked a posteriori by using the present analysis to estimate the displacement.   In this connection it should be noted that while the assumed exponential form is a reasonable representation of an underwater explosion pressure pulse until the pressure becomes small it is not representative of the subsequent stages during which incompressible flow (kinetic wave) effects are of equal or greater relative importance.   In particular, the last term of equation (27), corresponding as it does to an afterflow effect, must be considered as limited by the condition that q T is not too large when estimating the displacement due to the pressure pulse.

(2)   Direction of motion and diffraction effects.

G.I. Taylor has shown in a previous paper that a sphere which is just buoyant never reverses in motion when given an initial velocity.   A similar conclusion is not necessarily true for the motion produced by an underwater pressure pulse.   Thus, for the case of a short pulse from a distant source (X → ∞) we see from equation (56) that the velocity of the sphere dies away as a damped sine wave and thus becomes negative for certain periods; for this case, taking k = 3/2, it should be noted, however, that the maximum negative velocity is only .0043 times the maximum positive velocity so that quantitatively the reverse motion is relatively unimportant.

Some features of the reflection and diffraction of the incident wave by the sphere can be illustrated by considering the maximum unbalanced impulse acting on the sphere as tabulated for certain cases in Table 1.

Table 1 .....

<div align="center">TABLE 1.</div>

| | X | Maximum A/A_i | | Ratio $\frac{(a)}{(b)}$ | Maximum $\frac{If - Ib}{I}$ |
		(a) Fixed Sphere $k = 1$	(b) Buoyant Sphere $k = 1.5$		
Long Pulses	cu	2.09q	1.38q	1.56	--
Short Pulses	∞	1.29	.95	1.59	.175
	2	1.54	1.05	1.48	.122
	1.5	3.62	1.22	1.50	.091
	1.0	∞	∞	1.56	0

For a long pulse (q small) from a distant source we see from Table 1 that the maximum unbalanced impulse is small compared with the total incident impulse; physically, this is due to equalisation of pressure round the sphere when the pressure is maintained for a time long compared with that taken by a pressure wave to travel round the sphere.

For a short pulse from a distant source, however, the maximum unbalanced impulse is of the same order of magnitude as the incident impulse, corresponding in the case of a fixed sphere to an overall reflection factor of 1.29. A point specially worthy of notice, which is seen from equation (5a) with $X \to \infty$, is that the unbalanced impulse tends to zero with increasing time showing that, however short the pulse, its impulsive effect is eventually diffracted behind the sphere.

A similar effect is responsible for the fact shown by Table 1 that for short pulses from close sources $(X = 1)$ the maximum unbalanced impulse is much greater than the directly incident impulse. In such cases the major contribution to the maximum unbalanced impulse comes from diffraction of the incident pulse on to the part of the front of the sphere which is in the shadow and not from the small portion subjected directly to the incident pulse.

It should be noted that the values for $X = 1$ have been given in Table 1 to show the limits for small values of $X - 1$; such small values are possible for large q without invalidating the conditions discussed in paragraph (1) above.

(3)   Effect of fixing.

In view of present interest in the possible difference in damage sustained by a fixed and a suspended target, it is of value to see what evidence can be obtained from the present analysis comparing the two cases of $k = 1$ (fixed) and $k = 3/2$ (buoyant).

Comparing on the basis of unbalanced impulse it is seen from Table 1 that this is from 1/3 to 1/2 greater when the sphere is fixed. For long pulses from distant sources, however, the unbalanced impulse is small relative to the incident pulse whether the sphere be fixed or buoyant. Thus in this case, corresponding to a relatively large explosion at a large distance the main effect of the pressure pulse is a uniform impulse on fixed sphere which is large compared with any local increase, due to fixing, of the unbalanced impulse.

For short pulses from distant explosions, however, the unbalanced impulse is of the same order as the incident impulse and the possibility of appreciable effect of fixing cannot be dismissed on the present analysis.

The same is at first sight true of short pulses from near explosions but, on the other hand, in practical examples of this type the damaging effect tends to be concentrated in intensity over the portion of target close to the explosion.

In order to consider the effect of fixing on this near portion it is necessary to note that the complete solutions, of form equation (2), for the two cases of fixed and buoyant sphere differ only in the second term $j = 1$ which is also the term responsible for the total net force and the

<div align="right">unbalanced .....</div>

unbalanced impulse.   In view of this it is really shown that

$$i_f - i_b = \frac{3(A_f - A_b)}{4\pi a^2}$$ (39)

where the suffixes f and b denote fixed and buoyant sphere respectively, i is the impulse/unit area at the point of the sphere nearest the source while A as before is the unbalanced impulse.

Now for very short pulses the maximum value of i_f, which occurs initially and will be denoted by i', is approximately twice the incident impulse/unit area, whence

$$i' = \frac{2 \times A_1}{(x-1)\pi a^2}$$ (40)

From equations (39) and (40) we thus have

$$\frac{i_f - i_b}{i'} = \frac{3(x-1)}{8x} \frac{A_f - A_b}{A_1}$$ (41)

The maximum value of this expression is also tabulated in Table 1 and we see that for close small explosions it is small rising to order 17% for distance short pulses.

The present analysis is based on the assumption that the surface of the sphere is of itself rigid.   Any yielding of the front surface will, however, tend to lessen the bodily motion and where conclusions for any unyielding sphere indicate little effect of such motion they are not likely to be invalidated by yielding.

We can therefore still conclude, in the two cases of (i) large explosion (long pulse) at large distance and (ii) small explosion (short pulse) at near distance, that fixing has little effect on the impulse acting locally on the surface, this conclusion being limited in the second case to the part of the sphere near the explosion where in practice the major damage will generally occur.

The preceding conclusions regarding little effect of fixing on the magnitude of locally applied impulse can probably in most cases be interpreted as applying also to magnitude of resultant damage since this agrees with such experimental data on fixing as are available.

For any particular example it is probably best to check such interpretation by using the present analysis to estimate the maximum bodily velocity given to an equivalent buoyant sphere and compare with the maximum velocity given to local areas of the surface on assumptions such as that of the report "The pressure and impulse of submarine explosion waves on plates".   A numerical example of such comparison is given in Appendix B.

Appendix A.....

APPENDIX A.

The proof of the relation given in equation (3) follows analogous lines to the proof of Kirchoff's general solution of the wave equation given by Jeans, "The Mathematical Theory of Electricity and Magnetism", 4th Edition, paragraph 580, pages 522-524. Equation (543) of Jeans, with slightly changed notation, is

$$- \Sigma \int_{-t'}^{t''} dt \iint \left[\rho \, \frac{\partial G}{\partial n} - G \, \frac{\partial \rho}{\partial n} \right] dS$$

$$= \frac{1}{c^2} \left[\iiint \left[\rho \, \frac{\partial G}{\partial t} - G \, \frac{\partial \rho}{\partial t} \right] dx \, dy \, dz \right]_{-t'}^{t''} \tag{A1}$$

where ρ and G are any two solutions of the wave-equation, the summation is taken over all the surfaces bounding the region of the volume integral and in which the wave-equation holds, n is the normal to the surface drawn into this region and t'' and $-t'$ are positive and negative times respectively.

Since G can be any solution of the wave-equation we take it to be

$$G = \left[\frac{F'(ct+r)}{r} - \frac{F(ct+r)}{r^2} \right] \cos\theta \tag{A2}$$

whence

$$\rho \, \frac{\partial G}{\partial n} \quad G \, \frac{\partial \rho}{\partial n} = \frac{\rho}{r} \, \frac{\partial r}{\partial n} \, F''(ct+r) \, \cos\theta$$

$$- \left[\frac{\rho}{r} \frac{\partial r}{\partial n} + \frac{1}{r} \frac{\partial \rho}{\partial n} \right] F'(ct+r) \cos\theta$$

$$- \frac{\rho}{r} \frac{\partial \phi}{\partial n} F'(ct+r) \sin\theta$$

$$+ \left[\frac{\partial r}{\partial n} + \frac{1}{r^2} \frac{\partial \rho}{\partial n} \right] F(ct+r) \cos\theta$$

$$+ \frac{\rho}{r^2} \frac{\partial \phi}{\partial n} F(ct+r) \sin\theta \tag{A3}$$

Integrating the first three terms of (A3) by parts, we obtain,

$$\frac{1}{r} \frac{\partial r}{\partial n} \cos\theta \int_{-t'}^{t''} \rho F''(ct+r) \, dt = \frac{\partial r}{cr \, \partial n} \cos\theta \left[\rho F'(ct+r) - \frac{\partial \rho}{c \, \partial t} F(ct+r) \right]_{-t'}^{t''}$$

$$+ \frac{\partial r}{r \, \partial n} \cos\theta \int_{-t'}^{t''} \frac{\partial^2 \rho}{c^2 \, \partial t^2} F(ct+r) \, dt \tag{A4}$$

$$- \frac{\cos\theta}{r} \int_{-t'}^{t''} \left\{ \frac{2\rho}{r} \frac{\partial r}{\partial n} + \frac{\partial \rho}{\partial n} \right\} F'(ct+r) \, dt = - \frac{\cos\theta}{cr} \left[\frac{2\rho}{r} \frac{\partial r}{\partial n} + \frac{\partial \rho}{\partial n} F(ct+r) \right]_{-t'}^{t''}$$

$$+ \frac{\cos\theta}{cr} \int_{-t'}^{t''} \left\{ \frac{2}{r} \frac{\partial r}{\partial n} \frac{\partial \rho}{\partial t} + \frac{\partial^2 \rho}{\partial n \, \partial t} \right\} F(ct+r) \, dt \tag{A5}$$

$$\frac{\sin\theta}{r} \ \ldots$$

$$-\frac{\sin\theta}{r}\frac{\partial\theta}{\partial n}\int_{-t'}^{t''} \rho\, F'(ct+r)\, dt \;=\; -\frac{\sin\theta}{cr}\frac{\partial\theta}{\partial n}\left[\rho\, F(ct+r)\right]_{-t'}^{t''}$$

$$+\;\frac{\sin\theta}{cr}\frac{\partial\theta}{\partial n}\int_{-t'}^{t''}\frac{\partial\rho}{\partial t}\,F(ct+r)\,dt \tag{A6}$$

As Jeans, we now take F, which is as yet an arbitrary function, to be such that it and all its derivatives vanish except for zero argument, for which particular value F becomes infinite in such a way that its integral is unity. We also take t' sufficiently large so that, for all values of r considered, the value of r − ct' is negative, and we note that since t'' is positive, the value of r + ct'' is always positive. With these assumptions it is then seen firstly that the right-hand side of (A1) is zero at both limits and secondly that the integrated parts of (A4) (A5) and (A6) also vanish at both limits thus contributing nothing to the left-hand side of (A7). Finally the integrals on the right-hand sides of (A4), (A5) and (A6) and also the similar integrals of the last two terms in (A3) contribute to (A1) merely two values, at time t = − r/c, of the factors multiplying F(ct + r).

Collecting these terms together we then have

$$\sum\iint\left[\begin{array}{l}\dfrac{1}{r}\dfrac{\partial r}{\partial n}\dfrac{\partial^2\rho}{c^2\partial t^2} + \dfrac{3}{r^2}\dfrac{\partial r}{\partial n}\dfrac{\partial\rho}{c\,\partial t} \\[2mm] +\; \dfrac{1}{r}\dfrac{\partial^2\rho}{c\,\partial n\,\partial t} + \dfrac{2\rho}{r^3}\dfrac{\partial r}{\partial n} + \dfrac{1}{r^2}\dfrac{\partial\rho}{\partial n}\end{array}\right]_{t=-r/c}\cos\theta\, dS$$

$$+\;\sum\iint\left[\frac{1}{r}\frac{\partial\rho}{c\,\partial t} + \frac{\rho}{r^2}\right]_{t=-r/c}\sin\theta\,\frac{\partial\theta}{\partial n}\,dS = 0 \tag{A7}$$

Since the zero of time is arbitrary we have only to replace t = − r/c by t = t' − r/c to obtain equation (3) of the main paper.

Appendix B .....

§IX B.

As a numerical example of the relative effect of fixing a target let us consider a sphere of radius 5 feet subjected to the pressure pulse from a charge of 5 lbs. T.N.T. with its centre of gravity at 15 inches from the nearest point of the sphere. This case has been chosen as simulating the case of a half-scale Cylindrical target for which no difference in damage was found whether the target was suspended or resting on the bottom. The sphere has been chosen to have approximately the same volume as the Cylindrical target and we assume it just waterborne. The numerical values of constants for this case are then

$$x = 1.25 \qquad k = 3/2$$
$$q = 5 \qquad a = \sqrt{3}/2 \qquad (81)$$

and since $q (x - 1) = 1.25$ it should be noted that the case is one of a relatively close explosion where the present analysis, while it cannot give an accurate estimate, should give the correct order of maximum bodily velocity.

Using the values for sea-water of

$$\mu_0 = 64 \text{ lbs./cubic feet}$$
$$c = 4900 \text{ feet/second} \qquad (82)$$

and the experimental relation for T.N.T.,

$$p_0 = \frac{7 \, W^{1/3}}{D} \text{ tons/square inch} \qquad (83)$$

where W is weight of charge in lbs. and D is distance in feet we find, since D = 5,

$$v_0 = 63 \text{ feet/second} \qquad (84)$$

Using the values given by (81) and (84) we then find by using equation (25) that the maximum bodily velocity is

$$V_{max} = .20 \, v_0 = 12.6 \text{ feet/second} \qquad (85)$$

It may be noted that the bodily displacement of the sphere, as given by equation (27), during the time in which the pressure pulse communicates such a velocity is .15 inches which easily satisfies the assumption of the analysis that it is small relative to the radius (5 feet) of the sphere.

Thus, if the Cylindrical target had been strong enough to withstand the explosion without dishing, we should have expected the pressure pulse to give it a maximum bodily velocity of order 13 feet/second while in the presence of dishing the maximum velocity would tend if anything to be of lower order.

In order to consider whether a bodily velocity of this order is likely to affect the damage we note that the major damage was fairly concentrated near the charge and we then calculate the velocity given initially to the plating nearest the charge by using the results in the report "The pressure and impulse of submarine explosion waves on plates", assuming the plating leaves the water; for plating 0.45 inches thick we then obtain a plating velocity of 360 feet/second.

The energy communicated by the pressure pulse is thus mainly concentrated in the form of high plate velocity, of order 300 feet/second maximum, over the near portion of the target while on the other hand the total communicated impulse will only produce a bodily velocity of order 13 feet/second.

Owing to the concentrated nature of the blow there seems little possibility of the conditions on the back half of the target, i.e. whether fixed or opposed purely by its own and water inertia, being of any importance until after most of the energy has already been absorbed by dishing at the front of the target.

This conclusion is in agreement with the experimental results of which it is not, of course, a full explanation since the kinetic wave and pulsating gas bubble effects have not been considered but it seems probable that those effects, if of any importance, were also too concentrated to be affected by conditions on the back of the target.

APPENDIX C

Calculations for a buoyant sphere

Numerical calculations of velocity have been carried out for the case of a sphere which is just buoyant, i.e. of mean density equal to the density of the water.

From equation (21), $k = 3/2$, $m = \sqrt{3/2}$ for a buoyant sphere and inserting these values in equation (28) the non-dimensional ratio V/v_0 can be calculated as a function of the non-dimensional time T for given pairs of values of the parameters q and qX. If we use the term "pulse-length" as applied to an exponential pulse to mean the distance a/q the pulse has travelled while the pressure at any point decays in ratio $1/e$, then the parameter q is the ratio of sphere radius to "pulse-length". Similarly qX is the ratio of distance Xa, between pulse centre and sphere centre, to the "pulse-length".

The general shape of the velocity-time curves is similar for all cases calculated and a typical set is shown in Figure 1 corresponding to the limiting case $qX \to \infty$, i.e. a plane incident pulse.

Denoting the maximum bodily velocity by V_m, values of the ratio V_m/v_0 are given in Table 2, and in brackets in the same table we give values of T at which these maximum velocities occur. Thence the mean acceleration up to maximum velocity can be evaluated if desired.

TABLE 2.

Values of V_m/v_0 and (in brackets) of T at time of maximum velocity.

q/qX	2	5	10	20	∞
0.1	0.913 (2.7)	0.869 (2.5)	0.856 (2.5)	0.849 (2.4)	0.849 (2.4)
0.2	0.853 (2.5)	0.785 (2.2)	0.764 (2.1)	0.754 (2.1)	0.745 (2.1)
0.5	0.737 (2.2)	0.627 (1.8)	0.595 (1.7)	0.580 (1.7)	0.446 (1.7)
1.0	0.636 (2.0)	0.487 (1.6)	0.448 (1.5)	0.430 (1.4)	0.413 (1.4)
2.0	—	0.354 (1.4)	0.308 (1.2)	0.288 (1.2)	0.269 (1.1)
5.0	—	0.233 (1.5)	0.170 (1.1)	0.149 (0.95)	0.131 (0.85)

Intervals in T of 0.1 for $0 \leq T \leq 1$ and 0.2 for $1 < T \leq 3$ were used and the values of V_m/v_0 in Table 2 are correct to an error of one or two in the third digit whilst the values of T at $V = V_m$ are correct to about one quarter of an interval, i.e. to 0.05 for $T > 1$ and 0.025 for $T < 1$. Further sub-division of interval would have been necessary to obtain reasonably accurate values of maximum acceleration from the velocity calculations and this was not attempted. Graphical estimates were, however, obtained from the maximum slopes of curves such as those in Figure 1 and these indicated that the maximum acceleration varied between about 1.6 to 2.1 times the mean acceleration up to time of maximum velocity. Approximate estimates of maximum acceleration, correct to order 20% or less, can therefore be obtained by using Table 2 to derive mean acceleration and then multiplying by a factor 1.8. Accurate estimates for any particular case are best obtained by use of equation (23) which gives the net force on sphere at any time.

For short pulses $q \to \infty$, the ratio $V_m/v_0 \to 0$ but the product qV_m/v_0 remains finite and is given in Table 3, the values in which are correct to the third decimal place.

*Values of $q V_m/v_0$ for limiting case of
very short pulses $\alpha = \infty$*

$\frac{a}{X}$	0	0.161	0.300	0.423	0.534	0.636	0.732	0.824	0.913	1
$\frac{q V_m}{v_0}$	0.700	0.834	0.966	1.096	1.223	1.349	1.475	1.601	1.730	1.859

For application to the pressure pulse from an underwater explosion the calculations are subject of course to the limitations discussed in the main paper. In particular the entry for $qX = 5$, $q = 5$ in Table 2 corresponds to a contact explosion and is given only for interpolation purposes. A similar remark applies to the entry for $X = 1$ in Table 3.

Floating hemisphere subject to a pressure pulse from vertically below.

It may be noted that the analysis for the sphere can be applied also to the case of a hemisphere floating with diametral plane in the surface of the water and subjected to a pulse arriving vertically from below, i.e. the pulse centre is vertically below the sphere centre. In effect we have only to reflect this problem in the surface of the water and change the sign of the image pulse to see that it is equivalent to the problem of a buoyant sphere in an infinite liquid subjected to equal positive and negative pulses with centres diametrically opposite at equal distance from the sphere. Since the positive and negative pulses give equal contributions to the bodily motion of the sphere and reinforce one another the motion is similar to that due to the single positive pulse but of double magnitude.

Thus the results of Tables 2 and 3 can be immediately applied to the hemisphere problem by simply doubling the entries for V_m/v_0.

Figure 1. VELOCITY-TIME CURVES FOR PLANE PULSE
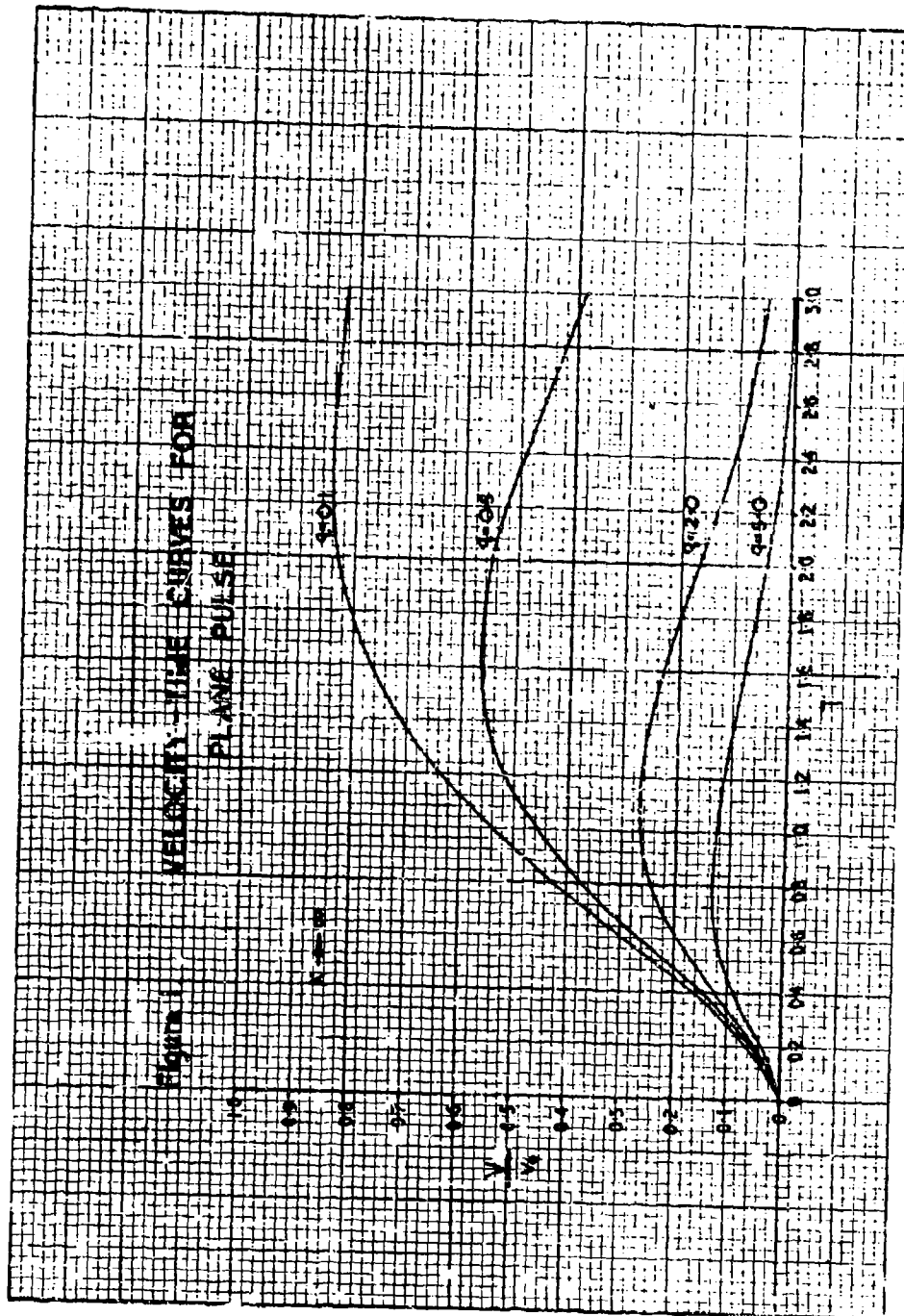
SUMMARY OF FORMULAE RELEVANT TO REFLECTION OF EXPLOSION PULSES
FROM A PISTON IN AN INFINITE FIXED WALL

E. N. Fox
Admiralty Undex Works, Rosyth, Scotland

British Contribution

March 1943

SUMMARY OF FORMULAE RELEVANT TO REFLECTION OF EXPLOSION PULSES FROM A PISTON IN AN INFINITE FIXED WALL

E. N. Fox

Admiralty Undex Works

March 1943

* * * * * * * *

A.1. **Compressible flow.**

The infinite wall is taken as the plene $x = o$, and all sources of pulses as lying to the right of this plane $(x > o)$, the total pressure in the incident pulse arriving at time t at any point on the plane $x = o$ being denoted by p_i.

From Kirchoff's general solution of the wave equation, the pressure p at time t at any point of the plane $x = o$ satisfies the equation

$$p = 2 p_i - \frac{1}{2\pi} \int\int \frac{1}{r} \left(\frac{\partial p}{\partial x}\right)_{t - \frac{r}{c}} dS \qquad (1)$$

where the surface integral is taken over $x = o$.

For a piston in an infinite rigid wall let

    ρ = mass density of water
    c = wave velocity
    S = area of piston
    s = perimeter of piston
    a = mass/unit area of piston
    U = velocity of piston away from sources
    ξ = displacement of piston away from sources
    $\xi_1 = \int_o^t \xi \, dt$

The boundary condition at $x = o$ is then

$$\frac{\partial p}{\partial x} = \rho \frac{dU}{dt} \quad \text{over } S$$

$$= o \quad \text{over rest of } x = o \qquad (2)$$

It is then merely a question of algebra and integration to derive the following formulae.

(a) Pressure at any point P within S is

$$p = 2 p_i - \rho c \, U(t) - \frac{\rho c}{2\pi} \oint \frac{U (t - \frac{r}{c}) \cos \nu}{r} \, ds \qquad (3)$$

where the line integral is taken round the perimeter s, r is the distance of p from any point of the perimeter and ν is the angle between the radius vector r and the inward normal to s (Figure 1).

(b) Pressure at any point Q on the wall outside the piston is

$$p = 2 p_i - \frac{\rho c}{2\pi} \oint \frac{U (t - \frac{r}{c}) \cos \nu}{r} \, ds \qquad (4)$$

with notation as before (Figure 1).

(c) .....

(c) Using bars to denote average values taken over the piston at any time, the mean pressure on the piston is

$$\bar{p} = 2\bar{p}_i - \rho c\, u(t) + \frac{\rho c^2\, s\, \dot{\xi}(t)}{\pi\, s}$$

$$- \frac{\rho c^2}{2\pi s} \oint ds_1 \oint \frac{\dot{\xi}\left(t - \frac{r}{c}\right) \cos\lambda_1 \cos\lambda_2}{r}\, ds_2 \tag{5}$$

where both line integrals are taken round s, r is the distance between ds_1 and ds_2, while λ_1 and λ_2 are the angles between the chord r and the inward normals to s at ds_1 and ds_2 respectively (Figure 2).

(d) For a circular piston of radius a equation (5) reduces to

$$\bar{p} = 2\bar{p}_i - \rho c\, u(t) + \frac{a\,\rho c}{\pi} \int_0^{\pi/2} u\left(t - \frac{2a \sin\theta}{c}\right) \cos^2\theta\, d\theta \tag{6}$$

the last two terms of which represent the relief pressure as given by Butterworth in equation (1) of the Appendix of the report "Note on the motion of a finite plate due to an underwater explosion".

(e) For a rectangular piston of sides 2a and 2b and diameter 2l, equation (5) gives

$$\bar{p} = 2\bar{p}_i - \rho c\, u(t) + \frac{\rho c^2 (a + b)}{\pi\, ab}\, \xi(t)$$

$$- \frac{\rho c^3}{2\pi\, ab} \left\{ \xi_1(t) - \xi_1\left(t - \frac{2a}{c}\right) - \xi_1\left(t - \frac{2b}{c}\right) + \xi_1\left(t - \frac{2l}{c}\right) \right\}$$

$$- \frac{\rho c^2}{\pi\, b} \int_0^{\tan^{-1}a/b} \dot{\xi}\left(t - \frac{2b \sec\theta}{c}\right) \cos\theta\, d\theta \tag{7}$$

$$- \frac{\rho c^2}{\pi\, a} \int_0^{\tan^{-1}b/a} \dot{\xi}\left(t - \frac{2a \sec\theta}{c}\right) \cos\theta\, d\theta$$

(f) If the piston is subject to an elastic restoring force the equation of motion is of form

$$m\frac{d^2\xi}{dt^2} + k\xi = \bar{p} \tag{8}$$

For a circular piston equations (6) and (8) give an integro-differential equation which can be solved step by step as in the report "Note on the motion of a finite plate due to an underwater explosion".

For a rectangular piston equations (6) and (8) involve the solution of ordinary linear differential equations with constant coefficients, but such solution would have to be carried out for successive intervals of time such as

$$0 \leqslant t \leqslant 2a/c, \quad 2a/c \leqslant t \leqslant 2b/c$$

depending on the relative magnitudes of a and b.

A.2. Incompressible flow.

The corresponding formulae for incompressible flow are obtained simply by letting $c \to \infty$ in the preceding equations.

For a circular piston subject to no elastic resistance equations (6) and (8) give

$$m\frac{du}{dt} = 2\bar{p}_i - \frac{8\rho a}{3\pi}\frac{du}{dt} \tag{9}$$

For .....

for a point source, at distance $\frac{x}{2}$ on the axis of the piston, emitting a wave of exponential form, $p_1 = p_0 e^{-nt}$ at centre of piston, the kinetic energy Ω_0 communicated finally to the piston is then given by

$$\frac{\Omega_0}{\Omega_1} = \frac{3\pi}{1 + \sin\theta} \left(\frac{x}{4a}\right) \frac{1}{1 + \frac{3\pi n}{8pa}} \tag{10}$$

where $\tan\theta = \frac{x}{a}$ $\tag{11}$

and Ω_1, the energy in the wave (neglecting afterflow contribution) directly incident on the piston is given by

$$\Omega_1 = \frac{\pi x^2 p_0^2 (1 - \sin\theta)}{\rho c n} \tag{12}$$

Equation (10) is the spherical wave analogue of Butterworth's equation (24) of report "note on the motion of a finite plate due to an underwater explosion" to which it reduces when $x \to \infty$ provided I in Butterworth's equation be correctly interpreted as twice the incident impulse.

A.3. Surface effect.

The effect of a free surface above the piston at right angles to the rigid wall which is then semi-infinite can be taken into account by the method of images. The problem then becomes that of an infinite wall containing two similar pistons subjected to the waves from positive and negative sources symmetrically situated with respect to the pistons. For a rectangular piston an equation similar to equation (7) but much more lengthy can be obtained in this way to allow for effect of surface, but in view of possible cavitation (see paragraph A.4) exact calculation of surface effect is of doubtful use.

For incompressible flow the energy communicated finally to a circular piston of radius a with centre at depth H below the surface can be expressed as $\alpha\Omega_0$ where Ω_0 is given by equation (10) and α is given approximately by

$$\alpha = \frac{(1 - \cos\psi)^2}{1 - \frac{3\pi a}{32 H \left(1 + \frac{3\pi n}{8pa}\right)}} \tag{13}$$

where $\tan\psi = \frac{2H}{x}$ $\tag{13}$

In equation (13) the denominator represents the effect of the "image piston" to the first order in a/H, while the numerator gives the effect of the "image source", the ratio of the mean incident pressures from the source and its image being taken approximately as the ratio of the incident pressures at the centre.

A.4. Effect of cavitation.

The preceding equations are all based on the assumption that no cavitation occurs, i.e. that tensions can be developed up to any required magnitude between the motor and the piston and in the water itself. A complete quantitative account of the effect of any cavitation seems unobtainable at present but two qualitative points seem worth mentioning.

Firstly, cavitation at or near the piston can be caused by the piston tending to move faster than the water at certain stages of the motion. The point to be noted in this case, neglecting surface effect considered later, is that after such cavitation the water will still be following up the piston and can thus communicate further energy if and when it catches up the piston. It is thus by no means certain that such cavitation will imply a drastic reduction in the energy communicated finally to the piston.

Secondly .....

224   - 4 -

Secondly, the tensile wave reflected from the free water surface will imply physically that
the water near the piston is being pulled away from the latter by the water near the surface.   If,
therefore, cavitation occurs due to this tensile wave, the water on the surface side of such
cavitation ceases to exert any pull on the water near the piston and the latter water will thus
more easily move in the direction of the piston.   Expressed otherwise the assumption of no
cavitation used in deriving equation (13) for α may imply quite large net tensions in the water
near the piston and it is difficult to see how such tensions can arrive near the piston since
they will probably have caused prior cavitation in the water near the surface.   It would therefore
seem that neglect of cavitation in calculating α as in equation (13) will imply if anything an
overcorrection for surface effect.
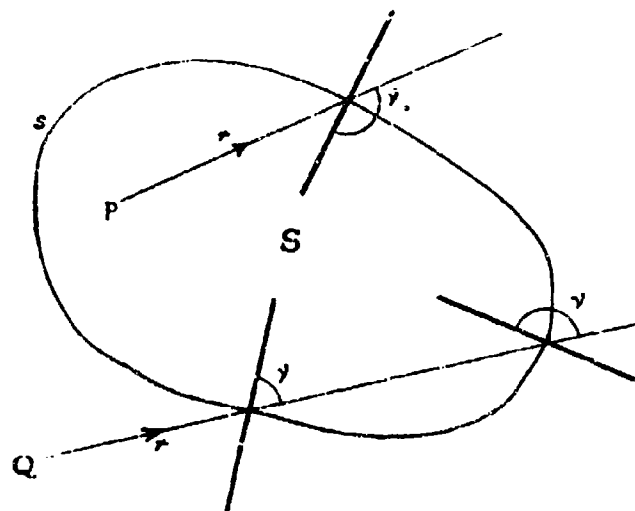
Figure 1.
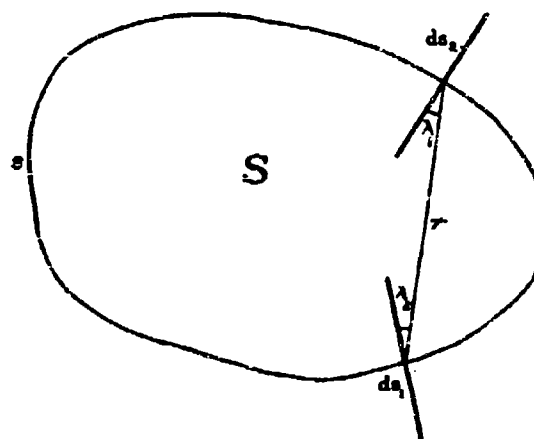
Figure 2.

EXPLOSIVE LOAD ON UNDERWATER STRUCTURES
AS MODIFIED BY BULK CAVITATION

E. H. Kennard
David W. Taylor Model Basin

American Contribution

May 1943

NOTATION

c speed of sound in water

g acceleration due to gravity

L a convenient linear dimension

m mass per unit area of a plate

n distance from a surface along its normal

p pressure

p_b breaking-pressure, at which cavitation occurs

p_c cavity pressure or pressure in cavitated region

p_h hydrostatic pressure

p , p'' pressure in incident and reflected wave-trains, respectively

p_0 see Equation [12] on page 12

q see Equation [16] on page 13

v particle velocity

v_x, v_y, v_z cartesian components of v

v_b particle velocity just ahead of a breaking-front, reckoned as positive away from the front

v_{bn} component of v_b normal to the boundary

v_c particle velocity in a cavitated region, reckoned as positive toward a breaking-front but away from other boundaries

v_{cn} component of v_c normal to the boundary

v_{cx}, v_{cy}, v_{cz} cartesian components of v_c

V_b velocity of propagation of a breaking-front

V_c velocity of propagation of a closing-front

x, y, z cartesian coordinates

α see Equation [12]

η fraction of space free of water in a cavitated region

ρ density of water

228

EXPLOSIVE LOAD ON UNDERWATER STRUCTURES
AS MODIFIED BY BULK* CAVITATION

ABSTRACT

Whereas cavitation is most commonly observed at the interface be-
tween water and a solid surface, there are indications that it may also occur
in the midst of a mass of water. Such cavitation may modify the action of
explosive pressure waves upon structures. This is possible wherever reflec-
tion of the wave gives rise to tension in the water. An extension of hydro-
dynamical theory to cover such cases is described in this report.

It is shown that cavitated regions should be formed through the
propagation of breaking-fronts moving at supersonic velocity. The cavitation
should usually take the form of small bubbles continuously distributed, rath-
er than of large voids. Subsequently the cavitation will be destroyed as the
boundary of the cavitated region contracts and acts as a closing-front. The
relevant mathematical formulas are cited.

Similitude relations are discussed, and the theory is applied to a
plane wave falling normally upon a plate, and to the explanation of the dome
that is formed over large charges exploded in the sea.

INTRODUCTION

The study of the behavior of ship structures when loaded by an un-
derwater explosion is a major project at the David W. Taylor Model Basin.
Good progress has been made toward an understanding of the pressure field
in open water, with all boundaries well removed, and to this extent the
groundwork has been laid for defining load. Important gaps still exist in
this line of information, however. The energy balance is still incomplete,
so that it is not yet possible to say what fraction of the explosive energy
is made available in the first cycle of pulsation of the gas globe. It is,
therefore, still impossible to evaluate the effect of the displacement of
the gas globe which may put its center at a point nearer the target at the
end of the first cycle than at its beginning. Questions of this sort have
led others also to conclude that sound fundamental data are still most
necessary (1).**

Questions relating to the properties of the *target*, as distinguished
from the load which the explosion puts on the target, are set aside for sepa-
rate consideration. It may be assumed that in this report the load is treated

---

* This term is rather new; it will be defined and discussed in the report.

** Numbers in parentheses indicate references on page 25 of this report.

in terms of   t rget of arbitrarily assumed properties, such as might serve
to measure   ctly the pressure in the water.

The behavior of an acoustical wave incident on a solid or free
boundary in water is rather fully understood; and the shock wave radiated
from an explosion in water partakes in large degree of the nature of an
acoustical wave. Even in such waves, however, the continuity of the medium
is believed to be broken at times by tensile effects to which the water re-
sponds by cavitation. In the shock wave, where pressures are a whole order
higher than in an acoustical wave, cavitation naturally has that much more
significance. Among the problems which must be solved before interactions
between field and target can be subjected to study by calculation, that of
cavitation must rank high in importance.

HYDRODYNAMICAL THEORY OF CAVITATION IN BULK

In practical experience cavitation usually originates between water
and a solid surface, such as a propeller blade. There are some indications,
however, that it may also occur in the midst of a mass of water, as for ex-
ample when explosive pressure waves are reflected from the surface of the sea.
To determine the effect of such cavitation upon the motion of the water, a
certain extension of hydrodynamical theory is required.

In the present report the necessary extension of the theory will be
described, but the complete mathematical details will be published elsewhere
(2). The theory is based upon certain simple assumptions, which are laid
down without entering upon the complicated question as to the nature of the
cavitation process itself. Two applications of the theory will be discussed,
dealing respectively with the impact of a pressure wave upon a plate, page 10,
and upon the surface of the sea, page 19.

The following assumptions will be made:

(a) cavitation occurs wherever the pressure in the water sinks
to a fixed value p_b, called the *breaking-pressure*;

(b) upon the occurrence of cavitation, the pressure instantly
becomes equal to a fixed value p_c, called the *cavity pres-
sure*, which cannot be less than p_b, so that

$$p_b \leqq p_c \tag{1}$$

(c) when the pressure rises above p_c, the cavitation disappears
instantly.

How far these assumptions correspond to the actual behavior of wa-
ter is not yet known. The value to be assigned to p_b is discussed briefly
on page 17. The cavitation will undoubtedly take the form of small bubbles

scattered through the water. Such bubbles have often been observed, but in
many cases they seem to contain air in addition to water vapor, and they do
not always disappear when the pressure is raised. All such complications
will be ignored here, however, in order to obtain a tractable analytical the-
ory. The bubbles may be supposed to be so small that the resulting innomo-
geneity of the water may be neglected; and p_e may be supposed to equal the
vapor pressure of the water.

The discussion will be limited to motion that is irrotational or
free from vortices, motion such as can be produced by the action of pressure
upon frictionless liquid. Furthermore, all variations of pressure will be
assumed to be small enough so that the usual theory of sound waves is appli-
cable to the unbroken water; but no limit need be set upon the magnicude of
its particle velocity.

BREAKING-FRONTS

Cavitation will begin, according to the assumptions just made, in
a region where the pressure is falling, and at a point of minimum pressure,
at the instant at which the pressure sinks to p_b. A cavity will form and
this cavity, for reasons lying outside the assumptions of the analytical the-
ory, will at once become subdivided into bubbles. Since, however, the pres-
sure will be sinking in the neighboring water also, the same process will
soon occur at neighboring points as well.
Thus a cavitated region will form, sur-
rounding the point of initiation. The
boundary of this region will sweep out
into the unbroken water as a breaking-
front, Figure 1. Since the pressure
gradient at the initial point of mini-
mum pressure is zero, the velocity of
advance of the breaking-front is seen
to be infinite at first, just as, when
a rounded bowl is lowered into water,
the boundary of the wetted region moves
out at first at infinite speed. Hence
cavitation occurs almost simultaneously throughout a considerable volume, re-
sulting in a fairly uniform distribution of bubbles; there is no reason to
expect the immediate formation of a large cavity anywhere.

Figure 1 - An Expanding Breaking-
Front, where $p = p_b$, Surrounding
a Cavitated Region

The speed of propagation of the breaking-front relative to the wa-
ter ahead of it, V_b, can be shown never to sink below the speed of sound, c.
Usually V_b is greater than c. This means that no influence can be propagated

past a breaking-front into the region ahead of it. The production of the
cavitated region is thus a consequence solely of processes occurring in the
unbroken water or on its boundaries, as a result of which the pressure in
successive portions is lowered to the breaking-pressure; the front is merely
a particular surface of constant pressure advancing in accordance with the
ordinary equations of wave propagation. Its speed of advance is found to
be (2)

$$V_b = \rho c^2 \frac{\frac{\partial v_x}{\partial x} + \frac{\partial v_y}{\partial y} + \frac{\partial v_z}{\partial z}}{\frac{\partial p}{\partial n}} \qquad [2]$$

where $\partial p/\partial n$ denotes the normal pressure gradient or the rate of increase of
the pressure along a normal to the front drawn into the unbroken water, and
v_x, v_y, v_z are components of the particle velocity taken in the directions
of cartesian axes. In order that the pressure may sink as the front ap-
proaches, the numerator in Equation [2] must be positive.

If p_b is less than p_c, there is a discontinuity of pressure at the
breaking-front, so that the pressure is p_b ahead of it and p_c behind it.
Thus, while the front is traversing an element of water, the element is
kicked forward by the excess of pressure acting on its rear face. If v_b is
the particle velocity just ahead of the front, and if v_{bn} is the component of
this velocity in a direction perpendicular to the front or to the boundary of
the cavitated region, taken positive toward the unbroken water, and if v_c and
v_{cn} denote corresponding quantities in the cavitated region just behind the
front, then the analysis (2) indicates that

$$v_{cn} = v_{bn} + \frac{p_c - p_b}{\rho V_b}. \qquad [3]$$

Components of velocity parallel to the boundary are, however, left unaltered.
Thus, if $p_b = p_c$, the particle velocity is left entirely unaltered by the
passage of the breaking-front, but if p_b is less than p_c there is a discon-
tinuity in its component perpendicular to the front.

THE CAVITATED REGION

Conditions within the region of cavitation must be comparatively
simple. Since there is no pressure gradient, and the pressure is uniformly
equal to p_c, the particle velocity must be constant in time, retaining the
value at which it was left by the passage of the breaking-front.

If $p_b = p_c$, the particle velocity, being unaltered by the passage
of the breaking-front, retains its expanding character. In this case, ac-
cording to our assumptions, the fraction η of the space that is occupied by

bubbles increases steadily from an initial value of zero. If p_b is less than p_c, however, a certain volume of space is freed at once by compression of the water as its pressure rises from p_b to p_c. The general formula for η at any point in the cavitated region at time t is (2)

$$\eta = \frac{p_c - p_b}{\rho c^2}\left[1 - \frac{c^2}{V_b^2}\right] + \int_{t_b}^{t}\left(\frac{\partial v_{cx}}{\partial x} + \frac{\partial v_{cy}}{\partial y} + \frac{\partial v_{cz}}{\partial z}\right)dt \qquad [4]$$

where t_b is the time at which cavitation occurred at this particular point and v_{cx}, v_{cy}, and v_{cz} are the components of the particle velocity v_c in the directions of the x, y, and z axes. Apparently, if p_b is less than p_c, η may either increase or decrease, or neither, after the breaking-front has passed.

THE CAVITATION BOUNDARY

When the boundary of the cavitated region, advancing as a breaking-front, arrives at a point beyond which V_b as given by Equation [2] would be less than the speed of sound, c, the analysis shows that it must halt abruptly. This may be regarded as happening either because the liquid ahead of the front is not expanding with sufficient rapidity, that is, the numerator in Equation [2] is too small, or because an excessive pressure gradient has been encountered, that is, the denominator is too large. The boundary may then do either of two things. Which it will do is found to depend in part upon the particle velocity in the neighboring cavitated region, but in larger degree upon conditions in the adjacent unbroken liquid.

One alternative is that the boundary may stand still as a *stationary boundary*, as shown in Figure 2, where any waves of pressure that may be incident upon it from the unbroken side are reflected as if from a free surface. This must occur whenever the incident waves are very weak.

The other alternative is that destruction of the cavitation may begin, that is, the boundary may recede toward the cavitated region, leaving the liquid unbroken again behind it. Such a boundary may be called a *closing-front*. Apparently it may be of either of two distinct types.

CLOSING-FRONTS

Closing of the cavitation may result from a contracting motion in the cavitated region itself, when the distribution of the values of v_c at different points are such that the bubbles tend to decrease in size. This can happen, however, only if p_b is less than p_c; for, as already remarked, if $p_b = p_c$
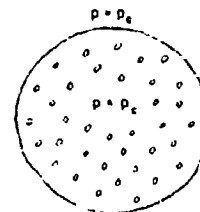
Figure 2 - A Stationary Boundary

the water retains the expanding motion which brought about the cavitation.
If contraction of the bubbles occurs near a part of the boundary at which
$\eta = 0$, this part of the boundary will advance into the cavitated region as
a closing-front. A closing-front of this type may be called an intrinsic
one; the analysis shows that it must advance at a speed exceeding the speed
of sound, else it will at once change into the other
type, to be described next.

When recession of the boundary of the cav-
itated region is caused by conditions in the un-
broken water, the boundary may be called a forced
closing-front, Figure 3. Its motion is essentially
an impact process, similar to that which occurs when
a locomotive picks up the slack in a long string of
cars. Layer after layer of the cavitated water is
compressed impulsively from p_c to some higher pres-
sure p, and its component of velocity normal to the
boundary is likewise changed. It is assumed in the
idealized theory, as already stated, that the cavitation bubbles close in-
stantly as the closing-front passes over them. If, in reality, they contain
a kernel of air or other foreign gas which requires time to redissolve in the
liquid, the process will be modified.

Figure 3 - A forced
Closing-Front

It can be shown that a forced closing-front cannot move faster than
sound, relatively to the unbroken liquid behind it, but exact equations cov-
ering its motion are difficult to formulate in the general case. The reason
can be said to lie in diffraction of the waves that are incident on the
boundary.

THE ONE-DIMENSIONAL CASE

The one-dimensional case, on the other hand, is easily treated in
more detail. If the motion is confined to one dimension, use may be made of
the familiar fact that any one-dimensional disturbance in unbroken liquid is
equivalent to two superposed trains of plane waves traveling in opposite di-
rections. One of these two trains will fall at normal incidence upon the
plane boundary of the cavitated region, while the other will be leaving it
continually as a reflected train of waves. Simple equations can then be
written in terms of these trains.

Let p' denote the pressure in the incident wave train, and let v_c
denote the particle velocity in the cavitated region, measured positively now
toward the cavitated side of the boundary. Then the analysis (2) indicates
that, if

$$p' \leq \frac{1}{2}(p_c + \rho c v_c)$$

the boundary remains at
rest, except, of course,
as it may move slightly
with the particle veloc-
ity of the water. The
incident waves are re-
flected as if at a free
surface at which the
pressure is always p_c;
see Figure 4. This case
will occur, for example,

Figure 4 - A Plane
Stationary Boundary
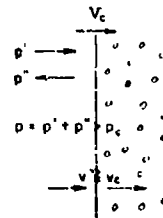
Figure 5 - A Plane Forced
Closing-Front advancing
toward the Right

whenever the incident waves are waves of tension but are not of sufficient
strength to cause fresh cavitation.

If, on the other hand,

$$p' > \frac{1}{2}(p_c + \rho c v_c)$$

the boundary advances toward the cavitated region as a forced closing-front;
see Figure 5. For the pressure p and the particle velocity v of the unbroken
water just behind the front, the latter taken positive toward the side of
cavitation, and for V_c, the speed of advance of the front relative to the
cavitated water ahead of it, the following formulas are obtained (2)

$$p - p_c = \frac{(1 - \eta)\rho c w^2}{2w + \eta(c - 2w)} \qquad [5]$$

$$v - v_c = w \frac{w + \eta(c - w)}{2w + \eta(c - 2w)} \qquad [6]$$

$$V_c = c \frac{w}{w + \eta(c - w)} \qquad [7]$$

where

$$w = \frac{1}{\rho c}(2p' - p_c) - v_c \qquad [8]$$

ρ is the density of water and c the speed of sound in it, and η is the frac-
tion of space that is occupied by bubbles.

According to Equation [7], $V_c = c$ if $\eta = 0$. The boundaries at
which $\eta = 0$ constitute, however, a singular case which will usually be of
momentary duration.

The most interesting example of such a boundary is a breaking-front
which has just ceased advancing. Usually the advance ceases because V_s has
sunk to c and would go below this value if the front advanced farther; then,
by Equation [4], $\eta = 0$ at the front. Furthermore, by Equation [3], in which

$v_{cn} = -v_c$, $v_{bn} = -v_b$, and in view of the differences in the choice of the positive direction for velocity, as illustrated in Figures 1 and 4,

$$v_c = v_b - \frac{p_c - p_b}{\rho c}$$

Here p_b and v_b represent pressure and particle velocity just behind the front, so that $p_b = p' + p''$ where p'' is the pressure in the reflected wave; whereas by the usual acoustic equations $\rho c v_b = p' - p''$. It follows that

$$p' = \frac{1}{2}(p_c + \rho c v_c)$$

Comparison of this equation with inequalities previously written involving p' shows that the further behavior of the boundary will depend upon the subsequent course taken by the incident pressure p'. If p' increases as time goes on, the boundary will at once start back toward the cavitated region as a forced closing-front; whereas, if p' remains constant or decreases, the boundary will remain stationary, constituting a free surface.

FINITE GAPS

Cavitation in the midst of a mass of liquid must ordinarily consist of small bubbles which can be assumed, for analytical purposes, to be continuously distributed. There appear to be only two ways in which large spaces or gaps can be formed in a liquid by hydrodynamic action not involving the motion of solids.

Rotational motion may have the effect of lowering the pressure to the breaking-point, as in an eddy, and then forming a cavity. Such motion, however, is excluded in the present discussion.

If the motion is of the irrotational or potential type a gap can form only if $p_b < p_c$, where a wave of tension falls upon the boundary of a cavitated region already formed and causes the surface of the unbroken water to withdraw. Such a gap will presumably take the form of a layer of especially large bubbles between the broken and unbroken water.

When cavitation results from the impact of a wave of tension upon the interface between water and a solid, its character will depend upon the relative magnitudes of the breaking-pressure for a water-solid and for a water-water surface. If the breaking-pressure between solid and water is higher than that within the water itself, breaking will occur first at the solid, with the formation of a gap or cavity. Otherwise continuously distributed cavitation will form in the water, a layer of which will be left in contact with the solid. What the facts are in the case of explosive pressure waves impinging upon painted or corroded steel is not yet known.

The subsequent closing of a gap, provided it does not contain an appreciable amount of air or other foreign gas, will result in the usual water-hammer effect. If the gap closes against a rigid boundary moving at fixed velocity v'', and v' is the particle velocity of the advancing water, the pressure rises instantaneously from p_c to $p_c + \rho c(v' - v'')$. When a gap closes in the midst of the water, however, with a difference $v' - v''$ in the particle velocities on the two sides of the gap, the impact pressure is only $\frac{1}{2}\rho c(v' - v'')$; here the pressure at the gap rises instantaneously from p_c to $p_c + \frac{1}{2}\rho c(v' - v'')$. The action is, in fact, the same as if the two masses of water had impinged simultaneously and from opposite sides upon a thin solid sheet moving with the mean velocity of the water or a velocity $\frac{1}{2}(v' + v'')$.

CAVITATION AND DYNAMICAL SIMILARITY

Cavitation in the midst of a liquid differs in its effect upon relations of similarity from cavitation at the surface of a solid.

A glance at the differential equations of sound, or at some of the equations written in this report, shows that, in constructing a possible motion similar to a given one, but on a different scale, it is necessary to preserve unchanged at corresponding points the values of the two dimensionless quantities

$$\frac{p}{\rho v^2}, \quad \frac{p}{\rho c^2},$$

where p is the pressure referred to any chosen datum or zero of pressure,
$\quad v$ is the particle velocity,
$\quad \rho$ is the density, and
$\quad c$ is the speed of sound in the liquid in question, here water.

In a given liquid, with fixed ρ and c, it follows that both p and the particle velocity must be preserved at corresponding points. The only transformation that is possible is thus the simple one, familiar in the discussion of underwater explosions, in which all linear dimensions and all times are changed in the same uniform ratio. The occurrence of cavitation at fixed values of p_b and p_c alters nothing in this conclusion so long as cavities of appreciable size do not form.

If large gaps occur, however, gravity may play a role in their neighborhood. Then, from such equations as $s = \frac{1}{2}gt^2$ and $p = \rho gh$, where s is the displacement in time t or h is the static head, it is evident that, for similarity to hold, an additional quantity must be preserved. This may be written in various forms, such as $gs\ t^2/s^2$ or

$$\frac{gL}{v^2}$$

where L is any convenient linear dimension. It is clear that L, like v^2, must be kept constant. Thus, if cavitation within the midst of a liquid is accompanied by the formation of cavities of considerable size, no transformation of similarity is possible at all.

The inclusion of effects of viscosity, on the other hand, requiring preservation of the quantity

$$\frac{\rho v L}{\nu}$$

where ν is the viscosity, is known to destroy the possibility of similarity, irrespective of whether cavitation occurs or not.

In experiments such as those on cavitating propellers, transformations of similarity can be made for two reasons. In the first place, the compressibility of the water can be neglected, as well as the viscosity effects, so that only two quantities need to be preserved in value, such as

$$\frac{p}{\rho v^2}, \quad \frac{gL}{v^2}$$

In the second place, only a single cavitation pressure is usually recognized, and this can be taken as the datum pressure which is held constant. The usual change of scale then becomes possible in which all linear dimensions and also the excess of pressure at each point over the cavitation pressure are changed in proportion to v^2. If, however, it became necessary to distinguish between two cavitation pressures, a breaking-pressure and a cavity pressure, then the fixed difference between these two would require all pressure differences to be fixed, and consequently similar motions on different linear scales could not occur.

APPLICATION: CAVITATION BEHIND* A PLATE

The simplest case to which the analytical theory of cavitation can be applied is that of plane waves of pressure falling at normal incidence upon a uniform plane sheet of solid material, where the sheet is so thin that elastic propagation through its thickness need not be considered; see Figure 6.

Various aspects of this case have been discussed in several reports (3) (4) (5) (6). If the pressure wave is of limited length and of sufficiently low intensity to make acoustic theory applicable, and if water can support the requisite tension, then it has been shown that the initial forward acceleration of the plate is followed by a phase during which it is brought to rest again by the action of tension in the water. The final displacement of the plate is equal to twice the total displacement of a particle

---

* On the side acted on by the explosion.

238

of water due to the incident wave, or the same as the displacement of the water surface when the plate is absent.

The effect of cavitation, on the other hand, will vary somewhat, according to the point at which it occurs. There are two possibilities:

1. The plate may break loose from the water, or

2. cavitation may occur first in the water itself.

1. The plate may break loose from the water; see Figure 7.

The pressure at which this occurs may be either the cavity pressure p_c or some lower pressure p_b'. In either case, the surface of the liquid then becomes a free surface at which the pressure is constant and equal to p_c, and the remainder of the incident wave is reflected from this free surface. The plate, meantime, will continue moving forward until it is arrested by other forces. The pressure p_h, atmospheric or otherwise, acting on
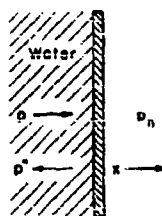
Figure 6 - Diagram representing Plane Waves of Pressure p in Water, falling upon a Large Thin Plate

This plate is backed by gas at the pressure p_h. A reflected wave of pressure p'' travels back into the water.
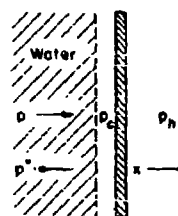
Figure 7 - Diagram illustrating the Case in which Cavitation occurs at a Thin Plate

Here the cavitation takes the form of a definite cavity in which the pressure is p_c.

the opposite face of the plate, may be assumed to exceed the pressure p_c in the cavity behind it; the difference, $p_h - p_c$, will suffice eventually to arrest the motion of the plate and to cause its return to contact with the water. There may also be other forces of elastic or plastic origin. It may happen, however, as suggested by Professor G.I. Taylor (5), that spray projected from the water surface will tend for a time to support the outward motion of the plate. When the returning plate strikes the water, an impact wave of pressure will be produced in the water as the plate comes exponentially to rest.

If the incident wave is of exponential form, explicit formulas are easily obtained. This case is discussed at length by Taylor (5), but a few details may be given here.

The equation of motion for the plate is

$$m \frac{d^2 x}{dt^2} = p + p''$$ [9]

where p is the excess of pressure in the incident wave above the hydrostatic
pressure p_k, which is assumed to be the same on both sides of the
plate,

p' is the excess of pressure over p_k in the reflected wave,

m is the mass of the plate per unit area,

x is the positional coordinate of the plate in a direction perpendicu-
lar to its surface, and

t is the time.

Elimination of p'' gives

$$m \frac{d^2 x}{dt^2} + \rho c \frac{dx}{dt} = 2p$$ [10]

where ρ is the density of water and c is the speed of sound in it. Compare
here Equations [9] and [10] on page 24 of TMB Report 480 (4).

The solution of Equation [10] for $p = 0$ is

$$\frac{dx}{dt} = u_0 e^{-\frac{\rho c t}{m}}$$ [11]

With a suitable choice of the constant u_0, this solution will represent the
motion of the plate after returning to contact with the water if t represents
the time measured from the instant of contact and u_0 is the velocity of the
plate at that instant.

To represent the impact of the pressure wave, we set $p = 0$ for
t less than 0 and, for t greater than 0,

$$p = p(t) = p_0 e^{-\alpha t}$$ [12]

in terms of two constants p_0 and α. It is assumed that the displacement of
the plate during the effective time of action of the wave is negligibly small.
The solution of Equation [10] that represents the plate as starting from rest
at $x = 0$ and $t = 0$ is then easily verified to be

$$\frac{dx}{dt} = \frac{2 p_0}{\rho c - \alpha m} \left(e^{-\alpha t} - e^{-\frac{\rho c t}{m}} \right)$$ [13]

see TMB Report 480, page 25.

The corresponding total pressure on the plate above hydrostatic is,
from Equations [9] and [13],

$$p + p'' = m \frac{d^2 x}{dt^2} = \frac{2 p_0}{\rho c - \alpha m} \left(\rho c e^{-\frac{\rho c t}{m}} - \alpha m e^{-\alpha t} \right)$$ [14]

If the simple assumption is now made that cavitation occurs at the surface of the plate as soon as the pressure sinks to a certain value p_b', the time at which it occurs can be found by putting $p + p'' = p_b' - p_h$ in Equation [14] and solving for t. The corresponding value of dz/dt as obtained from Equation [13] is then the velocity with which the plate leaves the water.

For the special case in which $p_b' = p_c = p_h$, this velocity is also the maximum velocity acquired by the plate and has the value

$$\frac{dz}{dt} = v_{max} = \frac{2p_0}{\alpha m} q^{\frac{q}{1-q}} \qquad [15]$$

where

$$q = \frac{\rho c}{\alpha m} \qquad [16]$$

as given on page 7 of TMB Report 489 (6). The formula for v_{max} can also be written

$$v_{max} = k \frac{p_0}{\rho c}, \quad k = 2q^{\frac{1}{1-q}} \qquad [17]$$

where k is a dimensionless number and $p_0/\rho c$ represents the particle velocity associated with the maximum pressure in the incident wave. A plot of k against q is shown in Figure 8.

If p_b' is less than p_h, the plate is slowed down somewhat by the action of the pressure p_h on its opposite face, assisted perhaps by tension in the water, so that it leaves the water with a velocity less than v_{max}.

The initial velocities of diaphragms acted on by explosive pressure waves as measured at the David W. Taylor Model Basin have always been less than the calculated v_{max}, but never less than half as great. Details will be reported elsewhere.

2. Cavitation may occur first in the water itself; see Figure 9.

Consideration of this case is new. If a fixed breaking-pressure p_b is assumed, the point at which cavitation starts may be found by examining the resultant pressure distribution in the water near the plate. The reflected pressure $p''(t)$ at the plate itself is, from Equations [12] and [14],

Figure 8 - Plot of the Coefficient k in Equation [17]

The broken curve continues the right-hand part of the curve backward on the same scale.

so long as cavitation does not occur,

$$p''(t) = \frac{p}{\rho c - \alpha m}\left[2\rho c\, e^{-\frac{\rho c t}{m}} - (\rho c + \alpha m)\, e^{-\alpha t}\right] \qquad [18]$$

Let x represent a distance from the plate, measured positively in the direction of propagation of the incident wave. Then the pressure at any point behind the plate, within the distance to which the reflected wave has traveled, will be

$$p = p\left(t - \frac{x}{c}\right) + p''\left(t + \frac{x}{c}\right) =$$

$$p_0\left[e^{-\alpha\left(t - \frac{x}{c}\right)} + \frac{2\rho c}{\rho c - \alpha m}\, e^{-\frac{\rho c}{m}\left(t + \frac{x}{c}\right)} - \frac{\rho c + \alpha m}{\rho c - \alpha m}\, e^{-\alpha\left(t + \frac{x}{c}\right)}\right] \qquad [19]$$

     Cavitation will begin where p as given by this equation first sinks to the breaking-pressure p_b. From this point a breaking-front will advance toward the plate, perhaps all the way up to it, while another one travels back into the water. The latter front travels forever, in the present case, provided p_b is less than 0, but the cavitation behind it soon becomes negligible. This is because the incident wave soon becomes inappreciable, and the receding breaking-front soon becomes indistinguishable from that particular reflected wave at which $p'' = p_b - p_A$ and travels with this wave at the speed of sound. Equation [4] then gives $\eta = 0$ behind the front.

     The particle velocity v_m ahead of the front becomes that of the reflected wave or $v_{bm} = -(p_b - p_A)/\rho c$; hence by Equation [3], in which $V_b = c$ and the signs of v_{cm} and v_{bm} must be changed to allow for the difference in the direction chosen for a positive velocity, the particle velocity behind the front is $-(p_c - p_A)/\rho c$. Thus the part of the reflected wave from $2p_0$ to p_b travels on, with a discontinuity at its rear face, leaving the pressure uniformly equal to p_c and the velocity uniformly equal to $-(p_c - p_A)/\rho c$ behind it. Only a limited region of cavitation is formed near the plate.

Figure 9 - Diagram illustrating the Case in which Bulk Cavitation occurs in the Water

     The process by which the plate, after being returned by other forces such as air pressure, destroys the cavitation again, can be followed by numerical integration in any particular case that may arise.

F   OP CAVITATION ON PRESSURE

The action of an exponential wave upon a plate is illustrated in Figures 10 and 11, which are drawn to represent very roughly the action of the shock wave from 300 pounds of TNT upon a plate of steel 1 inch thick, or from 1 ounce of TNT upon a plate 1/17 inch thick.

Figure 10 shows the excess pressure on the plate itself, above hydrostatic pressure, plotted
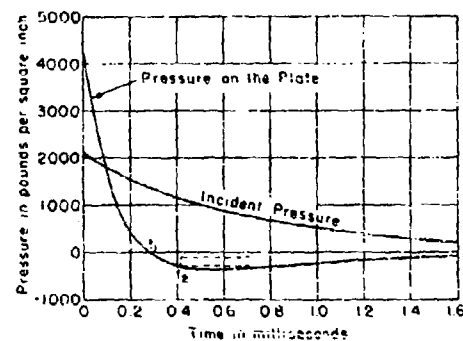
Figure 10 - Pressure on a Plate, in the Absence of Cavitation, plotted on a Time Base
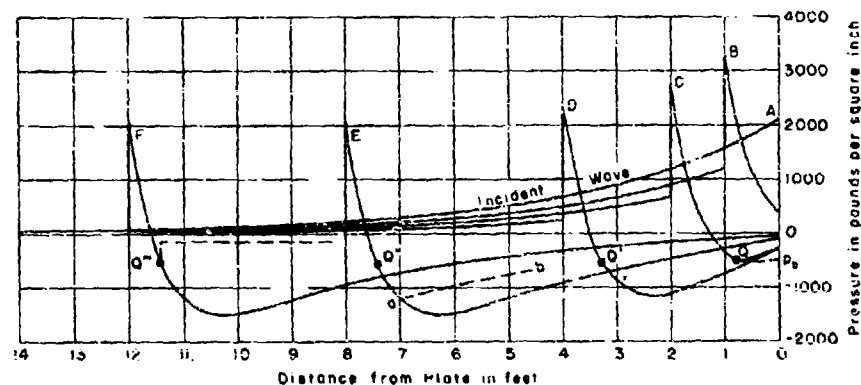
Figure 11 - Distributions of Pressure behind a Plate at Successive Instants of Time, in the Absence of Cavitation

The incident wave approaches from the left, hence distance from the plate is plotted in that direction.

on a basis of time. The time scale is labeled to correspond to 300 pounds of TNT; for 1 ounce the times would be 1/17 as great. One curve shows the incident pressure, or the pressure that would exist in the water at the location of the plate if the plate were absent, as given by Equation [12]. The other curve shows the actual pressure on the plate, as given by Equation [14]. This may be thought of as made up of the incident pressure p together with a component of pressure p″ due to a reflected wave that travels back into the water.
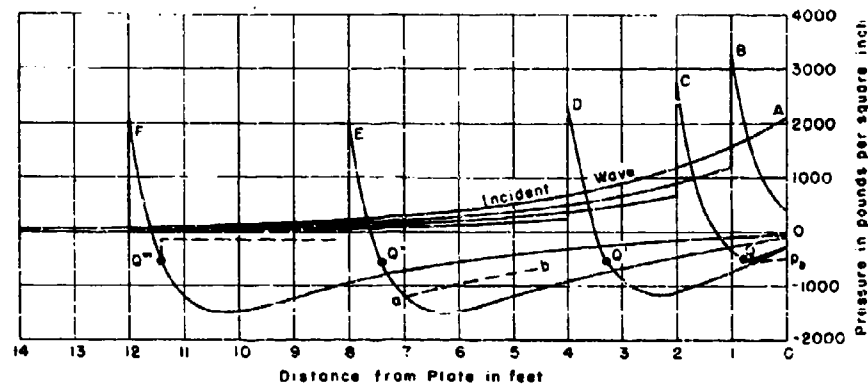
Figure 11 - Distributions of Pressure behind a Plate at Successive
Instants of Time, in the Absence of Cavitation

       Figure 11, on the other hand, shows the instantaneous distribution
of pressure in the water adjacent to the plate, plotted against the distance
from the plate. The distances shown in the figure correspond to 300 pounds
of TNT; for 1 ounce they would be 1/17 as great. The curves are calculated
by Equation [19] where $t + x/c$ is positive, and by Equation [12] elsewhere.
Curve A shows the distribution of pressure at the instant at which the pres-
sure wave first reaches the plate $(t = 0)$. Curve B shows the distribution
0.2 millisecond later $(t = 0.0002)$; at this time the reflected wave has ad-
vanced 1 foot from the plate. Curves C, D, E, F refer similarly to times
about 0.4, 0.8, 1.6, 2.4 milliseconds after the arrival of the incident wave.
Curve F serves also to represent the final form of the reflected wave; the
incident wave has by this time completely disappeared.

       These figures will be modified by the occurrence of cavitation in a
way that depends upon the laws governing the cavitation.

       Cavitation may occur *at the plate*. It may occur as soon as the
pressure sinks to the hydrostatic pressure p_h; this will be at the instant
marked t_1 in Figure 10. In this case the plate leaves the water with a ve-
locity equal to v_{max} as given by Equation [17], and the curve for the pres-
sure on the plate in Figure 10 coincides with the axis of zero pressure from
the time t_1 onwards. An alternative possibility, however, is that cavitation
may not begin until a lower pressure p_b' is reached, at a later time such as
that marked t_2 in Figure 10. In this case the plate leaves the water at the
time t_2 with a velocity less than v_{max}. The pressure on the plate after t_2
will then be the constant cavity pressure p_c. If $p_c = p_b'$, the curve will
extend horizontally from the point t_2, as shown by the lower of the broken

lines, instead of continuing downward. If, on the other hand, p_c is greater than p_b', the pressure on the plate will rise suddenly to the value p_c at the instant t_2 and will then remain constant, as illustrated by the upper of the two broken lines in Figure 10.

The distributions of pressure in the water, as plotted in Figure 11, will be modified in ways to correspond. The part of the reflected wave that is reflected from the water surface after the occurrence of cavitation will be modified so as to contain higher pressures, since the pressure at the water surface is higher than it would have been if the water had continued in contact with the plate. In Figure 11, on each of the later curves there will be a point representing the instantaneous position of that part of the reflected wave which was reflected just as cavitation began; such a point is indicated by a on Curve E. The press e to the right of this point contains a component that was reflected from the free water surface instead of from the plate and hence will lie somewhat higher than it would in the absence of cavitation, as is suggested in Figure 11 by the broken line ab.

As an alternative, cavitation might *begin in the water itself*. In such a case the analysis given in foregoing sections becomes applicable. Cavitation will start at a definite position as well as at a definite time. It might begin, for example, at Q in Figure 11; this point would then represent the position of that plane in the water, parallel to the plate, at which the pressure first sinks to the breaking-pressure p_b.

From this initial plane, a plane breaking-front will advance a short distance toward the plate, while another one will follow the reflected wave toward the left, moving a little more rapidly than this wave so as always to be in the position at which the total pressure equals p_b. Successive positions of the latter breaking-front are indicated in Figure 11 by Q', Q'', Q'''. Behind this front, or on the right in the figure, lies the cavitated region, in which the pressure equals the cavity pressure p_c. The boundary of this region on the side toward the plate is not shown in Figure 11, since its position can only be inferred from a more detailed study of the motion of the water near the plate. The uniform pressure p_c behind the breaking-front, on the assumption that p_c is greater than p_b, is illustrated for a certain instant of time by the broken line behind Q'''. Thus, the part of Curve F to the left of Q''', up to 12 feet from the plate, represents the part of the reflected wave that got past Q before cavitation began, diminished somewhat through being partially overtaken by the breaking-front which moves at first at supersonic velocity. The remainder of Curve F is replaced by the uniform pressure in the cavitated region or near the plate by an undetermined modified pressure.
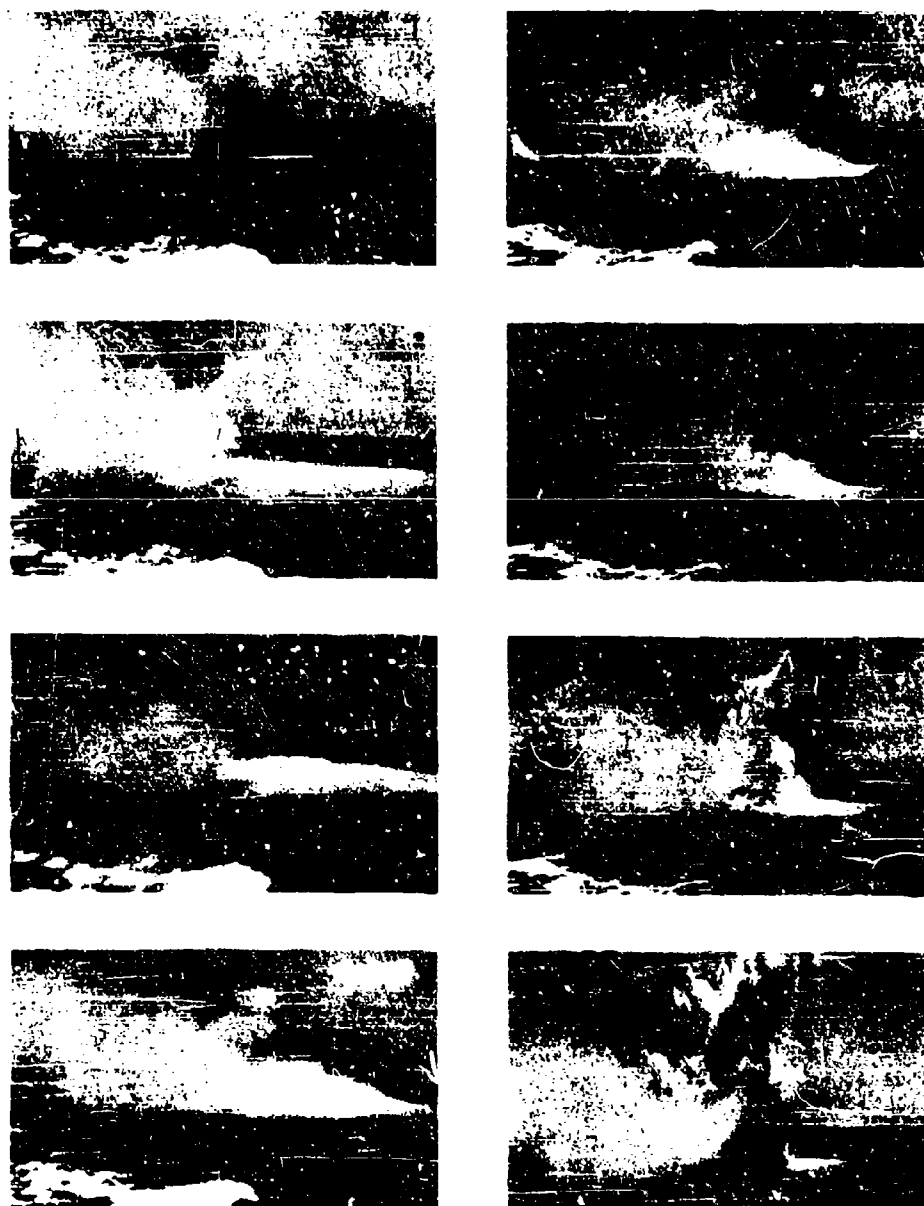
Figure 12 - Growth of a Dome and Plumes from an Underwater Explosion

The phenomenon is partially obscured by smoke from the ship from which the photographs were taken.

More complete figures are scarcely worth constructing until an actual known case presents itself for analysis.

CAVITATION UNDER THE SURFACE OF THE SEA

When a charge is exploded at a suitable depth in the ocean, a dome of white-appearing water is seen to rise somewhat above the surface, breaking after a moment into plumes of spray. The eight frames from a motion picture film, Figure 12, illustrate this phenomenon. The plumes are supposed to be associated with the escape of the explosion gases. The dome, however, has been ascribed to the occurrence of cavitation; a layer of water at the surface and just under it, after being kicked upward by the pressure wave, fails to be jerked to rest again by the action of a reflected wave of equal tension and continues rising until stopped by gravity and air pressure. This explanation will be considered briefly on the basis of the foregoing analysis.

It is necessary first to fix upon the value to be assumed for the breaking-pressure p_b. Hilliar (7) found that the dome was absent whenever, according to his measurements, the maximum pressure reaching the surface was under 0.3 ton or 670 pounds per square inch, and concluded that p_b was roughly of this magnitude. It will be assumed, therefore, for the moment, that $p_b = -600$ pounds per square inch.

To select a specific case for study, suppose that a charge of 300 pounds of TNT is detonated 50 feet below the surface. Then the pressure wave should be reflected from the surface as a wave of equal tension, diverging from the mirror image of the charge in the surface and decreasing in intensity as it progresses. Using Hilliar's data, it is easy to map out the lens-shaped volume within which the pressure would sink momentarily at least to -600 pounds per square inch if there were no cavitation.

Figure 13 - Diagram of Region of Reduced Pressure following Reflection of a Pressure Wave from the Surface

This volume is outlined roughly by the lower curve in Figure 13.

Application of the criterion obtained from the analysis for the propagation of a breaking-front indicates, on the contrary, that cavitation would in reality be confined to a much smaller region, which is shaded in Figure 13. To locate this region, it is necessary to estimate the magnitudes

of the incident and reflected waves as they become superposed upon each other
at various points and at various times. The pressure in each wave is assumed
to decrease in inverse proportion to the distance from its point of origin,
real or assumed; and allowance must be made for the time of propagation. It
is unnecessary to give details of the rather tedious calculations, which were
carried out only roughly.

By trial, it is found that the total pressure should first reach
the value of -600 pounds per square inch at a point situated directly over
the charge and about 1 foot under the surface. Cavitation will begin at this
point, according to the assumption made here, and from this point a closed
breaking-front will sweep out, moving at supersonic velocity. The upper side
of this front must obviously halt almost at once, for a tension of 600 pounds
per square inch cannot occur close to the surface; but the lower side may de-
scend to a considerable depth.

In Figure 14 are shown the estimated distributions of pressure
along a vertical line through the charge at two different times, distin-
guished by the numbers 1 and 2. Heavy curves are drawn to represent the ac-
tual pressures; light curves above the axis represent the component pressures
due to the incident wave, those below the axis the components due to the re-
flected wave.
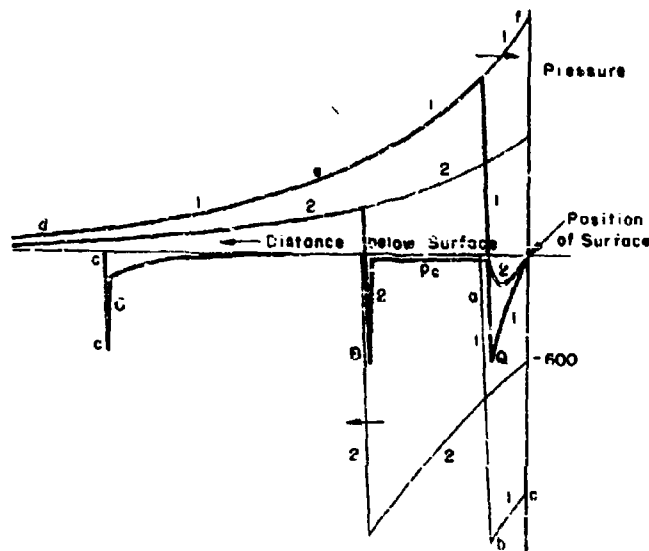
Figure 14 - Diagram illustrating the Distribution of Pressure below
the Surface of the Sea, as explained in the Text

At the instant 1, a small part of the incident wave has already been converted at the surface into the reflected wave, shown by the light curve abc; the remainder of the incident wave is represented by the curve def. Together these two components make up the total pressure represented by the heavy curve 1111. Cavitation is just beginning at Q, where the pressure has sunk to -600 pounds per square inch.

From this time onward, the curve of total pressure is clipped off at -600 pounds per square inch by the breaking-front. Hence, at the time 2, for example, the curve has its minimum at -600 at B, and to the right of this point, or toward the surface, lies a cavitated region, in which the pressure has the small negative value p_c. Just under the surface, however, in unbroken water, larger negative pressures will probably occur. The distribution of pressure at this instant will thus be as shown by the heavy curve 222.

The breaking-front will finally cease advancing when V_b as given by Equation [2] becomes equal to c. In applying this criterion, it is more convenient to transform Equation [2] by substituting, from the theory of sound waves,

$$\frac{\partial v_x}{\partial x} + \frac{\partial v_y}{\partial y} + \frac{\partial v_z}{\partial z} = -\frac{1}{\rho c^2}\frac{\partial p}{\partial t}$$

The actual formula employed in making the rough estimate was Equation [46] in Reference (2). Using the author's provisional estimate of the later part of the pressure curve, as represented on page 15 of Reference (6), it was concluded in the manner just described that cavitation might ultimately extend throughout a volume such as that shaded in Figure 14, or to a horizontal radius of nearly 100 feet, but only to a maximum depth in the center of 10 feet.

After the boundary of the cavitated region has ceased advancing as a breaking-front, it will undoubtedly begin to recede as a closing-front. No attempt has been made to follow this process, however, since it seems to be possible to infer the gross features of the subsequent motion of the water from more general considerations.

The particle velocity just behind the front may be estimated from Equation [3]. Just above the top of the cavitated layer, v_{bx}, representing the resultant particle velocity due to incident and reflected waves, adds numerically to the last term in Equation [3] and gives a total upward particle velocity v_{cx} in the cavitated layer of about 49 feet per second. The simultaneous value at the surface is twice that in the incident wave or perhaps 34 feet per second. Where the descending part of the front halts, however, the positive direction for v_{bx} is downward, whereas the actual particle velocity is due almost entirely to the reflected wave and is upward. Thus

v_{bn} is here nearly equal to $p_i/\rho c$, so that v_{bn} just about cancels the last term in Equation [3] and v_{cn} is small. It may safely be inferred that the particle velocity in the cavitated region will grade from a small value at the bottom to about 49 feet per second at the top.

The whole cavitated layer, 9 feet thick, should therefore rise, carrying a thin uncavitated sheet on top of it. This "solid" sheet will increase in thickness as its lower boundary travels downward in the form of a forced closing-front. The numerical values cited indicate that the center of gravity of the upper 10 feet of water will start upward with a velocity of perhaps 25 feet per second; and there should be a downward acceleration of g due to gravity and of $(34/10)g$ due to air pressure on the top, or a total of 4.4 g. The center of gravity should rise, therefore, not over $s = v^2/2g = 25^2/8.8 \times 32 = 2.2$ feet, during a time $v/4g$ or 0.2 second. The surface of the water will rise higher but certainly not more than twice as high or, at the utmost, 5 feet.

Now this picture as inferred from the analysis appears not to agree too well with the facts. Hilliar's observations indicate that, in the case considered, the dome would certainly be less than 60 feet in radius but would rise in a second or so to a height of 15 or 20 feet. The analytical estimate would be changed considerably if a different breaking-pressure were assumed, or if more recent values for the incident pressure were employed, but a large disagreement with observation would remain. The large rise that is actually observed could be explained only by supposing that the disintegration of the water extends up to the surface and serves to admit atmospheric pressure to the interior. Cavitation up to the surface might result from the initial presence of air bubbles in the upper few feet of water, which would effectively raise p_b, perhaps up to p_c. The whiteness observed in all explosions of this kind does, in fact, extend to the very edge of the dome in the photographs; see Figures 12 and 15. It is not easy to believe, however, that air can mix sufficiently rapidly with the cavitated water to relieve the vacuum effectively.

The jaggedness of the edge of the dome, so clearly revealed by the photographs, suggests a modified hypothesis. Perhaps the general mass of water really does rise only a few feet, as the analysis suggests, and what is seen as a white dome of considerable height is only an umbrella of spray thrown up from the surface.

The origin of the spray itself is perhaps to be found in an instability of the surface under impulsive pressure. The pressure gradient is equivalent to a momentary increase of gravity by a factor of 100 to 1000, followed by a reversal to similar values. If there are any small waves on
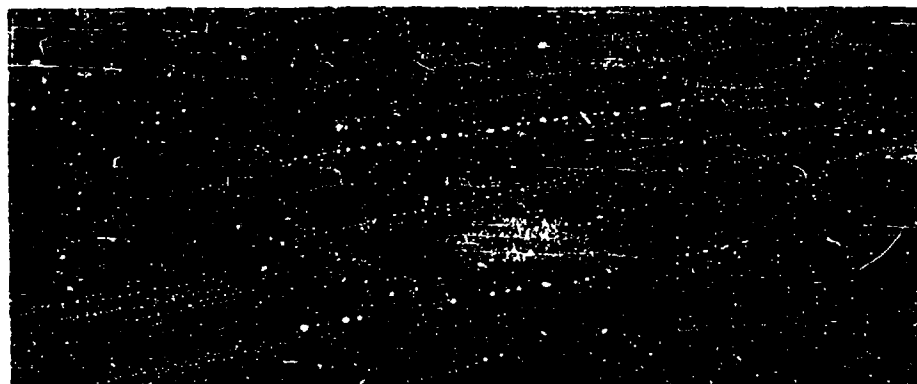
**Figure 15 - The Dome, 53 feet high, raised by a Charge of 1900 pounds
of Amatol, detonated 64 feet below the Surface**

This photograph is from Hilliar, Reference (7), Figure 62.

the surface, the lesser mass of water under the troughs will be accelerated
more violently than the greater mass under the crests, but the difference in
the accelerations will be greater during the pressure phase than during the
subsequent tension phase because the initial differential motion tends to
smooth out the waves or even to reverse them. The initial troughs should
thus tend to be thrown up as spray.

An indirect method of determining whether or not cavitation occurs
under the surface is by studying the reflected wave of tension itself. In
the absence of cavitation, this should be a reversed replica of the incident
wave, reduced somewhat by the greater distance of travel. If, however, cav-
itation occurs, only the very short initial part of the tension wave as pro-
duced at the surface, containing the rapid drop to the breaking-pressure p_b,
will continue traveling below the level at which the breaking-front halts.
It is readily seen that the lower boundary of the cavitated region should
stand still thereafter as a stationary boundary, as described on page 5.
For, as noted on page 8, $2p' = p_c + \rho c v_c$ when the breaking-front halts, where
p' is the positive pressure in the incident wave, and thereafter $2p' < p_c + \rho c v_c$
as p' decreases, so that the condition for a stationary boundary as stated
on page 7 is met. The tail of the incident wave will be reflected from this
boundary as a tension wave in which the pressure is $p'' = p_c - p'$. Thus the
total reflected wave as it occurs below the region of cavitation will be
qualitatively as sketched at C in Figure 14.

This conclusion is in general harmony with a series of piezoelec-
tric observations reported in 1924 (8). Only relatively small tensions were

found. Presumably an initial jab of high tension such as cc in Figure 14 would have little effect on the gage. The observed tensions would represent, therefore, merely the reflection of the tail of the incident wave from the bottom of the cavitated region, as is stated in the report.

The value of the breaking pressure may be inferred most easily from the minimum depth at which the reflected tension appears in full strength, indicating no cavitation. One of the observations mentioned points toward a relatively high value of p_b. A charge of 2 1/4 pounds of guncotton 60 feet below the surface gave a maximum pressure of 910 pounds per square inch on a gage placed 15 feet away and on the same level. Without cavitation, therefore, the maximum reflected tension should be about $910 \times 15/120 = 115$ pounds; but only 15 pounds was observed. Yet the maximum pressure at the surface would be only $910 \times 15/60 = 230$ pounds per square inch. If the gage was capable of measuring tensions effectively, the conclusion is justified that in this case the water must have cavitated at a tension scarcely exceeding 200 pounds.

It must be recognized, however, that cavitation at the gage might alter the conclusions materially. If cavitation over the gage occurs at higher pressures than it does in the water itself, then the tensions indicated by the gage set only a lower limit to the magnitude of the tension occurring in the water itself. The piezoelectric observations would be consistent with the assumption that no cavitation at all occurs in the midst of the sea.

A few remarks may be added concerning the similarity laws for surface phenomena. On page 9 it has been seen that the change to model scale, as it is commonly made in dealing with underwater explosions, is possible only so long as gravity effects can be neglected. In this change all linear dimensions and all times are changed in one and the same ratio; the pressures and velocities at corresponding points remain unchanged. It follows that the effects of air pressure upon surface phenomena will be relatively the same upon all scales. Insofar as these phenomena are influenced by gravity, however, similar motions on different scales are impossible. Similar motions would be possible only if the strength of gravity were changed in inverse ratio to the linear dimensions, so as to preserve the value of the quantity gL/v^2 or, since v^2 is unchanged, of gL itself; L is here any convenient linear dimension and v is the particle velocity. Small-scale phenomena thus correspond to large-scale ones occurring in a proportionately weaker gravitational field.

This conclusion is surprising, for it appears to mean that spray should be thrown to the same height by charges of all sizes. This would be

in conflict with the suggestion that the dome over large charges may consist chiefly of spray, for a charge of an ounce throws spray to a height of a few feet at most. The explanation of the difference may possibly lie in an influence of surface tension upon spray formation. Since the pressure under a curved surface is $p = 2T/r$ in terms of the surface tension T and the radius r, the relative effect of surface tension, when the pressures are unchanged, will be the same only if T is changed in the ratio of the linear dimensions. Thus surface tension, being actually constant, will have a much larger effect upon small-scale than upon large-scale phenomena.

On the other hand, as we have seen, a dome of superficially solid water is limited chiefly by air pressure, hence it should follow the usual linear scale. The absence of a noticeable dome over small charges is thus consistent with the estimate of possible dome heights as made in the forego-ing, and in turn constitutes evidence against the supposition that the dome over large charges consists largely of moderately disintegrated water.

It must be recognized, however, that other causes are possible for the difference in the surface phenomena on large and small scales. For one reason or another, cavitation might occur more easily in the salt water of the sea than in the fresh water in the laboratory. Or it might be that water can stand higher tension for the shorter times involved in the action of smaller charges. More evidence on these points is needed.

REFERENCES

(1) Work of the Explosion Research Laboratory at Woods Hole with piezo gages by R.H. Cole, in National Defense Research Committee Division 8 Interim Report of 15 November - 15 December 1942.

(2) "Cavitation in an Elastic Liquid," by E.H. Kennard, Physical Review, vol. 63, p. 172, 1943.

(3) Superintendent of Mining, Portsmouth (England) Report on "Explosive Trials against Ex-German Submarines," M.S. 3/21, Part II, dated 16 June 1921.

(4) "Report on Underwater Explosions," by E.H. Kennard, Volume I, of this compendium.

(5) "Pressure and Impulse of Submarine Explosion Waves on Plates," by G.I. Taylor, R.C. 235, 1941.

(6) "Effects of Underwater Explosions: General Considerations," by E.H. Kennard, TMB Report 489, 1942

(7) "Experiments on the Pressure Wave Thrown out by Submarine Explosions," by H.W. Hilliar, Department of Scientific Research and Experiment, R.E. 142/19, 1919.

(8) Admiralty Research Laboratory Report on the "Nature of the Pressure Impulse Produced by the Detonation of Explosives Under Water. An Investigation by the Piezo-Electric Cathode-Ray Oscillograph Method," A.R.L./S./12, C.B. 01670 (12), dated November 1924.

THEORETICAL INVESTIGATION OF CAVITATION PHENOMENA OCCURRING WHEN AN UNDERWATER PRESSURE PULSE IS INCIDENT ON A YIELDING SURFACE: I.

H. N. V. Temperley
Admiralty Undex Works, Rosyth, Scotland

THEORETICAL INVESTIGATION OF CAVITATION PHENOMENA OCCURRING WHEN AN UNDERWATER PRESSURE PULSE IS INCIDENT ON A YIELDING SURFACE: I.

H. N. V. Temperley

August 1944

*   *   *   *   *   *   *   *   *

Summary.

An account is given of the present position of the theory of the motion of a steel plate when subjected to an explosion pulse. Two approximations are in use, the infinite plate, and the piston in rigid wall. The former is considered to be a better approximation to a ship, the latter to a box model or diaphragm-gauge. Ships' plates of the thicknesses and strengths used in practice behave (towards explosion pulses) very much like free surfaces and negative pressures are consequently set up in the water. In certain circumstances cavitation occurs in the water, and some of the energy of the explosion pulse is transformed into kinetic energy of this water, which eventually collides with the plate. The plate thus receives energy which would be radiated away as a tension pulse if water were able to stand tension. Only a fraction of this kinetic energy is available to cause damage, nevertheless the investigation shows that the effect makes an important contribution to damage even if the plate is several inches thick. The theory is in qualitative agreement with experiment, and the modifications which will be necessary in order to take account of the effect of clamped edges or stiffeners are briefly discussed. Two effects which will have to be considered are diffraction of positive pressure from the immobile parts of the plate and impact of non-cavitated water with the plate after the disappearance of cavitation. Both of these effects, however, vanish for an infinite plate, which is the only case considered in the present report.

List of Symbols.

p_m = maximum pressure of incident pulse..

θ = time constant of incident pulse.

c = velocity of sound.

x = distance from origin of co-ordinates (also thickness of reconstituted layer of water)

y = deflection of plate.

ρ = density of plate.

a = thickness of plate.

ρ_0 = density of water.

$\phi \left(t - \frac{y}{c} \right)$ = pressure pulse reflected from plate.

$a = \dfrac{\rho \, a}{\rho_0 \, c \, \theta}$

$\theta_c = \dfrac{\theta \, a}{1 - a} \log \left(\dfrac{1}{a} \right)$ = Taylor cavitation time.

v_c = velocity of water at instant of cavitation.

ε_T = Taylor energy.

$\left. \begin{array}{c} \varepsilon_b \\ \varepsilon_c \end{array} \right\}$ defined in sub. paragraph "Energy Consideration"

●·····

256   - 2 -

ω = 2π x plastic seismic frequency of plate = $\sqrt{\frac{\sigma_0}{\rho R^2}}$

σ_0 = yield stress of plate.

R = radius of plate.

s = $\omega \theta a^b$ = ratio of time constant of pulse to that of plate.

$\ast$ means that the special non-dimensional units defined in sub. paragraph 8(b) must be used.

y_m, t_m, x_m = values of y, t and x when plate comes to rest.

Introduction.

The behaviour of a steel plate when subjected to an underwater explosion pulse has been treated theoretically by quite a number of workers. Butterworth summarised the earlier work on the subject and considered both an infinite plate backed by a spring and a piston moving in a circular aperture in a rigid wall. Taylor(1) considers the former model and shows that one gets increased damage if one supposes that the plate leaves the water as soon as the pressure in the water touching the plate falls below zero. He also suggests(2) that, in this case, the plate may gain still more energy if cavitation spreads outwards from the plate into the water. The resulting spray will be projected towards the plate and must eventually catch up and bombard it. This suggestion was partly explored by Fox and Rollo, who showed that such cavitation and follow-up of water would imply that, for a thin plate, virtually all the incident energy was trapped in the neighbourhood of the plate, and might conceivably contribute to damage. An actual mechanism of reloading has been considered by Kirkpod(3) who concludes that, in practical cases, almost all the energy expended in producing cavitation in water eventually contributes to damage. Unfortunately, only an abstract of this work is at present available. The general theory of the propagation of cavitation in water has been given by Kennard(4) who has applied it to a discussion of the effect on structures(5), and has given an account of the present position of the theory of the distortion of a plate by an explosion(6). It is the purpose of this report to obtain a definite numerical assessment of the extra energy communicated to an infinite plate by this process of cavitation and subsequent "follow-up" or bombardment with spray. Work is now proceeding on the similar problem for the piston in rigid wall, in order to assess the effect of the finite size of the plate, the importance of which is fully realised. It is hoped to deal with this in detail in a later report, but, in the meantime, a short discussion of the relation between the two types of theory seems appropriate.

Relation between the "Infinite Plate" and the "Piston in Rigid Wall" theories.

It is probable that the infinite plate on a spring is a reasonable representation of the behaviour of a ship, provided that one may assume that the effect of stiffeners, etc., is spread evenly all over the plates. If, however, the stiffeners are strong, it is necessary to know how the theory must be modified to allow for the fact that the parts of the plate near the stiffeners are practically immobile. This problem has been considered by Friedlander, who has obtained an estimate of the effect of stiffeners in delaying the onset of cavitation, and also of the effect of a slight curvature of an infinite plate on the time of onset of cavitation. Information on the effect of clamped edges is also wanted for the discussion of box models or diaphragm gauges, particularly when a baffle is fitted. For such cases the "piston in rigid wall" seems a definitely better approximation than the infinite plate.

Let us suppose, for the moment, that water is capable of standing tension. For ships' plates of the thicknesses used in practice, the reflected wave set up when they are acted upon by an explosion is almost entirely one of tension for a large plate so that the pressure at the plate quickly drops to zero and then to negative values. However, the pressure at the immobile wall remains positive, and a diffracted wave travels towards the centre of the plate, and thus enhances the damage. It is, in fact, shown by Butterworth that the effect of the diffracted wave may in a typical case be so great as to prevent the occurrence of tension at all, and that even when tension does occur, the diffracted wave eventually wipes it out, and urges the plate forwards again. In the infinite plate

case .....

case discussed by Taylor(1), this diffracted wave is absent, and tension, having once set in, persists indefinitely. It is clear that such a theory underestimates damage, and this can easily be seen to be true even if we assume that the plate leaves the water as soon as tension sets in.

If water cannot stand tension, then the plate will leave the water as soon as the pressure drops to zero, furthermore the water will cavitate as the tension-pulse set up by reflection at the plate travels outwards. Initially, the cavitated water will all be moving slower than the plate, but as the plate is brought to rest by the action of elastic and plastic stresses the water eventually catches up. For a very large plate it is clear that damage will be enhanced by this effect, and this is the case which is discussed below. Fox and Rollo have pointed out that, if cavitation occurs at a finite tension, the contribution to damage will vanish discontinuously if distance and weight of charge are changed continuously and bring the peak explosion pressure below a certain value. For a finite plate conditions will jump discontinuously from the "cavitation and follow-up" to the "diffracted wave" regimes in the same sort of way, and in such a case it is at present an open question which mechanism will be the more damaging. In any case, it seems clear that diffraction will predominate for a small plate, and cavitation for a large one, but it may be a matter of some difficulty to deal with the intermediate case, where both mechanisms are probably occurring together, cavitation at the centre, and diffraction near the edges.

Experimental evidence.

It is perhaps appropriate to mention at this point that the existence of cavitation in the water under such conditions has been established photographically beyond all possible doubt by Wright, Campbell and Senior in this country. U.S. Reports U.E. 10 and 19 are also relevant. In the latter papers it is also shown that cavitation is just prevented from occurring if conditions are such that the diffraction wave can reach the centre of the plate at the moment when the total pressure would otherwise have dropped to zero. Work on the motion of plates due to an explosion which also gives evidence that cavitation occurs is in hand at Road Research Laboratory(8), at the Taylor Model Basin(9) and at Admiralty Undex Works. This work is in qualitative agreement with theory, but until a method of allowing for edge effects has been worked out a quantitative comparison is not possible.

Little or no experimental evidence on the behaviour of sea-water under high rates of change of tension seems to be available. It is probably quite different from that of air-free water, which is what is usually studied in the laboratory. Even the static tension which pure water will stand does not seem to be known with any certainty.

Theory for an infinite plate.

(A)   Assumptions made.

As stated above, we shall be dealing with an infinite plate, and we shall also consider the case of a plane wave at normal incidence, so that conditions become effectively one-dimensional. We also assume that:-

(a)   The water cavitates at, or soon after, the instant at which the pressure drops to zero.

(b)   When the water catches up the plate after cavitation, it is brought to rest (relative to the plate) and does not rebound, so that a layer of "reconstituted" water gradually builds up on the plate. This water is treated as if it were incompressible.

Regarding assumption (a), there is considerable conflict of evidence on what the facts really are, and it is suspected that more than one parameter may in fact be involved. For example, it may well be that the rate of change of tension is important, as well as the tension itself.

Regarding assumption (b), the occurrences at the plate are probably very complex. Air-bubbles may persist so that cavitation does not disappear at once and pressure waves may be set up in the "reconstituted" water as the thickness of the layer grows. As the layer of "reconstituted" water turns out to be quite thin, any waves in this layer would probably soon be averaged out by reflection at the plate and at the surface. Very recently(9), some of the observed "kinks" in the deflection-time curves of diaphragms have been attributed to these waves.

(2) .....

(2) Taylor's theory.

The first stage of the motion has already been treated in detail by Taylor[1], so that a brief summary of his work is all that is needed, and we take up the problem at the point at which he leaves it.

Let y be the displacement of the plate in the direction of the incident pulse.

Let $\rho = \rho_m e^{-\frac{t}{\theta}} (t + \frac{x}{c})$ be the incident pulse coming from the positive direction.

$\rho = \phi (t - \frac{x}{c})$ be the reflected pulse (due to the motion of the plate).

ρ_a = mass of plate per unit area.

ρ_0 = density of water.

θ = the time constant of the pressure pulse (assumed exponential as usual).

The equation of motion of the plate is now:-

$$\rho_a \frac{d^2 y}{d t^2} = \rho_m e^{-\frac{t}{\theta}} + \phi (t) \tag{1}$$

Continuity at the surface of the plate requires that:-

$$\rho_0 c \frac{dy}{dt} = \rho_m e^{-\frac{t}{\theta}} - \phi (t) \tag{2}$$

Eliminating ϕ, we obtain the result:-

$$\rho_a \frac{d^2 y}{dt^2} + \rho_0 c \frac{dy}{dt} = 2 \rho_m e^{-\frac{t}{\theta}} \tag{3}$$

The solution of this, for which $y = \frac{dy}{dt} = 0$ at $t = 0$ is:-

$$\left.\begin{array}{l}
\dfrac{dy}{dt} = \dfrac{2 \rho_m}{\rho_0 c (1 - \alpha)} \; (e^{-\frac{t}{\theta}} - e^{-\frac{t}{\alpha\theta}}) \\[4mm]
y = \dfrac{2 \rho_m \theta}{\rho_0 c (1 - \alpha)} \; (1 - e^{-\frac{t}{\theta}} - \alpha + \alpha e^{-\frac{t}{\alpha\theta}})
\end{array}\right\} \tag{4}$$

where we have written α for $\dfrac{\rho_a}{\rho_0 c \theta}$. In Taylor's notation $\alpha = \frac{1}{\xi}$.

We assume with Taylor the result that, in any practical case, the effect of elastic and plastic forces on the motion of the plate is negligible during the time while the net pressure on the plate is positive. This fortunate circumstance has enabled us to drop the "spring" term in equation (1). In general also α is small compared with unity, $\alpha = 1$ would imply a plate about a foot thick for a 300 lb. charge, and about $\frac{1}{2}$ inch thick for a 1 oz. charge. The expression for the pressure at the plate is:-

$$p = \rho_m e^{-\frac{t}{\theta}} + \phi (t)$$

$$= \frac{2 \rho_m}{1 - \alpha} \left(e^{-\frac{t}{\alpha\theta}} - \alpha e^{-\frac{t}{\theta}} \right), \text{ using equations (2) and (4).} \tag{5}$$

The expression for the pressure in the water is obtained by taking account of the fact that ϕ represents a reflected pulse:-

$$p = \rho_a e^{-\frac{t}{\theta} - \frac{x}{\theta c}} + \rho_m e^{-\frac{t}{\theta} + \frac{x}{c}} - \frac{2\rho_m}{1 - \alpha} \left(e^{-\frac{t}{\theta} + \frac{x}{\alpha\theta c}} - e^{-\frac{t}{\alpha\theta} + \frac{x}{\alpha\theta c}} \right) \tag{6}$$

For .....

260 - 6 -

(a) Calculation of expression (C).

We require the quantity $\frac{\phi^2}{\rho_0 c^2}$ integrated, at the Taylor cavitation time, between $x = 0$, and $x = x_0$, where x_0 is the distance at which $\phi\left(t - \frac{x}{c}\right)$ vanishes at $t - C_c$, i.e. the co-ordinate of C at this time.

x_0 is determined by the equation:-

$$2\, e^{-\frac{\theta_c}{\overline{a\theta}}}\, e^{-\frac{x_0}{a\overline{a\theta}}} = (1 + a)\, e^{-\frac{\theta_c}{\theta}}\, e^{-\frac{x_0}{c\theta}} \tag{13}$$

Using the expression for ϕ obtained from equations (2) and (8). Performing the above integration, and using the above equation for x_0, we obtain for E_c the value:-

$$E_c = \frac{\rho_n^2 \theta}{\rho_0 c}\left[\frac{2a^2}{(1+a)}\left(\frac{4a}{(1+a)^2}\right)^{\frac{2}{a-1}} - (2a + \frac{1}{2})\right]\, a^{\frac{2a}{a-1}} \tag{14}$$

The total available energy is thus equal to $E + E_b + E_c$, which gives us:-

$$\text{Available energy} = \frac{2\rho_n^2\theta\,(1+a)^{\frac{1+a}{a-1}}}{\rho_0 c_a(1-\frac{1}{a})} \tag{15}$$

This agrees with the results given by Fox and Rollo but differs slightly from that used by Kirkwood which is equivalent to:-

$$\text{Available energy} = \frac{2\rho_n^2\theta}{\rho_0 c}\,(a + \frac{1}{2})\, a^{\frac{2a}{a}} \tag{16}$$

obtained by adding together E_T and E_b, but neglecting E_c.

The total energy that falls on unit area of plate is given by integrating the energy in the incident wave. It is simply:-

$$\text{Total energy} = \frac{\rho_n^2\theta}{2\rho_0 c} \tag{17}$$

Thus, the ratios of total energy to energy initially given to plate as kinetic energy, and to energy converted into kinetic energy of cavitated water or spray, can be expressed as functions of the single quantity a. The relevant information is given in Table 1.

TABLE 1.

Available damaging energy, as a fraction of the total energy, according to various assumptions.

a	.01	.05	.10	.15	.20	.25	.5	1	2
Taylor Energy (E_T)	.036	.16	.24	.31	.36	.80	.50	.55	.50
Available Energy ($E_T + E_b$) (Kirkwood)	.95	.88	.84	.92	.805	.80	.75	.66	.56
Total available energy ($E_T + E_b + E_c$)	.99	.97	.96	.935	.927	.91	.84	.74	.59

We are interested principally in the region of small a, and it is just here that we get the biggest gap between the Taylor energy, and the total available energy. The extra energy is in the form of kinetic energy of the cavitated water. When this water collides with the plate and a

layer ......

layer of water is built up upon it, it by no means follows that all this energy is available to cause plastic damage. In fact, this will only occur if the velocities of water and plate are nearly equal at the moment of collision, during the whole motion, which is not probable.

(4) The second phase of the motion.

In order to throw some light on this point, we must investigate the motion of plate and water after cavitation. Attempts were first made to do this by an application of Kennard's(6) theory of the propagation and disappearance of cavitation, but they proved ineffectual for two reasons. First, Kennard(6) uses Eulerian co-ordinates, whereas Lagrangian co-ordinates, which enable one to follow the motion of each particle of water, are much more appropriate to this problem. Secondly, it is not always possible to assume that the volume of "cavity" is everywhere small compared with the volume of water, and this invalidates some of Kennard's formulae.

Let us fix our attention on a particle of water, which, at the instant of cavitation, was at a distance x from the origin. Cavitation will occur here at a time given by equation (7) and the particle will start towards the plate with a velocity given by equation (8). The particle will travel effectively in a vacuum with undiminished velocity until it collides with particles ahead of it. Since the velocity given by equation (8) decreases with increasing x, the particle cannot overtake those ahead of it until they have been brought to rest, which can only happen if they collide with the plate or with the layer of "reconstituted" cavity-free water that is being built up on the plate. In other words, when our particle arrives at this layer, the water already in the layer will be just that which, before cavitation, was between our particle and the origin. Thus, neglecting a small correction, due to the compressibility of the water, the thickness of the reconstituted layer is just x. Meanwhile, the plate has moved in a distance y, so that the time at which our particle arrives at the "reconstituted" layer is given by the time the cavitation front takes to travel to x, plus the time the "bubbly" water or "spray" takes to travel back a distance y to reach the layer, which by this time has grown to just the thickness x. The mechanism may be compared with the transfer of a pack of cards, one by one, from hand to hand. The assumption that the same mass of water fills the same volume before and after cavitation is justifiable from the compressibility point of view if $\rho_a \ll \rho_o c^2$ which is the ordinary condition for the applicability of "acoustic" theory. It is, however, still possible that bubbles may persist for some time, e.g. if they are due to dissolved air or if they are fairly large so that their period of oscillation is appreciable. If we use the "spray" concept, the oscillation of the bubbles would be replaced by the rebound of some of the water from the "reconstituted" layer. From the mathematical point of view, it is immaterial whether we use the concepts of "spray" or of "bubbly water", and we cannot yet distinguish very clearly between them experimentally.

(5) The equations of motion of the plate.

On the basis of the above discussion, and using equations (7) and (8), we obtain one relation between t, x and y.

$$ t = \frac{\theta a}{1-a}\left[\frac{x}{a\,\theta\,c} - \log\left\{ \sinh\left(\frac{x}{\theta c}\right) + a\cosh\left(\frac{x}{\theta c}\right)\right\} \right] + \frac{y}{v_c} \tag{18} $$

where v_c is given as a function of x by equation (8). The second relation is obtained by momentum considerations. The momentum of the plate and reconstituted water is $(\rho_a + \rho_c x)\frac{\partial y}{\partial t}$. The rate at which momentum is brought up by the "bubbly" water is $\rho_o \frac{\partial x}{\partial t} v_c$. We thus have:-

$$ \frac{d}{dt}\left[(\rho_a + \rho_c x)\frac{\partial y}{\partial t}\right] - \rho_o \frac{\partial x}{\partial t} v_c + \rho a \omega^2 y = 0 \tag{19} $$

where $\frac{\omega}{2\pi}$ is the pseudo-frequency of the plate under whatever forces are acting upon it, in our case presumably plastic forces. For a plate made of material with yield stress σ_o and clamped along a circle of radius R, we have for ω^2 the result:-

$$ \omega^2 = \frac{8\sigma_o}{\rho R^2} \tag{20} $$

Equations (18) and (19) are sufficient to determine x and y as functions of t, our initial conditions being that at $t = \theta_c$, $x = 0$ and y and $\frac{dy}{dt}$ are given by equation (4). A complete discussion of the problem would require numerical integration of these equations for a set of values of two parameters,

one .....

one of them is α and the other specifies the strength of the spring. The remaining physical quantities can be combined into multipliers in various ways by a suitable choice of non-dimensional units. One possible choice is given below.

(a)   The case $\alpha = 0$.

In this case we have $v_c = \frac{2\,p_m}{p_0\,c}\;e^{-\frac{2x}{c}}$ and equation (18) becomes:— $y = \frac{2\,p_0}{p_0\,c}\,e^{-\frac{2x}{c}}\,(t - \frac{x}{c})$

so that numerical integration can be carried out quite easily. It will be noticed that if $\alpha = 0$ the equations are both satisfied by taking x to be permanently zero, meaning that, if the plate is unrestrained, it moves forward uniformly and never collects any water so it at all. Any restraint on the plate, however small, will eventually result in its collecting all the cavitated water, so that there seems to be a definite singularity in the solution of this equation at $\omega = 0$. This peculiarity persists for all values of α, and may account for the difficulties experienced in obtaining a solution valid for ω small, the case we are interested in.   For example, one can use successive approximations based on the solution $y = \frac{2\,p_x\,t}{p_0\,c}$ for $\omega = 0$, and this leads to a solution in ascending powers of $t^{\frac{1}{2}}$, but it is useless for calculating the maximum value of y because the convergence becomes very poor if $\alpha \sim 1$. A number of step-by-step calculations were carried out for different values of ω. These all suggested that x was nearly proportional to t, and an approximate solution based on this was also tried but failed for the same sort of reason. It is like trying to calculate $\frac{\pi}{2}$ by equating the series for $\cos\theta$ to zero.

(b)   The case $\alpha = 1$.

Equations (18) and (19) simplify somewhat in the apparently singular case $\alpha = 1$; many of the terms take an undetermined form, but can be evaluated without difficulty. The equations then take the form:—

$$\frac{d}{dt}\left[(1 + x)\,\frac{dy}{dt}\right] - \frac{e^{-2x}}{\beta}\,\exp\left[\frac{1 - e^{-2x}}{2}\right] + s^2\,y = 0 \qquad (21)\ \text{R}$$

$$y = \frac{e^{-2x}}{\beta}\,\exp\left[\frac{1 - e^{-2x}}{2}\right]\left[t - x + \frac{1 - e^{-2x}}{2}\right] \qquad (22)\ \text{R}$$

where we have introduced non-dimensional units as follows:—

Unit of $t = \theta$
Unit of $x = c\theta$
Unit of $y = 2\,p_x\,\theta/p_0\,c$
Unit of pressure = That pressure which acting against the spring under static conditions would produce a deflection y equal to one non-dimensional unit.
$\alpha = \dfrac{p_0}{p_0\,c}$
$s^2 = \alpha\,\omega^2\,\theta^2$

Equations involving such units will be denoted by R.

(6)   Solutions of these equations.

A complete understanding of the problem would involve a set of solutions of these equations over a range of values of the two parameters α and s^2, but only the cases $\alpha = 0$ and $\alpha = 1$ seem workable from a computational point of view (except at expense). For the present, however, it is doubtful if expert assistance is needed, as we are interested practically in small values of α (0.01 to 0.1, say) and the solutions for $\alpha = 0$ should give a fair idea of the behaviour of thin plates. Five cases were computed, for values of S ranging from 1 to 10^{-3}. $s = 1$ represents the condition where the time-constant of the plate under plastic stresses is comparable with the time-constant of the pressure-pulse. This is an extreme case, and would only hold, e.g. for a small diaphragm gauge. The theory cannot, however, be applied directly to such a gauge, on account of diffraction effect of the edges, which would be very important. An idea of the behaviour of thick plates can be obtained by solving the equation for $\alpha = 1$ in a representative case (actually $\beta = 1$, $s = 2^{-1}$). The results obtained are set out in Table 2, and the solutions for $S = 10^{-1}$, $\alpha = 0$ and $\alpha = 1$ are plotted in Figures 2 and 3

respectively .....

respectively, together with the pressure-time curves in the water at the "reloading front", (the surface of the reconstituted layer) and at the surface of the plate. The method of obtaining these curves is fairly straightforward, the quantity $\rho_0 v_c \frac{dx}{dt}$ represents the rate at which momentum is brought up by the water, and $\rho_0 \left(v_c - \frac{dy}{dt}\right) \frac{dx}{dt}$ therefore represents the pressure at the reloading front (rate of destruction of momentum). The pressure at the plate is obtained from this simply by subtracting $x \frac{d^2 y}{dt^2}$ (to correct for the pressure drop in the column of water of length x which is being accelerated). Actually $\frac{d^2 y}{dt^2}$ is negative so that the pressure at the plate is higher than that at the reloading front. For $c = 0$ the pressure at the plate must be nearly equal to the pressure of the spring $= \rho_a \omega^2 y$. Since the plate is stretching plastically, we have to stop the integration as soon as y reaches a maximum; thereafter, instead of equation (19) we have y = constant, v_c and x being still related to t by equations (8) and (18). By equation (8) v_c is given as a function of x, and by equation (18) t can then be found in terms of x. We can thus calculate the further growth of the reloading front and the pressure at it is given by the expression $\rho_0 v_c \frac{dx}{dt}$. After the plate comes to rest, the pressure at it and at the reloading front must be equal, so that we got a discontinuous drop in the pressure at the plate at the maximum of y. The pressure at the reloading front remains continuous but there is a jump in its time-derivative. Such discontinuities are common in plastic plate theory, and need not cause any alarm. In this case they have been caused by the fact that while $\frac{dy}{dt}$ is zero at the maximum of y, there is a finite jump in $\frac{d^2 y}{dt^2}$ to zero.

In any case, these discontinuities would be "rounded off" by the elastic recovery that always occurs, so that $\frac{d^2 y}{dt^2}$ would change continuously.

TABLE 2.

Final deflections of plate, and energy balance,
for various values of S.

S	1	.316	.1	.1	.01	.001	
α	0	0	0	1	υ	0	
y_c	.360	1.73	8.02	3.93	5.11	5.11	в
x_m	.357	.830	.866	.820	.563	.464	в
t_m	1.05	3.33	10.7	18.7	104	1040	η
Energy received before cavitation	0	0	0	54%	0	0	
Energy absorbed from cavitated water	47%	60%	64%	7%	67%	66%	
Energy falling on plate after it has come to rest	24%	18%	15%	5%	16%	16%	
Energy lost by collision at reloading front before plate comes to rest	27%	22%	21%	9%	17%	16%	
Energy carried away by reflected wave, before cavitation	0	0	0	25%	0	0	

y_m = Maximum deflection of plate.

t_m = Time at which maximum occurs.

x_m = Thickness of reconstituted layer at this instant.

(a)   Energy balance.

The fractions of the total energy falling on the plate, that appears as kinetic energy and that is reflected away into the water before cavitation follow at once from Taylor's work[1]. The remaining energy is converted into kinetic energy of the water. The energy absorbed by the plate can be inferred from the step-by-step solution. In non-dimensional units this as a fraction

of the .....

of the total energy falling on the plate, is simply $4S^2 y_m^2$ (8). When the plate has come to rest only the water which, before cavitation, lay between the origin and $x = x_m$ has contributed to damage. Since the velocity v_c is a decreasing function of x, it is clear that, once the plate has come to rest, the pressure can never again build up to a value large enough to set it in motion. Thus, the kinetic energy of the remaining "bubbly" water is all wasted. From the expression (8) for the velocity, we can write down the kinetic energy and integrate from x_m to infinity, the results also being entered in Table 2. Finally, by subtracting all these percentages from 100, we can obtain the energy lost by collision at the reloading front while the plate is actually moving. This can also be inferred directly from the step-by-step calculations, by a numerical integration of the quantity $\frac{dx}{dt}\left(\frac{dy}{dt} - v_c\right)^2$ (8) which can easily be shown to represent the rate of loss of energy in this way (the total energy being unity). The agreement of those two methods provide a satisfactory over-all check on the computations, which appear to be accurate to within 2% at most. Table 3 below gives an idea of the dissipation of energy (expressed as a percentage of the total energy) that has occurred up to a given instant. (Time expressed in non-dimensional units).

TABLE 3.

Energy lost by collision up to a given time (as percentage of total energy).

S = 10⁻¹ → $S = 10^{-1}$

Time	4	5	6	7	8	9	10.7	12	14	16	16	18.7	units	8
α = 0	2.5	4.5	7	9	12	15	20		comes to rest					5
α = 1		Less than 2%					2	2.5	3.5	5	7	9	(comes to rest)	5

The figures for α = 1 are approximate only.

(7)   The third phase of the motion.

It seems advisable here to call attention to yet another effect that is experimentally known to be important for a finite plate, though it vanishes for an infinite plate. The motion may not be complete, even though all the originally "bubbly" water has piled up on to the plate. There is still a gap left in the water, as the net result of the processes we have followed so far has been that the plate has been pushed in, and the cavitated water has all followed it. In any actual case, the resulting gap would be filled by water that has never cavitated, which would follow immediately after the last of the "bubbly" water, and would be driven inwards by its hydrostatic pressure. Now we have seen that an infinite plate in general comes to rest long before all the cavitation has disappeared, so that there may well be an interval between the second and third phases of the motion, as indeed experimental work suggests that there is. (See, for example,(9) T.M.B. report R.248. evidence suggesting the same thing is being obtained at Admiralty Undex Works). Whether or when the "build-up" of pressure caused by the filling up of the gap is enough to force the plate forwards again remains a matter for detailed investigation, but the following rough argument (based on energy considerations) shows that the effect will have to be considered. Consider a plate clamped along a circle of radius R. It receives energy of the order of magnitude $\frac{p_0^2 \theta}{2 \rho_0 c} \pi R^2$. The mean deflection of the plate is given

by equating this to the plastic energy $\frac{1}{2} \pi \lambda \sigma_0 y_m^2$ so that

$$y_m^2 \sim \frac{p_0^2 \theta}{\rho_0 c} \frac{R^2}{4 \lambda \sigma_0} \tag{24}$$

Volume of dish = $\pi R^2 y_m$ and the energy acquired by water at pressure p_0 entering this volume is $p_0 \pi R^2 y_m$, and this is comparable with the energy already acquired by the plate if:-

$$\frac{p_0}{p_m} \sim \sqrt{\frac{4 \lambda \sigma_0 c}{R^2 \rho_0 c}} \tag{25}$$

where ......

where p_o is the hydrostatic pressure. Insertion of numerical values shows that in the majority of cases this effect is one to be reckoned with. (It is prevented from being of importance for the infinite plate by the fact that the mass of unit area of plate and reconstituted water is infinite). It is emphasised that this effect is distinct from both the impact of cavitated water that we have been studying and also from any effects due to bubble oscillations, though it is hydrodynamically akin to both of these.

Discussion of results.

The conclusion that cavitation is an important factor in producing damage in thin plates is in agreement with Kirkwood's[3] work, and the investigation for a very thick plate has shown that cavitation may make an appreciable contribution even in this extreme case. There is, however, a serious discrepancy, in that Kirkwood[3] finds that nearly all the energy is absorbed by the plate, whereas we have arrived at a factor of the order of $\frac{1}{2}$. If all the energy is to be absorbed, then we must have the velocities of the plate and the velocities of the cavitated water just arriving at the reloading front equal, and this is definitely not possible according to the equations we have obtained. The cause of the discrepancy may lie in the distinction that Kirkwood[3] draws between the over-damped and under-damped cases. This cannot be understood without access to his full theory. In this report all practical cases start by being over-damped (owing to the radiation term $p_o c \frac{\partial y}{\partial t}$) but become under-damped directly cavitation sets in. The present investigation gives reasonable grounds for hoping that satisfactory rules for assessing the importance of the effect from an engineering point of view will eventually be found without a prohibitive amount of numerical work. The next step is clearly to try and work out some methods of assessing the effect of edges and stiffeners, and of oblique incidence of the pressure-pulse.

Conclusion.

Kirkwood's general conclusion that cavitation contributes largely to damage of thin plates has been substantiated, and application of the theory to a thick plate indicates that the effect is appreciable even here. The conclusion that nearly all the energy that would otherwise be radiated away can be reabsorbed by this cavitation mechanism is not agreed with, as it is believed that a certain amount of loss at collision is inevitable. It is not possible to decide the question experimentally, because the effect of the edges is unknown.

References.

(1)   Taylor.   "The pressure and impulse of submarine explosion waves on plates".

(2)   Taylor.   "The distortion under pressure of a diaphragm which is clamped along
                      its edge and stressed beyond the elastic limit."

(3)   Kirkwood.   U.S. Report U.E. 10.

(4)   Kennard.   Phys. Rev. March 1943.

(5)   Kennard.   Taylor Model Basin Report 511.

(6)   Kennard.   Taylor Model Basin Report 527.

(7)   U.S. Reports U.E. 18 and 19.

(8)   G.Charlesworth "Deflection-time curves, at the centre of box-model plates, resulting
                      from underwater explosions".

(9)   Taylor Model Basin Report R.248.
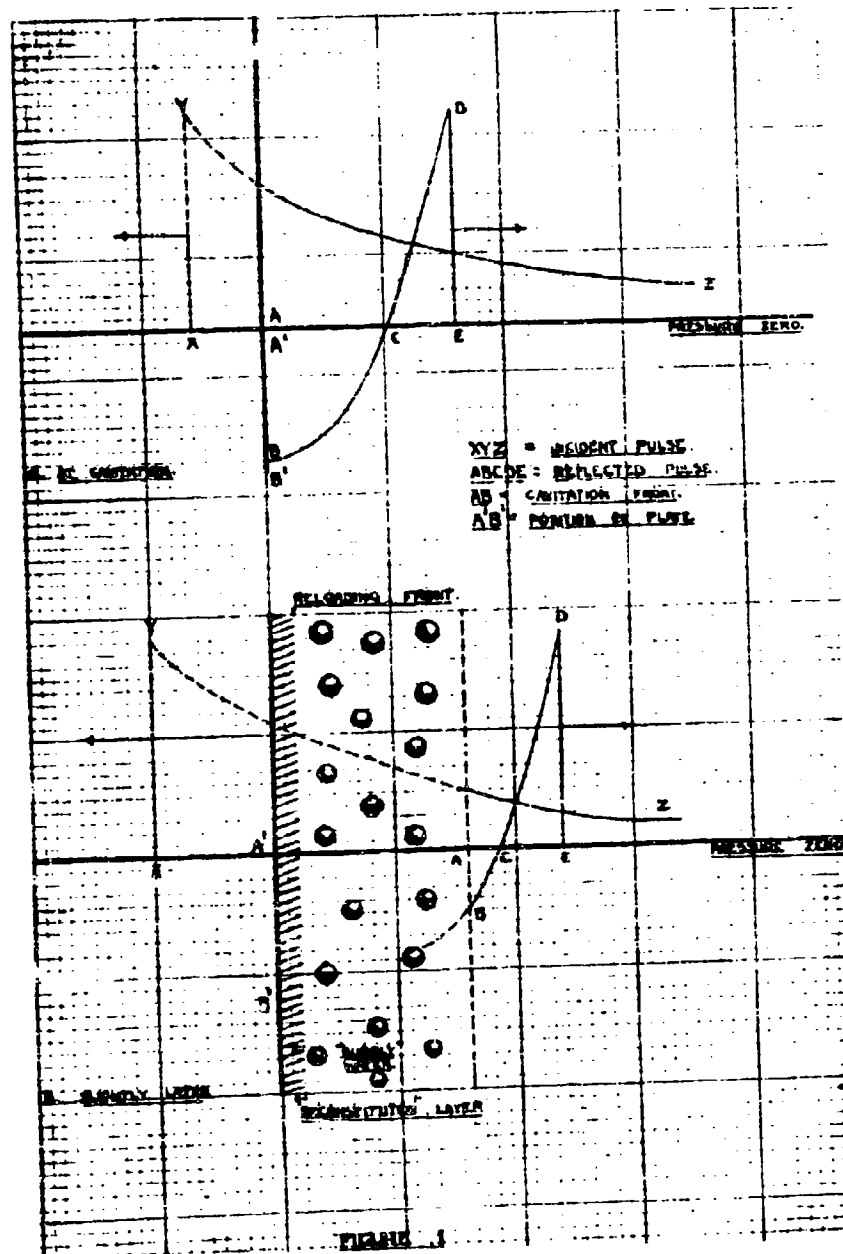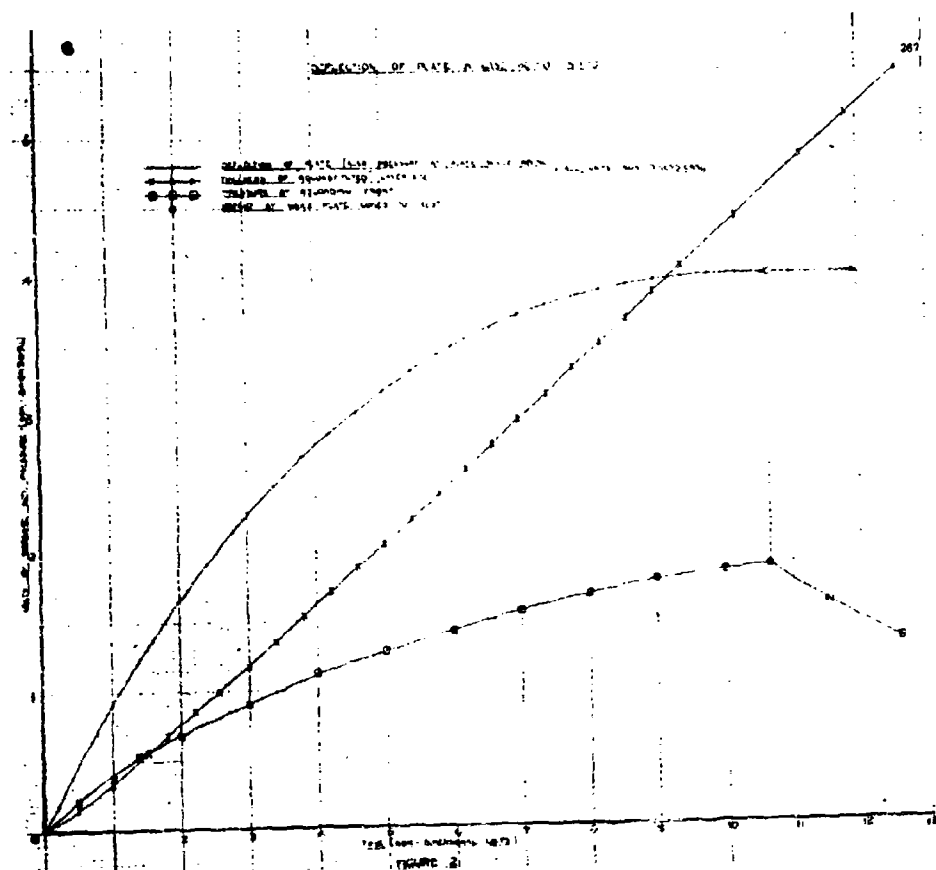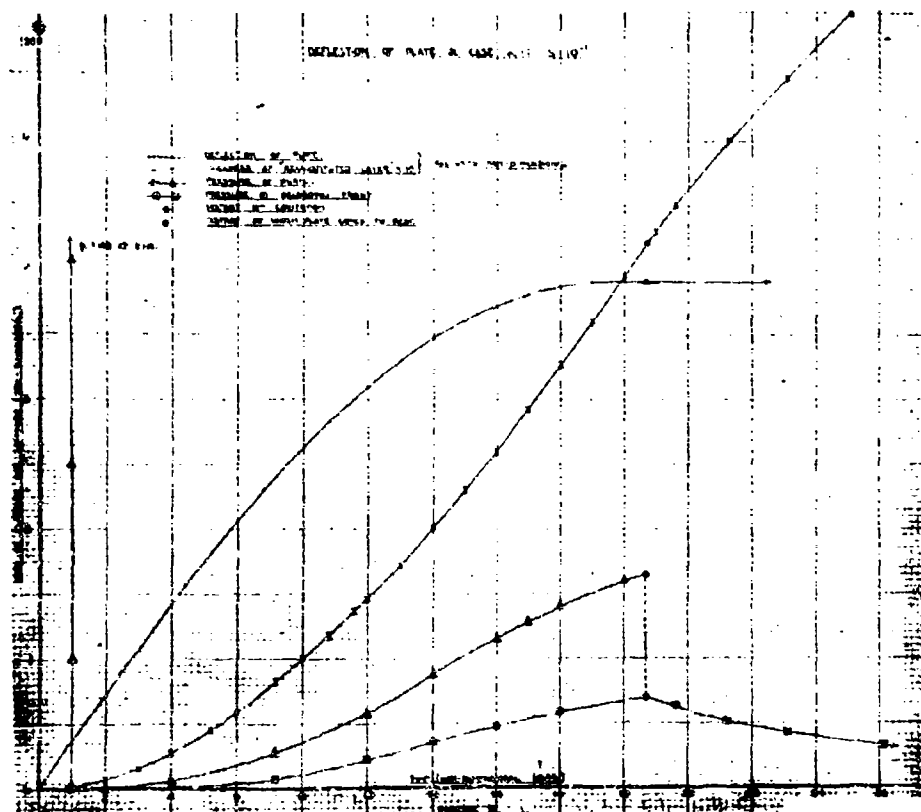
FIGURE 1

FIGURE 2

THEORETICAL INVESTIGATION OF CAVITATION PHENOMENA
OCCURRING WHEN AN UNDERWATER EXPLOSION IS
INCIDENT ON A YIELDING SURFACE - II

H. N. V. Temperley and Ll. G. Chambers
Admiralty Undex Works, Rosyth, Scotland

British Contribution

December 1944

THEORETICAL INVESTIGATION OF CAVITATION PHENOMENA OCCURRING WHEN AN UNDERWATER EXPLOSION IS INCIDENT ON A YIELDING SURFACE - ii

H. N. V. Temperley and Ll. G. Chambers

December 1944

*   *   *   *   *   *   . *   *

List of Symbols.

p_m =   maximum pressure of incident pulse.

p_i =   pressure in incident pulse.

p_r =   pressure in reflected pulse if plate were stationary.

p_ρ =   pressure due to motion of plate.

θ =   time constant of incident pulse.

c =   velocity of sound in water.

x =   distance from centre of plate along axis.

y =   deflection of plate.

R =   radius of plate.

r =   distance from centre of plate along radius.

s =   distance between two typical points on the plate.

ρ =   density of plate.

h =   thickness of plate.

σ_0 =   yield stress of plate.

ρ_0 =   density of water.

α = $\dfrac{\rho h}{\rho_0 c \theta}$

ρ = $\dfrac{\pi R}{2 c \theta}$

s = $\theta \sqrt{\dfrac{8 \sigma_0}{\rho R^2}}$

F =   force on plate.

u =   velocity of plate.

u_0 =   maximum velocity of plate.

$\equiv$ means that an equation is non-dimensional.

ψ, ω, n, γ are defined in the text.

270   - 2 -

Summary.

The problem of determining the history of cavitation and follow-up of water when an infinite plate is subjected to an exponential underwater explosion pulse has been considered in Report "Theoretical Investigation on Cavitation Phenomena occurring when an underwater Pressure Pulse is incident on a yielding surface — 1," referred to as I. In the present report a start is made on the problem of taking into account the modifications introduced if the plate is clamped at the edges and surrounded by an infinite rigid baffle. The consequences of the customary assumption of "proportional motion" are worked out in two specific cases, the "rigid piston" and the "paraboloid" approximations, and it is concluded that, in both, the cavitation time, as determined by vanishing pressure at the central point, is shortened, as compared with the infinite plate, due to the effect of the diffracted wave from the edge. It is found that the conditions at which cavitation just fails to occur also mark approximately the upper limit for the validity of incompressible theory and correcting terms are worked out for such a case.

The assumption of "proportional motion" is criticised on the ground that it is probably not valid during the early motion of the plate, and a more natural assumption is found to lead exactly to the criterion for cavitation at a finite plate suggested by Kirkwood (6), which is known to give good agreement with the experiments so far carried out. The criteria established for the occurrence of cavitation and for the failure of incompressible theory are applied to various types of diaphragm gauge. It is found that gauges of the "box model" type are so far removed from the critical region that the theory of I is probably valid, and that it should be fair to apply incompressible theory to gauges of the crusher type and to the smaller sizes of diaphragm gauge. The 6 inch copper diaphragm gauge appears to be a borderline case, where readings will be hard to interpret in terms of absolute values, though a corrected version of incompressible theory may prove satisfactory. Some suggestions for further work are outlined.

Introduction.

In a previous report (1) referred to hereafter as I, an account has been given of the present position of the theory of the motion of a clamped plate when subjected to an explosion pulse. It is there shown that a plate whose dimensions are large compared with the distance sound travels in the characteristic time of the assumed exponential pressure will behave very like a free surface, and, in particular, that finite tensions will first occur in the water near the plate, and will spread out into the water behind the reflected pulse. Taylor (2) solved the problem of the motion of such a plate, first on the assumption that water can stand tension everywhere, secondly on the assumption that water can stand tension, but that the interface between water and plate cannot, so that the plate leaves the water as soon as tension sets in, and acquires no further energy from it. In I, the same problem was solved, in some representative cases, on the assumption that water cannot stand tension at all, so that cavitation sets in wherever the pressure in the water drops to zero. The laws of the propagation of the cavitation front, and of the distribution of velocity in the cavitation zone, can easily be written down, and the equations governing the motion of the plate when bombarded by the cavitated water, accompanied by the disappearance of the cavitation, can also be formulated, but have to be solved numerically. It was found that the effect of the cavitated water colliding with the plate, thus communicating extra energy to it, may be very important for plates of thicknesses usual in ship construction, even though an appreciable percentage (of the order of 30%) of the kinetic energy of the cavitated water is lost on collision with the plate.

The modifications required by the fact that a plate may be clamped at the edges, as in a diaphragm gauge, and that the clamped edges may be surrounded by a practically rigid baffle, as in the box model, or again by the fact that a plate may be backed by stiffeners, as in a ship, were discussed qualitatively in I. To a first approximation, the effect of a baffle can be taken into account if we regard the plate as a piston moving in an aperture in a rigid wall. The relationship between this model and the infinite plate theory has been discussed by Butterworth and Wigglesworth (3), who showed that, provided cavitation does not occur, the motion of the piston could, in a typical case, have been represented by incompressible theory to a good approximation. It is the purpose of this report to examine this relationship a little more closely, and to try and set up a criterion to determine whether tension will occur or not. If tension does not occur, then one can be confident of the absence of cavitation, but if one is near the critical region it may be that some correction to the result given by incompressible theory is needed. If tension does occur, then one would expect the investigation given in I for an infinite plate to give satisfactory results provided that one were well away from the critical region, but near it one would have to take account simultaneously of diffraction and cavitation which would be very difficult. In this report we shall not attempt either of these last two problems.

The .....

The Equation of Motion of the Plate.

The investigation is based on an equation obtained by Butterworth and Wigglesworth. If the piston is at rest, it forms, in conjunction with the baffle, a rigid surface, and the pressure at it is just double that due to the incident wave above. If the piston is moving with a velocity U(t), there is a relief pressure due to this motion, which tends to decelerate the piston. By integrating the usual expression for the retarded potential over the surface of the piston, one gets the relief pressure at any point on the piston, and a second such integration gives the total force on the piston due to the relief pressure. It is (if U = 0 for t < 0)

$$ F = \rho_0 c - R^2 \left[u(t) - \frac{2c}{\pi R} \int_0^t \left(1 - \frac{c^2 t'^2}{4 R^2} \right)^{\frac{1}{2}} U(t - t') \, dt' \right] \tag{1} $$

where R is the radius of the piston, and ρ_0 and C are the density of and velocity of sound in water. For $t > \frac{2R}{c}$, the integration stops at $\frac{2R}{c}$. For a reason that will appear later, we shall not be concerned with times greater than $\frac{R}{c}$. For times up to this limit, the factor

$\left(1 - \frac{c^2 t'^2}{4 R^2} \right)^{\frac{1}{2}}$ is never less than $\sqrt{\frac{3}{2}}$, and since U is positive at any stage of the motion with

which we shall be concerned, it follows that the error in taking this factor equal to unity cannot possibly exceed 13% even in the very worst possible case (and in all ordinary cases it will be very much less than this). We may therefore assert with some confidence that the equation of motion obtained by Butterworth and Wigglesworth

$$ \rho h \, \frac{d^2 y}{dt^2} + \rho_0 c \, \frac{dy}{dt} - \frac{2 \rho_0 c^2}{\pi R} \, y = 2 p_m \, \rho^{-\frac{t}{\theta}} \tag{2} $$

is a good approximation for $t < \frac{R}{c}$. In this equation, y is the displacement of the piston, ρ its density and h its thickness, also p_m is the maximum pressure in the incident pulse and θ its time-constant. We introduce non-dimensional units as in I.

α = non-dimensional thickness of plate = $\dfrac{\rho h}{\rho_0 c \theta}$

β = non-dimensional radius of plate = $\dfrac{\pi R}{2 c \theta}$

Unit of displacement = $\dfrac{2 p_m \theta}{\rho_0 c}$

unit of time = θ

As in I, equations involving these units will be marked N. Equation (2) becomes

$$ \alpha \, \frac{d^2 y}{dt^2} + \frac{dy}{dt} - \frac{y}{\beta} = \rho^{-t} \qquad \text{N} \tag{3} $$

For a large plate, the term $-\frac{y}{\beta}$ becomes negligible, and the theory reduces to Taylor's (2) case. As in Taylor's work, the energy expended in stretching the plate has a negligible effect on the early part of the motion. The solution of equation (3), for which $y = \frac{dy}{dt} = 0$ at $t = 0$ is to the first order in $\frac{1}{\beta}$

$$ y = \frac{(1 + \beta) \alpha \beta}{(2\alpha + \beta)(1 + \beta - \alpha \beta)} \, \rho^{-t\left(\frac{1}{\alpha} + \frac{1}{\beta}\right)} - \frac{\beta \rho^{-t}}{(1 + \beta - \alpha \beta)} + \frac{(\alpha + \beta - \alpha \beta)}{(1 + \beta - \alpha \beta)(2\alpha + \beta)} \, \rho^{+\frac{t}{\beta}} $$

$$ \text{N} \quad (4) $$

Comparison ......

Comparison with Rayleigh's Work.

It is interesting to compare equation (1) with the apparently different equation obtained by Rayleigh (4) (see, for example, Theory of Sound, Volume II, paragraph 302) for the reaction pressure on a piston vibrating in an aperture in a rigid wall with a frequency $\omega/2\pi$ and maximum velocity U_o. The expression is

$$F = -\pi R^2 U_o \rho \, e^{i\omega t} \left[\rho_o C \left(1 - \frac{J_1(2kR)}{kR} + i \frac{H_1(2kR)}{kR} \right) \right] \tag{5}$$

where $k = \frac{\omega}{c}$, and J_1 and H_1 are respectively Bessel and Struve functions of order unity. Since any motion, periodic or not, can be represented by a Fourier integral, it is to be expected that equation (5) is equivalent to the more general form of equation (1) when $U(P)$ is not zero. This is in fact so, but the formal proof is rather long and is given in the Appendix. Equation (5) takes especially simple forms when kR is very large or very small.

(a)   **kR large:** $F \sim \pi R^2 U_o \rho \, e^{i\omega t} \left(\rho_o C + \frac{2i}{\pi} \frac{\rho_o c^2}{\omega R} \right)$ (6)

The first of these terms is the radiation damping term, corresponding to the second term on the L.H.S. of equation (2), while the second term (corresponding to the third term on the L.H.S. of equation (2)) measures the effect of diffraction on to the piston of the pressure-charges at the immobile walls. We thus conclude that equation (2) is likely to be a better approximation for a finite plate than Taylor's (2) infinite plate theory, which takes only the radiation damping term into account. This would have been sufficient justification for investigating the solutions of equation (2), but the argument in paragraph 2 is more precise, and enables us to set an upper limit to the error.

(b)   **kR small:** $F \sim \pi R^2 U_o \rho \, e^{i\omega t} \left(\frac{\rho_o \omega k R^2}{2} + \frac{8}{3\pi} \rho_o i \omega R \right)$ (7)

The second of these terms is proportional to the acceleration, and, in fact, arises from the "virtual mass" of the water moving with the piston that is obtained from incompressible theory. The first term is proportional to the differential coefficient of the acceleration, and also to $\frac{1}{c}$, and is therefore a correcting term, absent in incompressible theory. This suggests that we try the following equation as a correction to incompressible theory (expressed in non-dimensional units).

$$ - \frac{3\beta^2}{\pi^2} \frac{d^3 y}{dt^3} + \left(\frac{16}{3\pi} \beta + \alpha \right) \frac{d^2 y}{dt^2} = \rho^{-t} \tag{8}$$

Equation (8) (without the first term) is what would be obtained using incompressible theory. The correcting term tends to make the deflection smaller. A discussion of the effect of this correction on the final deflections is reserved for another report.

Regions of Validity of Equations (3) and (8).

The position is now as follows. The crude argument that the main contribution to the Fourier integral representing the motion of the plate will be from frequencies corresponding roughly to the inverse time-constant of the explosion, leads us to equation (3) for large plates and equation (8) for small ones, but gives no indication of the errors to be expected from their use. The more precise argument of paragraph 2 indicates that equation (3) will be best for short times and enables us to estimate the error. An argument due to Kennard (5) shows that the total impulse due to relief pressure plus diffraction from the edges vanishes for long times so that incompressible theory (or the improved version of it given by equation (8)) should be best for long time, provided that cavitation does not occur. His argument is based on the fact that the total pressure due to the motion of the plate is given by an integral involving the acceleration of the plate, so that the integral of this pressure between zero time and the time at which the plate comes to rest must vanish. We therefore use equation (3) in order to determine our cavitation criterion. Equation (8) could have been obtained directly from equation (1) by expansion of the second term in powers of $\frac{1}{c}$, integrating twice by parts.

Pressure .....

Pressure along the Axis of the Plate.

If we take the motion of the plate as given, we may calculate the pressure due to this motion at points along the axis, and in particular at the centre of the plate, without approximation. If $U(t)$ represents the velocity of the plate, x the distance along the axis, and r the distance from this point to a typical point on the plate, then we have, by the usual formula,

$$p_p = \frac{\rho_0}{2\pi} \int_x^{(x^2+R^2)^{\frac{1}{2}}} \int_0^{2\pi} \left(\frac{\partial u}{\partial t}\right)_{h-\frac{r}{c}} \, dr \, d\theta = -\rho_0 c \left[u(t-\frac{x}{c}) - u\left(t - \frac{(x^2+R^2)^{\frac{1}{2}}}{c}\right) \right] \quad (9)$$

which is rigorously correct along the axis. In our case U vanishes for negative times, so the two terms in equation (9) vanish for negative values of the argument. In addition to this, we have the pressure due to the incident pulse, and the pressure due to the pulse reflected by the rigid wall, expression (9) giving the modification to the latter due to part of the wall being movable. We thus have for the total pressure the complete expression

$$p = p_i + p_r + p_p = p_m^{-\frac{1}{\theta}(t+\frac{x}{c})} + p_m^{-\frac{1}{c}(t-\frac{x}{c})} - \rho_0 c\, u(t-\frac{x}{c}) + \rho_0 c\, u\left(t - \frac{(x^2+R^2)^{\frac{1}{2}}}{c}\right)$$

$$(10)$$

By means of this expression, we can discuss the complete history of pressure variations at points along the axis. The condition for cavitation is that expression (10) must be zero or negative. By the approximation used in spherical diffraction theory (that the plate may be taken as a portion of a sphere with the point in question as centre), one can also calculate the variation of pressure at points whose distance from the axis is small compared with x, but a complete expression for the pressure history at an arbitrary point does not seem to be possible, except as a definite integral or a series, even if we assume U to be given

The Onset of Cavitation.

If we use equation (3), or its approximate solution (4), in conjunction with equation (10), and put $x = 0$, we get the condition for the occurrence of zero pressure at the central point in the form

$$\rho^{-t}(1-\alpha\beta) - \frac{(\alpha+\beta-\alpha\beta)}{(2\alpha+\beta)}\rho^{+\frac{t}{\beta}} + \frac{(1+\beta)(\alpha+\beta)}{(2\alpha+\beta)}\rho^{-t\left(\frac{1}{\alpha}+\frac{1}{\beta}\right)} = 0 \qquad \qquad (11)$$

$$\left(t < \frac{R}{c\theta} = \frac{2\beta}{\pi} \right)$$

which reduces to Taylor's cavitation condition (2) for β very large.

This transcendental equation has been solved for various values of α and β, and the results are plotted in Figure 1. It will be seen that for $\beta > 10$ the plate may be effectively regarded as infinite, but that for smaller values the cavitation time begins to shorten appreciably. We now have to consider what happens for values of the non-dimensional time greater than $\frac{R}{c\theta}$ so that the final term in equation (10) becomes non-zero. This term always contributes a positive pressure, so tending to prevent cavitation. It can, in fact, be shown that if the pressure at the centre just vanishes at the critical time $t = \frac{R}{c}$ when the diffraction wave has just arrived at the centre, the time derivative of the pressure will be positive. This confirms Kirkwood's[?] suggested criterion for cavitation, that it occurs either before $t = \frac{R}{c}$, or not at all. Equation (10) shows, without difficulty, that cavitation is more likely to occur at the centre than at any other point on the axis. It also follows that the centre is more favourable than other points on the plate, because the diffraction wave arrives at any other point before it does at the centre. (It can be verified rigorously that for points near the centre the term $-\rho_0 cU$ is unaffected, but that the second term in equation (9) has to be modified to allow for the edge being nearer).

Insertion of the value $\frac{2\beta}{\pi}$ for the non-dimensional time in equation (11) gives us a critical curve relating to α and β. The following values have been worked out, and compared with what one gets if one uses Taylor's expression (2) $t = \frac{\alpha \log \alpha}{\alpha - 1}$ (4) for the cavitation time, i.e. neglects the effect of finite β.

Table 1 .....

TABLE 1.

Values of α and β for which cavitation is just prevented.

β	1.0	0.1	0.01
α (from equation 12)	No solution	0.124	0.012 9
α (neglecting effect of finite β)	1.00	0.015	0.000#

Thus, it will be seen that the effect of the diffraction at the edges, in "hurrying on" the onset of cavitation, may make cavitation possible at distinctly larger thicknesses of plate than we should deduce from infinite plate theory.

Propagation of Cavitation along the Axis.

Equation (10) can also be applied for non-zero values of x. One gets a transcendental equation slightly more complicated than equation (11), and can then obtain an idea of the extent of the cavitation zone by solving this equation for various values of x. The limit to the cavitation zone is set by the point at which the diffraction wave from the edge (represented by the fourth term in equation (10)) arrives at the instant when the pressure would otherwise drop to zero. The corresponding value of x should measure the length of the "beard" of bubbles that photographs show near the plates. Unfortunately, it seems that, in practical cases, the length of the "beard" is very sensitive to the other parameters, becoming very long compared with the radius of the plate even when one is not far off the critical conditions for the occurrence of cavitation at the centre of the plate. The reason for this is as follows. The position of the tip of the "beard" is determined by the diffraction wave, travelling a distance $(x^2 + a^2)^{\frac{1}{2}}$ with velocity of sound overtaking the cavitation front, which travels a distance x, slightly faster than sound but is slightly handicapped by the fact that cavitation does not begin until a finite time after the arrival of the incident pulse, whereas the diffraction wave starts off at this instant. If α is small, cavitation begins almost immediately so the handicap is small, and the cavitation front spreads a great distance into the water before the diffraction wave can overtake it. Since we are concerned, in practice, with small values of α, we should expect the theoretical length of the "beard" to be sensitive to α and hence to the time-constant of the pulse, and some specimen calculations showed that this was so. Attempts were made to compare the theory with the experimental results on the appearance of cavitation quoted in various U.S. reports (7), but the fact that the experimental knowledge of the time-constants of small charges is rather uncertain made it impossible to do more than verify that the theory gives results of the right order of magnitude.

The "Paraboloid" Approximation.

An objection to the "piston" approximation is that it does not allow for any bending of the plate. Since we should allow for the effect of immobilisation of the edges of a clamped plate, it would be better if we assumed the velocity to be distributed over the plate in such a way that the edge is at rest. The simplest assumption of this kind that one can make is that the velocity is distributed according to a parabolic law $u = 2u_0 \frac{a^2 - r^2}{a^2} f(t)$. Although the

observed final forms of dished plates are often not unlike this shape, it does not follow that the velocity of a given point is always the same fraction of the central velocity. Indeed, experimental work on the motion of various parts of a circular diaphragm and theoretical work on the mechanism of a "wave of fixity" travelling from edge to centre by which the diaphragm is brought to rest both make it likely that the approximation is only rough. Its consequences can, however, be investigated without much trouble, and it seems a more natural approximation than the "piston" one. Rayleigh's method for a piston vibrating with frequency $\frac{\omega}{2\pi}$ can be modified fairly easily, or we could derive an equation analogous to equation (5).

The .....

The Equation of motion of the plate according to this Approximation.

We take as our expression for the velocity of the plate

$$u = 2 u_0 \, e^{i\kappa t} \; \left(\frac{R^2 - r^2}{R^2}\right) \tag{12}$$

where r is the distance from the centre.

As the plate is now moving as a rigid body, it would not be correct to integrate up the pressure over the plate and then write down the equation of motion directly from this, as we did for the piston. We must first multiply the pressure at each point of the plate by the velocity at that point, and then integrate over the surface of the plate. This gives us the rate of doing work on the plate, which we can equate to the rate of change of kinetic energy of the plate to give the equation of motion. In equation (12) we have chosen the factor 2 in order this u_0 may represent the velocity of the "equivalent piston", i.e. the piston moving with a velocity u_0 would sweep out the same volume as the plate. The mean kinetic energy of the plate is given by

$$\varepsilon = \frac{1}{2} \, \rho_0 \, a \, u_0^2 \, \rho^2 \, e^{i\kappa t} \int_0^{2\pi} \int_0^R \; \left(\frac{u^2 - r^2}{R^2}\right)^2 \; r \, dr \, d\Omega = \frac{2 h}{3} \, R^2 \, u_0^2 \, \rho^2 \, e^{i\kappa t} \tag{13}$$

The relief pressure due to the motion of the plate is given, at a point distant r from the centre, by

$$p_p = \frac{\rho_0 \, i \omega \rho}{2\pi} \, e^{i\kappa t} \quad 2 u_0 \int \frac{R^2 - r^2}{R^2} \; \frac{e^{iks}}{s} \; dS,$$

where the integration is taken over the whole plate, and s is the distance between the point in question and a typical point on the plate. The rate of doing work on the plate is obtained by multiplying this integral by expression (12), and then again by $2\pi \, r dr$ and integrating from 0 to R. The multiple integral thus obtained can be evaluated by the method used by Rayleigh (4), the result for the rate at which the relief pressure does work being

$$\frac{8\pi \rho_0 \, u_0^2 \, c \rho^2 \, e^{i\kappa t}}{R^2} \quad \left| \; (J_1 \, (2 \kappa R) - i \, H_1 \, (2 \kappa R)) \left(-\frac{9}{R\kappa^2} + \frac{4R}{\kappa^2} \right) + \frac{5}{\kappa^3} \, (J_0 \, (2 \kappa R) - i \, H_0 \, (2 \kappa R)) \right.$$
$$\left. + \frac{\kappa^4}{6} + \frac{\kappa^4}{7\kappa^7} + \frac{201}{3\pi} \, \frac{R}{\kappa^3} \right| \tag{14}$$

The forms which expression (14) takes for κR large and κR small are respectively

$$8\pi \rho_0 \, u_0^2 \, c \rho^2 \, e^{i\kappa t} \; \left(\frac{R^2}{6} + \frac{1}{2\kappa^2} \right) \qquad (\kappa R \text{ large}) \tag{15}$$

and

$$8\pi \rho_0 \, u_0^2 \, c \rho^2 \, e^{i\kappa t} \; \left(\frac{125 \, R \, i\kappa}{315 \, \pi} + \frac{3}{16} \, R^2 \, \kappa^2 \right) \qquad (\kappa R \text{ small}) \tag{16}$$

These expressions, together with expression (14), suggest the following equation in place of equation (2).

$$\frac{R}{c\theta} \text{ large}; \quad \frac{2}{3} \, \rho h \, \frac{d^2 x}{dt^2} + \frac{2}{3} \, \rho_0 \, c \, \frac{dx}{dt} - \frac{2\rho_0 \, c^3}{R^2} \int_0^t y \, dt = 2 \, p_m^{-\frac{1}{2}} \hat{\theta} \tag{17}$$

and the following equation in place of equation (8)

$$\frac{R}{c\theta} \text{ small}; \quad -\frac{R^2}{m} \, \frac{d^2 y}{dt^2} + \left(\frac{1625 \, R}{m^2} + \frac{i\omega}{3} \right) \, \frac{d^2 y}{dt^2} + \frac{1}{2} \, s^2, = \rho^{-t} \qquad m \tag{18}$$

where y represents the central deflection and $s^4 = \dfrac{\theta^2}{\rho} \dfrac{8 \sigma_0}{R^4}$: ing a measure of the energy required to stretch the plate plastically, σ_0 being the yield stress. (In the "piston" approximation we cannot fix this coefficient unambiguously).

Comparison with the "Piston" Approximation.

Equation (18) is very similar to equation (8), differing from it only in the numerical coefficients. In a later report it is hoped to examine a case where the corrections to incompressible theory are not negligible, but where cavitation probably does not occur. Equation (17) differs from equation (2) both in the numerical coefficients and also in the fact that the first order correcting term is proportional to the time integral of y instead of to y itself. The reason for the latter difference is that the edge of the plate is being kept at rest, so that the effect of the diffraction wave is less abrupt, and therefore less important in the very early stages of the motion, than it is when the velocity jumps discontinuously to zero at the edge. The former difference means that, for a very large plate where both types of correction term are negligible, cavitation will set in according to the "piston" approximation at precisely the time given by Taylor's (2) simple theory, but according to the "paraboloid" approximation at an earlier time. The physical reason for this is that, in the latter case, the velocity of the central point (and therefore also the relief pressure at the centre) is $1\frac{1}{2}$ times larger (relative to the incident pressure) than in the former. As we decrease the radius of the plate the effect of the correction due to diffraction (tending to speed up the motion of the plate and thus to hasten cavitation) will presumably become important in the "piston" approximation before it does in the "paraboloid", so that it may be that the curves cross. Whether they do or not cannot be settled without a detailed calculation. This brings us to an important criticism of both models, which renders such a calculation rather superfluous.

Criticism of the Assumption of "Proportional Motion".

In both the models discussed above we have made a fundamental assumption, namely, that the law of distribution of velocity over the surface of the plate is the same for all times. For this reason we get the paradoxical result that an increase in the pressure near the edges tends to increase the velocity of the central point and thus to reduce the pressure there.   In the very early stages of the motion when the deformation of the plate is elastic, such a mechanism cannot be ruled out, as elastic stresses can be propagated from the edge to the centre of the plate faster than can the diffraction wave in the water.   In general, however, any lateral effects propagated elastically at such rates should be very small unless the plate is so thick that shear deflection is important.   The situation is even more definite if one assumes that practically the whole of the plate is stretched plastically (as seems likely if it is left with appreciable permanent deformation) since in this case lateral effects will be propagated along the plate at the comparatively slow velocity $\sqrt{\dfrac{\sigma_0}{\rho}}$ which is only of the order of 1% of the velocity of sound in water.   It   thus doubtful whether any appreciable effect on lateral motion can be propagated through the plate from edge to centre as fast as the diffraction wave through the water..   If this is a true representation of the situation, then it can only mean that the central portion of the plate will move according to Taylor's (2) original equation and that, apart from small elastic effects in the early stages of the motion, it will only "know" that it is part of a finite plate when the diffraction wave arrives. Although we cannot yet prove it rigorously, as we can in the rigid piston case, it seems fair to deduce that the same criterion for the occurrence of negative pressures will apply, i.e. that cavitation must occur either before the arrival of the diffraction wave at the central point or else not at all. On this assumption, we would deduce that Kirkwood's (6) cavitation criterion (that the Taylor cavitation time must be less than $\dfrac{R}{U}$) should be rigorously correct and not merely an approximation.

Experimental Evidence.

As these "plastic" and "proportional motion" assumptions lead in general to quite different results (see Table 1) for the critical thickness of plate at which cavitation occurs, and for the cavitation times, it should be possible to decide between them experimentally. A little evidence of this type is already available (7), similar charges being fired against various thicknesses of plate and the resulting cavitation photographed. So far, it appears

to point .....

to point definitely towards the second assumption. In that, to obtain agreement we have to use the Taylor cavitation time instead of the shorter time predicted for a rigid piston, but more work will be needed before this conclusion can be said to be finally established. In the meantime it is fair to point out that the fact that plastic waves cannot travel as fast as sound waves in water is one that is physically established, whereas the assumption of "proportional motion" was a purely artificial one, introduced in order to simplify the mathematics. This assumption is probably quite good enough for the purpose of determining the final deflection of the plate with reasonable accuracy, but the motion of the central point during the early motion will not be given correctly, and requires more elaborate investigation.

Criteria for the validity of incompressible Theory, and for the occurrence of Cavitation, applied to various Gauges.

The situation is now as follows. Inspection of equations (8) and (18) indicates that incompressible theory is likely to bcome a poor approximation if the non-dimensional quantity β is of the order of unity or greater. The assumption that the plate moves like a rigid piston suggests that cavitation is likely to set in if α is of the order of magnitude of β or less. The alternative and physically more plausible assumption introduced suggests that cavitation will set in if $\frac{q}{\rho} = \frac{\beta}{1} \frac{a}{a} \log \left(\frac{11}{\alpha}\right)$ or greater, that is $\frac{3\beta}{\#} = \frac{a}{3} \frac{\log a}{3} \frac{q}{a}$. It is

important to examine how nearly these criteria are satisfied for gauges and models used in practice. We have three variables, size of charge, unsupported area of plate (expressed by means of the radius of a circle of equal area) and thickness of plate.

TABLE 2

Criterion ($\beta = 1$) for failure of incompressible theory, assuming no cavitation.

Description of Gauge	Effective Radius	Critical Value of θ	Approximate Size of Charge	Typical Charges Used
D.N.C. Box Model	32"	.83 milliseconds	200 lbs.	8 lbs.
N.R.L. Box Model	8"	.21 "	28 lbs.	1 ounce
U.S. Drum Model	16.5"	.39 "	8 lbs.	8 lb.
12" Diaphragm Gauge	6"	.16 "	1 lb.	48 - 500 lbs.
6" Diaphragm Gauge	3"	.082 "	8 lb.	5 - 750 lbs.
3" Diaphragm Gauge	1.5"	.041 "	8 oz.	100 lbs.
1" Diaphragm Gauge	.5"	.018 "	$^2/_{60}$ oz.	10 lbs.
Hodugno Gauge	.5"	.018 "	$^1/_{60}$ oz.	5 lbs. upwards

Thus, it is clear that, quite apart from any question of cavitation, we could not hope to interpret the deflections of gauges of the box model type by means of incompressible theory, though it should be quite satisfactory for the smaller sizes of diaphragm gauge, and even more so for gauges of the "crusher" type, where the exposed area of piston is very small. Border-line cases are the 12 inches and 6 inches diaphragm gauges, where β would not be small compared with unity for the smaller charges. (It is proposed to apply the corrected form of incompressible theory to the 6 inches diaphragm gauge, in order to examine this point more closely).

Table 3a.....

-- 10 --

TABLE 3a.

Criterion $(\alpha = \beta)$ for appearance of cavitation according to "rigid piston" assumption.

Description of Gauge	Effective Radius	Material of Plate	Density of Plate	Thickness of Plate for $\alpha = \beta$	Typical Thickness used
D.R.C. Box Model	32"	Steel	8	6.3"	.2"
R.R.L. Box Model	8"	Steel	8	1.6"	.05"
U.S. Drum Model	10.5"	Steel	8	2.1"	.1"
12" Diaphragm Gauge	6"	Copper	9	1.0"	.05"
6" Diaphragm Gauge	3"	Copper	9	0.52"	.2"
3" Diaphragm Gauge	1.5"	Copper	9	0.26"	.2"
1" Diaphragm Gauge	.5"	Copper	9	0.09"	.1"
McDugne Gauge	.5"	Copper	9	0.09"	.05"

Extreme cases are gauges of the crusher type, in which the thickness of the piston is comparable with or greater than the radius. It will be quite safe to apply incompressible theory to such cases, but the smaller sizes of diaphragm gauge seem to be in or near the critical region. For the box models one can deduce that extensive cavitation will occur, and the same is likely to be true of ships' plates unless they are very much subdivided by stiffeners.

TABLE 3b.

Kirkwood's Criterion $\beta = \frac{\pi}{2} \frac{\sigma}{a - 1} \log \alpha$ for appearance of cavitation according to assumptions.

Description of Gauge	Thickness of Typical Plate	Weight of Typical Charge	Typical Value of α	$\frac{\alpha \log \alpha}{\alpha - 1}$	Critical Radius of Plate	Actual Radius
D.R.C. Box Model	.2"	5 lbs.	.10	.26	4.1"	32"
R.R.L. Box Model	.05"	1 ounce	.06	.18	0.6"	8"
U.S. Drum Model	.1"	¼ lb.	.11	.27	2.0"	10.5"
12" Diaphragm Gauge	.05"	45 lbs.	.01	.083	1.4"	6"
6" Diaphragm Gauge	.2"	5 lbs.	.11	.27	3.6"	3"
3" Diaphragm Gauge	.2"	100 lbs.	.09	.26	13.5"	1.5"
1" Diaphragm Gauge	.1"	10 lbs.	.05	.17	5.3"	.5"
McDugne Gauge	.05"	5 lbs.	.03	.11	1.7"	0.5"

This .....

This criterion gives larger values for the critical radius than would the criterion of Table 9a, so the smaller sizes of diaphragm gauge are probably safe from cavitation. The 6 inches diaphragm gauge appears to be a borderline case according to all three criteria, and a theoretical interpretation of the results is therefore likely to be difficult.

The Tables are set out in slightly different ways because:-

The criterion $R = 1$ is independent of thickness of plate, but depends on radius of plate and size of charge.

The criterion $\beta = a$ is independent of size of charge, but depends on radius and thickness of plate.

The criterion $\beta = \frac{\pi a \log a}{2(R-1)}$ depends on radius and thickness of plate, and also logarithmically on size of charge.

It will be noticed that none of the criteria depend on the maximum pressure. This would only come in if cavitation occurred at a finite tension.

Discussion.

We may therefore be confident that cavitation will occur with all the gauges of box model type, and probably also with ship's plates, and with the 12 inches copper diaphragm gauge. It should be safe to apply incompressible theory to gauges of the "crusher" type and to the smaller types of diaphragm gauge, but the 6 inches type appears to be a borderline case from the point of view both of failure of incompressible theory and of possible cavitation. There seems to be no a priori reason why one should get such a result as this, as the occurence of negative pressures (leading to cavitation) and the loss of energy by radiation (leading to the failure of incompressible theory) are physically quite distinct phenomena.

It will probably be safe to neglect the possibility of a small amount of cavitation at the centre when discussing the 6 inches diaphragm gauge, but it is very difficult to see how to deal with a case in which cavitation is occurring at the centre and over an appreciable fraction of the plate, while diffraction occurs at the edge. A perhaps easier problem, now under investigation, is to determine at what stage the theory of ! applicable to infinite plates breaks down for finite plates. Cavitation and follow-up will now be the main effects, the diffraction wave at the edges necessitating a correction, the order of magnitude of which will have to be worked out.

The results we have obtained should be compared with those of Friedlander (8), who considered an infinite plate divided up into a "chess-board" by immobile stiffeners, each "square" of the chess-board being constrained to move according to the parabolic law. Now, in our first two models, we found that relative to the infinite plate cavitation effect was hastened at the central point, whereas Friedlander (8) found that cavitation, reckoned as the instant at which the mean pressure over the plate dropped to zero, was later for his model than for the infinite plate. If we had based our own criteria on mean pressure rather than on pressure at the central point, we should, from equations (2) and (17), have deduced exactly the Taylor cavitation time for both "piston" and "parabolic" models, subject to the correction for the effect of the diffraction wave, which can only be in the direction of increasing mean pressure and so postponing the time at which it drops to zero. There is therefore no conflict with Friedlander's work. We have already pointed out that the effect of the diffraction wave in hastening cavitation at the centre is a consequence of the artificial assumption of "proportional motion", which probably does not represent the facts. The problem of finding a more representative model is now under investigation.

Conclusions and action recommended.

(a)   The best criterion for deciding whether or not cavitation occurs at a finite plate is probably that of Kirkwood (the Taylor cavitation time must be equal to $\frac{R}{c}$.)

(b) .....

(b)   If conditions are reasonably far removed from the critical region, one can probably regard the plate as infinite and apply the theory of I.   It is proposed to investigate how far away conditions must be for this to be possible.

(c)   It happens that this cavitation criterion is not very different from the criterion for the validity of incompressible theory, though this result could not have been predicted in advance.

(d)   The only type of diaphragm gauge in common use that is in this critical region appears to be the 6 inches type.   It is likely to be difficult to use this gauge as an absolute instrument, though it should be quite satisfactory for comparison purposes. The design of the smaller types of gauge might well be reconsidered, in order to remove them further from the critical region.

(e)   The assumption of "proportional motion", while probably satisfactory for predicting final deflections, is likely to give misleading results for cavitation times, and for the early motion.   It is proposed to look for a better model.

(f)   The pressure-time history of the central point of a plate cannot be taken as typical of the whole plate.

References.

1.   Temperley: "Theoretical Investigation of Cavitation Phenomena occurring when an Underwater Pressure Pulse is incident on a Yielding Surface - 1." (Referred to as I).

2.   Taylor: "The Pressure and Impulse of Submarine Explosion waves on Plates."

3.   Butterworth and Wigglesworth: "Damage to Ships' Plates by Underwater Explosions."

4.   Rayleigh: Theory of Sound: Volume II; paragraph 302.

5.   Kennard: "The Effect of a Pressure Wave on a Plate or Diaphragm."

6.   Kirkwood: O.S.R.D. Report 1115: "The Plastic Deformation of Marine Structures by an Underwater Explosion Wave: II to 15.11.42.

7.   Series of O.S.R.D. Interim Reports on Underwater Explosions and Explosives: No. 14 onward .

8.   Friendlander: "The Effect of an Underwater Explosion Pulse on a Framework Composed of Rectangular Panels."

Appendix .....

APPENDIX

Proof that equations (1) and (5) in the text are equivalent.

We assume that the velocity $U(t)$ is such that it can be expanded as a sum or integral of decreasing exponential functions of the time. We apply to equation (5) the operator $\frac{1}{2\pi i}\int_{-\infty}^{+\infty}\frac{d\omega}{\omega-in}$ which has the effect of changing $\rho^{i\omega t}$ into the function which takes the value zero for $t < 0$ and ρ^{-nt} for $t > 0$. This result follows by completing the contour by a semicircle below the real axis for $t < 0$ and above the real axis, for $t > 0$. In either case, the integral round the semicircle vanishes as $\omega = \infty$ by Jordan's Lemma and the result follows. The pressure on the piston due to a velocity U, which can be expanded as a sum or integral if such functions in the form $U = \sum_n A_n \rho^{-nt}$ is given by applying the same operator to the right hand side of equation (5). The integrals that result are very similar to those considered by Gallop (see Watson's Bessel Functions page #21) and are best evaluated by expression of the Bessel functions as integrals of Poisson's type and reversing the order of integration. Equation (5) thus gives us, for the reaction force due to such a velocity U, the expression:-

$$F = \sum_n -\frac{\rho_o C\pi R^2}{2\pi i}\int_{-\infty}^{+\infty}\frac{A\omega}{\omega-in}\rho^{i\omega t}\left(1-\int_0^{\frac{\pi}{2}}\sin^2\theta\,\rho^{-2\,ikR\cos\theta}\,d\theta\right)\,d\omega \qquad A(1)$$

For $t < 0$ the contour integrals both vanish. For $t > 0$ the first term becomes as before $-\rho_o C\pi R^2\sum_n A_n\rho^{-nt}$, while for the second term we must put the contour above the origin only for those values of θ for which $\omega t > 2$ $kR\cos\theta$, i.e. $t > \frac{2\,R\cos\theta}{c}$. Hence we have, if θ' is the critical value,

$$F = -\rho_o C\pi R^2 U +\sum_n \rho_o C\pi R^2 A_n \rho^{-nt}\int_{\theta'}^{\frac{\pi}{2}}\sin^2\theta\,\rho^{\frac{2n\,R\cos\theta}{c}}\,d\theta \qquad A(2)$$

Changing the variable so that $t' = \frac{2R}{c}\cos\theta$, it follows that A(2) is equivalent to equation (1) in the text. For $t > \frac{2R}{c}$ the integral in equation A(2) is from 0 to $\frac{\pi}{2}$ and that in equation (1) from 0 to $\frac{2R}{c}$.

The more general form of equation (1), when U is not zero for $t < 0$, is

$$F = -\rho_o C\pi R^2\int_0^{\frac{2R}{c}}\psi\left(\frac{ct'}{R}\right)\left(\frac{dU}{dt}\right)_{t-t'}\,dt' \qquad A(3)$$

where $\psi\left(\frac{ct'}{R}\right) = 1 - \frac{1}{\pi}(\sin 2\gamma + 2\gamma)$

where $\sin\gamma = \frac{ct'}{2R}$

Substituting $U = U_o\rho^{i\omega t}$ in equation A(3), it can be verified that the equation reduces to Rayleigh's expression (5). Thus the equivalence of the two methods is established.
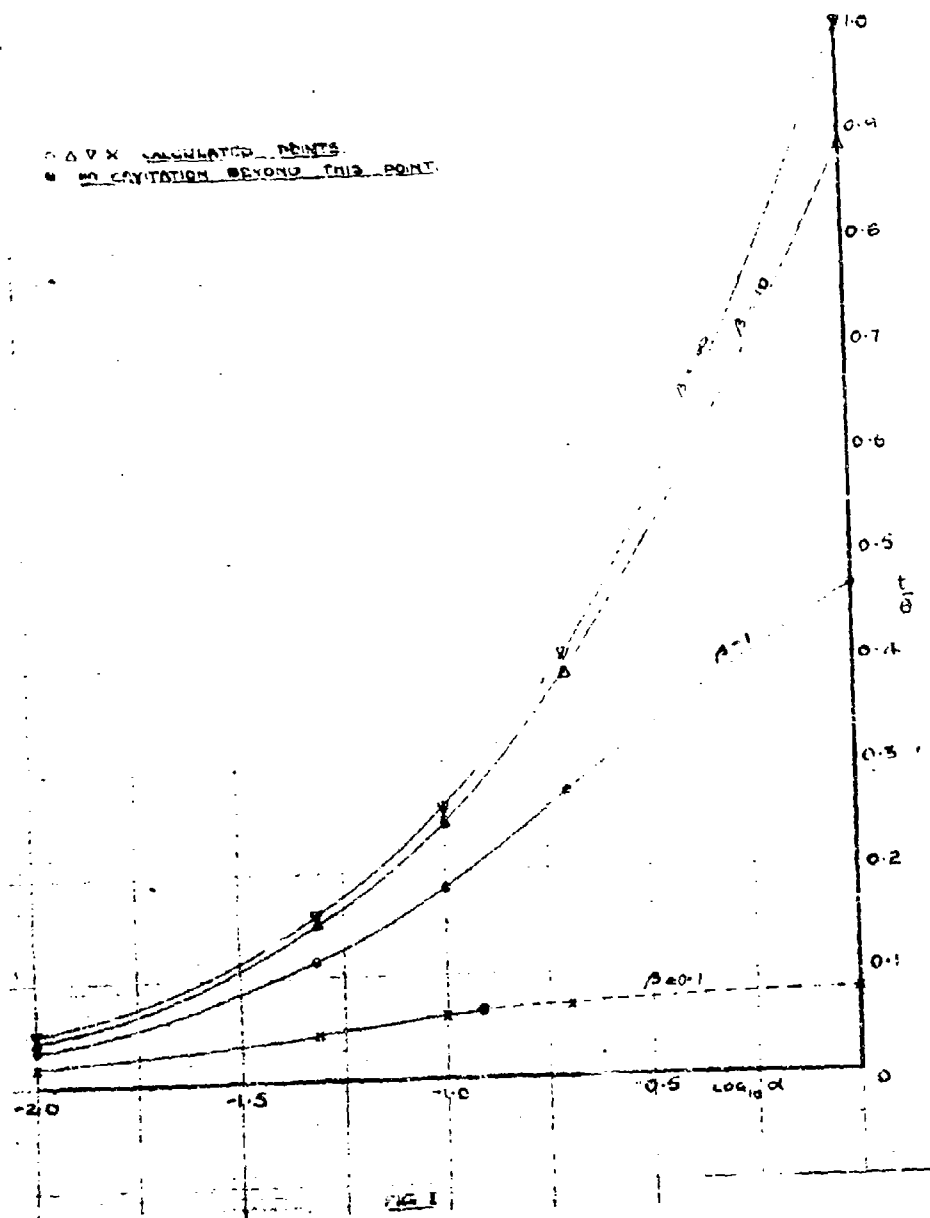
282

FIG. I

THEORETICAL INVESTIGATION OF CAVITATION PHENOMENA
OCCURRING WHEN AN UNDERWATER EXPLOSION IS
INCIDENT ON A YIELDING SURFACE - III

H. N. V. Temperley
Admiralty Undex Works, Rosyth, Scotland

THEORETICAL INVESTIGATION OF CAVITATION PHENOMENA OCCURRING WHEN AN UNDERWATER EXPLOSION IS INCIDENT ON A YIELDING SURFACE - III

H. N. V. Temperley

April 1945

* * * * * * * *

Summary.

In two previous reports, referred to as I(1) and II(2) the problem of damage to a plate with clamped edges and a baffle is considered on the alternative assumptions that water can or cannot stand tension, the plate being subjected to a normally incident exponential pulse. In the present report, some of this work is extended to oblique incidence, and, in addition, the effect of the plate being supported by stiffeners as well as at the edges, is being considered. For cases in which the radius of the plate is small compared with the "wave-length" of the pulse, it has already been shown in II that regions of tension in the water do not occur to any extent, so that the damage will be the same whether water can stand tension or not. It is therefore only necessary to consider cases in which the radius is comparable with or large compared with the "wave-length". The discussion shows that for radii large compared with the "wave-length" cavitation should increase damage, and that for a structure like a ship's bottom or a panel of plating divided up by stiffeners this should be true for practically all cases for which cavitation is important at all. For a structure like the box-model, on the other hand, there seems to be an appreciable region of values of the variables in which cavitation reduces damage, and this region seems to cover most of the cases occurring in practice. This last conclusion is only valid if it is possible to neglect the effect of diffraction if extensive cavitation occurs. Qualitative reasons for thinking this are given.

List of Symbols.

P_m = Maximum pressure of incident pulse.

ψ = Angle of incidence of pressure-pulse. (Acute angle between wave-front and plate).

θ = Time constant of incident pulse.

c = Velocity of sound in water.

ρ_0 = Density of water.

x = Distance from centre of plate along axis of plate. (Also thickness of layer of water on plate).

y = Deflection of plate.

z = Distance measured parallel to plate and in plane of propagation of pressure pulse.

D = Radius of plate.

N^2 = Number of sub-panels into which plate is divided by stiffeners.

ρ = Density of plate.

h = Thickness of plate.

σ_0 = Yield stress of plate.

a .....

$$a \quad = \quad \frac{\lambda}{A} -$$

$w \quad = \quad$ Weight of charge.

$D \quad = \quad$ Distance from charge.

$$\psi \left(\frac{ct'}{2R}\right) = 1 - \frac{1}{\pi} \left(\sin zy + zy\right)$$

$$\gamma \quad = \quad \frac{ct'}{2R}$$

$t \quad = \quad$ Time variable.

$t' \quad = \quad$ A variable of integration.

$$\lambda \quad = \quad \sqrt{\frac{3 \pi \rho_0 h}{\rho_0} \frac{y}{R^3}}$$

Introduction.

In two previous reports, referred to as I(1) and II(2) we have considered some of the modifications that have to be made in the theory of the motion of a clamped plate when subjected to an underwater explosion pulse, if we assume that water is incapable of standing any finite tension. Taylor (3) made a start on this problem for an infinite plate, considered as a mass backed by a spring, (the spring representing the elastic and plastic forces in the structure). He calculated the energy that was imparted to the plate up to the instant at which the pressure dropped to zero at the plate. In I we obtained explicit formulae governing the propagation of cavitation into the water subsequent to this instant, and formulated the equations governing the subsequent motion of the plate, as it is gradually brought to rest by the spring, but is subjected to the impact of the cavitated water which is thus given an opportunity to catch up. Solution of these equations showed that, for thin plates, the major portion of the damage would be caused by this "follow-up" mechanism, the final damage corresponding to about two-thirds of the energy brought up by the explosion pulse, the remaining third being partly reflected away before cavitation, and partly lost in the collision between water and plate. In II we investigated some of the modifications that would be needed for a finite plate. In particular, we found that Kirkwood's (4) suggested criterion for the occurrence of cavitation was probably correct, and also that it did not differ very much from the criterion that, in the absence of cavitation, incompressible theory would be a valid approximation for determining damage.

We have so far not attempted two of our main problems:

(a)   To determine whether damage is greater if cavitation occurs at zero pressure than it would be if water could stand tension.

(b)   The effect of a pressure-pulse at oblique incidence.

In this report, we shall attempt both of these problems for a large plate. For small plates neither question arises, because we have shown in II that, e.g. for diaphragm gauges, cavitation probably does not occur and that incompressible theory is probably a fair approximation. Further, if incompressible theory does apply, the damage would be practically independent of the angle of incidence, (as is, in fact, observed experimentally for diaphragm gauges).

The Effect of Oblique Incidence, if Cavitation occurs.

Taylor (3) was able to generalise his work to oblique incidence on the following two assumptions:

(a)   Conditions are not too near those of glancing incidence.

(b)   The motion of each element of the plate is independent of that of neighbouring elements, i.e. effects propagated through the plate may be neglected in comparison with effects propagated through the water.

Assumption .....

Assumption (a) is equivalent to the statement that diffraction effects due to the arrival of the pulse at the edge of the plate die away very quickly. The motion of the plate then becomes quasi-steady, every element of the plate having the same equation of motion, counting as zero the time at which the incident pulse arrives at the element. Since the incident pulse sweeps over the plate with a velocity $C/\sin\psi$, where ψ is the angle of incidence (defined as the acute angle between wave front and plate), this means that once we have calculated the motion of any element we can calculate that of any other element by "post dating" the time-scale by the appropriate values of $\frac{z\,\sin\psi}{C}$, where the z-axis lies in the plate and in a plane parallel to the direction of propagation of the wave-front.

Assumption (b) is similar to that introduced in I, in support of which both theoretical and experimental evidence was given. It is slightly less drastic in that in I it was applied to the diffraction wave, moving with precisely the velocity C, whereas here the pulse is sweeping over each element of the plate in turn with a velocity effectively greater than C (due to the tilt of the wave-front) and therefore the plastic and elastic forces will have still less chance of propagating themselves ahead of the incident wave-front than they have of propagating ahead of the diffraction wave.

If we make these two assumptions, the two boundary conditions at the plate can be satisfied, as Taylor (3) shows, by assuming that the effect of the plate can be represented as a simple reflected wave, the angle of reflection being equal to the angle of incidence. Besides the "post-dating" of the time-scale for elements of the plate with different z co-ordinates, the only other changes that have to be made in order to convert the theory for direct incidence into the theory for oblique incidence are, first that we must replace the quantity ρ_m by $\rho_m\cos\psi$ and ρ (the density of the plate) by $\rho\cos\psi$. When we come to consider the propagation of the cavitation front, the theory proceeds exactly as in I, except that we have x $\cos\psi$ in all the equations instead of x, (x being the co-ordinate whose axis is perpendicular to the plate). The fact that we have replaced ρ by $\rho\cos\psi$ necessitates our also replacing α by $\alpha\cos\psi$. The discussion of the various energies involved can also be taken over if we replace α by $\alpha\cos\psi$ and $\frac{\rho_m^2\theta}{\rho_0}$ by $\frac{\rho_m^2\theta}{\rho_0 c}\cos\psi$. This latter change is the same as replacing ρ_m by $\rho_m\cos\psi$ because k_T contains the factor ρc. For k_b, k_c and the total energy one of the factors $\cos\psi$ is removed when we integrate over the whole pulse.

It is a little more difficult to see what modifications have to be made to the theory of the "follow-up" stage of the motion. Since the angles of incidence and reflection are equal, it follows that the particles will have no velocity in the z-direction at the instant when the pressure drops to zero, and therefore that the velocity of the cavitated water will also be perpendicular to the plate. We can take over the argument of I, but here we leave x unchanged and do not replace it by x $\cos\psi$. We thus obtain, instead of equations (18) and (8) of I, the following relations between t, x, y, and vc, (vc being the velocity of the water at cavitation).

$$t = z\frac{\sin\psi}{c} + \frac{\theta\alpha\cos\psi}{1-\alpha\cos\psi}\left[\frac{x}{\alpha\theta c} - \log\left\{\sin R\left(\frac{x\cos\psi}{\theta c}\right)\right.\right.$$
$$\left.\left. + \alpha\cos\psi\cosh\left(\frac{x\cos\psi}{\theta c}\right)\right\}\right] + \frac{y}{z c} \qquad (1)$$

$$v = \frac{2\rho_m\cos\psi}{\rho_0 c}\left[\alpha\cos\psi\cosh\left(\frac{x\cos\psi}{\theta c}\right) + \sin R\left(\frac{x\cos\psi}{\theta c}\right)\right]\frac{\alpha\cos\psi}{1-\alpha\cos\psi}$$
$$xp - \frac{x\cos\psi\,(2-\alpha\cos\psi)}{\theta c\,(1-\alpha\cos\psi)} \qquad (2)$$

Since equation (19) in I is derived purely by momentum considerations, it cannot involve the quantity $\cos\psi$ directly. Also the thickness of the "reconstituted" layer of water on the plate is just x for when particles that were originally at a distance x from the origin are just arriving at the layer. In other words, equation (19) is exactly the same as in I, that is:—

$$\frac{d}{dt}\left[(\rho_m + \rho_0 x)\frac{dy}{dt}\right] - \rho_0\frac{dx}{dt}\,vc + \mu_m k^2 y = 0 \qquad (3)$$

Examination .....

- 4 -

Examination of these equations reveals the remarkable result that the corresponding equations of I can be made identical with them, if we make the very same changes in the variables that we have already introduced when discussing the motion of the plate up to cavitation, and the propagation of the cavitation front. For convenience, we recapitulate these changes here.

$$t \text{ becomes } t - \frac{r \sin \psi}{c}$$

$$p_m \text{ becomes } p_m \cos \psi$$

$$\rho \text{ becomes } \rho \cos \psi$$

$$a \text{ becomes } a \cos \psi$$

The other variables remaining unaltered, except that, consequent on the change in a, S^2 becomes $S^2 \cos \psi$. The corresponding changes in the non-dimensional units introduced in I are:-

Unit of x becomes $c \, \theta \sec \psi$ instead of $c \, \theta$

Unit of y becomes $\frac{2 p_m \theta}{\rho_0 c} \cos \psi$ instead of $\frac{2 p_m \theta}{\rho_0 c}$

the units of time and pressure being unaltered.

When we make the modifications in a and S, we can take over the information in Tables 1 and 2 of I without having to repeat the numerical work. The main result of this work is that for a thin plate about $\frac{2}{3}$ of the total energy falling on the plate appears as damage. The work in I shows that this figure is not very sensitive to S, and for a small it almost certainly only varies slowly with a, so we conclude that it is probably not very sensitive to ψ either. We thus conclude that, for a large plate, when cavitation occurs, the final damage corresponds to plastic energy of approximately $\frac{1}{3} \frac{p_m^2 \theta}{\rho_0 c} \cos \psi$ per unit area of plate which, if we assume p_m to to $\frac{W^{\frac{1}{3}}}{D}$ and θ to be proportional to $W^{\frac{1}{3}}$ where W is charge weight and D is distance, leads to a formula of the type

$$\text{Central Deflection} \propto \frac{(W \cos \psi)^{\frac{1}{3}}}{D} \tag{4}$$

The Effect of Cavitation on Damage.

We now examine various models of a structure undergoing damage to see what valid comparisons can be made between the consequences of the assumption that water can stand no tension at all, and of the assumption that water can stand unlimited tension. At first sight one would think that the answer is obvious, and that if a plate is free to leave the water when the pressure drops to zero it must always suffer more damage than if tensions can occur. For a sufficiently large plate this is certainly true, furthermore the work of I shows that if cavitation occurs, a further contribution to damage is made by impact of cavitated water with the plate. For a finite plate, however, one has to consider the effect of diffraction from the edges. For a very small plate, the effect of diffraction is to prevent tension occurring at all, and there will be no difference between the consequences of the two assumptions. Criteria for this are worked out in II). For a somewhat larger plate tension sets in before the arrival of the diffraction wave from the edges, and the pressure alternates in time between positive and negative values. It will be shown later that positive values predominate, so that the effect of diffraction is always to increase damage. For a sufficiently small plate this contribution is considerable, and it may well be that the effect of cavitation in preventing the diffraction wave from acting all over the plate more than balances the gains in damage due to the non-existence of tension at the plate and the effect of "follow-up".

(1) .....

(1)   The effect of cavitation on diffraction.

Owing to the simultaneous occurrence of cavitation and diffraction, it has, up to the present, been impossible to extend the work of I to a finite plate, but one can bring forward qualitative arguments which suggest that, for a sufficiently large plate, cavitation probably interferes seriously with the contribution to damage due to diffraction. Although the complete mapping out of the cavitation region would be a difficult matter, one can deduce enough about it for present purposes. In II we concluded that the cavitation time is probably independent of the radius of the plate, so that criterion for cavitation is simply that this time must be less than the time $\frac{a}{c}$ for the diffraction wave to arrive at the centre of the plate. By an extension of the arguments that led to this conclusion we deduce that cavitation occurs, at the Taylor cavitation time, over just that portion of the plate which the diffraction wave has not reached by then.   In II we also deduced that the position of the tip of the cavitation zone is sensitive to the thickness of the plate, so that even if the plate was a little below the critical thickness, the length of the "beard" would be several times the radius of the plate. We may therefore regard the cavitation zone as being, roughly, a cylinder.   The diffraction waves incident on the surface of this zone will be reflected as at a free surface.   Since we are assuming that water cannot stand any tension the effect will be to cause further cavitation and throw drops of water inwards at right angles to the surface.   Since this surface is nearly a cylinder, the drops will only have a small velocity component towards the plate, and will contribute little or nothing to damage.   We have also to consider the effect of diffraction on the outside portion of the plate, where cavitation does not occur.   The breadth of this portion is equal to the velocity of sound multiplied by the cavitation time, and its area therefore becomes a steadily smaller fraction of the total area of the plate, as its radius increases. It remains to consider whether diffraction would have any effect after cavitation has disappeared. In I we found that the plate came to rest (with any reasonable assumption about the strength of the spring) only at a time several times greater than the characteristic time θ of the explosion pulse, and that even then the layer of water built up on the plate is only about half the "wavelength" $C\theta$ of the pulse.   Reference to the theory of diffraction at a rigid piston shows that the main contribution of diffraction occurs within a time of the order of $\frac{dp}{c}$ so that if diffraction is to make any appreciable contribution after cavitation has disappeared R must be several times as big as $C\theta$ We shall show later that, if this is so, the effects of cavitation and "follow-up" (without any assistance from diffraction) are by themselves sufficient to make damage greater in the case when cavitation occurs.

Since we are trying to assess the effect of cavitation on damage for large plates it seems fair to compare the case treated in I (large rigid piston with cavitation occurring over the whole area) with the case partially treated in II (rigid piston moving in an aperture in a rigid wall, water being able to stand tension) as both these cases can be treated rigorously.   A comparison of the behaviour of these two models as the radius becomes large should give a fair idea of the critical conditions for the increase or decrease of damage due to the occurrence of cavitation.   The complete neglect of diffraction in the cavitational case is, for the reasons just given, probably justified as a first approximation.

(2)   The "spring" approximation.

When we are considering large plates the introduction and choice of a spring to replace the plastic forces in the plate needs some care.   We shall consider two types of case.   In the first we shall suppose the plate clamped at the edges only and surrounded by a rigid baffle. This will be referred to as the "box-model" set of assumptions.   In the second we shall suppose the plate to be supported at intervals by stiffeners, clamped at the edges, and surrounded by water on all sides.   This latter case corresponds closely to the case of an actual ship's bottom, so will be referred to as the "ship" set of assumptions.   It is customary to take account of the difference between "baffle" and "no baffle" simply by dropping the factor 2 representing the doubling in pressure in cases where diffraction is important but actually the point seems to merit a more careful investigation.

A second point that requires examination, if we are using the "box model" assumptions, is that the plate is actually brought to rest by plastic waves travelling in from the edges. For it to be possible to replace these by a spring one must first be certain not only that the ratio between deflection and energy for the spring is the same as that for the plate, but also

test during the time of movement of the piston and spring representing the plate, plastic waves from the edge have time to reach the centre of the plate. If this is not so, it is clear that the model is not fully representative, so the point must be checked for each model that we use. The test will be more stringent for the "box-model" case where the only clamping is at the edges than for the "ship" case where the plastic waves have only to travel from the stiffeners to the centre of each panel.

(3)   Comparison of various models for plates of large radius.

We shall carry out all the actual calculations with the "ship" model, which will be a panel of equivalent radius R divided up by stiffeners into N^2 panels each of equivalent radius $\frac{R}{N}$. We shall suppose that each of these sub-panels can be represented as a piston on a spring. It would be a better approximation to regard each sub-panel as deforming into a parabolic shape, as we could then regard the stiffeners as being at rest, but this leads to difficulties when we are considering the cases in which cavitation occurs. Our experience in the past has been that changing over from "piston" to "paraboloid" approximations does not alter the order of magnitude of the results (See II). In this report we are only trying to find approximate criteria for the effect of cavitation on damage, and the "piston" approximation should be satisfactory for this.

We need an expression for the strength of the spring per unit area of plate. A circular plate of radius $\frac{a}{N}$ when deformed into a cup of a sphere or paraboloid so that the mean deflection is y increases in area by $4\pi y^2$. This corresponds to a total plastic energy of $8\sigma_0 h \pi y^2$, where σ_0 is the yield stress and h the thickness of the plate, corresponding to an energy of $\frac{8\sigma_0 h N^2 y^2}{R^2}$

per unit area of plate. Thus, to represent the plastic forces we need a spring of strength $\frac{8\sigma_0 h N^2}{R^2}$ per unit mean deflection per unit area. We shall use this in all subsequent calculations. To go over to the "box-model" we simply put N = 1 and allow for the effect of the baffle as well as we can.

(3.1)   Incompressible theory.

The investigation given in II has shown us that incompressible theory is probably a good approximation for small plates, so it is of interest to see what results it gives for large R. The equation of motion, y in all cases representing mean deflection, is:-

$$\left(\rho h + \frac{9}{2\pi}\rho_0 R\right)\frac{d^2 y}{dt^2} + \frac{8 N^2 \sigma_0 h}{R^2}y = p_m\rho^{-\frac{t}{\theta}} \qquad (5)$$

where p_m is the maximum pressure in the explosion pulse, θ its time-constant, ρ the density of the plate and ρ_0 the density of the water. Since the plates are all moving as pistons, the "virtual mass" term $\frac{9}{2\pi}\rho_0 R$ will be the same as that for one large piston. For large R we may neglect ρh compared with this term. The solution of equation (5) is

$$y = \frac{3\pi p_m \theta^2}{8\rho_0 R(1 + \lambda^2\theta^2)}\left[\rho^{-\frac{t}{\theta}} + \frac{\sin\lambda t}{\lambda\theta} - \cos\lambda t\right] \text{ where } \lambda^2 = $$
$$\frac{3\pi\sigma_0 h N^2}{\rho_0 R^3} \qquad (6)$$

We suppose R and N to become large in such a way that $\frac{R}{N}$ remains fixed, corresponding to a fixed size of sub-panel. λ then becomes small, and the middle term in the bracket large compared with the other two. The maximum deflection is given by:-

$$y_m = \frac{(3\pi)^{\frac{1}{2}}}{8}\frac{R^{\frac{1}{2}}}{N}\frac{p_m\theta}{(\rho_0\sigma_0 h)^{\frac{1}{2}}} \qquad \text{(ship)} \qquad (7a)$$

thus tending to zero for large R. If, however, we take the "box-model" assumptions λ again becomes small for large R when we put N = 1 and the maximum deflection is now given by:

$$y_m = $$

$$y_m = \frac{(3\,m)^{\frac{1}{4}}}{4} \quad R^{\frac{1}{4}} \frac{\nu_2^{\;2}}{(\rho_0\,\sigma_0 h)^{\frac{1}{2}}} \qquad \text{(box-model)} \qquad (7b)$$

which becomes large for large R. In both these cases it can be verified that the spring approximation is satisfactory because the time to reach maximum deflection is proportional to $\frac{1}{\lambda}$, that is to $\frac{R^{3/2}}{m}$, whereas the time of travel of the plastic waves is proportional only to $\frac{R}{c}$.

(3.2) Motion of plate assuming cavitation.

It is shown in I that up to the time of cavitation the plate acquires a kinetic energy per unit area of $\frac{2\,v_m^2\,\sigma}{\rho_0\,c} \quad \alpha^{\frac{1+\alpha}{1-\alpha}}$ where $\alpha = \frac{\rho h}{\rho_0\,c\,\theta}$. If the plate acquires no further energy either from "follow-up" or diffraction, then the final deflection is given simply by equating this to the plastic energy, $\frac{\sigma_0 h}{R^2}\,\frac{h^2}{2}\,y^2$. We then have:

$$y_m = \alpha^{\frac{1}{2}\left(\frac{1+\alpha}{1-\alpha}\right)} \quad R \quad \frac{v_m\,\sigma^{\frac{1}{2}}}{(\omega\,\rho_0\,ch)^{\frac{1}{2}}} \qquad \text{(ship)} \qquad (8a)$$

The transition to the box model is made simply by putting $R = 1$. The doubling of the pressure is here retained in both models because for a large plate diffraction plays no part in the motion of the plate up to cavitation. We have therefore:

$$y_m = \alpha^{\frac{1}{2}\left(\frac{1+\alpha}{1-\alpha}\right)} \quad R \quad \frac{v_m\,\sigma^{\frac{1}{2}}}{(\rho_0\sigma_0\,ch)^{\frac{1}{2}}} \qquad \text{(box-model)} \qquad (8b)$$

If we make the alternative assumption that follow-up occurs but there is still no significant contribution from diffraction, (see section 2 for a discussion of this) then we have just the case treated in I. There we found that a rough rule was that about two-thirds of the incident energy was eventually converted into plastic work. The energy absorbed per unit area is now $\frac{\rho_0^2\,\theta}{3\rho_0\,c}$ and the factor $\alpha^{\frac{1+\alpha}{1-\alpha}}$ in equations (4a and b) is replaced by $\left(\frac{1}{12}\right)^{\frac{1}{2}}$. We now have to examine the validity of the "spring" assumption. Equations (8a and b) are based strictly on energy considerations and it is immaterial whether the energy communicated to the plate is absorbed by a spring or by plastic waves. The theory of I, however, assumes a uniform spring and a failure of this assumption might modify the factor of $\frac{2}{3}$. From the theory of I we find that the time to reach maximum deflection is of the order of magnitude $\frac{\theta}{S}$ where S is given by

$$\sqrt{\frac{\alpha\,\sigma_0\,h^2}{\rho\,R^2}}\sqrt{\frac{\sigma}{\rho_0\,c\,\theta}}. \quad \text{(It should be noted that in I we use a for thickness of plate while in}$$

II and this report we use h. We have also introduced the factor R^2 to allow for subdivision of the panel). The time for the plastic wave to reach the centre of the sub-panel is $\frac{c}{R}$ divided by the velocity $\sqrt{\frac{\sigma_0}{\rho}}$ of plastic waves. We thus see that, for the "spring" approximation to be valid we must have $R\alpha$ less than unity. Since α is not usually greater than 0.1 in practical cases and is often less, it appears that the spring assumption probably does not lead to serious error in this case, though the error does not diminish with increasing R as it does in the incompressible model.

(3.3) Motion of plate assuming that water can stand tension.

In II (Appendix, equation A.3) it was shown that for a piston moving in a rigid wall, the rigorous expression for the force on the unit area of plate due to the hydrodynamic forces is

$$- \rho_0\,c^2 \int_0^{c t/R} dt \left(\frac{ct}{R}\right)\left(\frac{d^2 z}{dt^2}\right)_{t-t'} \quad dt'. \quad \text{where } \psi\left(\frac{ct}{R}\right)$$

defined .....

defined as the function $1 - \frac{1}{\pi}(\sin 2\gamma + 2\gamma)$, $\sin \gamma = \frac{2Ct}{H}$ The equation of motion of the piston is therefore:

$$\rho \frac{d^2 y}{dt^2} + \rho_v c \int_0^{2H}_C \psi \left(\frac{ct'}{H}\right)\left(\frac{d^2 y}{dt^2}\right)_{t-t'} dt' + \frac{8\pi^2 \sigma_0}{H^4} hy = 2 \rho_m \rho^- \dot{\theta} \quad (9)$$

where we have used the same "spring" term as before. H becomes unity for a plate clamped at the edges only. For some purposes it is desirable to integrate the middle term once by parts, and we obtain: (cf. equation (1)).

$$\rho h \frac{d^2 y}{dt^2} + \rho_0 c \frac{dy}{dt} - \frac{2 \rho_0 c^2}{\pi R} \int_0^{2R}_C \left(1 - \frac{c^2 t'^2}{4R^2}\right)^{\frac{1}{2}} \left(\frac{dy}{dt}\right)_{t-t'} dt'$$

$$+ \frac{8\pi^2 \sigma_0}{R^2} hy = 2 \rho_m \rho^- \frac{1}{\theta} \quad (10)$$

It is possible to obtain the solution of either form of this equation in integral form by use of the Fourier transform, but the resulting integral is intractable. We can, however, deduce enough about the behaviour of the solution for the purposes of this report by simpler means.

We wish, first of all, to establish whether for large R, there is any case where diffraction can be neglected. For such a case one could, according to the discussion of section 3, deduce at once that cavitation will increase damage. If we assume that the effect of diffraction is negligible, we neglect the integral term in equation (10) and obtain the case of an infinite plate without cavitation treated by Taylor (3). The approximate solution of this equation is:

$$\frac{dy}{dt} = \frac{2 \rho_m}{\rho_0 c (1-\alpha)} \left(\rho^- \frac{1}{\theta} - \rho^- \frac{1}{\alpha \dot{\theta}}\right), \quad t > 0 \quad (11)$$

which leads to the following result for the final deflection:

$$y_m = \frac{2 \rho_m \theta}{\rho_0 c} \quad (12)$$

It can be shown that for any reasonable size and thickness of plate the effect of the spring term only introduces a small correction into expression (12). To assess the effect of diffraction we substitute the solution (11) into the integral term of equation (10). Since the expression (11) is always positive we can obtain an upper limit for the effect of diffraction by replacing the factor $\left(1 - \frac{c^2 t'^2}{4R^2}\right)^{\frac{1}{2}}$ by unity, and a lower limit by replacing it by $1 - \frac{c^2 t'^2}{4R^2}$. For large R these two quantities are nearly equal. The value of the integral is thus given in order of magnitude by:-

$$-\frac{4c\theta}{\pi R} \frac{\rho_m}{(1-\alpha)} \left[1 - \rho^- \frac{1}{\theta} - \alpha + \alpha^- \frac{1}{\alpha \dot{\theta}}\right]; \quad t < \frac{2R}{c} \quad (13)$$

$$-\frac{4c\theta}{\pi R} \frac{\rho_m}{(1-\alpha)} \left[\rho^- \frac{1}{\theta} \left(\rho^- \frac{2R}{c\theta} - 1\right) - \alpha \rho^- \frac{1}{\alpha \dot{\theta}} \left(\frac{2R}{c\theta} - 1\right)\right]; \quad t > \frac{2R}{c}$$

Tables of the basic integral have been prepared. Thus for equation (11) to be a satisfactory solution of equation (10), these two expressions must be small compared with the applied pressure $2 \rho_m \rho^- \dot{\theta}$. This requires in the first place that $\frac{c\theta}{R}$ should be small, i.e. R must be large compared with the "wave-length" $c\theta$ of the pulse, which is, in general well satisfied for a ship, and fairly well for the box-model. This criterion is, however, not sufficient, because, if it is satisfied, it implies that expression (13) contains an approximately constant term of order of magnitude $\frac{4c\theta \rho_m}{\pi R}$ and it is necessary to verify that the steady deflection such a pressure would cause against the spring is less than expression (11), for solution (10) not to be invalidated. The condition for this is:

$$\frac{4c\theta \rho_m}{\pi R} \div \frac{8 h' \sigma_0 \rho h}{\rho^2} < \frac{2 \rho_m \theta}{\rho_v c}$$

$$(14)$$

i.e. $\rho_0 c^2 R < 4 \pi h' \sigma_0 h$

this .....

This result indicates a difference between the "ship" case and the "box-model" case. If we put $N = 1$, it is impossible to satisfy the criterion (14) except if the thickness of the plate is several times its radius. The only practical case of this is a piston-type gauge, (such as the Hilliar copper crusher). In such a case $\frac{c\theta}{R}$ is not small, and the investigation of 11 then shows that cavitation cannot occur. It follows therefore that diffraction must always be considered in the box-model case, criterion (14) showing that solution (11) cannot be the correct limiting form for large R. The physical reasons for the two criteria are fairly obvious. Equation (11) implies that the plate is brought to rest by tension in the water rather than by the plastic forces. For tension to occur at all, we must have R at least comparable with $C\theta$, as was shown in 11. Criterion (14) implies that when the plate is brought to rest by tension, the plastic forces corresponding to this deflection are sufficient to prevent any further movement of the plate due to diffraction. We have seen that this implies that there must be considerable sub-division of the panel of plating. If we fix the size of the sub-panel, this implies fixing $\frac{R}{N}$ and criterion (14) is then satisfied in the limiting case of large R. If we take $\frac{R}{N}$ as one foot, corresponding roughly to a destroyer, and $h = \frac{1}{4}$ inch, N comes out at about $2^9 - 30$, corresponding to damage extending over an area of the order of 1500 square feet of the bottom. This is a not unreasonable value, but the criterion becomes increasingly difficult to satisfy for a ship with larger frame-spacing.

It might appear that we need another criterion in addition to (14). If we replace the spring by plastic waves, it is necessary for (11) to be a satisfactory approximation, that the plastic waves should have been able to reach every part of the plating by the time the diffraction wave has reached the centre. For a single plate ($N = 1$) this is obviously impossible, because the plastic waves only travel at a speed $\sqrt{\frac{\sigma_0}{\rho}}$, which is about 10% of t the velocity of sound in

water. Thus again, we deduce that N must be of the order of 20 and the criterion is practically the same for plastic waves as it is for the equivalent spring.

A failure of criterion (14) implies that the time for the plate to come to rest under plastic forces is greater than $\frac{R}{c}$. Then if θ is small compared with $\frac{R}{c}$, we may deduce that $\frac{d^2 y}{dt^2}$ will not change much in a time of the order of $\frac{R}{c}$ and we can take $\frac{d^2 y}{dt^2}$ outside the integral in equation (v) and neglect the difference between t and $t - t'$. The integral can now be evaluated and the equation of motion is just that given by incompressible theory, equation (5). The solution of this equation is given by equation (6), which for large R reduces to one term. To estimate the error caused by assuming incompressible theory we substitute this solution in equation (9) or (10) the integral term involving Bessel and Struve functions of order unity of the variable $\frac{2R\lambda}{c}$. Reference to tables of these functions shows that for $\frac{2R\lambda}{c} = 3$ the error is of the order of 10%. For incompressible theory to be a reasonable approximation in the absence of cavitation for a large plate ($R > c\theta$) we therefore have the approximate criterion $\frac{2R\lambda}{c} < 1$, or

$$\rho_0 \, c \, R \; > \; 12 \, \pi \, N^2 \, \sigma_0 h$$

This criterion is not the exact reverse of (14) which means that there is an intermediate region where neither incompressible theory nor equation (11) are satisfactory approximations. Actually the two theories give very much the same results in this region (they agree when $\rho_0 \, c^2 \, R = \frac{64}{\pi} \, N^2 \, \sigma_0 h$), which indicates that diffraction is probably not very important unless criterion (15) is satisfied.

It must be pointed out that the criterion (15) has nothing whatever to do with the criterion for the velocity of incompressible theory established in 11 for small plates, as the latter applies when θ is large compared with $\frac{R}{c}$, but criterion (15) is not applicable, unless, in addition, θ is small compared with $\frac{R}{c}$ so that it is possible to regard the velocity as communicated impulsively. These are both particular cases of Kennards "principle of reduction" (5).

(3.4)   Circumstances in which cavitation reduces damage.

By comparison of the various models it is now a simple matter to decide the effect of cavitation on damage if we assume that diffraction does not contribute significantly to damage when cavitation occurs. We may list the various possibilities as follows:-

(a) .....

(a)   For $R < C\theta$ the question falls to the ground, because cavitation either does not occur at all, or only over a small extent of the plate, and therefore probably does not affect damage.

(b)   For $R > C\theta$, we have two possibilities.   If $\rho_0 C^2 R < 4\pi N^2 \sigma_0 h$ we may be confident that the effect of diffraction is small, and that cavitation will therefore increase damage.   This criterion cannot, however, be satisfied in the "box-model" case but only in the "ship" case, with R of the order of 10 or more.   If $\rho_0 C^2 R > 4\pi N^2 \sigma_0 h$ diffraction becomes important, but incompressible theory remains a good approximation until R becomes somewhat larger.   We may then compare the results of sections (5.1) and (3.2) to find the effect of cavitation.   It seems best to assume complete "follow-up", as it is hard to imagine a mechanism by which the plate can leave the water when the pressure drops to zero, and receive no further damage either from cavitation or diffraction.   On this basis we conclude that cavitation will increase damage if the following criteria are satisfied:-

$$\left(\frac{3\pi}{5}\right)^{\frac{1}{4}} \quad R^{\frac{1}{4}} \quad \frac{p_m\,\theta}{(\rho_0\,\sigma_0\,R)^{\frac{1}{2}}} \quad < \quad \left(\frac{41}{16}\right)^{\frac{1}{4}} \quad \frac{R}{N} \quad \frac{p_m\,\theta}{(\rho_0\,\sigma_0\,C\,h)^{\frac{1}{2}}} \qquad \text{(ship)}$$

$$\frac{(3\pi)^{\frac{1}{4}}}{4} \quad R^{\frac{1}{4}} \quad \frac{p_m\,\vartheta}{(\rho_0\,\sigma_0\,h)^{\frac{1}{2}}} \quad < \left(\frac{1}{16}\right)^{\frac{1}{4}} \quad \frac{p_m\,\theta}{(\rho_0\,\sigma_0\,C\,h)^{\frac{1}{2}}} \qquad \text{(box model)}$$

which reduce simply to the following:-

$$\frac{R}{C} > \frac{9\pi\,\theta}{16} \qquad\qquad \text{(ship)} \qquad (16a)$$

$$\frac{R}{C} > \frac{9\pi\,\theta}{4} \qquad\qquad \text{(box model)} \qquad (16b)$$

The difference of a factor of 4 being due to the absence of the baffle.

Discussion.

For structures such as a ship's bottom, or panel backed by stiffeners and without any baffle, it will be seen that it needs a rather exceptional set of circumstances for cavitation to make any appreciable reduction in damage.   R must be comparable with $C\theta$ for cavitation to be extensive, and yet criterion (16a) must not be satisfied.   This fixes R within fairly narrow limits.   In addition N must be small enough for criterion (14) not to be satisfied, which restricts N to fairly small values.

For structures such as the box-model, although it is undoubtedly true that for sufficiently large R cavitation will increase damage, yet (16b) shows that for a baffled plate there is probably quite an extensive range of values of R for which extensive cavitation occurs and yet reduces damage.   Further, with N = 1, (no sub-division of plating) criterion (14) is never satisfied for any practical size of plate.   The range of values of R for which cavitation may be expected to diminish damage seems to include all types of box-model target in common use.

Conclusion.

The conclusion, on evidence at present available, appears to be that cavitation would almost certainly increase damage to such a target as a ship's bottom or plate sub-divided by stiffeners, but that it would, in general, reduce damage to targets of the "box-model" type consisting of a single plate and a baffle.

<div align="right">References .....</div>

References

(1) Temperley "The theoretical investigation of cavitation phenomena occurring when an underwater explosion pulse is incident on a yielding surface I". (Referred to as I).

(2) Temperley and Chambers, "The theoretical investigation of cavitation phenomena occurring when an underwater explosion pulse is incident on a yielding surface. (Referred to as II).

(3) Taylor. "The pressure and impulse of submarine explosion waves on plates".

(4) Kirkwood. "The plastic deformation of marine structures by an underwater explosion wave II to 15.11.42". C.S.R.D. Report 1115.

(5) Kennard. "The effect of a pressure-wave on a plate or diaphragm".

DIFFRACTION EFFECTS IN BUB   E DAMAGE
TO BOX MODEL PLATES ENERGY C NSIDERATIONS

G. Charlesworth
Road Research Laboratory, London

British Contribution

September 1945

DIFFRACTION EFFECTS IN BUBBLE DAMAGE TO BOX
MODEL PLATES ENERGY CONSIDERATIONS

G. Charlesworth

September 1945

*   *   *   *   *   *   *   *

Summary.

Bubble damage in box model experiments has indicated that energy is diffracted from the rigid flange on to the target plate. In this note, the effect of diffraction in a simplified system under conditions similar to those in box model tests is calculated approximately.

The system considered is that of a circular spring loaded piston moving in a finite fixed rigid circular baffle under the action of a plane bubble wave. The velocity of the water outside the baffle has been assumed equal to the particle velocity in the incident wave. An approximate solution of the equation of motion including the effect of compressibility is obtained and, in a representative numerical example, the deflection of the piston calculated from this solution is compared with the deflections for an infinite plate and for both finite and infinite baffles on non-compressive theory. The piston is assumed initially undeflected. It is found that the ratio of the maximum energy absorbed by the piston to that incident on it for the finite piston is of the same order of magnitude as that observed in box model experiments, which is not the case for the infinite plate or infinite baffle. It is also found that the maximum deflections for the finite baffle are about the same with the compressive and non-compressive approximation, though the deflection time-curves show that the deflection is greater at earlier times in the former case.

The calculations are then extended to the case of the piston deflected initially in a finite baffle for both the compressive and non-compressive cases. The ratio of maximum energy absorbed to incident energy is evaluated numerically for conditions similar to those in R.R.L. box model experiments. It is found that the energy ratio for the compressive approximation is in fair agreement with observation and is better than the non-compressive case.

It is concluded from the calculations that the observed extra energy absorbed by the plate above that directly incident on it in the bubble wave can be largely ascribed to diffraction effects from the flange.

Introduction.

In a recent series of box model experiments it was found that the energy absorbed by the target plate under the action of the bubble wave was more than twice that directly incident on it. It seems likely that most of this energy absorbed by the plate is due to diffraction from the rigid flange round the target plate. The present note is an attempt to determine approximately the effects of diffraction in a simplified system consisting of a piston moving in a baffle and is essentially an extension to bubble waves of Butterworth's analysis for shock waves (1).

Assumptions.

The system considered is a circular rigid spring loaded piston moving in a plane fixed rigid circular baffle of finite extent. The distribution of normal velocity over the plane of the piston and baffle is assumed to be over the piston, zero over the baffle and equal to the particle velocity in the incident wave outside the baffle. The assumed velocity outside the baffle is thus too well at points near the baffle and will lead to an overestimate of the energy absorbed by the piston. The incident wave is assumed to be plane. It is also assumed that the piston spring is 'plastic'.

Average .....

Average Pressure on the Piston.

Let $p(t)$ be the incident wave at any time t

$\nu(t)$ be the velocity of the piston at any time t away from the water

R_1 be the radius of the piston

R_2 be the radius of the baffle

ρc be the acoustic impedance of water

Then the average pressure on the piston is

$$\bar{p} = 2 p(t) - \rho c \, \nu(t) +$$

$$\frac{2}{\pi} \frac{\rho c}{R_1} \int_0^{2R_1} \nu\left(t - \frac{r}{c}\right) \sqrt{1 - \left(\frac{r}{2R_1}\right)^2} \; dr - \frac{2}{\pi R_1} \int_{R_2-R_1}^{R_2+R_1} p\left(t - \frac{r}{c}\right) \sqrt{1 - \frac{(r^2+R_1^2-R_2^2)^2}{(2rR_1)^2}} \; dr \qquad (1)$$

For an infinite piston, i.e. putting $R_2 = R_1$ and letting $R_1 \to \infty$, (1) reduces to the Taylor expression for an infinite plate provided the displacement of the piston and impulse remain finite:

$$\bar{p} = 2 p(t) - \rho c \, \nu(t) \qquad (2)$$

For an infinite baffle, i.e. $R_2 \to \infty$ (1) reduces to

Butterworth's expression

$$\bar{p} = 2 p(t) - \rho c \, \nu(t) + \frac{2 \rho c}{\pi R_1} \int_0^{2R_1} \nu\left(t - \frac{r}{c}\right) \sqrt{1 - \left(\frac{r}{2R_1}\right)^2} \; dr \qquad (3)$$

provided $p(-\infty)$ is zero.

If it is assumed that the velocity of the piston in the interval $t - \frac{2R_1}{c}$ to t is a linear function of time, (1) reduces to

$$\bar{p} = 2 p(t) - \frac{8 R_1}{3 \pi} \dot{\nu}(t) - \frac{2}{\pi R_1} \int_{R_2-R_1}^{R_2+R_1} p\left(t - \frac{r}{c}\right) \sqrt{1 - \frac{(r^2+R_1^2-R_2^2)^2}{(2r R_1)^2}} \; dr \qquad (6)$$

The non-compressive approximation, in which time retardations are assumed negligibly small, is obtained by letting $c \to \infty$ in (1) and gives

$$\bar{p} = p(t) - \frac{8 \rho R_1}{3 \pi} \dot{\nu}(t) \quad \text{for the finite baffle} \qquad (5)$$

and

$$\bar{p} = 2 p(t) - \frac{8 \rho R_1}{3 \pi} \dot{\nu}(t) \text{ for the infinite baffle} \qquad (4)$$

It is seen that the terms due to the motion of the piston in (1) reduce to the same factor in (4) as in (5) and (6).

Deflection of the Piston.

The equation of motion of the piston is

$$m\ddot{y} + ky = \bar{p} \qquad (7)$$

where y is the deflection of the piston

m is the mass/unit area of the piston

k is the stiffness of the spring/unit area of the piston.

Putting $\bar{p} = (...) - \frac{8\,\rho R_1}{3\,\pi}\,\dot{v}(t)$ (8)

(7) becomes $\left(m + \frac{8\,\rho R_1}{3\,\pi}\right)\ddot{y} + ky = f(t)$ (9)

from which

$$y = \frac{1}{Mq}\int_{-\infty}^{t} f(u)\,\sin q(t-u)\,du \qquad (10)$$

for the conditions $y = \dot{y} = o$ at $t = -\infty$
where

$$M = m + \frac{8\,\rho R_1}{3\,\pi}$$

$$q^2 = \frac{k}{M}$$

Application to Bubble Waves.

The bubble wave from 1 oz. charges may be represented approximately by

$$p(t) = p_o \exp\left(-\frac{n}{t}\right) \qquad (11)$$

Numerical evaluation of the last term in equation (8) using equation (11) for conditions typical of N.R.L. box model tests showed that its value was about the same as the equivalent term for the pressure at the centre point, viz. $p\left(t - \frac{R_2}{c}\right)$

The solutions of (10) are:

for finite baffle, equation (8), taking centre point value for the last term in (8)

$$\frac{My}{p_o} = \frac{\left\{2 - \exp\left(\frac{-nR_2}{c}\right)\right\}}{n^2 + q^2}\exp(nt) \qquad \text{for } -\infty < t < o$$

$$= \frac{2\exp(-nt) - \exp n\left(t - \frac{R_2}{c}\right)}{n^2 + q^2} + \frac{n}{n^2+q^2}\cdot\frac{\sin qt}{q} \quad \text{for } o < t < \frac{R_2}{c}$$

$$= \frac{\left(2 - \exp\frac{nR_2}{c}\right)\exp(-nt)}{n^2 + q^2} + \frac{2n}{q(n^2+q^2)}\left\{2\sin qt - \sin q\left(t - \frac{R_2}{c}\right)\right\} \text{ for } \frac{R_2}{c} < t < \infty$$

(12)

for finite baffle, equation (5)

$$\frac{My}{p_o} = \frac{\exp(nt)}{n^2+q^2} \qquad \text{for } -\infty < t < o$$

$$= \frac{\exp(-nt)}{n^2+q^2} + \frac{2n\,\sin qt}{q(n^2+q^2)} \qquad \text{for } o < t < \infty$$

(13)

for the infinite baffle, equation (6), the deflection is twice that in equation (13).

Piston .....

Piston Deflected Initially.

In box model experiments, the target plate is already dished by the shockwave before the arrival of the bubble wave. It is necessary therefore to consider the case of the piston deflected initially.

Let y_0 be the initial deflection.

Then the equation of motion of the piston (9) becomes

$$M\ddot{y} + ky = f(t) - ky_0 \qquad (14)$$

where y is the additional deflection above y_0 and no deflection occurs until $f(t) > ky_0$.

The solutions of (14) for the finite baffle are:

from equation (4) and taking the centre point value for the last term in (4)

$$\frac{My}{P_0} = \frac{2 - \exp(nR_2)}{\frac{c}{n^2 + q^2}} \exp(-nt) + \frac{2n}{q(n^2 + q^2)} \quad (2 \sin qt - \sin q(t - \frac{R_2}{c})$$

$$- \left\{ \frac{2 - \exp(-nR_2)}{\frac{c}{q^2}} \right\} \exp(-nt_0) \; \{1 + \sin\vartheta \sin (qt + qt_0 - \theta)\} \; \text{for} \; \frac{R_2}{c} < t < \infty \qquad (15)$$

where $\tan\theta = \frac{n}{q}$

and $ky_0 = \left(2 - \exp(-\frac{nR_2}{c})\right) p_0 \exp(-nt_0)$

from equation (5)

$$\frac{My}{P_0} = \frac{\exp(-nt)}{n^2+q^2} + \frac{2n \sin qt}{q(n^2+q^2)} - \frac{\exp(-nt_0)}{q^2} \; \{1 + \sin\theta \sin (qt + qt_0 - \theta)\}$$

$$\text{for} \; 0 < t \qquad (16)$$

where $ky_0 = p_0 \exp(-nt_0)$

Evaluation of y_0

The initial deflection y_0 is assumed due to the shock wave. In general, the distance of the charge from the target and the distance of the bubble minimum are not the same.

Let d_0 be the distance of the charge from the piston.

d be the distance of the bubble minimum from the piston.

P_0 be the maximum bubble wave pressure at unit distance, the corresponding value at any distance r being assumed to be P_0/r.

Then, assuming the total energy in the shock wave to be five times that in the bubble wave at the same distance, the total shock wave energy per unit area

$$= \frac{5}{\rho c} \frac{P_0^2}{d_0^2} \frac{1}{n}$$

It is now assumed, as observed experimentally, that the static energy absorbed in producing an initial deflection y_0 is equal to the total shock wave energy incident on the target. For the piston this condition is that

$$\frac{1}{2} k \ldots \ldots$$

$$\tfrac{1}{2} k y_o^2 = \frac{5}{\rho c} \frac{p_o^2}{d_o^2} \frac{1}{f}$$

Whence $\dfrac{ky_o}{p_o} = \dfrac{k \, y_o \, d}{p_o} = \left(\dfrac{10k}{\rho c n}\right)^{b} \dfrac{d}{d_o}$ (17)

Energy Absorption for Piston Deflected Initially.

If y_m is the maximum additional deflection above y_o, the energy absorbed by the piston per unit area is

$$\tfrac{1}{2} k (y_m + y_o)^2 - \tfrac{1}{2} k y_o^2$$

Putting $\quad y_m^1 = \dfrac{y_m}{p_o} \qquad\qquad y_o^1 = \dfrac{y_o}{p_o}$

then the ratio

$$\frac{\text{Energy absorbed by piston}}{\text{Energy incident on piston}} = \tfrac{1}{2} \rho c n k \, y_m^1 \, (y_m^1 + 2y_o^1) \tag{18}$$

Numerical Values.

Piston not deflected initially

Figure 1 shows the form of the deflection-time curves of the piston for the infinite plate, for the finite baffle as given by equations (12) and (13) and for the infinite baffle, for the following conditions typical of R.?.L. box model tests:-

$p_o = 4.34 \times 10^7$ dynes/sq.cm.

$n = 3.03 \times 10^3$ secs^{-1}

$\rho c = 1 \text{ } 4 \times 10^5$ gm/sec. sq.cm.

$m = 1.31$ gm/sq.cm.

$k = 8.122 \times 10^6$ dynes/sq.cm./cm.

$q = 6.507 \times 10^2$ sec^{-1}

$R_1 = 21.06$ cm.

$R_2 = 2R_1$

The values of $\bar{p}$ from equations (2), (4) and (5) are given in Figure 2, and the maximum deflections and ratios of maximum energy absorbed to energy incident on the piston are given in Table 1.

TABLE 1.

	Maximum deflection cms.	Energy absorbed / Energy incident
Infinite plate	0.36	0.12
Finite baffle equation (12)	2.26	4.9
Finite baffle equation (13)	2.19	4.6
Infinite baffle	4.38	18.4

It is .....

It is seen from Figure 1 that the effect of a baffle is to increase the deflection very considerably above that of the infinite plate which, as Figure 2 shows, is due to the increased net pressure on the piston due to diffraction. For the finite baffle, the non-compressive approximation results in an averaging out of the effects of diffraction from the baffle and region beyond. When compressibility is allowed for as in equation (4), the first effects of diffraction on the piston are due only to the baffle which results in larger deflections in the earlier stages than in the non-compressive case. Table 1 shows that the energy ratios for the finite baffle are of the same order of magnitude as observed in box model experiments, which is not the case for either the infinite plate or infinite baffle. The form of the net pressures in Figure 2 indicates that cavitation is unlikely to occur at box model plates for bubble waves even when the plate is not deflected initially.

Piston Deflected Initially.

Using equations (15), (16), (17) and (18), the ratios of energy absorbed to energy incident on the piston have been calculated for numerical values of the constants listed in the previous section. It has also been assumed that the movement of the bubble towards the target is the same as the calculated value for a 1 oz. charge towards a rigid disc. The results are shown in Figure 3, the energy ratio being plotted as a function of the distance of the charge from the piston.

It is seen that the non-compressive case leads to lower values of the ratio than equation (15). This is because neglect of compressibility results in lower pressures on the piston in the earlier stages of its motion.

The magnitude of the energy ratio is in reasonable agreement with observation in view of the approximations involved. It may be concluded that the observed energy ratio is due to the diffraction effects arising from the presence of the flange round the target plate.

Reference.

(1)   Notes on the motion of a finite plate due to an underwater explosion.

Incident wave $= 4.34 \cdot 10^7 e^{3.03 \cdot 10^3 t}$ dynes/sq.cm for $t < 0$

$= 4.34 \cdot 10^7 e^{-3.03 \cdot 10^3 t}$ dynes/sq.cm for $t > 0$

Infinite baffle
(non compressive case)

Finite baffle, equation (12)

Finite baffle, equation (13)
(non compressive case)

Infinite plate

DEFLECTION — Cm

0.4   0.8   1.2   1.6   2.0   2.4   2.8
TIME — Millisecs.
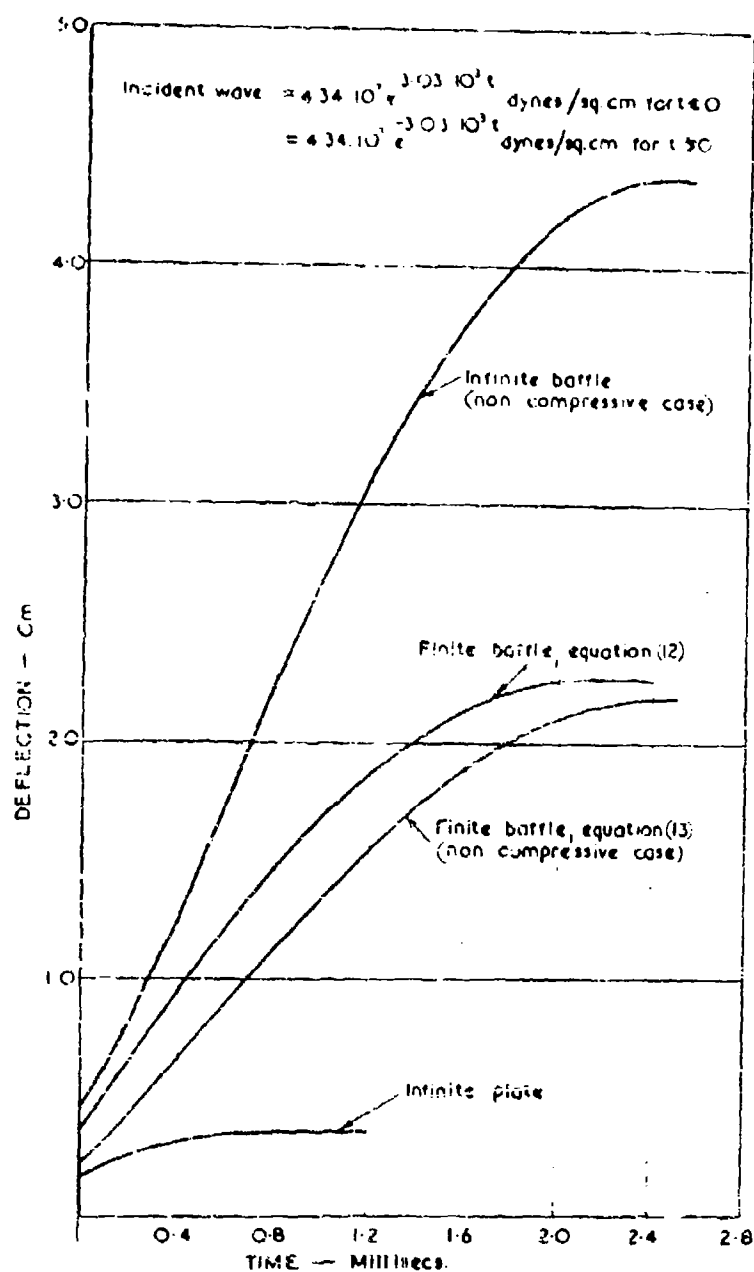
Fig. 1. DEFLECTION OF PISTON BY "BUBBLE WAVE" AS FUNCTION OF
TIME FOR VARIOUS CONDITIONS OF BAFFLE

302
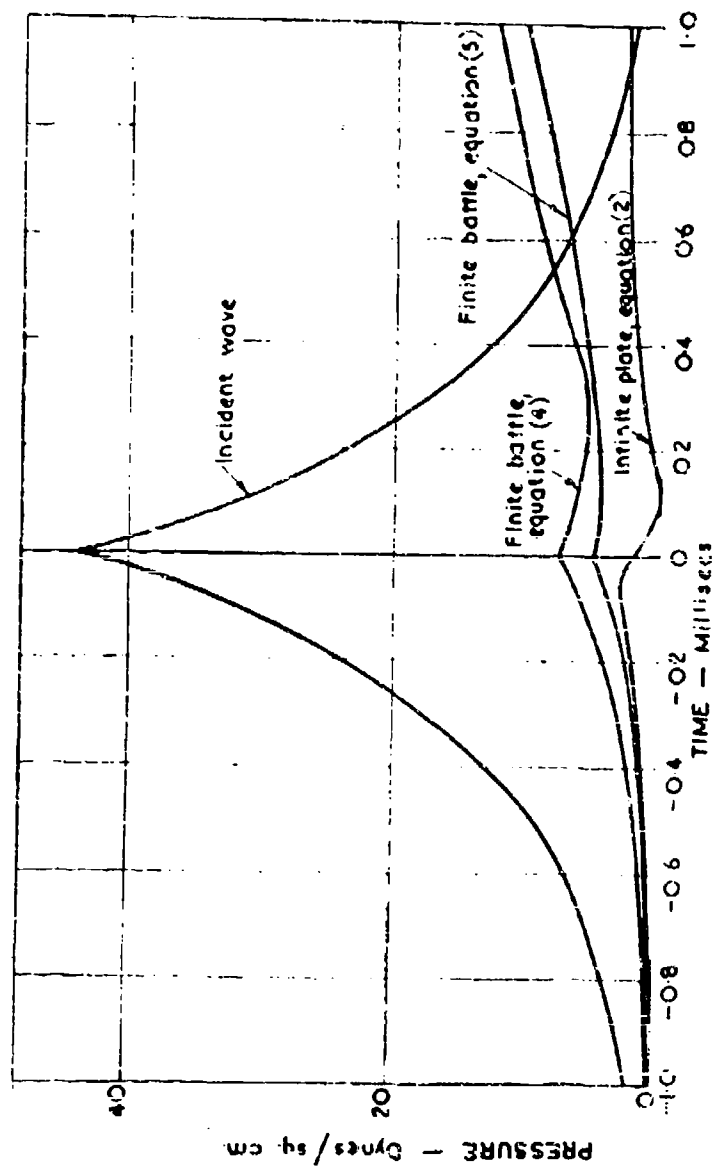
Fig.2 AVERAGE PRESSURE ON THE PISTON AS A FUNCTION OF TIME
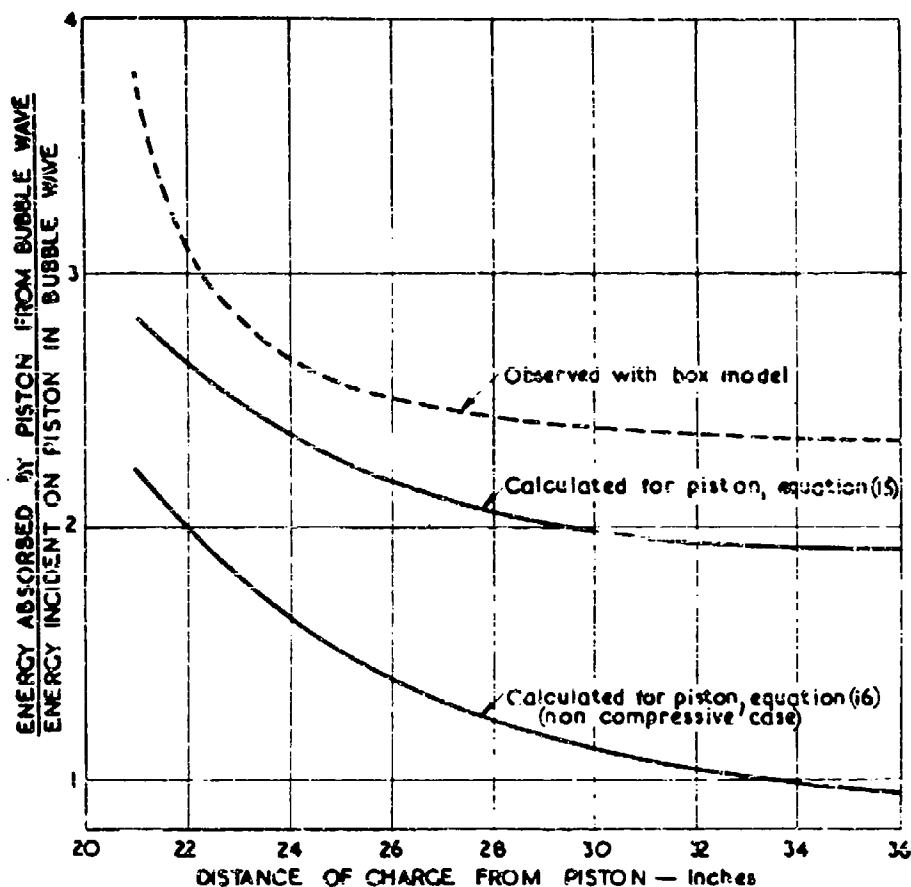
Fig. 3. RATIO OF ENERGY ABSORBED BY PISTON FROM BUBBLE WAVE
TO ENERGY INCIDENT ON PISTON IN BUBBLE WAVE FOR 1oz.
CHARGE AT VARIOUS DISTANCES FROM THE PISTON. CALCULATION
FOR PLANE WAVE AND FINITE BAFFLE WITH THE PISTON
DEFLECTED INITIALLY BY THE SHOCK WAVE

THEORY OF THE PLASTIC DEFORMATION OF THIN PLATES
BY UNDERWATER EXPLOSIONS

J. M. Richardson
Central Experimental Station
Bureau of Mines, Department of the Interior
Pittsburgh, Penna.

and

J. G. Kirkwood
California Institute of Technology

American Contribution

March 15, 1950

CONTENTS

306

CONTENTS (Cont.)

THEORY OF THE PLASTIC DEFORMATION OF THIN PLATES
BY UNDERWATER EXPLOSIONS

By John M. Richardson[a] and John G. Kirkwood[b]

ABSTRACT

The theory of a plastic deformation of thin plates is worked out for the case of axial symmetry. It is assumed that the stress-strain relations in the material are described by (a) vanishing strain for stresses too small to satisfy the von Mises plasticity condition and (b) for stresses satisfying the von Mises condition by incompressibility, and by the similarity of Mohr circles.

The linearized equations for the plate deformations are applied to a problem of damage by underwater explosions. In Parts II to V, inclusive, we consider in detail the deformation of circularly clamped plates without cavitation in the water and we make comparisons with experiment. In Part VI we consider the deformation of infinite plates with cavitation, and we attempt to extend the results to the problem of contact explosions.

a/ Physical chemist, Explosives Branch, Bureau of Mines, U. S. Department of the Interior.
b/ Professor of Chemistry, California Institute of Technology, Pasadena, California.

308

I. GENERAL THEORY OF THE AXIALLY SYMMETRIC DEFORMATION OF THIN PLATES

1. Introduction

The purpose of this part is the general formulation of the theory of the axially symmetric deformation of plates for the dynamic as well as static case. The treatment is limited to ductile materials whose stress-strain relations may be adequately described by incompressibility, a somewhat modified von Mises plasticity condition, and the principle of the similarity of Mohr circles for any nonvanishing strain. This description neglects the elastic domain of strain and hence corresponds to infinite elastic constants with a finite yield stress. Since terms proportional to powers of the thickness higher than the first are neglected, the theory is strictly applicable only to parts of the plate where the radii of curvature are much larger than the thickness. In the specific cases to be considered later the regions of inapplicability will be of negligible extent.

By the use of a parameter development of the nonlinear equations resulting from the above assumptions, relatively tractable equations are obtained as a first approximation. These equations are quite adequate for cases in which the angles between elements of plate in the initial and deformed states are not too large.

2. Model and Basic Assumptions

For the description of the deformation process cylindrical coordinates (r, ϕ, z) are used with an orientation such that the middle surface of the plate is initially coincident with r, ϕ -plane (see figure 1). Since axial symmetry is preserved, the coordinate ϕ is redundant. Overly specific statements about the boundary conditions are avoided as much as possible in

LEGEND

r_0 Initial radius

r Radius at time t

z Vertical displacement

u Radial displacement

a_0 Initial thickness

a Thickness at time t
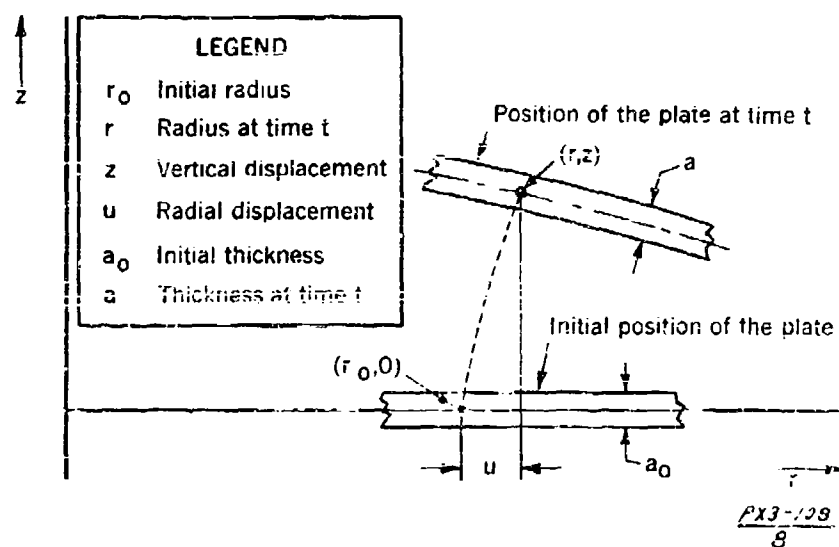
FIGURE 1 - Initial position and a later position of a section of the plate.

order not to limit unnecessarily the range of applicability of the theory.

The equations of the theory and the assumptions on which they are based are presented in the following paragraphs.

(a) *Equations and assumptions.* -- (1) *Equations governing axially symmetric motion of a plate.* The equations governing the axially symmetric motion of a plate, derived in Appendix A for the case of small thickness, are

$$\rho a \sqrt{1 + \left(\frac{\partial z}{\partial r}\right)^2}\, a_z - \frac{1}{r}\frac{\partial}{\partial r}\left(\frac{r \sigma_1 a \frac{\partial z}{\partial r}}{\sqrt{1 + \left(\frac{\partial z}{\partial r}\right)^2}}\right) = p, \tag{1}$$

$$\rho d \sqrt{1 + \left(\frac{\partial z}{\partial r}\right)^2}\, a_1 - \frac{1}{r}\frac{\partial}{\partial r}\left(r \sigma_1 d\right) + \frac{\sigma_2 d}{r} = 0, \tag{2}$$

where a_z and a_1 are the vertical and meridional accelerations, respectively, given by

$$a_z = D^2 z + \frac{\frac{\partial z}{\partial r}}{1 - \frac{\partial u}{\partial r}} D^2 u, \tag{3}$$

$$a_1 = \frac{\frac{\partial z}{\partial r}}{\sqrt{1 + \left(\frac{\partial z}{\partial r}\right)^2}} D^2 z + \frac{\sqrt{1 + \left(\frac{\partial z}{\partial r}\right)^2}}{1 - \frac{\partial u}{\partial r}} D^2 u, \tag{4}$$

where

$$D^2 z \frac{\partial^2}{\partial t^2} + \frac{2 \frac{\partial u}{\partial t}}{1 - \frac{\partial u}{\partial r}}\frac{\partial^2}{\partial r \partial t} + \left(\frac{\frac{\partial u}{\partial t}}{1 - \frac{\partial u}{\partial r}}\right)^2 \frac{\partial^2}{\partial r^2}. \tag{5}$$

In these equations r and z are the radial and vertical coordinates, respectively, of a point on the neutral surface of the plate (see figure 1), and u is the radial displacement of that point from its initial position to its

position (r, z) at time t ; ρ is the density of the plate material and δ is the actual thickness of the plate at the point (r, z) and at time t ; p is the pressure acting on the lower side of the plate at the radius r and at time t ; σ_1 and σ_2 are the principal stresses in the meridional and circumferential directions, respectively. Equations (1) and (2), expressed with a briefer but less explicit notation, have been derived in CSRD-4200.

(2) The modified von Mises plasticity condition. The biaxial reduced engineering stresses,

$$S_1 = \frac{\delta \sigma_1}{\delta_o \sigma_o},$$

and

$$\bar{S}_2 = \frac{\delta \sigma_2}{\delta_o \sigma_o},$$

(6)

are assumed to satisfy the von Mises condition in the plane-stress approximation, which in these terms may be written,

$$S_1^2 + S_2^2 - S_1 S_2 = 1.$$

(7)

Here δ_o is the initial thickness of the plate, and σ_o is the yield stress. Equation (7) is assumed to hold in the limit of vanishing strains implying ignoration of the elastic domain of strain.

(3) Incompressibility of material. The material is incompressible, or, in other words, Poisson's ratio equals 1/2. Incompressibility imposes the following relation on the ratio of the actual thickness δ to the initial thickness δ_o :

$$\frac{\delta}{\delta_o} = \frac{1}{(1 + \epsilon_1)(1 + \epsilon_2)} = \frac{\left(1 - \frac{u}{r}\right)\left(1 - \frac{\partial u}{\partial r}\right)}{\sqrt{1 + \left(\frac{\partial z}{\partial r}\right)^2}},$$

(8)

3

312

where ε_1 and ε_2 are the meridional and circumferential strains, respectively, given by

$$\varepsilon_1 = \frac{\sqrt{1 + \left(\frac{\partial u}{\partial r}\right)^2}}{1 - \frac{\partial u}{\partial r}} - 1, \tag{9}$$

$$\varepsilon_2 = \frac{1}{1 - \frac{u}{r}} - 1. \tag{10}$$

(4) Similarity of Mohr circles. A further relation is imposed on the stresses and strains by the principle of the similarity of Mohr circles[1], which, for the case treated here, may be expressed in the form,

$$\frac{\sigma_1 - \frac{1}{2}\sigma_2}{\sigma_2 - \frac{1}{2}\sigma_1} = \frac{S_1 - \frac{1}{2}S_2}{S_2 - \frac{1}{2}S_1} = \frac{\varepsilon_1}{\varepsilon_2}. \tag{11}$$

(b) Discussion of assumptions. — The equations of motion, Eqs. (1) and (2), as has been stated before, are rigorously true in the limit of vanishing thickness. If the stresses were linearly related to the strains as in the elastic case, neglected bending terms would be proportional to d^3. However, in the plastic stress-strain relationship as expressed by assumptions (2), (3), and (4), the bending terms are negligible, and consequently Eqs. (1) and (2) hold over a wider range of thickness than in the elastic case.

The von Mises condition as expressed in assumption (2) can be correlated only with biaxial tensile tests with plates.[2] It implies a

[1] Plasticity, by Nadai (McGraw-Hill, 1931).
[2] The condition as written implies isotropy only with respect to directions tangent to the plate making specialization to the linear tensile test illegitimate.

4

biaxial stress-strain relation in which the effect of strain hardening is exactly compensated by the effect of decreasing thickness, resulting in a somewhat closer fit to experimental results and a simplification of the higher approximations. As stated before, it also implies ignoration of the elastic domain of strain, an apparently justifiable approximation in the case of ductile materials such as steel and copper in which plastic flow can occur over relatively large domains of strain. In a rapid deformation process going well into the plastic domain of stress, the ignoration of the elastic domain is further justified by the fact that only the inertial terms of the equations of motion are important /at least in Eq. (1)/ when the strains are small.

The application of von Mises condition to all parts of the plate is valid only if the rate of strains keeps the same sign at each part. If the rate of strain changes sign anywhere, the equations of motion are tremendously complicated by unloading and hysteresis effects.

The experimental stress-strain curves deviate, of course, rather widely from the idealized one implied here. Moreover, the experimental curves are found to depend upon the rate of strain; however, these effects are manifested in a relatively small range of strain beyond the proportional limit. The yield stress σ_o may be regarded as a parameter adjusted to give the best agreement between the ideal and experimental curves. Hence it is easy to see that the ultimate tensile strength is a better value for σ_o than the stress at which yielding begins.

The principle of the similarity of the Mohr circles of stress and strain is usually assumed to hold only for stationary plastic flow. In the

5

absence of better information, it is assumed here to hold also for nonstationary flow.

The coincidence of the directions of principal stresses and strain, usually included among the rules describing plastic behavior, has not been stipulated here because it is automatically secured by the axial symmetry.

Before attempting a solution, it is desirable to recast Eqs. (1) to (11) in a more workable form. Using the reduced engineering stresses S_1 and S_2 exclusively, and combining some of the foregoing equations we get

$$\left(1 - \frac{u}{r}\right)\left(1 - \frac{\partial u}{\partial r}\right) a_z - \frac{c^2}{r}\frac{\partial}{\partial r}\left(\frac{r S_1 \frac{\partial z}{\partial r}}{\sqrt{1 + \left(\frac{\partial z}{\partial r}\right)^2}}\right) = \frac{p}{\rho a_o} \quad , \qquad (12)$$

$$\left(1 - \frac{u}{r}\right)\left(1 - \frac{\partial u}{\partial r}\right) a_1 - \frac{c^2}{r}\frac{\partial}{\partial r}\left(r S_1\right) + \frac{c^2}{r} S_2 = 0, \qquad (13)$$

where

$$c = \sqrt[4]{\sigma_o / \bar{r}} \quad ,$$

$$\frac{S_1 - \frac{1}{2} S_2}{S_2 - \frac{1}{2} S_1} = \frac{\left(1 - \frac{\partial u}{\partial r}\right)^{-1}\sqrt{1 + \left(\frac{\partial z}{\partial r}\right)^2} - 1}{\left(1 - \frac{u}{r}\right)^{-1} - 1} \quad , \qquad (14)$$

$$S_1^2 + S_2^2 - S_1 S_2 = 1, \qquad (15)$$

where a_z and a_1 are given by Eqs. (3) and (4). With the above equations should be included Eqs. (9) and (10) giving the strains.

3. Expansion in Terms of an Auxiliary Parameter and a Method of Successive Approximation

Since there is little hope of solving exactly the equations presented in assumptions (1) to (4), the desirability of a method of successive approximation is apparent. Following the introduction of a parameter α into the initial conditions and external forces in such a way that the dependent variables are analytic in α, the dependent variables in each equation are expanded in terms of α, and coefficients of the powers of α are collected. A method of successive approximation is immediately obtained by setting equal to zero the coefficient of each power of α.

The parameter α is introduced as follows.

$$\begin{aligned}
p(r,t) &= \alpha\, p^{(1)}(r,t) + \alpha^3\, p^{(3)}(r,t) + O(\alpha^5), \\
z(r,o) &= 0, \\
\frac{\partial z}{\partial t}(r,o) &= \alpha\, j(r), \\
u(r,o) &= 0, \\
\frac{\partial u}{\partial t}(r,o) &= \alpha^2\, k(r),
\end{aligned}\right\} \tag{16}$$

Now the independent variables z, u, S_1, and S_2 are functions of α, and furthermore they are analytic in α. Consequently, they can be expanded in power series in α with a radius of convergence hoped to be sufficiently large. It is apparent that changing the sign of α is equivalent to a reflection through the r,ϕ -plane, and that consequently z must be odd in α and u, S_1, and S_2 must be even in α. Both z and u vanish with α, whereas S_1 and S_2 approach a finite limit according to the idealized stress-strain relationship assumed in this treatment. In view of these considerations, the expansions take the form,

7

$$z(r,t,\alpha) = \alpha z^{(1)}(r,t) + \alpha^3 z^{(3)}(r,t) + O(\alpha^5),$$
$$u(r,t,\alpha) = \alpha^2 u^{(2)}(r,t) + \alpha^4 u^{(4)}(r,t) + O(\alpha^6),$$
$$S_1(r,t,\alpha) = S_1^{(0)}(r,t) + \alpha^2 S_1^{(2)}(r,t) + O(\alpha^4),$$
$$S_2(r,t,\alpha) = S_2^{(0)}(r,t) + \alpha^2 S_2^{(2)}(r,t) + O(\alpha^4).$$
$$(17)$$

The expansions given by Eqs. (17) are then introduced into Eqs. (12), (13), (14), and (15). A method of successive approximation can be obtained if the coefficient of each power of α is set equal to zero. The method thus obtained goes as follows.

(a) <u>First approximation</u>. -- The first approximation is

$$\frac{\partial}{\partial r}\left(r S_1^{(0)}\right) - S_2^{(0)} = 0, \tag{18}$$

$$\left(S_1^{(0)}\right)^2 + \left(S_2^{(0)}\right)^2 - S_1^{(0)} S_2^{(0)} = 1, \tag{19}$$

$$\frac{\partial^2 z^{(1)}}{\partial t^2} - \frac{c^2}{r}\frac{\partial}{\partial r}\left(r S_1^{(0)}\frac{\partial z^{(1)}}{\partial r}\right) = \frac{F^{(1)}}{\rho a_0}, \tag{20}$$

$$\left(S_1^{(0)} - \frac{1}{2} S_2^{(0)}\right)\frac{u^{(2)}}{r} - \left(S_2^{(0)} - \frac{1}{2} S_1^{(0)}\right)\left[\frac{\partial u^{(2)}}{\partial r} + \frac{1}{2}\left(\frac{\partial z^{(1)}}{\partial r}\right)^2\right] = 0. \tag{21}$$

In this approximation the strains are given by

$$\varepsilon_1 = \alpha^2\left[\frac{\partial u^{(2)}}{\partial r} + \frac{1}{2}\left(\frac{\partial z^{(1)}}{\partial r}\right)^2\right],$$
$$\varepsilon_2 = \alpha^2 \frac{u^{(2)}}{r}.$$
$$(22)$$

8

(b) Higher approximations. -- The nth ap,.oximation is obtained by setting equal to zero the coefficient of α^{2n-1} in Eq. (12), α^{2n-2} in Eq. (13), α^{2n} in Eq. (14), and α^{2n-2} in Eq. (15). Here the strains are, of course, given by the first n terms in Eqs. (9) and (10).

The reader will observe that in the nth approximation (except for $n = 1$) the dependent variables, $z^{(2n-1)}$, $u^{(2n)}$, $S_1^{(2n-2)}$, and $S_2^{(2n-2)}$, occur linearly, and that no variables with a higher superscript appear. Consequently, there will be no difficulties associated with nonlinearity except possibly in the first approximation. The solutions of all n-t approximations are to be fitted to the appropriate boundary and initial conditions before substitution in the nth approximation.

The foregoing method of successive approximation is applicable only to problems in which the initial conditions are expressible in the manner of Eq. (16) and the boundary conditions are expansible in α in such a manner that the vanishing of α corresponds to no motion of the plate. In order to use the initial and boundary conditions in the scheme of successive approximation, the coefficients of each power of α are set equal to zero, thereby obtaining conditions corresponding to each approximation.

The boundary conditions may take varied forms. Boundary conditions for the first approximation are considered in more detail in the next section. It is well to consider them separately for each anticipated special application of the general theory presented here. The parameter α will usually be assigned a physical meaning (that is, in the case of damage to infinite thin plates by projectiles, α is the ratio of the initial projectile velocity to the velocity of plastic waves), thus establishing a

obtained

.x-1 in

ins are,

xcept for

, and

:perscript

h nonlin-

f all n-t

tia con-

.cable

the

in

he plate.

f suc-

equal to

on.

condi-

the next

ed special

will

age to

projec-

a

connection between physical parameters and the error in the first approximation.

4. Thin-Plate Equations in the First Approximation

In obtaining the solution in the first approximation the first step is to solve Eqs. (18) and (19) for $\frac{\partial S_1^{(o)}}{\partial r}$ in terms of $S_1^{(o)}$ with the result:

$$\frac{\partial S_1^{(o)}}{\partial r} = \frac{1}{2r}\left\{ -S_1^{(o)} \pm \sqrt{4 - 3(S_1^{(o)})^2} \right\}. \tag{23}$$

Also

$$S_2^{(o)} = \frac{1}{2}\left\{ S_1^{(o)} \pm \sqrt{4 - 3(S_1^{(o)})^2} \right\}. \tag{24}$$

is obtained. Since having $S_1^{(o)}$ and $S_2^{(o)}$ both positive is the only case of interest here, only the positive sign in front of the radicals will be retained henceforth. It can be shown that $\partial S_1^{(o)}/\partial r$ possesses a saddle-point singularity at the point (0,1) in the $r, S_1^{(o)}$ -plane and that the orientation of the singularity is such that no integral curves except $S_1^{(o)} = 1$ cross the $S_1^{(o)}$ axis. It immediately follows from Eq. (18) that $0 \le S_1^{(o)} \le 1/\sqrt{3}$. The actual solution of Eq. (23) (using the plus sign) is

$$\log r = \frac{\sqrt{3}}{2}\left\{ -\frac{1}{\sqrt{3}} \log \left| \sqrt{1 - \frac{3}{4}(S_1^{(o)})^2} - \frac{1}{2}S_1^{(o)} \right| + \sin^{-1}\frac{\sqrt{3}}{2}S_1^{(o)} \right\} + C(\varepsilon), \tag{25}$$

with the limiting case,

$$S_1^{(c)} = 1. \tag{26}$$

Solutions (25) and (26) satisfy the qualitative restrictions already stated.
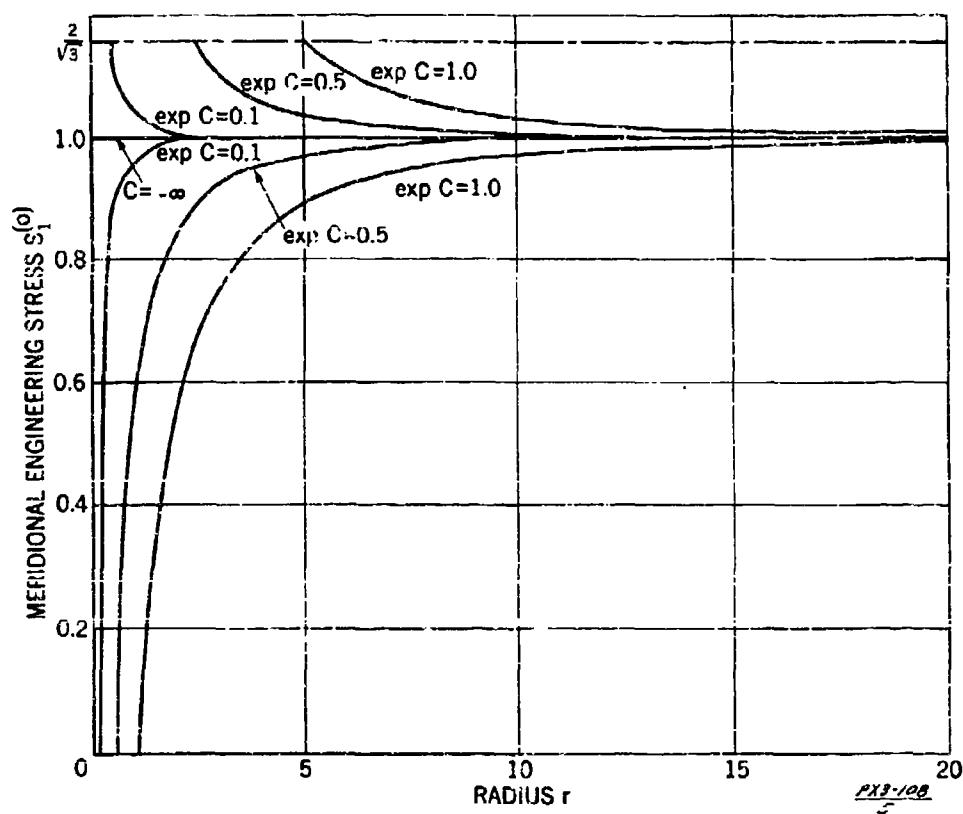
FIGURE 2 — The meridional engineering stress $S_1^{(o)}$ versus the radius r.

320

In figure 2 the solutions are plotted in the $r, S_1^{(o)}$-plane for several fixed values of $C(t)$.

Let the symbol D denote the range of r in which the basic equations describe the behavior of the plate. If the boundary conditions are such that D includes the point $r=0$, then, as one can easily see from figure 2, the stress distribution must be given by the contour $S_1^{(o)}=1$ to which corresponds also the contour $S_2^{(o)}=1$. If $S_1^{(o)}=S_2^{(o)}$ at any point in D, then $S_1^{(o)}=S_2^{(o)}$ at every point in D, even though D may not include the point $r=0$. The condition for the similarity of Mohr circles in conjunction with the last statement implies (in the first approximation, of course) that if the principal strains, ϵ_1 and ϵ_2, are equal anywhere in D, then they are equal everywhere in D, even though again D may not include $r=0$. If the boundary conditions are such that D does not include $r=0$, and such that $\epsilon_1 \neq \epsilon_2$ or $S_1^{(o)} \neq S_2^{(o)}$ for any r in D, the stress distribution will be given by one of the other contours of figure 2 corresponding to the general solution of Eq. (25) with $C(t)$ finite.

The prospective applications of the present theory are fortunately characterized by boundary conditions allowing the range D to include $r=0$, in which case the stress distribution is $S_1^{(o)}=S_2^{(o)}=1$. In view of the simplicity and wide range of applicability of the uniform stress distribution $S_1^{(o)}=S_2^{(o)}=1$, the solution of the first approximation will be resumed on that basis.

Setting $S_1^{(o)}$ and $S_2^{(o)}$ equal to unity in Eqs. (20) and (21) gives

11

$$\frac{\partial^2 z^{(1)}}{\partial t^2} - \frac{c^2}{r} \frac{\partial}{\partial r} \left(r \frac{\partial z^{(1)}}{\partial r} \right) = \frac{p^{(1)}}{\rho d_o} , \qquad (27)$$

$$\frac{\partial u^{(1)}}{\partial r} - \frac{u^{(1)}}{r} = - \frac{1}{2} \left(\frac{\partial z^{(1)}}{\partial r} \right)^2 . \qquad (28)$$

It is now apparent that in the first approximation the constant $c = \sqrt{\sigma_o / \rho}$ is the velocity of transverse plastic waves.

If the solution of Eq. (27) be known, the solution of Eq. (28) can be given in terms of it as follows:

$$\frac{u^{(1)}}{r} = \frac{1}{2} \int_{-}^{r^*(t)} \left(\frac{\partial z^{(1)}}{\partial r} \right)^2_{r=r'} \frac{dr'}{r'} , \qquad (29)$$

where $r^*(t)$ is a nonzero value of r at which the radial displacement vanishes. In the case of an infinite plate $r^*(t) = \infty$. The first approximation to the strains is given as an immediate corollary of Eq. (29) by

$$\varepsilon_1 = \varepsilon_2 = \frac{\alpha^2}{2} \int_{r}^{r^*(t)} \left(\frac{\partial z^{(1)}}{\partial r} \right)^2_{r=r'} \frac{dr'}{r'} . \qquad (30)$$

Since the integrand of Eq. (30) is always positive for every real solution of Eq. (27), the strains must always be greatest at $r = 0$, the center.

It should be noted that in this approximation the time enters explicitly only into Eq. (27), giving the profile $z^{(1)}$. This fact means that the membrane at a given instant of time t has the same radial-displacement distribution as a membrane statically constrained to the profile $z^{(1)}(r, t)$, with no tangential traction. An equivalent statement would be that tangential propagation effects occur with essentially infinite velocity.

12

322

It is instructive to compare the meridional strain ε_1, given by Eq. (30), with that obtained on the basis of normal motion to the same degree of approximation. If $x^{(i)}(r,t)$ is expressible in the form $T(t)R(r)$, and if $R(r)$ is of the parabolic form $A + B r^2$, the two assumptions give identical values for the meridional strain.[3/] However, if $R(r)$ is not of the above parabolic form, the quantity $\dfrac{d^2 R}{dr^2} - \dfrac{1}{r}\dfrac{dR}{dr}$ gives a measure of the deviations to be expected to occur between the two calculations of the meridional strain.

The plastic deformation of an infinite thin plate under various types of loading $\alpha\, p^{(i)}(r,t) + O(\alpha^3)$, of which the anticipated special applications can be considered special cases, reduces to the solution of

$$\frac{\partial^2 x^{(i)}}{\partial t^2} - \frac{c^2}{r}\frac{\partial}{\partial r}\left(r\frac{\partial x^{(i)}}{\partial r}\right) = \frac{p^{(i)}(r,t)}{\rho\, a_o}, \qquad (31)$$

and subsequently to the evaluation of

$$\varepsilon_1 = \varepsilon_2 = \frac{c^2}{2}\int_r^{r_o}\left(\frac{\partial x^{(i)}}{\partial r}\right)^2_{r=r'}\frac{dr'}{r'} \qquad (32)$$

to give the distribution of strains. The conditions for rupture are obtained by setting the time maximum of the central strain, $\varepsilon_1(o, t_m)$, equal to the critical rupture strain ε_c.

[3/] If $x^{(i)} = T(t)R(r)$, the assumption of normal motion gives for the meridional strain ε_1 (in the first approximation)

$$\varepsilon_1 = -\frac{c^2}{r}\int_0^t \frac{\partial x^{(i)}}{\partial r}\frac{\partial x^{(i)}}{\partial t}dt = -\frac{c^2}{2}\frac{T^2}{r}R\frac{dR}{dr}$$

and the assumption of similarity of Mohr circles [see Eq. (30)] gives

$$\varepsilon_1 = \frac{c^2}{2}\int_r^{r_o}\left(\frac{\partial x^{(i)}}{\partial r}\right)^2_{r=r'}\frac{dr'}{r'} = -\frac{c^2}{2}\frac{T^2}{r}R\frac{dR}{dr} - \frac{\alpha T^2}{2}\int_r^{r_o}R\left(\frac{d^2R}{dr^2} - \frac{1}{r}\frac{dR}{dr}\right)dr.$$

If the two results are to agree for r arbitrary, then

$$\frac{d^2R}{dr^2} - \frac{1}{r}\frac{dR}{dr} = 0$$

or $R = A + B r^2$.

13

II. HYDRODYNAMICS OF THE LOADING OF THE PLATE
BY AN UNDERWATER EXPLOSION WAVE

1. General Theory

In the last part we have treated the axially symmetric motion of
a thin plate under an arbitrary axially symmetric pressure $p(r,t)$. We
are ultimately interested in the behavior of an initially plane plate at-
tacked on the lower side by a plane underwater shock wave traveling in the
positive z-direction and backed by air (treated as vacuum here) on the upper
side. Here we seek the relation between the actual incident pressure $p(r,t)$
and the free-field pressure $p_o(t)$ of the shock wave.

Let this treatment be limited to the approximation corresponding
to coefficient of first power of α, $p^{(1)}(r,t)$, in the α-expansion of
$p(r,t)$ (Eq. (16) of Part I). It is then appropriate that we use linear-
ized hydrodynamics and, in considering the instantaneous geometry of the
system, neglect the deviations of the shell from its initial plane configu-
ration. The added approximation of treating the water as an inviscid fluid
allows us to use ordinary linear acoustical theory. In this theory we can
define a velocity potential ψ related to the pressure p and particle veloc-
ity $\vec{u}$ as follows,

$$\vec{u} = -\nabla\psi \ , \quad p = \rho_o \frac{\partial\psi}{\partial t} \ , \tag{1}$$

and satisfying the wave equation

$$\nabla^2\psi - \frac{1}{c_o^2}\frac{\partial^2\psi}{\partial t^2} = 0 . \tag{2}$$

In these equations, ρ_o and c_o are the density in and sound velocity of water
at zero pressure. If the notation of Part I were followed, the quantities

14

Ψ, p, and $\vec{u}$ should bear the superscript (1), indicating that they are coefficients of α in the α-expansions. We shall omit the superscripts here.

It should be mentioned at this point that the theory of this section is worked out on the assumption that cavitation does not occur. Mathematically speaking, this means that Eqs. (1) and (2) are assumed to hold everywhere in the fluid. Cavitation is discussed briefly and qualitatively in Section 2 of this Part. To avoid cavitation, it will be shown there that it is necessary (but not sufficient) to confine ourselves to the case of circularly clamped shells.

Getting back to the main current of the argument, it is known[1]/ the solution of (2) at a point in a volume (at every point of which (2) is satisfied) can be expressed as the sum of the retarded potentials due to distributions of simple and double sources on the surface of the volume. Consider two semi-infinite volumes above and below the r-ϕ-plane (in which the plate and other diffracting objects, if any, lie). Moreover, consider the velocity potential Ψ in each semi-infinite volume to vanish at infinity, and consider the Ψ in one volume to be given by the reflection through the r, ϕ-plane of the Ψ in the other volume. Under these conditions it follows that the Ψ at a point $\vec{r}$ below or on the r, ϕ-plane can be expressed in the form

$$\Psi(\vec{r}, t) = \frac{1}{4\pi} \int |\vec{r} - \vec{r}'|^{-1} \, \vec{u}(\vec{r}', t^*) \cdot \overline{dA}' , \tag{3}$$

$$t^* = t - |\vec{r} - \vec{r}'|/c_0 , \tag{4}$$

1/ Kirchhoff "Zur Theorie der lichtstrahien." Berl. Ber. 1882, p. 641 /Ges. Abh. i. 22/.

where the integration extends over the entire r,ϕ-plane, and $\overrightarrow{dA}$ is a vector element of area pointing in the negative z-direction. Henceforth our attention will be devoted exclusively to the case of $\overrightarrow{r}^0$ on the r,ϕ-plane.

In the case of interest, we wish to consider the actual ψ, p, and $\overrightarrow{u}$ in the water in relation to the corresponding free-field quantities, ψ_o, p_o, and $\overrightarrow{u}_o$ that would exist if the diffracting obstacle were absent. Let us apply Eq. (3) to the perturbations $\psi - \psi_o$ and $\overrightarrow{u} - \overrightarrow{u}_o$ of the free-field quantities ψ_o and $\overrightarrow{u}_o$ arising from the diffracting obstacle. Differentiating this result with respect to time, we obtain

$$p = p_o + \frac{\rho_o}{2\pi} \int |\overrightarrow{r}-\overrightarrow{r}'|^{-1} \left[\frac{\partial \overrightarrow{u}}{\partial t}(\overrightarrow{r}';t^*) - \frac{\partial \overrightarrow{u}_o}{\partial t}(\overrightarrow{r}';t^*) \right] \cdot \overrightarrow{dA}'. \quad (5)$$

Suppose the obstacle* extends over an area A_o in the r,ϕ-plane. Let the remainder of the r,ϕ-plane be denoted by A_1. In the area A_o let us use the relation $\rho_o \frac{\partial \overrightarrow{u}_o}{\partial t} = -\nabla p_o$. Eq. (5) then goes into the form

$$p = p_o + \frac{1}{2\pi} \int_{A_o} |\overrightarrow{r}-\overrightarrow{r}'|^{-1} \left[\nabla' p_o(\overrightarrow{r}';t) \right]_{t=t^*} \cdot \overrightarrow{dA}'$$

$$+ \frac{\rho_o}{2\pi} \int_{A_o} |\overrightarrow{r}-\overrightarrow{r}'|^{-1} \frac{\partial \overrightarrow{u}}{\partial t}(\overrightarrow{r}';t^*) \cdot \overrightarrow{dA}' \qquad (6)$$

$$+ \frac{\rho_o}{2\pi} \int_{A_1} |\overrightarrow{r}-\overrightarrow{r}'|^{-1} \left[\frac{\partial \overrightarrow{u}}{\partial t}(\overrightarrow{r}';t^*) - \frac{\partial \overrightarrow{u}_o}{\partial t}(\overrightarrow{r}';t^*) \right] \cdot \overrightarrow{dA}'.$$

---

* Here, we use the term "obstacle" in a somewhat generalized sense. It is meant to include all parts of a plane underwater structure offering resistance to the underwater explosion wave (e.g., plate and baffle).

Since we are interested only in pressures near the center of the obstacle, the contribution of the third integral in (6) (involving the difference $\vec{u} - \vec{u}_o$ in the area A_o outside the obstacle) will be quite small for most cases since this term represents the diffraction of the scattered (not the primary) wave. This is obviously true when the thickness of the pressure wave is small compared with the width of the obstacle. Consequently, we shall neglect this term obtaining the result,

$$p = p_o + \frac{1}{2\pi} \int_{A_o} |\vec{r} - \vec{r}'|^{-1} \left[\nabla' p_o(\vec{r}', t') \right]_{t' = t^*} \cdot \vec{dA}' \tag{7}$$

$$+ \frac{\rho_o}{2\pi} \int_{A_o} |\vec{r} - \vec{r}'|^{-1} \frac{\partial \vec{u}}{\partial t}(\vec{r}', t^*) \cdot \vec{dA}'.$$

Now let us specialize the above result to the case of an incident plane pressure wave and a circular plate of radius R_o clamped to a rigid baffle whose outside radius is R_1. In this case $p_o(\vec{r}, t) = p_o(t - x/c_o)$; thus $\nabla p_o(\vec{r}, t) = -\vec{1}_x p_o'(t)/c_o$ for $\vec{r}$ on the r, ϕ-plane. Also let $\vec{r}' - \vec{r} = \vec{r}^*$, and let $\vec{r}^* = r^*(\vec{1}_x \cos\phi^* + \vec{1}_y \sin\phi^*)$. (It should be emphasized that we are limiting $\vec{r}$ and $\vec{r}'$ to the r, ϕ-plane.) Finally, let z denote the displacement of the plate in the x-direction. With these assumptions and definitions, Eq. (7) becomes ($r < R_o$)

$$p(r,t) = 2 p_o(t) - \frac{1}{2\pi} \int_0^{2\pi} d\phi^* \, p_o(t - R_1^*/c_o) \tag{8}$$

$$- \frac{\rho_o}{2\pi} \int_0^{2\pi} d\phi^* \int_0^{R_o^*} dr^* \frac{\partial^2 z}{\partial t^2}(r', t - r^*/c_o),$$

where

$$r' = \left(r^2 + r^{*2} + 2 r r^* \cos\phi^* \right)^{1/2}, \tag{9}$$

and

$$R_o^* = -r\cos\phi^* + \sqrt{R_o^2 - r^2\sin^2\phi^*},$$
$$R_1^* = -r\cos\phi^* + \sqrt{R_1^2 - r^2\sin^2\phi^*}. \quad (10)$$

In some instances it may be more convenient to express the second integral of (8) in the form

$$-\frac{\rho_o}{2\pi}\int_0^{2\pi}d\phi'\int_0^{R_1}dr'\,\frac{r'}{r^*}\frac{\partial^2 z}{\partial t^2}(r';t - r^*/c_o), \quad (11)$$

where

$$r^* = (r^2 + r'^2 - 2rr'\cos\phi')^{1/2}. \quad (12)$$

For use in subsequent applications, we list several special forms of (8). For $r=0$, we get

$$p(o,t) = 2p_o(t) - p_o(t - R_1/c_o) - \rho_o\int_0^{R_o}dr'\,\frac{\partial^2 z}{\partial t^2}(r';t - r'/c_o). \quad (13)$$

Suppose τ is a characteristic time for the deformation process. If $c_o\tau \gg R_1$, we obtain to a good approximation,

$$p(r,t) = p_o(t) - \frac{\rho_o}{2\pi}\int_0^{2\pi}d\phi'\int_0^{R_o}dr'\,\frac{r'}{r^*}\frac{\partial^2 z}{\partial t^2}(r';t). \quad (14)$$

If $R_o \ll c_o\tau \ll R_1$, we get

$$p(r,t) = 2p_o(t) - \frac{\rho_o}{2\pi}\int_0^{2\pi}d\phi'\int_0^{R_o}dr'\,\frac{r'}{r^*}\frac{\partial^2 z}{\partial t^2}(r';t). \quad (15)$$

2. Cavitation

In the initial stages of the impact between the plate and the explosion wave, large negative pressures may under some circumstances develop at the surface of the plate due to the reflected rarefaction wave. Since water, especially dirty water, cannot support a tension of great

magnitude, it has been proposed that cavitation will occur when the pressure in the wave becomes negative. This is assumed by G. I. Taylor[2] in his theory of plastic damage. The hydrodynamic theory developed in the last section as applied to thin circular plates in Parts III, IV, and V fails when cavitation is well-developed. Consequently, it is imperative that the results of this part be amended by a reliable cavitation criterion.

During the initial stages of its motion, the central part of the circularly clamped plate will behave as a free plate, since it will take a finite time R_0/c_0 for a pressure wave in the water starting from the periphery of the plate to perturb the pressure distribution near the center. Furthermore, it will take a considerably longer time R_0/c for a plastic wave in the plate to travel from the periphery to the center (see Part IV, Sec. 4). It has been shown by Kennard[3] that for a pressure wave of the form $p_s(t) = p_m e^{-t/\theta}$ impinging upon a free plate of thickness a_0 and density ρ, the pressure will drop to zero in a time

$$\theta_c = \frac{\theta\,\theta_1}{\theta - \theta_1}\, \log \frac{\theta}{\theta_1}$$

$$\theta_1 = \rho\, a_0 /\rho_0 c_0$$

If this time is reached before the arrival of the pressure wave from the periphery a negative pressure will certainly be developed and we assume that cavitation will occur. Thus we propose the following criterion:

$$R_0/c_0 > \theta_c \quad - \quad \text{cavitation}$$
$$R_0/c_0 < \theta_c \quad - \quad \text{cavitation}$$

(17)

If this criterion is in error, it probably underestimates the critical value of R_0/c_0 above which cavitation occurs.

[2] Private communication.
[3] E. H. Kennard, David Taylor Model Basin Report, No. 480 (1941).

III. APPROXIMATE THEORY OF CIRCULARLY CLAMPED PLATES
CONSTRAINED TO A PARABOLIC PROFILE

1. Introduction

Since experiments on the plastic deflection of clamped plates (Modugno gauges, etc.) by underwater explosion waves show the final profile to be very nearly parabolic in most cases, it seems likely that a simple theory using a parabolic constraint should give satisfactory results. This supposition has been well confirmed experimentally as will be shown in Part V.

Since in this treatment it is possible to confine our attention to the center of the plate ($r = 0$), a more rigorous treatment of the water loading including retardation effects is tractable. In Part IV, where the plate deformation is treated without constraints on the profile, a comparably rigorous treatment of the water loading would be excessively difficult, and consequently only the incompressive approximation is considered there.

Since a constrained or minimum system becomes the enlarged is stiffer and more massive, one will expect the treatment of this Part to give smaller deflections and longer deflection times than the otherwise equivalent unconstrained treatment.

2. Equations of Motion

If we substitute the expression for a parabolic profile

$$z(r,t) = z_o(t)[1 - (r/R_o)^2],\qquad (1)$$

where $z_o(t)$ is the central deflection

Eq. (27) of Part I (with $\alpha = 1$, and cor

neglecting terms of the order of α^4) we obtain

$$\frac{d^2 z_o}{dt^2} + \omega_o^2 z_o = \frac{p}{\rho A_o} \, , \tag{2}$$

$$\omega_o^2 = 1/\Theta_1 \Theta_o \quad , \quad \Theta_1 = \rho A_o/\rho_o c_o \quad , \quad \Theta_o = \rho_o c_o R_o^2/4 a_o \sigma_o ,$$

where for convenience in the subsequent discussion, the plastic frequency has been factored into two times, a damping time Θ_1 and a plastic time Θ_o.

When the parabolic profile, Eq. (1), is substituted in Eq. (13) of Part II and one lets $R_f \to \infty$, corresponding to a very large baffle, one obtains for the pressure at the center of the plate,

$$p = 2 p_o(t) - \rho_o c_o \left[\frac{dz}{dt} + \frac{2}{\Theta_2} z_o (t - \Theta_2) - \frac{2}{\Theta_2^2} \int_{t-\Theta_2}^{t} z_o(t') dt' \right] \tag{3}$$

$$\Theta_2 = R_o/c_o \, .$$

When t is less than Θ_2, the time required for the diffracted wave to travel from the edge to the center of the plate, Eq. (3) reduces approximately to

$$p = 2 p_o(t) - \rho_o c_o \frac{dz_o}{dt} \, , \tag{4}$$

based upon geometrical acoustics. When t is greater than Θ_2 and the third and higher time derivatives of z_o can be neglected, a Taylor's expansion in Θ_2 of the right hand side of Eq. (3) yields the "incompressive" approximation,

$$p = 2 p_o(t) - \frac{2 \rho_o c_o \Theta_2}{3} \frac{d^2 z_o}{dt^2} \, . \tag{5}$$

Unfortunately, neither of the two limiting cases represented by Eqs. (4) and

practical inter-

l phase of the

motion and Eq. (5) is approached in the latter phase. A theory based upon Eq. (4) will give final deflections which in general are too small, since the damping term $\rho_0 c_0 \, dz_0/dt$ fades away for times greater than θ_1, and the second term of Eq. (5), by increasing the effective inertia of the plate, retards its deceleration in the later phase of the motion.

The complete deflection equation, obtained by substituting Eq. (3) into Eq. (2), has the form

$$\frac{d^2 z_0}{dt^2} + \frac{1}{\theta_1}\frac{dz_0}{dt} + \frac{1}{\theta_1}\left[\frac{z_0}{\theta_0} + \frac{2}{\theta_2}z_0(t-\theta_2)\right.$$

$$\left. - \frac{2}{\theta_2^2}\int_{0-\theta_2}^{t} z_0(t')\,dt'\right] = \frac{2p_0(t)}{\rho\,z_0}. \tag{6}$$

This is an integro-differential difference equation, which can be solved by the method of Laplace transforms. The initial condition subject to which Eq. (6) is to be solved is $z_0(t) = 0$ for $t \le 0$.

3. Deflection of Circular Diaphragm by an Exponential Wave.

It has been found that the initial pressure pulse immediately following the shock front of an underwater explosion wave has a pressure-time curve which is closely approximated by the exponential formula

$$p_0(t) = p_m \, e^{-t/\theta}, \tag{7}$$

where p_m is the peak pressure. It is therefore a matter of interest to investigate the solution of Eq. (6) for an exponential wave. In discussing the solution of Eq. (6), we shall neglect the change in phase of the explosion wave due to the plate deflection. We will first consider the case of an infinite baffle.

We shall employ the Laplace transform $L(\omega)$ of $z_o(t)$, defined as

$$L(\omega) = \int_o^{\infty} z_o(t) e^{-\omega t} dt .$$
(8)

After taking the Laplace transform of both sides of Eq. (6) and integrating by parts, one obtains

$$L(\omega) = \frac{2 p_m}{\rho \, a_o} \frac{\omega}{(\omega + 1/\theta) F(\omega)} ,$$

$$F(\omega) = \omega^3 + \frac{\omega^2}{\theta_1} + \frac{\omega}{\theta_1 \theta_o} - \frac{2}{\theta_1 \theta_2} + \frac{2}{\theta_1 \theta_2} (1 + \omega \theta_2) e^{-\omega \theta_2} ,$$

$$z_o(t) = \frac{p_m}{\pi \iota \rho a_o} \int_{c-i\infty}^{c+i\infty} \frac{\omega e^{\omega t}}{(\omega + 1/\theta) F(\omega)} d\omega ,$$
(9)

where ι is the imaginary unit $\sqrt{-1}$, and C is any real constant greater than the least value of ω for which the transform $L(\omega)$ exists. If one determines the zeros ω_n, with vanishing or negative real parts, of $F(\omega)$,

$$F(\omega_n) = 0,$$
(10)

one may evaluate the integral of Eq. (9) by the theory of residues to obtain

$$z_o(t) = \frac{2 p_m \theta}{\rho_o a_o} G(t),$$

$$G(t) = \sum_n \frac{\omega_n}{1 + \omega_n \theta} \frac{e^{\omega_n t}}{\theta_1 F'(\omega_n)} - \frac{e^{-t/\theta}}{\theta_1 \theta^2 F(-1/\theta)} ,$$
(11)

$$F'(\omega_n) = 3\omega_n^2 + \frac{2\omega_n}{\theta_1} + \frac{1}{\theta_1 \theta_o} - \frac{2\omega_n}{\theta_1} e^{-\omega_n \theta_2} .$$

The permanent deflection of the plate, with possible neglect of a small

elastic recovery, is given by

$$
\left.\begin{aligned}
z_m &= \frac{2 P_m \phi}{\rho_0 c_0} \, G_m \, , \\
G_m &= G(t_m) \, , \\
G'(t_m) &= 0 \, ,
\end{aligned}\right\} \tag{12}
$$

where the time t_m of deflection is determined by the condition that the derivative $G'(\theta_m)$ of G vanish.

If $1/F(\omega)$ of Eq. (9) is expanded in powers of $e^{-\omega \theta_1}$ and C is chosen greater than the greatest real part of the roots ω_n of

$$
F_0(\omega_n) = 0 \, , \tag{13}
$$

$$
F_0(\omega) = \omega^3 + \frac{\omega^2}{\theta_1} + \frac{\omega}{\theta_1 \theta_0} - \frac{2}{\theta_1 \theta_1^2} \, ,
$$

it may be shown that for $t < \theta_1$, the deflection $z_p(t)$ is given by Eq. (11), except that the sum extends over the zeros of $F_0(\omega)$ rather than over those of $F(\omega)$.

If, on the other hand, $e^{-\omega \theta_1}$ is expanded in powers of $\omega \theta_1$ and terms of the order ω^4 are neglected, $F(\omega)$ is approximated by the expression

$$
\left.\begin{aligned}
F(\omega) &= \omega \left[\left(1 + \frac{2\theta_1}{3\theta_1}\right) \omega^2 + \frac{1}{\theta_1 \theta_0} \right] \, , \\
\omega_1 &= 0, \pm i \omega_0^* \, , \\
\omega_0^* &= \left(\frac{4\sigma_0}{\rho R_0^2 (1 + 2\theta_1/3\theta_1)} \right)^{1/2} \, .
\end{aligned}\right\} \tag{14}
$$

Eq. (14) represents the incompressive approximation to $F(\omega)$, in which the apparent plastic frequency ω_0^* differs from that of the free plate due to the loading effect of the water. When $\omega_0^* \theta_1$ is small relative to unity,

it may be verified that $\pm i\omega_0^*$ closely approximate two of the zeros of the exact $F(\omega)$ of Eq. (9). With the neglect of other zeros of $F(\omega)$, we obtain the complete incompressive solution from Eq. (11):

$$z_o(t) = \frac{2p_m\theta}{\rho_o c_o}\frac{\omega_0^*\theta_o}{1+\omega_0^{*2}\theta^2}\left[\sin\omega_0^* t + \omega_0^*\theta\left(e^{-t/\theta}-\cos\omega_0^* t\right)\right]. \quad (15)$$

Using Eq. (12), we finally obtain for the maximum deflection and duration of deflection

$$\left.\begin{array}{c} z_m = \frac{2p_m\theta}{\rho_o c_o}\,\omega_0^*\theta_o\,\sin\beta\ , \\[2mm] t_m = \beta/\omega_0^*\ , \\[2mm] \cos\left(\beta - \tan^{-1}\omega_0^*\theta\right) = \frac{e^{-\beta/\omega_0^*\theta}}{(1+\omega_0^{*2}\theta^2)^{1/2}}\ . \end{array}\right\} \quad (16)$$

When $\omega_0^*\theta$ is small relative to unity, β is approximated by $\pi/2$, the deflection is proportional to the momentum of the incident wave, and the duration t_m equal to one-fourth the plastic period $2\pi/\omega_0^*$ of the loaded plate. When $\omega_0^*\theta$ is large relative to unity, $\sin\beta$ is approximated by $1/\omega_0^*\theta$, the deflection becomes proportional to the peak pressure, and the duration equal to the half-period. Thus a diaphragm gauge which measures momentum for small charges might well measure peak pressure for very large charges.

It is of interest to put Eqs. (16) in a more convenient form for numerical use. We denote by I the impulse $p_m\theta$ of the incident wave in psi-milliseconds, and we express the yield stress σ_o^- in psi and the densities ρ_o and ρ of water and plate in grams/cm^3. With these units, Eqs. (16)

become

$$z_m = \frac{0.1084}{(\rho\sigma_0)^{1/2}}\left(\frac{R_0}{d_0}\right)\frac{I\sin\beta}{(1+2\rho_0 R_0/3\rho d_0)^{1/2}} \quad \text{inches},$$

$$t_m = 9.65\left(\rho R_0\left(\frac{\rho}{\sigma_0}\right)^{1/2}\left(1+2\rho_0 R_0/3\rho d_0\right)^{1/2}\right) \text{ millisec.,} \Bigg\} \quad (17)$$

$$\omega_0^* \theta = \frac{0.2068\,\theta}{R_0}\left(\frac{\sigma_0}{\rho}\right)^{1/2}\left(1+2\rho_0 R_0/3\rho d_0\right)^{-1/2},$$

where R_0, the radius of the plate is expressed in inches and θ, the duration parameter of the wave, in milliseconds. In Table I β and $\sin\beta$ are presented for several values of $\omega_0^* \theta$.

TABLE I

$\omega_0^* \theta$	β	$\sin\beta$
0.0	1.57	1.00
.5	2.02	.90
1.0	2.28	.76
2.0	2.55	.56
3.0	2.68	.45
5.0	2.82	.31

     If the plate is supported in one end of a long cylinder of radius R, with axis parallel to the direction of propagation of the incident wave, an approximate treatment of the diffracted wave can be given, since the walls of the cylinder do not diffract the primary wave, but only diffract the scattered wave from the end of the cylinder. Thus in first approximation, we can neglect the influence of the walls. This case is of interest since it corresponds roughly to the experimental arrangement of the diaphragm gauges employed in the Explosives Research Laboratories at Bruceton and Woods Hole.

The plane in which the plate is supported is now finite, and thus we use Eq. (13) of Part II with R_1 finite, which we repeat here:

$$p = 2 p_o(t) - p_o(t-\theta_s) - \rho_o \int_0^{R_o} dr' \frac{\partial^2 z}{\partial t^2}(r', t-r'/c_o), \bigg\} \quad (18)$$
$$\theta_s = R_1/c_o .$$

The deflection $z_o(t)$ for a parabolic profile becomes

$$z_o(t) = \frac{P_m \theta}{\rho_o c_o}\left[2 G(t) - G(t-\theta_s)\right]. \quad (19)$$

In the incompressive approximation corresponding to Eq. (16), one gets

$$z_m = \frac{2 p_m \theta}{\rho_o c_o} \omega_o^* \theta_o \, g(\rho) ,$$
$$g(\rho) = \sin \rho - \tfrac{1}{2} \sin (\rho - \omega_o^* \theta_s) ,$$
$$t_m = \rho/\omega_o^* , \quad (20)$$
$$\tan(\rho - \tan^{-1}\alpha) = \frac{(2 - e^{\theta_s/\theta}) e^{-\rho/\omega_o^* \theta}}{[(1 + \omega_o^{*2}\theta^2)(1 + 8 \sin^2 \omega_o^* \theta_s/2)]^{1/2}} ,$$
$$\alpha = \omega_o^* \theta - \frac{(1 + \omega_o^{*2}\theta^2)^2 \sin \omega_o^* \theta_s}{2 - \cos \omega_o^* \theta_s + \omega_o^* \theta \sin \omega_o^* \theta_s} .$$

When θ_s is small relative to θ , a deflection z_m equal to one-half that of a plate supported in an infinite wall is approached. When θ_s is greater than the time of deflection calculated by Eq. (16), the result for the infinite wall is obtained, since $G(t-\theta_s)$ and its derivatives vanish for $t-\theta_s$ less than zero.

On general grounds, we may surmise that z_m will approach proportionality with the impulse I of the incident wave when t_m is large compared with θ , while it will approach proportionality with the peak pressure p_m when t_m is small compared with θ . In the incompressive approximation,

Eq. (16), we find that the first case is realized when $\omega_o^*\theta$ is small rela-
tive to unity, and the second case when $\omega_e^*\theta$ is large relative to unity.
In other words, impulse or peak pressure is the decisive damage factor, ac-
cording to whether the plastic period of the plate is large or small relative
to the duration parameter θ of the incident wave.

IV. THE PLASTIC DEFORMATION OF A THIN, CIRCULAR PLATE WITH AN UNCONSTRAINED PROFILE

1. Introduction

In Part III an analysis of the plastic deformation of a thin cir-
cular plate by an underwater explosion wave was presented for the case of the
profile constrained to a parabolic shape. Here, a more exact solution is ob-
tained without artificial constraints by expanding the deflection in a series
of Bessel functions. By this means, proper account is taken of the frequency
shifts and interaction of the deflection modes arising from the water load-
ing. Because of the excessive difficulty in treating the retardation effects
in the water loading for this case, only the incompressive approximation is
considered.

Detailed calculations are made for the case in which the first two
terms of the Bessel function series are retained, corresponding to the funda-
mental mode and one overtone. The final deflections so obtained do not differ
greatly from those calculated with the parabolic profile. The times of de-
flection are about 20% lower than in the parabolic treatment (with incompres-
sive water loading). The maximum central deflection is about 25% higher for
impulsive loading and not significantly different for loading by a wave of
duration long compared with the period of the fundamental mode.

338

2. Equation of Motion

We consider a circular plate of radius R_o and thickness δ_o, composed of material of yield stress σ_o and density ρ. The edge of the plate is assumed to be clamped to a rigid supporting structure extending a negligible distance beyond the edge of the plate. It is also assumed to be backed by air on the upper side, and to be in contact with water of density ρ_o on the lower side. The explosive wave advancing in the positive z-direction is assumed to be of acoustical intensity and to be of exponential form $p_o = p_m e^{-t/\theta}$.

We will use the linearized equation of motion derived in Part I for the vertical deflection z. For convenience, we repeat this equation (Eq. (27), Part I) here with the expansion parameter α set equal to unity and with the dropping of the superscripts referring to the first approximation:

$$\left. \begin{array}{c} \dfrac{\partial^2 z}{\partial t^2} - c^2 \dfrac{1}{r} \dfrac{\partial}{\partial r}\left(r \dfrac{\partial z}{\partial r}\right) = \dfrac{p}{\rho \delta_o}, \\[2mm] c^2 = \sigma_o/\rho \end{array} \right\} \tag{1}$$

Here, we treat the water loading in the incompressive approximation, thereby neglecting retardation effects. In this case it is appropriate to use Eq. (14) of Part II:

$$\left. \begin{array}{c} p = p_o - \dfrac{\rho_o}{2\pi} \displaystyle\int_0^{2\pi} d\phi \int_0^{R_o} dr' \dfrac{r'}{r^*} \dfrac{\partial^2 z}{\partial t^2}(r';t), \\[3mm] r^* = \left(r^2 + r'^2 - 2rr'\cos\phi\right)^{1/2}. \end{array} \right\} \tag{2}$$

This result corresponds to a small or nonexistent baffle; for an infinite baffle, the term p_o must be multiplied by 2.

29

The elimination of p between Eqs. (1) and (2) with the introduction of the dimensionless variable $x = r/R_o$ yields the result

$$[1 + \lambda O] \frac{\partial^2 z}{\partial t^2} - \frac{\omega_o^2}{x} \frac{\partial}{\partial x} \left(x \frac{\partial z}{\partial x} \right) = \frac{p_o(t)}{\rho s_o}, \tag{3}$$

where

$$\omega_o^2 = c^2/R_o^2 = \sigma_o/\rho R_o^2 \quad , \quad \lambda = R_o \rho_s/2_o \rho$$

and O is an integral operator defined by

$$O F(x,t) = \frac{1}{2\pi} \int_0^{2\pi} d\phi \int_0^1 dx' x' \left(x^2 + x'^2 - 2xx' \cos\phi \right)^{-1/2} F(x';t).$$

The quantity ω_o is equal to the reciprocal of the time required for a transverse plastic wave to travel the radius of the plate. The parameter determines the magnitude of the inertial effect of the surrounding water.

Eq. (3) is an integro-differential equation whose solution is subject to the following initial and boundary conditions:

$$z = 0, \ \frac{\partial z}{\partial t} = 0 \ ; \ t = 0, \ 0 \leq x \leq 1 \ ; \\ z = 0, \ t \geq 0, \ x = 1. \tag{4}$$

In solving Eq. (3) under the conditions (4), it is convenient to expand z in a series of Bessel functions

$$z(x,t) = \sum_{i=1}^{\infty} z_i(t) J_o(k_i x), \tag{5}$$

where $J_o(u)$ is the zero order Bessel function of u and k_i is the i-th zero of $J_o(u)$. The details of the solution are given in Appendix B. The solution in the case of an exponential wave

$$p_o(t) = p_m e^{-t/\theta} \quad , \quad t \geq 0, \tag{6}$$

is

$$z(x,t) = p_m s \, \zeta(x,t), \tag{7}$$

340

where

$$f(x,t) = \frac{1}{\rho c_o} \sum_{i,\ell=1}^{\infty} \frac{\omega_\ell^*}{\omega_\ell^{*2}} C_{i\ell}(\lambda)\, g_\ell(t)\, J_o(k_i x), \qquad (8)$$

$$C_{i\ell}(\lambda) = -\sum_{j=1}^{\infty} \frac{2 k_i\, \Delta_{ji}\left(\frac{\omega_\ell^2}{\omega_\ell^{*2}}\right)}{J_1(k_i)\, k_j^2\, \Delta'\left(\frac{\omega_\ell^2}{\omega_\ell^{*2}}\right)}, \qquad (9)$$

$$g_\ell(t) = \frac{\sin \omega_\ell^* t + \omega_\ell^* \theta \left(e^{-t/\theta} - \cos \omega_\ell^* t\right)}{1 + \omega_\ell^{*2} \theta^2}, \qquad (10)$$

in which

$$\left.\begin{array}{l} \Delta(\beta) = |B_{ji} - \beta \delta_{ji}|, \\[2mm] \Delta'(\beta) = \dfrac{\partial}{\partial \beta} \Delta(\beta), \end{array}\right\} \qquad (11)$$

$\Delta_{ij}(\beta)$ is the cofactor of the ij element of $\qquad$ (12)
the determinant $\Delta(\beta)$,

$\dfrac{\omega_\ell^2}{\omega_\ell^{*2}}$ is the ℓ-th root of $\quad \Delta(\beta)$, $\qquad (13)$

$$B_{ji} = \frac{\delta_{ji} + \lambda A_{ji}}{k_i k_j}, \qquad (14)$$

$$\delta_{ji} = \begin{cases} 0 & j \neq i, \\ 1 & j = i, \end{cases} \qquad (15)$$

$$A_{ji} = \frac{1}{\pi J_1(k_i) J_1(k_j)} \int_0^1 x\,dx \int_0^1 x'\,dx' \int_0^{2\pi} d\phi\, \frac{J_o(k_i x)\, J_o(k_j x')}{\sqrt{x'^2 + x^2 - 2 x x' \cos\phi}}. \quad (16)$$

In Eqs. (7), (8), and (9), ω_ℓ^* is the 1-th frequency of the water loaded

31

diaphragm and ω_i is the i-th frequency of the free diaphragm (all modes of vibration are radially symmetric). The matrix B_{ij} depends on λ only (except for zeros of J_o), therefore $\frac{\omega_o^2}{\omega_i^2}$ the roots of Δ depend only on λ, and consequently the same for the coefficients C_{il}.

It is of particular interest to calculate the maximum central deflection

$$z_m = z(o, t_m), \tag{17}$$

where t_m is the smallest positive value of t satisfying

$$\frac{\partial}{\partial t} z(o, t) = 0. \tag{18}$$

It happens that z_m is given by the relatively simple formula

$$z_m = p_m \otimes f_m,$$
$$f_m = \frac{1}{\rho d_o} \sum_{i,l=1}^{\infty} \frac{\omega_i^+}{\omega_o^2} C_{il} \sin \omega_l^* t_m, \tag{19}$$

in which t_m can be obtained by solving Eq. (18) by successive approximation.

The permanent plastic deflection of the diaphragm, as has been previously shown, will differ from $z(x, t_m)$ by a small amount, usually less than one percent. It can be shown that the center point of the diaphragm reaches its maximum deflection first. As the rate of strain changes sign at the center an unloading wave travels out toward the center with acoustical velocity. The diaphragm passes in a very short time from the plastic to the elastic state during the unloading and continues to vibrate elastically until the residual kinetic energy is radiated. Since the elastic recovery is small, the diaphragm takes a permanent set in very nearly

the position it occupied at the time t_m when the center point reached its maximum.

We remark here that an accurate description of the early stage of the motion requires the retention of a large number of terms in the series (5). The approximate solution to be used in Sec. 3, in which only two terms are retained, while adequate for the later phase of the motion, is not very accurate for times less than, say, .3 of the total time of deflection.

3. Solution of Equation of Motion Using Two Terms in Bessel Function Expansion of the Deflection. Presentation of Numerical Results

When the Bessel function series (8) is approximated by the first two terms, the deflection of the diaphragm takes the form,

$$z = p_m \theta \, f(x,t) , \qquad (20)$$

where $x = r/R_o$,

and

$$f(x,t) = \frac{\omega_1^*}{\rho a_o} \left[\frac{C_{11}}{\omega_1^2} J_o(k_1 x) + \frac{C_{21}}{\omega_2^2} J_o(k_2 x) \right] g_1(t)$$
$$+ \frac{\omega_2^*}{\rho a_o} \left[\frac{C_{12}}{\omega_1^2} J_o(k_1 x) + \frac{C_{22}}{\omega_2^2} J_o(k_2 x) \right] g_2(t) ,$$

when the free field pressure of the   osion wave is given by

$$p_o(\beta) = p_m e^{-t/\theta} \qquad (21)$$

Supplementary data concerning Eq. (20) are presented in Appendix C. The frequency ω_i is the i-th frequency of the free diaphragm and ω_ℓ^* is the ℓ-th frequency of the water loaded diaphragm; a_o is the thickness and ρ is the density of the diaphragm.

The nondiagonal terms $B_{ij}(i \neq j)$ in the secular determinant $\triangle$ have a small effect on the fundamental frequency and the first overtone. This point is discussed in Appendix C. Also C_{12} and C_{21} are much smaller than C_{11} or C_{22}. These results mean that the hydrodynamic interaction between the two principal modes of vibration is small, and that the nondiagonal terms B_{ij} could have been neglected without large error (at least in the two-mode treatment).

The maximum central deflection z_m is found by methods described at the end of Sec. 2. It is found mathematically that the part of the diaphragm midway between the center and the periphery reaches its maximum at a time about 20% greater than t_m, the time of maximum central deflection. This is not important because of reasons mentioned in Sec. 2.

In the presentation of numerical results, appropriate dimensionless variables are chosen. Accordingly, in Tables I-A, II-A, III-A, and IV-A, $\omega_0 t_m$ and $\frac{V_0}{P_m} \frac{1}{\omega_0 \theta} \frac{d_0 z_m}{R_0^2}$ are presented as functions of $1/\omega_0 \theta$ for four values of $\lambda = R_0 \rho_0 / d_0 \rho$. These tables allow us to find the time of deflection t_m and the maximum central deflection z_m if the diaphragm parameters, R_0, d_0, ρ, and σ_0, the shock-wave characteristics, p_m and θ, and the density ρ_0 of water are given.

The diaphragm profiles, z/z_m vs. r/R_0, are given as functions of the reduced time τ/t_m for several values of $1/\omega_0 \theta$ and λ in Tables I-B, I-C, I-D, II-B, II-C, II-D, III-B, III-C, III-D, IV-B, IV-C, and IV-D. The appropriate values of z_m and t_m are found by consulting the tables mentioned in the previous paragraph. The tables considered thus far are grouped according to values of λ, the tables having a Roman numeral I

corresponding to the smallest value of λ , etc.

In Figures 1, 2, 3, and 4 some of the data from the above tables
is presented for the special case of the USRL diaphragm gauge. For this
case we have the

thickness	= 0.078 in.
radius	= 1.675 in.
yield stress	= 50,000 p.s.i.
and density	= 7.8 gm./cm^3.

These specifications of the diaphragm and a value of 1.007 gm./cm^3. for the
density of sea water at 20° C. yield a value of 2.75 for λ and 4.94 msec.$^{-1}$
for ω_0 . Specimen values of the maximum central deflection z_m and the time
of deflection t_m, for typical values of p_m and Θ , are given in the fol-
lowing table:

(msec.)	(p.s.i.)	(in.)	(msec.)
0.101	4000	0.49	0.29
0.505	2000	0.49	0.36
1.01	2000	0.57	0.39

In the above tables and graphs the profile for $t/\Theta_m = 1$ is rather
peaked in the case of Θ small and resembles a circular arc in the case of
Θ large (in particular, compare figures 1 and 3). In the case of Θ small,
the peaked condition is what one should expect since in the case of impulsive
loading the diaphragm would tend to be deflected to a conical shape, if the
water loading were evenly distributed. In the case of Θ large, the resem-
blance of the profile to a circular arc is easy to see if one considers the
fact that the diaphragm under the influence of a static pressure is deflected

FIGURE 1 - Plate profiles (θ = 0.101 msec.).

346
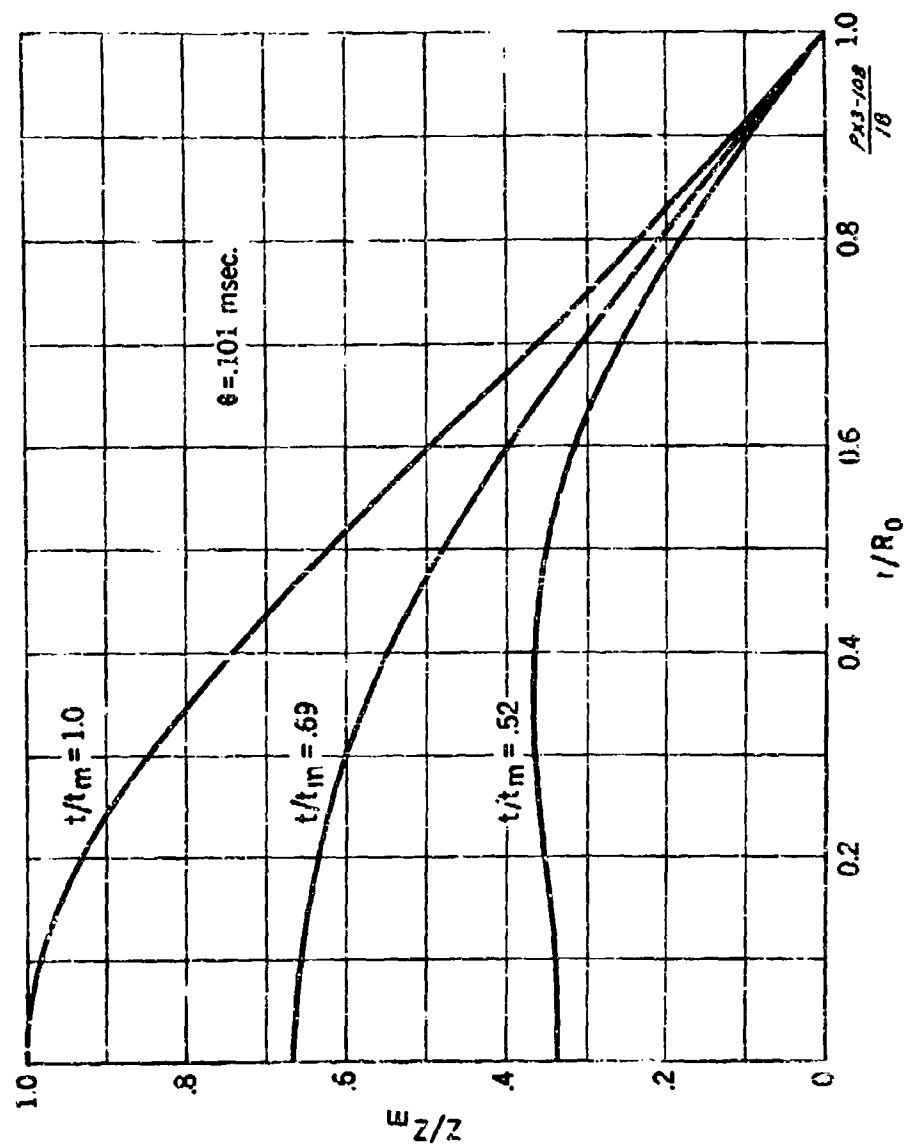
FIGURE 2 — Plate profiles (θ = 0.505 msec.).
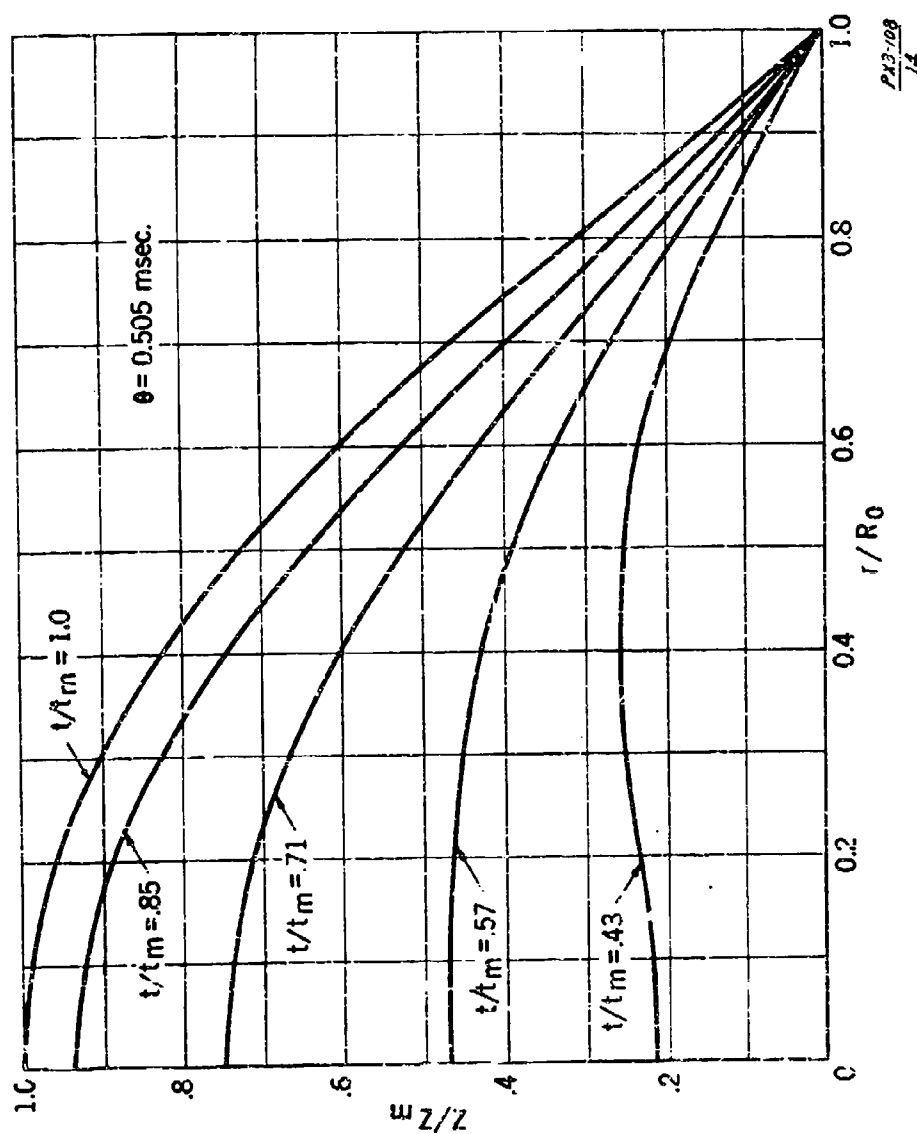
FIGURE 5 – Plate profiles ($\theta = 1.01$ msec.).

348
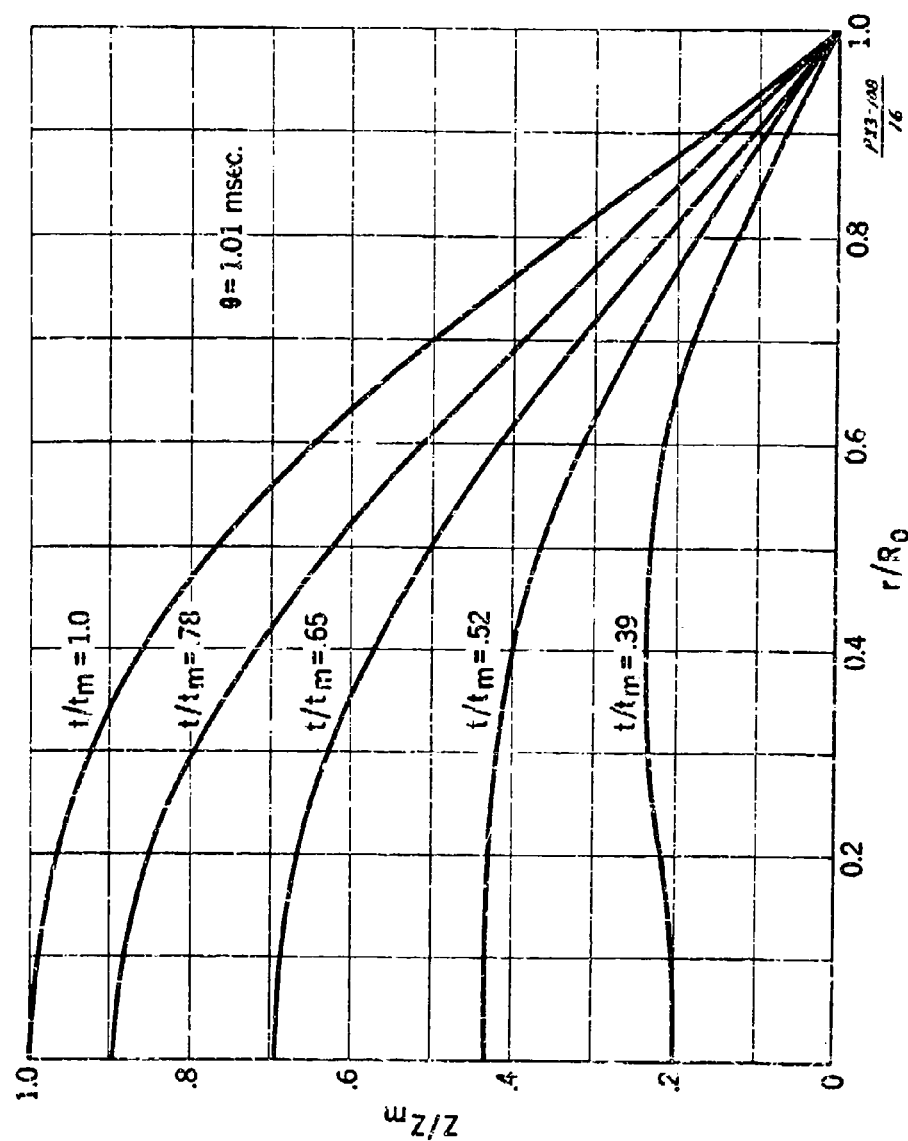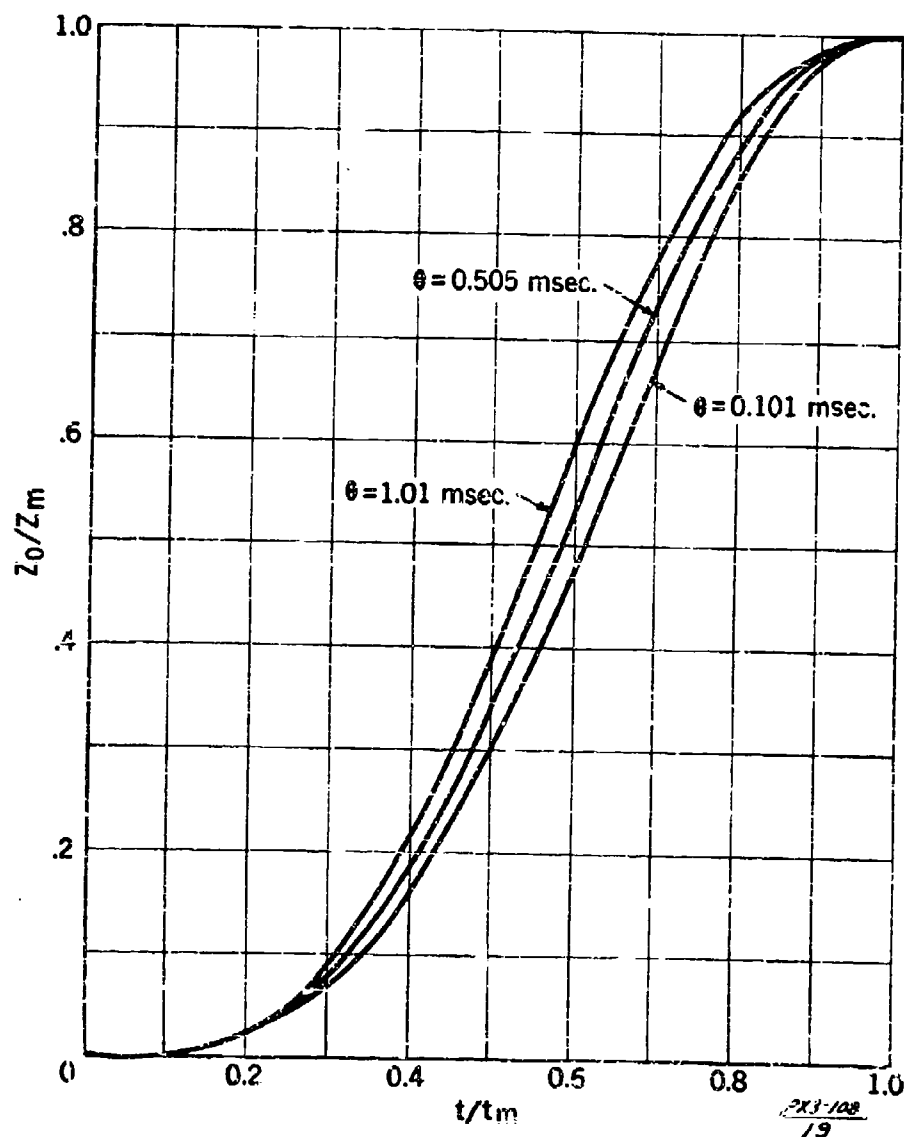
FIGURE 4 - Central deflection versus time for several
values of θ.

to a spherical shape. The profiles for small values of t/t_m are of questionable accuracy, since the treatment using two Bessel functions breaks down for small values of the time. However, the convexity in these profiles may not be entirely fictitious because of the nonuniform distribution of water loading.

In Table V the results of the treatment assuming a parabolic profile (Part III) are compared with the results of the more exact treatment with parameters appropriate to the UERL diaphragm. It is significant that the values of z_m are in close agreement except for small values of Θ, the more exact treatment giving larger deflections than the parabolic. This discrepancy is evidently due to the fact that the profile is more nearly conical than parabolic for waves of very short duration, as mentioned above. The values of t_m for the more exact treatment are about 20% lower than those for the parabolic. A corresponding difference is found in the fundamental frequencies.

TABLE I-A. — Maximum central deflection and time of deflection
as a function of $\omega_o\theta$ for $\lambda = 0.6875$

Units: θ, t_m — msec; ω_o — msec^{-1}; δ_o, z_m, R_o — in.; σ_o,
P_m — p.s.i.; ρ — gm.cm^{-3}.

$\dfrac{1}{\omega_o\theta}$	$\omega_o t_m$	$\dfrac{\sigma_o}{P_m}\dfrac{1}{\omega_o\theta}\dfrac{\delta_o z_m}{R_o{}^2}$
0.2	1.40	0.0932
0.4	1.35	0.165
0.6	1.32	0.225
0.8	1.28	0.275
1.0	1.26	0.317
1.2	1.23	0.354
1.4	1.21	0.384
1.6	1.20	0.411
1.8	1.18	0.435
2.0	1.16	0.455
2.2	1.15	0.473
2.4	1.14	0.489
2.6	1.13	0.504
2.8	1.12	0.517
3.0	1.11	0.528
3.2	1.10	0.538

$$\omega_o = 0.1034 \frac{1}{R_o}\left(\frac{\sigma_o}{\rho}\right)^{1/2}$$

37

TABLE I-B. – Diaphragm profile as a function of time

$$\lambda = 0.6875 \quad 1/\omega_0\theta = 2.0$$

		z/z_m	
r/R \ t/t_m	0.64	0.86	1.00
0	0.578	0.920	1.00
0.1	0.573	0.905	0.983
0.2	0.567	0.857	0.924
0.3	0.549	0.784	0.837
0.4	0.517	0.689	0.726
0.5	0.468	0.579	0.601
0.6	0.400	0.461	0.470
0.7	0.314	0.339	0.341
0.8	0.214	0.220	0.218
0.9	0.106	0.106	0.104
1.0	0	0	0

TABLE I-C. – Diaphragm profile as a function of time

$$\lambda = 0.6875 \quad 1/\omega_0\theta = 0.40$$

		z/z_m	
r/R_0 \ t/t_m	0.54	0.74	1.00
0	0.426	0.766	1.00
0.1	0.427	0.756	0.986
0.2	0.428	0.730	0.946
0.3	0.423	0.685	0.880
0.4	0.410	0.622	0.790
0.5	0.380	0.542	0.680
0.6	0.332	0.447	0.554
0.7	0.265	0.340	0.417
0.8	0.183	0.226	0.275
0.9	0.091	0.111	0.134
1.0	0	0	0

38

TABLE I-D. — Diaphragm profile as a function of time

$$\lambda = 0.6875 \qquad 1/\omega_o \theta = 0.20$$

| r/B_o \ t/t_m | z/z_m | | |
	0.54	0.71	1.00
0	0.393	0.718	1.00
0.1	0.394	0.709	0.986
0.2	0.395	0.687	0.947
0.3	0.393	0.647	0.881
0.4	0.381	0.590	0.792
0.5	0.354	0.527	0.684
0.6	0.311	0.428	0.558
0.7	0.249	0.327	0.421
0.8	0.172	0.218	0.278
0.9	0.086	0.107	0.135
1.0	0	0	0

TABLE I-B. - Diaphragm profile as a function of time

$$\lambda = 0.6875 \qquad 1/\omega_o \theta = 2.0$$

r/R_o	t/t_m		
	z/z_m		
	0.64	0.86	1.00
0	0.578	0.920	1.00
0.1	0.573	0.905	0.983
0.2	0.567	0.857	0.924
0.3	0.549	0.784	0.837
0.4	0.517	0.689	0.726
0.5	0.468	0.579	0.601
0.6	0.400	0.461	0.470
0.7	0.314	0.339	0.341
0.8	0.214	0.220	0.218
0.9	0.106	0.106	0.104
1.0	0	0	0

TABLE I-C. - Diaphragm profile as a function of time

$$\lambda = 0.6875 \qquad 1/\omega_o \theta = 0.40$$

r/R_o	t/t_m		
	z/z_m		
	0.54	0.74	1.00
0	0.426	0.766	1.00
0.1	0.427	0.756	0.986
0.2	0.428	0.730	0.946
0.3	0.423	0.685	0.880
0.4	0.410	0.622	0.790
0.5	0.380	0.542	0.680
0.6	0.332	0.447	0.554
0.7	0.265	0.340	0.417
0.8	0.193	0.226	0.275
0.9	0.091	0.111	0.134
1.0	0	0	0

TABLE I-D. – Diaphragm profile as a function of time

$$\lambda = 0.6875 \qquad 1/\omega_0 \theta = 0.20$$

r/R₀ \ t/tₘ	z/zₘ		
	0.54	0.71	1.00
0	0.393	0.718	1.00
0.1	0.394	0.709	0.986
0.2	0.395	0.687	0.947
0.3	0.393	0.647	0.881
0.4	0.381	0.590	0.792
0.5	0.354	0.517	0.684
0.6	0.311	0.428	0.558
0.7	0.249	0.327	0.421
0.8	0.172	0.218	0.278
0.9	0.086	0.107	0.135
1.0	0	0	0

TABLE II-A. – <u>Maximum central deflection and time of deflection</u>
<u>as a function of $\omega_o \Theta$ for $\lambda = 1.375$</u>

Units: Θ, t_m – msec; ω_o – msec^{-1}; a_o, x_m, R_o – in.; σ_o, p_m – p.s.i.; ρ – gm. cm^3.

$\dfrac{1}{\omega_o \Theta}$	$\omega_o t_m$	$\dfrac{\sigma_o}{p_m} \dfrac{1}{\omega_o \Theta} \dfrac{a_o x_m}{R_o^2}$
0.2	1.57	0.0884
0.4	1.51	0.153
0.6	1.48	0.208
0.8	1.43	0.252
1.0	1.38	0.289
1.2	1.35	0.320
1.4	1.33	0.347
1.6	1.31	0.370
1.8	1.29	0.390
2.0	1.27	0.407
2.2	1.26	0.423
2.4	1.24	0.436
2.6	1.23	0.447
2.8	1.22	0.458
3.0	1.21	0.468
3.2	1.20	0.476

$$\omega_o = 0.1034 \frac{1}{R_o} \left(\frac{\sigma_o}{\rho} \right)^{1/2}.$$

TABLE II-B. - <u>Diaphragm profile as a function of time</u>

$\lambda = 2.375$ $\qquad$ $1/\omega_0 \theta = 2.0$

		z/z_m	
r/R_0	t/t_m 0.59	0.78	1.00
0	0.472	0.825	1.00
0.1	0.469	0.813	0.983
0.2	0.472	0.776	0.927
0.3	0.467	0.718	0.842
0.4	0.450	0.640	0.734
0.5	0.417	0.546	0.611
0.6	0.364	0.441	0.481
0.7	0.290	0.330	0.351
0.8	0.199	0.216	0.225
0.9	0.100	0.105	0.108
1.0	0	0	0

TABLE II-C. - <u>Diaphragm profile as a function of time</u>

$\lambda = 1.375$ $\qquad$ $1/\omega_0 \theta = 0.40$

			z/z_m	
r/R_0	t/t_m 0.50	0.66	0.83	1.00
0	0.330	0.643	0.905	1.00
0.1	0.330	0.636	0.892	0.987
0.2	0.339	0.620	0.855	0.951
0.3	0.343	0.588	0.795	0.891
0.4	0.340	0.542	0.713	0.807
0.5	0.322	0.480	0.613	0.701
0.6	0.287	0.401	0.499	0.577
0.7	0.232	0.309	0.375	0.438
0.8	0.162	0.208	0.247	0.291
0.9	0.082	0.102	0.121	0.142
1.0	0	0	0	0

TABLE II-D. - <u>Diaphragm profile as a function of time</u>

$$\lambda = 1.375 \qquad 1/\omega_o\theta \approx 0.20$$

r/R$_0$	t/t$_m$ 0.48	0.64	0.79	1.00
			z/z$_m$	
0	0.298	0.589	0.848	1.00
0.1	0.298	0.583	0.837	0.987
0.2	0.307	0.570	0.805	0.952
0.3	0.312	0.544	0.751	0.891
0.4	0.310	0.503	0.677	0.808
0.5	0.295	0.448	0.585	0.703
0.6	0.263	0.377	0.479	0.579
0.7	0.213	0.291	0.362	0.439
0.8	0.149	0.196	0.240	0.292
0.9	0.075	0.097	0.117	0.141
1.0	0	0	0	0

TABLE III-A. – <u>Maximum central deflection and time of deflection as a function of $\omega_0\theta$ for $\lambda = 2.75$</u>

Units: θ, t_m – msec; ω_0 – msec^{-1}; a_0, x_m, R_0 – in.; σ_0, P_m – p.s.i.; ρ – gm. cm^{-3}

$\dfrac{\lambda}{\omega_0\theta}$	$\omega_0 t_m$	$\dfrac{\sigma_0}{P_m} \cdot \dfrac{1}{\omega_0\theta}$	$\dfrac{a_0 x_m}{R_0^2}$
0.2	1.92	0.0795
0.4	1.77	0.138
0.6	1.68	0.181
0.8	1.62	0.221
1.0	1.58	0.252
1.2	1.54	0.277
1.4	1.51	0.298
1.6	1.48	0.316
1.8	1.46	0.332
2.0	1.44	0.346
2.2	1.42	0.357
2.4	1.41	0.367
2.6	1.39	0.376
2.8	1.38	0.384
3.0	1.37	0.391
3.2	1.36	0.397

$$\omega_0 = 0.1034 \, \frac{1}{R_0} \left(\frac{\sigma_0}{\rho}\right)^{1/2}$$

TABLE III-B. - <u>Diaphragm profile as a function of time</u>

$$\lambda = 2.75 \qquad 1/\omega_o\theta = 2.0$$

r/R_o	r/s_m 0.52	0.69	1.00
	t/t_m		
0	0.337	0.665	1.00
0.1	0.337	0.657	0.944
0.2	0.351	0.637	0.929
0.3	0.361	0.601	0.847
0.4	0.363	0.549	0.728
0.5	0.349	0.482	0.619
0.6	0.314	0.400	0.490
0.7	0.256	0.307	0.358
0.8	0.180	0.205	0.231
0.9	0.091	0.101	0.111
1.0	0	0	0

TABLE III-C. - <u>Diaphragm profile as a function of time</u>

$$\lambda = 2.75 \qquad 1/\omega_o\theta = 0.4$$

r/R_o	r/s_m 0.43	0.57	0.71	0.85	1.00
	t/t_m				
0	0.219	0.471	0.746	0.937	1.00
0.1	0.218	0.468	0.736	0.924	0.968
0.2	0.233	0.455	0.710	0.888	0.959
0.3	0.247	0.452	0.665	0.827	0.905
0.4	0.255	0.428	0.603	0.744	0.820
0.5	0.251	0.390	0.525	0.642	0.729
0.6	0.230	0.335	0.432	0.524	0.608
0.7	0.191	0.264	0.328	0.396	0.464
0.8	0.135	0.180	0.218	0.261	0.311
0.9	0.068	0.090	0.107	0.127	0.153
1.0	0	0	0	0	0

44

TABLE III-D. - Diaphragm profile as a function of time

$\lambda = 2.75$ $1/\omega_o\theta = 0.2$

r/R_o \ t/t_m	s/s_m 0.39	0.50	0.65	0.78	1.00
0	0.198	0.431	0.694	0.894	1.00
0.1	0.199	0.427	0.686	0.882	0.989
0.2	0.213	0.427	0.664	0.850	0.969
0.3	0.225	0.417	0.625	0.795	0.925
0.4	0.233	0.397	0.570	0.719	0.859
0.5	0.230	0.364	0.499	0.624	0.765
0.6	0.211	0.314	0.414	0.512	0.645
0.7	0.174	0.248	0.316	0.388	0.500
0.8	0.123	0.170	0.211	0.257	0.337
0.9	0.063	0.085	0.103	0.126	0.166
1.0	0	0	0	0	0

TABLE IV-A. — <u>Maximum central deflection and time of deflection</u>
<u>as a function of $\omega_o \ell$ for $\lambda = 5.5$</u>

Units: Θ, t_m — msec; ω_o — msec^{-1}; a_o, z_m, R_o — in.;
σ_o, P_m — p.s.i.; ρ — gm. cm^{-3}.

$\dfrac{1}{\omega_o \Theta}$	$\omega_o t_m$	$\dfrac{\sigma_o}{P_m}\dfrac{1}{\omega_o \Theta}\dfrac{a_o z_m}{R_o^2}$
0.4	2.98	0.0763
0.6	2.21	0.121
0.6	2.03	0.156
0.8	1.94	0.187
1.0	1.88	0.210
1.2	1.83	0.229
1.4	1.79	0.244
1.6	1.75	0.257
1.8	1.72	0.268
2.0	1.70	0.278
2.2	1.68	0.286
2.4	1.66	0.293
2.6	1.64	0.299
2.8	1.62	0.304
3.0	1.61	0.309
3.2	1.60	0.313

$$\omega_o = 0.1034 \frac{1}{R_o}\left(\frac{\sigma_o}{\rho}\right)^{1/2}$$

46

TABLE IV-B. -- <u>Diaphragm profile as a function of time</u>

$$\lambda = 5.50 \qquad 1/\omega_o\theta = 2.0$$

r/R_o	t/t_m = 0.44	0.59	0.74	1.00
0	0.196	0.447	0.738	1.00
0.1	0.199	0.448	0.728	0.984
0.2	0.223	0.450	0.697	0.930
0.3	0.248	0.444	0.647	0.847
0.4	0.268	0.427	0.580	0.743
0.5	0.274	0.395	0.556	0.620
0.6	0.258	0.344	0.405	0.490
0.7	0.218	0.274	0.304	0.359
0.8	0.156	0.188	0.200	0.232
0.9	0.060	0.094	0.097	0.111
1.0	0	0	0	0

TABLE IV-C. -- <u>Diaphragm profile as a function of time</u>

$$\lambda = 5.50 \qquad 1/\omega_o\theta = 0.40$$

r/R_o	t/t_m = 0.34	0.45	0.57	1.00
0	0.113	0.242	0.512	1.00
0.1	0.116	0.283	0.508	0.949
0.2	0.135	0.294	0.500	0.968
0.3	0.155	0.301	0.481	0.923
0.4	0.173	0.301	0.450	0.856
0.5	0.180	0.289	0.404	0.761
0.6	0.172	0.259	0.343	0.641
0.7	0.147	0.211	0.268	0.496
0.8	0.106	0.148	0.182	0.334
0.9	0.054	0.075	0.090	0.165
1.0	0	0	0	0

47

TABLE IV-D. - Diaphragm profile as a function of time

| | $\lambda = 5.50$ | $1/\omega_0 \theta = 0.20$ | | |
| | | s/s_m | | |
r/R_0 $\quad$ t/t_m	0.25	0.34	0.42	1.00
0	0.092	0.235	0.432	1.00
0.1	0.095	0.235	0.428	0.989
0.2	0.111	0.245	0.423	0.963
0.3	0.128	0.252	0.410	0.915
0.4	0.144	0.235	0.386	0.843
0.5	0.150	0.246	0.350	0.745
0.6	0.144	0.221	0.299	0.624
0.7	0.123	0.181	0.234	0.480
0.8	0.088	0.126	0.159	0.322
0.9	0.045	0.064	0.079	0.159
1.0	0	0	0	0

TABLE V. – <u>Comparison of parabolic treatment with the two-term Bessel-function treatment for a UERL diaphragm gauge</u>

Units: z_m – in.; p_m – p.s.i. – sec.; θ, t_m – msec; $\hat{f}_p(\theta)$, $\hat{f}(\theta)$ – in. (psi. sec.)$^{-1}$; ω_o^*, ω_1^*, ω_2^* – msec.$^{-1}$.

Parabolic profile $z_m = p_m \theta \hat{f}_p(\theta)$			Two term Bessel function profile $z_m = p_m \theta \hat{f}(\theta)$		
θ	$\hat{f}_p(\theta)$	t_m	θ	$\hat{f}(\theta)$	t_m
0.1	0.92	0.36	0.1	1.23	0.29
0.2	0.75	0.40	0.2	0.90	0.32
0.3	0.63	0.43	0.3	0.70	0.34
0.4	0.54	0.45	0.4	0.58	0.35
0.5	0.47	0.46	0.5	0.50	0.36
0.6	0.41	0.47	0.6	0.44	0.36
0.7	0.37	0.47	0.7	0.39	0.37
0.8	0.34	0.48	0.8	0.35	0.38
0.9	0.31	0.48	0.9	0.32	0.38
1.0	0.28	0.49	1.0	0.29	0.39
$\omega_o^* = 5.86$			$\omega_1^* = 6.82$		$\omega_2^* = 21.27$

The quantities z_m and t_m are the maximum central deflection and time of deflection respectively of an unbaffled UERL diaphragm of 1.675 in. radius, 0.075 in. thickness, 7.8 gm. cm.$^{-3}$ density, and with a yield stress of 50,000 p.s.i.

4. The Initial Phase of the Plastic Deformation of a Thin Plate

In Sections 2 and 3 of this Part, the equation of motion of a thin plate, loaded by an exponential explosion wave, was solved by expansion of the deflection in a series of Bessel functions. Since the series does not converge very rapidly in the early phase of the motion, another type of solution is presented here, in which the propagation of the transverse membrane wave from the edge to the center of the diaphragm, is explicitly treated. At the same time, the solution given here is less general than our previous one, since it is only possible to carry it through in the approximation of uniform water loading at all points on the diaphragm.

As surmised by Bohnenblust and von Karman, by analogy with the case of the string, the center portion of the plate remains flat out to the point reached by the incoming transverse plastic wave at the given time. For impulsive loading, there is a kink in the profile at this point. For loading with a finite duration, the second derivative, but not the first, is discontinuous. If the nonuniform distribution of water loading were properly taken into account, the center portion would not, of course, be exactly flat.

The equation of motion of the plate loaded with a shock wave of free field pressure $p_0(t)$ may, in the incompressive approximation, be written

$$\left(1+\lambda G\right)\frac{\partial^2 z}{\partial t^2} - \omega_o^2 \frac{1}{x}\frac{\partial}{\partial x}\left(x\frac{\partial z}{\partial x}\right) = \frac{p_0(t)}{\rho a_o} , \qquad (22)$$

where $x = r/R_o$,

$$\omega_o^2 = \sigma_o/\rho R_c^2 \quad , \quad \lambda = R_c p_o/a_o \rho$$

and G is an integral operator defined by

$$O F(x,t) = \frac{1}{2\pi} \int_0^{2\pi} d\phi \int_0^1 x' dx' \left(x'^2 + x^2 - 2xx' \cos\phi \right)^{-1/2} F(x',t).$$

The diaphragm has a radius R_0, thickness a_0, and is constructed of material of density ρ and yield stress σ_o. At time t the diaphragm is deflected an amount z at a distance r from the center. ρ_o is the density of water. $R_0 \omega_o$ is the velocity of transverse plastic waves in the free (unloaded) plate.

In solving Eq. (22) we replace the operator O by unity as a first approximation. If the diaphragm moves as a piston, this replacement gives the correct water loading at the center, but gives too large a water loading some distance from the center. We now have

$$(1+\lambda) \frac{\partial^2 z}{\partial t^2} - \omega_c^2 \frac{1}{x} \frac{\partial}{\partial x} \left(x \frac{\partial z}{\partial x} \right) = \frac{p_o(t)}{\rho a_o} . \tag{23}$$

Taking the Laplace transform of both sides we get

$$\omega^2 (1+\lambda) L - \omega_o^2 \frac{1}{x} \frac{d}{dx} \left(x \frac{d}{dx} L \right) = \frac{L_p}{\rho a_o} , \tag{24}$$

where $L = \int_0^\infty z(x,t) e^{-\omega t} dt$,

and $L_p = \int_0^\infty p_o(t) e^{-\omega t} dt$.

The solution of Eq. (24) is

$$L = \frac{1}{\rho a_o} \frac{L_p}{(1+\lambda) \omega^2} \left(1 - \frac{J_o(ikx)}{J_o(ik)} \right) , \tag{25}$$

where $k = (1+\lambda)^{1/2} \omega/\omega_o$. Inverting the Laplace transform we obtain immediately the solution of Eq. (23):

$$z = \frac{1}{\rho a_o (1+\lambda)} \frac{1}{2\pi i} \int_{c-i\infty}^{c+i\infty} \frac{L_p}{\omega^2} \left(1 - \frac{J_o(ikx)}{J_o(ik)} \right) e^{\omega t} d\omega . \tag{26}$$

Now we wish to obtain an asymptotic expression for Eq. (26) suitable for small values of t. To accomplish this, we make an asymptotic development of the integrand of the integral in (26) valid for large ω. We make use of the fact that

$$J_o(u) \simeq \frac{\cos(u - \frac{\pi}{4})}{\sqrt{\frac{1}{2}\pi u}} \tag{27}$$

for large u. From this we immediately obtain

$$\frac{J_o(ikx)}{J_o(ik)} \simeq x^{-1/2} e^{-k(1-x)}. \tag{28}$$

Substituting (28) into (26) we obtain the result

$$z = \frac{1}{\rho a_o (1+\lambda)} \left[h(t) - x^{-1/2} h(t^*) \right], \tag{29}$$

where $t^* = t - \frac{(1+\lambda)^{1/2}(1-x)}{\omega_o}$,

and $h(t) = \frac{1}{2\pi i} \int_{c-i\infty}^{c+i\infty} \frac{L_p e^{\omega t}}{\omega^2} d\omega = \int_0^t dt' \int_0^{t'} dt'' p_o(t'')$, $t > 0$,

$$= 0, \quad t \leq 0.$$

On account of the incompressive approximation we must not take t too small (i.e., $t \leq R_o/c_o$, where c_o is the velocity of sound) in using Eq. (28). On the other hand, the asymptotic development breaks down if we take t too large (i.e., $t \sim (1+\lambda)^{1/2}/\omega_o$, which is the time required for a transverse plastic wave to traverse the radius of the loaded plate).

The meaning of Eq. (29) is perhaps clearer if we rewrite it in the form

$$z = \frac{1}{\rho a_o (1+\lambda)} h(t), \quad 0 \leq z \leq 1 - \frac{\omega_o t}{(1+\lambda)^{1/2}},$$

$$= \frac{1}{\rho a_o (1+\lambda)} \left[h(t) - x^{-\frac{1}{2}} h(t^*) \right], \quad 1 - \frac{\omega_o t}{(1+\lambda)^{1/2}} \leq x \leq 1, \tag{30}$$

where

$$t^* = t - \frac{(1+\lambda)^{1/2}(1-x)}{\omega_o} .$$

The first of Eqs. (30) is the equation of motion of a free plate. Thus we see that the central area of the diaphragm moves initially as a free plate and is consequently flat; however, the flatness is destroyed by a transverse wave represented by the second of Eqs. (30) traveling in from the periphery with a velocity $R_o \omega_o (1+\lambda)^{-1/2}$ ($R_o \omega_o$ is the velocity of transverse plastic waves in the unloaded diaphragm, the factor $(1+\lambda)^{-1/2}$ takes account of the water loading).

If $p_o(t)$ is bounded, it follows that $h(t)$ is continuous and has a continuous derivative; consequently, in such a case the deflection z and its derivatives with respect to the time t and the reduced radius x respectively are continuous. However, suppose that $p_o(t)$ is not bounded and, to be more specific, suppose it has a singularity at $t = 0$ such that

$$\int_0^t p_o(t') dt' = I > 0 , \quad t > 0 ,$$

$$= 0 , \quad t \leq 0 .$$

Then the time derivative of the deflection is discontinuous at the initial instant and the radial derivative and time derivative are both discontinuous at

$$x = 1 - \omega_o t / (1+\lambda)^{1/2} .$$

FIGURE 5 - Plate profiles during the initial phases

($\theta = 0.1$ msec.).

388
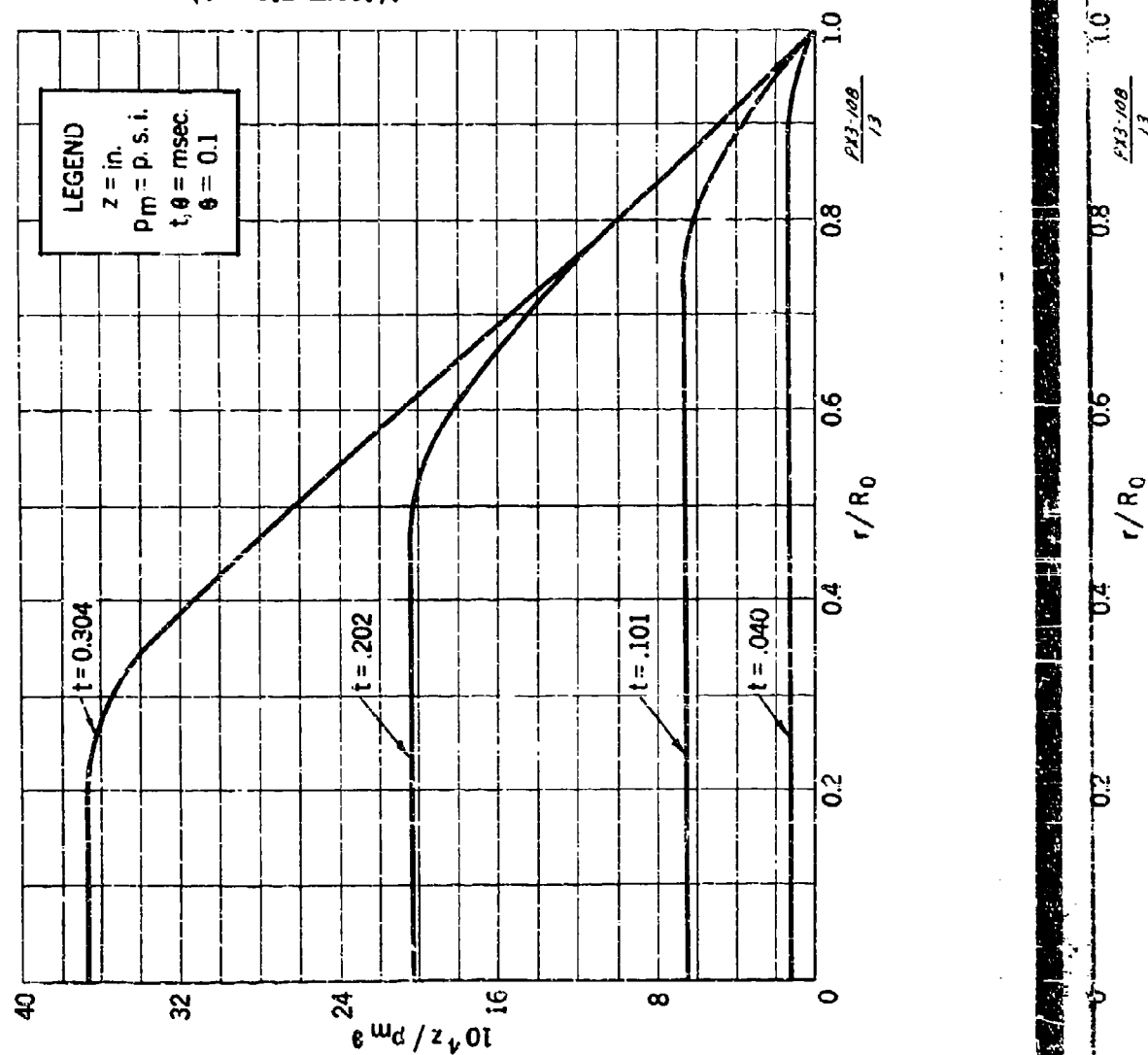
FIGURE 6 - Plate profiles during the initial phase.

(θ = 1.0 msec.).
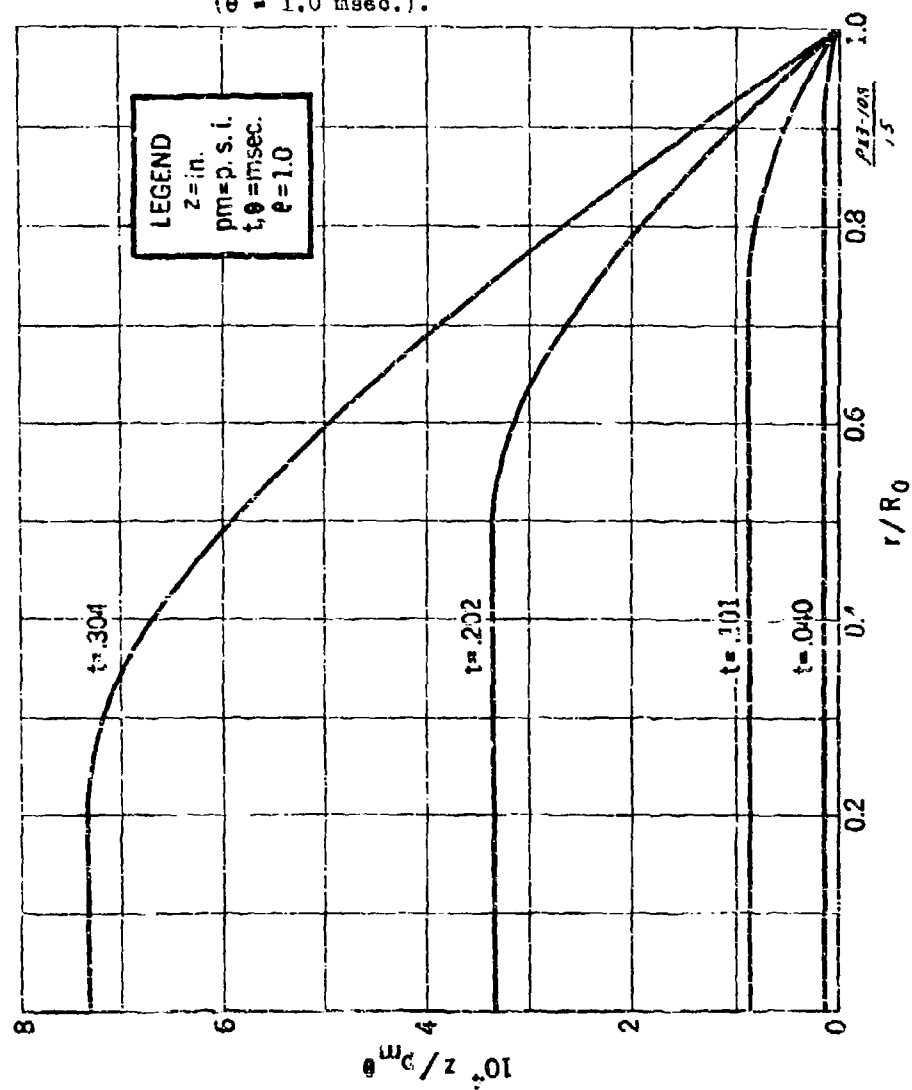
In other words, in the case of impulsive loading the diaphragm profile has a kink which is propagated inward with a velocity $R_0 \omega_0 (1+\lambda)^{-1/2}$.

In the case of an exponential wave of the form

$$p_e(t) = p_m e^{-t/\theta}, \quad t > 0,$$
$$= 0 \qquad , \quad t \leq 0,$$

we have

$$\left. \begin{array}{l} h(t) = p_m \theta \left[t - \theta (1 - e^{-t/\theta}) \right], \quad t \geq 0, \\ = 0, \quad t \leq 0. \end{array} \right\} \tag{31}$$

In the limiting case of impulsive loading, that is, with an infinitesimal value of the duration θ, we have

$$\left. \begin{array}{l} h(t) = I t, \quad t \geq 0, \\ = 0, \quad t \leq 0, \end{array} \right\} \tag{32}$$

where

$$I = \int_0^\infty p_e \, dt = \lim_{\theta \to 0} p_m \theta.$$

In figures 5 and 6 are shown diaphragm profiles for various times, i.e., $z/p_m \theta$ vs. r/R_0 for various values of t, calculated with $p_0 = p_m e^{-t/\theta}$, and with $R_0 = 1.675$ in., $\sigma_0 = 50,000$ p.s.i., $a_0 = 0.078$ in., $\rho = 7.8$ gm./cm.^{3}, which correspond to the standard UERL diaphragm gauge. In figure 5, $\theta = 0.1$ msec., corresponding to rather impulsive loading, and in figure 6, $\theta = 1$ msec., corresponding to much longer duration. It is apparent that the diaphragm bends much more sharply at the edge of the flat central portion in figure 5 than in figure 6.

V. COMPARISON OF THE THEORIES OF PARTS III AND IV WITH EXPERIMENT

The ultimate object of experimental and theoretical work on the underwater damage to diaphragms is the prediction of damage to ships attacked by a given explosive under specified conditions. To have engineering significance, certain aspects of the theory must be tested by comparison with experiment. In this part, we compare theoretical results with experimental results obtained at the Underwater Explosion Research Laboratory at Woods Hole.

Here we present comparisons on the basis of both the parabolic theory (Part III) and the two-mode Bessel-function theory (Part IV, Section 3) using both empirical and theoretical pressure-time curves for the shock wave. The incompressive approximation to the water loading is used in both theories and a small baffle is assumed. Consequently, for the parabolic theory Eqs. (17) of Part III are used with a factor of 1/2 multiplied into the expression for z_m to take account of the small (instead of infinite) baffle. For the two-mode Bessel-function case the tables of Part IV, Section 3 are used without modification.

The agreement between theoretical and experimental values of the maximum deflection is very good in most cases. The agreement among the various sets of theoretical values themselves is satisfactory but not excellent. The theoretical values are on the average about 15% higher than the experimental values. The values calculated from the two-mode Bessel-function theory are on the average about 7% higher than those from the parabolic theory, the discrepancy being most conspicuous for small charge weights.

55

The comparisons are made for the UERL gauge using a thin steel diaphragm whose specifications are as follows:

Radius, R_0 = 1.65 in.

Thickness, a_0 = 0.085 in.*

Yield Stress, σ_0 = 60,000 p.s.i.[†]

Density, ρ = 7.8 gm. cm.$^{-3}$

The diaphragm is mounted on a steel block such that it is backed by air. The mounting block weighs about 25 lbs. and is fastened to a large steel ring. The face of the block extends only a small distance beyond the edge of the diaphragm; consequently, the calculations are made on the assumption of a small baffle.

In Table I we compare the calculated and experimental[1] values of the maximum central deflection z_m of the diaphragm after attack by a shock wave from Mark 6 depth charges at a distance R. The charges were loaded with a weight W of cast TNT whose density lies between 1.55 and 1.60 gm. cm.$^{-3}$. Three sets of calculated values are given: (1) calculated from the two-mode Bessel-function treatment using theoretical pressure-time curves;[2] (2) calculated from the two-mode Bessel-function treatment using the following empirical pressure-time curves:[3]

$$P_m = 20,400 \left(\frac{R}{W^{1/3}}\right)^{-1.14}$$

$$\theta = 0.0735 \left(\frac{R}{W^{1/3}}\right)^{-.14} W^{1/3}$$

---

* In the experiments considered "Lot III" plates were used with values of the thickness scattered closely about the value given above. The experimental values of the maximum deflection are corrected for the deviations of the thickness from the value of 0.085 in.

[†] Value quoted by the supplier.

1/ OSRD Report UE-13, p. 10; OSRD Report UE-14, p. 10.
2/ OSRD Report 2022 (1943).
3/ OSRD Report UE-16, p. 9.

r. The

ing.

the

a

ies of

shock

aded

pu. cm.$^{-3}$.

o-mode

?) cal-

g empir-

of the
imental
of the

TABLE I. - Comparison of calculated and experimental damage to diaphragms by large charges of cast TNT

Charge weight W (lbs.)	Charge distance R (ft.)	Maximum central deflection z_m (in.)			
		Calc. (1)*	Calc. (2)*	Calc. (3)*	Expt.
185.2	35	0.58	0.50	0.46	0.42
190.5	"	0.59	0.51	0.47	0.44
"	"	"	"	"	0.43
289	"	0.71	0.61	0.57	0.55
290.4	"	0.72	0.61	0.57	0.56
292	"	0.72	0.61	0.57	0.53
"	"	"	"	"	0.52
294	"	"	"	"	0.55
"	"	"	"	"	0.54
295	"	"	0.62	"	0.57
"	"	"	"	"	0.55
589	45	0.73	"	0.59	0.58
185.2	50	0.39	0.34	0.31	0.29
190.5	"	0.40	0.34	0.32	"
289	"	0.48	0.41	0.38	0.36
290.4	"	0.48	0.41	0.38	0.37
292	"	"	"	0.39	0.35
294	"	"	"	"	0.37
295	"	"	"	"	"
185.2	60	0.32	0.28	0.26	0.24
190.5	"	"	"	"	"
289	"	0.39	0.34	0.31	0.29
290.4	"	"	0.33	0.32	0.33
292	"	"	0.34	"	0.26
"	"	"	"	"	0.29
294	"	"	"	"	"
295	"	"	"	"	"
589	"	0.53	0.45	0.43	0.40
633	"	0.54	0.46	0.44	0.55
589	75	0.41	0.35	0.33	0.30

|	Av. Dev. from Expt.	Av. Dev. from Expt.	Av. Dev. from Expt.
	31%	12%	5.2%

* (1) Two-mode Bessel-function treatment; theoretical pressure-time curves
  (2) Two-mode Bessel-function treatment; empirical pressure-time curves.
  (3) Parabolic treatment; empirical pressure-time curves.

where p_m is the peak pressure in p.s.i., θ the time constant in msec., R the distance in feet, and W the charge weight in lbs.; and (3) calculated from the parabolic treatment using the empirical pressure-time curves above. In figure 1 curves corresponding to the third set of calculated values in table I are compared with the experimental values.

In table II we present comparisons of calculated and experimental values of the maximum diaphragm deflections for the case of small charges of loose tetryl, density 0.97 ± 0.05. Two sets of calculated values are given: (1) calculated from the two-mode Bessel-function treatment, and (2) calculated from the parabolic treatment. All of the calculated values are based upon the theoretical pressure-time curves[2]/ for tetryl, density 1.00. Cases for which cavitation is believed to occur by the criterion of Part II, Section 2, are marked by asterisks at the left of the table; however, it is believed that cavitation is not well developed and that the theories of Parts III and IV may roughly apply. In figure 2 curves corresponding to the second set of calculated values in table II are compared with the experimental values.

The calculated values of the deflection, except those calculated from the parabolic treatment for small tetryl charges, are considerably higher than the experimental values. For large charges of case TNT (table I and figure 1), the deflections calculated from the two-mode Bessel-function treatment using theoretical pressure-time curves are on the average 31% higher than the experimental deflections, those calculated from the same treatment using empirical pressure-time curves are 12% higher, and finally those calculated from the parabolic treatment using the same empirical pressure-time curves are 5.2% higher. For small charges of loose

574

FIGURE 1 - Comparison of calculated and experimental
damage to thin circular plates by large
charges of cast TNT.
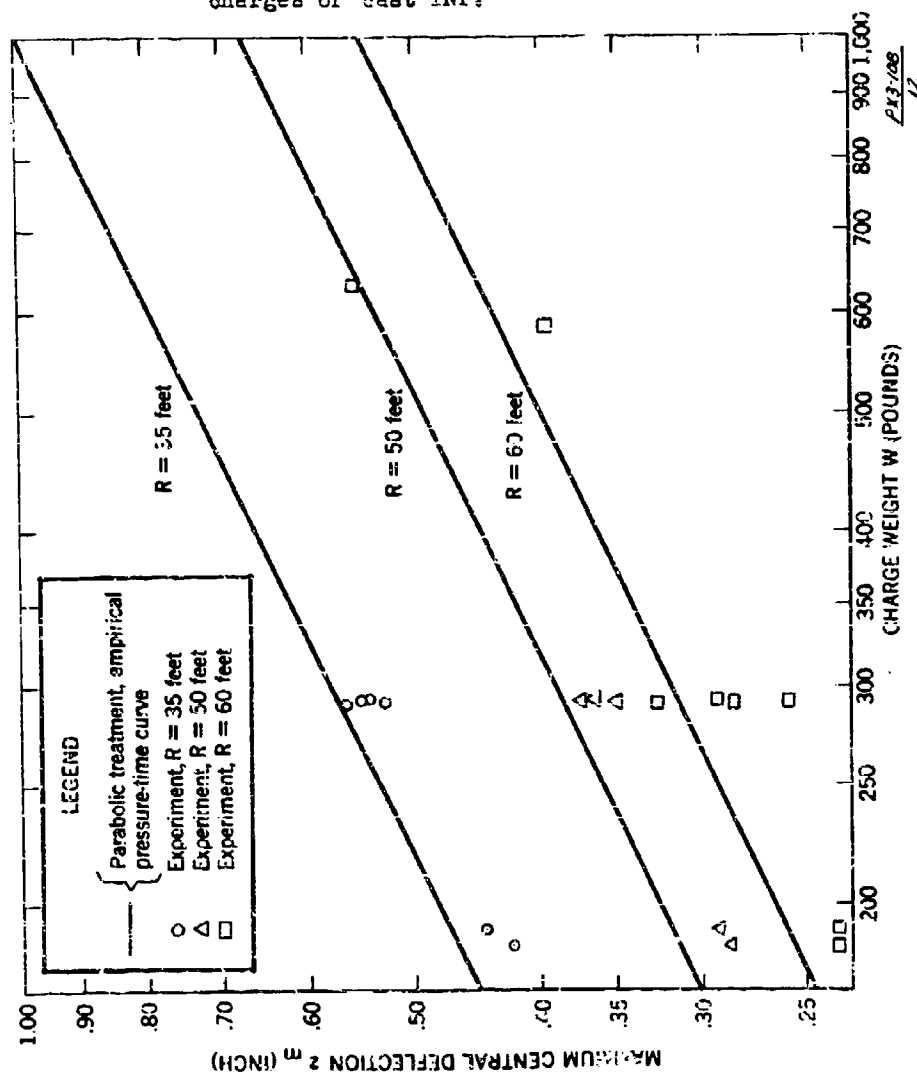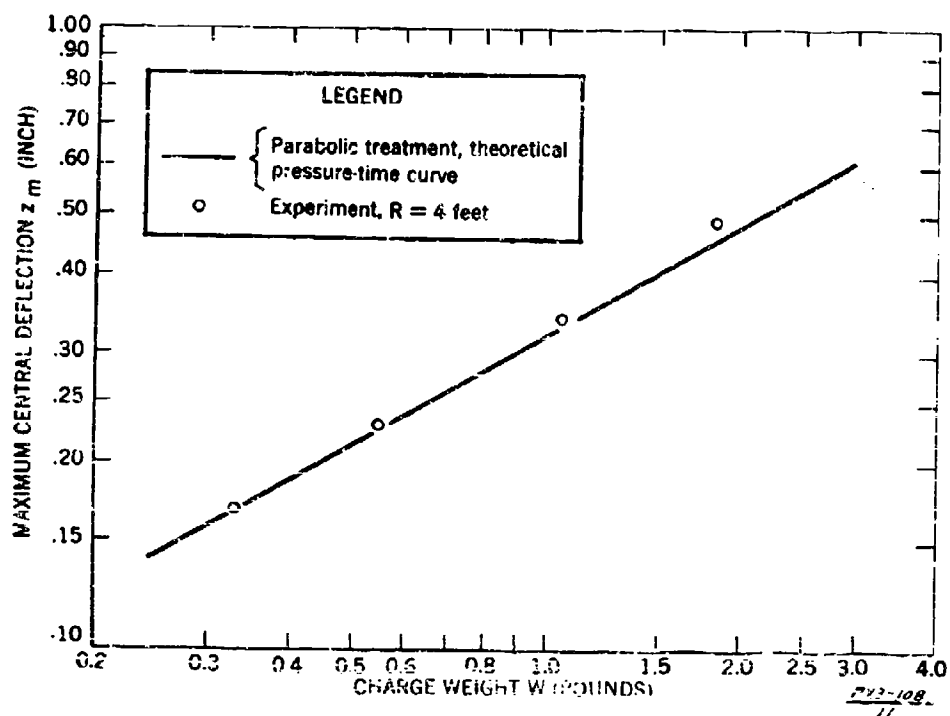
FIGURE 2 — Comparison of calculated and experimental
damage to thin circular plates by small
charges of loose Tetryl.

TABLE II. - <u>Comparison of calculated and experimental damage to diaphragms by small charges of loose tetryl</u>

Charge weight W (lbs.)	Charge distance R (ft.)	Maximum central deflection z_m (in.)		
		Calc. (1)**	Calc. (2)**	Expt.
* 0.331	4	0.258	0.169	0.169
* 0.552	4	0.241	0.227	0.230
1.060	4	0.488	0.335	0.343
1.823	4	0.647	0.457	0.492

	Av. % Dev. from Expt.: +40%	Av. % Dev. from Expt.: -3.7%

* Cavitation.

** (1) Two-mode Bessel-function treatment.
(2) Parabolic treatment.

tetryl (table II and figure 2), the deflections calculated from the two-
mode Bessel function treatment are on the average 40% higher than the ex-
perimental deflections, and those calculated from the parabolic treatment
are 3.7% lower, the theoretical pressure-time curves being used in both
cases. It must be admitted that the excellent agreement between the para-
bolic theory and experiment for small charges is due to an accidental can-
cellation of errors. The two-mode Bessel-function treatment is in a sense
in better agreement with experiment in that it involves errors which are
rather insensitive to variations of the charge weight, whereas additional
error of opposite sign which rapidly increases in absolute magnitude as the
charge weight becomes quite small causing the cancellation mentioned above.
The nature of the additional error peculiar to the parabolic theory will
be discussed later.

The greatest contribution to the discrepancy between theory and
experiment is probably due to the idealization of the stress-strain curve
and to the use of the value of the yield stress quoted by the supplier in
lieu of better information. Another contribution of importance may be due
to the yielding of the diaphragm mounting which in the calculations was as-
sumed to be rigid. The theoretical pressure-time curves, of course, contrib-
ute error to the cases in which they are used. The rectification of any of
the above-mentioned errors would be to tend to lower the calculated values
of the deflection, possibly bringing them nearer to the experimental values.
There are numerous minor sources of error, among which may be mentioned the
neglect of the effect of diaphragm curvature on the diffracted wave, the
neglect of all other nonlinear terms in the deflection, and the incompressive
approximation in treating the diffracted wave.

The reason for the discrepancy between the parabolic and two-mode Bessel-function theories is the artificial restraint of a parabolic profile in the former. For large charges, producing shock waves of long duration, the two theories give values of the maximum deflection only a few percent apart; but for very small charges, producing shock waves of very short duration, the results are conspicuously divergent. This situation is made understandable by the fact that the two-mode Bessel-function treatment gives a final profile which is almost parabolic for waves of long duration but which is quite peaked with an abnormally raised center for waves of short duration. The two theories also give rather different times of deflection, the parabolic theory giving values of this quantity roughly 20% higher. The calculated times of deflection have not been compared with experiment, since there are no data yet available for noncavitating cases.

In conclusion, the parabolic theory gives deflections which agree more closely with experiment than do those given by the more elaborate two-mode Bessel-function theory, the better agreement supposedly being due to a partial cancellation of errors common to both theories by an error associated with the restraint of a parabolic profile. However, the parabolic theory gives results for large charges differing little from the results of the more elaborate theory, and is more practical for actual computation because of its greater simplicity. Where empirical pressure-time curves have been used, the agreement of both theories with experiment is very good in view of the numerous possible sources of error.

VI. DAMAGE TO INFINITE PLATES BY UNDERWATER EXPLOSIONS

1. Introduction

The problem of damage to infinite plates—that is, plates having linear surface dimensions many times greater than the charge distance—is treated here as an infinite plastic membrane under impulsive loading. The behavior of an infinite membrane is qualitatively quite different from that of a circularly clamped membrane whose radius is relatively small compared with the charge distance. In particular, in the case of the infinite membrane the maximum central strain calculated on the basis of normal motion is about ten times greater than that calculated on the basis of the similarity of Mohr circles (leading to the equality of principal strains), whereas in the case of the circularly clamped membrane the calculations on the two bases give ~~practically~~ virtually identical results. Consequently, the case under consideration is one in which it is imperative to use the correct theory of strain (on the basis of the similarity of Mohr circles).

In Sec. 2, the problem of damage to plates (in the first approximation) under an arbitrary loading is considered with particular emphasis on impulsive loading. In Sec. 3, the more special case of impulsive loading giving an initial velocity distribution of the form $(R^2 + r^2)^{-\nu}$ is considered and explicit solutions in terms of elementary functions are given for the profile and strain distribution in the cases of $\nu = 1/2$, $3/2$, and $5/2$. The variable $\underline{r}$ is the radius in cylindrical coordinates in which the z-axis coincides with the center of symmetry of the system. In the case of underwater explosions, $\underline{R}$ is the distance between the middle

surface of the plate and the charge center. Because of considerations advanced in Sec. 4, the pertinent solutions for $\nu = 3/4$ are found by interpolation.

In Sec. 4, an attempt is made to apply the foregoing results to damage by underwater explosions. In the absence of a detailed solution of the hydrodynamical problem associated with loading, certain rough semi-empirical assumptions are made. It is assumed that each element of plate absorbs almost instantaneously in the form of kinetic energy a constant fraction of the energy incident in the solid angle subtended by that element. This assumption leads immediately to an initial velocity distribution proportional to $(R^2 + r^2)^{-3/4}$; hence the special emphasis on $\nu = 3/4$. Since the velocity of sound in water is much greater than the velocity of transverse plastic waves in the plate, retardation effects in the explosion wave are neglected. A formula is obtained giving the critical weight W of a given explosive necessary to cause rupture when exploding in contact with a plate of thickness a_0. The results of this formula are compared with the results of rupture experiments performed at the David Taylor Model Basin. Attention is centered on the values of χ, the fraction of the total energy of explosion delivered to the plate, giving agreement between the theoretical and experimental results for rupture by contact explosions. The values of χ so obtained are scattered in a range of values of reasonable magnitude (0.1 to 0.2). The χ values apparently depend on the plate thickness in a relatively regular fashion, the explanation of which is as yet unclear. Although the results do not appear very satisfactory from the standpoint of predicting rupture, they may be regarded as fairly conclusive evidence

in favor of the strain theory advocated in this report over the alternative one based upon normal motion. A theory based upon normal motion would give unreasonable values of α about one-tenth as large as those obtained here.

The treatment presented in Secs. 2 and 3 may seem overly elaborate in relation to the crude use made of it in Sec. 4. However, it is hoped that the results presented in Sec. 3 may be used more fully and satisfactorily at some future time when a more successful attack is made upon the hydrodynamical problem.

2. Solution for impulsively loaded infinite plastic membrane

The equation giving the first approximation to the vertical displacement of an infinite thin diaphragm under no external forces may be written

$$
\left.
\begin{aligned}
&\frac{\partial^2 z^{(1)}}{\partial t^2} - c^2 \frac{1}{r} \frac{\partial}{\partial r}\left(r \frac{\partial z^{(1)}}{\partial r}\right) = 0, \\
&z = \alpha z^{(1)} + 0 \ (\alpha^3),
\end{aligned}
\right\}
\tag{1}
$$

where z is the vertical displacement, α the expansion parameter, r the radial coordinate, t the time, and $c\left[=\sqrt{\sigma_o/\rho}\right]$ the velocity of transverse plastic waves in the plate. The initial velocity distribution is assumed to be of the form

$$
\frac{\partial z}{\partial t}(r,0) = \alpha c g\left(\frac{r}{R}\right),
\tag{2}
$$

where R is some representative linear dimension of the system. The initial displacement is, of course, taken to be zero.

For convenience, the foregoing equations are put into nondimensional form. By introducing the variables $x = r/R$, $y = z^{(1)}/R$, and $\tau =$

382

ct/R, Eqs. (1) and (2) may be reduced to

$$\frac{\partial^2 y}{\partial t^2} - \frac{1}{x}\frac{\partial}{\partial x}\left(x\frac{\partial y}{\partial x}\right) = 0 \tag{3}$$

and

$$\frac{\partial y}{\partial t}(x,0) = g(x). \tag{4}$$

The general solution of Eq. (3) is very simply obtained by the use of the Laplace transform and the Hankel transform with respect to the variables t and x, respectively. Application of the Laplace transform gives

$$s^2 L - \frac{1}{x}\frac{\partial}{\partial x}\left(x\frac{\partial L}{\partial x}\right) = g(x), \tag{5}$$

where

$$L(x,s) = \int_0^\infty y(x,t) e^{-st} dt. \tag{6}$$

Application of the Hankel transform to Eq. (5) gives

$$(s^2 + k^2) H = G, \tag{7}$$

where

$$H(k,s) = \int_0^\infty L(x,s) J_0(kx) x\, dx$$
$$= \int_0^\infty \int_0^\infty y(x,t) e^{-st} J_0(kx) x\, dx\, dt, \tag{8}$$

and

$$G(k) = \int_0^\infty g(x) J_0(kx) x\, dx. \tag{9}$$

65

In using the Hankel transform the boundary conditions that y vanish at $x = \infty$ and $\partial y/\partial x$ vanish at $x = 0$ have been used.

Solving Eq. (7) for $\underline{y}$ and inverting the Laplace and Hankel transforms, the solution is immediately obtained in the form

$$y(x,\tau) = \frac{1}{2\pi i} \int_{\substack{\gamma - i\infty \\ \gamma > 0}}^{\gamma + i\infty} \int_0^\infty G(k) J_0(kx) e^{s\tau} \frac{k\,dk\,ds}{s^2 + k^2} \,. \tag{10}$$

Using the fact that

$$\frac{1}{2\pi i} \int_{\gamma - i\infty}^{\gamma + i\infty} \frac{e^{s\tau}}{s^2 + k^2} \, ds = \frac{\sin k\tau}{k} \,, \tag{11}$$

Eq. (10) can be simplified to

$$\left. \begin{aligned} y(x,\tau) &= \int_0^\infty G(k) \sin k\tau \, J_0(kx)\,dk, \\ &= \mathscr{I}_m \int_0^\infty G(k) e^{ik\tau} J_0(kx)\,dk \,. \end{aligned} \right\} \tag{12}$$

the existence of a reduced pressure

$$\mu(x,\tau) = \frac{R p(\eta,t)}{\rho c^2 a_0} \,, \tag{13}$$

in addition to the initial impulse, gives a more general solution,

$$\left. \begin{aligned} y(x,\tau) &= \int_0^\infty G(k) \sin k\tau \, J_0(kx)\,dk \\ &+ \int_0^\tau \int_0^\infty M(k,\tau') \sin k(\tau-\tau') J_0(kx)\,dk\,d\tau' \end{aligned} \right\} \tag{14}$$

384

where

$$M(k, \tau') = \int_0^\infty p(x, \tau') J_0(kx) x \, dx. \tag{15}$$

This result is obvious if the pressure is regarded as a superposition of impulses.

The first approximations to the meridional and circumferential strains, ξ_1 and ξ_2, respectively, are given as a function of position and time by

$$\xi_1 = \xi_2 = \frac{x^2}{2} h(x, \tau), \tag{16}$$

where

$$h(x, \tau) = \int_x^\infty \left(\frac{\partial \eta}{\partial x}\right)_{x=x'}^2 \frac{dx'}{x'}. \tag{17}$$

These are nothing more than Eq. 32 of Part I, recast in nondimensional form.

The case of interest here, impulsive loading of the plate by an underwater explosion wave, involves an initial velocity distribution of the form

$$\frac{\partial \eta}{\partial t}(x, 0) = \frac{1}{(1+x^2)^\nu} = g^{(\nu)}(x), \tag{18}$$

the particular value of 3/4 for ν being of greatest interest. Here, x is equal to the radius r divided by the distance R between the plate and the center of the explosive charge. In Sec. 4 of this Part the determination of the values of κ and ν on a physical basis will be discussed. In the

cases of $\nu = 1/2,\ 3/2,\ 5/2,\ \ldots$, one is able to obtain the functions $y(x,\gamma)$ and $h(x,\gamma)$ in terms of elementary functions. The solutions for these special values of ν will be considered in the next section, with the ultimate intention of finding the functions y and h for $\nu = 3/4$ by interpolation.

3. Solutions with initial velocity distributions of the form $(1 + x^2)^{-n-1/2}$

It is the purpose of this section to obtain the functions $y(x,\gamma)$ and $h(x,\gamma)$ in terms of elementary functions when the initial velocity distribution is given by

$$g^{(\nu)}(x) = \frac{1}{(1+x^2)^\nu}\ ,\qquad \nu = \tfrac{1}{2},\tfrac{3}{2},\tfrac{5}{2},\cdots \tag{19}$$

The entire set of solutions may be obtained from one solution by differentiation and integration with respect to a parameter β introduced into Eq. (19) for $\nu = 3/2$ as follows

$$g^{(3/2)}(x,\beta) = \frac{1}{(\beta^2 + x^2)^{3/2}}\ . \tag{20}$$

The Hankel transform of Eq. (20) is

$$G^{(3/2)}(k,\beta) = \frac{e^{-\beta k}}{\beta}\ . \tag{21}$$

The solution of Eq. (3) becomes[1]

$$g^{(3/2)}(x,\tau,\beta) = \int_0^\infty G^{(3/2)}(k,\beta)\,\sin k\tau\,J_0(kx)\,dk\,,$$

$$= \mathscr{Im}\,\frac{1}{\beta}\int_0^\infty e^{(-\beta+i\tau)k}J_0(kx)\,dk = \mathscr{Im}\frac{1}{\beta\left[(\beta-i\tau)^2 + x^2\right]^{1/2}}\ . \tag{22}$$

---

[1] Bessel functions, by G. N. Watson (2nd ed., Cambridge 1944), p. 384

It is quite clear that any linear operation with respect to β which transforms $g^{(\nu)} \longrightarrow g^{(\nu')}$ also transforms $y^{(\nu)} \longrightarrow y^{(\nu')}$. Consequently, the functions $y^{(1/2)}(x,\tau)$ and $y^{(5/2)}(x,\tau)$ can be derived from $y^{(3/2)}(x,\tau,\beta)$ as follows:

$$y^{(1/2)}(x,\tau) = y^{(1/2)}(x,\tau,1) = \int_1^\infty y^{(3/2)}(x,\tau,\beta)\,\beta\,d\beta = \int_1^\infty \left\{ \ell n \frac{1}{[(\beta-i\tau)^2+x^2]^{1/2}} \right\} d\beta, \quad (23)$$

$$y^{(5/2)}(x,\tau) = y^{(5/2)}(x,\tau,1) = -\frac{1}{2}\,\mathcal{I}m\left[\frac{\partial}{\partial\beta}\, \frac{1}{\beta[(\beta-i\tau)^2+x^2]^{1/2}} \right]_{\beta=1}$$

$$= \frac{1}{2}\mathcal{I}m\left[\frac{x^2+(1-i\tau)+(1-i\tau)^2}{[(1-i\tau)^2+x^2]^{3/2}} \right]. \quad\quad (24)$$

The functions $h^{(1/2)}(x,\tau)$ and $h^{(5/2)}(x,\tau)$ can in a similar fashion be derived from a function

$$h^{(3/2)}(x,\tau,\beta,\beta') = \int_x^\infty \frac{\partial y^{(3/2)}}{\partial x}(x',\tau,\beta)\, \frac{\partial y^{(3/2)}}{\partial x}(x',\tau,\beta')\, \frac{dx'}{x'} \quad\quad (25)$$

as follows:

$$h^{(1/2)}(x,\tau) = h^{(1/2)}(x,\tau,1,1) = \int_1^\infty \int_1^\infty h^{(3/2)}(x,\tau,\beta,\beta')\,\beta\beta'\,d\beta\,d\beta', \quad\quad (26)$$

$$h^{(5/2)}(x,\tau) = h^{(5/2)}(x,\tau,1,1) = \frac{1}{4}\left[\frac{\partial^2}{\partial\beta\partial\beta'} h^{(3/2)}(x,\tau,\beta,\beta') \right]_{\substack{\beta=1 \\ \beta'=1}}. \quad\quad (27)$$

The functions $y^{(\nu)}$ and $h^{(\nu)}$ and some of their properties are listed in the following for $\nu = 1/2$, $3/2$, $5/2$. Higher values of ν will not be considered here.

Case (1). $\nu = 1/2$.

The solution for this case is

$$y^{(1/2)}(x,t) = \tan^{-1}\left\{\frac{\tau + \sqrt{\frac{1}{2}(\zeta^2 - 1 - x^2 + \tau^2)}}{1 + \sqrt{\frac{1}{2}(\zeta^2 + 1 + x^2 - \tau^2)}}\right\} , \tag{28}$$

$$\zeta^2 = \sqrt{(1 - \tau^2 + x^2)^2 + 4\tau^2} . \tag{29}$$

Some qualitative aspects of the plate profile for this type of loading are implied by the following properties of $y^{(1/2)}(x,\tau)$:

$$y^{(1/2)}(0,\tau) = \tan^{-1}\tau ; \tag{30}$$

$$y^{(1/2)}(x,\tau) \simeq \frac{\tau}{\sqrt{1+x^2}} , \qquad \tau \ll 1 ; \tag{31}$$

$$y^{(1/2)}(x,\tau) \simeq \frac{\tau}{x} , \qquad \frac{\tau}{x} \ll 1 , x \gg 1 ; \tag{32}$$

$$y^{(1/2)}(x,\tau) \simeq \frac{\pi}{2} - \frac{1}{\tau - \frac{x^2}{4\tau}} , \qquad \frac{x}{\tau} \ll 1 , \tau \gg 1 . \tag{33}$$

The function $h^{(1/2)}(x,\tau)$ takes the form

$$h^{(1/2)}(x,\tau) = \frac{1}{2(1+\tau^2)^2}\left\{\tau\tan^{-1}\left(\frac{2\tau}{1-\tau^2+x^2}\right) - \frac{1}{2}(1+\tau^2)\left(\frac{1+x^2+\tau^2-\zeta^2}{x^2}\right)\right.$$

$$\left. - \frac{1-\tau^2}{2}\log\left[\frac{(1+\tau^2+x^2+\zeta^2)(1-\tau^2)-2x^2\tau^2}{2\zeta^2(1+\tau^2)}\right]\right\} , \tag{34}$$

388

where ζ^2 is given by Eq. (29).

The function $h^{(1/2)}(x, \gamma)$ has the following properties:

$$h^{(1/2)}(0, \tau) = \frac{1}{2(1+\tau^2)^2}\left\{-\tau^2 + \tau \tan^{-1}\left(\frac{2\tau}{1-\tau^2}\right) - \frac{1-\tau^2}{2}\log(1+\tau^2)\right\},\qquad (35)$$

$$h^{(1/2)}(x, \tau) \approx \frac{\tau^2}{4}\frac{1}{(1+x^2)^2}, \qquad \tau \ll 1. \qquad (36)$$

The properties of $h^{(1/2)}$ as well as $h^{(3/2)}$ and $h^{(5/2)}$ for large γ will not be considered here because they have little physical significance in this range for reasons to be stated near the end of this section. This limitation applies also to $y^{(1/2)}$, $y^{(3/2)}$, and $y^{(5/2)}$; however, the behavior of these functions is considered for large γ because of its intrinsic interest.

The functions $y^{(1/2)}(x, \gamma)$ and $h^{(1/2)}(x, \gamma)$ are presented in Tables I and II, respectively.

The maximum value of $h^{(1/2)}(x, \gamma)$ occurs at $x = 0$ and $\gamma = \gamma_m^{(1/2)} = 1.10$ and has a value $h_m^{(1/2)} = h^{(1/2)}(0, \gamma_m^{(1/2)}) = 0.07222$.

Case (2), $\nu = 3/2$

The solution for this case is

$$y^{(3/2)}(x, \tau) = -\frac{1}{\xi}\zeta^2 \qquad (37)$$

where ζ^2 is given by Eq. (29). Some properties of $y^{(3/2)}(x, \gamma)$ are:

$$y^{(3/2)}(0, \tau) = \frac{\tau}{1+\tau^2}; \qquad (38)$$

$$y^{(3/2)}(x, \tau) \approx \frac{\tau}{(1+x^2)^{3/2}}, \qquad \tau \ll 1; \qquad (39)$$

71

Table I. - The function $y^{(1/2)}(x, \gamma)$.

$$x = r/R, \qquad \gamma = ct/R$$

x \ γ	0.4	0.8	1.2	1.6	2.0	4.0
0	0.3805	0.6749	0.8762	1.012	1.178	1.326
0.2	.3746	.6688	.8721	1.010	1.177	1.325
.4	.3555	.6514	.8599	0.9990	1.172	1.325
.6	.3348	.6235	.8392	.9887	1.163	1.323
.8	.3108	.5875	.8101	.9696	1.152	1.321
1.0	.2808	.5464	.7732	.9437	1.136	1.318
1.2	.2553	.5040	.7300	.9109	1.114	1.315
1.4	.2324	.4629	.6824	.8714	1.087	1.311
1.6	.2122	.4250	.6341	.8259	1.054	1.306
1.8	.1946	.3908	.5877	.7772	1.013	1.300
2.0	.1793	.3606	.5445	.7273	0.9666	1.293
2.4	.1542	.3104	.4701	.6337	.7966	1.274
2.8	.1348	.2714	.4108	.5549	.7034	1.248
3.2	.1196	.2403	.3636	.4908	.6228	1.210
3.6	.1069	.2155	.3256	.4388	.5563	1.156
4.0	.0971	.1950	.2944	.3964	.5016	1.082

Table II. The function $h^{(1/2)} (x, \tau)$.

$$x = r/R, \qquad \tau = ct/R$$

x \ τ	0.1	0.8	1.2
0.2	0.02886	0.06249	0.07130
.4	.02436	.05827	.06884
.6	.01883	.05048	.06456
.8	.01358	.04132	.05854
1.0	.00955	.03191	.05095
1.2	.00656	.02372	.04237
1.4	.00455	.01719	.03375
1.6	.00315	.01237	.02601
1.8	.00224	.00894	.01961
2.0	.00160	.00652	.01460
3.0	.00042	.00170	.00383
4.0	.00013	.00060	.00130

73

$$y^{(3/2)}(x,\tau) \simeq \frac{\tau}{x^6}, \qquad \frac{\tau}{x} \ll 1, \quad x \gg 1; \tag{40}$$

$$y^{(3/2)}(x,\tau) \simeq \frac{1}{\tau}\left(1 - \frac{1}{\tau_2} + \frac{x^2}{2\tau_2}\right), \quad \frac{x}{\tau} \ll 1, \quad \tau \gg 1. \tag{41}$$

The function $h^{(3/2)}(x, \tau)$ takes the form

$$h^{(3/2)}(x,\tau) = \frac{1}{8}\left\{\frac{1}{2\tau^2}\left(1 - \frac{1+x^2-\tau^2}{\zeta^2}\right) - \frac{(1+x^2+\tau^2)^2 - 4x^2}{\zeta^3}\right\}, \tag{42}$$

where ζ^2 is given by Eq. (29).

The function $h^{(3/2)}(x, \tau)$ has the following properties:

$$h^{(3/2)}(0,\tau) = \frac{1}{8} \frac{9\tau^2 + 2\tau^4 + \tau^6}{(1+\tau^2)^4}, \tag{43}$$

$$h^{(3/2)}(x,\tau) \simeq \frac{9\tau^2}{8(1+x^2)^4}, \qquad \tau \ll 1. \tag{44}$$

The functions $y^{(3/2)}(x, \tau)$ and $h^{(3/2)}(x, \tau)$ are presented in Tables III and IV, respectively.

The maximum value of $h^{(3/2)}(x, \tau)$ occurs at $x = 0$ and $\tau = \tau_m^{(3/2)} = 0.578$ and has a value $h_m^{(3/2)} = h^{(3/2)}\left(0, \tau_m^{(3/2)}\right) = 0.1315$.

Case (3). $= 5/2$

The solution for this case is

$$y^{(5/2)}(x,\tau) = \frac{1}{2\zeta^6}\left\{\tau\left(1-x^2+\tau^2\right)\sqrt{\frac{1}{2}\left(\zeta^2+1+x^2-\tau^2\right)}\right. \tag{45}$$

$$\left. + \left[2-3(x^2+\tau^2) + (x^2-\tau^2)^2\right]\sqrt{\frac{1}{2}\left(\zeta^2-1-x^2+\tau^2\right)}\right\},$$

where as before ζ^2 is given by Eq. (29). Some properties of $y^{(5/2)}(x, \tau)$ are

$$y^{(5/2)}(0,\tau) = \frac{\tau}{(1-\tau^2)^2}\left(1 + \frac{1}{2}\tau^2\right); \tag{46}$$

TABLE III. – The function $y^{(3/2)}(x, \Upsilon)$.

$x = r/R,$ $\quad \Upsilon = ct/R$

x \ Υ	0.4	0.8	1.2	1.6	2.0	4.0
0	0.3448	0.4878	0.4918	0.4494	0.4000	0.2353
0.2	.3306	.4792	.4892	.4910	.4003	.2355
.4	.2925	.4531	.4805	.4478	.4012	.2361
.6	.2413	.4099	.4638	.4446	.4022	.2372
.8	.1891	.3529	.4363	.4378	.4029	.2387
1.0	.1438	.2896	.3960	.4248	.4022	.2407
1.2	.1080	.2290	.3440	.4025	.3985	.2431
1.4	.0813	.1771	.2861	.3685	.3891	.2460
1.6	.0617	.1359	.2297	.3275	.3713	.2495
1.8	.0474	.1046	.1807	.2721	.3425	.2534
2.0	.0369	.0812	.1410	.2212	.3031	.2579
2.4	.0234	.0507	.0870	.1392	.2108	.2680
2.8	.0156	.0333	.0560	.0879	.1351	.2786
3.2	.0108	.0229	.0377	.0578	.0868	.2849
3.6	.0078	.0163	.0265	.0396	.0579	.2748
4.0	.0058	.0120	.0193	.0283	.0403	.2331

TABLE IV. The function $h^{(3/2)}(x, \gamma)$.

$x = r/R$, $\gamma = ct/R$

x \ γ	0.4	0.8	1.2
0.2	0.09319	0.11452	0.07051
.4	.06886	.10319	.06927
.6	.04248	.08451	.06647
.8	.02280	.06128	.06105
1.0	.01122	.03897	.05199
1.2	.00530	.02214	.03973
1.4	.00251	.01167	.02680
1.6	.00120	.00594	.01617
1.8	.00061	.00302	.00904
2.0	.00031	.00156	.00487
3.0	.00002	.00009	.00 6
4.0	0	.00001	.00003

$$y^{(5/2)}(x,\tau) \simeq \frac{\tau}{(1+x^2)^{5/2}}, \qquad \tau \ll 1; \tag{47}$$

$$y^{(5/2)}(x,\tau) \simeq \frac{\tau}{x^5}, \qquad \frac{\tau}{x} \ll 1, \ x \gg 1; \tag{48}$$

$$y^{(5/2)}(x,\tau) \simeq \frac{1}{2\tau}\left(1+\frac{1}{\tau^2}+\frac{x^2}{2\tau^2}\right), \ \frac{x}{\tau} \ll 1, \ \tau \gg 1. \tag{49}$$

The function $h^{(5/2)}(x,\tau)$ takes the form

$$h^{(5/2)}(x,\tau) = \frac{1+3\tau^2}{96\,\xi^7}\left(1-\frac{w^2}{\xi^2}\right) - \frac{1+\frac{3}{2}\tau^2}{48\,\xi^2}\frac{w^2}{\xi^6} + \frac{1}{18\,\xi^6} - \frac{1}{72\,\xi^8}(w^4-4\tau^2)$$

$$- \frac{1}{18\,\xi^{12}}\left(w^6+6\tau^2 w^4 - 12\tau^2 w^2 - 8\tau^4\right) \tag{50}$$

$$- \frac{1}{16\,\xi^{16}}\left[(1-\tau^2)(w^8-24\tau^2 w^4+16\tau^2)+16\tau^2 w^6-64\tau^4 w^2\right],$$

where

$$w^2 = 1 + x^2 - \tau^2;$$

and where, again, ξ^2 is given by Eq. (29).

The function $h^{(5/2)}(x,\tau)$ has the following properties:

$$\left.\begin{aligned}
h^{(5/2)}(0,\tau) &= \frac{1+3\tau^2}{48\tau^2(1+\tau^2)} - \frac{(1+\frac{3}{2}\tau^2)(1-\tau^2)}{48\tau^2(1+\tau^2)^3} + \frac{1}{18(1+\tau^2)^3} - \frac{(1-5\tau^2)}{72(1+\tau^2)^4} \\
&\quad - \frac{1-9\tau^2-5\tau^4+5\tau^6}{18(1+\tau^2)^6} - \frac{1+3\tau^2-46\tau^4+30\tau^6+13\tau^8-\tau^{10}}{18(1+\tau^2)^8}
\end{aligned}\right\} \tag{51}$$

$$h^{(5/2)}(x,\tau) = \frac{25}{12}\frac{\tau^2}{(1+x^2)^5}, \qquad \tau \ll 1. \tag{52}$$

The functions $y^{(5/2)}(x,\tau)$ and $h^{(5/2)}(x,\tau)$ are presented in Tables V and VI, respectively.

TABLE V. The function $y^{(5/2)}(x,\gamma)$.

$$x = r/R, \quad \gamma = ct/R$$

x \ γ	0.2	0.3	0.4	0.5	0.8	1.2	1.6	2.0	4.0
0	0.1874	0.2601	0.3131	0.3385	0.3609	0.2983	0.2340	0.1867	0.0877
0.2	.1717	.2410	.2940	.3300	.3547	.2986	.2351	.1875	.0878
.4	.1339	.1931	.2438	.2814	.3341	.2983	.2393	.1902	.0882
.6	.0923	.1363	.1801	.2190	.2957	.2944	.2430	.1945	.0888
.8	.0589	.0917	.1168	.1537	.2407	.2815	.2475	.2004	.0898
1.0	.0362	.0559	.0773	.1006	.1786	.2541	.2490	.2074	.0910
1.2	.0214	.0344	.0480	.0639	.1224	.2110	.2423	.2143	.0926
1.4	.0137	.0224	.0298	.0395	.0797	.1597	.2223	.2182	.0946
1.6	.0086	.0134	.0187	.0248	.0507	.1215	.1874	.2149	.0970
1.8	.0055	.0086	.0120	.0156	.0323	.0739	.1438	.1993	.1000
2.0	.0037	.0055	.0079	.0104	.0208	.0478	.1017	.1697	.1040
2.4	.0017	.0026	.0036	.0048	.0092	.0202	.0445	.0937	.1130
2.8	.0009	.0013	.0018	.0024	.0044	.0092	.0192	.0417	.1261
3.2	.0005	.0007	.0010	.0012	.0023	.0046	.0080	.0182	.1437
3.6	.0003	.0003	.0006	.0007	.0013	.0024	.0045	.0085	.1437
4.0	.0002	.0003	.0003	.0004	.0007	.0014	.0024	.0043	.1226

TABLE VI. – The function $h^{(5/2)}(x, \gamma)$.

$x = r/R$, $\gamma = ct/R$

x \ γ	0.2	0.4	0.6	0.8	1.0
0	0.04154	0.10817	0.12207	0.09100	0.04867
0.2	.03359	.09648	.11495	.08913	.04859
.4	.02204	.06755	.09361	.08227	.04821
.6	.00888	.03691	.06281	.06805	.04689
.8	.00627	.01660	.03380	.04921	.04333
1.0	.00273	.00689	.01219	.02754	.03592
1.2	.00162	.00302	.00622	.01214	.02479
1.4	.00135	.00157	.00277	.00511	.01406
1.6	.00080	.00096	.00133	.00221	.00661
1.8	.00060	.00066	.00062	.00109	.00286
2.0	.00045	.00057	.00056	.00064	.00129
3.0	.00012	.00013	.00013	.00013	.00015
4.0	.00005	.00005	.00006	.00005	.00007

79

The maximum value of $h^{(5/2)} (x, \gamma)$ occurs at $x = 0$ and $\gamma = \gamma_m^{(5/2)} = 0.513$ and has a value $h_m^{(5/2)} = h^{(5/2)}\left(0, \gamma_m^{(5/2)}\right) = 0.1253$.

It is perhaps interesting to note that the function $y^{(\nu)} (x, \gamma)$ giving the plate profile as a function of time approaches a nonvanishing constant value for $\nu = 1/2$ as the time becomes infinite, but approaches zero for $\nu = 3/2, 5/2$. This behavior is presumably related to the fact that the velocity distribution given by $g^{(\nu)} = (1 + x^2)^{-\nu}$ corresponds to an infinite kinetic energy for $\nu = 1/2$ and to a finite kinetic energy for $\nu > 1/2$. Also it may be noted that the central part of the plate remains concave downward for all time in the case of $\nu = 1/2$, whereas it becomes convex downward after some time in the case of $\nu = 3/2, 5/2$. These remarks apply only to a membrane under constant tension and are perhaps somewhat academic on that account. A real material is subject to stress relief when the rate of strain changes sign; consequently, the behavior of the functions $y^{(\nu)} (x, \gamma)$ and $h^{(\nu)} (x, \gamma)$ is significant only in the interval $0 \leq \gamma \leq \gamma_c^{(\nu)}$ of the reduced time where $\gamma_c^{(\nu)}$ is the value of the reduced time at which the rate of strain first changes sign at any point on the plate. At a given point x on the plate, the rate of strain changes sign at a value of γ given by $\partial h^{(\nu)} (x, \gamma)/\partial \gamma = 0$. It will be stated but not proved here that the rate of strain changes sign first at the center $x = 0$ (this behavior is illustrated in the tables); consequently $\gamma_c^{(\nu)}$ is given by $\partial h^{(\nu)} (0, \gamma)/\partial \gamma = 0$. Thus the time of maximum central strain is equal to the time at which the rate of strain first changes sign anywhere, or, in short, $\gamma_c^{(\nu)} = \gamma_m^{(\nu)}$.

Although $y^{(\nu)}$ (x, γ) is evidently discontinuous with respect to ν for $\gamma = \infty$, both $y^{(\nu)}$ (x, γ) and $h^{(\nu)}(x, \gamma)$ are analytic in ν for finite values of γ. Furthermore, it is hoped that these functions are so related to ν that three-point interpolation with respect to ν (constant x and γ) among $\nu = 1/2$, $3/2$, $5/2$ gives adequate accuracy for functions at intermediate values of ν when $0 \leq \gamma \leq 4$, say. The intermediate value of $3/4$ for ν is of particular interest here. In Table VII and Figure 1 the interpolated function $y^{(3/4)}$ (x, γ) is presented numerically and graphically, respectively. This function gives the behavior of the plate profile (if there is no stress relief) when the plate has an initial velocity distribution given by $g^{(3/4)}$ $(x) = (1 + x^2)^{-3/4}$. In Table VIII and Figure 2 the interpolated function $h^{(3/4)}$ (x, γ) is presented. This function gives the strain distribution as a function of time (if, again, there is no stress relief). In the case of a real plate subject to stress relief, both of the functions $y^{(3/4)}$ and $h^{(3/4)}$ give the correct behavior—within the approximations inherent in the general theory—of the profile and strain distribution up to the time of maximum central strain.

By three-point interpolation it is found that $h_m^{(3/4)} = 0.0932$ and $\gamma_m^{(3/4)} = 0.927$.

The foregoing treatment of the structural behavior of a plastic plate is exact within the limits of the general theory for the special forms of the initial velocity distribution considered. When the initial velocity distribution is due to an underwater explosion, one has to treat a hydrodynamical problem made quite formidable by cavitation and finite amplitude effects. In the next section only a very crude attempt is made

TABLE VII. – Ine function $y^{(3/4)}(x,\gamma)$.

$$x = r/R, \qquad \gamma = ct/R$$

γ / x	0.4	0.8	1.2	1.6	2.0	4.0
0	0.3712	0.6225	0.7622	0.8389	0.9306	0.9649
0.2	.3629	.6153	.7583	.8370	.9297	.9643
.4	.3384	.5944	.7466	.8292	.9268	.9646
.6	.3084	.5608	.7261	.8206	.9208	.9637
.8	.2757	.5174	.6961	.8046	.9134	.9629
1.0	.2399	.4686	.6568	.7818	.9019	.9617
1.2	.2103	.4195	.6098	.7511	.8857	.9607
1.4	.1853	.3738	.5580	.7122	.8633	.9591
1.6	.1645	.3336	.5062	.6660	.8338	.9571
1.8	.1473	.2992	.4578	.6156	.79 \	.9546
2.0	.1331	.2702	.4146	.5645	.7510	.9516
2.4	.1111	.2250	.3447	.4726	.6062	.9431
2.8	.0953	.1923	.2932	.4008	.5168	.9292
3.2	.0831	.1675	.2547	.3466	.4450	.9056
3.6	.0735	.1484	.2250	.3049	.3896	.8647
4.0	.0662	.1332	.2015	.2723	.3464	.8004

82

400

FIGURE 1 – The function $y^{(3)}_2(z, \tau)$ versus z for various values of τ.

PX3-108

TABLE VIII.   The function $h^{(3/4)}$ (x, γ).

$$x = r/R, \qquad \gamma = ct/R$$

x \ γ	0.4	0.8	1.2
0.2	0.05066	0.08276	0.07308
.4	.03978	.07567	.07096
.6	.02748	.06372	.06705
.8	.01733	.04931	.06106
1.0	.01053	.03541	.05281
1.2	.00634	.02411	.04286
1.4	.00394	.01274	.03693
1.6	.00250	.01051	.02352
1.8	.00168	.00709	.01656
2.0	.00113	.00490	.01159
3.0	.00027	.00114	.00261
4.0	.00008	.00039	.00086

402

FIGURE 2 – The function $h^{(3)}(x, \tau)$ versus x for various values of τ.
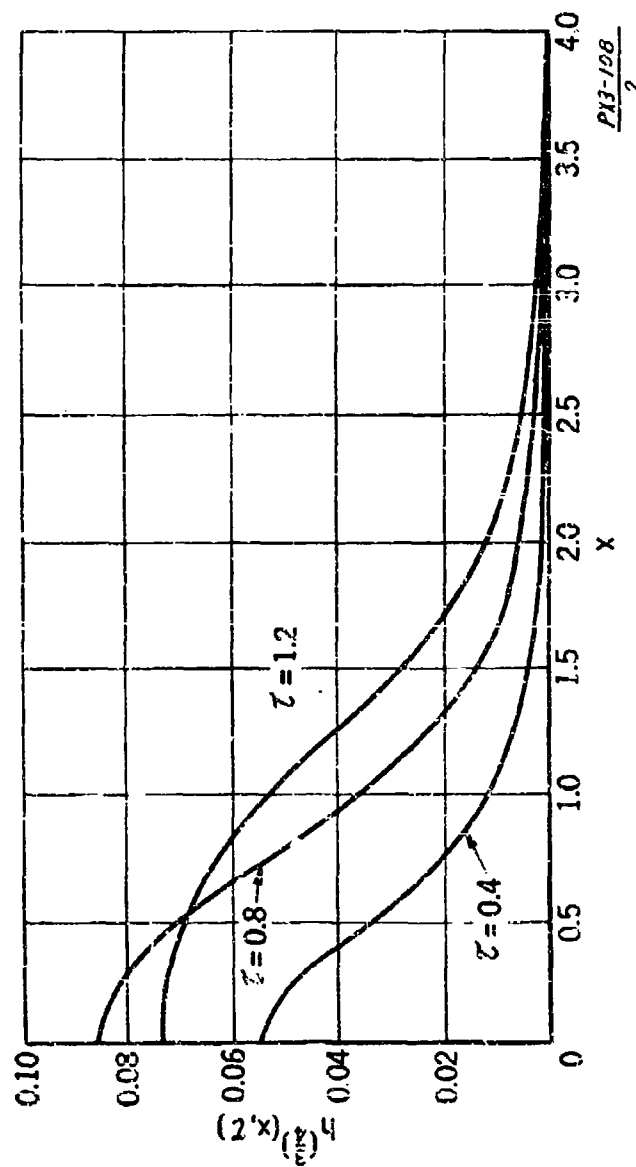
to solve this hydrodynamical problem in conjunction with the results
of the present section. Hence the accuracy of the structural part
of the final results in the next section is somewhat masked by the
uncertainties in the hydrodynamical part, perhaps thereby causing the
results of the present section to seem overly elaborate. However, it
is hoped that the results of the present section may be more fully
utilized when a more successful attack is made upon the associated
hydrodynamical problem.

4. Application to damage by underwater explosions

In this section the foregoing theory is applied to the case
of an infinite thin plate loaded by an underwater explosion wave. It
is assumed that the plate is backed by air, and, further, that the
underwater pressure wave impinging upon the front surface is of suffi-
ciently short duration to cause well-developed cavitation within a
relatively short period of time, that is, short compared with the time
of deformation. Under these assumptions the plate may be treated ap-
proximately as moving freely with an initial velocity distribution
related to the properties of the explosive.

The problem of determining the loading from the properties
of the explosion wave--that is, determining the actual pressure acting
on the plate from the free field pressure in the incident wave--has not
been solved. The problem is complicated by cavitation and in some cases
by nonacoustical effects due to finite amplitude. In the absence of any
solution, the procedure will be based on certain ad hoc semi-empirical
assumptions. It is assumed that the energy delivered to a plate element

is a constant fraction of the energy incident in the solid angle subtended by that element. It is also assumed that in passing from the explosive to a plate element the energy flux density decreases as the inverse square of the distance.[2] Using this assumption and also taking

---

[2] The fact that the energy-distance curve in air explosions is approximately inverse square for several charge radii suggests the possibility of an analogous situation existing in underwater explosions. Since the central strain depends critically only on the plate profile near the center ($r < 2R$, say) it would seem that the assumption of inverse-square attenuation of the energy might be a good approximation.

---

account of the oblique angle of incidence on off-center elements, one obtains a surface density of kinetic energy in the plate proportional to $(R^2 + r^2)^{-3/2}$, where r is the radius and R is the distance between the charge center and the middle surface of the plate. Since the velocity of sound in water is much greater than the velocity of transverse plastic waves in the plate, it is assumed that the energy can be treated as though it were delivered to all parts of the plate at the same instant. Consequently, under these assumptions the initial velocity distribution is given by

$$\frac{\partial z}{\partial t}(r,0) \propto c\alpha \frac{\partial y^{(3/4)}}{\partial \tau}(x,0) = \frac{c\alpha}{(1+x^2)^{3/4}}, \tag{53}$$

where $x = r/R$, $y = z/R$, and $\gamma = ct/R$, the quantities z and t being the vertical displacement and the time, respectively. The quantity c is, as before, the velocity of transverse plastic waves in the plate. The expansion parameter α will be assigned a value on the basis of the amount of energy delivered to the plate. Equating the fraction γ of the

total energy of explosion E to the initial kinetic energy of the
plate gives the following value for α^2:

$$\alpha^2 = \frac{1}{\pi} \frac{\gamma E}{\sigma_0 a_0 R^2},\qquad (54)$$

where a_0 is the initial thickness of the plate and σ_0 is the yield
stress of same.

Beyond the assumption that it is a constant, the energy
fraction γ will be treated as an empirical constant. If the energy
delivery were 100 percent efficient in each element of solid angle
cutting the plate, γ would equal $1/2$, since the plate subtends a solid
angle of 2π out of a maximum of 4π. If the energy delivery were
50 percent efficient, corresponding roughly to utilization of only the
primary shock-wave energy, then γ would equal $1/4$, and so forth. These
statements are offered only as a guide in interpreting the empirical
values of γ to be obtained.

The distribution of strains is given by

$$\varepsilon_1 = \varepsilon_2 = \frac{\alpha^2}{2} h^{(3/4)}(x,\tau),\qquad (55)$$

with α^2 given by Eq. (54), and where ε_1 and ε_2 are the meridional
and circumferential strains, respectively. The function $h^{(3/4)}(x,\tau)$
is discussed and tabulated in Sec. 3. The maximum central strains are
given by

$$\varepsilon_1 = \varepsilon_2 = \varepsilon_m = \frac{\alpha^2}{2} h_m^{(3/4)}.\qquad (56)$$

The dimensionless constant $h_m^{(3/4)}$ is equal to 0.0932. The criterion
of rupture, the principal thing of interest here, is then given by the

scheme:

$$\text{Rupture:} \quad \xi_m > \xi_c \, , \\ \text{No Rupture:} \quad \xi_m < \xi_c, \quad \Bigg\} \qquad (57)$$

where ξ_c is the critical rupture strain and is an intrinsic property of the material. Combination of Eqs. (54) and (56) with the critical condition for rupture, $\xi_c = \xi_m$, leads to the result

$$\xi_c = \frac{1}{2\pi} h_m^{(3/4)} \frac{\gamma E}{\sigma_0 a_0 R^2} \, , \qquad (58)$$

giving the conditions under which rupture just occurs. Introducing $\underline{\xi}$, the energy per unit weight of explosive, and $\underline{N}$, the weight of explosive, Eq. (58) may be rewritten:

$$\xi_c = \frac{1}{2\pi} h_m^{(3/4)} \gamma \xi \left(\frac{\sigma_c a_c}{W^{1/3}} \right)^{-1} \left(\frac{R}{W^{1/3}} \right)^{-2}. \qquad (59)$$

It is of interest to determine the minimum weight $\underline{W}$ of a spherical charge of a given explosive causing rupture when exploding in contact with a plate of thickness a_0 and yield stress σ_0. In this case the distance $\underline{R}$ between the middle surface of the plate and the charge center is equated to the sum of the charge radius and one-half of the plate thickness with the result:

$$R = \left(\frac{3W}{4\pi \rho_e} \right)^{1/3} + 1/2 a_0, \qquad (60)$$

where ρ_e is the density of loading of the explosive. Substituting Eq. (60) into Eq. (59) the desired relation between a_0, σ_0, and $\underline{W}$ is obtained in the form

$$\varepsilon_c = \frac{1}{2\pi} h_m^{(3/4)} \frac{\gamma \xi}{\sigma_o} \left(\frac{a_o}{W^{1/3}} \right)^{-1} \left[\left(\frac{3}{4\pi \rho_c} \right)^{1/3} + \frac{1}{2} \frac{a_c}{W^{1/3}} \right]^{-2}. \tag{61}$$

Experiments on the rupture of steel plates by the contact explosion of loose Tetryl charges have been conducted at the David Taylor Model Basin, and some data obtained therefrom have been kindly supplied to the author by Commander C. H. Gerlach of the Bureau of Ships. The comparison of the results of Eq. (61) with these data is restricted to the case of single-ply steel plates, the applicability of the theory to laminated plates being uncertain. The value of the energy fraction γ, adjusted to bring Eq. (61) and experimental data into agreement as regards the relation between the charge weight W and the plate thickness a_o, is used as a criterion of comparison. Using $h_m^{(3/4)} = 0.0932$, $\xi = 1.02$ kcal/gm, (for loose Tetryl), and $\mathcal{E}_c = 0.25$, Eq. (61) may be specialized to

$$\varepsilon_c \approx 4.24 \gamma \left(\frac{a_o}{W^{1/3}} \right)^{-1} \left(1.875 \rho_c^{-1/3} + \frac{1}{2} \frac{a_c}{W^{1/3}} \right)^{-2}, \tag{62}$$

giving γ as a function of $a_o/W^{1/3}$ and σ_o. In Eq. (62) and henceforth a_o is expressed in inches, W in pounds, and σ_o in pounds per square inch. In Table IX are tabulated values of γ along with the experimental values of a_o and W from which they were calculated. The yield stress σ_o assumed for each kind of steel is also tabulated.

It is seen that the values of γ given in Table IX vary from roughly 0.1 to 0.3 in the order of increasing thickness. It might be

TABLE IX. -- Values of the energy fraction bringing the theoretical and experimental results into agreement

$$\rho_d = 0.90$$

Plate thickness, a_0 (in.)	Type of steel*	Yield stress, $\overline{y_0}$ (lb/in.)	Charge weight, $\underline{w}$ (lb)	$a_0/w^{1/3}$	Energy fraction $\underline{x}$
0.500	MC	60,000	0.219	0.83	0.260
.500	MS	60,000	.234	.81	.250
.500	GLS	75,000	.310	.74	.280
.500	HTS	100,000	.250	.63	.300
.500	MS	60,000	.125	1.00	.330
.500	MS	60,000	.188	.87	.280
.500	MS	60,000	.234	.81	.250
.375	MS	60,000	.187	.66	.188
.375	MS	60,000	.188	.66	.188
.250	GLS	75,000	.154	.54	.183
.250	MS	60,000	.110	.52	.141
.125	MS	60,000	.0485	.36	.0915
.125	GLS	75,000	.0551	.39	.120
.125	MS	60,000	.0485	.36	.0915
.125	MS	60,000	.0485	.36	.0915
.125	MS	60,000	.0584	.39	.0985
.125	MS	60,000	.0595	.39	.0992
.0625	HTS	100,000	.0198	.27	.108

*MS, mild steel; HTS, high tensile steel; GLS, Great Lakes steel.

supposed that this variation is due to cavitation; however, quantitative estimates of the cavitation effect based upon the Taylor cavitation time show no such dependence on the plate thickness. The larger values of $\underline{\gamma}$ are of reasonable magnitude and thus the comparison with experiment may be considered a partial verification of the treatment of strain used here since the alternative treatment based upon normal motion leads to unreasonably small values of $\underline{\gamma}$ (about one-tenth as large). From the standpoint of predicting rupture, the theory as it stands cannot be considered very satisfactory.

The theory is by no means limited to contact explosions, nor is it limited to infinite plates. The essential restriction on its application is that the charge distance and the distance from the point of attack to the nearest edge be so related that a transverse plastic wave starting from the nearest edge does not reach the point of attack during the rupture process. This condition may be stated in the form

$$\frac{r_e}{R} > \gamma_m^{(3/4)} = 0.927, \tag{62}$$

where r_e is the distance to the nearest edge.

APPENDIX A

DERIVATION OF THE EQUATIONS OF MOTION OF THIN PLATES
SUBJECT TO AXIALLY SYMMETRIC DEFORMATIONS

In Part I, Section 2 (Eqs. (1) and (2)), the equations of motion
of thin plates were stated without proof. Here we give an elementary der-
ivation of these equations employing a procedure similar to that used by
M. P. White[1] for the case of static equilibrium.

We now consider the geometrical descrip-
tion of the deformation. Strictly speaking, the position of a particle in
the deformed plate is described by the Euler coordinates (r, ϕ, x) which
are related by a time-dependent transformation to the initial or Lagrange
coordinates (r_o, ϕ_o, x_o) of the particle. Since we consider only
axially symmetric loading, there is no dependence on ϕ. Since the plate
is very thin, we shall employ the plane stress approximation, and neglect
bending. We now write for points on the middle section,

$$r = r(r_o, t),$$
$$x = x(r_o, t).$$

Holding t constant, these expressions are the parametric equation of the
surface of the plate. Holding r_o constant in the above expressions we ob-
tain the parametric equations of the trajectory of a particle whose radial
Lagrange coordinate is r_o. The radial and vertical components of the ac-
celeration of an element of the plate are consequently denoted by $(\partial^2 r/\partial t^2)_{r_o}$
and $(\partial^2 x/\partial t^2)_{r_o}$ respectively.

Before going to the derivation of the equation of motion, we make
the assumption that the diaphragm is sufficiently thin for the bending stresses

---

[1] M. P. White, Div. 2 report, A-167.

to be neglected in comparison with the membrane stresses. Since the former
is proportional to the cube of the thickness while the latter is propor-
tional to the first power, the above assumption is applicable to thin dia-
phragms. There is another assumption (seldom mentioned because it is ob-
viously valid for practically all cases of interest) that the time of
travel of a wave front through the thickness of the diaphragm is very small
compared with the decay time of the incident shock wave.

Taking advantage of the axial symmetry we consider the forces act-
ing on an infinitesimal segment of the circumferential strip included be-
tween r, $r + dr$, ϕ, and $\phi + d\phi$. We make use of the unit basis vec-
tors $\vec{1}_z$, $\vec{1}_r$, $\vec{n}$, and $\vec{e}$ which are related to each other as
follows:

$$\vec{n} = \vec{1}_r \sin\vartheta + \vec{1}_z \cos\vartheta,$$
$$\vec{e} = \vec{1}_r \cos\vartheta - \vec{1}_z \sin\vartheta,$$
(A-1)

where ϑ is the angle between $\vec{n}$ and $\vec{1}_z$ and is given by

$$\vartheta = -\tan^{-1}\left(\partial z / \partial r\right)_z.$$
(A-2)

Before proceeding further we assume that two of the principal stresses σ_1
and σ_2 are in the meridional ($\vec{e}$) and circumferential ($\vec{e} \times \vec{n}$) directions
respectively and that the third principal stress in the normal direction
($\vec{n}$) may be neglected in comparison with the first two. The force acting
on the element included between r, $r + dr$, ϕ, and $\phi + d\phi$, due to cir-
cumferential tension is

$$d\vec{f}_c \, d\phi = -\vec{1}_r \cos\vartheta \cdot 2 \sigma_2 \, dr \, d\phi.$$
(A-3)

The force due to the incident pressure p is

$$d\vec{f}_p \, d\phi = \vec{n} \sec\vartheta \, p \, r \, dr \, d\phi.$$
(A-4)

412

The force acting at r due to meridional tension is

$$\vec{f}_m(r)d\phi = \vec{e} \, r a \, \sigma_1 d\phi. \tag{A-5}$$

The acceleration of the element is

$$\vec{a} = \vec{1}_r \left(\frac{\partial^2 r}{\partial t^2}\right)_{r_o} + \vec{1}_z \left(\frac{\partial^2 z}{\partial t^2}\right)_{r_o}, \tag{A-6}$$

and the mass is

$$dm \, d\phi = a \cos\vartheta \, a \, \rho \, r \, dr \, d\phi. \tag{A-7}$$

Equating the total force and the product of mass and acceleration we obtain

$$\vec{f}_m(r+dr) - \vec{f}_m(r) + d\vec{f}_c + d\vec{f}_p = \vec{a} \, dm \tag{A-8}$$

after division by $d\phi$.

Substituting (A-3), (A-4), (A-5), (A-6), and (A-7) into (A-8) and taking the vertical ($\vec{1}_z$) and meridional ($\vec{e}$) components then dividing by r we obtain

$$\rho a \cos\vartheta \, a_z + \frac{1}{r} \frac{\partial}{\partial r} \left(r \sigma_1 a \sin\vartheta\right) = p, \tag{A-9}$$

$$\rho a \cos\vartheta \, a_1 - \frac{1}{r} \frac{\partial}{\partial r} \left(r \sigma_1 a\right) + \frac{\sigma_2 a}{r} = 0, \tag{A-10}$$

where

$$a_z = \vec{1}_z \cdot \vec{a} = \left(\frac{\partial^2 z}{\partial t^2}\right)_{r_o}, \tag{A-11}$$

$$a_1 = \vec{e} \cdot \vec{a} = \cos\vartheta \left(\frac{\partial^2 r}{\partial t^2}\right)_{r_o} - \sin\vartheta \left(\frac{\partial^2 z}{\partial t^2}\right)_{r_o}. \tag{A-12}$$

With the aid of Eq. (A-2), the trigonometric functions of ϑ may be expressed in the form

93

$$\sin \mathcal{V} = - \frac{\frac{\partial z}{\partial r}}{\sqrt{1 + \left(\frac{\partial z}{\partial r}\right)^2}} , \qquad (A-13)$$

$$\cos \mathcal{V} = \frac{1}{\sqrt{1 + \left(\frac{\partial z}{\partial r}\right)^2}} . \qquad (A-14)$$

The substitution of these expressions into (A-9) and (A-10) gives Eqs. (1) and (2) of Part I.

To complete the derivation, we must find explicit expressions for a_z and a_r. Introducing the radial displacement $u = r - r_0$ we may write

$$\left(\frac{\partial}{\partial t}\right)_{r_0} = \frac{\partial}{\partial t} + \left(\frac{\partial u}{\partial t}\right)_{r_0} \frac{\partial}{\partial r} , \qquad (A-15)$$

$$\left(\frac{\partial^2}{\partial t^2}\right)_{r_0} = \frac{\partial^2}{\partial t^2} + 2\left(\frac{\partial u}{\partial t}\right)_{r_0} \frac{\partial^2}{\partial r \partial t} + \left(\frac{\partial u}{\partial t}\right)_{r_0}^2 \frac{\partial^2}{\partial r^2} + \left(\frac{\partial^2 u}{\partial t^2}\right)_{r_0} \frac{\partial}{\partial r} , \quad (A-16)$$

in which the partial differentiations with respect to r and t are understood to be performed at constant t and r, respectively. Operating on u by (A-15) and (A-16) we obtain after some manipulation

$$\left(\frac{\partial u}{\partial t}\right)_{r_0} = \frac{\frac{\partial u}{\partial t}}{1 - \frac{\partial u}{\partial r}} , \qquad (A-17)$$

$$\left(\frac{\partial^2 u}{\partial t^2}\right)_{r_0} = \frac{D^2 u}{1 - \frac{\partial u}{\partial r}} , \qquad (A-18)$$

where

$$D^2 = \frac{\partial^2}{\partial t^2} + 2 \frac{\frac{\partial u}{\partial t}}{1 - \frac{\partial u}{\partial r}} \frac{\partial^2}{\partial r \partial t} + \left(\frac{\frac{\partial u}{\partial t}}{1 - \frac{\partial u}{\partial r}}\right)^2 \frac{\partial^2}{\partial r^2} . \qquad (A-19)$$

(A-13)

(A-14)

(1)

for

te

(A-15)

(A-16)

der-

on u

(A-17)

(A-18)

(A-19)

Inserting these results in (A-16) we get

$$\left(\frac{\partial^2}{\partial 6^2}\right)_{r_0} = D^2 + \frac{(D^2 u)}{1 - \frac{\partial u}{\partial r}} \frac{\partial}{\partial r} \cdot \qquad (A-20)$$

The substitution of (A-20) along with (A-13) and (A-14) into (A-11) and (A-12) yields Eqs. (3) and (4) of Part I.

APPENDIX B

DETAILS OF THE SOLUTION IN SECTION 2, PART IV

The equation of motion (3), Part IV, to be solved is,

$$(1 + \lambda O) \frac{\partial^2 z}{\partial t^2} - \omega_o^2 \frac{1}{x} \frac{\partial}{\partial x}\left(x \frac{\partial z}{\partial x}\right) = \frac{P_o(t)}{\rho a_o} , \qquad (B-1)$$

where

$$\omega_o^2 = \sigma_o'/\rho R_o^2 , \qquad \lambda = R_o \rho_o /a_o \rho ,$$

and O is an integral operator defined by

$$O F(x,t) = \frac{1}{2\pi} \int_0^{2\pi} d\phi \int_0^1 x' dx' (x'^2 + x^2 - 2xx'\cos\phi)^{-1/2} F(x',t) .$$

Eq. (B-1) is most conveniently solved by the method of Laplace transforms.
Taking the Laplace transform of both sides, we get

$$\omega^2 (1 + \lambda O) L(x,\omega) - \omega_o^2 \frac{1}{x} \frac{d}{dx}\left(x \frac{d}{dx} L(x,\omega)\right) = \frac{L_p(\omega)}{\rho a_o} , \qquad (B-2)$$

where

$$L(x,\omega) = \int_o^\infty z(x,t) e^{-\omega t} dt ,$$

and

$$L_p(\omega) = \int_o^\infty P_o(t) e^{-\omega t} dt .$$

If the deflection $z(x,t)$ is expanded in a series of Bessel functions as in Eq. (5), Part IV,

$$z(x,t) = \sum_{i=1}^\infty z_i(t) J_o(k_i x) \qquad (B-3)$$

where $J_o(u)$ is the zero order Bessel function of u, and k_i is the i-th zero

of $J_o(\omega)$, it follows that

$$L_n(z, \omega) = \sum_{i=1}^{\infty} L_i(\omega) J_o(k_i z), \qquad (B-4)$$

where

$$L_i(\omega) = \int_0^{\infty} x_i(t) e^{-\omega t} dt .$$

Substituting the expression (B-4) into Eq. (B-2), multiplying by $x J_o(k_i x)$, and integrating with respect to x from 0 to 1, we obtain the following set of equations,

$$\sum_{i=1}^{\infty} [(\delta_{ij} + A_{ij}\lambda)\omega^2 + \delta_{ij} \omega_i^2] \frac{1}{2} J_1(k_i) J_1(k_j) L_i(\omega) \qquad (B-5)$$
$$= \frac{J_1(k_j)}{k_j} \frac{L_p(\omega)}{\rho a_o}, \quad j = 1, 2, \ldots$$

where

$$\omega_i^2 = \omega_o^2 k_i^2 = \sigma_o k_i^2 / \rho R_o^2 ,$$
$$\delta_{ij} = \begin{cases} 0, & i \neq j, \\ 1, & i \neq j, \end{cases}$$

and

$$A_{ij} = \frac{1}{\pi J_1(k_i) J_1(k_j)} \int_0^1 x \, dx \, J_o(k_i x) \odot J_o(k_j x)$$

as in Eq. (16), Part IV. It is apparent that $A_{ij} = A_{ji}$.

It is possible to reduce the system of Eqns. (B-5) to the standard form

$$\sum_{i=1}^{\infty} \left(B_{ij} + \frac{\omega_o^2}{\omega^2} \delta_{ij} \right) k_i J_1(k_i) L_i(\omega) \qquad (B-6)$$
$$= \frac{2}{k_j^2} \frac{1}{\rho a_o} \frac{L_p(\omega)}{\omega^2}, \quad j = 1, 2, \ldots$$

where $\quad B_{ij} = \dfrac{\delta_{ij} + A_{ij}\lambda}{k_i k_j} \quad, \quad B_{ij} = B_{ji}$.

Let $\Delta(\beta) = |B_{ij} - \beta \mathcal{E}_{ij}|$ and let $\Delta_{ij}(\beta)$ be the cofactor of the ij-th element of the determinant $\Delta(\beta)$. The solution of Eq. (B-6) is

$$L_i(\omega) = \frac{1}{\rho \delta_o} \frac{L_p(\omega)}{\omega^2} \sum_{j=1}^{\infty} \frac{2\,\Delta_{ji}\left(-\frac{\omega_o^2}{\omega^2}\right)}{k_i k_j^2\, J_1(k_i)\, \Delta\left(-\frac{\omega_o^2}{\omega^2}\right)} \quad . \tag{B-7}$$

The quantity Δ_{ji}/Δ may be expanded in a sum of partial fractions as follows: if $\Delta(\beta)$ has the roots β_ℓ, $\ell = 1, 2, \ldots$, all of multiplicity one, we have

$$\left. \begin{aligned} \frac{\Delta_{ji}(\beta)}{\Delta(\beta)} &= \sum_{\ell=1}^{\infty} \frac{\Delta_{ji}(\beta_\ell)}{(\beta - \beta_\ell)\,\Delta'(\beta_\ell)} \quad, \\[2mm] \Delta'(\beta) &= \frac{d}{d\beta}\,\Delta(\beta) \ . \end{aligned} \right\} \tag{B-8}$$

Using (B-8) the solution (B-7) becomes with $\beta_\ell = \omega_o^2/\omega_\ell^{*2}$

$$L_i(\omega) = \frac{-1}{\rho \delta_o} \frac{L_p(\omega)}{\omega^2} \sum_{\ell, j=1}^{\infty} \frac{2}{k_i k_j^2 J_1(k_i)} \; \frac{\omega^2 \omega_\ell^{*2} \Delta_{ji}\left(-\frac{\omega_o^2}{\omega_\ell^2}\right)}{\omega_o^2 (\omega^2 + \omega_\ell^{*2}) \Delta'\left(-\frac{\omega_o^2}{\omega_\ell^{*2}}\right)} \tag{B-9}$$

$$= \frac{I}{\rho \delta_o \omega_o^2} \sum_{\ell=1}^{\infty} \frac{C_{i\ell}\, \omega_\ell^{*2}\, L_p(\omega)}{I(\omega^2 + \omega_\ell^{*2})} \quad,$$

where

$$C_{i\ell} = -\sum_{j=1}^{\infty} \frac{2 k_i}{k_j^2 J_1(k_i)} \; \frac{\Delta_{ji}\left(-\frac{\omega_o^2}{\omega_\ell^2}\right)}{\Delta'\left(-\frac{\omega_o^2}{\omega_\ell^{*2}}\right)} \quad; \tag{B-10}$$

and $I = \displaystyle\int_o^{\infty} p_o(t)\,dt$.

The inversion of the Laplace transform gives

$$z_i(t) = \frac{1}{2\pi i} \int_{C-i\infty}^{C+i\infty} L_i(\omega) e^{\omega t} d\omega$$
$$c > 0$$

$$= \frac{I}{\rho a_o} \sum_{\ell=1}^{\infty} \frac{\omega_\ell^*}{\omega_i^2} C_{i\ell} \, g_\ell(t),$$

(B-11)

where

$$g_\ell(t) = \frac{\omega_\ell^*}{2\pi i \, I} \int_{C-i\infty}^{C+i\infty} \frac{L_p(\omega) e^{\omega t} d\omega}{\omega^2 + \omega_\ell^{*2}} .$$

The function $g_\ell(t)$ can also be written

$$g_\ell(t) = \frac{\int_o^t p_o(t') \sin \omega_\ell^* (t-t') dt'}{\int_o^\infty p_o(t') dt'} .$$

(B-12)

In the case of an exponential wave,

$$p_o(t) = p_m e^{-t/\theta} \quad , \quad t \geqslant 0,$$

(B-13)

Eq. (B-12) becomes

$$g_\ell(t) = \frac{\omega_\ell^* \theta \left(e^{-t/\theta} - \cos \omega_\ell^* t \right) + \sin \omega_\ell^* t}{1 + \omega_\ell^{*2} \theta^2} .$$

(B-14)

In this case the complete expression for z is

$$z = \sum_{i=1}^{\infty} z_i(t) J_o(k_i x)$$

$$= \frac{I}{\rho a_o} \sum_{\ell, i=1}^{\infty} \frac{\omega_\ell^*}{\omega_i^2} C_{i\ell} \, g_\ell(t) J_o(k_i x) ,$$

(B-15)

where $I = p_m \theta$ and $g_\ell(t)$ is given by (B-14).

APPENDIX C

SUPPLEMENTARY DATA CONCERNING THE SOLUTION IN
SECTION 3, PART IV

Eq. (20), Part IV, contains several quantities which are here written out in expanded form.

$$\Delta(\rho) = \begin{vmatrix} B_{11} - \rho & B_{12} \\ B_{21} & B_{22} - \rho \end{vmatrix} \; ,$$

$$\Delta'(\rho) = 2\rho - B_{11} - B_{22}$$

$$= (\rho - \rho_1) + (\rho - \rho_2) \; , \qquad \text{(See C-5)}$$

$$B_{11} = \frac{1 + A_{11}\lambda}{k_1^2} \; , \qquad\qquad A_{11} = 0.746 \; , \tag{C-1}$$

$$B_{12} = B_{21} = \frac{A_{12}\lambda}{k_1 k_2} \; , \qquad\qquad A_{12} = 0.158 \; ,$$

$$B_{22} = \frac{1 + A_{22}\lambda}{k_2^2} \; , \qquad\qquad A_{22} = 0.260 \; ,$$

$$k_1 = 2.405 \; , \qquad\qquad k_2 = 5.520 \; ,$$

$$J_1(k_1) = 0.5191 \; , \qquad\qquad J_1(k_2) = 0.3403 \; , \tag{C-2}$$

$$\Delta_{11}(\rho) = B_{22} - \rho \; ,$$

$$\Delta_{12}(\rho) = \Delta_{21}(\rho) = -B_{21} = -B_{12} \; , \tag{C-3}$$

$$\Delta_{22}(\rho) = B_{11} - \rho \; .$$

The roots ρ_1 and ρ_2 are obtained by solving

$$\Delta(\beta) = (B_{11} - \beta)(B_{22} - \beta) - B_{12}^2 = 0, \qquad \text{(C-4)}$$

giving

$$\left. \begin{array}{l} \dfrac{\omega_o^2}{\omega_1^{*2}} = \beta_1 = \frac{1}{2}(B_{11} + B_{22}) + \left[\frac{1}{4}(B_{11} - B_{22})^2 + B_{12}^2\right]^{1/2}, \\[2mm] \dfrac{\omega_o^2}{\omega_2^{*2}} = \beta_2 = \frac{1}{2}(B_{11} + B_{22}) - \left[\frac{1}{4}(B_{11} - B_{22})^2 + B_{12}^2\right]^{1/2} \end{array} \right\} \qquad \text{(C-5)}$$

It is obvious that β_1 and β_2 are real and that β_1 is positive; β_2 is positive if $\begin{vmatrix} B_{11} & B_{12} \\ B_{21} & B_{22} \end{vmatrix} > 0$, which can be easily verified.

For the case of $\lambda = 2.75$ (corresponding to the URRL diaphragm),

$$B_{11} = 0.528$$
$$B_{12} = B_{21} = -0.0328$$
$$B_{22} = 0.0563$$

$$\omega_o^2/\omega_1^{*2} = \beta_1 = 0.5286 \qquad \omega_1^{*} = 1.382\,\omega_o$$
$$\omega_o^2/\omega_2^{*2} = \beta_2 = 0.5513 \qquad \omega_2^{*} = 4.305\,\omega_o$$

It is apparent that if the nondiagonal terms B_{12} and B_{21} in were neglected, one would obtain for the roots β_1 and β_2, the values B_{11} and B_{22} which differ little from the values actually obtained for the roots. Compare the numerical values given for β_1 and B_{11}, and β_2 and B_{22} above. This means that the interaction terms B_{12} and B_{21} cause only small perturbations in the frequencies ω_1^{*} and ω_2^{*}. The coefficients C_{ig} are

$$C_{11} = \frac{2k_1}{(\beta_1 - \beta_2) J_1(k_1)} \left[\frac{\beta_1 - B_{22}}{k_1^2} + \frac{B_{12}}{k_1^2}\right],$$

$$C_{12} = \frac{2k_1}{(\beta_1 - \beta_2)\, J_1(k_1)}\left[\frac{\beta_{22} - \beta_2}{k_1^2} - \frac{\beta_{12}}{k_2^2}\right] ,$$

$$C_{22} = \frac{2k_2}{(\beta_1 - \beta_2)\, J_1(k_2)}\left[\frac{\beta_{11} - \beta_2}{k_1^2} - \frac{\beta_{12}}{k_2^2}\right] ,$$

$$C_{21} = \frac{2k_2}{(\beta_1 - \beta_2)\, J_1(k_2)}\left[\frac{\beta_1 - \beta_{11}}{k_1^2} + \frac{\beta_{12}}{k_2^2}\right] .$$

For $\lambda = 2.75$

$$c_{11} = 1.619, \qquad c_{21} = 0.0863,$$

$$c_{12} = 0.01663, \qquad c_{22} = 0.991 .$$

BUCKLING INSTABILITY OF THIN CYLINDRICAL SHELLS

J. M. Richardson
Central Experimental Station
Bureau of Mines, Department of the Interior
Pittsburgh, Penna.

and

J. G. Kirkwood
California Institute of Technology

American Contribution

February 28, 1950

423

CONTENTS

ABSTRACT

BUCKLING INSTABILITY OF THIN CYLINDRICAL SHELLS

By

John M. Richardson[a] and John G. Kirkwood[b]

The buckling instability of thin cylindrical shells is here
treated under static loading. The Poisson-Love theory of shells as corrected
by Epstein is applied to the case of cylindrical shells with numerical re-
sults that differ rather little from the von Mises treatment based upon
the uncorrected Poisson-Love theory.

[a] Physical Chemist, Explosives Branch, Bureau of Mines, U. S. Depart-
ment of the Interior.
[b] Professor of Chemistry, California Institute of Technology, Pasadena,
California.

BUCKLING INSTABILITY OF THIN CYLINDRICAL SHELLS

EXTERNAL STATIC LOADING

1. Introduction and General Theory

The buckling of cylindrical shells closed at both ends under external hydrostatic loading has been treated by von Mises[1] using the

---

[1] von Mises, Stodola Festschrift, p. 418 (1929)
Experimental Model Basin Report 366 (1933)
Saunders and Windenburg, A.S.M.E. Trans. vol. 53 (1931)
Windenburg and Trilling, A.S.M.E. Trans. vol. 56 (1934)

Poisson-Love theory of shells. Recently Epstein[2] has corrected certain

---

[2] Epstein, Jour. Math. and Phys., vol. XXI, 198, (1942)

---

errors in the second-order terms in the equations of the classical theory of shells. They arise in part from incorrect expressions for the curvatures, and in part from the premature introduction of the plane stress approximation into the membrane terms of the shell equations.

It is our purpose here to develop the theory of buckling of cylindrical shells under static loading on the basis of the corrected shell equations. Although the numerical corrections to the buckling pressure are not large, it seemed to us worthwhile to present corrected tables and graphs. Moreover, the theory of static buckling is presented from a different point of view than the usual one. Envisaged from the dynamical point of view, the condition for static buckling is found to be equivalent to the condition for dynamical instability for small displacements, in the sense that one or more of the shell frequencies become complex when the

critical load is exceeded.

Although the formulation of the dynamic theory of buckling is somewhat more involved than that of the usual static theory and yet leads to the same results for static loading, it has several advantages. First, it may be generalized in a natural way to yield conditions of stability under dynamic loading. Second, it shows that the critical pressure of the static theory really defines the limit of stability for the structure under small perturbations. This is important in connection with the nonlinear buckling theory of von Karman, 3/ since it shows that, even if

---

3/ von Karman, Enz. d. Math. Wiss., Bd. IV, 428 (1910)
  Friedricks and Stoker, Am. Jour. Math., vol. LXIII, 839 (1941)

---

static modes of buckling are possible at lower loads than the critical load of the linear theory, they could only be excited by large perturbations.

We consider a cylindrical shell of radius R, thickness a, and length L, closed at both ends and in equilibrium with a uniform external hydrostatic pressure P. We denote by u, v, w the axial, circumferential, and inwardly directed radial components of the supplementary displacements produced by additional loading due to an excess pressure $p(\theta, z, t)$ where θ and z are cylindrical coordinates specifying position on the surface of the undeformed shell, and t is the time. Buckling can of course be excited by out-of-roundness as well as by a supplementary load. However, the excitation function for out-of-roundness can be regarded as an equivalent excess pressure. Supplementing the Epstein4/ shell equations with the

---

4/ Epstein, Work cited in footnote 2.

---

membrane term due to the uniform load P, we have the following equations of motion for the shell excited by the excess load p.

$$\frac{\partial^2 w}{\partial \tau^2} + (D_{11} - \mathcal{G} B_{11})w + D_{12} v + D_{13} u = \frac{p}{\omega_0^2 \rho a}$$

$$\frac{\partial^2 v}{\partial \tau^2} + D_{21} w + D_{22} v + D_{23} u = 0$$

$$\frac{\partial^2 u}{\partial \tau^2} + D_{31} w + D_{32} v + D_{33} u = 0$$

(1)

$$\tau = \omega_0 t \qquad \omega_0^2 = \frac{E}{\rho R^2(1-\nu^2)} \qquad \mathcal{G} = \frac{1-\nu^2}{E} \frac{R}{a} P$$

where E is the elastic modulus, ν Poisson's ratio, and ρ the density of the material of the shell. The shell operators D_{ik} and the buckling operator B_{ij} are given in Appendix A. In Equations (1), terms of order α^4 and $\alpha^2 \mathcal{G}$ have been neglected and will also be neglected in the expansion of determinants entering into their solution. Many of the terms in the Epstein operators are really redundant, since after elimination between Equations (2) they would be found to contribute only to terms of higher order.

The boundary conditions for the problem considered are satisfied by the Fourier series

$$w = \sum_{n=-\infty}^{+\infty} \sum_{\ell=1}^{\infty} w_{n\ell} \sin\left(\frac{\pi\ell x}{L}\right) e^{in\theta} ,$$

$$v = \sum_{n=-\infty}^{+\infty} \sum_{\ell=1}^{\infty} \frac{v_{n\ell}}{in} \sin\left(\frac{\pi\ell x}{L}\right) e^{in\theta} ,$$ (2)

$$u = \sum_{n=-\infty}^{+\infty} \sum_{\ell=1}^{\infty} u_{n\ell} \cos\left(\frac{\pi\ell x}{L}\right) e^{in\theta} ,$$

The boundary conditions are single-valuedness of all displacements in θ, vanishing of w and v at cylinder ends due to support by rigid frames, and vanishing of the supplementary axial strain at the ends. The last

condition at first glance appears to limit the solutions of (2) to cases
for which the supplementary pressure p vanishes on the cylinder ends.
This limitation is actually not implied if only the terms for the axial
mode, $\ell = 1$, are retained in Equation (2), since in this approximation
the equations of motion and the orthogonality of the trigonometric func-
tions show that there is no interaction between the terms of Equations (2)
and terms in u of the form $\sin(\pi \ell z/L)$, excited by supplementary pressure
on the cylinder ends. It is understood that terms for n = 1 are to be
omitted from the sums (2), since they correspond to uniform translation
perpendicular to the axis without deformation.

Substitution of the series (2) into Equations (1) and use of
the orthogonality of the trigonometric functions yields for each Fourier
component a set of Equations of the form,

$$\frac{d^2 w_{n\ell}}{d\tau^2} + (A_{11}^{(n\ell)} - \gamma C_{11}^{(n\ell)}) w_{n\ell} + A_{12}^{(n\ell)} v_{n\ell} + A_{13}^{(n\ell)} u_{n\ell} = \frac{P_{n\ell}(t)}{\omega_s^2 \rho a}\,,$$

$$\frac{d^2 v_{n\ell}}{d\tau^2} + A_{21}^{(n\ell)} w_{n\ell} + A_{22}^{(n\ell)} v_{n\ell} + A_{23}^{(n\ell)} u_{n\ell} = 0\,,$$

$$\frac{d^2 u_{n\ell}}{d\tau^2} + A_{31}^{(n\ell)} w_{n\ell} + A_{32}^{(n\ell)} v_{n\ell} + A_{33}^{(n\ell)} u_{n\ell} = 0\,, \tag{3}$$

and

$$P_{n\ell}(t) = \frac{1}{2\pi L} \int_0^L \int_0^{2\pi} p(x,\theta,t) \sin\left(\frac{\pi \ell x}{L}\right) e^{in\theta} dx\, d\theta\,.$$

The matrix elements $A_{ik}^{(nl)}$ and $C_{11}^{(nl)}$ are given in Appendix A. The solu-
tions of Equation (3) appropriate to vanishing values of the displacements

4

and velocities at the initial instant of time $T = 0$, are readily found to be (most conveniently with the aid of Laplace transforms),

$$u_{n\ell}^r(t) = \sum_{\beta=1}^{3} \frac{W_{n\ell}(\lambda_\beta^{(n\ell)})}{\omega_s^2 \rho \alpha} \int_0^\tau P_{n\ell}(s) \sin \lambda_\beta^{(n\ell)}(\tau-s)\, ds ,$$

$$V_{n\ell}(t) = \sum_{\beta=1}^{3} \frac{V_{n\ell}(\lambda_\beta^{(n\ell)})}{\omega_\beta^2 \rho \alpha} \int_0^\tau P_{n\ell}(s) \sin \lambda_\beta^{(n\ell)}(\tau-s)\, ds , \qquad (4)$$

$$w_{n\ell}(t) = \sum_{\beta=1}^{3} \frac{U_{n\ell}(\lambda_\beta^{(n\ell)})}{\omega_0^2 \rho \alpha} \int_0^\tau P_{n\ell}(s) \sin \lambda_\beta^{(n\ell)}(\tau-s)\, ds ;$$

$$W_{n\ell}(\lambda) = -\frac{2\Delta_{11}^{(n\ell)}(\lambda)}{\Delta'^{(n\ell)}(\lambda)} , \qquad V_{n\ell}(\lambda) = -\frac{2\Delta_{12}^{(n\ell)}(\lambda)}{\Delta'^{(n\ell)}(\lambda)} ,$$

$$U_{n\ell}(\lambda) = -\frac{2\Delta_{13}^{(n\ell)}(\lambda)}{\Delta'^{(n\ell)}(\lambda)} , \qquad \Delta'^{(n\ell)}(\lambda) = \frac{d}{d\lambda}\Delta^{(n\ell)}(\lambda) , \qquad (5)$$

where $\Delta_{ik}^{(n l)}$ is the ik minor of the shell frequency determinant, $\Delta^{(n l)}(\lambda)$

$$\Delta^{(n\ell)}(\lambda) = \begin{vmatrix} A_{11}^{(n\ell)} - \rho C_{11}^{(n\ell)} - \lambda^2 & A_{12}^{(n\ell)} & A_{13}^{(n\ell)} \\ A_{21}^{(n\ell)} & A_{22}^{(n\ell)} - \lambda^2 & A_{23}^{(n\ell)} \\ A_{31}^{(n\ell)} & A_{32}^{(n\ell)} & A_{33}^{(n\ell)} - \lambda^2 \end{vmatrix} , \qquad (6)$$

and the quantities $\pm\ \lambda_\beta^{(n l)}$; $\beta = 1, 2, 3$ are the six roots (assumed non-degenerate in Equations (4 and 5)) of the secular equation.

$$\Delta^{(n l)}(\lambda) = 0. \qquad (7)$$

Thus the $\lambda_\beta^{(n l)}$ are the ratios of the shell frequencies for the nl mode to the fundamental frequency ω_0. From Equation (4), it is seen that a given

mode becomes unstable if one or more of the three frequencies ceases to be real. A sufficient condition for instability, under which at least one frequency is pure imaginary, is

$$\Delta^{(nl)}(0) < 0. \tag{8}$$

Thus a given mode becomes unstable when

$$\Delta^{(nl)}(0) = 0. \tag{9}$$

This is precisely the condition for static buckling, which allows the equilibrium equations to have nonvanishing solutions for vanishing supplementary load. Other types of dynamical instability of the shell are of course possible with selected values of the shell parameters, but we shall not examine them here. They would correspond to complex frequencies with nonvanishing real parts.

When the determinant $\Delta^{(nl)}(0)$, Equation (6), is expanded, and terms of $O(\alpha^4)$ and $O(\alpha^2\phi)$ are dropped, it takes the relatively simple form,

$$\Delta^{(nl)}(0) = \frac{1-\nu}{2}\left(b + d\alpha^2 - c\phi\right),$$

$$b = (1-\nu^2)\mu^4,$$

$$c = (n^2+\mu^2)^2\left(n^2+\tfrac{1}{2}\mu^2 - 1\right),$$

$$d = (n^2+\mu^2)^4 - 2n^6 + n^4\left(1 - 2(3+\nu)\mu^2\right)$$
$$+ n^2\left[4\mu^2 - (1-\nu)^{-1}(7 - 15\nu - 3\nu^2 + 6\nu^3 - 2\mu^4)\mu^4\right]$$
$$+ (1+\nu)(1+3\nu)\mu^7 - (1-\nu)^{-1}(1-\nu^2+2\nu^3)\mu^6, \qquad \mu = n\pi R/L. \tag{10}$$

Buckling instability in a given shell mode occurs at a critical value of ϕ, given by

$$\phi_c = \frac{b + d\alpha^2}{c}, \tag{11}$$

6

Buckling of the shell takes place in the mode which gives the least critical value of ϕ_c, at pressures exceeding a critical pressure Pc, corresponding to this value of ϕ. We have

$$P_c = \frac{a}{R} \frac{E}{1-\nu^2} \phi c, \tag{12}$$

unless $E\phi c/(1-\nu^2)$ exceeds the yield stress σ_o of the material of construction, in which case

$$P_c = a\sigma_o/R. \tag{13}$$

It is found that the buckling mode corresponds to $\lambda = 1$ and to a value of n, equal to the number of circumferential lobes excited, which increases with decreasing ratio of shell length to diameter.

2. Tables and Graphs of the Critical Buckling Pressure and the Number of Lobes as a Function of the Shell Parameters

The buckling pressure Pc of cylindrical shells has been calculated as a function of the parameters a/2R and L/2R, the ratios of wall thickness and shell length or frame spacing to the diameter, with the use of equations (10), (11), (12), and (13). The following values of Young's modulus, Poisson's ratio, and yield stress were employed.

$$E = 3 \times 10^7 \text{ p.s.i.}$$
$$\nu = 0.3$$
$$\sigma_o = 3 \times 10^4 \text{ p.s.i.}$$

The results are presented in numerical form in the accompanying tables and graph (figure 1). In the tables, the lobe zones are marked out with solid lines and the boundary between the plastic and elastic zones is indicated by a dotted line. In Figure 1, the buckling pressure Pc is

7

ast

e Pc,

(12)

f con-

(13)

valua

in-

calcu-

wall

the use

Young's

bles

t with

is

is

432

plotted as a function of L/2R for constant values of a/2R. The lobe zones are marked out with the dotted curves.

Our buckling pressures differ but a few percent from those of the von Mises theory over a considerable range of shell parameters. Although the differences *have* no practical importance, we hope that our tabulations of the results of the theory will prove useful because of their comprehensiveness and convenience *t* form.

Critical Buckling Pressure

P (p.s.i.)

$\frac{a}{2E}$ \ $\frac{L}{2R}$	n	0.15	0.16	0.17	0.13	0.19	0.20	0.21	0.22	0.23	n
		20		19		18			17		
0.00125	20	32.0	29.8	27.9	26.2	24.8	23.4	22.4	21.2	20.2	17
0.0015	19	49.9	46.5	43.7	41.1	39.0	36.6	34.8	33.2	31.5	16
0.0020	18	103	96.0	90.5	85.0	80.7	76.2	73.0	68.8	65.6	15
0.0025		150	150	150	150	147	139	132	125	119	14
0.0030		180	180	180	180	180	180	180	180	180	
0.0035		210								210	
0.0040		240								240	
0.0045		270								270	
0.005		300								300	
0.006		360								360	
0.007		420								420	
0.008		480								480	
0.009		540								540	
0.010		600								600	
0.0125		750								750	
0.015		900								900	
0.0175		1050								1050	
0.020		1200								1200	
0.0225		1350								1350	
0.025		1500								1500	
0.0275		1650								1650	
0.030		1800	1800	1800	1800	1800	1800	1800	1800	1800	

9

434

Critical Buckling Pressure

P (p.s.i.)

$\frac{a}{2R}$ / $\frac{L}{2R}$	0.24	0.25	0.26	0.27	0.28	0.29	0.30	0.32	0.34	
	n	16			15				14	n
0.00125	16									14
0.0015		30.0	28.8	27.8	26.5	25.5	24.6	23.9	22.1	20.8	
0.0020	15	62.3	60.0	57.5	55.2	53.2	51.7	49.0	45.9	43.2	13
0.0025	14	115	110	105	100	97.0	93.5	90.0	83.7	79.0	12
0.0030		160	174	168	161	154	149	144	136	125	11
0.0035		210	210	210	210	210	210	210	195	184	
0.0040		240	240	240	240	240	240	240	240	240	
0.0045		270								270	
0.005		300								300	
0.006		360								360	
0.007		420								420	
0.008		480								480	
0.009		540								540	
0.010		600								600	
0.0125		750								750	
0.015		900								900	
0.0175		1050								1050	
0.020		1200								1200	
0.0225		1350								1350	
0.025		1500								1500	
0.0275		1650								1650	
0.030		1800	1800	1800	1800	1800	1800	1800	1800	1800	

10

Critical Buckling Pressure

P (p.s.i.)

$\dfrac{t}{2R}$ \ $\dfrac{L}{2R}$	0.36	0.38	0.40	0.42	0.44	0.46	0.48	0.50	0.55	
n		12				11				n
0.00125										11
0.0015										
0.0020	12	40.5	38.1	36.2	34.5	32.8	31.2	29.8	28.7	25.8	10
0.0025		75.0	70.0	66.1	63.2	60.8	57.5	54.5	52.1	47.8	
0.0030		118	112	106	100	95.5	91.3	87.9	84.2	75.3	9
0.0035	11	176	164	155	148	142	135	128	122	112	
0.0040	10	235	221	210	202	189	180	172	165	152	
0.0045		270	270	270	270	245	243	233	224	201	8
0.005		300	300	300	300	300	300	300	295	265	
0.006		360	360	360	360	360	360	360	360	360	
0.007		420								420	
0.008		480								480	
0.009		540								540	
0.010		600								600	
0.0125		750								750	
0.015		900								900	
0.0175		1050								1050	
0.020		1200								1200	
0.0225		1350								1350	
0.025		1500								1500	
0.0275		1650								1650	
0.030		1800	1800	1800	1800	1800	1800	1800	1800	1800	

11

Critical Buckling Pressure

P (p.s.i.)

$\frac{a}{2R}$ \ $\frac{L}{2R}$	0.60	0.65	0.70	0.75	0.80	0.85	0.90	0.95	1.00	
n	10		9			8			7	n
0.00125										
0.0015	10									
0.0020	23.6	21.9	20.2							
0.0025	43.0	39.5	37.2	34.0	31.6	29.8	28.4	26.7	25.1	7
0.0030	9	69.5	63.2	58.1	54.2	51.1	48.1	44.6	41.9	39.8
0.0035	102	92.0	85.7	80.8	74.8	69.5	65.5	62.4	59.8	
0.0040	8	137	126	119	108	100	94.0	89.2	85.3	81.8
0.0045	184	172	158	145	136	128	122	115	108	6
0.005	244	224	205	191	181	172	161	150	141	
0.006	360	352	327	306	289	265	248	236	225	
0.007	420	420	420	420	420	387	366	350	337	
0.008	480	480	480	480	480	480	480	480	470	5
0.009	540	540	540	540	540	540	540	540	540	
0.010	600								600	
0.0125	750								750	
0.015	900								900	
0.0175	1050								1050	
0.020	1200								1200	
0.0225	1350								1350	
0.025	1500								1500	
0.0275	1650								1650	
0.030	1800	1800	1800	1800	1800	1800	1800	1800	1800	

12

Critical Buckling Pressure

P (p ...)

$\frac{a}{2R}$ \ $\frac{L}{2R}$	1.1	1.2	1.3	1.4	1.5	1.6	1.7	1.8	1.9	
n		7			6			5		n
0.00125										5
0.0015	7									
0.0020										
0.0025	22.7	21.0								
0.0030	36.6	33.2	30.1	27.8	26.3	25.0	23.2	21.6	20.1	
0.0035	54.0	48.2	44.5	41.9	39.9	36.3	33.6	31.6	29.9	
0.0040	72.0	65.7	61.1	57.5	52.6	48.7	45.8	43.5	41.8	
0.0045	97.5	90.0	85.0	76.2	70.6	66.0	63.0	60.0	57.9	
0.005	129	120	109	100	93.5	88.1	84.0	81.0	76.0	
0.006	208	186	170	159	151	144	137	124	115	
0.007	300	270	250	236	227	211	193	178	167	4
0.008	418	382	357	338	314	286	264	247	234	
0.009	540	517	490	458	411	378	351	332	316	
0.010	600	600	600	578	527	487	459	435	418	
0.0125	750	750	750	750	750	750	750	750	750	
0.015	900								900	
0.0175	1050								1050	
0.020	1200								1200	
0.0225	1350								1350	
0.025	1500								1500	
0.0275	1650								1650	
0.030	1800	1800	1800	1800	1800	1800	1800	1800	1800	

13

Critical Buckling Pressure

P (p.s.i.)

$\frac{a}{2R}$	$\frac{L}{2R}$	2.0	2.5	3.0	3.5	4.0	5	6	7	8
	n	5			4			3		n
0	.00125									
	0.0015									
	0.0020									
5	0.0025									3
	0.0030									
	0.0035	28.5	22.6							
	0.0040	40.2	30.5	25.6	23.0	20.4				
	0.0045	54.8	41.6	35.9	32.4	26.0	20.7			
	0.005	70.5	54.3	47.8	40.9	33.4	26.5	24.1	23.0	
	0.006	108	88.0	77.8	60.8	52.0	44.0	40.5	32.5	25.4
4	0.007	158	133	109	87.5	77.2	67.2	62.5	44.4	35.6
	0.008	223	192	145	122	110	99.0	81.8	60.7	49.1
	0.009	304	248	192	167	152	138	103	78.1	65.2
	0.010	402	316	250	221	204	183	126	99.5	85.5
	0.0125	750	520	440	400	377	281	206	171	154
	0.015	900	820	720	668	640	408	317	285	253
	0.0175	1050	1050	1050	1040	850	570	468	419	393
	0.020	1200	1200	1200	1200	1110	790	685	602	575
	0.0225	1350	1350	1350	1350	1350	1050	910	840	808
	0.025	1500	1500	1500	1500	1500	1350	1210	1133	1095
	0.0275	1650	1650	1650	1650	1650	1650	1590	1500	1450
	0.030	1800	1800	1800	1800	1800	1800	1800	1800	1800

14

Critical Buckling Pressure

P (p.s.i.)

$\frac{a}{2R}$ $\frac{h}{R}$		9	10	15	20	30	
	n			2			n
0.00125							
0.0015							
0.0020							
0.0025							
0.0030							
0.0035							
0.0040							
0.0045							
0.005							
0.006		21.8					
0.007		30.9	28.3	24.0	23.2	22.7	
0.008	2	43.8	40.7	35.3	34.5	34.0	2
0.009		58.9	55.6	49.6	48.8	48.2	
0.010		76.0	73.8	68.0	67.0	66.5	
0.0125		145	139	131	130	129	
0.015		241	234	227	225	224	
0.0175		380	372	358	355	353	
0.020		560	550	534	531	529	
0.0225		789	770	759	752	750	
0.025		1075	1060	1039	1030	1026	
0.0275		1425	1410	1385	1375	1370	
0.030		1795	1792	1789	1787	1785	

15

440

Figure 1 - The buckling pressure P and number of lobes n as functions
of the parameters L/2R and a/2R.
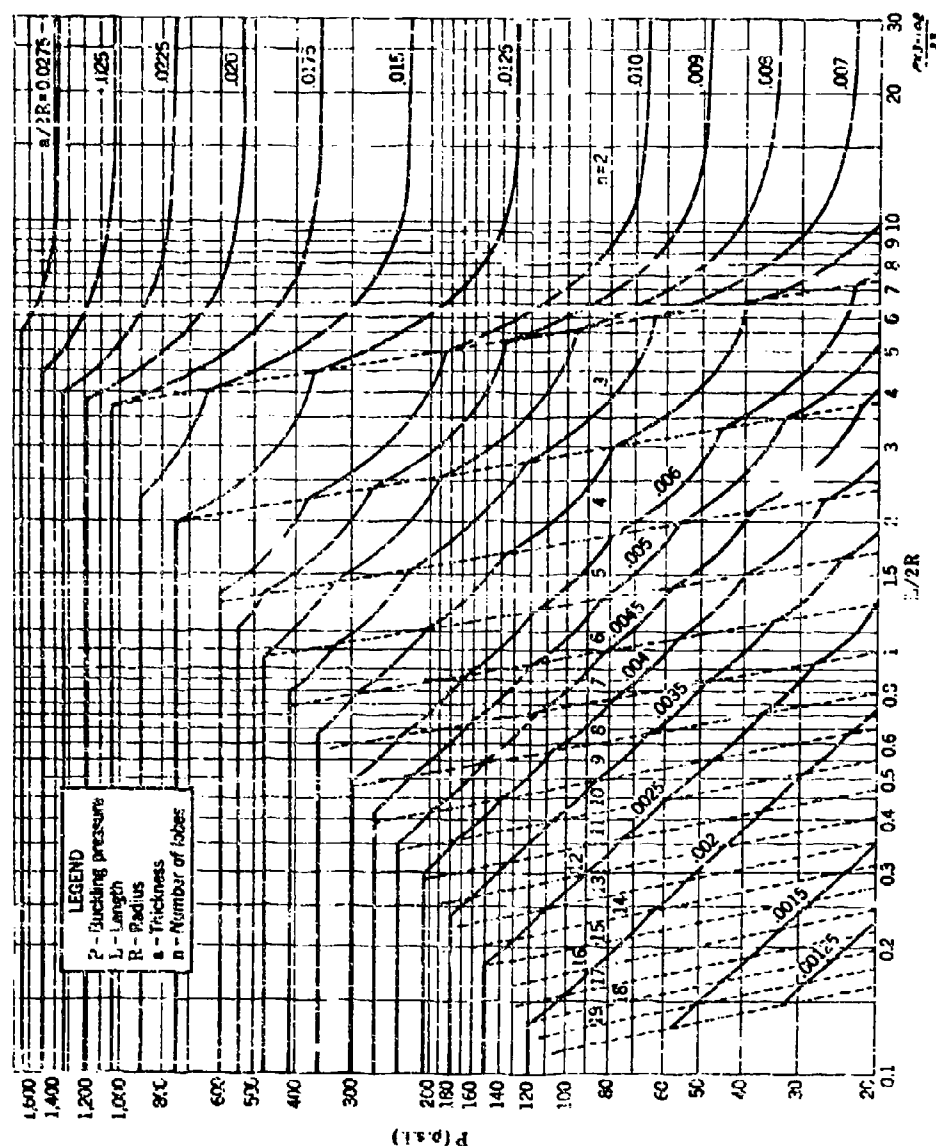
APPENDIX A

Definitions of the Operators D_{ik} and B_{11}, and the Matrix Elements $A_{ik}^{(n\ell)}$ and $C_{11}^{(n\ell)}$

For the convenience of the reader we repeat here the definitions of the shell operators D_{ik} and the buckling operator B_{11} of OSRD 3780[2] and the corresponding matrix elements $A_{ik}^{(n\ell)}$ and $C_{11}^{(n\ell)}$. The symbols to be used are defined as follows:

Symbol	Definition
α^2	$a^2/12R^2$
μ	$\pi R\ell/L$
σ	$1/(1-\nu)$
a	Shell thickness
R	Mean radius of cylinder
L	Length of cylinder
(r,θ,z)	Cylindrical coordinates with the origin at one end of the cylinder and with the z-axis coincident with the axis of the cylinder
ν	Poisson's ratio
n,ℓ	Defined by Eqs. (7)

The definitions of Epstein shell operators D_{ik} and the buckling operator B_{11} are

$$B_{11} = -\frac{\partial^2}{\partial \theta^2} - \frac{R^2}{2}\frac{\partial^2}{\partial z^2} - 1.$$

$$D_{11} = 1 + \alpha^2\left\{(4\sigma-3)+\tfrac{1}{2}(2\sigma^2-3\sigma+10)\frac{\partial^2}{\partial\theta^2}+\left(\frac{\partial^2}{\partial\theta^2}+R^2\frac{\partial^2}{\partial z^2}\right)^2+\tfrac{1}{10}(3\sigma^3-6\sigma^2+3\sigma-1)R^2\frac{\partial^2}{\partial z^2}\right\},$$

$$D_{12} = -\frac{\partial}{\partial\theta}-\alpha^2\left\{\frac{\sigma}{2}(\sigma-1)+\frac{\sigma}{2}(\sigma^2+2\sigma+3)\frac{\partial^2}{\partial\theta^2}+\tfrac{1}{10}(3\sigma^3-6\sigma^2+2\sigma+3)R^2\frac{\partial^2}{\partial z^2}\right\}\frac{\partial}{\partial\theta},$$

16

$$D_{13} = -\nu R \frac{\partial}{\partial z} - \alpha^2 \left\{ \frac{\sigma-1}{\sigma} (4\sigma-3) + \frac{1}{2\sigma}(3\sigma^3-6\sigma^2+10\sigma-3)\frac{\partial^2}{\partial\theta^2} - \frac{(\sigma-1)^2}{2}R^2\frac{\partial^2}{\partial z^2}\right\}R\frac{\partial}{\partial z},$$

$$D_{21} = \frac{\partial}{\partial\theta} + \frac{\alpha^2}{2}\left\{(\sigma^2+4\sigma-15)+(2\sigma^3-\sigma-1)\frac{\partial^2}{3\partial\theta^2}+\frac{1}{\sigma}(2\sigma^3-3\sigma^2-2)R^2\frac{\partial^2}{\partial z^2}\right\}\frac{\partial}{\partial\theta},$$

$$D_{22} = -\left(\frac{\partial^2}{\partial\theta^2}+\frac{1-\nu^2}{2}R^2\frac{\partial^2}{\partial z^2}\right)-\frac{\alpha^2}{2}\left\{(\sigma^2+\sigma-13)+2(\sigma-1)^2\left(\frac{\partial^2}{\partial\theta^2}+R^2\frac{\partial^2}{\partial z^2}\right)\right\}\frac{\partial^2}{\partial\theta^2},$$

$$D_{23} = -\frac{1+\nu}{2}R\frac{\partial^2}{\partial\theta\partial z}-\frac{\alpha^2}{2}\left\{(\sigma^2+3\sigma-19)+\frac{12}{\sigma}+2(\sigma-1)^2\left(\frac{\partial^2}{\partial\theta^2}+R^2\frac{\partial^2}{\partial z^2}\right)\right\}R\frac{\partial^2}{\partial\theta\partial z},$$

$$D_{31} = \nu R\frac{\partial}{\partial z}+\frac{\alpha^2}{2}\left\{(\sigma^2+3\sigma-6)+\frac{1}{\sigma}(2\sigma^3-\sigma^2-2\sigma-2)\frac{\partial^2}{\partial\theta^2}+(2\sigma^2-3\sigma-1)R^2\frac{\partial^2}{\partial z^2}\right\}R\frac{\partial}{\partial z},$$

$$D_{32} = -\frac{1+\nu}{2}R\frac{\partial^2}{\partial\theta\partial z}-\frac{\alpha^2}{2\sigma}\left\{(\sigma^3+2\sigma-1)+2\sigma(\sigma-1)^2\left(\frac{\partial^2}{\partial\theta^2}+R^2\frac{\partial^2}{\partial z^2}\right)\right\}R\frac{\partial^2}{\partial\theta\partial z},$$

$$D_{33} = -\left(\frac{1+\nu}{2}\frac{\partial^2}{\partial\theta^2}+R^2\frac{\partial^2}{\partial z^2}\right)-\frac{\alpha^2}{2\sigma}\left\{\frac{\partial^2}{\partial\theta^2}+(\sigma-1)(\sigma^2-3\sigma-6)R^2\frac{\partial^2}{\partial z^2}+2\sigma(\sigma-1)^2\left(\frac{\partial^2}{\partial\theta^2}+R^2\frac{\partial^2}{\partial z^2}\right)R^2\frac{\partial^2}{\partial z^2}\right\}.$$

The definitions of corresponding matrix elements $A_{ik}^{(n\ell)}$ and $C_{ik}^{(n\ell)}$ are

$$C_{11}^{(n\ell)} = n^2 + \frac{1}{2}\mu^2 - 1,$$

$$A_{11}^{(n\ell)} = 1+\alpha^2\left[(4\sigma-3)-\frac{1}{2}(3\sigma^2-3\sigma+2)n^2+(n^2+\mu^2)^2-\frac{1}{4\sigma}(3\sigma^3-6\sigma^2+7\sigma-2)\mu^2\right],$$

$$A_{12}^{(n\ell)} = -1-\alpha^2\left[\frac{\sigma}{2}(\sigma-1)-\frac{3}{2}(\sigma^2-2\sigma+3)n^2-\frac{1}{2\sigma}(3\sigma^2-6\sigma^2+2\sigma+3)\mu^2\right],$$

$$A_{13}^{(n\ell)} = \nu\mu+\mu\alpha^2\left[\frac{\sigma-1}{\sigma}(4\sigma-3)-\frac{1}{2\sigma}(3\sigma^3-6\sigma^2+10\sigma-3)n^2+\frac{(\sigma-1)^2}{2}\mu^2\right],$$

$$A_{21}^{(n\ell)} = -n^2-n^2\alpha^2\left\{\frac{1}{2}(\sigma^2+4\sigma-15)-\frac{1}{2}(2\sigma^3-\sigma-1)n^2+\frac{1}{2\sigma}(2\sigma^3-3\sigma^2-2)\mu^2\right\},$$

$$A_{22}^{(n\ell)} = n^2+\frac{1-\nu^2}{2}\mu^2+\frac{1}{2}n^2\alpha^2\left[(\sigma^2+\sigma-13)-2(\sigma-1)^2(n^2+\mu^2)\right],$$

$$A_{23}^{(n\ell)} = -\frac{1+\nu}{2}n^2\mu - \frac{1}{4}n^2\mu c^2\left[\sigma^2+3\sigma-14+\frac{12}{\sigma}-2(\sigma-1)^2(n^2+\mu^2)\right],$$

$$A_{31}^{(n\ell)} = \nu\mu + \mu n^2\left[\frac{1}{2}(\sigma^2+3\sigma-6)-\frac{1}{2\sigma}(2\sigma^3-\sigma^2-2\sigma-2)n^2-\frac{1}{2}(2\sigma^2-3\sigma-1)\mu^2\right],$$

$$A_{32}^{(n\ell)} = -\frac{1+\nu}{2}\mu - \mu c^2\left[\frac{1}{2\sigma}(\sigma^2-2\sigma-1)-(\sigma-1)^2(n^2+\mu^2)\right],$$

$$A_{33}^{(n\ell)} = \frac{1-\nu}{2}n^2+\mu^2+c^2\left[\frac{n^2}{2\sigma}+\left(\frac{\sigma-1}{2\sigma}\right)(\sigma^2+3\sigma-6)\mu^2-(\sigma-1)^2(n^2+\mu^2)\mu^2\right].$$

443

·],

)μ²].

TIME-DISPLACEMENT STUDIES OF DIAPHRAGMS DEFORMED
BY EXPLOSIVE LOADING

G. E. Hudson and C. T. Johnson
David W. Taylor Model Basin

American Contribution

May 1944

TIME-DISPLACEMENT STUDIES OF DIAPHRAGMS DEFORMED
BY EXPLOSIVE LOADING

By G. E. Hudson and C. T. Johnson

INTRODUCTION

The experiments, described in TMB Report 509 (10)[*], in which a thin, circular, steel diaphragm mounted in the bottom of a steel boat is attacked by a small charge of explosive, have been extended to a much wider range of distances between charge and diaphragm. In the meantime about five times as many diaphragms have been tested by the methods described, without an essential change in the technique or the apparatus. A great deal more information has been gained, owing as much to the more detailed and more extended analyses of the data as to the greater number of tests. All of these data and analyses will be described in a subsequent TMB report.

The aim of the present report is to furnish to other workers on diaphragms a detailed time history of the motion of the diaphragms as observed in these more recent experiments. This description covers details of the first swing of the diaphragm that are not given in the previous report (10). The description includes an account of the subsequent motion and vibrations of the boat after the shock wave impinges upon it, as well as an account of the subsequent bulging of the diaphragm as a result of the pressure pulses emitted from the oscillating gas globe.

Although not all details of the motion are fully understood, attempts are made at explanations of certain phases of it. Such explanations are presented chiefly as hypotheses to be tested by further observations and experiments.

TEST APPARATUS AND PROCEDURE

The diaphragms used in these tests were of furniture steel, having a yield stress σ_y of 43.5×10^3 pounds per square inch, and radius a of 5.125 inches. Their uniform initial thickness h_0 was 0.0567 inch. Each charge weighed 0.8 ounce and consisted of 22 grams of tetryl plus a detonator cap.

The diaphragms were welded at the rim to steel holding rings 1 inch thick, which in turn were bolted to a mounting ring, so that the combination was about 2 inches thick. The mounting ring was bolted to the bottom plate of a flat-bottomed steel boat. The bottom plate of the boat was of steel 1 inch thick, 5 feet wide by 5 1/2 feet long. The total weight of the boat was about 1400 pounds. The charges were detonated in the water beneath the boat and on the axis of symmetry of the diaphragms, at distances varying from 5 inches to 32 inches. All other pertinent dimensions are given in Figure 21.

[*] Numbers in parentheses indicate references at the end of this paper.
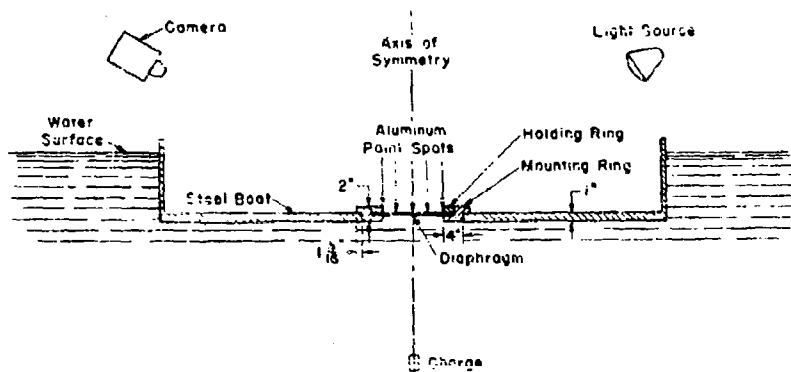
Figure 21 - Schematic Diagram of Underwater Explosion Apparatus
Arranged for Streak Photography

Observations of the motion of the diaphragms and the boat were made
by streak photography. As explained in Reference (10) such photographs show
the motion of spots of aluminum paint situated at various points on the dia-
phragm and boat. One spot called the center spot was at the center of each
diaphragm; two spots called the mid-spots were placed midway between the cen-
ter and edge on a diameter; and two called the edge spots were painted on the
holding ring at the extremities of the diameter on which the other spots were
located. The film was run at various speeds up to a maximum of about 1200
inches per second. If it was desired to obtain good resolution of the ini-
tial motion, which lasted about 2 milliseconds, it was obtained at high film
speeds, giving a record as shown in Figure 22a; if an overall picture of the
motion was desired it was obtained at low film speeds, giving a record like
that shown in Figure 22b. An intermediate speed yielded a streak photograph
such as that in Figure 22c.

MOTION OF DIAPHRAGM AND HOLDING RING

When the shock wave from a charge reaches a diaphragm it imparts to
the diaphragm and the holding ring an initial velocity normal to the original
plane of the diaphragm. As far as can be determined from the streak pictures
with the present limit of resolution the action appears to be impulsive. When
the charge is sufficiently far from the diaphragm, that is, when its distance
exceeds 8 to 10 inches or one diameter, the shock wave reaches all parts of
the diaphragm at about the same instant, so that the initial velocity of the
diaphragm material is practically uniform. Except for the material near the
edge, which is jerked to rest almost immediately, the diaphragm seems to be-
have initially quite like a free plate.
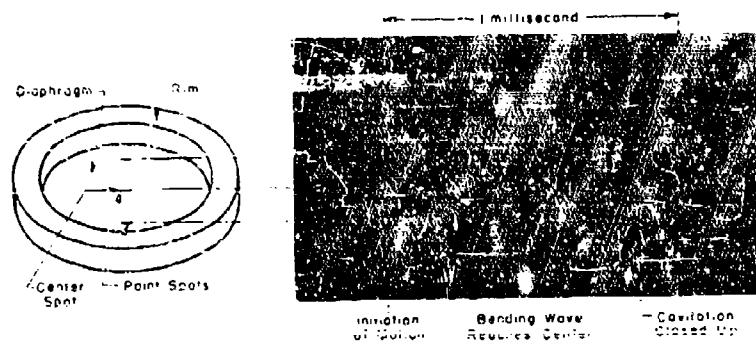
Figure 22a – High-Speed Streak Photograph
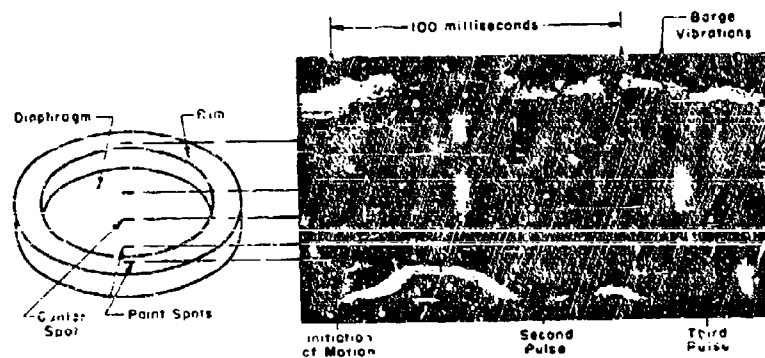
Figure 22b – Low-Speed Streak Photograph
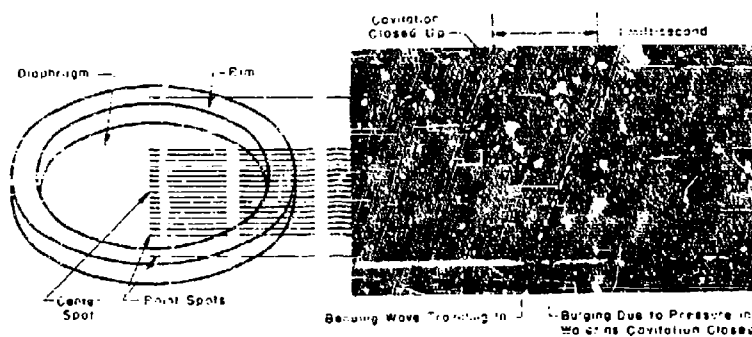
Figure 22c – Medium-Speed Streak Photograph

More than three spots were painted on the diaphragm to show more clearly
the transit of the bending wave.

Figure 22 – Typical Streak Photographs of Motion of Diaphragms

The diaphragm velocities observed vary from about 4.1×10^3 inches per second at a charge distance of 5 inches to 0.64×10^3 inches per second at a charge distance of 32 inches. On the other hand, the initial velocities of the edge spots were much lower, varying from about 0.6×10^3 inches per second to 0.1×10^3 inches per second over the same range of charge distance.

If the actual distance from the charge to a diaphragm spot is multiplied by the observed initial velocity of that spot, a constant is obtained which is independent of the charge distance. This may be expressed by the relation

$$v = \frac{20.48}{d} \text{ inches per millisecond}$$

where v is the velocity of the spot under consideration and d is the distance of the charge from that spot in inches. The dimensions of the numerical coefficient is inches^2 per millisecond. The product of the edge spot velocities v_E by their respective charge distances is also independent of the charge distance. This is expressed by the relation

$$v_E = \frac{3.23}{d_E} \text{ inches per millisecond}$$

where the subscript E indicates that the quantities refer specifically to the edge spots. The dimensions of the numerical coefficient is inches^2 per millisecond. The root mean square deviation from the mean of these constants is ± 1.41 inches^2 per millisecond for the diaphragm spots and ± 0.50 inches^2 per millisecond for the edge spots.

A theoretical calculation* based on the theory of the behavior of a free plate, developed by Kennard (11), leads to the values

$$17.26 \text{ inches}^2 \text{ per millisecond}$$

and

$$2.63 \text{ inches}^2 \text{ per millisecond}$$

for the diaphragm constant and the edge constant respectively. The reason for the discrepancy between these values and those obtained from the streak photographs is not evident. The differences appear to be larger than the experimental error.

---

* In this calculation, the assumption is made that cavitation occurs as soon as the pressure in the water drops to zero. The incident pressure wave is assumed to be described by the formula

$$p = \frac{68.5}{d} \cdot e^{-\frac{t}{38.77}} \times 10^3 \text{ pounds per square inch}$$

where t is in microseconds and d is in inches. The numerical coefficients in this formula are calculated on a similarity basis from the peak pressure and time constants, measured by Dr. E. Shapiro of the Taylor Model Basin staff, for 27.2 grams of tetryl at 3 feet (12).

The diaphragm bulges outward at time t_2, possibly
due to impulse received when cavitation closes up.

The bending wave reaches center and all motion
ceases temporarily.

The jerky motion of material appears in the flat
central region of the diaphragm, shown by broken
lines, possibly due to vibrations in a layer of
water left on undersurface of diaphragm.

The diaphragm acquires uniform initial velocity.
Cavitation takes place between reflected shock
wave and diaphragm.

Diaphragm 1 millisecond after initiation of Motion

Diaphragm at Time t_2

Diaphragm at Time t_1

Bending Wave
Diaphragm at Time t_0'''

Bending Wave
Diaphragm at Time t_0''

Bending Wave
Diaphragm at Time t_0'

Diaphragm at initial instant of Motion

Cavitation Region

Reflected Shock Wave
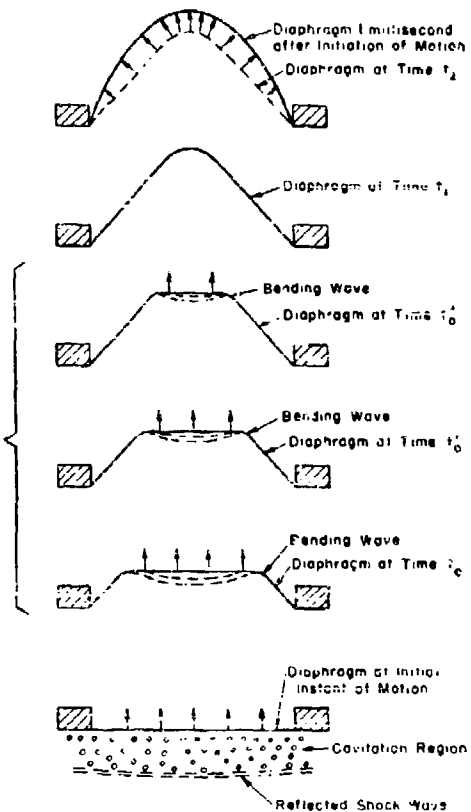
Figure 23 - Various Stages of Motion of a Diaphragm

As soon as the diaphragm begins to move, a bending wave, carrying
the news of the retarding presence of the edge, travels radially inward to-
ward the center, as in Figure 23. The material in the central region of the
diaphragm, interior to this bending wave, continues to move with almost its
initial uniform velocity until the wave reaches it. Near the center a small
but definite jerking motion is superimposed on this velocity, as seen in the
typical displacement-time curves in Figures 24a and 24b, of the center spots
on the diaphragms. In general, there seem to be four separate pauses, occur-
ring at times t_0, t_0', t_0'', and t_1. The material in the central region re-
gains sufficient velocity, after times t_0 and t_0', and in about one-half to
two-thirds of the cases after time t_0'', to more than make up for the velocity
lost at these times. That is, in this region up to time t_0'', and in about
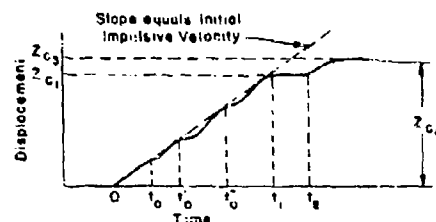
Figure 24a - An Idealized Displacement-Time Curve of the Center of a Diaphragm of the U-Class. The existence of the pause at time t_0 is uncertain.
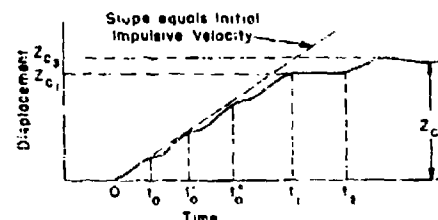
Figure 24b - An Idealized Displacement-Time Curve of the Center of a Diaphragm of the L-Class

Figure 24 - Typical Displacement-Time Curves of Center Spots on the Diaphragms

one-half to two-thirds of the cases up to time t_1 the overall displacement is about what it would have been if the jerking motion had not been present. At time t_1 the bending wave reaches the center, as illustrated in Figure 23, which then comes to rest or undergoes a slight elastic return.

There appear to be two different modes of vibration in the diaphragms. This divides the diaphragms into two classes corresponding to these modes of vibration. In the first class, referred to as the upper or U-class, the diaphragms regain at the time t_1 the entire displacement lost during the pauses, as shown in Figure 24a. In the other class, referred to as the lower or L-class, the lost deflection is not fully regained as in Figure 24b, and the deflection at the center is less than if the motion had continued at a uniform rate. The origin of the jerking motion in the flat central region is not known, nor is it known why there seem to be two different modes of this type. One suggestion* is that the jerking is due to a pressure wave reflected back and forth between the central area of the diaphragm and a cavitated region in the water. In other words it may be caused by vibrations in a layer of water left on the undersurface of the diaphragm as it is displaced.

Figures 25, 26, and 27 show the variation with charge distance of the measured times t_0', t_0'', and t_1 respectively. The data on t_0 were too meager and difficult to measure to indicate any significant variation with distance. The measurements which were made, however, give an average for t_0 of about 0.12 millisecond. The time t_0' decreases slightly from 0.2 millisecond at a charge distance of 8 inches to about 0.16 millisecond at a charge distance of 13 inches. At greater charge distances this value remains practically unchanged.

----

* This suggestion was first made to the writer in a discussion with Dr. ?. Fye of the Woods Hole Oceanographic Institution.
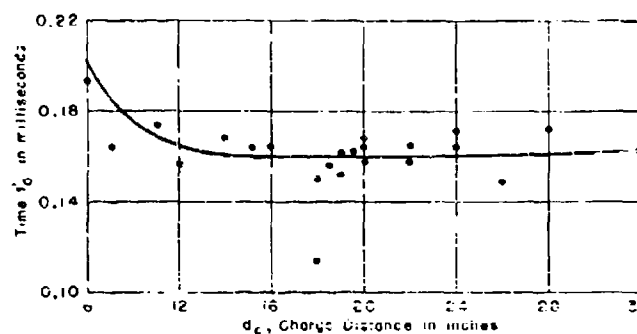
Figure 25 - Time t_0' of Second Hesitation in the Motion of the Center Spot
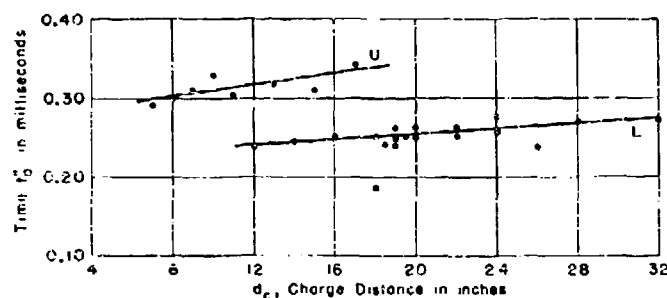
Figure 26 - Time t_0'' of Third Hesitation in the Motion of the Center Spot
Note separation into upper, U, and lower, L, classes.
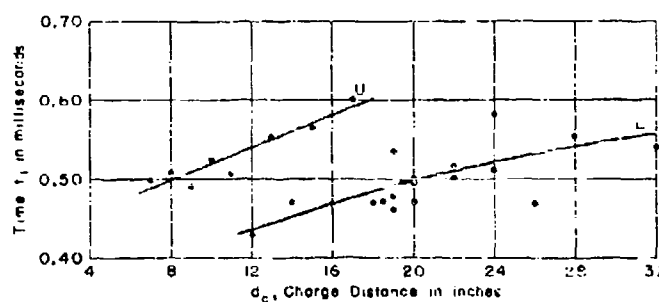
Figure 27 - Time t_1 of the Arrival of the Bending Wave at the Center
This is the swing time of the diaphragm.

First evidence of the separation of the data into two groups appears in the graph of t_o'' in Figure 26, which consists of two branches. The U-branch is practically rectilinear, extending from 0.30 millisecond at 7 inches to 0.34 millisecond at a charge distance of 18 inches. The L-branch is also linear with charge distance and extends from 0.24 millisecond at 12 inches to 0.275 millisecond at 32 inches charge distance. The two groups are separated still farther in the t_1-graphs, Figure 27. The U-branch is rectilinear and extends from 0.49 millisecond at 7 inches to 0.6 millisecond at 18 inches. The L-branch exhibits a slight tendency to depart from linearity. It extends from 0.435 millisecond at a charge distance of 12 inches to about 0.56 millisecond at 32 inches, with considerable scatter in the data.

The fact that t_1, frequently referred to as the swing time of the diaphragms, is not constant, but seems to increase slowly with charge distance in both the U and the L groups, is probably a combined result of many separate effects. The major part of this variation, however, may very likely be ascribed to the increase in plastic stress due to increased strain rates at shorter charge distances. The result of this increase in stress would be to increase the velocity of the bending wave, thereby cutting down its time of transit from edge to center.

At time t_1 the diaphragm appears to be almost conical in shape. The departure from a cone may be attributed, in part at least, to the strain-rate
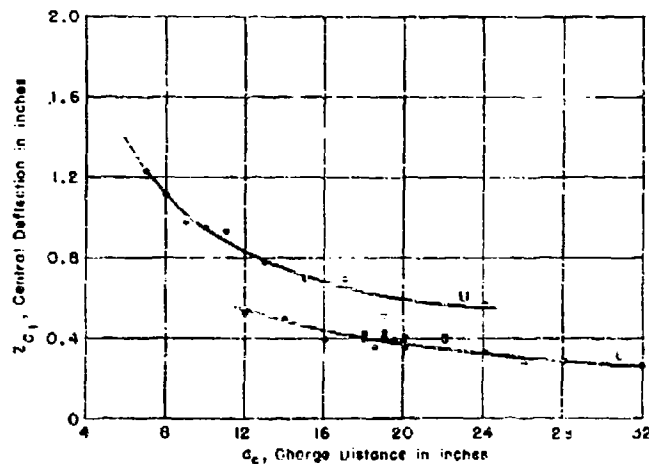
Figure 28 - Central Deflection Z_{C_1} at the Time of Arrival
of the Bending Wave from the Edge

Note that, at a charge distance of 6 inches, the deflection is large because the center has received the blow caused by closing up of cavitation before the bending wave arrives.

effect mentioned in the previous para-
graph. The central deflection Z_{c_1} at
this time, varies from 1.2 inch at a
charge distance of 7 inches to 0.26
inch at a charge distance of 32 inches.
Z_{c_1} is plotted in Figure 28 and shows
the characteristic splitting into a
U- and L-graph.

The splitting is not quite
as obvious in the graphs of central
deflection against charge distance as
it is in the graphs of time against
charge distance. However, it should
be emphasized that the double-branch
phenomenon is not due simply to a ran-
dom scatter. This is quite clear from
an examination of the displacement-
time curves. Moreover, the diaphragms
which appear in the U-branch of one
graph also appear in the U-branch of
the other graphs. The same statement
applies to the diaphragms of the
L-class.

Figure 29 - An Enlarged Streak Record
This record was traced from a photograph. It
shows the bending wave traveling to the center
of the diaphragm, and the effect of the blow
received at the center as cavitation closes.

Just before, or, more frequently, a few tenths of a millisecond
after the time t_1 at which the bending wave reaches the center, an additional
impulse is received by the diaphragm. This takes the appearance, as in Fig-
ure 29, of a sharp increase in velocity near the center, which region has al-
ready come to rest when the charge distance exceeds 7 inches. The impulse is
accompanied by a bulging of the outer portions of the diaphragm. This phe-
nomenon is thought to be due to a kind of water-hammer effect when the cavi-
tation in the water closes up under the influence of the pressures in the
tail of the shock wave. The time t_3 of occurrence of the blow at the center
is plotted in Figure 30 which again exhibits the splitting of the data into
the two groups, U and L. The trends are quite definite in this graph and
show, as the charge distance is increased, a comparatively rapid increase in
the time at which the blow is received.

At about 1.1 millisecond after the initiation of the motion, the
diaphragm finally comes to rest relative to the holding ring save for a
slight elastic motion of very small amplitude. The central deflection Z_{c_3}
at this time t_3 is shown in Figure 31 plotted against charge distance. The

Figure 30 - Time t_2 Plotted against Charge Distance

t_2 is the time at which an additional blow is received at the center of the diaphragm. This blow is supposedly caused by the closing up of the cavitated region in the water.
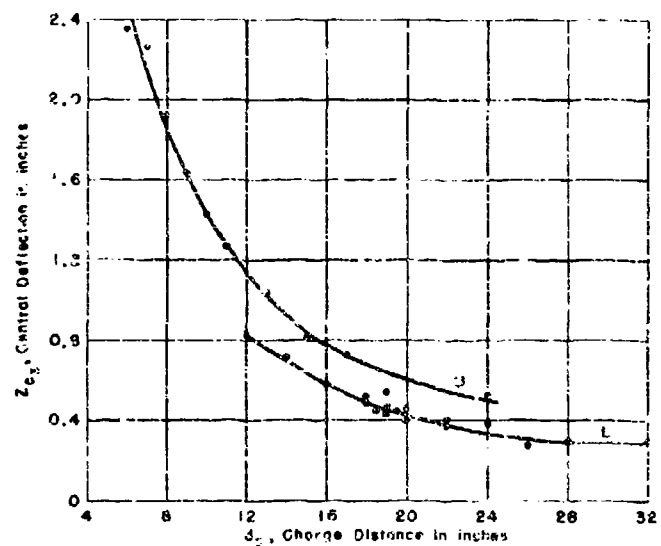
Figure 31 - The Central Deflection Z_{c_2} after the Cavitation Blow Has Been
Received and the Diaphragm Has Reached Its Maximum Deflection
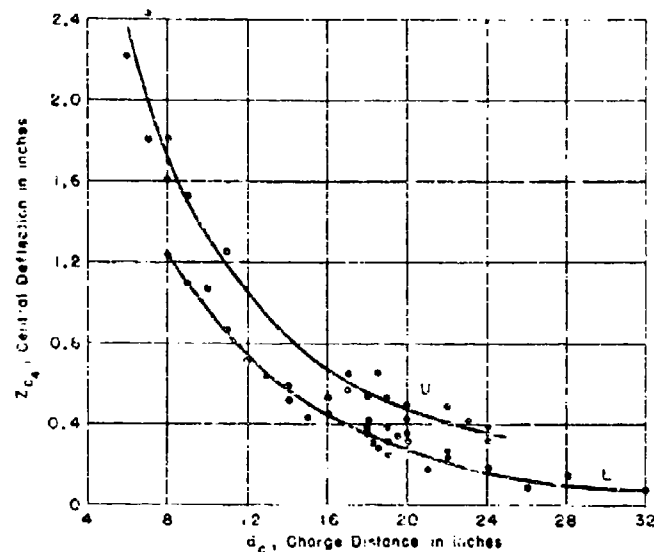
Figure 31 - The Central Deflection after the Diaphragm Has
Returned Elastically from the Maximum Deflection Z_{C_3}

separation into two groups is still in evidence in this graph. The effect of
the water-hammer blow is also evident if the graph is compared with that of
Z_{C_1}, Figure 28. The deflection has increased to about 2.25 inches at a charge
distance of 7 inches, an increase of about 1 inch relative to the U-branch of
Figure 28. At 32 inches the deflections are 0.29 inch in Figure 31 and 0.26
inch in Figure 28. The elastic return somewhat decreases these central de-
flections, as shown by the curves of Figure 32 in which the central deflec-
tion Z_{C_4}, observed about 2 or 3 milliseconds after the initiation of the mo-
tion, is plotted against charge distance.

The displacement of the diaphragm thus far has been described rela-
tive to the holding ring which is bolted to the mounting ring in the bottom
of the boat. The streak pictures show that the motion of the holding ring
is as follows: On the impact of the shock wave it is given an initial veloc-
ity upward, as discussed previously, on which there is superimposed a damped
vibratory motion of large amplitude having a frequency of about 60 cycles per
second. This frequency agrees roughly with that calculated for the free vi-
bration of a rectangular plate of the same dimensions as the bottom of the
boat. The holding ring and part, at least, of the bottom of the boat to
which it is attached jump to a height of about 2.8 inches when the charge is
fired 20 inches from the diaphragm. The holding ring is then accelerated
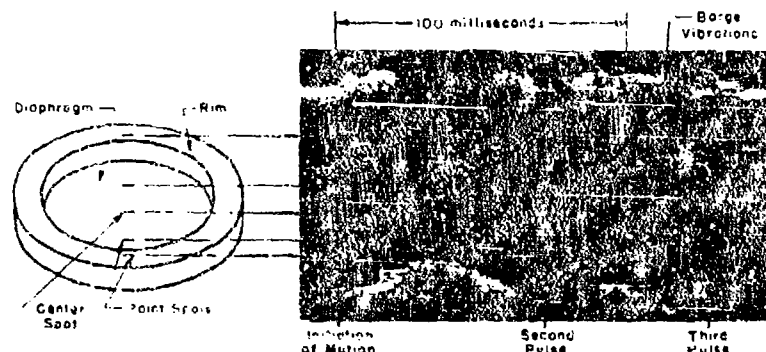
Figure 22b – Low-Speed Streak Photograph

downward, presumably under the influence of gravity and air pressure, and returns to the original level at about 75 milliseconds.

Simultaneously with this return of the holding ring, the diaphragm receives another blow which appears to be not quite so impulsive in nature yet strong enough under the proper conditions to do considerably more damage to the diaphragm. This contributes the major part of the "C-phase" damage, inferred in Reference (10). Indeed, at charge distances less than 18 inches, the diaphragms invariably rupture during the application of this second blow. Because the time interval between the initiation of the motion and the second blow agrees so closely with the period of oscillation of the explosion-gas globe, it seems quite probable that the increase in damage is due mainly to the pressure wave sent out from the gas globe on recompression. It is also quite possible that the return of the boat to the water level just in time to receive the second pressure pulse might fortuitously have increased its damaging effect. That is, the results obtained in tests of this kind almost certainly depend upon the nature of the supporting structures.

That little, if any, work is done on a diaphragm in the time interval between 2 milliseconds after the initiation of the motion and the time t_s 75 milliseconds later just before it receives the second blow is evident from comparison of the central deflections Z_{C_5}, measu   e latter time and plotted in Figure 33, with the central deflections $_{s'}$ nown in Figure 32. It is found possible to measure the central deflections Z'_{C_5} of a few of the unruptured diaphragms after the second blow. These are plotted in Figure 34; because of the paucity of data and because of the screening effect of the second blow, the data are not separated into two branches.

After the tests were completed the diaphragms were cut from the holding rings and their profiles were drawn. Measurements on these yielded
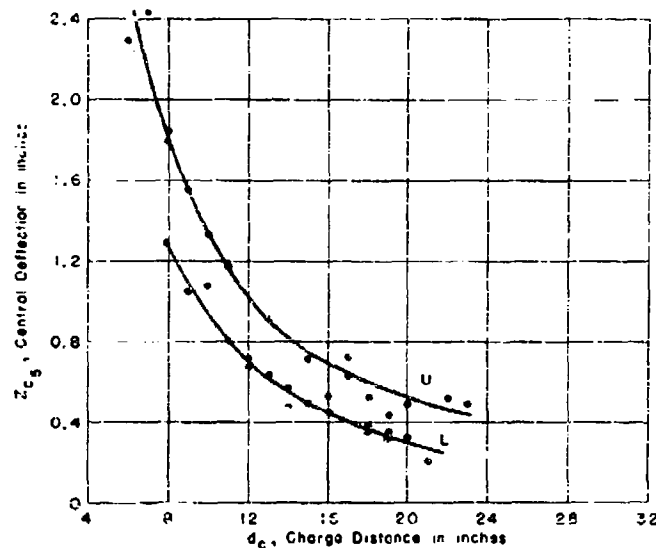
Figure 33 - Central Deflection Just before Arrival cf the Second Pulse
Caused by the Globe Oscillations

Compare with Figure 32.
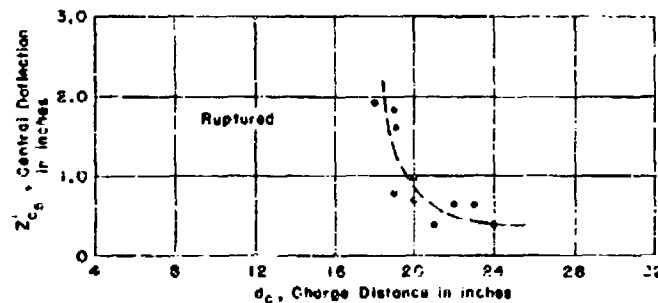
Figure 34 - Central Deflection Just after the Second Pulse,
from the Gas-Globe Oscillations, Has Done Its Damage

the final central deflections Z_{c_F} plotted in Figure 35. For the ruptured
diaphragms, estimates of the central deflections were made by assuming par-
abolic shapes in the torn central region. These doubtful deflection values
are distinguished by plotting them as crosses. Of course, there is consider-
able scatter among these latter points, but the break in the curve at the
critical rupture distance is quite clear. Little damage is done to the dia-
phragms after the second blow, as can be verified by comparing Figure 35 with
Figure 34.
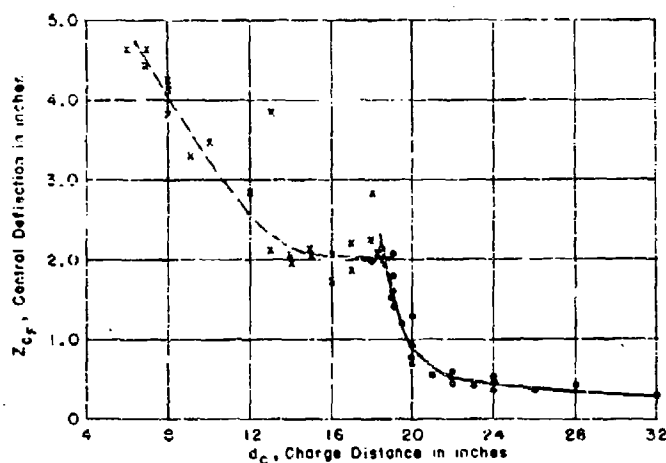
Figure 35 - Final Central Deflection Z_{C_F} As Measured
from the Diaphragm Profiles

The crosses denote estimated central deflection of the ruptured diaphragms. The curve through
the unruptured diaphragms agrees well with that of Figure 34.

It may be noted from Figure 22b that the 60-cycle vibrations of the
bottom plate of the boat are again excited by the second blow, and again by
the third blow. This can be verified by an inspection of the streak photo-
graph. The time interval between the second and the third blows has been
measured and found to be about 58 milliseconds, which is shorter than the
interval between the first and the second blows. This probably results from
the shortened period of oscillation of the gas globe as it loses some of its
energy in the successive pressure waves emitted during its compression phases.
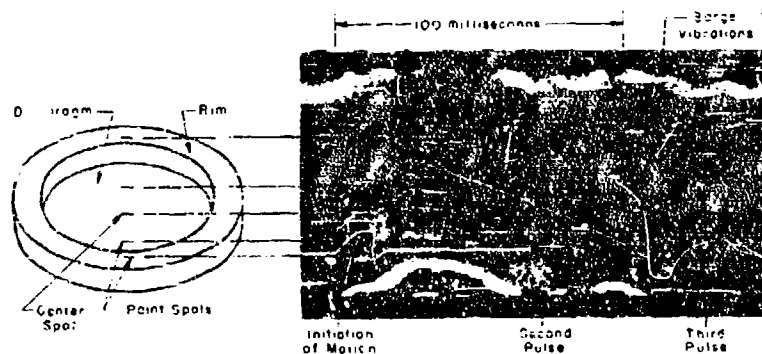
Figure 22b - Low-Speed Streak Photograph

The radial displacement-time curves of the particles in the diaphragm have not yet been studied This experimental investigation will be made as soon as the requisite apparatus becomes available. It should furnish information about the thinning of the diaphragm during the deformation and therefore about the all-important question of rupture by underwater attack. Incidental to this study, considerable light may be shed on the interesting jerking motion of the material in the center of the diaphragm.

CONCLUSIONS

The observations described in this report bear out in detail the hypothesis put forth in Reference (10) that the C-phase pressures are effective in producing damage when the charge distance is less than a certain critical one. Moreover, quantitative evidence supports the contentions of (10) that (a) the pressures between the closing up of cavitation and the second blow do little damage, and (b) the initial impulsive velocities of parts of the diaphragm are proportional to the inverse first power of their distances from the charge. That is, the initial kinetic energy of the diaphragm at the larger charge distances is roughly proportional to the solid angle subtended by the diaphragm at the charge.

REFERENCES:

(10) "Early and Ultimate Damage due to Underwater Explosions against 10-inch Diaphragms," by G. E. Hudson, Ph.D., TMB Report 509, August 1943.

(11) "Effects of Underwater Explosions, General Considerations," by Professor E.H. Kennard, TMB Report 489, September 1942.

(12) "Progress Report on Underwater Explosion Research - Bureau of Ships Symbol E139 - Part 2 - The Pressure-Time Curve for Underwater Explosions of Very Small Charges of Tetryl," by M.M. Shapiro and E.T. Habib, TMB Report R-202, February 1944.

AN IMPROVED TECHNIQUE FOR HIGH SPEED PHOTOGRAPHY

D. A. Senior and C. O. J. Grove-Palmer
Naval Construction Research Establishment
Rosyth, Scotland

British Contribution

January 1950

AN IMPROVED TECHNIQUE FOR HIGH SPEED PHOTOGRAPHY

D. A. Senior and C. O. J. Grove-Palmer

Naval Construction Research Establishment
Rosyth

January 1950

* * * * * * * *

Abstract.

A technique is described for high speed cine-photography of the phenomena which take place when small explosive charges are fired under water. At the same time, the explosive pressures are recorded by piezo-electric technique. Pressure records are obtained for a period of 60 milliseconds, and high speed photographs are taken by means of a 16 mm. Fastax camera at speeds up to 4,000 frames/second. At the maximum speed, a cine record in black and white or colour is obtained for a period of 60 milliseconds. The layout of equipment is described, and details of time marking and sequence timing arrangements are given.

Introduction.

In studying phenomena associated with the detonation of small explosive charges under water, the problem arose of taking motion pictures of an area 3 feet 6 inches square through nine feet of water at speeds up to 4,000 frames/second. The illumination of limited areas for this purpose may readily be provided by means of continuous light sources, but the power requirements are considerable if the area to be photographed is extensive. (Calculations showed that in this instance, colour photography would require about 1,000 k.w. of photoflood lighting, which was clearly impracticable).

High intensities of illumination may, however, be provided for limited periods by means of photoflash bulbs (1), (2), (3), and the technique which is described is based upon this principle. Photographs are taken simultaneously of phenomena above and below the water surface. The equipment has been designed so as to synchronize the photography with other methods of recording.

The photographs cover a period of 60 milliseconds at maximum speed, and therefore give the general history of the explosion phenomena. First information is obtained by projecting the records as a film at normal speed. From a study of the film it is possible to decide at which points more detail and time resolution are required. The detailed study is then carried out by taking microsecond flash photographs at suitable times from the instant of detonation.

Water treatment.

Experiments have been carried out in a cylindrical tank of diameter 12 feet and depth 9 feet around which has been built a laboratory to provide cover over the tank itself and accommodation for control and recording equipment.

Water clarity is maintained by careful exclusion of dust and continuous filtration (the filter handles one tank volume per day). An alkalinity of $pH.8$ is maintained by the addition of sodium carbonate (about 6 g of the anhydrous salt per day). The addition of 0.6 g potassium alum per day then ensures coagulation of suspended matter and its removal by the filter.

Photographic equipment.

Camera.

The Western Electric 16 mm. Fastax camera has been used. This camera has a maximum speed of 4,000 frames/second, the exposure time then being 80 microseconds.

Two modifications have been found desirable. The lens provided by the makers (of focal length 2 inches) does not give a sufficiently large field of view. It has therefore been replaced

By A. ....

by a Dallmeyer 'Reverse Telephoto' lens which has an effective focal length of 1 inch.   The comparatively large distance of 2 inches from the rear component to the focal plane makes it possible to use this lens in spite of the space occupied by the rotating glass block which is a feature of the camera.

No time marker is available with the camera as manufactured.   A crater tube (Sylvania Type R.1130.3) has therefore been installed to operate at a tuning fork controlled frequency of 5 kc/s.   The light is focussed, by means of a small mirror and lens, on to the film on the sprocket wheel in the space between the perforations and the edge of the film.   The arrangement is shown in Figure 2.

Light source.

Light is provided by firing a sequence of flash bulbs, the wire-filled type being used in preference to those with foil filling.   The advantages are that, with the wire-filled variety, the time interval between the application of voltage and maximum light output is constant within close limits; the percentage of bulbs which fail to fire is very small; the bulbs do not fire sympathetically and may thus be mounted compactly in groups without the use of partitions.   They are, moreover, robust, and able to resist explosive shock.

Reflector units have been built to take twelve or twenty-four bulbs which are fired at intervals of 10 milliseconds.   Their light outputs overlap to give an even illumination throughout the sequence.

Provision is made for firing a maximum number of 192 bulbs in groups over periods varying from 60 to 320 milliseconds.   The following formula, derived experimentally, gives the number of flash bulbs required (bulbs used being Philips P.F. 56 with an output of 56,000 lumen seconds):-

$$N = \frac{f^2 \, d^2 \, e^{D/10}}{30 \, Z}$$

where f is the lens aperature.

 d is the distance from the light source to the subject in feet.

 D is the water path in feet traversed by the light between light source and camera.

 S is the speed of the camera in thousands of frames/second (with the Fastax camera the exposure time is approximately one third the time per frame).

 Z is a factor which varies inversely with the speed of the film used and has a value of unity for Kodachrome.

 N is the number of bulbs in each group, the number of groups being determined by the length of record required.

Photographic layout.

The layout is shown in Figure 1.   The camera is mounted with its axis running vertically through the centre of a 1 inch plate glass window in the bottom of a brass box (the waterscope). The function of the waterscope is to eliminate optical distortion by the water surface.   A mirror is arranged beneath the waterscope at an angle of about 45° to the vertical the depth and angle of the mirror both being adjustable.   A surface silvered mirror is introduced between the camera and waterscope when photographs above the water surface are required.

Photography is carried out by reflected light against a black background.   The reflector units are clipped on to vertical poles which may be withdrawn from the water in order to change the bulbs.   No waterproofing is provided as the bulbs operate quite satisfactorily under water.

The explosive charge, a 15 grain electric detonator, is supported upon stiff wires which serve also as firing leads.   Orange and green coloured cable is used so that the colour rendering may be checked in colour films.

Pressure recording.

Shock wave pressures are recorded for a period of 50 milliseconds by piezo-electric technique.   Two ½ inch diameter tourmaline crystal gauges are connected to amplifiers and the pressures recorded by an oscilloscope and drum camera.

Time .....

Time marking is provided by means of a crater tube operating in parallel with the tube in the Fastax camera. The two records are synchronized by interrupting the timing traces for 0.2 milliseconds about 16 milliseconds after firing the charge.

In order to facilitate comparison of pressure records, the drum camera speed is adjusted to 750 r.p.m. before the Fastax camera is started, the speed being checked as follows:- a radial line painted upon the driving pulley of the drum is illuminated by means of a neon stroboscope operating at a tuning fork controlled frequency of fifty flashes per second. When the drum is running at 750 r.p.m. the line is seen as a cross. The charge is fired when the cross appears stationary.

Sequence timing.

Sequence of events.

The technique of timing the photographic and pressure records is influenced by features of the design of the oscillograph recording camera which will first be described with the aid of Figure 2. The film is wrapped around a drum 7 feet in circumference, the ends of the film being threaded through a slot in the periphery of the drum and held in place by means of a wedge. Exposure of the film during one revolution of the drum is regulated by the shutter S (Figure 2). The shutter consists of a brass plate, constrained to fall vertically, a slot in the plate permitting exposure of the film as the shutter passes the gate in the body of the camera.

The shutter is released by the electromagnetic trigger T at such a time that exposure of the film begins a few inches after the join in the film has passed the gate. Timing is effected by means of the contactor C mounted on the spindle of the camera drum, the angular position of the contactor segment being adjustable with respect to the position of the join in the film.

The whole sequence will now be made clear by Figures 2 and 3. The drum camera is first run up to speed. When the speed is steady at 750 r.p.m. the Fastax camera is started; thereafter timing is regulated by two circuits. The first, a simple delay circuit, governs the time of firing the charge relative to the start of the Fastax camera. Contacts are closed at a predetermined time after the start of the camera. (This circuit is not required in cameras such as the Eastman High-speed camera, which incorporates a mechanical switching device).

This closure completes the circuit to the contactor C. When the contactor segment reaches the brush, the second control circuit is set in operation. Details of this circuit, which is built around a Post Office uniselector, are given below. On receipt of the signal from the contactor, relays are operated which allow the uniselector to perform one cycle.

The cycle is performed in twenty-five steps at intervals of 16 milliseconds. The flash bulbs are fired on step number 2 and on subsequent steps. (The number of steps used depends upon the length of record required).

A signal is supplied to the circuit which operates the drum camera shutter on step number 1. The charge is fired on step number 4. On step number 5 a synchronization pulse is injected into the time marker supply.

Control circuit.

This circuit is designed (1) to time the opening of the shutter in the drum camera used in pressure recording, (2) to provide a synchronization pulse to the time markers on the Fastax and drum cameras, (3) to fire a sequence of photoflash bulbs and (4) to fire the charge. These operations are performed by a Post Office uniselector (Type 421). The remainder of the circuit starts the uniselector at the appropriate time, ensures that it performs one cycle only, and permits the testing of the uniselector without firing the flash bulbs.

The circuit is shown in Figure 4; it is operated by connecting the terminal marked "start" to the negative side of the 110 volt supply. The duration of this contact may be either prolonged or as short as a few milliseconds. In either case, the uniselector performs one cycle and then stops. If the switch S is in the open position the circuit resets itself automatically when the starting contact is removed. When the switch S is closed, the circuit must be re-set by hand before another cycle is performed.

This feature (hand re-set) is necessitated by the nature of the contact which operates the circuit in practice. As has been mentioned this circuit is started by the rotary contactor on the drum camera. Consequently, once the circuit to this contactor has been made, impulses of

about .....

about 2 milliseconds duration are repeated at intervals of 80 milliseconds – once for each
revolution of the drum. Without automatic re-setting between impulses the uniselector would operate
repeatedly with consequent

The control circuit must thus fulfil two conditions: (1) it must operate on a short
duration starting pulse and (2) it must then provide power to the uniselector for a long enough
period to make one step. After this the uniselector takes control. The power supply must,
however, be removed before the completion of the whole cycle in order to avoid the initiation
of a further cycle.

The first condition is achieved by the rapid closure of the double wound Relay X
(Figure 4). This relay is energised initially on a voltage of 110 volts through the contacts
X_3 which are normally closed. This permits a surge of current to flow until operation of the
relay opens the contacts X_3. Relay X is then maintained by the reduced current which flows
through the series resistor R_2. Under these conditions the operation of relay X is sufficiently
rapid to respond to the starting pulse (which is of duration 2 milliseconds).

The relay is also maintained by the operation of contacts X_2 which connect the second
exciting coil of the relay to the negative end of the supply through the switch S (which is shown
closed in the position for "hand re-set").

The operation of the contacts X, completes the circuit to the driving magnet M of the
uniselector through the first wiper W_1 and the single contact on which the wiper normally rests.
After the first step the wiper gains contacts with the "homing" arc H. The driving current
through the magnet M and the self drive contacts Dr is then maintained until the uniselector has
completed a cycle of 25 steps. The wiper W_1 then comes to rest again on the single contact
mentioned above.

By this time, the circuit to the positive end of the supply must be broken if a second
cycle is to be avoided. This is brought about by the contacts Y_1. Relay Y is operated by the
closure of the contacts X_2. It is loaded with a capacitor C_1 and supplied through the resistor
R_4 and therefore closes relatively slowly. Consequently, current is supplied to the driving
magnet of the uniselector during the interval between the operation of relays X and Y. This
interval is adjusted, by choice of the values of R_4 and C_2, and is just sufficiently long for
the wiper W_1 to gain contact with the "homing" arc H.

Operation of relay Y also causes the contacts Y_2 to open. The circuit may therefore be
re-set by opening and closing the switch S. This de-energises relay X which in turn breaks the
supply to relay Y. Relay Y is then maintained for a short time by C_1, so that the contacts X_1
open before Y_1 recloses and re-setting does not initiate any cycle. The contacts X_2 also
operate a pilot lamp which is alight when relay X is not energised, i.e. when the circuit is ready
for operation.

Automatic re-setting is arranged by leaving the switch S open. Operation of relay Y causes
the contacts Y_2 to open. Relay X is de-energised at this stage or when the starting contacts are
opened if this should occur later. This in turn de-energises relay Y and leaves the circuit ready
for operation.

Contacts 2 to 23 inclusive on the second bank of the uniselector are brought out to
socket to which the reflector units are plugged. Arrangements are made to fire the bulbs on
contacts 2 to 6, 2 to 12 or 2 to 23.

Provision is made for testing the control unit and checking the speed of the uniselector
without firing the flash bulbs. K_1 and K_2 are contacts on a non-locking test key. Closure of
K_1 maintains the uniselector for as many cycles as are desired. Relay Z operates when K_2 is
closed and is maintained via contacts Z and the homing arc until the end of the cycle during
which K_2 is opened. The contacts Z_2 break the circuit to the flash bulbs which consequently do
not fire during testing. The pilot lamp P_2 is wired so as to light once per cycle as wiper No. 4
passes over the last 4 contacts of the bank.

The speed of the uniselector is controlled by means of the variable resistor R.6.

Results .....

Results.

Typical photographs from a high speed cine record are given in Figure 5.   These show
the water phenomena associated with the detonation of small charges below the water surface.
In each case the lower portion of the picture shows the bubble formed in the water by the
products of the explosion.   The upper portion shows the formation of the surface phenomena
typical of an underwater explosion.

Acknowledgements.

The writers wish to thank Mr. O.R. Leah, B.Sc., A.M.I.E.E., for his assistance with the
design of the control circuit, Messrs. W.J. Millar and F. Winfield for their work during the
development of the technique.

References.

(1)   Lester, H.H.   G.E. Review. 47 (April, 1944)

(2)   Palme, A.   American Photography (January, 1945)

(3)   Lester, H.H.   J. Soc. Mot.Pict.Engrs.45, (November, 1945).

FIG. 1. Photographic Layout.

G_1
PIEZO-ELECTRIC GAUGES
G_2

Amplifier

AMPLIFIER

DRUM CAMERA

BRUSH

CONTACTOR

TIME MARKER

CATHODE RAY
OSCILLOSCOPE

TIME MARKER

SHUTTER
CONTROL
CIRCUIT

TIME MARKER
AMPLIFIER

DELAY
CIRCUIT

FLASH CONTROL CIRCUIT

REFLECTOR
UNIT

FLASH CIRCUIT

CHARGE

CAMERA
CONTROL
CIRCUIT

FASTAX CAMER

TIME
MARKER
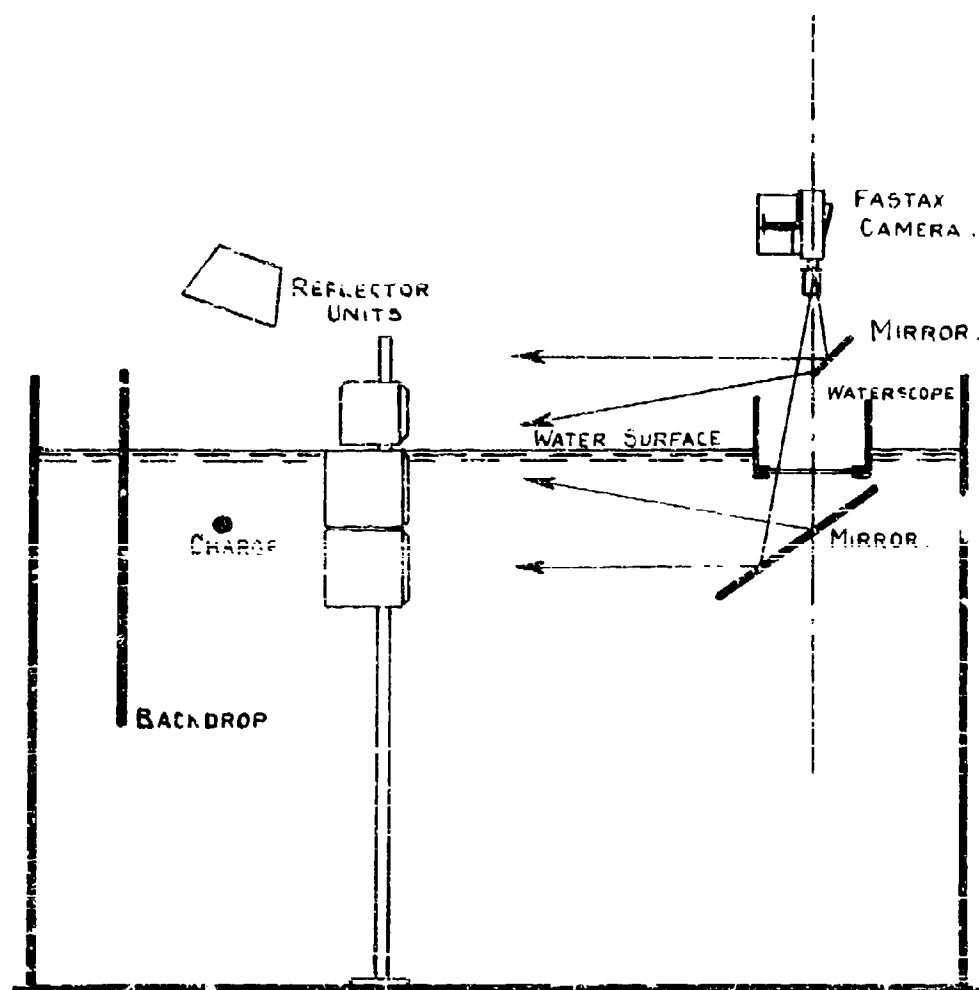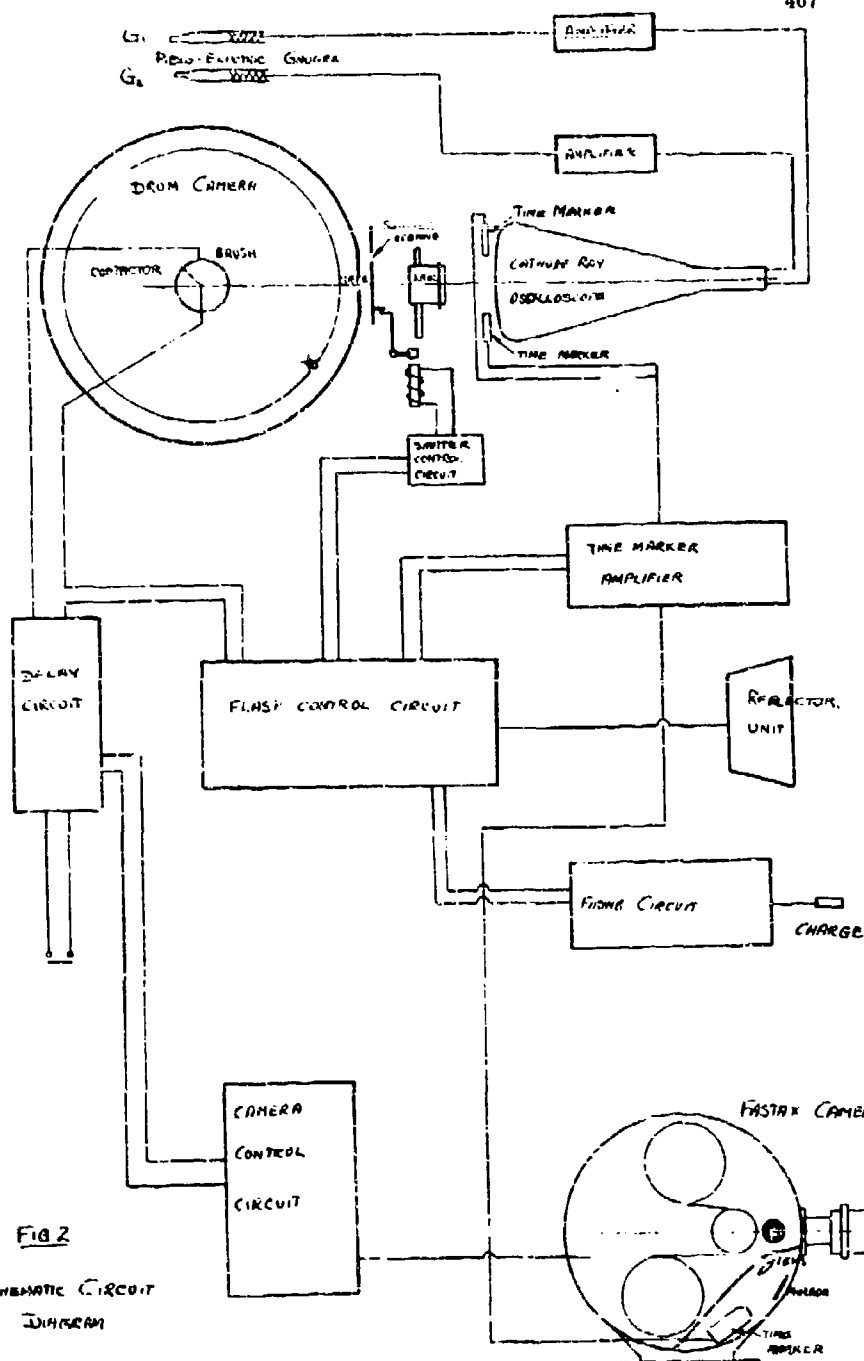
FIG 2

SCHEMATIC CIRCUIT
DIAGRAM

488

FIG 3. SEQUENCE OF EVENTS

- FASTAX CAMERA STARTS
- 0.96 SEC FOR A CAMERA SPEED OF 4000 FPS
- DELAY CIRCUIT CONTACTS CLOSE
- 0 TO 80 M.SEC DEPENDANT ON POSITION OF CONTACTOR WHEN CIRCUIT CLOSES
- DRUM CAMERA CONTACTOR CLOSES
- 16 M.SEC — UNISELECTOR STARTS
- 16 M.SEC — CONTACT N° 1 SIGNAL TO SHUTTER CONTROL CIRCUIT SHUTTER BEGINS TO FALL
- 16 M.SEC — N° 2
- 16 M.SEC / 8 M.SEC — JOIN IN FILM PASSES GATE / SHUTTER OPENS / N° 3
- 16 M.SEC — N° 4 CHARGE FIRED
- 16 M.SEC — N° 5 SYNCHRONISATION PULSE
- 16 M.SEC — N° 6
- 10 M.SEC — SHUTTER CLOSES
- 10 M.SEC — JOIN IN FILM AGAIN PASSES GATE
- 252 M.SEC
- N° 23
- FASTAX CAMERA STOPS

DRUM CAMERA SHUTTER OPEN

FLASH BULBS FIRED

1.5 SEC

Fig. 6. Control Circuit

$C_1 = 0.6 \mu F$ $C_3 = 0.1 \mu F$

$C_2 = 0.1 \mu F$

$C_4 = 0.1 \mu F$

$R_1 = 100 \Omega$ $R_5 = 15,000 \Omega$ $R_7 = 20 \Omega$

$R_2 = 1000 \Omega$ $R_4 = 100 \Omega$

$R_3 = 1000 \Omega$ $R_6 = 100 \Omega$

489

470

Figure 5

FRAME ENLARGEMENTS FROM THREE TYPICAL MOTION PICTURE RECORDS

O·25 M.SEC   2·25 M.SEC   17·5 M.SEC   25 M.SEC   41 M.SEC
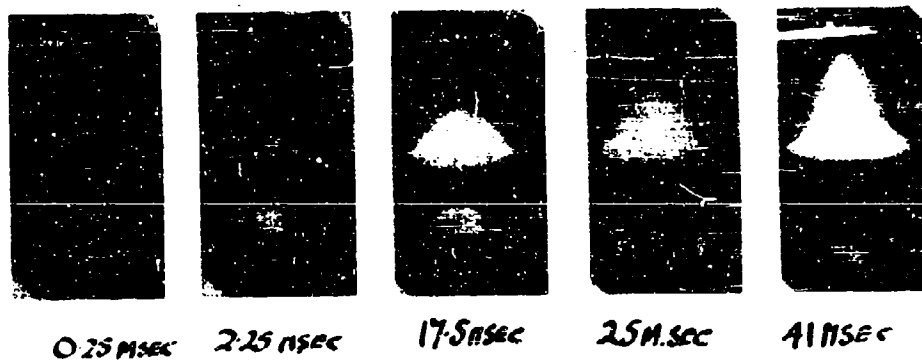
PRELIMINARY STATIC TEST OF A BOX MODEL TARGET PLATE

E. N. Fox
Admiralty Undex Works, Rosyth, Scotland

British Contribution

.

May 1943

PRELIMINARY STATIC TEST OF A BOX MODEL TARGET PLATE

E. N. Fox.

May 1943

: * * * * * * * *

Summary.

(1)   Results are given of a static test on a Box Model target plate subjected to uniformly distributed lateral pressure.

(2)   The shape of the deflected plate is in reasonable agreement with that expected theoretically on the assumption, as made by Professor G. I. Taylor in the report "The distortion under pressure of a diaphragm which is clamped along its edge and stressed beyond the elastic limit" (hereafter called report A), of uniform stress in the plate.   The load-deflection curve is also in reasonable agreement with the theory of report A if, due to strain hardening, the uniform stress in the plate is assumed to increase as the deflection increases with pressure.

(3)   Permanent strains, as measured along the centre lines, were greater near the edges than at the centre.   This result is attributed mainly to the influence of strain hardening.

Introductory Note.

The test described in this report was of an exploratory nature carried out with restricted facilities and both the accuracy and scope of the measurements were necessarily limited.

Since it has not yet been possible to carry out a more comprehensive trial it is thought that the results obtained in this preliminary test are of sufficient interest to warrant the present report.

Arrangements for trial.

The Box Model used for the test was of welded construction built by N.C.D. Portsmouth immediately prior to the test and since used for explosion trials in conjunction with the older models of similar design but of riveted construction.

The Model is essentially a rectangular box upon at one face around which an external angle section forms a flange to which the mild steel target plate (5 lbs./square feet nominal poundage) was fastened by bolts passing through a flat clamping plate of the same width (6 inches) as the flange.   Views of the model, taken after the test, are shown in Plates 1 to 4.

The Model was rested on its back with target plate horizontal and is shown in Plate 1 without clamping frame but with the arrangement devised by N.C.D. Portsmouth for measuring deflections during the trial.   This arrangement consists of nine wooden rods, of square section with pointed lower end, constrained to move vertically by guiding holes in the channel frames seen in Plate 1. These rods were marked off on one face with scales to $\frac{1}{10}$th inch, readings of which were taken where they were crossed, for each group of three rods, by a thin thread stretched horizontally between the vertical angle sections supporting the overhead channels.   These threads (not shown in Plate 1) were not quite touching the rods to ensure their not moving with the rods and the scales were read during the test by the use of binoculars at a short distance from the Model.   This latter arrangement was adopted as a safety precaution since it was not known prior to the test at what pressure or in what manner the plate would fail.   No difficulty was experienced in reading the scales to the nearest marking, i.e. to $\frac{1}{10}$th inch, by this method.

The .....

The Model was filled with water and connected to a hydraulic supply, the pressure so applied being measured by a gauge connected to the Model at the hole marked X in Plate 1. This gauge read up to 260 lbs./square inch in 5 lbs./square inch intervals while an additional gauge, reading to 650 lbs./square inch in intervals of 10 lbs./square inch, was connected to the inflow pipe at a distance of about 10 feet from the Model. There was no significant difference between the readings given by the two gauges.

In addition to readings taken during the trial by the preceding method, measurements of permanent deflection after the trial were taken at the points on the plate indicated in Figure 1 and Table 2.

Measurements of final pull-in at the edges were also taken as indicated in Figure 2 and Table 4 while measurements of permanent strain were made along the centre lines $\overline{oo}_1$, LL_1 (Figure 1) by taking strain rubbings, before and after trial, of centre punch marks spaced at approximately 1 inch intervals.

Description of trial.

It was intended prior to the trial that the pressure should be increased in stages, at the end of each stage the pressure being held constant while the deflection scales were read. This procedure was adopted for the pressures shown in Table 1 up to and including 120 lbs./square inch but at this latter pressure a slight leak developed at the edge fixings and it became difficult to maintain the pressure at a steady value. An immediate decision was accordingly made to continue the trial by increasing the pressure slowly and to concentrate on reading the central deflection scale only. In this way the central deflections shown in Table 1 for pressure above 120 lbs./square inch were recorded. It should be noted that in this second stage the central deflection increased by less than 6 inches in a matter of minutes so that any inertia resistance offered by the plate was completely negligible compared with the applied pressure.

At a pressure of 275 lbs./square inch the trial ceased abruptly by shearing of a clamping bolt in the middle of a long side and with water issuing rapidly at this point the pressure dropped suddenly to zero.

Discussion of Results.

1. Shape of deflected plate.

To avoid shearing of the plate round the edges the inner edge of the clamping frame was rounded off to about $\frac{1}{16}$ inch radius as shown in Figure 1, and the unsupported target plate area was thus given by the dotted lines in Figure 1 at the commencement of the trial but decreased slightly during the trial. To the order of accuracy of the measurements the unsupported area of plate can be taken as 6 feet by 6 feet while the points 1 to 9, at which deflections were measured during the trial, are the quarter-points of this area.

The deflections taken during the trial are tabulated in Table 1 while the permanent deflections after the trial are given in Table 2. The deflections quoted in Table 1 for zero pressure correspond to an initial asymmetric slackness in the plate. Comparison of deflections, in both Tables 1 and 2, for points, e.g. 2 and 8, nominally symmetrically situated with respect to the centre of the plate show that the deflection of the plate under the uniform pressure and after its release was reasonably symmetrical.

In report A, Professor G. I. Taylor developed the theory of a plate strained plastically by uniform lateral pressure and obtained a solution for a rectangular plate on the assumption that the plate behaved as a membrane exerting uniform stress in all directions in its plane. With this assumption the shape of the deflected plate is the same as that well-known for a soap film; contours of which shape are shown by the dotted curves in Figure 2 in which the full curves give the contours of the deflected plate after trial as plotted from the data in Table 2. In the comparison the contours have been drawn for equal central deflection and it is seen that the theoretical and observed contours are in reasonable agreement. As a further check the theoretical ratio of central to mean deflection is 1.72 while from Table 3 the corresponding ratio was 2.03 after

trial .....

trial and from 1.93 to 2.04 for pressures of 40 - 120 lbs./square inch during trial.   Both figure 3 and Table 3 thus show that the shape of the deflected plate is in reasonable agreement with the theory of report A.

2.   Load-deflection curve.

The relation between applied pressure and central deflection is plotted in Figure 4 where the experimental points from Table 1 are shown connected by a faired curve.

If the plate behaved as a membrane exerting a constant stress the load-deflection curve would be a straight line through the origin given, from equation 36 of report A with changed notation, by

$$Z_c = \frac{0.179 \ p a^2}{s_o h} \tag{1}$$

where Z_c = central deflection
          p = applied pressure
          a = half long span (36 inches)
          h = plate thickness (0.1114 inches)
          s_o = yield stress

Comparing this equation with the curve of Figure 4 it should first be noted that in the initial stages the theory would not be expected to apply in view of the elastic nature of small deflections and of the initial slackness of the plate.   Considering pressures above 60 lbs./square inch the experimental curve, while it cannot be approximated closely by a straight line through the origin over the whole of its length, is nevertheless not in disagreement with theoretical expectation if allowance is made for strain hardening.   Thus if we assume the stress in the plate to be constant over the surface but, due to strain hardening, to increase with increasing deflection then equation (1) will still hold at any particular deflection.   The stress s_o will now be, however, an increasing function of Z_c, and thus the load-deflection curve will become concave to the pressure axis.   Conversely from Figure 4 we can estimate the variation of s_o which would be necessary to give agreement between equation (1) and the experimental data. In this way we find that for pressures from 60 lbs./square inch to 275 lbs./square inch the calculated value of s_o varies from 18 tons/square inch to 23.5 tons/square inch.

As the test was a preliminary one intended originally to explore the possibilities of static tests rather than to obtain definite data, the plate used was taken arbitrarily from dockyard stocks; when it was realised that the data obtained was of sufficient interest to warrant analysis no spare piece of plate was available to carry out a tensile test.   It can, however, be said that the preceding values, deduced from Figure 4, of s_o increasing from 18 tons/square inch to 23.5 tons/square inch seem reasonable in view of the ultimate strength of 26 - 30 tons/square inch required by specification for the stock of plates from which the particular plate used in the trial was taken.

If we assume as indicated by Table 3 that the deflected plate is approximately constant in shape corresponding to a mean value $Z_c = 1.99$ then the volume of the deformed plate is directly proportional to the maximum deflection and from Figure 4 the total work done by the applied pressure can then be calculated to give a value of 185,000 foot lbs.   This can be regarded as divided between elastic strain energy, energy in permanent straining of unsupported target plate area and work done in pull-in at the edges.   From Table 1 and Table 2 it is seen that the measured elastic recovery at the centre was only 0.05 inches so that even allowing for an experimental error of 0.1 inches the work done in elastic deformation is only 1 - 2% of the total. An estimate of the work done in pull-in at the edges is given by multiplying $s_o h$ by the total area of pull-in as given in Table 4.   As discussed previously s_o may be taken as varying between 18 and 23.5 tons/square inch whence using a mean value of 21 tons/square inch we find that the work done in pull-in at the edges is 25,000 foot lbs. which is about 25% of the total work done.   We are thus left with about 160,000 foot lbs. of work done in stretching the original unsupported target plate area of 24 square feet again using $s_o = 21$ tons/square inch on the membrane assumption this work done corresponds to an increase of 370 square inches in the original area.   This estimated average area extension of 10.7% corresponds to an average lineal

                                                                                          strain .....

strain of about 5% which is not inconsistent with the measured strains recorded in Figures 5 and 6 for the centre lines.

3. Strain measurements.

To obtain estimates of permanent strain punch marks were made on the two centre-lines at approximately 1 inch centres and rubbings of these marks taken before and after trial. Owing to the thinness of the plate these punch marks could only be lightly made and it was found that the rubbings were not in general distinct enough to get sufficiently accurate measurements on 1 inch intervals. The rubbings were accordingly measured up in successive over-lapping pairs at three inch intervals, i.e. between punch marks 1 and 4, 2 and 5, etc., since in this way errors due to ill-definition of rubbings contribute only one third the error to the mean strain as compared with measurements over 1 inch gauge length. The mean strains in these successive overlapping three-inch intervals are shown plotted as ordinates in Figures 5 and 6 against the mid-points of the intervals as abscissa. Rubbings of several of the punch marks were too ill-defined to give any reliable measurements and there are corresponding missing points in Figures 5 and 6; it is unfortunate that punch marks near the edges comprised most of this category.

Due to inaccuracy of measurement no significance can be attached to minor variations from point to point on Figures 5 and 6 but on the other hand the general trend showing strain increasing towards the edges is undoubtedly a result not arising from experimental error. This result was rather unexpected since for an ideal plastic material yielding at a constant stress the analysis of report A showed the converse effect that for both a circular and an elliptical plate the strain decreases from a maximum at the centre to zero at the edges. A qualitative explanation of the observed result can, however, be given if work hardening is taken into account.

Thus if we consider an infinitely long plate under uniform lateral pressure each element of the plate is constrained to have no movement parallel to the edges and if work hardens under load the transverse strain will be a single-valued function of the transverse stress. This latter will, however, be constant over the span, in order to satisfy the equation of equilibrium in the place of the plate and thus the strain will also be constant over the span. To account for the strain being actually greater at the edges than at the centre it is only necessary to assume that due to the bolt-holes the plate is rather weaker near the edge, i.e. the stress-strain curve for an element near the edge is assumed to lie below that for an element near the centre. Since equilibrium will still demand a transverse stress constant over the span, a greater strain will be produced at the edges than at the centre. The preceding explanation is regarded as tentative since firstly, Figures 5 and 6 do not rule out the possibility of the strain decreasing rapidly very near the edges and secondly, the theoretical result for no strain hardening quoted from report A refers to a circular or an elliptical plate and the corresponding theoretical solution, yet to be obtained, for a rectangular plate might yield a different result.

4. Type of failure.

The cause of cessation of trial, namely by shearing of a clamping bolt, was unexpected since in explosion trials failure at the fixings takes place by tearing of the plate along the line of bolt holes at the centre of one or both of the long edges. Moreover when failure does not occur in explosion trials but the deflection is appreciable the bolt holes are always considerably more elongated than in the static trial.

It is not thought that the static failure was fortuitous due to a weak bolt since adjacent bolts were appreciably sheared and it would be improbable that the bolts used for the static trial were weaker than any used in the many explosion trials. This apparent relative weakness of the bolts may be due, however, to the fact that in the static trial the pressure was outwards and the bolts were thus subjected not only to shear as in explosion trials but also to tension. If this were the complete explanation it would be expected that that failure would have occurred at a smaller deflection in the static trial whereas in point of fact the static deflections both maximum and mean were 10 - 20% greater than any that have been obtained in explosion trials without rupture. It thus seems necessary to postulate, not only that the bolts have a possibly lower resistance under the conditions of the static trial but that the plate has a lower resistance at the bolt-holes in the explosion trials. Regarding this latter, the suggestion offered is that in explosion trials the plastic wave set up in the clamped edge of the plate by the deflecting unsupported central portion has difficulty in traversing the relatively weak line of bolt-holes. Consideration of such propagation of a plastic wave across a line of weakness lies outside the scope of the present paper but is a problem it is hoped to consider in the future.

495

TABLE 1.

Pressure lbs/sq →	DEFLECTION IN INCHES DURING TEST AT POINTS 1 TO 9 (FIGURE 1.)								
	5	2	8	4	6	1	3	7	9
0	0.69	.5.	0.6?	0.41	0.64	0.21	0.21	0.10	0.37
40	1.94	1.71	1.69	1.56	1.54	1.26	1.31	1.25	1.32
60	3.04	2.61	2.7-	2.21	2.39	1.91	2.01	1.95	1.82
100	4.54	3.91	4.04	3.41	3.59	3.01	3.01	3.00	2.97
120	5.14	4.51	4.54	4.01	4.04	3.61	3.51	3.40	3.32
130	5.54								
140	5.84								
150	6.14								
160	6.44								
170	6.74								
180	7.04								
190	7.34								
200	7.64								
210	8.04								
220	8.44								
230	8.64								
240	9.04								
250	9.54								
260	9.94								
275	10.74								

TABLE 2.

FINAL DEFLECTIONS AT INTERSECTIONS OF AA, HH, ETC., FOR FINAL PRESSURE OF 275 LBS./SQ.IN. (FIGURE 1)

	HH	JJ	KK	LL	MM	NN	OO
AA	0.89	1.28	2.31	2.56	2.31	1.25	0.59
BB	1.10	2.25	4.32	5.00	4.16	2.25	1.19
CC	2.00	3.56	6.91	8.44	6.72	3.63	2.06
DD	2.70	4.75	8.91	10.64	8.94	4.62	2.50
EE	2.31	3.81	6.91	8.31	6.80	3.52	2.10
FF	1.75	2.63	4.50	5.38	4.86	2.51	1.31
GG	0.94	1.50	2.63	3.13	2.31	1.22	0.66

TABLE 3.

MEAN DEFLECTION AND RATIO OF MAXIMUM TO MEAN DEFLECTION.

Pressure lbs/sq in.	40	60	100	120	275
Z	0.99	1.49	2.29	2.65	5.27
Z_c/Z	1.98	2.04	1.98	1.95	2.03
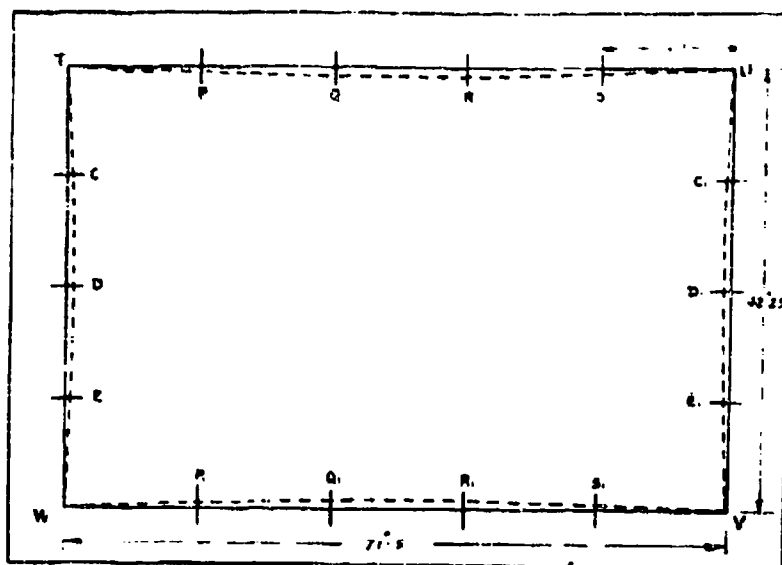
FIG. 7. PLAN SHOWING POINTS AT WHICH "PULL IN" AT EDGES WAS MEASURED.

TABLE 4.

MEASUREMENTS OF "PULL IN" AT EDGES.		
POSITION.	SEATING.	PLATE.
P₁	3/32"	7/32"
C₁	9/32"	7/32"
R₁	6/32"	7/32"
S₁	4/32"	6/32"
P	3/32"	6/32"
Q	6/32"	11/32"
R	6/32"	9/32"
S	4/32"	5/32"
C	NIL	7/32"
D	NIL	7/32"
E	NIL	6/32"
C₁	NIL	5/32"
D₁	NIL	7/32"
E₁	NIL	5/32"

AREA OF "PULL IN" (SQ. INS.).			
EDGE	SEATING	PLATE EXCLUDING SEATING	TOTAL.
W V	8.8	11.9	20.7
T U	9.1	13.2	22.3
T W	NIL	7.5	7.5
U V	4.0	6.9	6.9
	SUM TOTAL		57.4

477

FIG 1. PLAN OF PLATE & FRAME SHOWING POINTS AT WHICH
DEFLECTIONS WERE MEASURED.

478
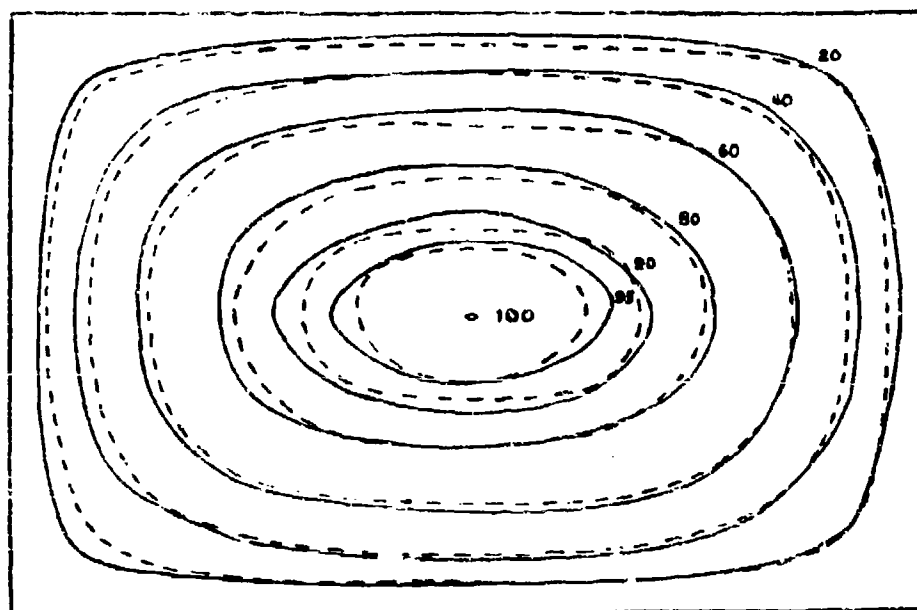
OBSERVED.

THEORETICAL.

NUMBERS TO CONTOUR LINES DENOTE PERCENTAGE OF MAXIMUM DEFLECTION

FIG. 3   COMPARISON OF OBSERVED & THEORETICAL CONTOURS AFTER
LOADING TO A PRESSURE OF 275/LBS/SQ.INCH & RELEASING
THE LOAD.

479

MAXIMUM DEFLECTION IN INCHES.
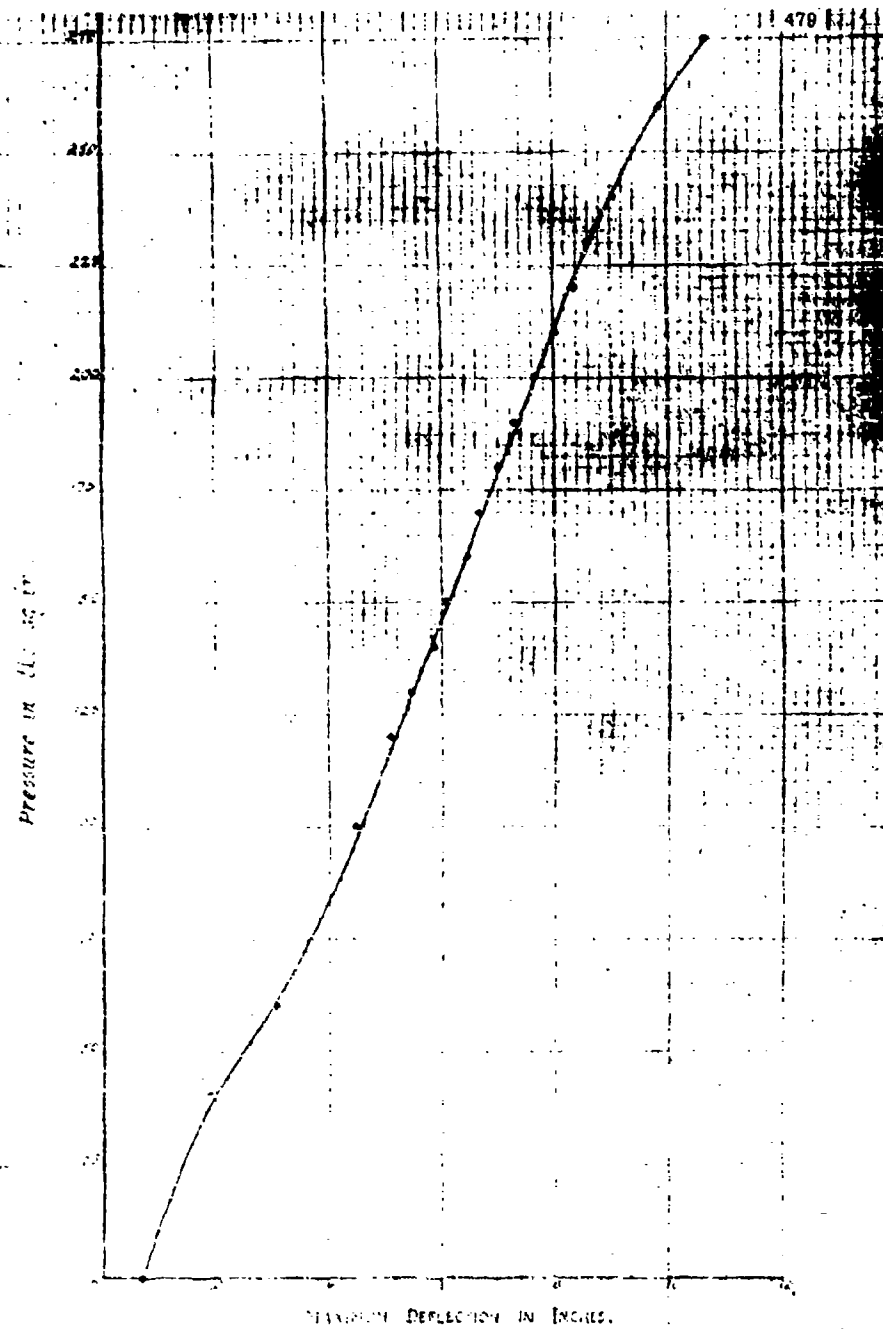
Fig. 4. Variation of Central Deflection with Pressure.
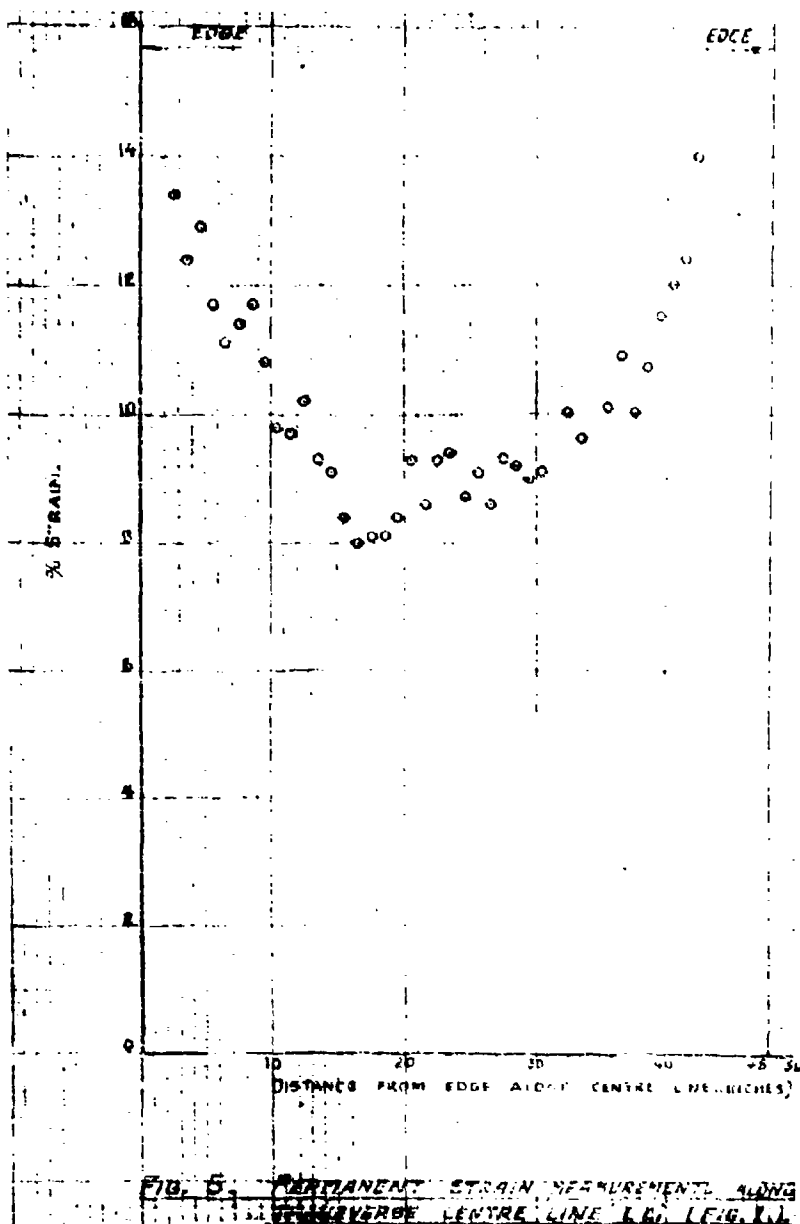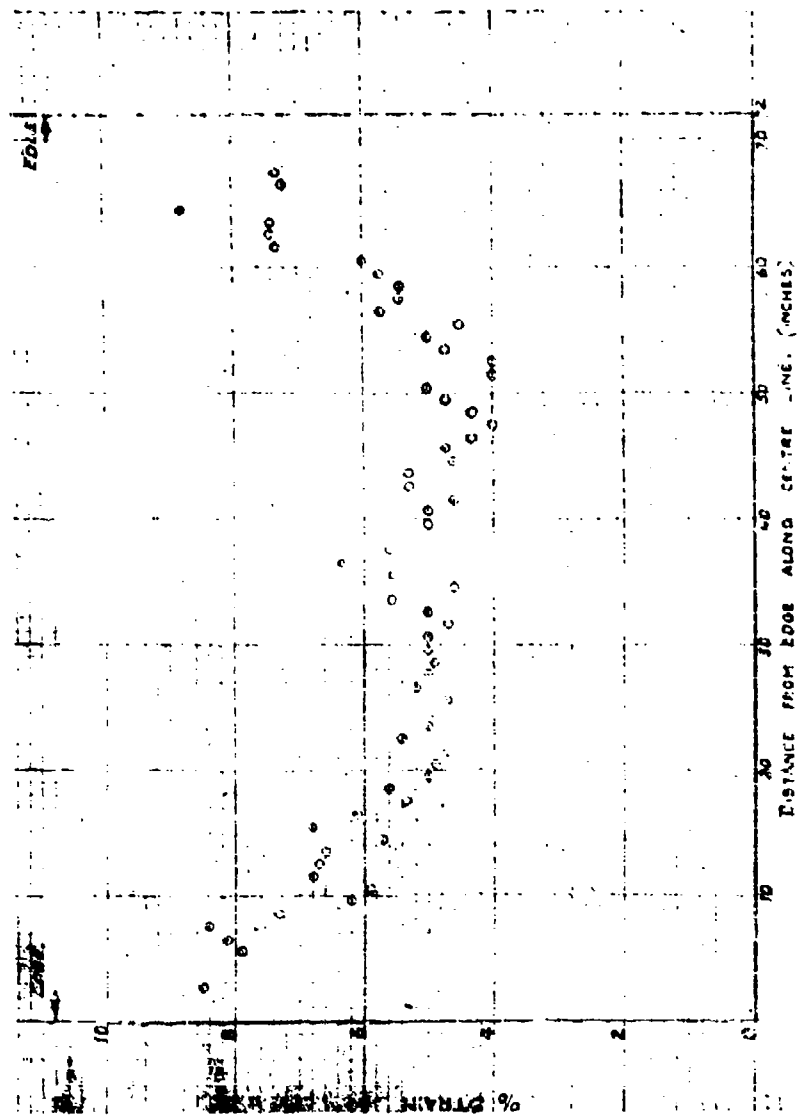
480

FIG. 5. PERMANENT STRAIN MEASUREMENTS ALONG TRANSVERSE CENTRE LINE E.G. (FIG. 1.)

FIG. 6. PERMANENT STRAIN MEASUREMENTS ALONG LONGITUDINAL CENTRE LINE J.DI (FIG.1).

DISTANCE FROM EDGE ALONG CENTRE LINE, INCHES.

FIG. 6   PERMANENT STRAIN MEASUREMENTS.
ALONG LONGITUDINAL CENTRE LINE 0-01 (FIG.1)
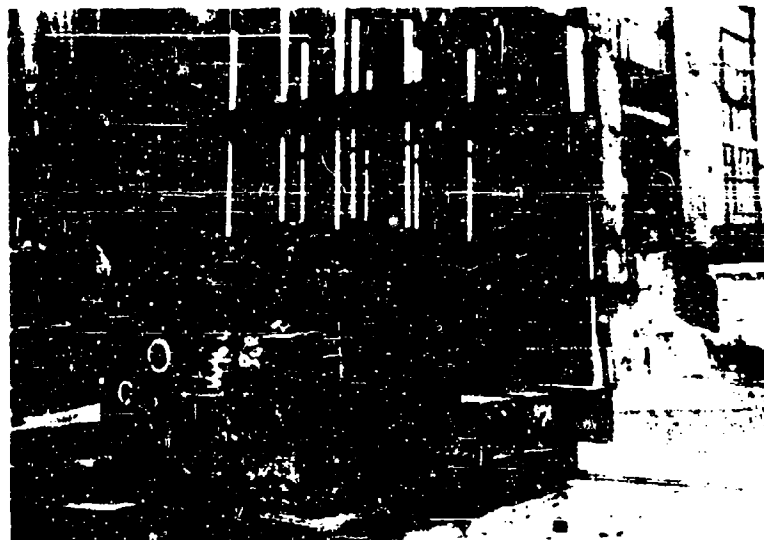
PLATE 1. ARRANGEMENT FOR MEASURING DEFLECTIONS DURING TRIAL.
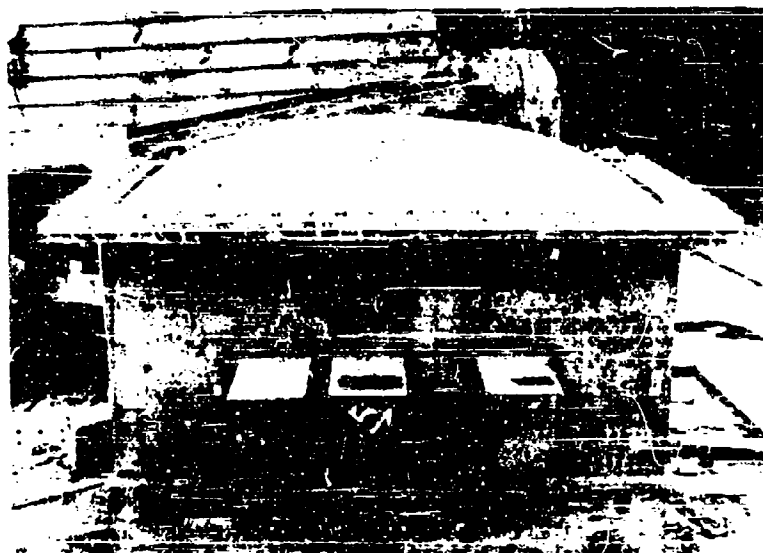
PLATE 2. SIDE VIEW OF DEFLECTED PLATE AFTER TRIAL
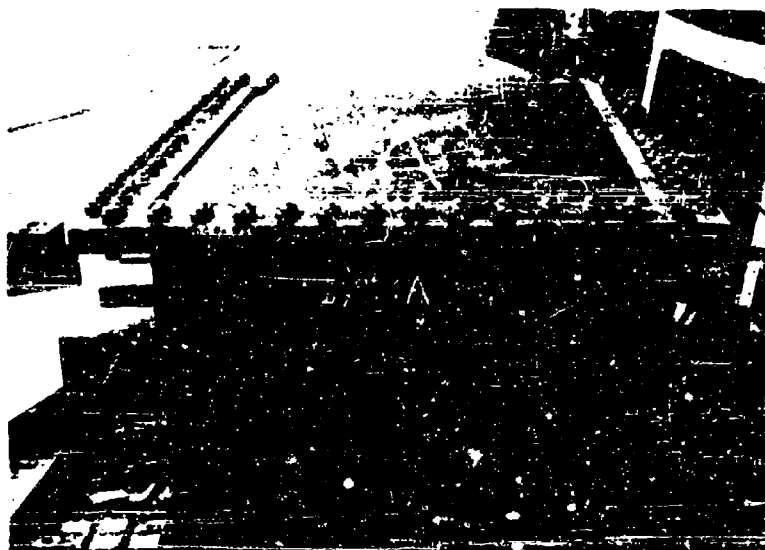
PLATE 3. END VIEW OF DEFLECTED PLATE AFTER TRIAL.
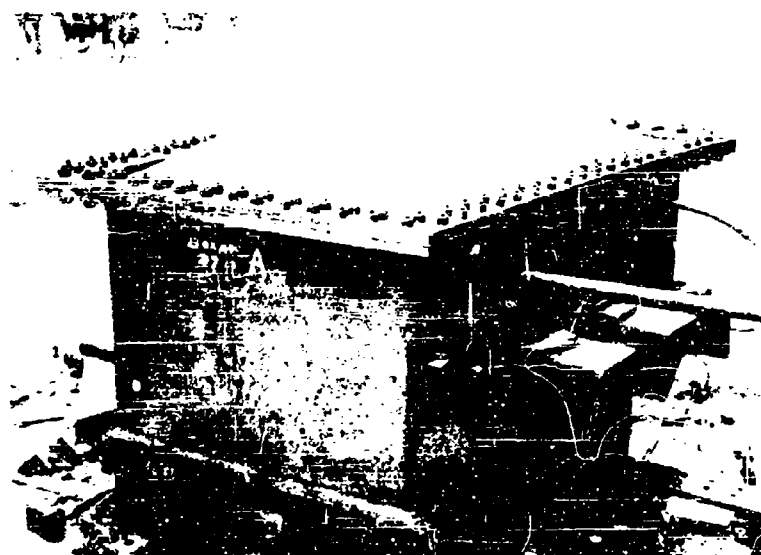
PLATE 4. DIAGONAL VIEW OF DEFLECTED PLATE AFTER TRIAL.

ANALYSIS OF PULL-IN AT EDGE FIXINGS IN BOX MODEL TRIALS

E. N. Fox
Admiralty Undex Works, Rosyth, Scotland

British Contribution

September 1945

ANALYSIS OF PULL-IN AT EDGE FIXINGS
IN BOX MODEL TRIALS

E. N. Fox

September 1945

*   *   *   *   *   *   *   *

Summary.

An approximate theory is developed for the behaviour under impulsive loading of a rectangular plate which is relatively weak at the edges, it being assumed that the edge fixings exert a mean membrane tension T_1 per unit length of periphery which is less than the mean membrane tension T_0 required to stretch the material in the unsupported area of the plate.

For a given type of loading the theory indicates that there will be a critical magnitude of load and a corresponding critical final mean deflection below which all increase of unsupported area takes place at the edges. For greater final mean deflections corresponding to more severe loading the increase in area will be due both to edge pull-in and plate stretching, the fractional contribution of the latter increasing steadily with increasing final mean deflection corresponding to increasing magnitude of load.

Experimental data on edge pull-in of the target plate in Box Model trials are in general qualitative agreement with the theory and quantitative comparison leads to an estimate that $(T_0 - T_1)/T_0$ is of order 5% or less for all shots.

It is concluded that estimates of energy absorbed by the target plate which have been given in previous reports on the assumption that there is no edge weakness only erred by 5% or less due to neglect of this particular phenomenon.

Object of analysis.

In previous analyses [1][2] of the results of Box Model trials, it was found that for some shots the estimated energy absorbed in plastic deformation of the target plate was considerably larger than the energy communicated by the shock-wave as estimated on different theories of loading.

Several possible sources for this difference were suggested and the present report is concerned with one of these, namely, that the energy absorbed, as calculated on the assumption that the plate was raised to its yield stress everywhere, might be seriously over-estimated if pull-in at the edge fixings could occur at a mean stress much lower than the yield stress for the plate.

In order to examine this possibility, measurements of the pull-in at the edges of the target plate were made as a routine procedure in all Box Model trials from shot 274 onwards. At the same time an approximate theoretical analysis was undertaken for application to these measurements with a view to estimating the resistance to pull-in relative to resistance to plate stretching. The present report gives the results of this application.

Outline of theory.

The detailed theory is given in the Appendix and we shall therefore give only the main assumptions and results.

(1)   Physical assumptions.

The plate is assumed to behave according to the more familiar "coal-bubble" approximation [1] i.e., any increase in area occurs under a constant membrane tension

$$T_0 = s_0 h$$

where s_0 is the yield stress and h is the original thickness assumed uniform over the plate.

By .....

By analogy with the plate assumption, we assume that the edge fixings exert a mean tension T_1 per unit length of edge when pull-in is occurring, and we assume

$$T_1 < T_0$$

corresponding to the edge fixings being relatively weaker than the plate.

We neglect any elastic effects, all energy absorption in plate or at edges thus being assumed irreversible.

The plate is assumed to be initially plane and at rest.

The impulsive pressure is assumed to be of the form

$$p = P(t) \, f_0 \, (x,y)$$

where x,y are rectangular co-ordinates in the plane of the plate and t is time, and the solution is obtained for the two specific cases of $P(t)$:

    (a)   Load communicated instantaneously as an initial velocity.

    (b)   Load suddenly applied and then maintained constant, i.e., $P(t) = H(t)$ where $H(t)$ is Heaviside's unit function.

(2)   Method of analysis.

Using the preceding assumptions an approximate theory is developed in the Appendix, using the method of an earlier report, the deflection w and the displacements, u, v in the plane of the plate being assumed to be of constant distribution in space as given by equations (1) to (3) in the Appendix.

The deflection w and displacements u, v are assumed sufficiently small to neglect terms higher than second order in w or first order in u and v.

As a further simplification, the solutions are carried through on the assumption that $(T_0 - T_1)/T_0$ is small, this being justified later by application of the theory to the experimental results.

(3)   Nature of motion and main results of theory.

For the particular loads assumed, it is shown in the Appendix that the motion will consist of successive stages of one or other of the following types:—

    Type I: Plate stretching and pulling-in at edges.

    Type II: Plate inextensional but pulling-in at edges.

The interesting qualitative result is then obtained that for either type of load the motion will consist entirely of Type II if the load is of sufficiently small magnitude corresponding to sufficiently small final mean deflections W_m. This result is exhibited in Figure 2, where it is seen that below a certain critical final mean deflection W_1 or W_2 ($= 1.89 \, W_1$) depending on type of load, all the increase of area S_m occurs at the edges implying that all the energy is absorbed there. Above the critical value W_1 or W_2, a progressively smaller fraction of S_m occurs at the edges and consequently more and more energy is absorbed in plate stretching.

It may be noted that the two curves in Figure 2 for the two different types of load are for practical purposes of the same shape over the range plotted since, if the curve (b) were plotted with abscissae W_m/W_2, it becomes virtually coincident with curve (a). This is a somewhat remarkable fact, since the equations for the two curves are not mathematically identical and no obvious physical reason can be suggested for such near-coincidence. However, this result does suggest that the qualitative shape of the curve is not very dependent on the particular form of loading assumed in the analysis.

In .....

In addition to Figure 2, the other main result of the theory is equation (109) of the Appendix, namely:

$$\frac{T_o - T}{T_o} = K \frac{W_1^2}{4ab} = \frac{9}{32} K \frac{W_2^2}{4ab} \tag{109}$$

where from equations (131) and (132) we should take $K = 26$ as a reasonable probable value and $K = 40$ as a probable overestimation of K.

Experimental data.

The Box Model, described in an earlier report, consists essentially of a rectangular steel box open at one side which is covered during the trial by a target plate held in position between the box and a stout flat frame by two rows of $\frac{7}{8}$" B.S. bolts passing through the frame and through an angle bar fastened round the edge of the box (Figure 1). The internal dimensions of the target plate were 7 feet by 5 feet, while those of the large plate were 9 feet by 8 feet. In two shots (206 and 209) the large plate frame was replaced by a small frame of 7 feet by 5 foot external dimensions.

Due to minor repairs after damaging shots, the unsupported area of target plate was not exactly constant, but for the present purpose it is sufficient to note that its area was $70 \times 86 = 3120$ square inches correct to 5% for all shots.

Shots involving rupture at the edge fixings are not amenable to analysis, and all shots considered are thus non-rupture shots. In all cases the target plate was mild steel and was suspended vertically with charge and centre of target plate at a depth of 7 feet. Details of charge conditions and plate thicknesses do not enter into the present analysis but are included in Table 1 for sake of completeness.

In order to measure the edge pull in, a line was scribed on the target plate at the inside edge of the clamping frame before the shot and the displacements of this line relative to the frame measured after the shot. The final values for total area of pull-in are given in Table 1 and, except for Shots 206 and 209, it is considered that they are correct to an experimental error of about 5% or less.

For shots 206 and 209, the very rigid large plate frame was replaced by a small frame for a reason not concerned with the present analysis, and, as a result, the frame and box suffered slight distortion, the total pull-in of the target plate being appreciably greater than that measured relative to the frame. Unfortunately, the subsidiary role of the pull-in measurements led to this distortion of the frame remaining unnoticed until after the second shot so that it is not possible to give any accurate correction for frame distortion for each shot separately.

However, the final total pull-in of the frame for the two shots was approximately equal to the combined pull-in relative to the frame in the two shots and the values of the latter were accordingly multiplied by a factor of two to give the corrected values of S'_m shown in Table 1. These corrected values for Shots 206 and 209 may be up to about 25% in error.

Comparison of theory and experiment.

(1)   Preparation of data for analysis.

In order to analyse the experimental data by means of the theory, it is necessary first to estimate the total increase of area S_m due to both pull-in and plate stretching. This can be calculated from:

$$S_m = \frac{1}{2} A_1 W_m^2$$

where W_m is the final mean deflection and A_1 is given by equation (9) of the Appendix if $f_1(x,y)$ is the final shape. The mean deflection W_m is calculated from the observed deflections by a curvature formula as described in a previous report and is tabulated in Table 1. In paragraph A.13 of the Appendix it is shown that for smooth shapes the value of A_1 varies but little with exact shape

of .....

of deflection and that as a mean value it is reasonable to assume $A_1 = 31.6$. We can thus calculate the ratio S'_m/S_m from the formula

$$\frac{S'_m}{S_m} = \frac{S'_m}{15.8 \, W_m^2}$$

to obtain the values given in the last column of Table 1.

The combined error in S'_m/S_m due to errors in S'_m and errors in estimating S_m are considered to be at most 10% with the exceptions of Shots 206 and 209, for which the error may be as much as 50%.

(2) General comparison of theory and experiment.

The values of S'_m/S_m in Table 1 have been plotted against W_m in Figure 3, and it will be seen that in spite of a considerable scatter there is a definite indication that S'_m/S_m increases as W_m decreases (a statistical check indicating that this is significant) and varies in general in much the way that the theory predicts. Some of the scatter is undoubtedly due to the possible experimental error in S'_m/S_m discussed in the previous section; in particular the value S'_m/S_m = 1.07 for Shot 221 must err from this cause since by definition $S_m > S'_m$. However, the experimental results cover a large variety of shots with differing charge conditions and plate thicknesses, so that even if S'_m/S_m could be accurately measured a considerable scatter is in any case conceivable due to variations in type of loading and of $(T_o - T_1)/T_o$ from shot to shot.

Thus the curves drawn in Figure 3 correspond to the theoretical curves of Figure 2 with $W_1 = 1.0°$ and $W_2 = 1.89°$ and since they bracket the experimental points, all scatter could be due purely to variation in type of loading from shot to shot. Since the second pulse due to bubble collapse is of much longer effective duration than the initial shock wave, such a variation in type of loading is quite feasible from shot to shot depending on the relative contributions to damage of shock-wave and second pulse.

Now if we put $W_1 = 1°$ or $W_2 = 1.89°$ in equation (109) with 4ab = 3220 square inches and K = 25 from equation (131), we then find that $(T_c - T_1)/T_o = 0.008$. Thus, if we assume the scatter in Figure 3 to be due primarily to variation in type of loading between instantaneous impulse and H(t), we should then expect $(T_o - T_1)/T_o$ to be about 1% for all shots.

However, we cannot rule out the possibility that the scatter may be equally or more dependent on a variation of $(T_o - T_1)/T_o$ from shot to shot.

Since, as previously stated, the shapes of the two curves (a) and (b) in Figure 2 are virtually the same, we can interpret the curves in Figure 3 not only as $W_1 = 1°$, $W_2 = 1.89°$ corresponding to different loading and same $(T_o - T_1)/T_o$, but also as $W_1 = 1°$, $W_2 = 1.89°$ for pure impulse loading corresponding from equation (109) (with K = 25, 4ab = 3220 square inches) to $(T_o - T_1)/T_c = 0.008$ and 0.028. Similarly, we could interpret these curves in Figure 3 as $W_2 = 1°$, $W_2 = 1.89°$ corresponding to H(t) loading with $(T_o - T_1)/T_o = 0.002$ and 0.008. Conversely, it follows that, provided the type of loading is such as to give a theoretical curve in Figure 2 lying between curves (a) and (b), then the values of $(T_o - T_1)/T_o$ for all shots are deduced to lie in the range 0.002 to 0.028. Further, the upper estimate of this range would only be increased for other types of loading if these could give a curve lying to the left of curve (a) in Figure 2. This does not seem possible since the instantaneous impulse is the most sudden loading we can assume and we should expect, as indicated by the relative positions of curves (a) and (b), that the less sudden the loading the greater the tendency for pull-in as opposed to plate stretching, i.e., the more the curve lies to the right in Figure 2. Thus, our upper estimate of 0.028 based on pure impulse should be a true upper estimate for all types of loading. On the other hand, our lower limit of 0.002 based on H(t) loading is so small that it is relatively unimportant that even lower estimates could be obtained by assuming types of loading giving curves lying to the right of curve (b) in Figure 2.

We thus estimate that, whatever the type of loading actually occurring, the values of $(T_o - T_1)/T_o$ for all shots lie in a range from virtually zero to about 0.03. This latter is based on a probable mean value K = 25 but even if we assume K = 40, which is probably too large (see A-2F), our estimates of $(T_o - T_1)/T_o$ still remain small, being less than 0.05. This implies, of course, the relatively small variation of less than 5% in T_1/T_o from target to target. This is not unreasonable if the main resistance to pull-in is the resistance against the plate stretching at the

bolt-holes ......

bolt-holes. The ratio of this latter to the resistance to stretching in the main body of the plate would be expected to be independent of the plate thickness and dependent only on the plate material and on the geometrical pattern of the bolts, both of which factors were nominally the same for all targets. There remains therefore only the contribution to T_1 of the frictional resistance which will depend on bolt tightness while its ratio to T_0 will probably decrease with plate thickness. However, this frictional resistance, although variable, is probably only a small part of the resistance to pull-in even initially, and, once the plate commences to thin due to stretching at the bolt holes, the frictional resistance will rapidly become negligible. On the whole, therefore, the smallness of the variation of T_1/T_0 from target to target is not unexpected. On the other hand, variations in the small frictional resistance could conceivably produce appreciable variations in the small difference $(T_0 - T_1)$ and could thus be in part or even mainly responsible for the scatter of the experimental points in Figure 3.

Finally, we can now consider how neglect of pull-in affects estimates of energy absorbed by the target plate.

Thus, if we neglect the relative weakness of the energy fixings and assume all increase in area to take place against the mean membrane stress T_0, the energy absorbed is

$$\Omega_0 = T_0 S_m$$

On the other hand, the true estimate, taking account of a relative weakness at the edge, is

$$\Omega'_p = T_0 (S_m - S'_m) + T_1 S'_m$$

whence

$$\frac{\Omega'_p}{\Omega_p} = 1 - \frac{(T_0 - T_1)}{(T_0)} \frac{S'_m}{S_m}$$

Since $S'_m/S_m < 1$ and $(T_0 - T_1)/T_0 < 0.05$ we conclude that neglect of edge weakness only implies an error of order 5% or less in the estimated energy absorbed by the target plate. In particular, such neglect cannot therefore account for the much large differences, recorded previously[1][2], between energy absorbed by target plate and energy communicated according to various theories.

Conclusions.

(1) The agreement between the approximate theory and the experimental results is reasonable bearing in mind that the large scatter of the experimental points, as plotted in Figure 3, is to be expected in view of probable variation in type of loading and/or small variations in edge resistance from shot to shot, due to the large variety of charge and target conditions in the experiments.

(2) The mean membrane stress T_1 round the periphery is estimated to differ by less than 5% from the mean membrane stress in the unsupported area of plate.

(3) Estimates of energy absorbed by the target plate given in previous reports[1][2] are not likely to be in error by more than about 5% due to neglect of the pull-in phenomenon.

References.

(1)   Taylor, G.I.   "The Distortion under pressure of a diaphragm which is clamped
                          along its edge and stressed beyond the elastic limit".

(2)   Fox, E.N., and Rollo,   "Analysis of Box Model Trials. II".
          W.T.

(3)   Fox, E.N., and Craig,J. "The optimum distribution of weight between plating and stiffeners
                          for maximum resistance to impulsive loading - first theoretical
                          analysis".

APPENDIX

Mathematical theory of pull-in at edges.

A.1   Nomenclature:

t	=	time
x,y	=	rectangular co-ordinates in plane of plate.
$2a, 2b$	=	lengths of sides of unsupported plate area.
w	=	$w(t) \, f_1(x,y)$ = deflection at point of plate.
u	=	$u(t) \, f_2(x,y)$
v	=	$v(t) \, f_3(x,y)$ } = displacement in plane of plate.
h	=	thickness of plate.
ρ	=	mass density of plate.
S_0	=	increase of plate area due to stretching.
S_1	=	increase of plate area due to pull-in.
S	=	$S_0 + S_1$
S_m	=	final maximum value of S.
S'_m	=	final maximum value of S_1
W_m	=	final mean deflection = maximum value of W.
W_1, W_2	=	borderline values of W_m for no stretching in the two loading cases considered
$p(t,x,y)$	=	$P(t) \, f_0(x,y)$ = applied impulsive pressure.
v	=	initial mean velocity due to instantaneous impulse.
P_1	=	magnitude of $P(t)$ when load is suddenly applied and maintained constant.
T	=	generalised uniform membrane tension per unit length in plate.
T'	=	generalised uniform tension per unit length round edges of unsupported plate area.
T_0	=	constant value of T when plate is stretching.
T_1	=	constant value of T' when edges are pulling-in.
Δ_0	=	areal strain at centre of plate.
$(\Delta_0)_m$	=	final strain at centre of plate.
θ	=	$\alpha \, t$
θ_c, t_0	=	values of θ and t at commencement of plate stretching.
θ_1, t_1	=	values of θ and t at cessation of plate stretching.
A_0		is defined by equation (18).

$A_1\ B_1\ C_1$ are defined by equation (9)

$A_2\ B_2\ C_2$ "   "   "   "   (13)

A_3 is   "   "   "   (26)

$\phi\,(t)$ "   "   "   "   (39)

α "   "   "   "   (74)

β "   "   "   "   (122)

γ "   "   "   "   (46)

κ "   "   "   "   (106)

$F_1\ F_2\ F_3$ are "   "   equations (110), (111), (112).

$K_1\ K_2\ K_3\ K_4$ "   "   "   equation (117)

r =   general variable of integration.

Dots are used to denote differentiation with respect to time t, while the four subsidiary symbols δ, y, ω, and θ'_1, which are used only temporarily, are defined where they occur.

A. 2   *Expressions for surface increases.*

The forms assumed for the displacements are:

$$w \;=\; W(t)\ f_1\,(x,y) \tag{1}$$

$$u \;=\; U(t)\ f_2\,(x,y) \tag{2}$$

$$v \;=\; V(t)\ f_3\,(x,y) \tag{3}$$

where U, V and W are to be determined, while specific forms for f_1, f_2 and f_3 will be assumed later. We note for present use that f_1, f_2, f_3 must satisfy the following boundary conditions:

$$f_1 \;=\; 0 \quad \text{along edges } x = \pm a$$
$$\text{and } y = \pm b \tag{4}$$

$$f_2 \;=\; 0 \quad \text{along edges } y = \pm b$$

$$f_2 \;\leq\; 0 \quad \text{along edge } x = a \qquad\qquad\Bigg\} \tag{5}$$

$$f_2 \;\geq\; 0 \quad \text{along edge } x = -a$$

$$f_3 \;=\; 0 \quad \text{along edges } x = \pm a \qquad\qquad\Bigg\}$$

$$f_3 \;\leq\; 0 \quad \text{along edge } y = b \qquad\qquad \tag{6}$$

$$f_3 \;\geq\; 0 \quad \text{along edge } y = -b$$

The inequalities in (5) and (6) merely specify without loss of generality the signs of U and V (namely positive) in the light of the physical condition that the plate is pulling-in at edges. Also without loss of generality we can specify:

$$\frac{1}{4ab} \int_{-a}^{a} \int_{-b}^{b} f_1\ dx\ dy \;=\; 1 \tag{7}$$

so that W is identified with the mean deflection.

To .....

To the first order in u and v and to the second order in w the increase in area of the original unsupported plate area is:

$$S_0 = \int_{-a}^{a} \int_{-b}^{b} \frac{\partial u}{\partial x} + \frac{\partial v}{\partial y} + \frac{1}{2}\left(\frac{\partial w}{\partial x}\right)^2 + \frac{1}{2}\left(\frac{\partial w}{\partial y}\right)^2 \quad dx\,dy$$

$$= \frac{1}{2} A_1 w^2 - B_1 u - C_1 v \tag{8}$$

where

$$A_1 = \int_{-a}^{a} \int_{-b}^{b} \left(\frac{\partial f_1}{\partial x}\right)^2 + \left(\frac{\partial f_1}{\partial y}\right)^2 \quad dx\,dy$$

$$B_1 = \int_{-b}^{b} \left[\; f_2(-a,y) - f_2(a,y)\;\right] \; dy \tag{9}$$

$$C_1 = \int_{-a}^{a} \left[\; f_3(x,-b) - f_3(x,b)\;\right] \; dx$$

We may note that:

$$A_1 \geq 0$$
$$B_1 \geq 0 \tag{10}$$
$$C_1 \geq 0$$

the first being obvious from the expression for A_1, while the latter two follow from the boundary conditions (5) and (6).

The total area of pull-in at edges is given by integration round the edges as:

$$S_1 = \int_{-b}^{b} - u\, f_2(a,y)\; dy + \int_{-b}^{b} u\, f_2(-a,y)\; dy$$

$$+ \int_{-a}^{a} - v\, f_3(x,b)\; dx + \int_{-a}^{a} v\, f_3(x,-b)\; dx$$

whence from (9):

$$S_1 = B_1 u + C_1 v \tag{11}$$

A.3   Energy expressions.

The originally unsupported area of plate may be regarded as a closed system subjected to a lateral load and a tensile force round its edges.

The total kinetic energy of the system is then, using (1), (2) and (3),

$$\frac{1}{2}\rho h \int_{-a}^{a} \int_{-b}^{b} (\dot{w}^2 + \dot{u}^2 + \dot{v}^2)\, dx\,dy \;=\; \frac{1}{2}\rho h\, (A_2 \dot{w}^2 + B_2 \dot{u}^2 + C_2 \dot{v}^2) \tag{12}$$

where

$$A_2 = \int_{-a}^{a} \int_{-b}^{b} f_1^2 \, dx \, dy$$

$$B_2 = \int_{-a}^{a} \int_{-b}^{b} f_2^2 \, dx \, dy \qquad (13)$$

$$C_2 = \int_{-a}^{a} \int_{-b}^{b} f_3^2 \, dx \, dy$$

Using the concept of a generalised mean stress[3] to cover the case when the plate is not stretching, then the potential energy of plate stretching is given by use of (6) as:

$$\int_{c}^{S_0} T \, d S_0 = \int_{0}^{W} T \, A_1 \, d W - \int_{0}^{U} T \, B_1 \, d U - \int_{0}^{V} T \, C_1 \, d V \qquad (14)$$

in which T may be regarded as a function of time and is equal to T_0 at any time when the plate is stretching.

Similarly, the potential energy of pull-in is by use of (11):

$$\int_{0}^{S_1} T' \, d S_1 = \int_{0}^{U} T' \, B_1 \, d U + \int_{0}^{V} T' \, C_1 \, d V \qquad (15)$$

where T' may be regarded as a function of time and is equal to T_1 at any time when pull-in is occurring.

Fuller consideration of T and T' is given later (paragraph A.5).

Finally, if the applied impulsive pressure is of the form:

$$p(t, x, y) = P(t) f_0(x, y) \qquad (16)$$

then the potential energy of this pressure can be written as:

$$\int_{-a}^{a} \int_{-b}^{b} \int_{0}^{t} p \frac{dw}{dt} \, dt \, dx \, dy = - A_0 \int_{0}^{W} P(t) \, d W \qquad (17)$$

where:

$$A_0 = \int_{-a}^{a} \int_{-b}^{b} f_0(x, y) \, f_1(x, y) \, dx \, dy \qquad (18)$$

Hence, we have finally from (12), (14), (15) and (17) that:

$$\text{Total K.E.} = \tfrac{1}{2} \rho h \left[A_2 \dot{W}^2 + B_2 \dot{U}^2 + C_2 \dot{V}^2 \right] \qquad (19)$$

$$\text{Total P.E.} = A_1 \int_{0}^{W} T W \, dW - B_1 \int_{0}^{U} (T - T') \, d U$$

$$- C_1 \int_{0}^{V} (T - T') \, d V - A_0 \int_{0}^{W} P(t) \, d W \qquad (20)$$

A.4 .....

A.4 *Equations of motion.*

We now apply Lagrange's equations to the expressions (19) and (20) to obtain:

$$\rho h\, A_2\, \ddot{W} + A_1\, T\, W = A_0\, P(t) \tag{21}$$

$$\rho h\, B_2\, \ddot{U} = (T - T')\, B_1 \tag{22}$$

$$\rho h\, C_2\, \ddot{V} = (T - T')\, C_1 \tag{23}$$

The initial condition of rest gives:

$$
\left.
\begin{aligned}
W &= \dot{W} = 0 \\
U &= \dot{U} = 0 \\
V &= \dot{V} = 0
\end{aligned}
\right\} \quad \text{when } t = 0 \tag{24}
$$

Now from (22), (23) and (24) it follows immediately that:

$$\frac{B_1}{B_2}\, U = \frac{C_1}{C_2}\, V \tag{25}$$

whence by virtue of (11) U and V can both be expressed in terms of S_1 by the relations:

$$
\left.
\begin{aligned}
U &= \frac{B_1\, S_1}{B_2\, A_3} \\[2mm]
V &= \frac{C_1\, S_1}{C_2\, A_3} \\[2mm]
\text{where} \quad A_3 &= \frac{B_1^{\,2}}{B_2} + \frac{C_1^{\,2}}{C_2}
\end{aligned}
\right\} \tag{26}
$$

From (22), (25) and (26) it then follows that the equation of motion for S_1 is

$$\rho h\, \ddot{S}_1 = A_3\, (T - T') \tag{27}$$

with initial conditions:

$$S_1 = \dot{S}_1 = 0 \quad \text{when } t = 0 \tag{28}$$

If we denote S as the total increase of area of dished plate due both to stretching and to pull-in, then from (8) and (11):

$$S = \tfrac{1}{2} A_1\, W^2 = S_0 + S_1 \tag{29}$$

From (29), (27) and (21) we note for future use that:

$$\rho h\, \ddot{S}_0 = \frac{A_1\, A_0}{A_2}\, W\, P(t) + \rho h\, A_1\, \dot{W}^2 + A_3(T' - T) - \frac{A_1^{\,2}}{A_2}\, T\, W^2 \tag{30}$$

We now have the three equations (21), (27) and (29) for five unknowns W, S_0, S_1, T and T' and we therefore require two more equations which will now be derived from consideration of the physical type of motion.

A.5 *Physical conditions restricting type of motion.*

We shall restrict ourselves to the case where the applied load is always of one sign and we can then without loss of generality assume that:

$$A_1\, P(t) \geqslant 0 \tag{31}$$

since .....

since this merely states that we are measuring w in the direction of applied load.

We also bear in mind that the constants A_1 B_1 C_1, A_2 B_2 C_2, A_3 as defined earlier by equations (9), (19) and (20) are all positive.

In order to consider which types of motion are possible, we first collect together some consequences of our physical assumptions.

Firstly, the assumption that the plate stretches under constant tension T_0 implies that:

$$\left. \begin{array}{l} T = T_0 \quad \text{when} \quad \dot{S}_0 > 0 \\[2mm] T \leqslant T_0 \quad \text{when} \quad \dot{S}_0 \leqslant 0 \end{array} \right\} \tag{32}$$

and similarly for the edge pull-in we have:

$$\left. \begin{array}{l} T' = T_1 \quad \text{when} \quad \dot{S}_1 > 0 \\[2mm] T' \leqslant T_1 \quad \text{when} \quad \dot{S}_1 \leqslant 0 \end{array} \right\} \tag{33}$$

Secondly, our assumption that the edge fixing is relatively the weaker implies that:

$$T_0 > T_1 > 0 \tag{34}$$

and thence as a corollary from (32), (33), (34) and (27) we have:

$$\ddot{S}_1 > 0 \quad \text{when} \quad \dot{S}_0 > 0 \tag{35}$$

Finally, we shall need to show that there is no tendency of the plate or edges to buckle or compress since this is not physically obvious.   For this purpose we can assume our general equations (21) and (27) to hold provided T and T' are compressive and not tensile, i.e., we must have:

$$\left. \begin{array}{l} T \leqslant 0 \quad \text{when} \quad \dot{S}_0 < 0 \\[2mm] T' \leqslant 0 \quad \text{when} \quad \dot{S}_1 < 0 \end{array} \right\} \tag{36}$$

since otherwise we should be extracting energy from the plate or edge fixings which is contrary to our assumption that the dishing is plastic with irreversible absorption of energy.

A.6   Continuity conditions.

On physical grounds the displacements U, V, w and therefore S, S_0, C_1 must be continuous: we must also assume that T and T' are finite and then from (27) it follows that $\ddot{S}_1$ is always finite and therefore that $\dot{S}_1$ is continuous.   Also, if w > 0, then from (30) and (31) $\dot{S}_0$ will be finite or positively infinite, the latter corresponding to the concept of an instantaneous impulse; thus $\dot{S}_0$ will be either continuous or will increase discontinuously provided w > 0.

The continuity conditions are thus:

$$\left. \begin{array}{l} \text{w, } S_0\text{, } S_1\text{, } \dot{S}_1 \text{ continuous.} \\[2mm] \dot{w}\text{, } \dot{S}_0 \text{ continuous or increasing discontinuously.} \end{array} \right\} \tag{37}$$

It follows that if at the end of any particular type of motion we have:

$$\left. \begin{array}{l} w \geqslant 0 \\[2mm] \dot{S}_0 \geqslant 0 \\[2mm] \dot{S}_1 \geqslant 0 \end{array} \right\} \tag{38}$$

then these same relations will be satisfied by the initial conditions for the succeeding type of motion.

A.7 ......

A.7   *Possible types of motion.*

We now introduce ϕ, a function of time defined by:

$$\phi(t) = \frac{A_1 A_0}{A_2} \, W \, P(t) + \rho h \, A_1 \dot{k}^2 \tag{39}$$

whence equation (31) implies that:

$$\dot{\phi} \geqslant 0 \tag{40}$$

at any time when $W \geqslant 0$ and therefore in particular when the relations (38) are satisfied.

Using this function, it then follows from (30) and (27) that

$$\rho h \, \bar{S}_0 = \phi + A_3 (T' - T) - \frac{A_1^2}{A_2} \, T \, W^2 \tag{41}$$

$$\rho h \, \bar{S}_0 + \rho h \, \bar{S}_1 = \phi - \frac{A_1^2}{A_2} \, T \, W^2 \tag{42}$$

We can now prove the following Lemmas.

Lemma A.   If $W \geqslant 0$, $\dot{S}_0 > 0$, $\dot{S}_1 \geqslant 0$ initially, then $\dot{S}_0 > 0$, $\dot{S}_1 > 0$ in the ensuing stage of motion.

For $\dot{S}_1 > 0$ by the previous continuity considerations and therefore $\bar{S}_1 > 0$ by (35). Thence since $\dot{S}_1 \geqslant 0$ initially, $\dot{S}_1 > 0$ in ensuing motion.

Lemma B.   If $W \geqslant 0$, $\dot{S}_0 = 0$, $\dot{S}_1 \geqslant 0$ initially, then $\dot{S}_0 \geqslant 0$ in ensuing stage of motion.

Assume Lemma is false and that $\dot{S}_0$ becomes < 0, then we must have $\bar{S}_0 < 0$ since $\dot{S}_0 = 0$ initially and further $T \leqslant 0$ from (36). But $\bar{S}_0 < 0$ and $T \leqslant 0$ together imply $\bar{S}_1 > 0$ from (42) and therefore imply that $\dot{S}_1$ becomes > 0 since $\dot{S}_1 \geqslant 0$ initially. But $\bar{S} \geqslant 0$, $\dot{S}_1 > 0$ together imply that $T > T' = T_1 > 0$ from (27), (33) and (34), and, therefore, since $T \geqslant C$, we cannot have $\dot{S}_0$ becoming negative. Thus, if Lemma is false, we arrive at contradiction and therefore Lemma must be true.

Lemma C.   If $W \geqslant 0$, $\dot{S}_0 \geqslant 0$, $\dot{S}_1 \geqslant 0$ initially, then $\dot{S}_1 \geqslant 0$ in ensuing stage of motion.

Firstly, if $\dot{S}_1 > 0$ initially, then $\dot{S}_1 > 0$ in ensuing stage by continuity conditions.

Secondly, if $\dot{S}_1 = 0$ initially, then if Lemma is false and $\dot{S}_1$ becomes negative, then $\bar{S}_1$ also becomes negative. But $\dot{S}_1 < 0$, $\bar{S}_1 < 0$ imply $T < T' \leqslant 0$ from (27) and (36) and thence from (40) and (41) we must have $\bar{S}_0 > 0$ and therefore $\dot{S}_0 < 0$ since $\dot{S}_0 \geqslant 0$ initially. But $\dot{S}_0 > 0$ implies $T = T_0$ from (32), thus contradicting $T < 0$ already proved to hold if Lemma is false. Thus Lemma must be true.

The preceding Lemmas thus show that the stage of motion succeeding initial conditions satisfying (38) must be one of the three types.

Type   i. $\dot{S}_0 > 0$, $\dot{S}_1 > 0$

Type   ii. $\dot{S}_0 = 0$, $\dot{S}_1 > 0$.

Type iii.   (Plate at rest) $\dot{S}_0 = 0$ $\dot{S}_1 = 0$.

Now the initial conditions of rest prior to motion as given by (24) and (26) satisfy the relations (38) and thus the initial stage of motion must be of Type I or Type II during either of which S_1 is increasing, S_0 is constant or increasing and W is increasing so that W becomes positive and thus the conditions (38) will be satisfied throughout this initial stage and by our previous continuity considerations they will be satisfied at the beginning of the second stage. This must then in turn be of Type I, II or III by the preceding Lemmas and thus by induction it follows that all stages of the whole motion will be of Types I, II or III; in effect, we have shown that there is no tendency for the plate or edge fixings to go into compression when the load is of one sign and the energy absorption is irreversible.

We have .....

We have therefore to consider the motion as compounded of successive stages in which the plate may be either (1) stretching and pulling in at edges, or (2) inextensional but pulling in at edges, or (3) at rest. We have throughout considered the condition of rest as a type of motion because, while trivial if it forms the final stage, it could in fact be an intermediate stage between stages of actual motion in the case where the applied load is of oscillating magnitude, i.e., the plate could cease moving when the load was decreasing and then commence to move again when the load had subsequently increased to a sufficient magnitude. We can now write down the relevant equations which hold in the different stages.

A.8   Equations governing each type of motion.

__TYPE I.__   Plate stretching and pulling-in at edges.

The physical conditions are:

$$\left. \begin{array}{l} \dot{s}_0 > 0 \\[2mm] \dot{s}_1 > 0 \end{array} \right\} \tag{43}$$

whence from (32) and (33):

$$\left. \begin{array}{l} T = T_0 \\[2mm] T' = T_1 \end{array} \right\} \tag{44}$$

Thence from (21) and (27):

$$\rho h \, A_2 \, \ddot{W} + A_1 \, T_0 \, W = A_0 \, P(t) \tag{45}$$

$$\ddot{\xi}_1 = \frac{A_3 (T_0 - T_1)}{\rho h} = Y \tag{46}$$

defining a new parameter Y.

We thus have four equations for the four unknowns T, T', W and S_1 and thence $\dot{s}_0$ and S are given by (29). It may be noted for future use from (29) and (46) that:

$$\ddot{s}_0 = (\ddot{S} - Y) \tag{47}$$

during this type of motion. The solution of the preceding equations will be invalid if it violates the conditions (43).

__TYPE II.__   Plate inextensional but pulling-in at edges.

The physical conditions imply in view of (32) and (33) that:

$$\left. \begin{array}{l} \dot{s}_1 > 0 \\[2mm] T < T_0 \end{array} \right\} \tag{48}$$

$$\left. \begin{array}{l} \dot{s}_0 = 0 \\[2mm] T' = T_1 \end{array} \right\} \tag{49}$$

whence the equations of motion (21) and (27) become:

$$\rho h \, A_2 \, \ddot{W} + A_1 \, T \, W = A_0 \, P(t) \tag{50}$$

$$\rho h \, \ddot{s}_1 = A_3 (T - T_1) \tag{51}$$

and equations (29) and (49) give:

$$\dot{S} = A_1 \, W \, \dot{W} = \dot{s}_1 \tag{52}$$

We thus ......

We thus have six equations given by (49), (50), (51) and (52) for the six unknowns T, T', W, S, S_0 and S_1. The equations are only valid so long as the conditions (48) are satisfied.

From (50), (59) and (49) we note that:

$$T\left(A_3 + \frac{A_1^2 W^2}{A_2} \right) = \dot{\phi} + A_1 T_1 \tag{53}$$

so that during Type II motion we have by virtue of (48) that:

$$T > 0 \tag{54}$$

Also from (51) and (52):

$$\frac{A_3 (T_0 - T)}{\rho n} = \dot{Y} - \ddot{S} \tag{55}$$

so that (48) may be replaced by:

$$\left. \begin{array}{l} \dot{S}_1 > 0 \\[2mm] \ddot{S} \leqslant \dot{Y} \end{array} \right\} \tag{56}$$

For future use we also note, from (51), (52), (53) and (39), that

$$\rho n \ddot{S} \left[1 + \frac{A_1^2 W^2}{A_2 A_3} \right] = \rho n A_1 \dot{W}^2 + \frac{A_1 W}{A_2} \left(A_0 P(t) - T_1 A W \right) \tag{57}$$

TYPE III.   Plate at rest.

The physical conditions are:

$$\left. \begin{array}{l} \dot{S}_1 = 0 \\[2mm] \dot{S}_0 = 0 \end{array} \right\} \tag{58}$$

whence from (29), (21) and (27):

$$\left. \begin{array}{l} \ddot{W} = 0 \\[2mm] \dot{S} = 0 \\[2mm] T = T' = \dfrac{A_0 P(t)}{A_1 W} \end{array} \right\} \tag{59}$$

Thus we have six equations for the six unknowns T, T', W, S_1, S_0 and $\dot{S}_1$. Also from (58), (52) and (53) the state of rest will only be possible so long as:

$$\left. \begin{array}{l} T' \leqslant T_1 \\[2mm] T \leqslant T_0 \end{array} \right\} \tag{60}$$

whence from (59) and (58) the plate can remain at rest provided:

$$A_0 P(t) \leqslant T_1 A_1 W \tag{61}$$

4.0   The energy equation.

Having shown that, with our assumptions of initial rest and pressure always positive, the motion is compounded of stages of Type I, Type II or rest in which S_0 and S_1 are either constant or increasing, it follows that the energy absorbed in the plate at any stage is:

$$\int T \, d \ \cdots$$

$$\int T \, d S_0 + \int T^* \, d S_1 = T_0 S_0 + T_1 S_1 = \tfrac{1}{2} T_0 A_1 W^2 - (T_0 - T_1) S_1 \qquad (62)$$

Also from (12) and (26) the kinetic energy at any time is:

$$\tfrac{1}{2} \rho h \left(A_2 \dot{W}^2 + \frac{\dot{S}_1^2}{A_3} \right) \qquad (63)$$

while from (17) the work done by the applied load is

$$A_0 \int_0^W F(t) \, d W$$

The energy equation is thus:

$$\tfrac{1}{2} \rho h \left(A_2 \dot{W}^2 + \frac{\dot{S}_1^2}{A_3} \right) + \tfrac{1}{2} T_0 A_1 W^2 - (T_0 - T_1) S_1 = A_0 \int_0^W e(t) \, d W \qquad (64)$$

This equation can also be obtained from the equations (21) and (27) by multiplying by $\dot{W}$ and $\dot{S}_1/A_3$ respectively, adding and integrating, and using equation (62).

A. 10 *Introduction of assumption that* $(T_0 - T_1)/T_0$ *is small.*

Now in either Type I or Type II motion we have $T^* = T_1$ in (27) and multiplying this equation by $\dot{S}_1$ and integrating we obtain:

$$\tfrac{1}{2} \rho h \dot{S}_1^2 = A_0 \int_0^{S_1} (T - T_1) \, d S_1$$

and since $\dot{S}_1 > 0$, $T \le T_0$, while initially $\dot{S}_1 = S_1 = 0$ we therefore obtain

$$0 \le \tfrac{1}{2} \rho h \dot{S}_1^2 \le A_3 (T_0 - T_1) S_1 \qquad (65)$$

by use of (29). But the energy equation (64) can be written with regrouped terms in the form:

$$\tfrac{1}{2} \rho h A_2 \dot{W}^2 + \tfrac{1}{2} T_0 A_1 W^2 (1 - \delta) = A_0 \int_0^W F(t) \, d W \quad .$$

where

$$\delta = \frac{S_1}{S} \left[1 - \frac{\rho h \dot{S}_1^2}{2 A_3 (T_0 - T_1) S_1} \right] \left[\frac{T_0 - T_1}{T_0} \right] \qquad (65a)$$

and we have shown that $S_0 > 0$, $S_1 > 0$ throughout the motion so that $S = S_0 + S_1 \ge S_1 \ge 0$ and therefore, using (65), we must have:

$$0 \le \delta \le \frac{T_0 - T_1}{T_0} \qquad (65b)$$

It therefore follows that if we now assume:

$$\frac{T_0 - T_1}{T_0} \quad \ll 1 \qquad (66)$$

then, neglecting terms of this order in (65a), we obtain:

$$\tfrac{1}{2} \rho h A_2 \dot{W}^2 + \tfrac{1}{2} T_0 A_1 W^2 = A_0 \int_0^W F(t) \, d W \qquad (67)$$

for .....

for both Type I and Type II motion. This equation gives on differentiation

$$\rho h\, A_2\, \ddot{W} + T_0\, A_1\, W = A_0\, P(t) \tag{68}$$

which is the same as equation (45). Thus, on the assumption (66), we obtain the same equation for W in both Types I and II motion. While the particular cases of load to be considered later can be solved explicitly without making the assumption that $(T_0 - T_1)/T_0$ is small, the simplicity introduced by only one equation for W during all the motion is very great. Since this assumption will be found reasonable, a posteriori, in application to the Box Model, and since any attempt at great accuracy is meaningless for such application in view of the approximate nature of both method of analysis and physical assumptions, we shall adopt the assumption (66) that $(T_0 - T_1)/T_0$ is small in the remainder of our analysis.

We shall thus use equation (68) for both Types I and II and for any given type of load we can then evaluate W as a function of time. Thence from (29) we can obtain $\dot{S}$ as a function of time and the various stages can then easily be identified by virtue of the following geometrical properties of the curves for $\dot{S}$ and $\dot{S}_1$ against time.

(a)   During Type I motion, (46) indicates that $\dot{S}_1$ is a straight line of positive slope Y which must lie below the $\dot{S}$ curve to satisfy (43).

(b)   During Type II motion, (52) indicates that the $\dot{S}_1$ curve is coincident with the $\dot{S}$ curve which must have a slope $\leqslant$ Y by (56).

(c)   During rest, $\dot{S} = \dot{S}_1 = 0$ so that both curves become coincident with the time axis and will remain so provided (61) is satisfied.

Since $\dot{S} > 0$ for Types I, II or rest, which have alone been proved possible, we must not continue the solution of (68) for negative values of W and $\dot{S}$, i.e., we first consider only the portion of the $\dot{S}$ curve up to where it cuts the axis of time. Immediately prior to this time, the motion will be of Type II since in Type I motion $\dot{S}_1$ increases steadily and at the end of Type I motion we must therefore have $\dot{S} = \dot{S}_1 > 0$; this is also geometrically obvious from (a) above. But if the motion is of Type II and the $\dot{S}$ curve is cutting the time axis, whence $\dot{S} = \ddot{W} = 0$, then from (57) this can only happen if $A_0\, P(t) - T_1\, W$ is becoming negative and this in turn implies from (61) that a state of rest is possible. This state of rest will then continue indefinitely unless P(t) subsequently increases to violate (61) and further motion will then ensue. Such further motion can then be treated in the same way by using equation (68) and considering the $\dot{S}$ curve, the conditions at the recommencement of motion being the same as initially save that W = 0 but is equal to the value of W at the first cessation of motion. In the two specific cases of load we will now consider, P(t) does not increase after the first cessation of motion, so that no recommencement of motion is possible and it is only necessary to consider the $\dot{S}$ curve up to the time when it first cuts the time axis.

4.22   *Summary of procedure for solution.*

Summing up from the preceding section, our procedure for solution with any given form of load P(t) is as follows:

(1)   Equation (46) is solved with initial conditions $W = \dot{W} = 0$.

(2)   The curve for $\dot{S}$ versus t is then obtained up to the time at which it first cuts the time axis.

(3)   If the slope of the $\dot{S}$ curve is always $\leqslant$ Y, then Type I motion is not possible and the motion is thus of Type II throughout. In this case the $\dot{S}_1$ curve is identical with the $\dot{S}$ curve throughout the motion.

(4)   If the slope of the $\dot{S}$ curve exceeds Y over a finite portion of the curve then Type I motion will commence directly the slope exceeds Y and the curve for $\dot{S}_1$ versus t will become a line of slope Y. Type I motion will cease and Type II ensue when this line cuts the $\dot{S}$ curve. In this case the $\dot{S}_1$ curve follows the $\dot{S}$ curve until $\dot{S}$ first exceeds Y and $\dot{S}_1$ then proceeds along a chord of slope Y until this cuts the $\dot{S}$ curve when the $\dot{S}_1$ curve again follows the $\dot{S}$ curve; this process may be repeated if the $\dot{S}$ curve is oscillatory so that $\dot{S}$ later again exceeds Y.

(5) .....

(5)   The $\dot{S}_1$ curve must become coincident with the $\dot{S}$ curve prior to cutting the time axis and when this latter occurs a period of rest will ensue.   There will be no further motion unless P(t) subsequently increases sufficiently to violate (61).

Since the equation to the $\dot{S}$ curve is obtained from (68) and (29) with initial conditions,

$$w = \dot{w} = 0 \tag{69}$$

the application of the preceding geometrical criteria becomes a matter of simple analytical geometry.

When the $\dot{S}_1$ curve has thus been determined any of the remaining variables S_1, T, etc., can be determined by using the relevant equations from paragraph A.8 according to type of motion.   Since observable quantities in box model trials are the final deflection and pull-in, we shall confine attention to the values of:

$$
\left.
\begin{array}{ll}
w_m & = \text{final mean deflection.} \\[1em]
S_m = \tfrac{1}{2} A_1 w_m^2 & = \text{area under } \dot{S} \text{ curve} \\[1em]
S'_m & = \text{final area of pull-in} = \text{area under } \dot{S}_1 \text{ curve}
\end{array}
\right\} \tag{70}
$$

in the two specific forms of P(t) which we now proceed to consider.

A.22   *Motion due to an instantaneous impulse.*

If we let P(t) become infinitely great but of infinitely short duration, the impulse remaining finite, then from our general equations (21) and (29) and the initial conditions (24) and (69), the conditions after the impulse will be:

$$
\left.
\begin{array}{l}
w = 0 \\[1em]
\dot{w} = \dfrac{A_0}{\rho h A_2} \displaystyle\int_0^{t=0} P(t)\, dt = V \\[1em]
S_1 = 0 \\[1em]
\dot{S}_1 = 0 \\[1em]
\dot{S} = 0 \\[1em]
S = 0
\end{array}
\right\} \quad t = +0 \tag{71}
$$

with the equation (68) for w becoming:

$$\rho h A_2 \ddot{w} + T_0 A_1 w = 0 \qquad\qquad t > 0 \tag{72}$$

The solution for w from (72) and (71) is thus:

$$w = w_m \sin \alpha t \tag{73}$$

where

$$\alpha = \sqrt{\dfrac{A_1 T_0}{\rho h A_2}} \tag{74}$$

$$w_m = V/\alpha \tag{75}$$

Thence from (29), (73) and (75):

$$S = \tfrac{1}{2} A_1 w^2 = \tfrac{1}{2} A_1 w_m^2 \sin^2 \alpha t \tag{76}$$

$$\dot{S} = A_1 w \dot{w} = \tfrac{1}{2} A_1 \alpha w_m^2 \sin 2\alpha t \tag{77}$$

$$\ddot{S} = A_1 V^2 \cos 2\alpha t \tag{78}$$

Thus .....

Thus the curve of $\dot{S}$ against t will be a half sine curve as shown in Figure 4, the motion ceasing when $\dot{S}$ becomes zero at time $t = \pi/2\alpha$ with no further recommencement since $P(t) = 0$ thereafter.

The geometrical criteria of the preceding section are now easily applied since we note from (78) that the slope $\dot{S}$ decreases steadily from $A_1 v^2$ at $t = 0$ to $-A_1 v^2$ at $2\alpha t = \pi$. We thus have the following cases:

(a)　$\underline{A_1 v^2 \leqslant Y.}$

In this case criterion A.11(3) applies and the motion is of Type II throughout so that the $\dot{S}_1$ curve is identical with the $\dot{S}$ curve.

(b)　$\underline{A_1 v^2 > Y.}$

In this case criterion A.11(4) applies and the motion will then commence with Type I, the $\dot{S}_1$ curve then being the line OB of slope Y as illustrated. This type ceases at the point B corresponding to time t_1 given by:

$$Y t_1 = \tfrac{1}{2} A_1 \alpha w_m^2 \sin 2\alpha t \tag{79}$$

and the remainder of the motion is of Type II since the slope of $\dot{S}$ curve does not again increase to become $> Y$. The $\dot{S}_1$ is thus composed of the line OB and the curve BC.

If we now define W_1 as the borderline value of W_m corresponding to $A_1 v^2 = Y$, then from (75), (78) and (86):

$$W_1^2 = \frac{Y}{A_1 \alpha^2} + \frac{A_2 A_1}{A_1^2}\left(\frac{T_0 - T_1}{T_0}\right) \tag{80}$$

If we further put:

$$\theta_1 = \alpha t_1 \tag{81}$$

then from (79) and (80):

$$\frac{w_m^2}{w_1^2} = \frac{2\theta_1}{\sin 2\theta_1} \tag{82}$$

For the maximum values S_m and S'_m we then have from (70), (76) and Figure 4:

$$\left.\begin{array}{l} S_m = \tfrac{1}{2} A_1 w_m^2 \\[4pt] S'_m = S_m \text{ for } W_m < W_1 \\[4pt] S'_m = \tfrac{1}{2} Y t_1^2 + S_m - \tfrac{1}{2} A_1 W_m^2 \sin^2\alpha\, t_1 \text{ for } W_m > W_1 \end{array}\right\} \tag{83}$$

Then using (79) the ratio S'_m/S_m is given in terms of W_m/W_1 by the following equations:

$$\frac{S'_m}{S_m} = 1 \text{ for } \frac{W_m}{W_1} \leqslant 1 \tag{84}$$

$$\left.\begin{array}{l} \dfrac{S'_m}{S_m} = \tfrac{1}{2}\left(1 + \cos 2\theta_1 + \theta_1 \sin 2\theta_1\right) \quad \dfrac{W_m}{W_1} > 1 \\[10pt] \dfrac{w_m^2}{w_1^2} = \dfrac{2\theta_1}{\sin 2\theta_1} \quad\quad\quad\quad 0 \leqslant \theta_1 \leqslant \pi/2 \end{array}\right\} \tag{85}$$

Using θ_1 as a parameter, we then obtain the values given in Table 2 and plotting in Figure 2.

A.19 ......

A.13   Motion due to load suddenly applied and then maintained constant.

If the load is of the form:

$$p(t) = 0, \quad t < 0$$
$$= p_1, \quad t > 0 \tag{86}$$

then equation (68) becomes:

$$\rho_0 A_2 \ddot{S} + A_1 T_0 W = P_1 \tag{87}$$

and the initial conditions rest (69) we obtain as solution:

$$W = \tfrac{1}{2} W_m (1 - \cos \alpha t) \tag{88}$$

where:

$$W_m = \frac{2 P_1}{A_1 T_0} \tag{89}$$

while α is given by (74) as in the preceding section.

Then S and its derivatives are given by:

$$S = \tfrac{1}{2} A_1 W^2 = \tfrac{1}{4} S_m (1 - \cos \alpha t)^2 \tag{90}$$

$$\dot{S} = \tfrac{1}{2} \alpha S_m \sin \alpha t (1 - \cos \alpha t) \tag{91}$$

$$\ddot{S} = \tfrac{1}{2} \alpha^2 S_m (\cos \alpha t - \cos 2\alpha t) \tag{92}$$

where:

$$S_m = \tfrac{1}{2} A_1 W_m^2 = \frac{2 P_1^2}{A_1 T_0^2} \tag{93}$$

The motion must cease when $\dot{S} = \dot{W} = 0$ and $\alpha t = \pi$ and change to state of rest as considered in the section A.11(5).

Further, when $\alpha t = \pi$, we have from (88) and (89) and (90) that:

$$\dot{S} = \dot{W} = 0$$
$$A_1 T_1 W = A_1 T_1 W_m = \frac{2 P_1 T_1}{T_0} > P_1 \tag{94}$$

since $T_0 \sim T_1$ per assumption (66). As the load P(t) remains constant for $\alpha t \geq \pi$, equation (94) will thus be satisfied indefinitely and no further motion will occur. Physically this means that for $\alpha t \geq \pi$ the deformed plate remains at rest in statical equilibrium with the load P_1, the resulting tension in plate and at edges being too small to produce any yielding.

Since there is no further motion, it follows that W_m and S_m as given by (89) and (93) are the final maximum values of W and S, as their notation anticipated.

In order to decide the types of motion during $0 \leq \alpha t \leq \pi$, the curve for $\dot{S}$ from (91) is shown in figure 5. As will be seen from equation (93), the slope $\ddot{S}$ of the S curve increases steadily from 0 at t = 0 up to a maximum value $9 \alpha^2 S_m/16$ at $\cos \alpha t = \tfrac{1}{4}$ and hence decreases steadily to a negative value at $\alpha t = \pi$.

If we now define W_2 as the borderline value of W_m corresponding to the maximum $\ddot{S} = Y$, then, using (46):

$$W_2^2 = \frac{32 Y}{9 \alpha^2 A_1} = \frac{32}{9} \frac{A_3 A_2}{A_1} \left(\frac{T_0 - T_1}{T_0} \right) \tag{95}$$

Thence .....

Thence, applying the criterion of paragraph A.11 to figure 5, we have:

(a) $W_m \leq W_2$

The slope of the $\dot{S}$ curve is always $\leq Y$ so that the motion is always of Type II, and in particular:

$$S'_m = S_m, \qquad W_m \leq W_2 \tag{96}$$

(b) $W_m > W_2$

The motion will be of Type II until the point A where $\dot{S} = Y$ and will then change to Type I, the $\dot{S}_1$ curve then becoming the line AC of slope Y in Figure 5; AC is therefore the tangent at A to the $\dot{S}$ curve since $\dot{S}$ is continuous. The motion will revert to Type II at the point C and will remain of this type since the slope $\dot{S}$ is decreasing steadily and is $< Y$ on CD for all possible positions of C.

If the point A corresponds to:

$$\theta = \alpha t = \theta_0 \tag{97}$$

then from (92) θ_0 is given by:

$$\tfrac{1}{2}\alpha^2 S_m (\cos\theta_0 - \cos 2\theta_0) = Y \tag{98}$$

and similarly if the point C corresponds to:

$$\theta = \alpha t = \theta_1 \tag{99}$$

then it is easily shown from the tangency property of AC and the equation (91) for $\dot{S}$ that:

$$\sin\theta_1 (1 - \cos\theta_1) - \sin\theta_0 (1 - \cos\theta_0) = (\theta_1 - \theta_0)(\cos\theta_0 - \cos 2\theta_0) \tag{100}$$

Thence from (70), (90) and (91) it follows that:

$$\frac{S'_m}{S_m} = 1 - \tfrac{1}{4}(1 - \cos\theta_1)^2 + \tfrac{1}{4}(1 - \cos\theta_0)^2$$
$$+ \tfrac{1}{4}(\theta_1 - \theta_0) \times \{ \sin\theta_0 (1 - \cos\theta_0) + \sin\theta_1 (1 - \cos\theta_1) \} \tag{101}$$

for $W_m > W_2$.

The first two terms in (101) correspond to the area under CD, the third term to the area under DA and the remaining terms to the area under AC.

Further, from (93), (95) and (98), it follows that:

$$\left(\frac{W_2}{W_m}\right)^2 = \tfrac{8}{9}(\cos\theta_0 - \cos 2\theta_0) \tag{102}$$

for $W_m > W_2$ the corresponding range of θ_0 being:

$$\cos^{-1}\tfrac{1}{4} > \theta_0 > 0 \tag{103}$$

From (100), (101), (102) and (96) we can thus evaluate S'_m/S_m as a function of W_m/W_2. In the calculations for $W_m > W_2$ it is most convenient to regard θ_0 as the basic parameter and θ_1 as an intermediate parameter given by (100). The only involved part of the calculations is this calculation of θ_1 since (100) is an implicit equation for θ_1; this evaluation was performed by obtaining a first approximation graphically and then correcting this by (100).

Thus we plotted the curve of ordinate y (say) and abscissa θ,

$$y = \sin\theta (1 - \cos\theta) \tag{104}$$

corresponding in shape to the $\dot{\sigma}$ curve, and the tangent AC (Figure 5) at $\theta = \theta_0$ is then given by:

$$Y = \sin \theta_0 (1 - \cos \theta_0) + (\sigma - \theta_c)(\cos \theta_0 - \cos 2\theta_c) \qquad (105)$$

This tangent was then drawn by calculating from (105) two points on it, namely, the point where it cuts $Y = 0$ and the point where it cuts either $\theta = \pi$ or $\theta = \pi/2$ the latter being used for the steeper tangents to avoid the points being too widely spaced. (The use of the graphical property of tangency as such would be relatively inaccurate). Where this tangent cut the curve (104) then gave a first approximation θ'_1 (say).

Now, if we put $\theta_1 = \theta'_1 + \epsilon$ in (100), expand in powers of ϵ and neglect powers higher than the first, we obtain:

$$\epsilon (\cos \theta_0 - \cos 2\theta_0 - \cos \theta'_1 + \cos \theta'_1) \qquad (106)$$

$$= \sin \theta'_1 (1 - \cos \theta'_1) - \sin \theta_0 (1 - \cos \theta_0) - (\theta'_1 - \theta_0)(\cos \theta_0 - \cos 2\theta_0)$$

Using therefore the graphical value of θ'_1 in (106), we obtained ϵ and thence a corrected value of θ_1 for given θ_0. Since ϵ was in all cases small, no further correction by successive substitution in (106) was found necessary.

The results for S'_m/S_m as a function of W_m/W_1 are given in Table 2 but are not plotted as such in Figure 2 since the somewhat remarkable fact was noted that this curve was virtually indistinguishable from the curve S'_m/S_m versus W_m/W_1 for the instantaneous impulse over the range plotted. Mathematically there does not seem any obvious connection between the set of equations (85) and the set (100), (101) and (102) while physically no explanation can be offered. However, this does not mean that the relative area of bull-in is the same in the two cases for a given central deflection, since from (90) and (95):

$$W_2^2 = \frac{32}{9} W_1^2$$
$$\text{i.e. } W_2 = 1.89 W_1 \qquad (107)$$

In order to bring out this difference, the ratio S'_m/S_m for the present case has been plotted in Figure 2 against the same abscissa W_m/W_1 as for the instantaneous impulse.

A.24   *Numerical values of parameters.*

For numerical application to Box Model results, we note that the qualitative variation of S'_m/S_m with W_m/W_1 in Figure 2 does not depend on the numerical values of the parameters A_1 etc., but that W_1 depends on the constant K(say) defined by:

$$K = \frac{4\pi D A_1^2}{A_2 A_3} \qquad (108)$$

whence from (90) and (95) we have:

$$\frac{T_0 - T_1}{T_0} = K \frac{W_1^2}{4ab} = \frac{9}{32} K \frac{W_2^2}{4ab} \qquad (109)$$

The constant K depends on the six parameters defined in (9) and (13) but not on A_0, and we must therefore make specific assumptions regarding the forms of the displacement functions of $f_1 f_2 f_3$ of equations (1), (2) and (3). We assume them to be of the simple type:

$$\frac{w}{W} = f_1 (x,y) = F_1 \left(\frac{x}{a}\right) F_1 \left(\frac{y}{b}\right) \qquad (110)$$

$$\frac{u}{U} = f_2 (x,y) = F_2 \left(\frac{x}{a}\right) F_3 \left(\frac{y}{b}\right) \qquad (111)$$

$$\frac{v}{V} = f_3 (x,y) = F_3 \left(\frac{x}{a}\right) F_2 \left(\frac{y}{b}\right) \qquad (112)$$

It will .....

It will be noted that each is the product of an x and y factor and there is assumed to be no essential difference between the x and y direction. We shall further assume that the load and therefore the resulting displacements are symmetrical so that:

$$F_1\left(\frac{x}{a}\right), F_3\left(\frac{x}{a}\right) \text{ are even functions of } \frac{x}{a}$$

$$F_2\left(\frac{x}{a}\right) \text{ is an odd function of } \frac{x}{a} \tag{113}$$

Also from (7) and (110) we choose:

$$\int_0^1 F_1(r)\, dr = 1 \tag{114}$$

so that w is identified with the mean deflection and similarly without loss of generality we may take:

$$F_2(-1) = -F_2(1) = 1$$

$$\int_0^1 F_3(r)\, dt = 1 \tag{115}$$

which implies that U and V are identified with the mean pull-in along the two pairs of opposite edges.

Substituting in (9) and (15) from (110), (111) and (112), we then find after simplification:

$$A_1 = 4\left(\frac{a}{b} + \frac{b}{a}\right) K_1 K_2$$

$$B_1 = 4b$$

$$C_1 = 4a$$

$$A_2 = 4ab\, K_1^2$$

$$B_2 = C_2 = 4ab\, K_3 K_4 \tag{116}$$

where:

$$K_1 = \int_0^1 \left[\, F_1(r)\,\right]^2 dr$$

$$K_2 = \int_0^1 \left[\, F'_1(r)\,\right]^2 dr$$

$$K_3 = \int_0^1 \left[\, F_3(r)\,\right]^2 dr$$

$$K_4 = \int_0^1 \left[\, F_3(r)\,\right]^2 dr \tag{117}$$

From (26) and (116) we then obtain:

$$A_3 = \frac{4\left(\frac{b}{a} + \frac{a}{b}\right)}{K_3 K_4} \tag{118}$$

and thence from (108) and (116) we find:

$$K = u K_2^2 K_3 K_4 \left(\frac{a}{b} + \frac{b}{a}\right) \quad (119)$$

In order to evaluate K we have now to assign specific forms to F_1, F_2 and F_3. For F_1 the final shape of the deflected plate in Box Model trials suggests as reasonable alternatives:

$$F_1(r) = \frac{\pi}{2} \cos \frac{\pi r}{2}$$

$$\text{or} \quad F_1(r) = \frac{3}{2}(1 - r^2) \qquad (120)$$

for which from (117) we find $K_2^2 = 9.5$ or 9 respectively.

Similarly, the final shape of pull-in at the edges in Box Model trials suggests that the same forms are reasonable shapes for F_3 also, i.e., we may take:

$$F_3(r) = \frac{\pi}{2} \cos \frac{\pi r}{2}$$

$$\text{or} \quad F_3(r) = \frac{3}{2}(1 - r^2) \qquad (121)$$

which give $K_3 = 1.19$ or 1.2 respectively.

Thus the four combinations of (120) and (121) give values of $K_2^2 K_3$ ranging from 10.8 to 11.4. The smallness of this range indicates that K is not very sensitive to the precise forms for F_1 and F_3.

The choice of a form for F_2 is not so easy since we have no direct experimental evidence to help and we therefore seek guidance from the exact solutions given by Taylor(1) for a circular and an elliptical panel under uniform static pressure.

We shall thus assume a two-term polynomial:

$$F_2(r) = \rho(r - r^3) - r^3 \qquad (122)$$

which satisfies (113) and (115) while the ρ term is similar to that given by Taylor(1) both for the radial displacements in a circular panel and the centre-line displacements in an elliptical panel under uniform static pressure.

In order to estimate ρ we note from (111) and (116) that:

$$\frac{S_1}{4ab} = \frac{u}{a} + \frac{v}{b} \qquad (123)$$

while, since w is even in x and y the central areal strain Δ_0 (say) in the plate is from (111) and (112):

$$\Delta_0 = \left[\frac{\partial u}{\partial x} + \frac{\partial v}{\partial y}\right]_{\substack{x=0 \\ y=0}} = \left[\frac{u}{a} + \frac{v}{b}\right] F'_2(0) F_3(0) \qquad (124)$$

Now from the report "The distortion under pressure of a diaphragm which is clamped along its edge and stressed beyond the elastic limit, it can also be shown that the central areal strain is twice the mean areal strain for both the circular and elliptical panels under uniform static pressure. This suggests that we assume the same ratio to hold in our problem for the final areal strain at centre and mean areal strain due to stretching, i.e., we assume:

$$(\Delta)_{0'm} = 2 \frac{S_m - S'_m}{4ab} \qquad (125)$$

whence from (123) and (124) we obtain:

$$F'_2(0) F_3(0) = 2 \frac{S_m - S'_m}{S'_m} \qquad (126)$$

Now .....

Now, using (121) we have $F_2(0) = \pi/2$ or 1.5. and, taking the latter for simpler arithmetic, we obtain from (122) and (126):

$$\beta = F'_2(0) + \frac{4}{3} \frac{S_m - S'_m}{S'_m} \qquad (127)$$

For all Box Model shots $S'_m \geq \frac{1}{3} S_m$ so that:

$$\beta < \frac{8}{3} \qquad (128)$$

while from (122) and (117) we find:

$$K_4 = \frac{1}{30\varepsilon} (\varepsilon_m{}^2 \quad 22 \beta + 40) \qquad (129)$$

It is then easy to show that in the range $0 \leq \beta \leq \frac{8}{3}$,

$$0.1 \leq K_4 < 0.5 \qquad (130)$$

We have previously seen that $K_2{}^2 \dot{\varepsilon}_3 \sim 11$ so that, for $a/b = 1.52$ as in Box Model shots we find from (119) and (130) that K lies in the range 10 to 40.

We shall therefore assume that:

$$K = 25 \qquad (131)$$

gives a reasonable expected value for K, while:

$$K = 40 \qquad (132)$$

probably overestimates K.

As a final point, we require a value for A_1 in order to estimate S_m from the mean deflection by use of (70).

Using (120) or (121) and $a/b = 1.52$ we find from (117) and (116) that

$$\left.\begin{array}{l} A_1 = 32.7 \text{ for cosine shape} \\[2mm] A_1 = 31.4 \text{ for parabolic shape} \end{array}\right\} \quad \frac{a}{b} = 1.52 \qquad (133)$$

further, the value of A_1 for the soap bubble shape and $a/b = 1.5$ is implicit in equation (38) of the report mentioned on the previous page, and is:

$$A_1 = \frac{16}{3} \times 5.76 = 30.8 \text{ for soap bubble shape } \frac{a}{b} = 1.5 \qquad (134)$$

The difference in A_1 for a/b varying from 1.5 to 1.52 is undoubtedly negligible so that for the three shapes of cosine, parabola and soap bubble we find A_1 varying from 32.7 to 30.8. It may be noted that the same three shapes give values 2.47, 2.25 and 2.06 respectively for the ratio of central to mean deflection and this range covers most of the box model shots. For smooth shapes, A_1 is thus relatively insensitive to the precise shape and we shall take:

$$A_1 = 31.6 \qquad (135)$$

as a mean value for application to Box Model trials. This value would only lead to pronounced error if "ripples" were present since such ripples give a relatively large contribution to increase of area compared with any contribution to mean deflection. Fortunately the dishing in Box Model trials is relatively smooth and the use of (135) is unlikely to introduce errors of more than about 5% in the deduced value of S_m.

TABLE 1.

EXPERIMENTAL DATA FOR NON-CONTACT SIDE SHOTS AGAINST BOX MODEL.
ALL TARGET PLATES MILD STEEL WITH CHARGE AT DEPTH OF 7 FT.

Shot No.	Charge			Plate Thickness	Mean Deflection W_m	Total Pull-In S'_m	Ratio $\frac{S'_m}{S_m}$
	Type	Weight	Distance				
		oz.	ft.	ins.	ins.	sq.ins.	
174	T.N.T.	20.2	2.0	0.355	2.81	73.3	0.59
181 R.	T.N.T.	20.2	2.0	0.350	2.83	78.5	0.62
239 R.R.	T.N.T.	20.2	2.0	0.366	2.24	58.0	0.73
175	M.II	20.3	2.0	0.357	3.60	112.8	0.50
180 R.	M.II	20.3	2.0	0.354	3.56	99.6	0.50
176	T.N.T.	20.2	3.0	0.225	2.64	61.6	0.56
185 R.	T.N.T.	20.2	3.0	0.229	2.40	45.3	0.50
240 R.R.	T.N.T.	20.2	3.0	0.243	2.02	40.4	0.63
177	M.II	20.2	3.0	0.232	3.57	88.1	0.44
182	M.II	20.1	5.0	0.182	3.19	82.0	0.51
183	T.N.T.	20.2	5.0	0.182	3.22	71.1	0.44
186	M.II	16.4	5.0	0.162	2.62	57.9	0.53
187	T.N.T.	16.4	5.0	0.163	1.79	41.5	0.82
196 R.	T.N.T.	16.4	5.0	0.150	2.43	44.3	0.48
188	T.N.T.	16.4	3.0	0.228	2.06	44.1	0.66
195 R.	T.N.T.	16.4	3.0	0.223	2.22	52.6	0.68
189	M.II	16.4	3.0	0.244	2.94	64.4	0.47
194 R.	M.II	16.5	3.0	0.226	3.02	72.9	0.51
190	M.II	16.5	2.0	0.352	3.30	90.6	0.53
192 R.	M.II	16.5	2.0	0.323	3.31	91.6	0.53
191	T.N.T.	16.4	2.0	0.350	2.54	65.5	0.65
193 R.	T.N.T.	16.4	2.0	0.323	2.51	65.0	0.65

TABLE 1 (Continued)

EXPERIMENTAL DATA FOR NON-CONTACT SIDE SHOTS AGAINST BOX MODEL.
ALL TARGET PLATES MILD STEEL WITH CHARGE AT DEPTH OF 7 FT.

Shot No.	Type	Charge Weight oz.	Charge Distance ft.	Plate Thickness ins.	Mean Deflection W_m ins.	Total Pull-in S'_m sq.ins.	Ratio $\frac{S'_m}{S_m}$
200	E.G.H.	36.1	3.5	0.319	3.40	88.9	0.49
205 R.	E.G.H.	36.1	3.5	0.316	3.38	83.6	0.46
201	E.G.L.	37.0	3.5	0.319	3.61	97.1	0.47
204 R.	E.G.L.	37.0	3.5	0.316	3.52	99.9	0.51
202	E.G.H.	36.1	2.5	0.369	3.45	100.8	0.54
206	T.N.T.	34.0	7.0	0.126	2.16	(55.0)	(0.75)
209 R.	T.N.T.	29.2	7.0	0.130	1.96	(42.6)	(0.70)
207	E.G.L.	37.0	8.5	0.131	2.42	47.9	0.52
210 R.	E.G.L.	37.0	8.5	0.117	2.33	47.8	0.56
208	E.G.H.	35.8	8.5	0.130	2.69	58.5	0.51
211 R.	E.G.H.	36.0	8.5	0.112	1.74	41.7	0.87
214	E.G.H.	35.5	5.0	0.225	2.61	72.1	0.67
215	E.G.L.	37.0	5.0	0.226	2.68	73.1	0.65
218	T.N.T.	32.6	3.5	0.311	2.71	70.5	0.61
219 R.	T.N.T.	33.0	3.5	0.311	2.67	66.2	0.59
220	T.N.T.	32.0	8.5	0.111	1.89	41.0	0.73
221	T.N.T.	74.1	6.0	0.242	1.42	34.2	1.07
222	T.X.1.	20.6	3.0	0.243	3.14	82.2	0.53
223 R.	T.X.1.	20.6	3.0	0.24	2.95	83.3	0.60
224	T.X.1.	20.5	5.0	0.171	2.77	71.3	0.59

TABLE 1. (Continued)

EXPERIMENTAL DATA FOR NON-CONTACT SIDE SHOTS AGAINST BOX MODEL.
ALL TARGET PLATES MILD STEEL WITH CHARGE AT DEPTH OF 7 FT.

Shot No.	Charge			Plate Thickness	Mean Deflection W_m	Total Pull-in S'_m	Ratio $\frac{S'_m}{S_m}$
	Type	Weight os.	Distance ft.	ins.	ins.	sq.ins.	
235	T.X.1.	20.5	2.0	0.361	3.14	80.1	0.51
236 R.	T.X.1.	20.5	2.0	0.359	3.11	71.7	0.47
237	T.N.T.	33.2	6.5	0.166	2.26	34.2	0.42
241	T.N.T.	32.5	3.5	0.243	2.72	56.6	0.48
242	T.N.T.	32.6	7.0	0.125	2.50	38.8	0.39

Bracketed values for Shots 206 and 209 are corrected values

R after Shot Number denotes nominal repeat of preceding shot in Table.

R.R. after Shot Number denotes nominal repeat of preceding two shots in Table.

M.II = Minol II

T.X.1 = Torpex I.

E.G.H. = Ex-German (high H.N.D).

E.G.L. = Ex-German (low H.N.D).

TABLE 2.

THEORETICAL VARIATION OF S'_m/S_m with W_m/W_1.

Loading by instantaneous impulse			Load varying as $H(t)$				
θ_1 degrees	$\frac{W_m}{W_1}$	$\frac{S'_m}{S_m}$	θ_0 degrees	θ_1 degrees	$\frac{W_m}{W_2}$	$\frac{W_m}{W_1}$	$\frac{S'_m}{S_m}$
0	1	1	75.5	75.5	1	1.89	1
20	1.042	0.995	60	104	1.06	2.00	0.99
30	1.100	0.977	50	123	1.17	2.21	0.94
40	1.191	0.931	40	176	1.38	2.60	0.815
50	1.331	0.843	30	153	1.76	3.32	0.605
60	1.555	0.703	20	166	2.54	4.70	0.54
65	1.721	0.613	10	176	4.99	9.45	0.101
70	1.950	0.510	0	180	∞	∞	0
75	2.288	0.394					
80	2.858	0.269					
85	4.134	0.136					
90	∞	0					

513
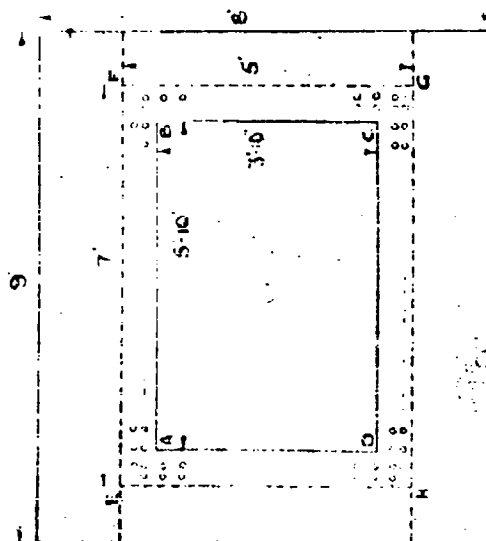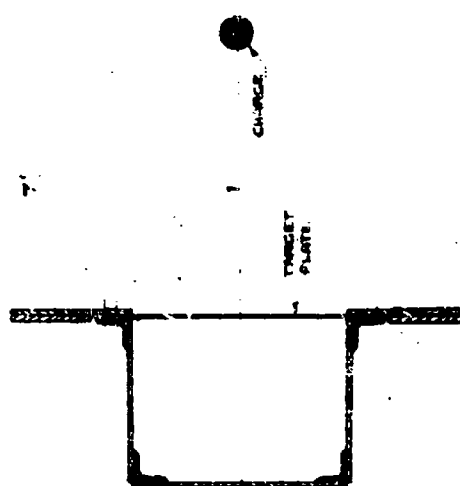
GENERAL SCHEMATIC ARRANGEMENT OF TRIALS.
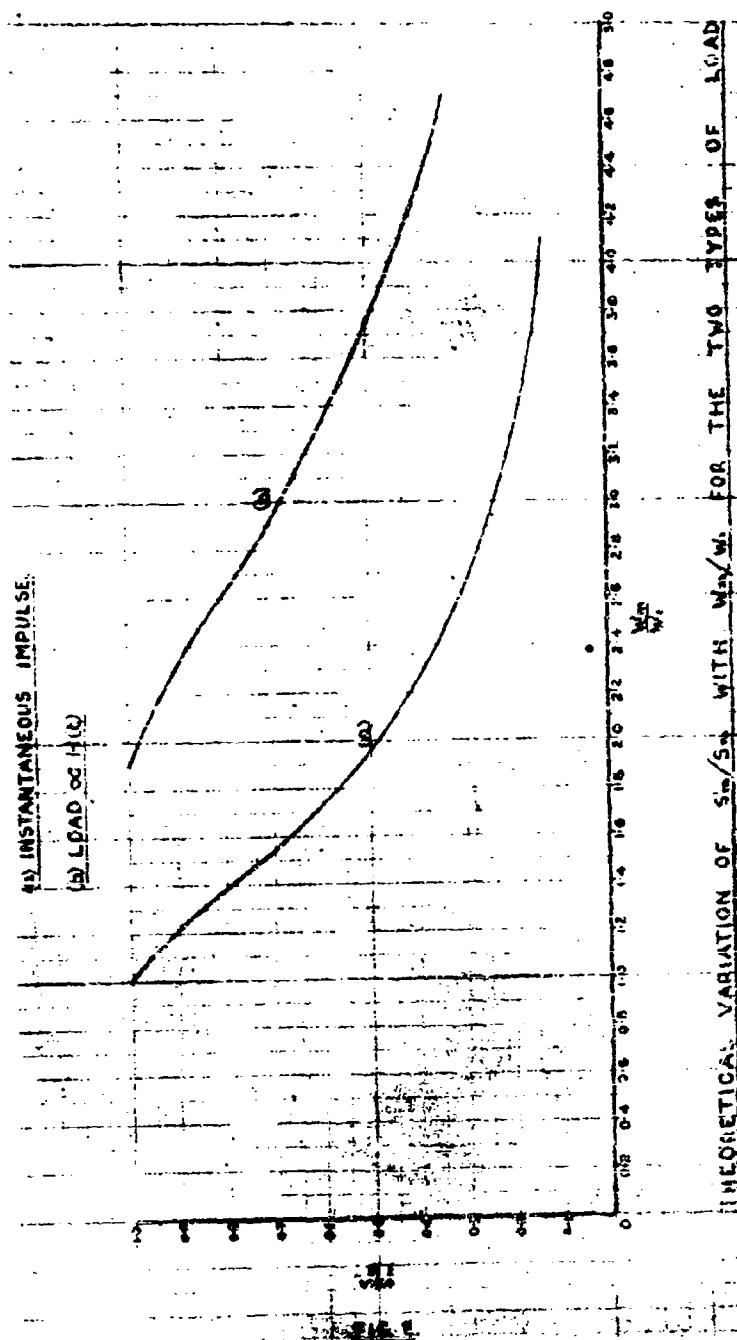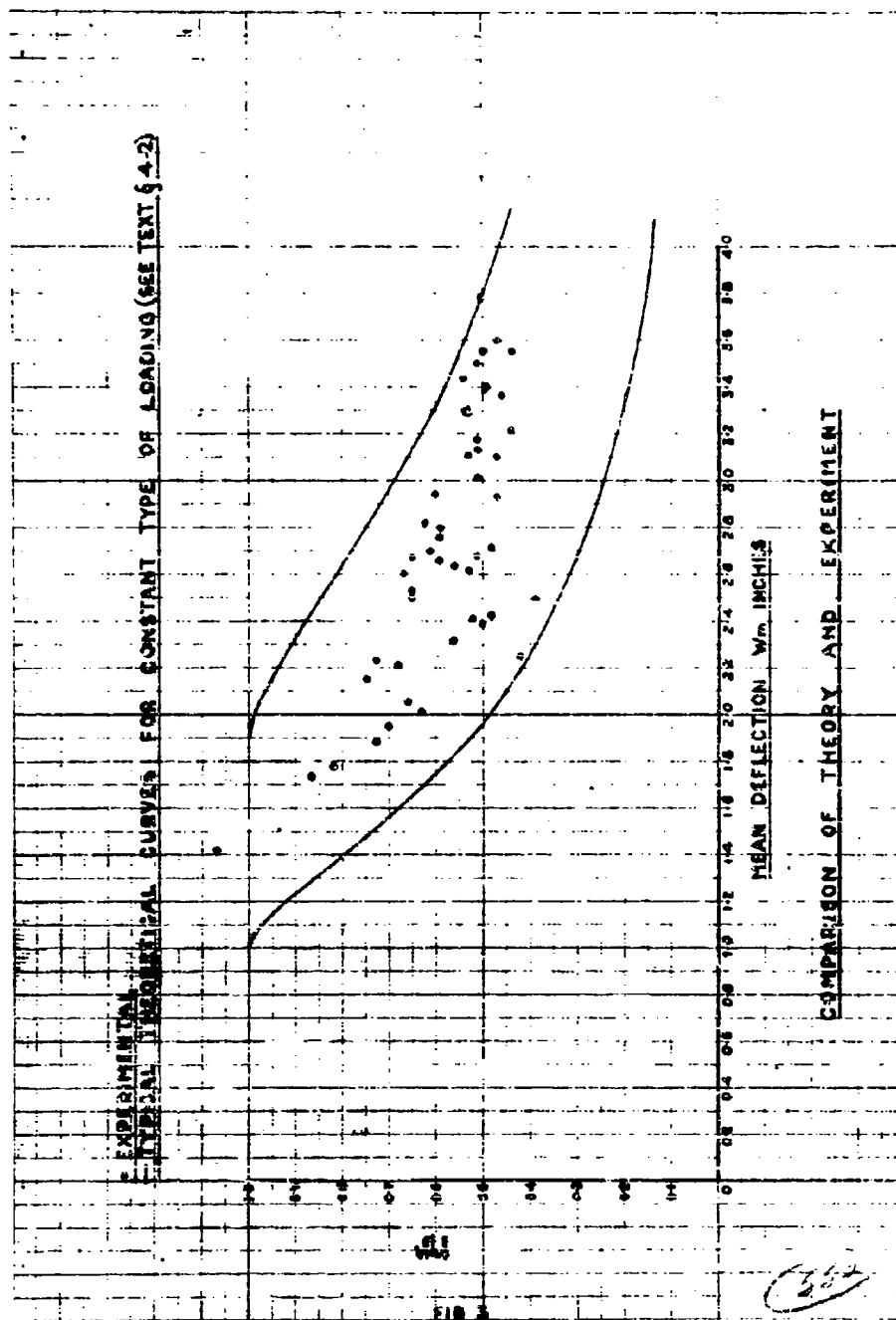
FIG. 1

(i) INSTANTANEOUS IMPULSE.

(b) LOAD ∝ H(t)

THEORETICAL VARIATION OF S_m/S_g WITH W_m/W_t FOR THE TWO TYPES OF LOAD

EXPERIMENTAL THEORETICAL CURVES FOR CONSTANT TYPE OF LOADING (SEE TEXT § 4-2)

MEAN DEFLECTION Wm INCHES

COMPARISON OF THEORY AND EXPERIMENT

FIG 3

516

OB IS OF SLOPE Y
SHADED AREA = PLATE STRETCHING
UNSHADED AREA EDGE PULL-IN
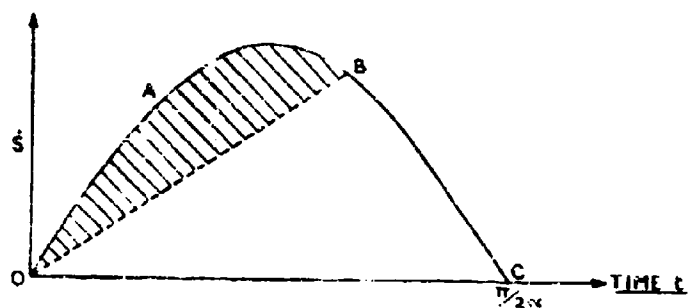
VARIATION OF S WITH TIME FOR INSTANTANEOUS IMPULSE

FIG 4

AC IS OF SLOPE Y
SHADED AREA = PLATE STRETCHING
UNSHADED AREA = EDGE PULL-IN
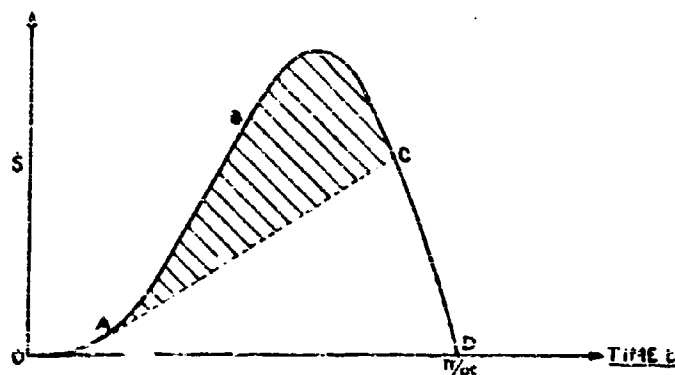
VARIATION OF S WITH TIME FOR LOAD ∝ H(t)

FIG 5

DIAPHRAGM GAUGE STUDIES OF UNDERWATER EXPLOSIONS

P. M. Fye and J. E. Eldridge
Underwater Explosives Research Laboratory
Woods Hole Oceanographic Institution

American Contribution

March 1951

ABSTRACT

This report, which describes a great variety of experiments with a simple type of underwater gauge, should be of interest to anyone concerned with the damaging power of underwater explosions. It not only describes the construction and use of this gauge for comparing explosives but also a variety of experiments which throw light on the way in which damage is produced in structures by underwater explosions. It provides an illuminating illustration of the precautions and care which are required in order that accurate and precise conclusions can be drawn from even simple scientific investigations.

Principally to compare various explosives with respect to their underwater damaging power and to investigate the various factors controlling damage by underwater explosions, a type of diaphragm gauge was constructed for use at this laboratory. It consisted of a circular steel or copper diaphragm, about 1/16 in. thick, clamped across the open end of a strong steel cup, the inside diameter of which was 3.3 in. The diaphragm formed a watertight seal over the cup so that on submersion the gauge remained air-filled. By exposing the gauge sufficiently close to an underwater explosion, the diaphragm was permanently deformed; the depression at the point of maximum deformation was measured and arbitrarily defined as the damage produced. The more important results obtained with this gauge using small charges (up to 25 lbs.) are outlined below.

1. The equation $D = k \dfrac{W^m}{d^n}$ was found to apply over a considerable

range of experimental conditions. In this equation, D is the maximum depression of the diaphragm, k is a constant for a given type of explosive and a given type of diaphragm, W is the charge weight, d is the charge-to-gauge distance, m and n are constants for a given type of diaphragm. It was found experimentally that m and n for a given diaphragm material were approximately in the ratio 1 to 2. For steel diaphragms, m and n were found to be about 0.6 and 1.2, respectively; for copper, m and n were respectively 0.4 and 0.8.

2. For steel diaphragms, the damages observed experimentally agreed closely with those predicted by the theoretical studies of diaphragm deformation carried out by J. G. Kirkwood and others.

3. When half-scale gauges were exposed to underwater explosions in which all other linear dimensions of the experiment were decreased by one-half, the damage produced was one-half that obtained with the regular gauges under normal conditions. In other words, Hopkinson's scaling rule was found to hold for a two-to-one variation.

4. If the gauges were held in place by a simple wooden framework instead of by an encompassing steel ring, the damage could be decreased by as much as 50%. This was indicated to be due to rarefaction waves reflected from the wood and consequent cancellation of a portion of the pressure wave from the explosion.

518

5. Surrounding the front face of the gauge with a steel disc or baffle increased the resulting damage by as much as 50%.

6. In ordinary use with small charges, the time required for the complete deformation of the diaphragm was about 3 times the time-constant* of the primary shock-wave. Subsequent pulses from the bubble had no appreciable effect on the final deformation unless the experiment was set up so that the bubble migrated toward the gauge during its oscillation. In this case, bubble pulses increased the deformation as much as 80%, and the time required for final deformation was correspondingly increased.

7. It was proved by flash photographs that cavitation was formed in the water in front of these diaphragms during deformation under certain conditions but not for most of the experiments described herein. Although exhaustive tests were not conducted, the theoretically derived criterion for the formation of cavitation was found to agree with observations.

8. If the mass of the diaphragm was increased by a factor of about 7.7 without a corresponding change in mechanical strength, the damage was decreased by about 50%.

9. Gauges placed in the Mach region of two intersecting shock-waves from a pair of charges recorded up to 50% more damage than gauges placed the same distance from a single charge of the same total weight.

10. The bubble from one charge was found to shield a damage gauge from the effects of a second charge detonated on the other side of the first charge, provided that the two charges were not too close.

---

* The time required for the pressure to fall to $1/e$, or 36.8% of its maximum value.

I. INTRODUCTION

When underwater explosives research was begun by the NDRC in the spring of 1941, two of the most important tasks undertaken were (1) the study of the factors which influence underwater explosion damage, and (2) the comparison of various underwater explosives with respect to their damaging power. Since "damage" is a loosely defined term, there can be no such instrument as a "damage gauge"; yet, there could be no solution to the above mentioned problems without some means, arbitrary though it may be, of measuring damage. Accordingly, in the summer of 1941, a gauge consisting of a strong steel cylinder, closed at one end, and covered at the other end with a relatively thin metal diaphragm was put into use.[1,2,3] The "damage" measured by the gauge was the amount of deformation suffered by the diaphragm on exposure to the underwater explosion.

Although this gauge was an arbitrary one, it was used successfully for comparison of explosives in the weight range from about one ounce to 25 lbs. as well as for testing service weapons. It was of particular value in the period during which the more elaborate techniques of explosion measurement were being developed.

II. DESCRIPTION OF THE UERL DIAPHRAGM GAUGE

1. Construction

This diaphragm gauge was designed and constructed in 1941 at the Explosives Research Laboratory, Bruceton, Pennsylvania[1] as follows. (See Figures 1 and 2.) The edges of a section of steel pipe, 4-1/2 in. O.D. x 3-1/8 in. I.D. x 3 in. long, were beveled for fillet welding. A solid steel plate 7 x 7 x 1/2 in. was welded over one end of the pipe section, and the second plate 7 x 7 x 1/2 in. with a central hole of nearly 3-1/4 in. diameter was welded over the other end of the pipe. The outside face of this second plate was milled flat, and the hole was accurately finished to a diameter of 3.270 in. The edge between the side of the hole and the milled face was then rounded off into a 90° arc of 1/16 in. radius. A third steel plate, 7 x 7 x 1/2 in., was milled flat on one face and a tapered hole 4.582 x 3.432 in. bored in the center, the narrower end of the hole being at the milled face. Smaller holes were drilled through the two milled plates, and the holes in one were tapped to take 1/2 in. x 13 thread cap screws so that the two plates could be bolted tightly together. Provision was made for eight cap screws spaced around the main hole. The first gauges were so constructed that the cap screws were inserted through the welded plate to engage threads in the cover plate; this proved to be cumbersome and subsequent gauges were made with holes tapped in the welded plate. A hole was drilled also in each corner of the two plates so that pins could be inserted to assure reproducible alignment of the two plates.

---

[1] This gauge has been previously described by Fye and Alexander in OSRD Report No. 1035, November 1942.

[2] Wilson, Cole and Fye, OSRD Report No. 1220, February 1943.

[3] A diaphragm gauge was already in use by the British, cf, Mine Design Department, Summary No. M. S. 940/42, A.C. 3338, October 1942.

520

7"

TAP $\frac{1}{2}$"−13
4 CORNER HOLES

A

7"

6" DIA.

22$\frac{1}{2}$°

A A

$\frac{5}{8}$"

$\frac{1}{2}$"

3.432"

3.270"

$\frac{1}{2}$"x 1" HEX BOLT
BOTH FACES
SURFACE GROUND

41°

DRILL $\frac{1}{2}$"
ALL HOLES

$\frac{1}{16}$ RADIUS

TAP $\frac{1}{2}$−13
ALL HOLES

4" DOUBLE EXTRA
STRONG STEEL PIPE

$\frac{3}{8}$" CONTINUOUS FILLET WELD

$\frac{1}{4}$" CONTINUOUS FILLET WELD

TAP $\frac{1}{2}$−13
4 CORNER HOLES

SECTION A—A

FIG. I
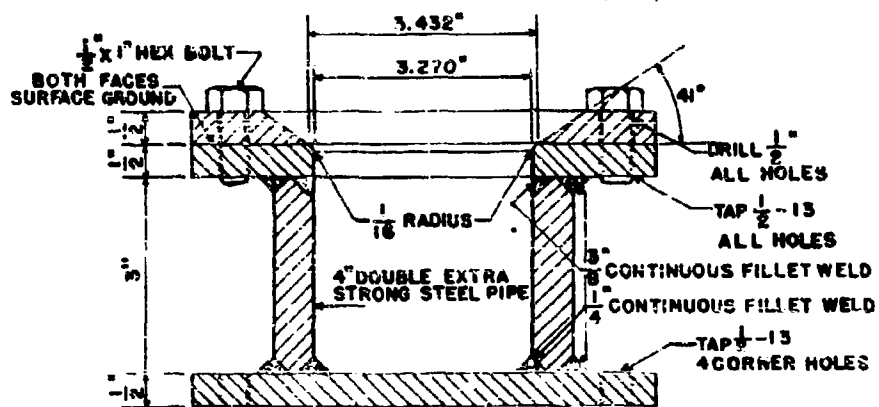
DETAIL OF DIAPHRAGM GAUGE

UERL   WOODS HOLE, MASS

DRAWN BY HRC
1−24−46

Diaphragm
Cap screws
Clamping plate

Front View

Diaphragm
Cap screws
Clamping plate
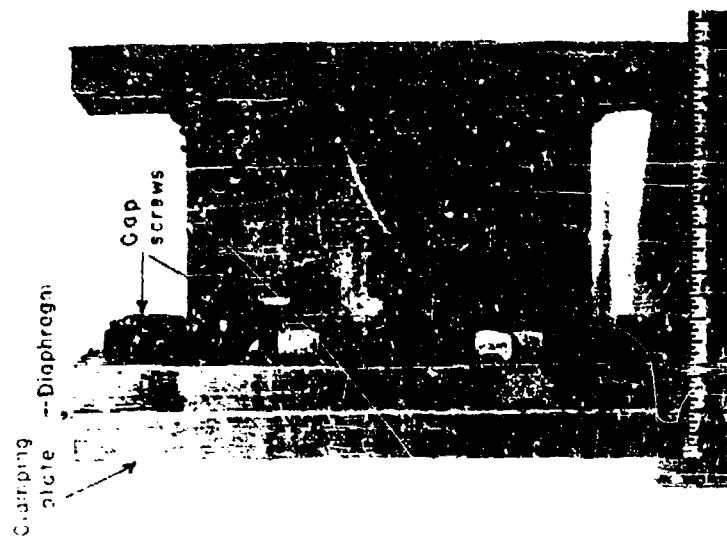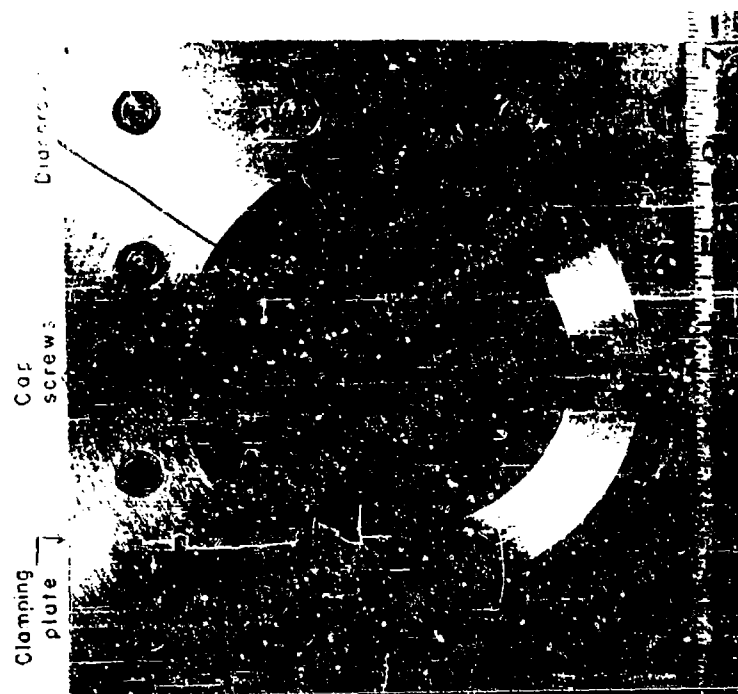
Side View

Fig. 2. Photographs of UERL Diaphragm Gauge

522

The diaphragm used in this type of gauge was steel or copper and was 7 x 7 x ca. 1/16 in. thick. Before use, it was drilled with twelve holes around the edge to correspond with the pin and cap screw holes and all rough edges were smoothed off. The diaphragm was then clamped between the milled faces of the gauge plates.

2. Method of Using the Gauge

Most shots were conducted in the following manner. Four damage gauges were mounted on a framework in the center of which was fixed the explosive charge. The gauges all pointed toward the charge and were spaced at approximately 90° intervals about the charge.

Before clamping the diaphragm in place, a medium-bodied motor oil (e.g., SAE-40) was applied with a paint brush to both of the milled faces of each gauge to aid in keeping the gauge watertight.

If the charge was sufficiently small (ca. 1/2 lb.) the whole rig (frame, gauges and charge) could be lowered into the water from a boom on the dock. In most cases, however, larger charges (up to 25 lbs.) were used which necessitated working on a raft anchored out in the harbor and suspending the rig after it had been lowered into the water either from the raft or from a buoy attached by a horizontal line to the raft. When the shot had been fired, the rig was raised to the surface and new diaphragms installed in the gauges for the next shot. Photographs of the larger rafts are shown in Figures 3 and 4 and the smaller raft is shown in Figure 5. This pontoon-floated raft is particularly convenient for this type of work. It is rectangular in shape (23 ft. x 28 ft.) with a 13 ft. x 16 ft. opening in the center. One end has a 12 ft. x 23 ft. apron for a work space and the other end has a gangway which can be removed for floating gear out of the center away from the raft. An overhead quadrupod with cables to a winch permits lowering and raising gear. When the raft is anchored in a current with the open end down stream the gauges and gear can be lowered until they are supported by a floating buoy and then the buoy and gear floated down stream to a safe distance for firing the charge.

Most of the charges used were cast in cylindrical cardboard or tin can containers, and were boostered with pressed tetryl pellets.[4]/ The booster was usually half-submerged in the explosive. The tetryl pellets were initiated by a DuPont No. 8 electric detonator set into a small well provided in the top pellet. Putty placed around the detonator and tetryl waterproofed the latter sufficiently up to depths of 40 ft.

3. Diaphragm Materials

Both copper and hot-rolled steel were used as diaphragm materials. The copper was annealed until it was dead-soft before use[1]/. The steel

4/ Philip Newmark and Ernest Patterson, OSRD Report No. 6259, NDRC Report No. A-361.
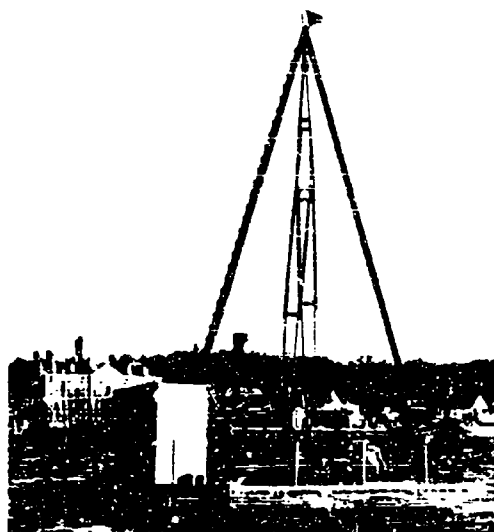
Fig. 3. Large raft.

Fig 5 Small raft.
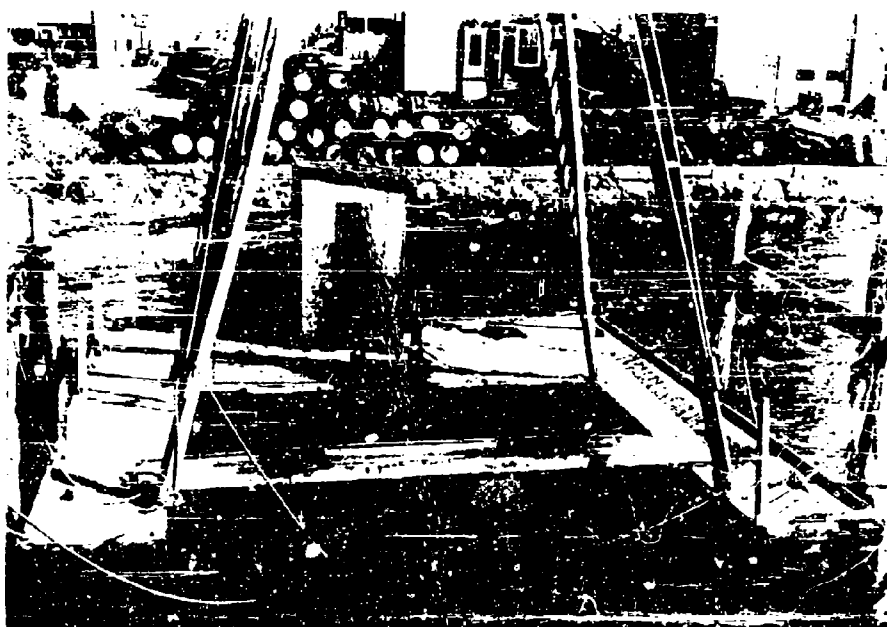
Fig. 4 Deck of large raft

used in the tests herein reported was from five separate lots; the
physical properties of the various lots are given in Table I. Yield
stresses and tensile strengths for the first four lots and Lot 5b are
quoted from the supplier's specifications; other Lot 5 values (in
parenthesis) for the yield stress and tensile strength were determined
at the David Taylor Model Basin.

Table Ia. Physical properties of various steels
used in diaphragm gauge tests

Lot No.	Nominal Diaphragm Thickness (in.)	Yield Stress (lbs/in.^{2})	Tensile Strength (lbs/in.^{2})
1	.064	-	60,000
2	.064	-	48,500
3	.075-.095	60,000	-
4	.073	-	-
5 (thick)	.150	$(40,310 \pm 1,014)$	$(69,324 + 704)$
5 (medium)	.080	$(50,149 \pm 629)$	$(72,803 \pm 462)$
5a (thin)	.040	$(42,608 \pm 2,336)$	$(59,355 \pm 2,467)$
5b (thin)	.040	39,000	54,000

Lot 5 steel was used most extensively for this and other work
requiring sheet metal[5]. The three thicknesses were specially obtained
from the American Rolling Mill Company and all were from the same melt
of steel and had compositions as uniform as possible. Additional tests
on part of Lot 5 by the Materials Testing Laboratory of Massachusetts
Institute of Technology furnished the data of Table Ib.

Table Ib. Additional Lot 5 Data

Lot No.	Young's Modulus (lbs/in.^{2})	Yield Strength (lbs/in.^{2})	Ultimate Strength (lbs/in.^{2})	Elongation (fraction of original length)
5 (medium)	28.5×10^6	46,590	69,880	0.323
5b (thin)	25.5×10^6	36,800	59,650	0.352

III. THEORETICAL PREDICTION OF DEFORMATION OF DIAPHRAGMS

The study of circular diaphragm deformation by means of fluid
pressure has been pursued on a theoretical basis by several groups,

5/ J. C. Decius and Paul M. Fye, OSRD Report No. 6247, NDRC Report No. A-369.

such as that of G. I. Taylor[6] in Britain, and those led by R. W. Goranson[7], by E. H. Kennard[8] and by J. G. Kirkwood[9] in the United States. The work of the Kirkwood group has been connected rather closely with that of the UERL and, in addition to their general calculations, they have made calculations which are specific for the UERL damage gauge.

Without going into the development of the Kirkwood calculations which have already been reported[9], it may be illustrative to cite the result of some of their work made applicable to the UERL diaphragm gauge.

If the following assumptions, among others, are made:

(1) that the diaphragm is affected only by the primary shock-wave from an underwater explosion,
(2) that "cavitation" does not occur in the water in front of the diaphragm during the damage process,
(3) that the profile of the plastically deformed diaphragm is parabolic, then

$$Z_m = \frac{103.4 \, P_m \, \theta}{(\rho \, \sigma_0)^{1/2}} \left(\frac{R_0}{a_0}\right) g \left(1 + \frac{2}{3} \frac{R_0}{\rho} \frac{\rho_0}{a_0}\right)^{-1/2} \quad \text{(in.)} \qquad (1)$$

$$\omega = \frac{206.8}{R_0} \left(\frac{\sigma_0}{\rho}\right)^{1/2} \left(1 + \frac{2}{3} \frac{R_0}{\rho} \frac{\rho_0}{a_0}\right)^{1/2} \quad \text{(sec}^{-1}) \qquad (2)$$

In the above equations,

Z_m is the final central deflection of the diaphragm

a_0 is the diaphragm thickness in inches

R_0 is the radius of the diaphragm, equal to 1.64 in. for this gauge.

ρ is the density of the diaphragm in gm/cm^3

ρ_0 is the density of the water in gm/cm^3

σ_0 is the yield stress of the diaphragm material in lbs/in.^{2}

[6] G. I. Taylor, Sept. 1, 1942, S.W. 24, II-5-2799.
[7] Lt.Cdr. R. W. Goranson, USNR, August 1943, Bureau of Ships, U.S.Navy, Underwater Explosion Report No. 1942-4.
[8] E. H. Kennard, March 1944, Taylor Model Basin, U. S. Navy, Report No. 527.
[9] J. G. Kirkwood and J. M. Richardson, September 30, 1944, OSRD 4200.

P_m is the peak pressure of the shock-wave (assumed exponential) in lbs/in.^{2}

θ is the time (sec) required for the pressure of the shock-wave to fall to P_m/e, where e = 2.718 and

g   is a function of $\omega\theta$ as given in Table II below.

Table II.   Values of g corresponding to various values of $\omega\theta$

$\omega\theta$	g	$\omega\theta$	g	$\omega\theta$	g
0.2	0.491	3.0	0.219	7.0	0.117
0.4	0.456	3.5	0.197	7.5	0.110
0.6	0.435	4.0	0.179	8.0	0.105
0.8	0.406	4.5	0.165	8.5	0.100
1.0	0.378	5.0	0.152	9.0	0.0946
1.5	0.321	5.5	0.141	9.5	0.0904
2.0	0.276	6.0	0.132	10.0	0.0865
2.5	0.246	6.5	0.124		

Equations (1) and (2) combined with Table II allow a calculation to be made of the diaphragm deformation to be expected with a UERL damage gauge for given experimental conditions. Further details may be found in reference 9.

IV. COMPARISON OF THEORY AND EXPERIMENT

1. Steel Diaphragms

The Kirkwood equations given in Section III have been used to predict damage versus charge weight curves for Lot 3 and Lot 5 steel diaphragms in regular UERL damage gauges. These curves are shown in Figures 6 and 7 where experimental data are also plotted to indicate the excellent agreement between theory and experiment under these conditions.

For determining the theoretical curves the following data were used.

a_0 = 0.065 in. for Lot 3 diaphragms

a_0 = 0.080 in. for Lot 5 diaphragms

ρ = 7.8 gm/cm^3

ρ_0 = 1.01 gm/cm^3

σ_0 = 60,000 lb/in.^{2} for Lot 3 diaphragms

σ_0 = 68,000 lb/in.^{2} for Lot 5 diaphragms
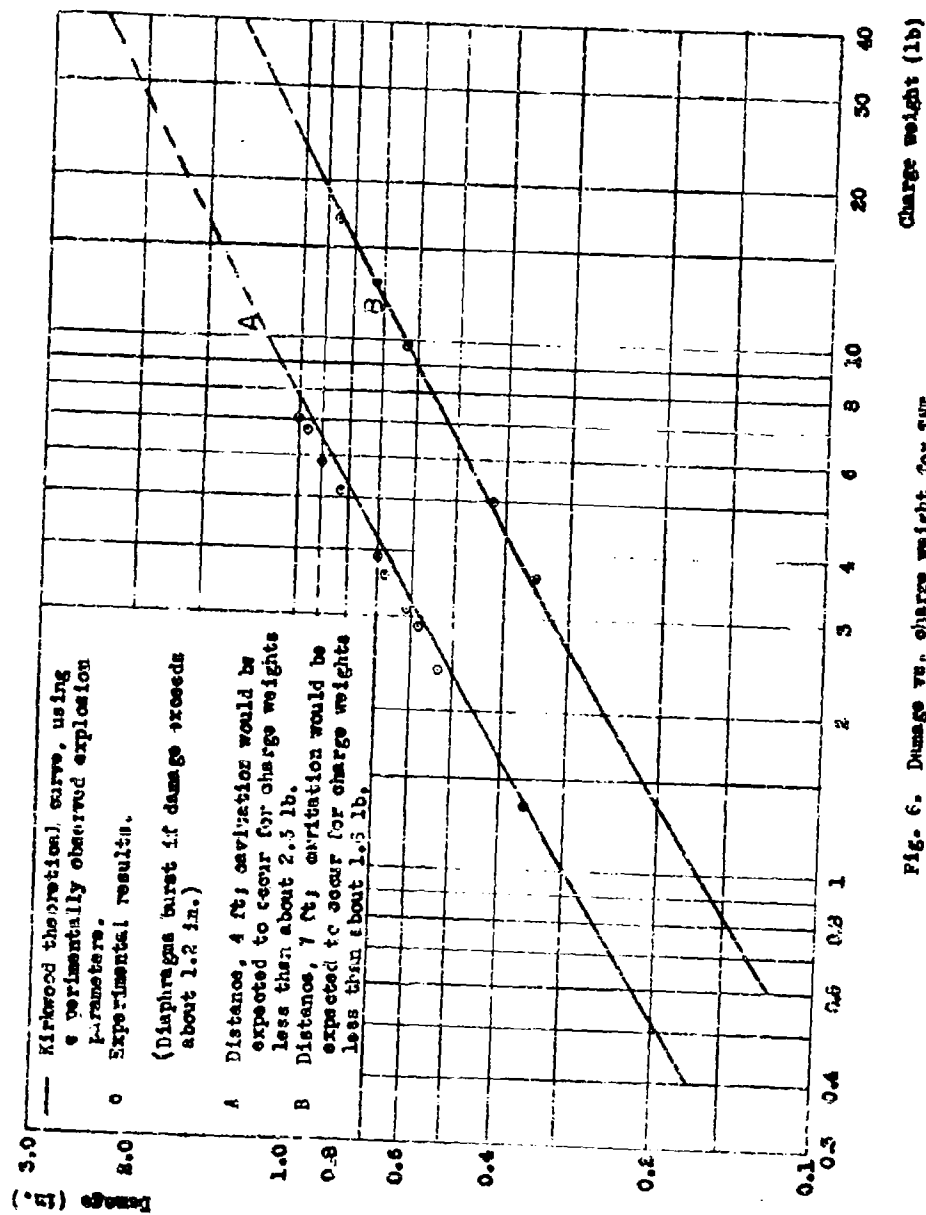
Fig. 6. Damage vs. charge weight for TNT.
.ot 3 steel diaphragms; gauges mounted on steel ring.

528

Lot 3 steel diaphragms; gauges mounted on steel ring.
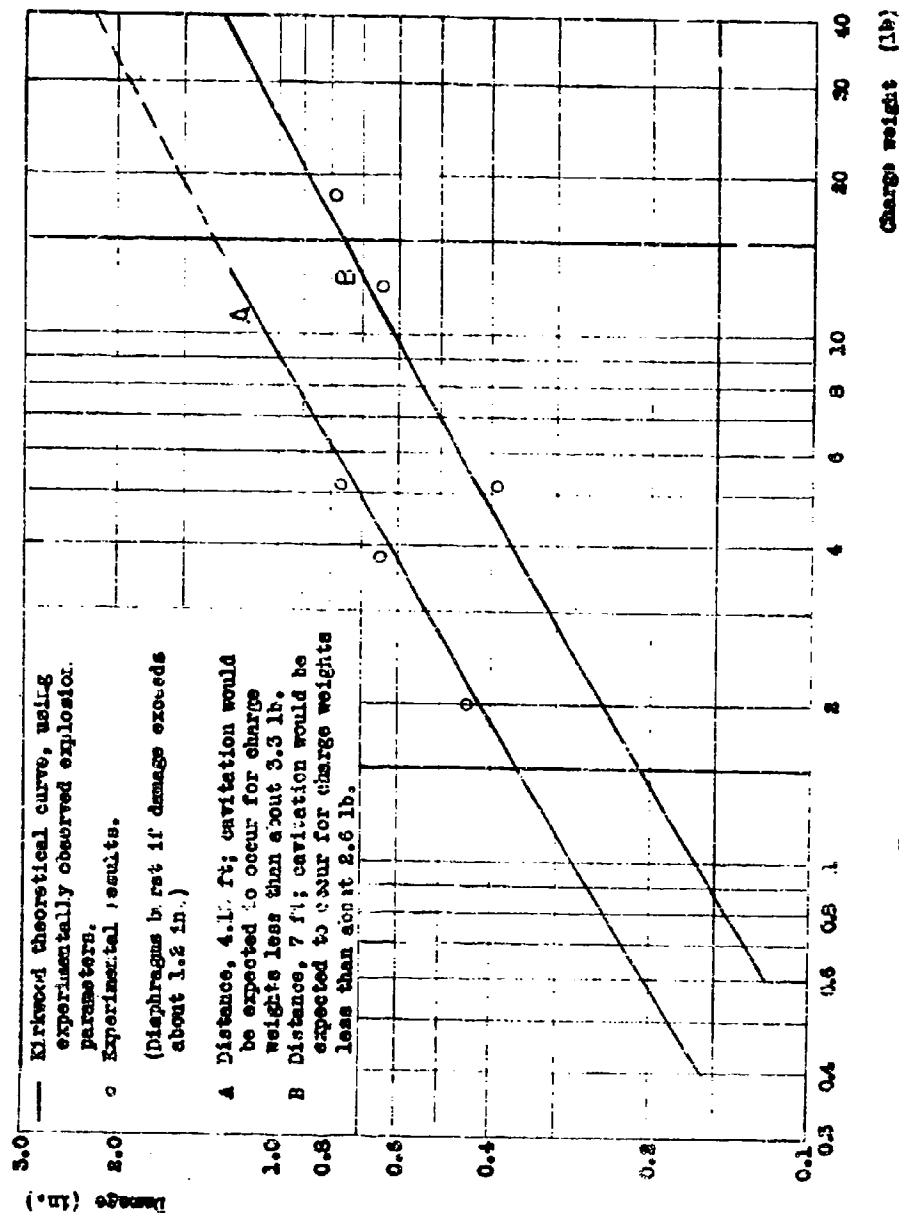
Fig. 7. Damage vs. charge weight for TNT.
Lot 5 steel diaphragms; gauges mounted on steel ring.

The peak pressure p_m and impulse I were calculated using the empirical expressions

$$p_m = 20,400 \left(\frac{W^{1/3}}{R} \right)^{1.1} \quad \text{lb/in.}^2 \tag{3}$$

$$I = 1.50 \frac{W^{2/3}}{R} \quad \text{lb-sec/in.}^2 \tag{4}$$

where W (lb) is the weight of TNT and R (ft) is the charge-to-gauge distance. The relation between p_m and I is assumed to be given by

$$I = p_m \theta \tag{5}$$

so that the time constant θ may be calculated from the following expression

$$\theta = 73.5 W^{0.29} R^{0.14} \text{ } \mu\text{sec}, \tag{6}$$

which will be used later.

The above expressions for the explosion parameters p_m and I were determined by piezoelectric measurements of explosions from full-scale charges[10]. Although some error may be introduced in scaling these values down to small charges, it is felt that they are probably more reliable than those obtained with small charges where instrumentation difficulties made it necessary to apply considerable corrections to apparent values.

Although somewhat outside the scope of this report, it is interesting to note the effect on the theoretical damage-weight curve if theoretical shock-wave parameters are substituted for the empirical values. Table III lists the scaled empirical values with those predicted theoretically[11] for small TNT charges of density 1.59 gm/cm^3.

Table III.   Comparison of theoretical and experimental explosion parameters

(Distance from charge 4 feet)

Charge Weight	Peak Pressure (lbs/in.^{2})		Impulse (lbs-sec/in.^{2})		Time-constant θ (μ sec)	
(lbs TNT)	Theo.	Expt.	Theo.	Expt.	Theo.	Expt.
0.4	3300	2960	0.26	0.204	80	69
1.0	4850	4200	0.48	0.379	98	95
4.0	8700	7120	1.12	0.944	128	133
10.0	12900	10100	1.91	1.75	149	173
40.0	27000	17100	4.3	4.38	178	256

10/ "Underwater Explosions", Princeton University Press pg 242 by R.H. Cole.
11/ Kirkwood, Brinkley, and Richardson, OSRD No. 2022, p.22, Nov. 1944.

Figure 6 shows the comparison between a theoretical damage versus weight curve based on theoretical shock-wave parameters and the experimental damage results. Considering the fact that the only experimental values used in determining the theoretical curve were the dimensions of the gauge and the yield stress of the diaphragms, the agreement (ca. 15%) is excellent.

2. Copper Diaphragms

It is difficult to apply Kirkwood's damage equations to copper diaphragms because copper does not have a definite yield stress like that of steel nor was the theory intended to apply to copper. Figure 9 shows that a theoretical curve based on a yield stress of 5,000 lbs/in.^{2} passes through the empirical damage-weight curve, but has a markedly greater slope. The slope of the theoretical curve is gradually decreased by assuming greater yield stress, but such a procedure rapidly changes the absolute level of the curve, as is illustrated by the example in which the yield stress was taken as 20,000 lbs/in.^{2} It is evident that the low weight exponent (i.e., slope of the damage-weight curve plotted on log-log paper) found for copper diaphragms is difficult to reconcile with the Kirkwood damage equations. It is possible that work hardening is a relatively important factor in the damage process for copper.

V. RESULTS OF EXPERIMENTS

1. The Empirical Equation of Damage

The "damage" recorded by a deformed diaphragm can be measured in terms of two simple parameters of the deformation, namely, the volume of the "dish", or the maximum depth of this dish. Since the latter measurement was easier to make accurately, and since it seemed to be reproducible, only this measurement was made for most work, and it was arbitrarily defined as damage.

It had previously been found[1],[12] that the maximum depth of depression of a deformed diaphragm could be expressed fairly accurately over a considerable range of experimental conditions by the following empirical equation:

$$D = k \frac{W^m}{d^n} \tag{7}$$

where D is the maximum depth of depression, or damage,

k is a constant determined by the properties of the explosive, the properties of the diaphragms, and by the units used for the other quantities,

W is the weight of the explosive charge,

12/ Cf. for instance, reports from the Mine Design Department of the British Admiralty
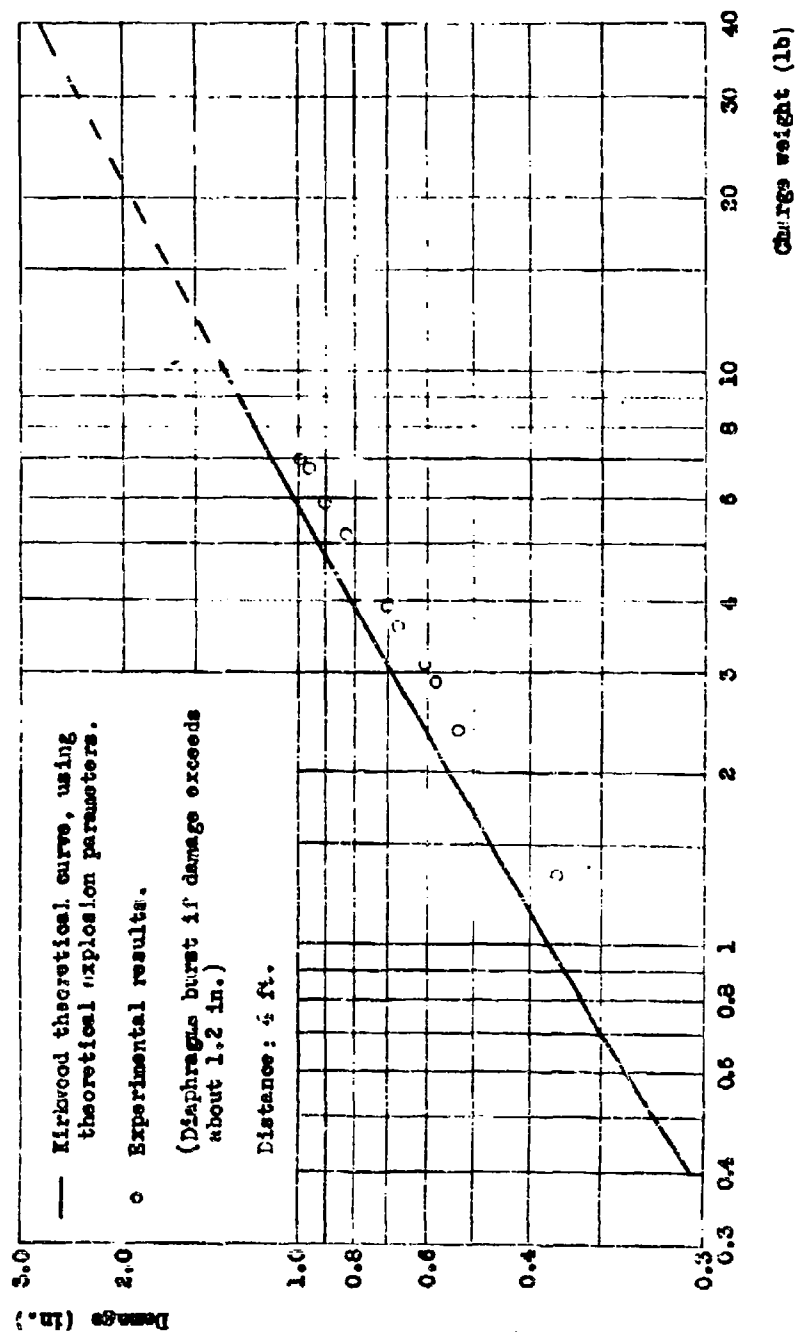
Fig. 4. Damage vs. charge weight for T.T.

Lot 5 steel diaphragms; gauges mounted on steel ring.
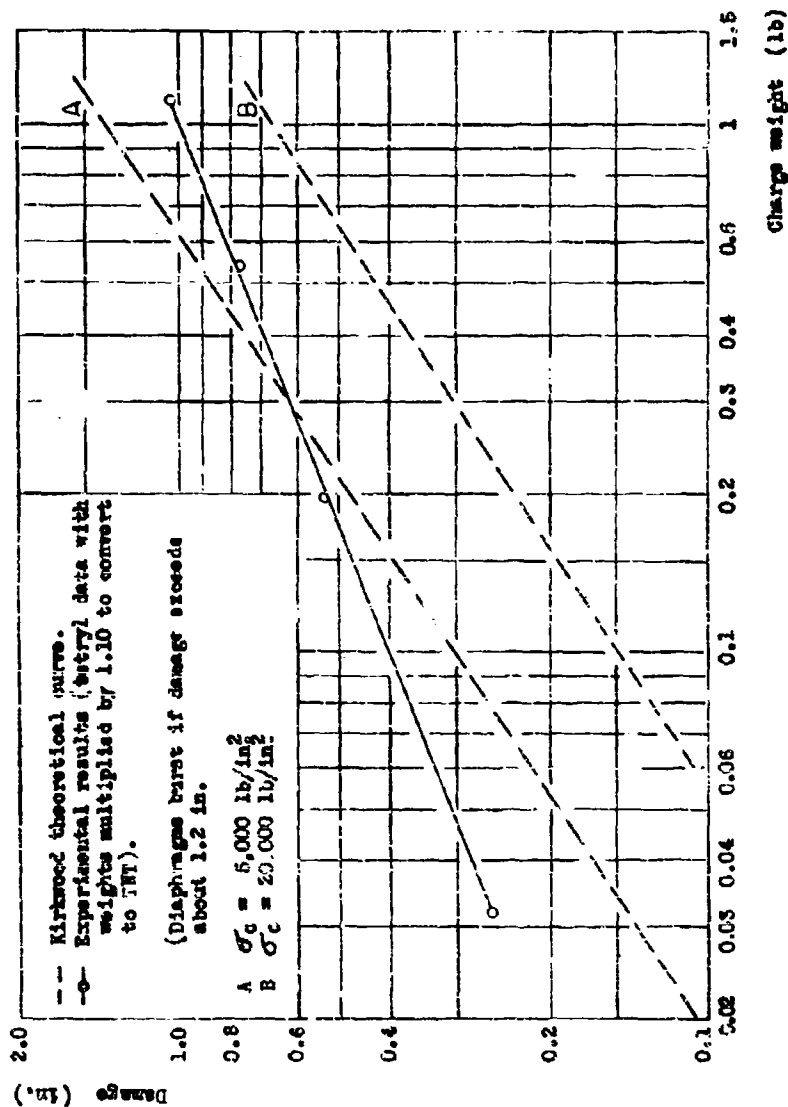
Fig. 9. Damage vs. charge weight for TNT. Copper
diaphragms annealed (semi soft, gauges mounted on steel
ring. Diaphragm thickness: 0.0652 in. Charge-to-gauge
distance: 4 ft.

<u>d</u> is the charge-to-gauge distance, and

<u>m</u> and n are constants determined by the properties of the diaphragm

The constants m and n were found not to be mutually independent, but were in the ratio of about 1:2 for both the copper and steel diaphragms. For the copper diaphragms, m and n were about 0.4 and 0.8 respectively; for the steel diaphragms, m and n were about 0.6 and 1.2 respectively. These values for the constant m were determined over a limited range of charge weights, in most cases from 1 to 10 lbs. Weight and distance exponents determined from 300 and 600 pound charges and steel diaphragms were approximately 0.49 and 1.13[13].

To illustrate some of the uses of the damage Equation (7) let us suppose that two explosives, A and B, are being compared by means of gauges and using two different diaphragm materials, 1 and 2. If we fire one shot with each explosive for each diaphragm material, we may express the results by the following four equations

$$D_{A1} = k_{A1} \frac{\left(W_{A1}\right)^{m_1}}{\left(d_{A1}\right)^{n_1}} \qquad (8)$$

$$D_{B1} = k_{B1} \frac{\left(W_{B1}\right)^{m_1}}{\left(d_{B1}\right)^{n_1}} \qquad (9)$$

$$D_{A2} = k_{A2} \frac{\left(W_{A2}\right)^{m_2}}{\left(d_{A2}\right)^{n_2}} \qquad (10)$$

$$D_{B2} = k_{B2} \frac{\left(W_{B2}\right)^{m_2}}{\left(d_{B2}\right)^{n_2}} \qquad (11)$$

If the experiment has been performed so that the charge weights and distances were held constant for the shots represented by Equations (8) and (9), and constant also for Equations (10) and (11), then damage ratios for the two explosives will be obtained.

13/ J. S. Coles, OSRD Report No. 6240, NDRC Report No. A-362.

$$\frac{D_{A1}}{D_{B1}} = \frac{k_{A1}}{k_{B1}} \tag{12}$$

$$\frac{D_{A2}}{D_{B2}} = \frac{k_{A2}}{k_{B2}} \tag{13}$$

These two damage ratios will generally be unequal, due to the different physical properties of the two diaphragm materials.

However, the two explosives may be compared according to other criteria in which the result will be independent of the diaphragm material if the ratio between m and n is independent of the diaphragm material. For example, different weights of the two explosives may be chosen so that equal damages will be produced at a given charge-to-gauge distance, or the same weight of each explosive may be fired at different distances so chosen that equal damages will be produced. In either case, Equations (8) and (9) combine to give

$$k_{A1} \frac{\left(W_{A1}\right)^{m_1}}{\left(d_{A1}\right)^{n_1}} = k_{B1} \frac{\left(W_{B1}\right)^{m_1}}{\left(d_{B1}\right)^{n_1}} \tag{14}$$

and Equations (10) and (11) result in

$$k_{A2} \frac{\left(W_{A2}\right)^{m_2}}{\left(d_{A2}\right)^{n_2}} = k_{B2} \frac{\left(W_{B2}\right)^{m_2}}{\left(d_{B2}\right)^{n_2}} \tag{15}$$

If the experiment has been conducted with d_{A1} and d_{B1} the same, and with d_{A2} and d_{B2} the same, then equivalent weight ratios for the two explosives are determined:

$$\frac{W_{A1}}{W_{B1}} = \left(\frac{k_{B1}}{k_{A1}}\right)^{1/m_1} \tag{16}$$

$$\frac{W_{A2}}{W_{B2}} = \left(\frac{k_{B2}}{k_{A2}}\right)^{1/m_2} \tag{17}$$

If the experiment has been performed with W_{A1} and W_{B1} the same, and with W_{A2} and W_{B2} the same, then the following equivalent distance ratios are obtained:

$$\frac{d_{B1}}{d_{A1}} = \left(\frac{k_{B1}}{k_{A1}}\right)^{1/n_1} \tag{18}$$

$$\frac{d_{B2}}{d_{A2}} = \left(\frac{k_{B2}}{k_{A2}}\right)^{1/n_2} \tag{19}$$

If, now, the equivalent weight ratios and equivalent distance ratios are independent of the diaphragm material,

$$\left(\frac{k_{B1}}{k_{A1}}\right)^{1/m_1} = \left(\frac{k_{B2}}{k_{A2}}\right)^{1/m_2} \tag{20}$$

and

$$\left(\frac{k_{B1}}{k_{A1}}\right)^{1/n_1} = \left(\frac{k_{B2}}{k_{A2}}\right)^{1/n_2} \tag{21}$$

Equations (20) and (21) can be written

$$\frac{k_{B1}}{k_{A1}} = \left(\frac{k_{B2}}{k_{A2}}\right)^{m_1/m_2} = \left(\frac{k_{B2}}{k_{A2}}\right)^{n_1/n_2} \tag{22}$$

Equation (22) will be true if $\frac{m_1}{m_2} = \frac{n_1}{n_2}$; or $\frac{m_1}{n_1} = \frac{m_2}{n_2}$,

which was one of the premises.

It is, therefore, evident that results of somewhat more general significance will be obtained if explosives are compared on the basis of equivalent weights, equivalent volumes, or equivalent distances (all independent of diaphragm material), rather than on the basis of relative damage produced. In practice, it was found more convenient

536

to compare explosives at constant charge-to-gauge distances rather than
at constant weights or volumes, so the equivalent weights of explosives
were the quantities determined directly. The other ratios can easily
be calculated if one ratio, the exponents a and n, and the explosive
densities are known.

For example, if the equivalent weight ratio W_A/W_B (D and d held
constant) is designated as W_{Dd}; the equivalent volume ratio V_A/V_B
(D and d held constant) as V_{Dd}; the equivalent distance ratios
d_B/d_A (D and W held constant) and d_B/d_A (D and V held constant) as
d_{DW} and d_{DV}, respectively; and the density ratio W_A/W_B (V held constant)
as W_V, then

$$V_{Dd} = \left(W_V\right)^{-1}\left(W_{Dd}\right) , \tag{23}$$

$$d_{DV} = \left(W_V\right)^{-m/n}\left(W_{Dd}\right)^{m/n} , \tag{24}$$

and

$$d_{DW} = \left(W_{Dd}\right)^{m/n} \tag{25}$$

2. The Effect of Wooden Frames

In tests with damage gauges, some sort of framework for fixing the
orientation of gauges and charge-to-gauge distances is essential. The
first type of frame used at UERL consisted of a wooden cross at the center
of which the charge was fastened. One gauge was mounted on the end of
each of the four arms of the cross so that it faced the charge. The
whole rig was lowered by a rope or wire cable into the water with safety
lines connected to the gauges. A top view sketch of this type of frame
is shown in Figure 10.
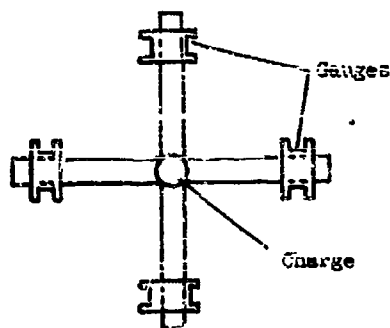
Figure 10. First frame type

A frame of this construction was, of course, good for only one shot.

Partly in an effort to avoid constant replacement of frames, and partly due to a presentiment that a foreign object so close to the charge might be affecting the results, a second type of wooden frame, shown in Figure 11 was soon put into use. The charge in this case was positioned by twine tied between it and the sides of the frames.

Position of gauge
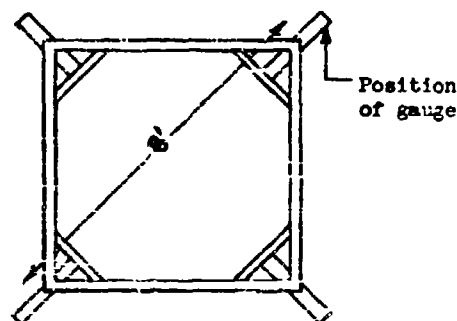
Figure 11. Second Frame Type.

By an unfortunate coincidence, the damage recorded by the gauges when mounted on this frame was the same, within experimental error, as that obtained with the cross frame, and it was concluded that the frame in neither case had any significant effect on the damage gauge results, particularly since the primary interest was in comparing other explosives relative to a standard explosive (TNT). However, because the second type frame seemed to be an improvement in technique, it was retained in use although frames of this type also were almost invariably destroyed by a single shot.

Another experiment which led to the belief that the method of mounting the gauges had little effect on damage was the following. In order to determine whether an increase of inertia of the damage gauges would increase the damage, several charges varying in weight from 0.8 to 4.2 lbs. were fired at steel diaphragms at distances of 36 and 48 in. The weight of each gauge, weighing 30 lbs. normally, was successively increased by 15, 30, and 50 lbs. In no instance was there an increase in damage to the diaphragm until the charge and distances were such that the diaphragm was damaged more than 80% of the maximum damage possible without rupture. Beyond 80% of maximum depression, doubling the weight of the gauge (total weight 60 lbs.) increased the damage by 5%.

Increasing the weight of the gauge by 50 lbs. (total weight 80 lbs.) did not further increase the damage. It was concluded, therefore, that increasing the inertia of the gauges considerably did not materially change the damage results.

Early in the summer of 1943, however, a new shipment of lumber used for constructing the frames was received which produced markedly different damage results. This led to the investigation of several types of supporting frames.

The usual type of frame, Figure 11, made of 3 x 3/4 in. furring, was varied by "quartering" each member to decrease the strength of the frame, and by "doubling" to increase the strength. The doubled frame was constructed simply by nailing together two members for the side pieces of the frame shown in Figure 11 so that the dimensions of these sections were 3 x 1-1/2 in. It should be noted that for this type frame the closest edge of the wooden frame was closer to the charge than the gauge diaphragms. Figure 12 shows a partially doubled frame in which the sections between C and D, and B and D have been doubled in the same fashion. Figure 13 shows a frame constructed so that all parts of the wooden frame were farther from the charge than the diaphragms in the gauges. Weakened and doubled frames were investigated for this style frame as well. Finally, tests were made with the gauges mounted rigidly on a steel ring (Figure 14). The ring was made of 1-1/2 in. solid round stock and the gauges were mounted (1) on spruce blocks, (2) on oak blocks, and (3) on mounts made of 1-1/2 in. angle iron. The results varied with each type of mounting. The ring was not significantly affected by the shots.

Our conclusions from these experiments were as follows. The data are listed in Tables IV to VII.

(a) The regular frames (Figure 11) produced a definite decrease in damage when strengthened by means of the doubled sides, and an increase in damage when weakened by use of the quartered sides. An increase in damage was also shown when the frame members were decreased from 3 x 3/4 in. to 2 x 3/4 in. The data for these shots are shown in Table IV. Here it may be seen that strengthening the frame by doubling may decrease the damage as much as 17% and weakening the frame by quartering the frame increase it as much as 49%. This was also shown in shots in which frames were unsymmetrically strengthened as shown in Figure 12. The data in Table V indicate that less damage occurred for those gauges mounted on the doubled sections of the frame.

(b) The use of the "outside" frames (Figure 13) for which all charge-to-frame distances were greater than the charge-to-gauge distance resulted in a damage greater than with the frames of Figure 11. The increases in damage were as much as 78%, as indicated in Table VI. The weakening of this type of frame by changing from 3 x 3/4 in. members to the 2 x 3/4 size and the doubling of the frame had comparatively little effect. Increasing the distance d of the gauge from the frame tended to increase the damage.
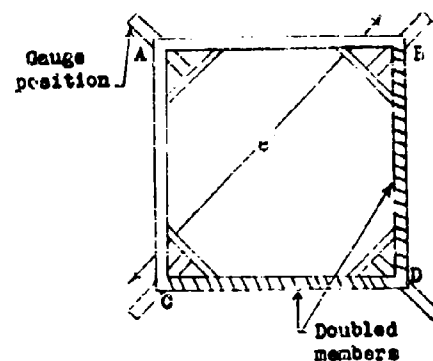
Fig.12. Partially doubled frame.
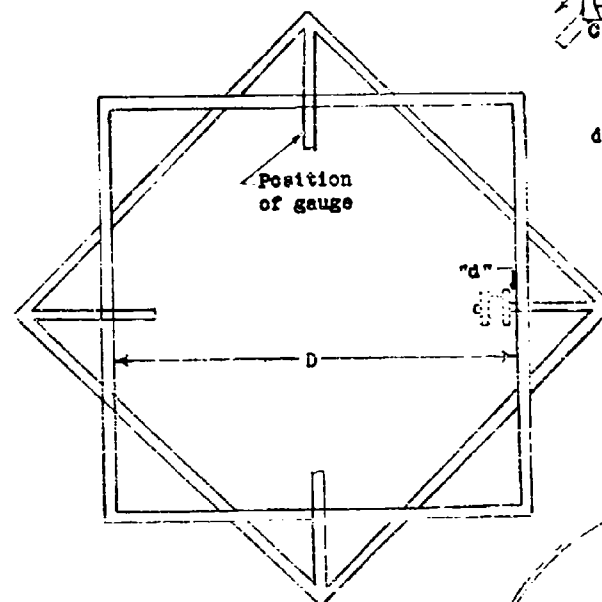
Fig.13. "Outside" frame.
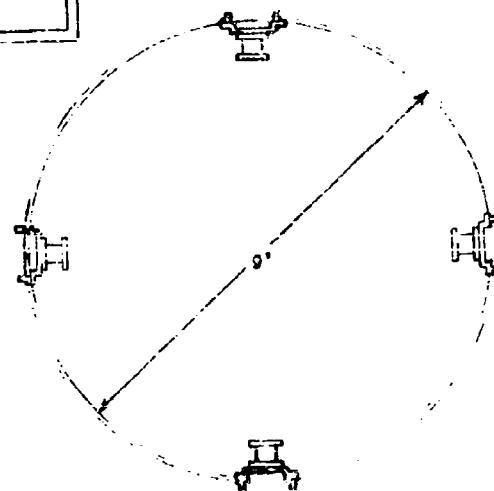
Fig.14. Steel ring frame.

Table IV. Results with frame style shown in Figure 11.

Charge-to-gauge distance 48 in.

Size of stock	Charge (gm)		Average Damage (10^{-2}in.)a/	Percentage Variation
	TNT	Tetryl		
Regular, 3 x 3/4 in.	1300	100	32.2 ± 0.6	0
			32.3 ± 0.5	0
	975	100	25.3 ± 1.2	0
	--	980	25.8 ± 0.6	0
"Doubled" 3 x 1-1/2 in.	1300	100	27.9 ± 0.4	-13
			27.2 ± 0.4	-16
	975	100	22.1 ± 0.6	-13
	--	980	22.6 ± 0.4	-12
"Quartered" 1-1/2 x 3/8 in.	1300	100	47.8 ± 0.6	+49
2 x 3/4 in.	1300	100	41.7 ± 0.8	+30
			41.6 ± 2.2	+27
	1300	100	43.4 ± 0.8b/	+35
			43.8 ± 0.8b/	+36
	975	100	36.3 ± 1.6b/	+43
2 x 1-1/2 in.	1300	100	34.3 ± 0.8	-17 c/
			40.7 ± 1.6d/	- 2

a/ Corrected to 0.085-in. thickness. The correction of damage results to compensate for variations in diaphragm thickness is discussed in Part V, Sec. 5(a)
b/ Wood used was hemlock, all others were pine.
c/ Compared with 2 x 3/4-in. stock.
d/ Braced with broken members.

Table V. Results with partially doubled frame (Figure 12)

Charge (gm)		Damage Gauge A $(10^{-2}$in.$)$	Damage Gauge B $(10^{-2}$in.$)$	Percentage Variation of B from A	Damage Gauge D $(10^{-2}$in.$)$	Percentage Variation of D from A
TNT	Tetryl					
1300	100	33.4	31.3	-6.3	28.3	-15.4
		31.8	29.8	-6.3	28.0	-12

Table VI. Results with "outside" frames (Figure 13)

Frame Type	Charge (gm)		d (in.)	Damage $(10^{-2}$in.$)$a/	Percentage Variation Compared with Regular Frames of Table IV	
	TNT	Tetryl			2 x 3/4 in.	3 x 3/4 in.
Fig.13 style, 3 x 3/4-in. stock	1300	100	0	49.6 ± 1.1	+18	+54
	1300	100	0	53.8 ± 1.2	+33	+67
	1300	100	1-1/2	52.3 ± 0.6	+26	+62
	975	100	2-1/2	45.1 ± 0.6		+78
	1300	100	3	55.1 ± 1.3	+33	+71
Fig.13 style, 2 x 3/4-in. stock	1300	100	2-1/2	55.0 ± 0.2	+33	+71
		930	3	44.3 ± 0.1		+72
Fig.13 style, "Doubled" 3 x 1-1/2-in. Stock	1300	100	1/2	48.3 ± 0.9	+17	+50

a/Corrected to 0.065-in. thickness.

542

Table VII. Results with steel-ring frame (Figure 14)

Charge (gm)		Gauge Backing	Average Damage (10⁻²in.)	No. of Shots	Percentage Variation Compared with Regular Frames of Table IV	
TNT	Tetryl				2 x 3/4 in.	3 x 3/4 in
1300	100	Spruce	57.2 ± 0.9	2	+30	+77
975	100		50.6 ± 1.1	1	+40	+100
--	980		50.7 ± 0.4	1	+40	+98
1300	100	Oak	59.8 ± 0.6	4	+37	+86
975	100		51.3 ± 0.9	3	+41	+99
--	980		52.5 ± 0.7	4	+45	+106
1300	100	Steel	61.4 ± 0.8	4	+41	+91
975	100		53.5 ± 0.6	3	+47	+110
--	980		54.5 ± 0.3	4	+51	+110

(c) The mounting of gauges on a steel ring (Figure 14) resulted in greater damage than any type of wooden frame mounting. This increase varied from 6 to 10% over the type shown in Figure 13 to 30 to 100% over the regular type of Figure 11. The change in type of gauge backing from spruce to oak increased damage 2 to 4%. Typical results with the steel ring are shown in Table VII.

An additional experiment in which a chain was stretched between gauges mounted on a regular wooden frame (Figure 11) to prevent their swinging away from the explosion more than about 1 in. resulted in no increase in damage over that usually produced.

It was concluded that, in general, the lighter the wooden frame the more the damage, and the greater the charge-to-frame distance, the more the damage.

A suggested explanation for the remarkable increase in damage (25 to 100%) when gauges were mounted on a steel ring rather than at the corners of a square wooden frame was that the wood, being a medium less dense than water, reflected a rarefaction wave which partially destroyed the shock-wave. Another proposed explanation was that the damage was increased by the more rigid backing of the steel ring. To test the reflection theory independently of the rigidity with which the gauges were mounted, shots under three sets of frame conditions were fired. One was a frame consisting only of the ring; another consisted of the ring and an "outside" wooden frame (Figure 13); and the last consisted of the ring and an "inside" wooden frame (Figure 11). For this and the following frame experiments, except where otherwise noted, Lot 4 steel diaphragms were used, the charge-to-gauge distance was 48 in., the charge employed for each shot was 2.31 lbs. TNT, and two shots were fired for each arrangement.

It was found that the average ratio of the damage obtained with the outside frame and ring, to the damage obtained with the ring alone was 0.90; the average ratio of the damage obtained with the ring and inside frame to the damage obtained with the ring alone was 0.59.

To make sure that the decreased damage found in these cases was caused by reflection of the shock-wave from the wood and not by some phenomenon involving actual contact of the wood and the gauges, the following experiment was next performed. Shots were fired in which (1) boards were lashed to the ring outside the circle of the gauges; (2) boards were lashed to the ring within the circle of the gauges but below the plane of the gauges so as not to be directly between the charge and the gauges; (3) boards half as wide as in (2) were lashed to the ring as in (2). The average ratios of the damages obtained compared with the damage obtained with the ring alone were found to be 1.00, 0.82, and 0.90, respectively.

To investigate the possible effect of movement of the gauge as a whole on the damage of the diaphragm, shots were fired using the ring alone in which one, two, and three gauges were used. In the

cases in which two and three gauges were used, the gauges were spaced at 90° intervals. In all of these cases, then, the shock-wave would tend to move the whole ring, and the damage could be compared to damages obtained in the usual case in which four gauges were mounted at 90° intervals about the ring so that the latter had no tendency to move. No important differences were found.

In order to obtain evidence as to the effect of the ring itself on damage, two types of shots were fired and compared with the usual shots. In the first type, sheet iron was wired to the ring. The sheet iron was 6-1/2 in. high and extended all around the outside of the ring. In the second type, the gauges were mounted on rubber shock mounts about 3/8 in. thick between the gauges and the ring. This experiment was to test the effect of the rigidity of the mounting on damage. Neither the sheet iron nor the shock mounts were found to have any significant effect on damage, so it would appear that the reflections from the ring and the rigidity of the ring make no appreciable contributions to damage.

Two shots were also fired using Lot 3 steel diaphragms, 3.78 lb. TNT charges, and an inside wooden frame (Figure 11) in addition to the ring. These shots were compared with two previous shots in which the ring was not used. The average ratio of the damage obtained with the wooden frame and ring to the damage obtained with the wooden frame alone was found to be 1.07. Of eight such ratios, however, the spread was considerable (0.95 to 1.24), due perhaps to the variability in the wood. This indicates that the major portion of the "frame effect" is due to the presence of the wood and not the break-up of the frame or the movement of the gauges.

3. Results Using Wooden Frames

A considerable number of tests were conducted with damage gauges before the importance of the effect of wooden frames on damage was discovered. These experiments are described in the following subdivisions. It should be kept in mind that, in general, a new frame was used for every shot and that, therefore, an important variable was not controlled except insofar as the same kind of lumber was used until it was used up. It is probably unsafe to compare results of shots which were separated by a considerable time interval. Shot numbers indicate the order in which the tests were conducted.

(a) Determination of time of damage. A simple method was devised for determining the approximate time during which deformation of the diaphragms in URRL damage gauges occurred. The method consisted of firing shots in which the gauges and charge were suspended in a plane parallel to the water surface and successively decreasing the depth of the rig until the gauges began to record markedly less damage. The decrease in damage was caused by the reflection of a rarefaction (tension) wave from the water-air interface which cut off the latter part of the pressure wave. At the critical depth where the deformation first

appears to be affected, the path difference between direct and reflected waves, divided by the velocity of the shock-wave (ca. the velocity of sound in water), gives the time delay in the arrival of the reflected wave, and thus (if we disregard deformation of the diaphragm caused by its own inertia) the time required for normal deformation. Comparison of the deformation time with the pressure time curve of the shock-wave will show what part of the shock-wave caused the damage. It will be noted that no account has been taken of the contribution of bubble pulse waves to the deformation, but other experiments (Section V, 4,c) have shown that in normal use of the gauge the contributions of bubble pulses were negligible.

The results of these tests are listed in Table VIII, and some of the results are shown graphically in Figures 15 and 16. The deformation times range from 240 to 360 microseconds.

(b) Double shots. According to Kirkwood, curved diaphragms with the convex side toward the charge should be deformed more than those exposed with the concave side toward the charge. To determine the relative capacities of convex and concave diaphragms to withstand deformation, the following experiments were carried out. The first experiment consisted of reversing a damaged diaphragm in the gauge and firing a second charge identical with the first. That is, for the second shot the dent of the damaged diaphragm was bulged out toward the charge. The result of the second shot was a deformation in the opposite direction in which the maximum depression (measured from the original undeformed plane surface as reference point) was greater by 25 to 40%. The dent from the second shot had an asymmetrical contour, having the greatest depression two-thirds of the way toward the side of the bulge near the bottom of the gauge.

In the second experiment, diaphragms were exposed to the explosions of two similar charges in succession without removing the diaphragms from the gauges. It was found that the damage was increased by the second shot but not to the same extent as on the reversed diaphragms discussed above. Table IX lists the data.

(c) Study of errors. A series of experiments were conducted in which we investigated the various sources of errors in our use of the UERL damage gauges. This was done by making various deliberate changes of the sort that might occur accidentally in the experimental set-up and then determining the extent that the damage was affected by this change. Charges of approximately 4 lbs. loose tetryl (density about 1 gm/cm^3) were used so that no initiator other than a No. 8 DuPont cap would be necessary. Charge-to-gauge distance was 48 in. for these tests, unless otherwise specified.

(i) Due to variation of charge-to-gauge distance. When the gauges were displaced with respect to the charge, the change in damage was about 3% per inch of displacement. Hence, if the charge should shift 1 in. toward one gauge, that gauge would have 6% more damage than the one opposite it. The damage averaged over the two opposite gauges should
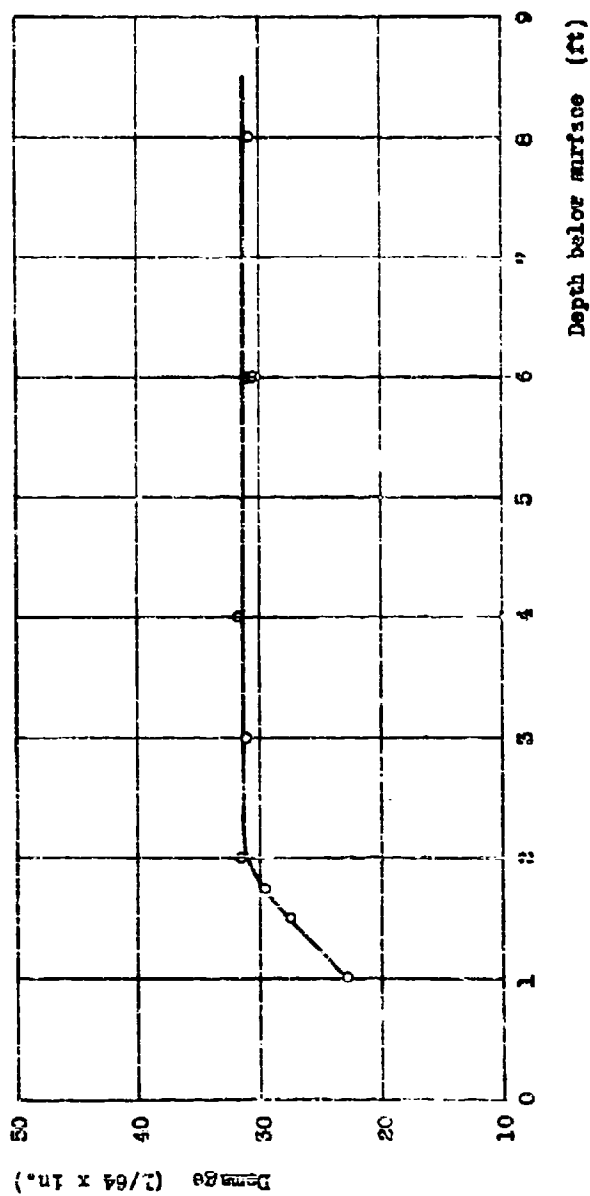
Fig. 15. Effect of depth on damage; 100 gm loose tetryl; copper diaphragms at 48 in.
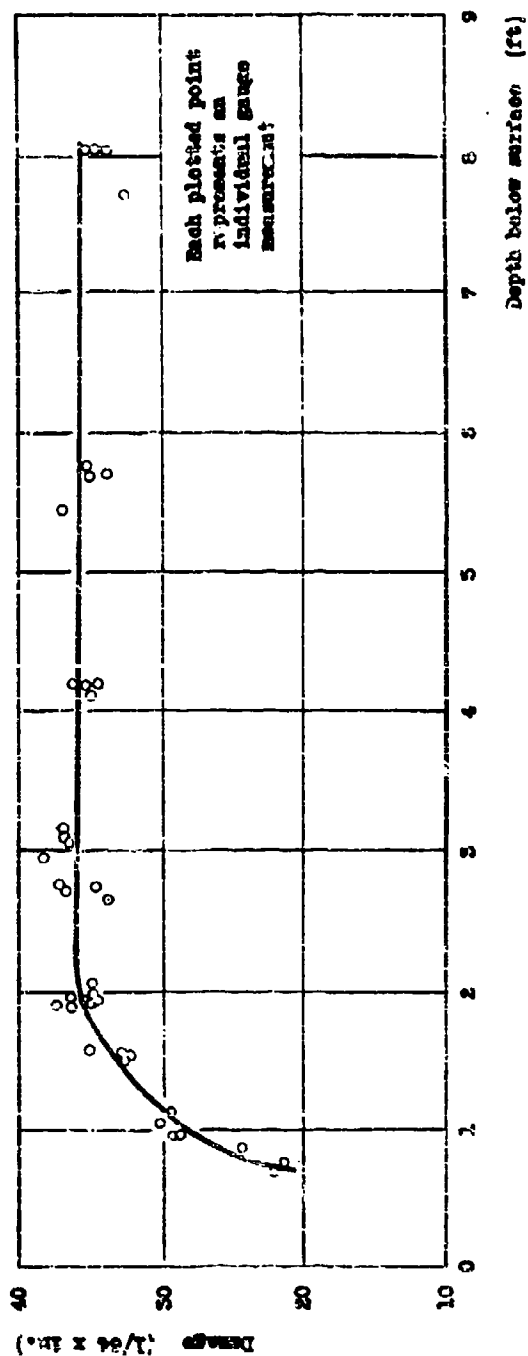
Fig. 16. Effect of depth on damage: 4 lb cast TNT; steel diaphragms at 48 in.

548

Table VIII. Results obtained by varying depth of immersion.[a/]

Copper diaphragms used except as noted.

Charge (gm)		Charge-to-Gauge Distance (in.)	Critical Depth Below Surface (in.)	Damage (1/64 in.)	Cutoff Time (msec)	Peak Pressure (lb/in²)	Pressure at Cutoff Time
TNT	Tetryl						
50	15	15	15	60.0	0.31	7550	<1% peak
100	15	24	15	52.8	.24	5500	<2% peak
--	100 loose	24	24	--	.33	5220	<1% peak
--	15 loose	30	21	36.3	.36	1960	<1% peak
--	15	48	24	32.3	.33	1140	<1% peak
--	100 loose	48	24	31	.33	2370	<1% peak
--	300 loose	48	24	41	.33	3590	<2% peak
4 lb[b/]	--	48	22	37	.29	7100	790 lb/in²

a/Peak pressures and pressures at the cutoff time calculated assuming
$p(t) = p_m e^{-t/\theta}$ and using Equations (3) and (5) for p_m and θ.
b/Steel diaphragm used.

Table IX. Results of double shots with steel diaphragms.

Experiment	Number of Diaphragms	Loose Tetryl Charge (gm)	Average Damage (1/64 in.)		Percentage Increase
			1st shot	2nd shot (total)	
Diaphragm reversed in gauge for second shot	4	975	28.1 ± 1.4	39.8 ± 0.8	41.7
	8	1280	36.0 ± 0.4	48.0 ± 1.4	33.3
Diaphragm left in gauge for second shot	12	975	28.8 ± 0.7	36.8 ± 0.6	27.8
	12	1280	35.8 ± 0.8	43.9 ± 0.6	22.6

be constant to within 1% for such a displacement of the charge from
position. Thus for our set-up of 4 gauges at 90° intervals around the
charge, a gauge displacement would have a more serious effect on the
average result than a charge displacement, but was much less likely to
occur. Table X gives the data.

Table X. Variation of damage with distance

(Charge 2000 gm loose tetryl)

Number of Diaphragms	Distance (in.)	Damage (in. x 100)
4	54	44.6 ± 0.2
4	51	48.6 ± 0.3
4	48	50.0 ± 0.3
4	45	59.2 ± 2.0
4	42	62.0 ± 0.1

(ii) Due to variation of charge level and tilt. Since in normal
practice the charge was tied into the center of a square frame by four
tie-lines of marlin (twine), it was of interest to know how much error
might be introduced by a change in level, or tilt of the charge. By
placing the charge above and below the level of the gauges it was shown
that a displacement of 1 ft. in a line perpendicular to the plane of the
gauges changed the damage about 4%.

Results on tilt of the charge varied widely but indicated that an
inclination of 30° of the charge axis did not result in more than a 5%
variation in damage.

(iii) Due to variation in gauge orientation. Gauges were twisted
so that the angle between the diaphragms and the charge-to-gauge axis
was 120°, 135°, and 180°. In the customary set-up the diaphragm is
perpendicular to this axis. When the diaphragm was parallel to the
charge-to-gauge axis (180° angle), the damage was decreased 5%, in the
other cases, about 3%.

(iv) Due to miscellaneous variations. Some of the steel diaphragms
were slightly warped by the shearing process. These could be straightened
by a pressure of a few pounds and the amount of warping was never greater
than about 1/64 in. (measured perpendicular to the diaphragm). Warping
to this extent introduced no measurable error.

Variation in cap screw tightness (see Section II) was found to
introduce errors as large as 10% with copper diaphragms and somewhat
smaller errors with steel diaphragms. Having one man tighten all cap
screws with a 10 in. wrench an equal amount seemed to be satisfactory.

In test with service weapons, the best results were obtained using a torque wrench which slipped after a predetermined torque was reached.

In usual practice the damaged diaphragms were measured after removal from the gauges. A series of diaphragms were measured in the gauges before and after the shot and the difference compared with the usual measurements. The measurements in the gauges averaged .003 in. greater than out of the gauges. This was less than 1% of the ordinary damage and either method was considered adequate as long as it was used consistently.

The thickness of the diaphragm in the region which remained undamaged, that is, protected by the clamping plate of the gauge, was measured before and after the shot and found to remain the same within .001 in. However, by marking diaphragms with parallel lines about 1/2 and 1-1/2 in. from the edge, it was shown that there is movement toward the central or damaged portion of the diaphragm. The amount of slippage was roughly proportional to the damage and varied from 0.20 mm to 0.60 mm for a damage change of 0.32 to 0.46 in.

(v) Summary. If then, for a typical experiment, we assume the following errors, we can calculate deviations for a single shot using 4 gauges.

Assumed Errors	% Deviation in Damage
±2 in. Gauge-to-charge distance (variation due to charge displacement only)	±3.5%
±6 in. Charge displacement (vertical)	± 2%
±15° Charge tilt	± 1%
± 5° Gauge orientation	± 1%

Then if there were no other variables we should have the following precision:

Standard deviation of a single observation   ± 4.3%

Probable error of a single observation   ± 3.2%

These results are to be compared to the standard deviation and probable error as determined from the distribution curves plotted in Figures 17 and 18. To obtain these curves we have used 212 damaged diaphragms. These were damaged by 2 to 4 lb. charges all at 48 in.

In Figure 17 the actual deviations in hundredths of an inch from the mean for each series is plotted against frequency of occurrence. Figure 18 shows the percentage deviation from the mean for each series. The absolute deviation is nearly constant independent of amount of damage, so Figure 17 is considered more useful than Figure 18.
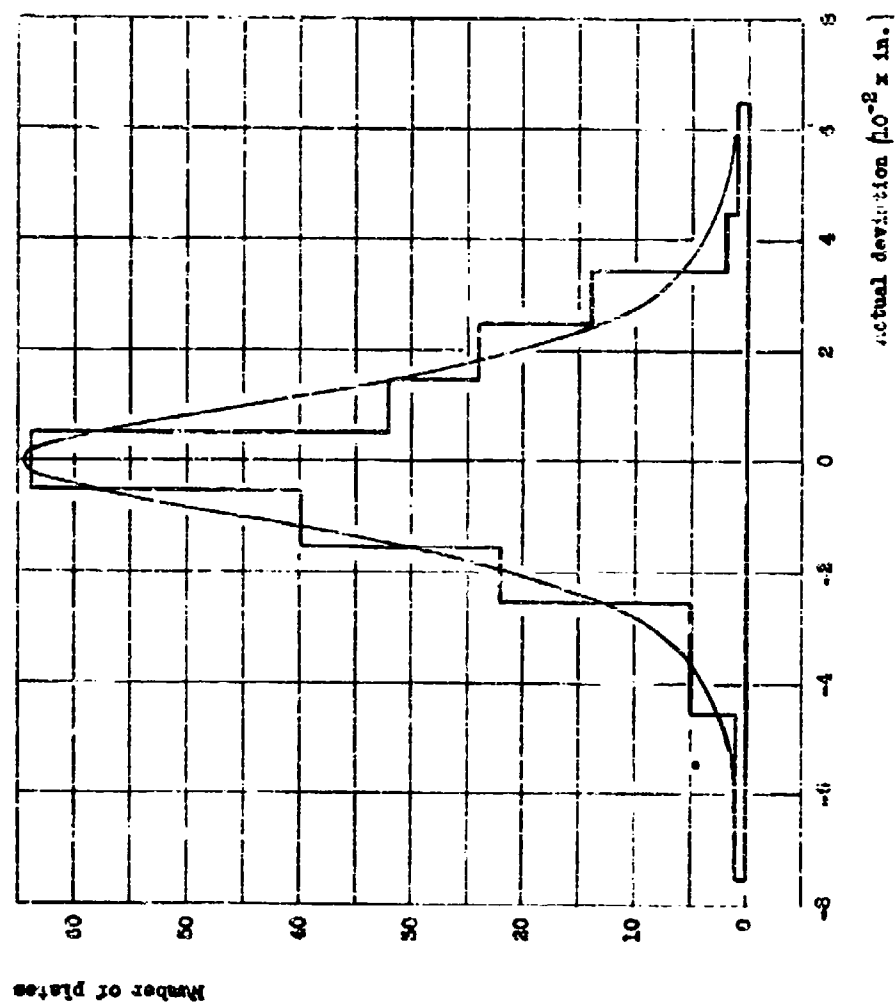
Fig. 19. Distribution of actual deviation in damage for 212 plates.

Fig. 1". Distribution of actual deviation in damage for 212 plates.
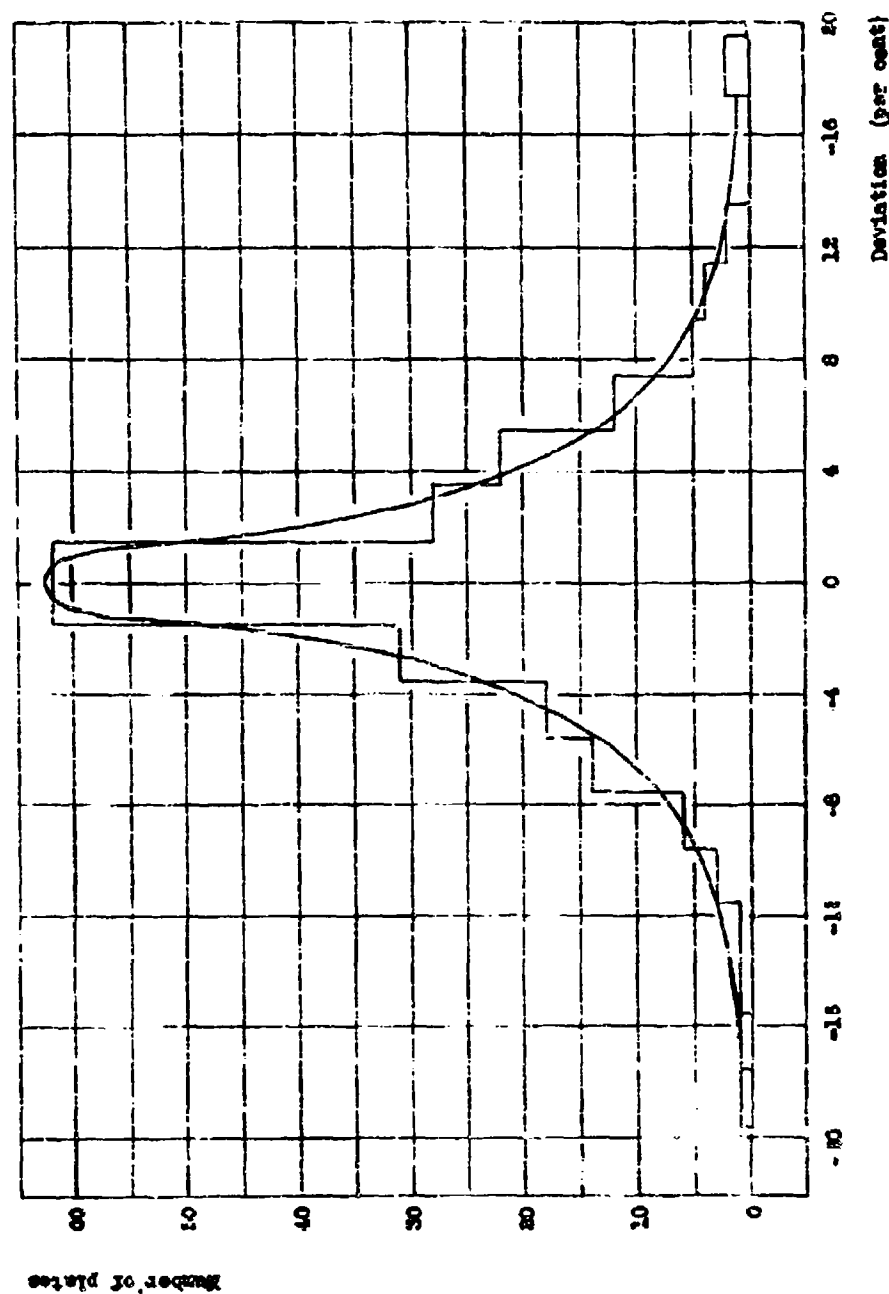
Fig. 1f. Distribution of percentage deviation in damage for 212 plates.

From these distribution curves the standard deviation and probable error of a single observation may be calculated. These are given in Table XI.

Table XI. Deviation measures for 212 damaged diaphragms

Deviation Measure	Absolute Deviation	Percentage Deviation
Standard deviation of a single observation	± 0.018	± 5.1%
Probable error of a single observation	± 0.012	± 3.4%

(d) Test of Hopkinson's scaling rule. In order to test the well known Hopkinson scaling rule[14], half-scale models of the regular UERL diaphragm gauge were constructed. Each linear dimension of the regular gauge was carefully reduced by one-half. To insure that the properties of the half-scale diaphragms would be the same as those of the full size diaphragms, we used copper diaphragms annealed under the same conditions and at the same time. 20 BS gauge (thickness .032 in.) was used in the small gauges and 14 BS gauge (thickness .065 in.) was used in the regular gauges. To eliminate the necessity of scaling boosters and subsequent difficulties of detonating cast charges, loose tetryl charges were used throughout. In each case the container used for the charge with the small gauges was scaled from the larger container (except for wall thickness) and the weight of explosive was 1/8 that of the larger charge.

The results listed in Table XII indicated that the damages scaled on the average to within 2%, the largest deviation being 5%. The shapes of the pairs of diaphragms had the same appearance. If there was any change in the strength of the copper diaphragm with rate of strain in the range of rates encountered here, it must have been masked by compensating errors. Any such "speed effect" should cause a deviation from Hopkinson's rule. It should be noted that part of the shots were with wooden frames and the others with steel rings. When the steel ring support was used, copper diaphragms showed the same weight and distance exponents as previously obtained for copper diaphragms using wooden frames (0.4 and 0.8 respectively).

14/ "the damage inflicted on a given structure by a given charge at a given distance will be reproduced to scale if the linear dimensions of the charge and the structure and the distance between them are all increased or decreased in the same ratio"; RC 142/19 Submarine explosions, p. 18, H. W. Hilliar.

Table XII. Scaling experiments

Gauge Scale	Charge Weight[a] (gm)	Charge-to-Gauge Distance (in)	Average Damage[b] (10^{-2} in.)	$\dfrac{D_{\text{Full scale}}[c]}{D_{\text{Half scale}}}$
Shots made with wooden frames				
Half	31.75	18	41.6 ± 0.4	
	31.75	18	41.9 ± .5	
(mean)	31.75	18	41.75 ± .4	
Full	250.5	36	80.5 ± 1.5	
	250.5	36	82.2 ± 1.7	
	250.5	36	83.2 ± 1.1	
(mean)	250.5	36	81.9 ± 1.4	1.98
Shots made with steel ring frames				
Half	30.0	24	39.1 ± 0.2	
	63.0	24	53.7 ± .5	
	95.5	42.2	40.7 ± .3	
	195.5	42.1	51.6 ± 1.4	
Full	250.5	47.7	76.5 ± 0.6	1.95
	516.5	47.7	107.2 ± .7	1.96
	774.5	83.6	83.1 ± 1.0	2.01
	1558.5	83.7	108.7 ± 0.9	2.10

a/ The charge was loose Tetryl but the weight listed here includes 0.5 gm for Du Pont No. 8 detonator.

b/ Average of 4 gauges for each shot with average deviation of a single diaphragm.

c/ Ratio includes a weight or distance correction where necessary.

4. Experiments Designed to Test Predictions of Diaphragm Deformation Theory.

(a) Effect of variation in diaphragm thickness on deformation. When Lot 3 steel diaphragms were first received, it was found that the thickness of these diaphragms varied from .075 to .094 in. In Lot 1 and Lot 2 diaphragms the variance had not been greater than .002 in. If Lot 3 diaphragms were to be used, it was necessary to establish a method of correcting the damage obtained with a diaphragm of a given thickness so that it would be comparable with that of a diaphragm of another thickness.

(1) Derived from theory. Consider Equation (1) and Equation (2) of Section III. Substituting typical values for the constants σ_0 , ρ , ρ_0 , and a_0 in Equation (2), namely 60,000, 7.8, 1.01, and 0.085, respectively, the value 6610 sec^{-1} is obtained for ω . If a_0 is not 0.085 but 0.075, ω becomes 6340 sec^{-1}, a change of 4.1%. For none of the small scale work discussed in this report was the time-constant (θ) of the shock wave at the gauge positions greater than 0.25×10^{-3} sec (the time-constant of a shock wave 3 ft. from a 25 lb. TNT charge[15]) so an upper limit for the value of $\omega\theta$ would be about 1.65. Then a diaphragm thickness variation from .085 in. to .075 in. or to .095 in. would change the corresponding value of g by 2% at the most (much less for a single shot), see Table II.

Let us now assume that g is independent of a_0 over the range of variation of a_0 encountered, and consider the ratio of damages predicted by Equation (1) for two diaphragms of different thicknesses, other conditions being held constant. It is easily deduced that the ratio of damage (Z_m') of a diaphragm of a given thickness (a_0') to the damage (Z_m) of a diaphragm of standard thickness (a_0) is

$$\frac{Z_m'}{Z_m} = \left[\frac{c_0}{a_0'} \left(\frac{a_0 + .145}{a_0' + .145}\right)\right]^{1/2} = \frac{1}{X} \tag{26}$$

If the diaphragm thickness is varied from a standard value of .085 in. to .075 in., the damage is increased 9%.

It appears, then, that the contribution of the g term variation to the variation in Z_m caused by different diaphragm thicknesses is of second order, in no case more than about 10% of the total damage variation due to different thicknesses for the experimental conditions employed. This enables the calculation from Equation (26) of a reasonably accurate set of correction factors, independent of the yield stress of the steel and of the peak pressure and time-constant of the particular shock wave

15/ NDRC Division 8 Interim Report Underwater Explosives and Explosions, UE-16, p. 10, December 1943.

ion

.

the
l and
f
ethod
ness

(2)
, ρ ,

ot
: of
: (θ)
iec
?)
a
in.
.ess

of
licted
con-
of
ie (z_m)

(26)

in.

on to
f
ariation
yed.
curate
steel
wave

———

sions,

producing the damage, by means of which the damage for a diaphragm of a
given thickness can be reduced to that for a diaphragm of standard
thickness. A plot of these cor--- on factors as a function of diaphragm
thickness is given in Figure 19   e given damage is simply multiplied by
the proper correction factor (X) obtain the damage which would have been
obtained with a diaphragm of standard (.085 in.) thickness. More accurate
correction factors may be computed by including the contribution of the
variation in g, but this is not necessary as long as the total correction
is small.

This treatment can be applied similarly to copper diaphragms.

(ii) Empirical determination. (aa) Lots 3 and 5 steel diaphragms.
By suitably choosing diaphragms of different thicknesses for the four
damage gauges used in single shots, the effect of thickness variations on
damage was determined experimentally. For example, two diaphragms .085
in. thick and two diaphragms .075 in. thick would be damaged under the
same conditions, and the correction factor for .075 in. diaphragms ob-
tained directly. Having obtained such information for diaphragms of all
thicknesses in the Lot 3 range it was then possible to compare the results
for different shots in which diaphragms of different thicknesses were used.

In Figure 19, the empirical correction factor is plotted as a function
of diaphragm thickness and compared with the curve obtained from Kirkwood's
theory (V, 4, a). The data for the empirical curve was all obtained using
the steel ring mounting, although similar results (with respect to thick-
ness correction) were obtained when gauges were mounted on wooden frames.
The deviation from the theoretical curve is greatest for th thickest
diaphragms. Although the majority of the data used in determining the
empirical curve have been for damages of about 0.70 in., there is some
evidence that this correction curve is not a function of the amount of
damage. In a series of shots in which diaphragms of .075 in. thickness
were compared with .093 in. diaphragms, the mean percentage increase of
damage for thin over thick diaphragms was constant at 20 $\pm$ 1% for damages
of 0.23 in., 0.53 in., 0.71 in., and 0.98 in. (Cf results with copper
diaphragms below).

The theoretical thickness correction was partially corroborated also
by results obtained with larger charges. A 50 lb. chemical series of
12 charges of various compositions was shot[16] with two UERL diaphragm
gauges 25 ft. from the charge and two gauges 35 ft. from the charge. A
Lot 5a (ca. 0.038 in. thick) diaphragm was placed in one of the two
gauges at each of these distances, while a Lot 5 (ca. 0.080 in. thick)
diaphragm was placed in the second gauge at these distances. The actual
diaphragm thicknesses were measured before the shot and the maximum
depressions were corrected to standard thickness (.038 in. for thin
diaphragms and .085 in. for medium diaphragms). The corrected damages
obtained for the thin diaphragms were then compared with the corrected
damages for the medium diaphragms subjected to the same explosive shock
wave; the mean damage ratio was found to be 2.13 ($\sigma_m = 0.018$) for the
25 ft. distance and 2.16 ($\sigma_m = 0.006$) for the 35 ft. distance.

16/ Reported in OSRD No. 6240 and 6241.
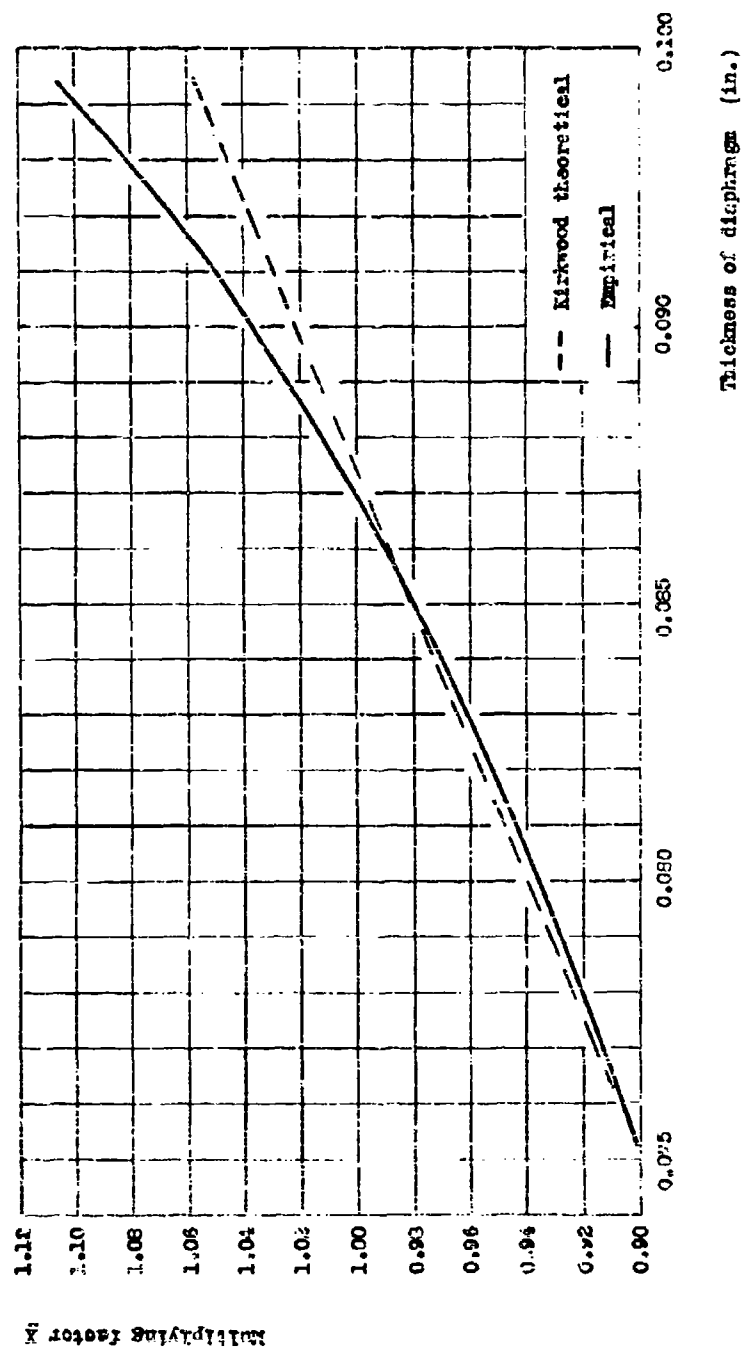
Fig. 19. Thickness correction; multiplying factor for Lot 3 steel diaphragms.

The ratio predicted from Equation (1) and Equation (2) in Section III for these conditions was 2.22. For this calculation the following constants were used:

$$a_0 \text{ (thin)} = 0.035 \text{ in.}$$

$$a_0 \text{ (medium)} = 0.085 \text{ in.}$$

$$\sigma_0 \text{ (thin)} = 42,600 \text{ lbs/in}^2$$

$$\sigma_0 \text{ (medium)} = 50,100 \text{ lbs/in}^2$$

$$\theta = 0.368 \times 10^{-3} \text{ sec}$$

(bb) Copper diaphragms. In studying the effect of thickness of diaphragms on damage for copper diaphragms, two thicknesses, .032 in. and .064 in. were used. All the copper diaphragms were annealed at the same time until dead soft so that the properties other than thickness might be held constant. Eight shots were fired in each of which thin diaphragms were placed in two opposite gauges and thick diaphragms in the other two gauges, all supported by a steel ring. The results are tabulated below:

Table XIII. Damages of thick and thin copper diaphragms

Charge (gm tetryl)	Charge to-gauge distance (in.)	Average Diaphragm Thickness[a]/ (in. x 100) Thick	Thin	Average Damage[a]/ (in. x 100) Thick	Thin	% Increase in Damage:[b]/ $\frac{\text{Thin-thick}}{\text{thick}} \times 100$
19.5	48	65.3	32.1	25.7	40.0	55.3
81.5	48	64.9	32.1	53.0	76.5	44.0
224.5	48	66.1	31.9	76.7	109.7	42.5
461.5	48	64.7	32.0	103.1	Burst	-
38.5	84	66.0	32.5	26.5	40.7	52.9
217.5	84	64.2	32.1	52.8	75.8	43.2
600.5	84	65.5	33.0	75.8	106.3	39.9
1232.5	84	65.1	31.8	100.0	Burst	-

a/ Average of two diaphragms
b/ Based on damages corrected for small variations of distance from 48. in. and 84 in.

It is evident from these data that the ratio of thin to thick damage was not constant. It may be shown that this ratio is a function of damage and that the function is approximately the same for the two distances.

This may be represented by the analytical equation:

$$[\Delta] = K \, (D_{.064 \text{ in.}})^{0.73} \tag{27}$$

$[\Delta]$ represents the difference in damage between thin and thick diaphragms. K is a constant, $D_{.064 \text{ in.}}$ is the damage of the thick diaphragm.

No significant difference was observed in the weight exponents found for the thin and thick diaphragms.

(b) **The baffle effect.** The Kirkwood Damage Theory predicts greater damage for a diaphragm held in a rigid "infinite" plane disc (which will reflect the shock wave and momentarily double the pressure) than for a diaphragm held in the center of a disc of finite radius because of the lower pressure wave moving in from the edge. Actually, the "infinite" disc is one whose radius is larger than a limiting value; this limit is such that for a longer radii damage is complete before the diffracted shock wave can reach the diaphragm. The "infinite" disc must also be thick enough that reflections from the back surface will be so late in occurring that they can have no effect on the deformation of the diaphragm. The limiting radius can be found by multiplying the velocity of sound by damage time[17]/ and is about 1-1/2 ft. for regular UERL small charge work with steel diaphragms in the standard gauge. The effect of size of baffle on damage is predicted by the theory, and comparison of predicted and actual results provides a test of the theory.

(1) **Theoretical predictions.** The following analysis is based on the assumption that the baffle is not fixed but is able to move almost freely during the time interval required for the deflection of the diaphragm. This assumption conforms with the conditions of the experiments discussed below. The assumption is further made that the baffle is of infinite radius.

Consider an initially flat circular diaphragm of thickness a_0, radius R_0, density ρ, and yield stress σ_0 mounted in an infinite baffle of mass m per unit area. Suppose that the baffle is surrounded on both sides by water and that the diaphragm is in contact with water in front but is backed by air. During an interval of time t after the front of an exponential pressure wave of the form

$$p(t) = p_m e^{-t/\theta}. \quad t > 0;$$
$$p(t) = 0, \qquad t \leq 0; \tag{28}$$

has struck the system, the diaphragm undergoes a displacement $z_0(t)$ with reference to the baffle, which in turn undergoes a displacement $z_1(t)$. At low pressures the sound velocity in water is c_0 and the density of water is ρ_0. The differential equations of motion of the center of the

---

17/ Cf J. G. Kirkwood, OSRD 1115, Eq. (3.11) December 1942.

the diaphragm (assuming parabolic profile) and the baffle respectively are[17]

$$\left(1 + \frac{2}{3}\lambda\right)\left[\frac{d^2 Z_0(t)}{dt^2} + \bar{\omega}_0^2\, Z_0(t)\right] + \frac{d^2 Z_1(t)}{dt^2} + \frac{1}{\Theta_1}\frac{dZ_1(t)}{dt} = \frac{2p_m e^{-t/\Theta}}{\rho_0 s_0},\quad (29)$$

$$\frac{d^2 Z_1(t)}{dt^2} + \frac{1}{\Theta^*}\frac{dZ_1(t)}{dt} = \frac{2p_m e^{-t/\Theta}}{m},\qquad (30)$$

where

$$\lambda = \frac{\rho_0 R_0}{s_0},\qquad\qquad \Theta_1 = \frac{\rho s_0}{\rho_0 c_0},$$

$$\bar{\omega}_0 = \frac{2}{R_0}\sqrt{\frac{\tau_0}{\rho}}\left(1 + \frac{2}{3}\lambda\right)^{-1/2},\qquad \Theta^* = \frac{m}{2\rho_0 c_0}.$$

Equations (29) and (30) are to be solved for Z_0 subject to the following initial conditions

$$Z_0(0) = Z_0'(0) = 0,\qquad\qquad (31)$$
$$Z_1(0) = Z_1'(0) = 0.$$

One obtains

$$Z_0(t) = \frac{1}{2}\left[(1 - \beta)\, z_0^0\,(\Theta,t) + \frac{\Theta}{\Theta^*}\beta z_0^0(\Theta^*,t)\right],\qquad (32)$$

where

$$\beta = \frac{\Theta^* - \Theta_1}{\Theta - \Theta^*};$$

and

$$z_0^0\,(\Theta,t) = \frac{2p_m \Theta}{\bar{\omega}_0\,\rho s_0}\frac{\left[\sin\bar{\omega}_0 t + \bar{\omega}_0\Theta\left(e^{-t/\Theta} - \cos\bar{\omega}_0 t\right)\right]}{\left(1 + \frac{2}{3}\lambda\right)\left(1 + \bar{\omega}_0^2\Theta^2\right)}.\qquad (33)$$

The quantity $z_0^0\,(\Theta,t)$ may be interpreted as the deflection at time t of a diaphragm mounted in an infinite rigidly supported baffle when struck

by an exponential wave with a peak pressure p_m and time constant θ (Equation 28). The quantity Z_o^0 (θ^*, t) is obtained by replacing θ by θ^* in Equation 33. With an exponential wave, (Equation 28) the deflection at time t of an unbaffled diaphragm mounted in a fixed frame is $1/2$ Z_o^0 (θ, t).

The time of deflection t_m is equal to the lowest positive value of t satisfying

$$\frac{dZ_o\ (t)}{dt} = 0 \tag{34}$$

Correspondingly the maximum deflection Z_m is $Z_o\ (t_m)$.

The standard UERL steel diaphragm has the following specifications:

Radius $\qquad R_o = 1.64$ in.

Thickness $\qquad a_o = 0.078$ in.

Yield stress $\quad \sigma_o = 60,000$ lbs/in^2

Density $\qquad \rho = 7.8$ gm/cm^3

For such a diaphragm we have:

$$\theta_1 = 10.4 \text{ microsec}$$

$$\bar{\omega}_o = 6.44 (\text{millisec})^{-1}$$

$$\lambda = 2.75$$

If this diaphragm is mounted in an infinite free baffle having an average thickness of 1 in. and a density of 7.8 gm/cm^3,

$$\theta^* = 66.7 \text{ microsec}$$

An 840 gm. charge of TNT (density 1.59) placed at a distance of 48 in. produces a shock wave which can be approximated by an exponential wave in which $p_m = 6200$ lbs/in^2 and $\theta = 112$ microsec.

This wave should theoretically produce the following deflections under the conditions indicated:

Description of Baffle	Z_m(in.)	t_m (microsec.)
None	0.56	340
Infinite fixed	1.12	340
Infinite free (1 in. steel plate)	0.64	310

562

(11) Experimental results. For the experimental work baffles of
three different radii were used in conjunction with regular UERL damage
gauges and baffles of four different types were used with half-scale
gauges.

Tests with the regular gauges are summarized in Table XIV. The
baffles were cut out of 1 in. steel armor plate with a square hole at
the center for the gauge; the baffle and gauge were rigidly held to-
gether by inch-thick steel bars bolted on in back so that the front
face of the gauge and the baffle-face were one plane surface without
obstructions except for the heads of the gauge cap screws. Two baffled
gauges were fastened opposite each other at the points spaced 90° from
the unbaffled, control gauges. All gauges were mounted in the usual
fashion on a steel ring.

A 12 in. radius baffle was made and tried first. Since it was
feared that the large area exposed to the shock wave might cause the
ring to be pushed out of shape, small charges were first tried before
using the size charge for which calculations were made. It was found
on the contrary that the ring was pulled in (toward the explosion) along
the axis of the baffles. Since the ring was distorted by each shot,
the experiment was carried on by moving all gauges 90° around the ring
after each shot to get the baffled gauges on the long axis and reverse
the distortion. A distance correction was applied using distances to
the charge before the shot; this correction is valid only if damage is
completed before distortion occurs. The correction for both baffled
and unbaffled gauges was made by using the distance exponent (1.21) as
determined with the unbaffled gauges. It gave consistent results when
used in addition to the thickness correction (Sec. V, 4, a), and two
shots in which wire cable was run across the ring to decrease the dis-
torting motion showed no difference in results. To find out if possible
diffraction through the crack between gauge and baffle had any effect,
two shots were fired with the crack plugged with lead and sealed with
"Bostik" (a rubber cement); there was no difference in results.

With 6 in. radius baffles, the same distortion occurred to a
smaller extent; the method used was the same and the results were treated
in the same way. Two shots in which the crack between gauge and baffle
was covered with sheet steel showed no difference in results.

Infinite baffles were obtained by using a baffle with a 24 in.
radius (well beyond the theoretical limiting radius), and by placing
gauges, with and without baffles, flush with the sandy bottom of the
ocean. In the latter case, the charge was supported 48 in. above the
gauge. A special rig was necessary to force the gauge and baffle down
until the face was flush with the bottom, and a diver had to examine
the gauge and set the charge on its support. Results were not very
reproducible because the charge distance was uncertain, the gauge could
not be set perfectly flush with the bottom, and the bottom itself was
not perfectly reproducible.

In a supplementary experiment, a few thin (.025 in.) diaphragms were damaged in the regular type gauge and with a 25 in. baffle, hung free. The increase in damage with the baffle was 22%.

The work with the half-scale damage gauges (Cf. Sec. V, 3, d) is summarized in Table XV. According to the theory, baffle radii scale with gauge size, and the 8 in. and 10 in. radium baffles for the half-scale gauges are about at the theoretical limit for an infinite baffle. In general, the infinite baffle produced a 25% to 30% increase over the damage occurring with the gauge alone.

In a special experiment to obtain an infinite baffle all parts of which would be reached by the shock wave at the same time, a hemispherical baffle (1/8 in. thick) of 17 in. radius was used with a half-scale gauge at the pole and the charge at the center. Eight shots were fired (4 shots of 41 gm. loose tetryl, 4 of 95 gm. tetryl; charge distance 15 to 17 in.) with this baffle, and for comparison, six shots were fired using the same charges and distances with the unbaffled gauge. The increase in damage over the unbaffled gauge was about 20%.

(iii) Comparison of theory with experiment. The ratio of the maximum deflection in the case of the infinite free baffle to that in the case of no baffle is predicted by the theoretical treatment given in (V, 5, (b), 1) to be 1.14, calculated on the assumption that regular damage gauges are used, with Lot 3 diaphragms, and a baffle 1 in. thick, and that the charge consists of 840 gm. TNT placed 48 in. from the gauge. The experimental ratio found for these conditions is about 1.22 (Table XIV-A). The discrepancy may possibly be ascribed to a small departure of the motion of the part of the baffle near the gauge pot from free plate motion due to bending resistance, causing the value calculated theoretically to be too small.

(c) The time required for the diaphragm deformation. Kirkwood's theoretical work has predicted among other results the deformation of a diaphragm exposed to an underwater explosion wave as a function of time for various experimental conditions. The empirical determination of the time required for diaphragm deformation as applied to UERL damage gauges will be discussed here. (Cf. also Sec. V, 3, a).

To determine if the secondary pulse from the second bubble expansion was responsible for any appreciable fraction of the depression of a diaphragm under normal use of the damage gauge, experiments were carried out using an electrical contact inside the gauge and arranged to close a circuit when about 90% of the final depression was attained. The circuit was connected to a cathode-ray oscillograph with a time base triggered by the break of the circuit in the detonator cap of the charge. Lot 3 steel diaphragms (.075 to .085 in. thick) were used and the gauge was mounted on a steel ring.

In one set of shots, a single dummy gauge was mounted opposite the gauge used. The charges were of loose tetryl (100 gm. at 18 in., 250 gm. at 6-1/4 in., and 250 gm. at ca. 30 in.) and the rig was lowered to a depth of about 8 ft. for firing. The total depth was 20 ft. in the other shots, 2200 gm. cast TNT was employed at a distance of 7 ft. and depths of 20 and 25 ft. In this case, three dummy gauges were fastened to the ring. The total depth was roughly 70 ft.

Table XIV-A - Comparative damages -- baffled vs. unbaffled

Gauges mounted on steel ring; charge-to-gauge distance, 48 in.

Baffle Radius (in.)	Charge (gm)		Damage[a]	(10^{-2} in.)	Increase of Damage of Baffled Gauge over Unbaffled (exp) (percent)
	Tetryl	TNT	Baffled	Unbaffled	
Lot 3 Plates					
12	50	--	8.5	5.6	53.5[b]
12	150	--	21.7	16.9	28.3
12	250	--	29.2	23.0	27.0
12	480	--	43.4	34.3	26.5
12	625	--	59.9	49.2	22.0
Lot 4 Plates[c]					
12	480	--	53.6	44.2	21.2
12	90	743	69.2	58.3	18.4
12	90	743	69.3	58.2	19.0
12	90	743	68.9	58.8	17.1 (Avg. 18.7)
12	90	743	70.0	58.1	20.4
8	90	743	66.6	57.9	15.0
8	90	743	66.0	58.8	12.2
8	90	743	67.3	58.7	14.5 (Avg. 13.7)
8	90	743	66.9	58.9	13.6
8	90	743	66.6	58.9	13.9

a/ Average of 2 diaphragms per shot. Corrected for distance and thickness variation.
b/ Result doubtful because of small damage.
c/ Lot 3 and Lot 4 plates give different absolute values because they differ in strength and thickness.

585

Table XIV-B - Comparative damages -- baffled vs. unbaffled gauges.

Baffled gauge set on bottom; charge-to-gauge distance, 48 in.

Baffle Radius (in.)	Charge (gm) Tetryl	Charge (gm) TNT	Damage (10⁻²in.) Baffled	Damage (10⁻²in.) Unbaffled	Increase of Damage of Baffled Gauge over Unbaffled (exp) (percent)	Increase of Damage of Baffled Gauge Over Unbaffled For Infinite Baffle (theo) (percent)	Damage When on Bottom Minus Damage When on Ring (10⁻²in.)
					Lot 3 Plates		
12	90	175	28.2	24.0 a/	17.5	72	
12	90	428	43.2	35.0 a/	23.2	73	
					Lot 4 Plates		
12	90	743	75.5	58.5 b/	29.1	82	5.9
12	90	743	75.5	58.5	29.1	81	5.9
8	90	743	73.6	58.5	25.9	81	6.9
8	90	743	73.3	58.5	25.2	81	6.6
Unbaffled gauge	90	743	70.1	58.5	19.9	81	11.6

a/ Interpolated from other Lot 3 data.
b/ Average of 18 diaphragms.

Table XIV-C - Partial Summary of Baffled-Gauge Data

Regular UXRL damage gauges
Charge, 745 gm TNT plus 90 gm Tetryl
Lot 4 steel diaphragms; thickness, 0.073 in.
Charge-to-gauge distance, 48 in.
Baffle thickness, 1 in.

Gauge Mounting	Hung Free	On Steel Ring	On Bottom
Baffle Radius (in.)		Damage[a]/(in.)	
4 (gauge alone)	0.576 (2)	0.585 (18)	0.756 (2)
8	.655 (2)	.667 (10)	.732 (4)
12	.688 (2)	.694 (8)	.755 (2)
24	.655 (6)		.732 (2)

a/ The number in parentheses after each average damage indicates the number of diaphragms from which the average was obtained.

Table XV - Comparative Damages - Baffled vs. Unbaffled Half-Scale Gauges

Half-scale damage gauges
Charge, 95 gm Tetryl
Lot 4 steel diaphragms
Charge-to-gauge distance, 24 in.
Baffle thickness, 1/2 in.

Gauge Mounting	Hung Free	On Steel Ring
Baffle Radius (in.)	Damage[a]/ (in.)	
2 (gauge alone)		0.134 in. (10)
8		.174 in. (6)
10		.170 in. (4)
24	0.164 (4)	

a/ The number in parentheses after each average damage is the number of diaphragms from which the average was obtained.

In all tests the contact closed within a few milliseconds although the secondary pulse came very much later. There was some chatter but the time at which the final closure occurred was still only a fraction of the bubble period. For some of the 250 gm. charges a piezoelectric gauge alongside the damage gauge recorded the primary and secondary pulses as a rough check on the time interval. This interval was of the order of 165 msec.

This experiment was repeated using wooden frames instead of the steel ring as a mounting for the gauges. The same result was obtained, i.e., the damage was produced by the shock wave.

Next, a series of measurements of the deformation of steel diaphragms in UERL damage gauges on a steel ring versus time after incidence of the primary shock wave was made, so that an empirical deformation-time curve could be obtained. The experimental arrangement was similar to that used previously, a contact being placed known distances behind the diaphragm. When closed, this contact connected a stop voltage to a single sweep oscillograph. The contact was sufficiently yielding that it had no appreciable affect on the final damage. The pressure-time curve of the explosion wave was recorded simultaneously by a piezoelectric gauge placed at the same distance from the charge (30 in. from 250 gm. loose tetryl). In this way, closing of the contact produced a sharp cutoff of the piezo gauge record. The circuit is shown in Figure 20.
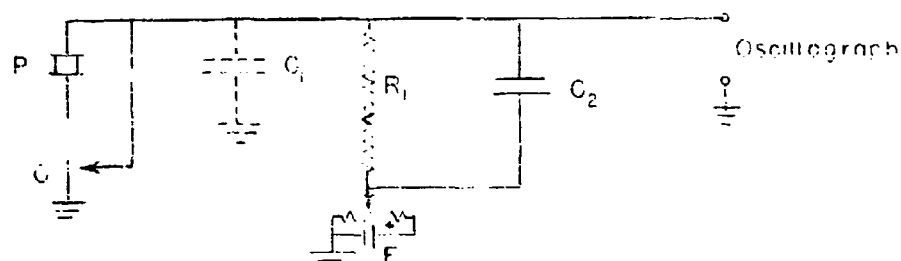
P - Piezoelectric gauge   C - Contact behind the damage gauge
R_1 - 0.3 or 20 megohms C_1 - Cable capacity of about 5000 $\mu\mu f$
R_2 - 5000 ohms C_2 - Padding capacity of about 2000 $\mu\mu f$
E - 6 volts

Fig. 20. Circuit employed for determination of times of deformation.

The time scale was calibrated against a 25 kc/sec crystal controlled oscillator, and checked by time intervals on the record known in terms of the shock wave velocity. Lot 3 steel diaphragms, .075 to .080 in. thick, were used as before.

The data obtained are given in Table XVI and plotted in Figure 21.

TABLE XVI - Time of central deflection for Lot 3 steel diaphragms.

250 gm. loose Tetryl at 30 in.; contact method

Depth of Contact d_c (10^{-3}in.)	Maximum Damage d_d (10^{-3}in.)	$\frac{d_c}{d_d}$ (percent)	t (μsec)	Diaphragm Thickness (10^{-3}in.)
51	433	11.7	26.6	76.0
48	402	11.9	31.0	80.0
47	424	11.1	26.6	76.8
101	389	26	51.0	79.5
104	419	25	53.0	75.3
103	413	25	53.0	75.5
199	398	50	80.4	79.6
205	402	51	80	79.2
200	411	49	85	78.1
200	413	48	78	76.9
199	420	47	79	76.9
302	422	72	111	76.0
300	419	72	105	79.4
302	414	73	99	80.1
299	416	72	111	76.8
383	426	90	140	75.1
386	431	90	146	74.7
410	418	98	147	76.5
410	407	101	144	79.4
410	431	95	141	76.1

The general shape of the curve is qualitatively what one would expect. The time for maximum depression cannot be fixed with great accuracy from such a curve but is about 155 microseconds. Possibly a less ambiguous figure is the time of 82 microseconds for half the final deformation. These figures are comparable with the duration of the incident shock wave (time constant 54 microseconds) and show that for the experimental conditions in this case the influence of the secondary and later impulses is negligible.

The theoretically predicted damage time curve for these conditions[18] is also given in Figure 21. However, since cavitation occurs for this case (cf. Table XVIII) the theory does not apply here but is considered more typical of most of the work where cavitation did not exist.

The deformation time curve was determined also by the method discussed earlier (Sec. V, 3, a) in which the depth of the charge and damage gauges below the surface was varied and the corresponding effect on damage, due to the rarefaction wave reflected from the surface, noted.

The results of this experiment are shown in Figure 22. The dotted curve shows the damage and cut-off times plotted against the depth. This time is calculated on the assumption that a tension wave is reflected from the surface and cuts off the tail of the direct wave. Acoustic velocities were assumed. The minimum time which will give full damage is clearly not easy to determine with any accuracy but seems to be about 215 ± 40 microseconds (a depth of 15 ± 2 in.). This is higher than the values of 138 - 177 microseconds found by the electrical contact method. However, it may well be that the last few per cent of the damage require a relatively long time; if so, the results obtained by the contact method might easily be somewhat in error.

(d) Deformation of water-backed diaphragms. In connection with the tests investigating the effect of variations in diaphragm thickness on damage (Sec. V, 4, a), several shots were fired using thick and thin copper diaphragms clamped between the face plates of regular gauges so that the diaphragms were water-backed. Thin diaphragms were placed in two opposite gauges and thick diaphragms in two other gauges, all supported by a steel ring. The ratio found for the damage of the thin diaphragms to the damage of the thick diaphragms was about the same as that found with air-backed gauges. The data are listed in Table XVII and are comparable with the data given in Table XIII.

Table XVII. - Damages of thick and thin copper diaphragms

(Water-backed gauges)

Charge (gm)		Charge-to-gauge Distance	Average[a] Diaphragm Thickness $(10^{-3}$ in.$)$		Average[a] Damage $(10^{-2}$ in.$)$		Increase in Damage[b]
TNT	Tetryl	(in.)	Thick	Thin	Thick	Thin	(percent)
	461.5	48	65.4	32.3	20.1	32.3	59.8
	980.0	48	64.7	32.1	29.2	45.1	53.9
	2153.5	48	66.6	32.5	46.9	68.2	45.4
3300	110	48	64.8	31.8	53.8	79.4	46.0
6300	320	84	65.2	31.9	40.1	57.1	41.9

a/Average of two diaphragms.
b/Increase in damage defined as difference in damage for thin and thick diaphragms expressed as percent of damage for thick diaphragms. Based on damages corrected for small variations of distance from 48 in. and 84 in.

18/OSRD No. 4200, p.46 (Fig. 4); p.55. The parameter θ was determined as in Section IV.
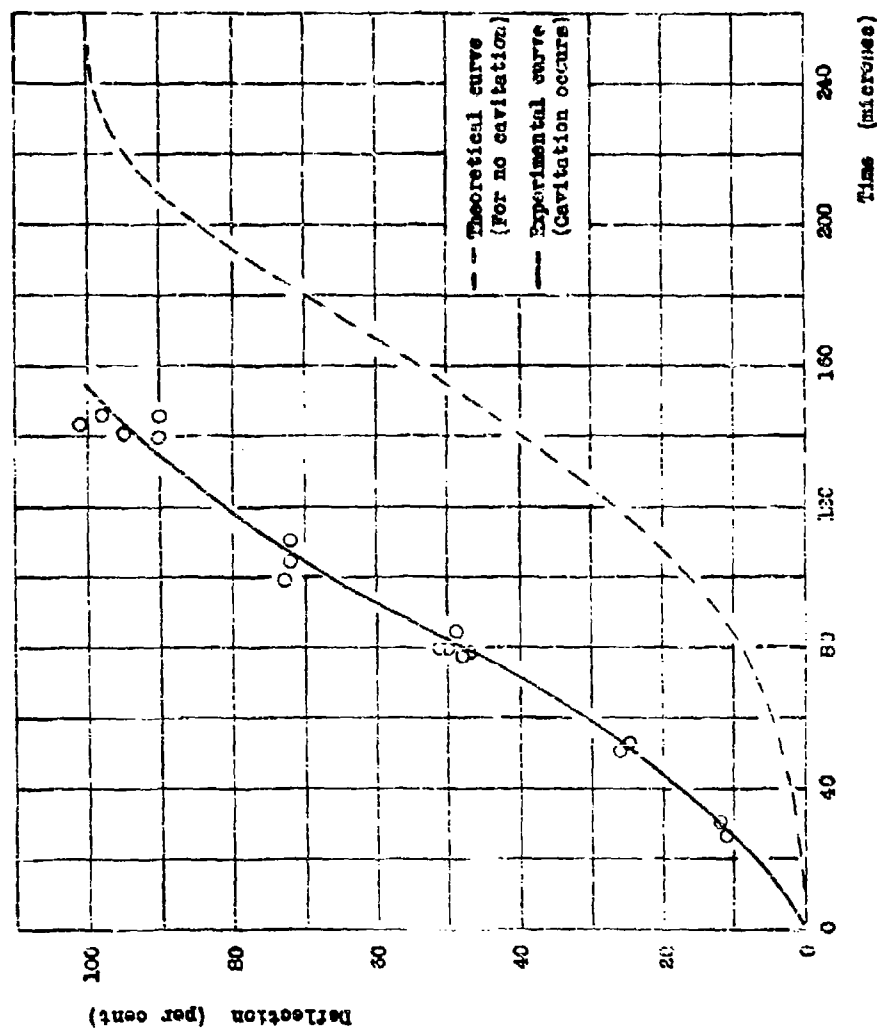
Fig. 21. Per cent damage vs. time.
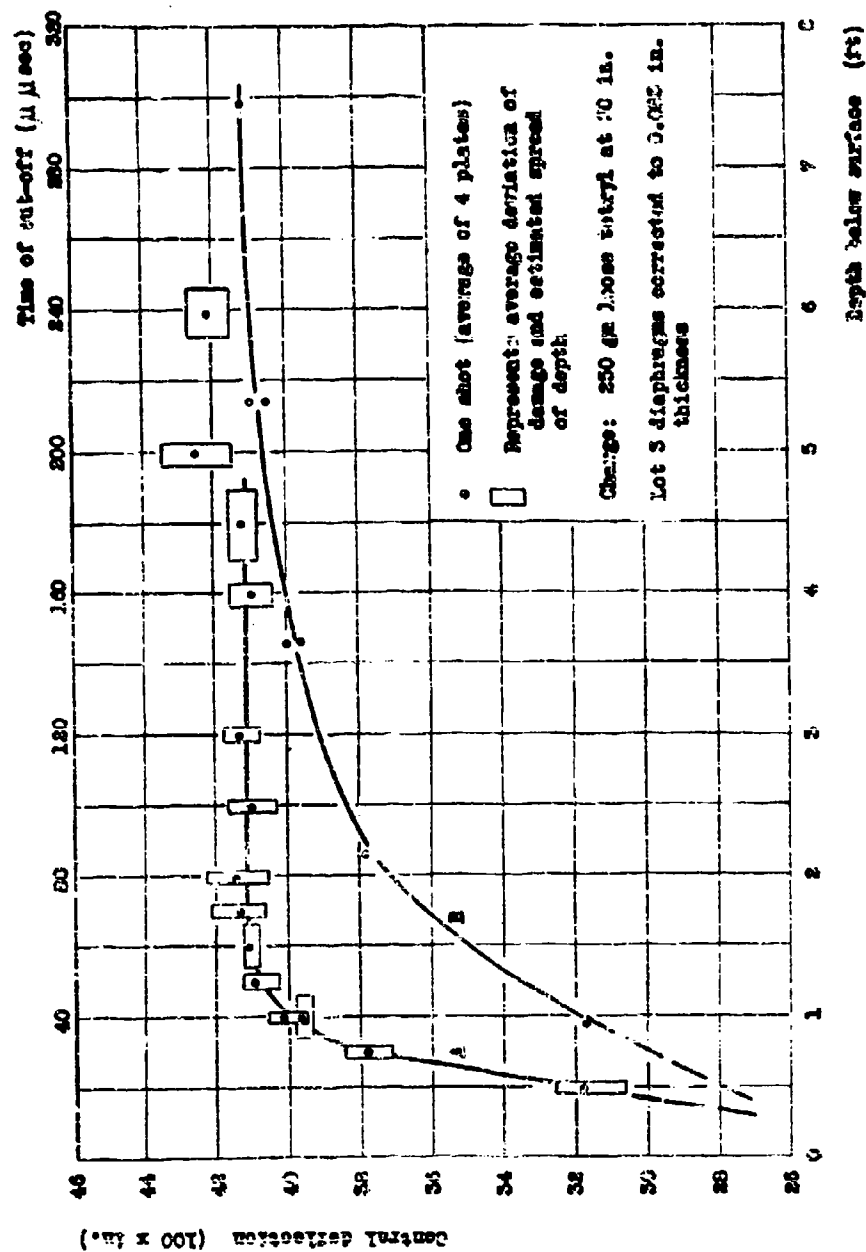
Fig. 22. A - Diaphragm gauge damage vs. depth below surface.
         B - Diaphragm gauge damage vs. time of cut-off.

There appears to be about a 30% increase in the weight exponent for the water-backed diaphragms over the air-backed diaphragms, however.

The shape of the damage of the water-backed diaphragm was distinctly different from the usual parabolic profile. This was noticed particularly on the thin diaphragms when the damage exceeded half an inch. On these diaphragms there was an additional dent in the center of the diaphragm which also showed excessive thinning. This may in part explain the higher weight exponents since damage is measured in terms of maximum central deflection. Profiles of air-backed and water-backed diaphragms are shown in Figure 23, A and B, respectively. The unusual shape of B may perhaps be qualitatively explained by assuming that the time of damage of the diaphragm is of the same order of magnitude as the time required for the shock wave to pass from the front face of the gauge around to the central region in the back of the diaphragm. Then the diffracted wave in the rear of the diaphragm will cause a disproportionate damage, acting more near the edge than at the center. This explanation has been tested by mounting the gauge against one end of a 2-1/2 ft. pipe, leaving the other end of the pipe open to the water. The profile of the resulting damage is shown in Figure 23, C. The appearance of the diaphragm qualitatively verified this hypothesis in that the additional central dent is removed and the shape is more nearly the usual one.

(e) Cavitation. (i) Effect of cavitation on damage. In the deformation of a diaphragm by an "explosion[19] wave, large negative pressures may under some circumstances develop at the surface of the diaphragm due to the reflected rarefaction wave emitted in the geometrical acoustical phase of the motion. Since water cannot support a tension of great magnitude, it has been suggested that cavitation will occur if the pressure in the wave falls to zero or less". The chief role of cavitation is to prevent loss of kinetic energy from the diaphragm by radiation in the reflected rarefaction wave. Neglect of cavitation in cases where it occurs therefore leads to the theoretical prediction of too little damage.

(ii) Conditions required for the formation of cavitation. "For[19] an exponential wave impinging on a free plate with damping time $\theta_1 = \rho a_0 / \rho_0 c_0$, the pressure will fall to zero at a time θ_c given by

$$\theta_c = \frac{\theta\theta_1}{\theta-\theta_1} \quad \log_e \quad \frac{\theta}{\theta_1}" \tag{35}$$

The derivation of this equation is given in reference 21. The terms are described below.[20] "This time (θ_c) will be lengthened somewhat by the

---

[19] Quoted sections have been taken from CSRD No. 1115, J. G. Kirkwood, Dec. 1942.

[20] ρ and ρ_0 are the densities of the diaphragm material and the water, respectively; a_0 is the thickness of the diaphragm; c_0 is the velocity of sound in water, and θ is the time constant of the shock wave (Section III).

Fig. 22. A = Diaphragm gauge damage vs. depth below surface.
B = Diaphragm gauge damage vs. time of cut-off.

Depth below surface (ft)
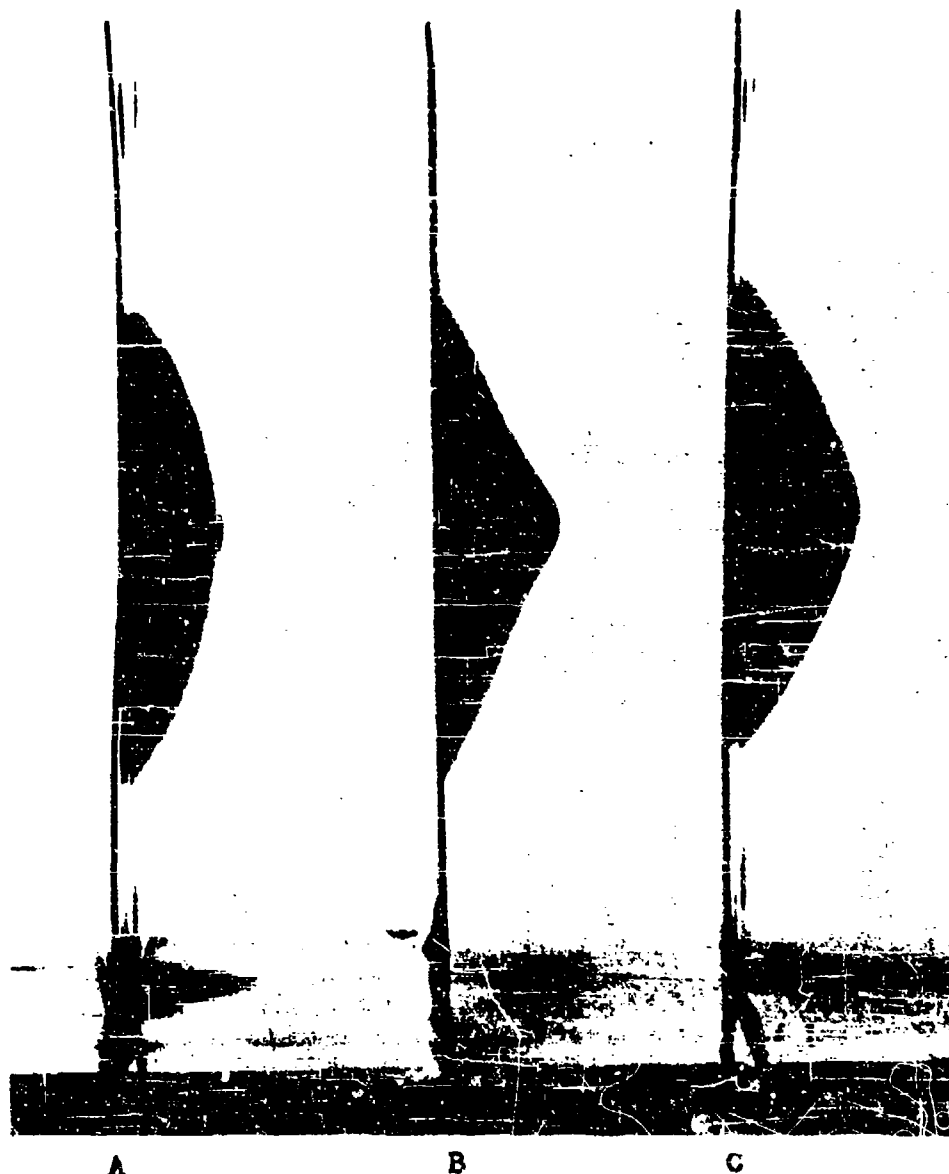
Fig. 23. Shapes of air-backed and water backed
deformed copper diaphragms.

574

resistance of the (diaphragm) to deformation both in the elastic and plastic domains." However, according to Kirkwood. a good criterion for the occurrence or non-occurrence of cavitation is the following:

$$\theta_2 > \theta_c \qquad \text{Cavitation}$$

$$\theta_2 < \theta_c \qquad \text{No cavitation}$$

where θ_2 is equal to R_0/c_0, the time required for the diffracted pressure wave to travel from the periphery of the diaphragm to the center of the diaphragm. (R_0 is the radius of the unsupported part of the diaphragm.) On this basis, "we would expect cavitation in the case of very thin (diaphragms) of large diameter under the impact of a wave of short duration produced by a small charge of explosive."

(iii) Proof of the existence of cavitation. To furnish an empirical test of the criterion for cavitation derived theoretically, several under-water photographs[21] of about 1 microsecond exposure were taken of damage gauges in the process of diaphragm deformation. A sample photograph showing cavitation bubbles is reproduced in Figure 24, and the data for all photographs are summarized in Table XVIII.

Table XVIII - Data for cavitation photographs

Diaphragm Thickness (in.)	Charge Weight (gms)	Distance (in.)	θ (μsec)	θ_c (μsec)	θ_2 (μsec)	Cavitation Observed
.013	50	13.5	35	5	29	Yes
.025	50	24	40	9	29	Yes
.039	50	24	40	12	29	Yes
.038	500	48	80	15	29	Yes
.074	50	12	35	18	29	Yes
.078	250	30	55	21	29	Yes
.156	50	12	35	27	29	No
.156	250	30	55	33	29	No

It is shown in the above table that only in one border-line case, where θ_2 exceeds θ_c by only 2 microseconds, does the theoretical cavitation criterion not apply. The figures are of course not this accurate.

Theory and experiment both indicate that cavitation does not usually occur in the use of this gauge as in this report.

21/ J. E. Eldridge, Paul M. Fye and R. W. Spitzer, Photography of Underwater Explosions I, NDRC Report A-368, OSRD 6246.

Fig. 24. Sample photograph of damage gauge in process of diaphragm deformation. Bubbles indicate cavitation.

(f) Effect of increasing mass of diaphragm on damage. Since the density of the diaphragm material occurs as a parameter in the damage equations of the Kirkwood Theory (cf. Section III), a partial test of the theory could be made by "loading" the diaphragm so as to change the effective density without altering the mechanical strength of the diaphragm. The following methods of loading were tried.

(1) A lead disk was soldered to the back of the diaphragm with two series of grooves cut into the disk almost down to the diaphragm; they were 1/4 in. apart and at right angles to each other so as to reduce the strength of the lead. (A few solid lead disks were tried and proved unsuccessful.)

(2) The gauges were hung face down, so that the diaphragm was parallel to the charge-to-gauge line, with (a) mercury and (b) putty lying free on the back of the diaphragm.

(3) Putty was packed into a thin-walled steel tube soldered to the back of the diaphragm. The gauge was set in the normal vertical position and a cardboard disk was used to hold the putty in place.

(4) Mercury was loaded on the back of a vertically held diaphragm by means of a second diaphragm clamped in a fitting inside the gauge. This second diaphragm consisted of (a) cellulose acetate sheeting, and (b) this sheeting plus a 1/4 in. sheet of rubber.

A load of about 530 gm, which is 6.7 times the weight of the steel diaphragm (79 gm.) was used. The charge range was 200 to 2400 gm. at distances of 4 to 4-1/2 ft. Results are given in Table XIX. Since in some of these tests the diaphragm was heated to solder material to it, five diaphragms were given similar heat treatments and then damaged with no loading. The heating was found to affect the damage by no more than 2 to 3%.

In general it may be concluded from these tests (a) that a rough agreement with theory has been found; (b) that in the cases of mercury loading and of lead loading where the lead completely left the diaphragm, the lower damage of loaded diaphragms results from the fact that the loading material left the diaphragm in the deceleration stage carrying energy with it; (c) that the horizontal gauges show less damage and somewhat less effect of loading than the vertical gauges.

(g) Effect of bending radius on nature of rupture of diaphragms. The damage gauges used at UERL have been constructed with a bending radius of 1/16 in. (Sec. II.1). It was observed that steel diaphragms in these gauges ruptured at the edge, while copper diaphragms burst in the center. It was suggested that rupture should occur at the edge because of the finite time required for the plastic wave to propagate to the center. Kirkwood in his theory ignores this propagation time and predicts that rupture should occur in the center, provided that the bending radius is great enough to avoid rupture by bending as opposed to tension. In order

Table XIX - Comparison of damages of loaded and unloaded diaphragms

(All charges included 90 gm. tetryl in addition to the TNT listed)

Charge Weight TNT (gm.)	Charge-to-Gauge Distance (in.)	Method of Loading	Damage [a] (in.)		Damage Ratio of Loaded Diaphragm to Unloaded Diaphragm		Weight Ratio of Loaded Diaphragm to Unloaded Diaphragm
			Diaphragm Loaded	Diaphragm Unloaded	Experimental	Calculated [b]	
(a) Gauge Vertical -- Normal Position							
100	43	1. . Pb	0.119	0.219e/f/	0.54	0.54	7.78
690	48	1. . Pb	.288c/	.543e/	.53	.57	7.66
690	47	3. . Putty	.279	.563	.53	.57	7.74
690	47.6	4a. Fe	.204	.553	.37	.57	7.74
690	47.6	4b. Fe	.251	.557	.45	.57	7.74
2300	48	1. . Pb	.463d/	1.02e/	.47	.58	7.78
2300	47.1	3. . Putty	.569	1.02	.55	.58	7.74
2300	47.5	4a. Hg	.429	(0.941s/)	.47	.58	7.74
2300	47.5	4b. Hg	.435	.996	.44	.59	7.43
(b) Gauge Horizontal -- Face Down							
690	53	2b. Putty	0.255	0.394	0.65	0.57	7.74
690	54.6	2a. Hg	.181	.470	.39	.57	7.74
2300	54.6	2b. Putty	.475	.750	.62	.58	7.74
2300	55	2a. Hg	.421	.711	.59	.58	7.74

a/ Damages have been corrected to standard thickness of 0.073 in. for Lot E steel diaphragms.
b/ The theory of Kirkwood. See OSRD Report No. 1115, by J. G. Kirkwood.
c/ Lead disk partially torn loose from plate.
d/ Lead disk completely torn loose from plate.
e/ Average of two diaphragms -- all others are single diaphragm.
f/ Cavitation may exist in front of diaphragm.
g/ Water in gauge; abnormally low damage.

to observe the effect of the size of the bending radius on the damage
of steel diaphragms in general, and the point of rupture in particular,
a gauge was altered to have a bending radius of 1/8 in.

Damages were obtained ranging from 1/2 in. to the bursting limit
and in general were .01 to .02 in. greater than for the normal gauge.
Steel diaphragms in the gauge with the 1/8 in. radius burst in the center
and had a bursting limit of about 1.25 in. as compared with 1.10 in. for
the normal gauge.

(h) Shape of deformation profile. Kirkwood predicts[22] that if a
diaphragm is exposed to an impulsive shock
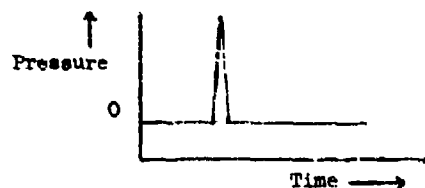
i.e., a shock wave of very short duration relative to the diaphragm
deflection time, the shape of the deformation will tend to be conical.
On the other hand, if the diaphragm is exposed to a step shock,
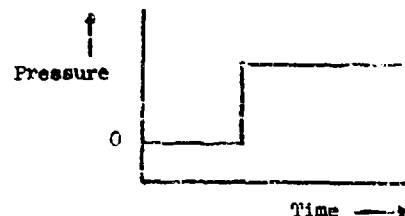
where the duration of the pressure is very long compared to the deflection
time, he predicts a spherical deformation. Ordinary shock wave durations
in diaphragm gauge work fall between these two limits, but it is interest-
ing to note that Kirkwood's predictions are borne out at least qualitatively
as these limits are approached. In Figures 25 and 26 the central profiles
of two sets of damaged steel diaphragms are reproduced. The maximum de-
flection for the diaphragms of each set are approximately equal, and the
change in shape of the profiles for shock waves of increasing duration is
evident. Thin (.038 in.) diaphragms were chosen to demonstrate this
effect since sharp bends would tend to be "ironed out" by thicker diaphragms.

Another demonstration of change of shape with wave form is clearly
shown in the experiments wherein the shock-wave is cut off by bringing the
gauges and charge successively closer to the surface (cf. Sections V, 3, a
and V, 4, c). Here the shape becomes more conical as the cut-off time is
shortened.

22/ J. G. Kirkwood and J. M. Richardson OSRD No. 4200, p. 40

(i) Thinning of diaphragms during deformation. The thickness of the diaphragms mentioned in the preceding subsection (h) was measured at several points to determine the thinning caused by the deformation. Kirkwood gives the equation[23]/

$$\frac{a}{a_0} = \frac{1}{(1+y_0^2)^2} \tag{36}$$

for the central thinning, where a is the thickness at the point of maximum deflection, a_0 is the initial thickness, and y_0 is the maximum deflection divided by the diaphragm radius. For diaphragms 0.038 in. thick initially, the central thickness after deformation is predicted from this equation to be 0.029 and 0.033 in. for central deflections of 0.64 and 0.46 in., respectively. Inspection of the measured thicknesses indicated in Figures 25 and 26 shows reasonably good agreement between theory and experiment. Kirkwood gives also an equation for the thinning at any other point in the deformed area. This equation requires the thinning to decrease as the distance from the center is increased, corresponding qualitatively with the experimental measurements.

(j) Effect of weight and mounting. Inspection of Equations (1) and (2) of Section III will show that the maximum deformation suffered by a diaphragm exposed to an underwater explosion is not a function of the mass of the mounting which supports it. In other words, it is tacitly implied that the gauge as a whole will not move enough during the time of deformation to affect the deformation significantly. The independence of damage on the weight of the mounting was demonstrated empirically in experiments with wooden frames (Section V, 2, 3) and also in the course of some full scale weapon tests. In these tests two gauges were fastened in a light (70 lb.) mounting and two gauges in a heavy (220 lb.) mounting; both mountings were the same distance from the charge. Table XX lists the mean damage ratios and the standard deviations from the means.

Table XX. Mean ratios of light mount/heavy mount diaphragm depressions

Charge Weight (lbs.)	No. of Shots	Distance (ft.)	Light Mount Depression / Heavy Mount Depression (mean)	σ_m
200	17	50	1.01	.01
250	8	50	1.03	.02
300	8	60	1.01	.02

[23]/ OSRD No. 4200, p.37

as of
ured at
n.

(36)

of
ximum
3 in.
cted
ions of
cknesses
etween
:hinning
the
l.

a (1)
fered
ion of
ls
uring
The
rated
and also
wo gauges
:avy
he charge.
s from the

...	σ m
	.01
	.02
	.02

25 gm loose tetryl at 15.5 in.
Measured deformation: 0.451 in.

250 gm loose tetryl at 4 ft, 2 in.
Measured deformation: 0.438 in.

50 lb charge at 35 ft
Measured deformation: 0.491 in.

253 lb charge at 75 ft
Measured deformation: 0.472 in.

Scale
½ in.
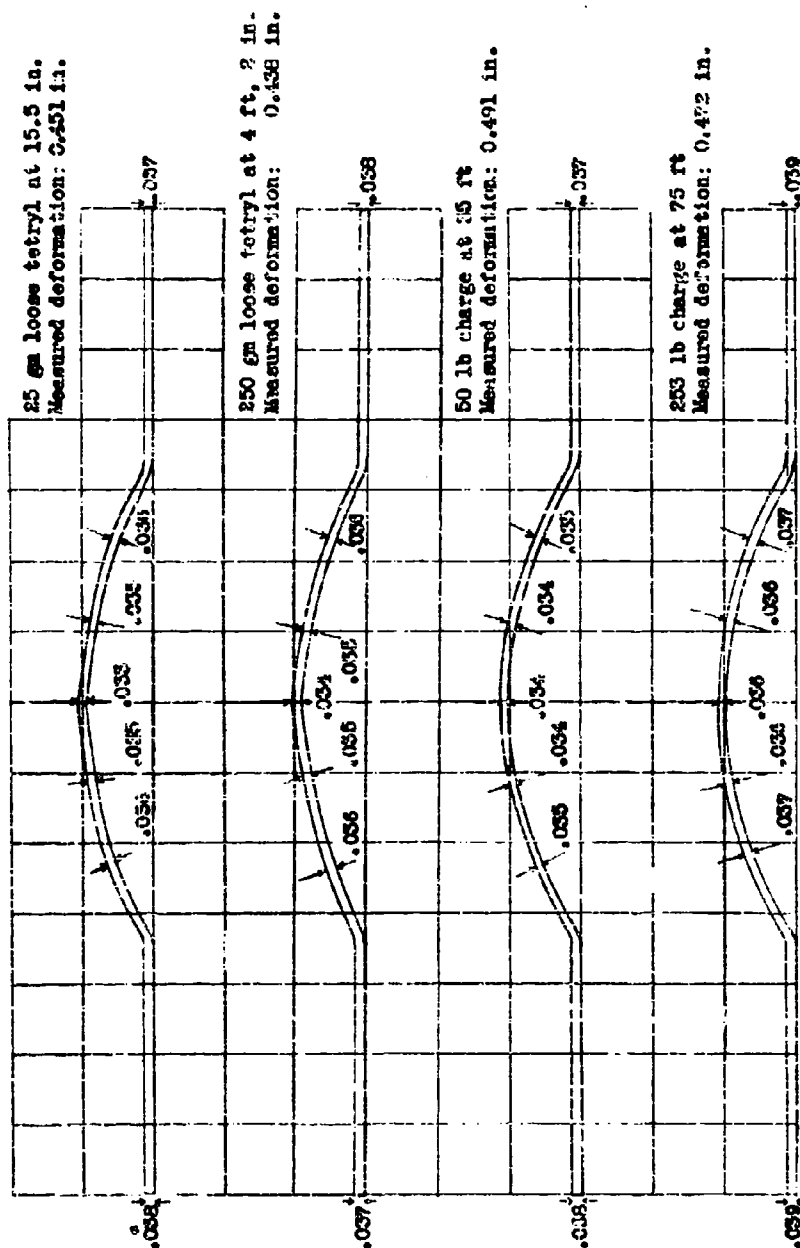
Fig. 25. Central profiles for typical Lot 5 steel diaphragms.

Fig. 26. Central profiles for typical Lot 5 steel diaphragms.

100 gm loose tetryl at 22.5 in.
Measured deformation: 0.659 in.

500 gm loose tetryl at 4 ft, 2 in.
Measured deformation: 0.649 in.

50 lb TNT at 25 ft
Measured deformation: 0.616 in.

292 lb TNT at 50 ft
Measured deformation: 0.655 in.

Scale
½ in.

582
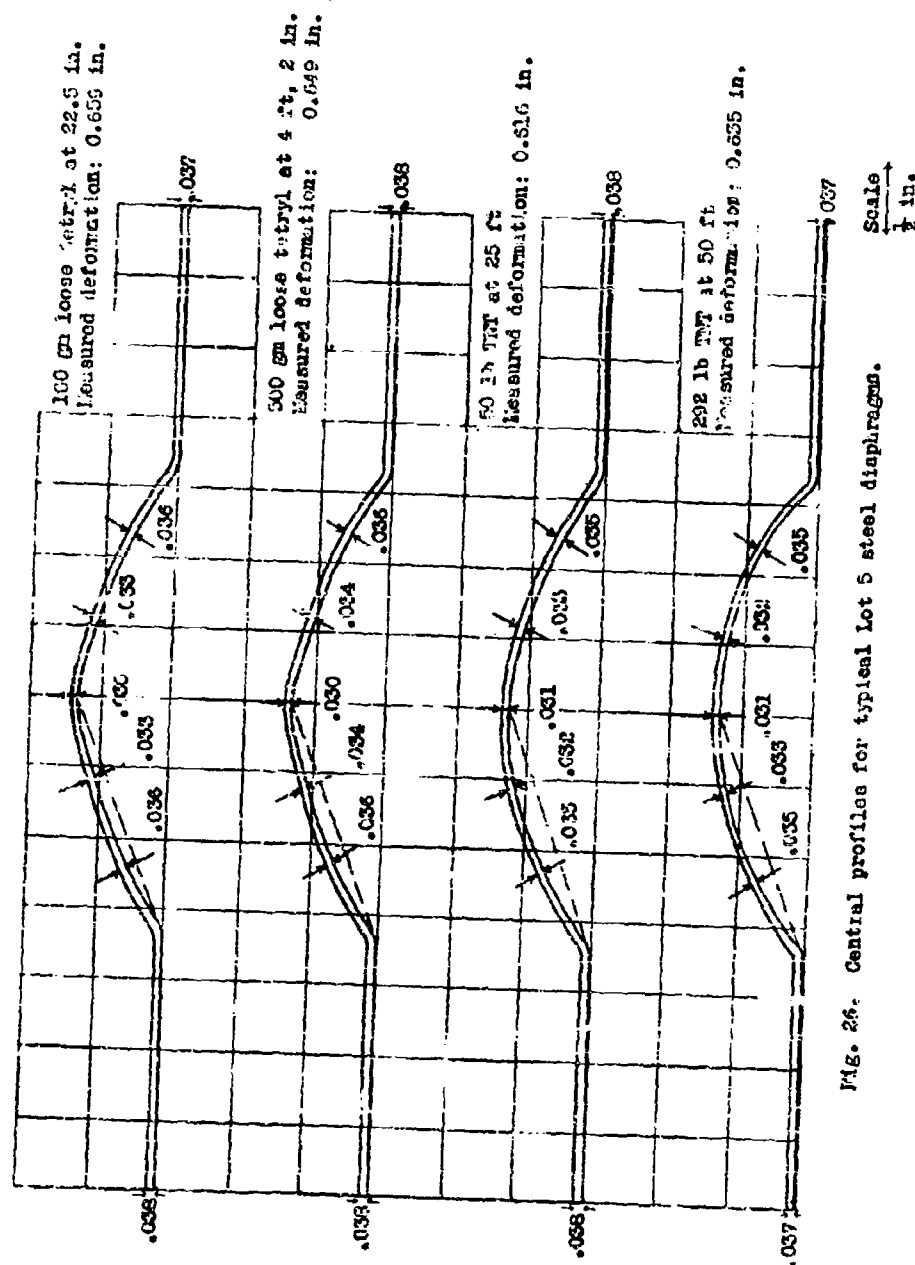
A statistical study of the results showed further that the per cent differences between the reading of the two gauges in a given block were not significantly different for the light and heavy blocks. In other words, the reproducibility of results was not affected by the weight of the mountings over the range of conditions employed.

5.   Miscellaneous Experiments

(a) Increased damage to diaphragm gauges placed above the charge and its explanation in terms of bubble pulses. It was found that under certain circumstances at USRL damage gauge recorded from 10 to 80% greater damage when mounted vertically above a small charge than when mounted at the same level to the side, the charge being at the same depth in the two experiments. This result immediately suggested that the secondary pulses from the rising gas bubble were causing extra damage. Therefore, a contact was placed in the gauge above the charge to measure the time required for final deformation. This time was found to be very great, approximately 250 msec., much greater than the time previously reported for the gauge in the same horizontal plane as the charge (Section V, 4, c). Furthermore, calculation showed that the time observed for the over-the-charge case corresponded closely with the expected time of arrival of the third wave from the explosion (i.e., the second bubble pulse) and that the center of the bubble at this time should have risen practically to the gauge itself.

The data for these experiments are summarized in Table XXI. Gauges were mounted in the usual manner on a steel ring, which was, however, suspended with its plane vertical instead of horizontal. The charge was cylindrical with its axis horizontal, i.e., perpendicular to the plane of the ring. It was found that the increased damage occurred only when the line from the charge to the gauge was within 10° or so of the vertical. The contour of the damaged diaphragm was rounder than usual and the ring was considerably distorted near the top gauge, with bad damage to the gauge mounting bracket.

The time of maximum damage was measured with the contact oscillograph technique (Section V, 4c) in another set of tests. A gauge was mounted 42 in. above a charge of 200 gm. loose tetryl. Lot 4 steel diaphragms were used. The charge depth was 12 ft. A second damage gauge was used as a control in two of the shots, the line from it to the charge making an angle of 36° with the vertical. The damage to the gauge above the charge was quite variable, making it difficult to get many results on the time of maximum damage.

The results which were obtained are listed in Table XXII.

Figure 27 shows the results of an approximate calculation of the bubble period, radius, and rise under gravity. This is based on Bancroft's[24] maximum radius measurement for 50 gm. tetryl at a depth of 10 ft., the observed pulse time for 200 gm. tetryl at a depth of 11 ft.[25]

24/ Division 8, NDRC, OSRD, Interim Report UE-8, p.13.
25/ Ibid., UE-11, p.7
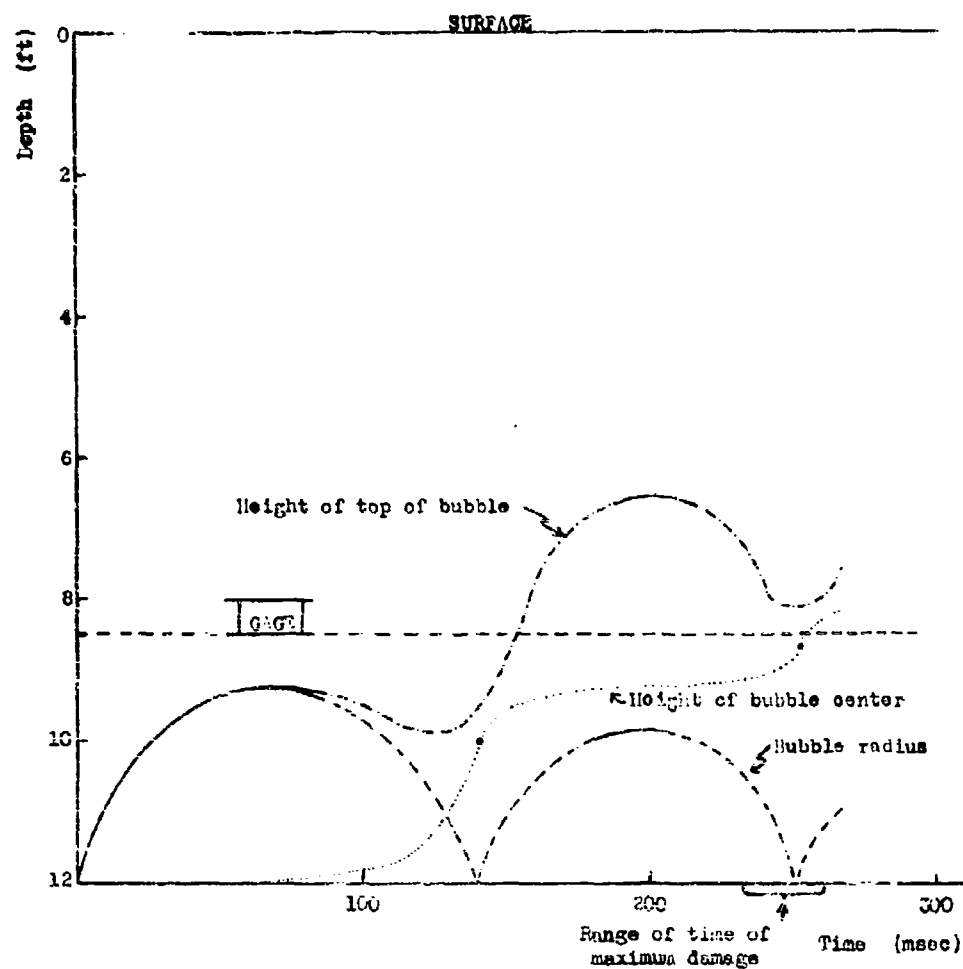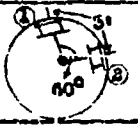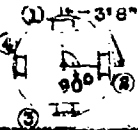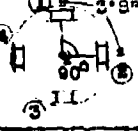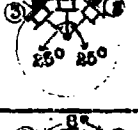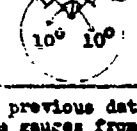
Fig. 27. Movement of the bubble of a 200 gm charge of tetryl 12 ft below the sea indicated by parameters given in the text. The effect of the surface and of the damage gauge is neglected.

584

Table XXI. Results with damage gauges placed above the charge
Charge depth, 18 ft; total depth, 25 ft.

Charge Weight Tetryl (gm)	Charge Distance (in.)	Conditions (Ring Diam: 5 ft)	Damage (10⁻²in.)				Normal Damage (10⁻²in.)	Increase Top Gauge (1) over Normal (percent)
			1	2	3	4		
200	28-1/4		Burst at edge	53.2			55$^{a/}$	>80
200	42		44.0	30.0			29$^{a/}$	52
200	42		47.2	30.9			28$^{a/}$	62
100	22-1/2		50.4	43.0	43.0	43.0	45$^{b/}$	10
100	22-1/2		55.7	44.2	43.9	42.6	43$^{b/}$	30
100	22-1/2		46.4	44.8	44.1		43$^{b/}$	7
100	22-1/2		46.3	46.6			43$^{b/}$	9

a/ Estimated from previous data.
b/ Average of side gauges from fourth and fifth shots.
c/ Ring diameter; 9 ft.

anter

radius

300

e (msec)

yl 12 ft
ffect of

Table XXII - Time for maximum damage, gauge above charge

d_c is the depth of the contact beneath the diaphragm;

d_p the final central damage;

<u>D</u> the damage to the control diaphragm mounted ca. $36°$ from the vertical.

d_c (in.)	d_p (in.)	d_c/d_p (%)	D (in.)	d_p/D (%)	t (msec)
0.445	Burst	-	0.277		262
0.455	0.463	97	0.284	164	258
0.435	Burst	-			4
0.455	0.453	100		162	233
0.447	0.555	81		198	>192

Table XXIII - Summary of diaphragm-gauge measurements in the Mach region of intersecting shock waves

Lot 4 steel plates   Firing depth 10 ft.
Total charge weight, 224 gm loose Tetryl

α (deg)	Distance (in.) Between Charges	a	b	Max. Depression (10^{-2}in.) Gauge No. 6	17	5	8	Mean of 6 and 17 (10^{-2}in.)	Damage Ratio[a]
62	52.1	56.1	23.5	23.4	27.9	42.0	42.8	25.6	1.08
65.1	44	54.3	28.0	26.2	35.1	34.2	34.0	30.6	1.29
69	37.6	53.4	30.7	28.8	27.1	28.3	29.8	28.0	1.17
72	31.9	52.2	33.5	34.1	29.4	27.3	27.7	31.8	1.34
75	26.3	51.4	36.3	32.7	31.7	23.6	24.5	32.2	1.35
80	17.5	50.5	40.9	38.6	31.4	21.6	21.6	35.0	1.7
85.1	8.5	50.0	45.0	31.7	33.7	23.1	23.5	32.7	1.37
90	0	49.5	49.5	23.6	23.7	24.0	22.9		
90	0	49.5	49.5	24.5	24.3	24.0	23.3		

a/Ratio of mean of 6 and 17 to mean of all maximum depressions for the two $90°$ shots (23.8 ± 0.4).

and the observed rise for second and third pulses and the time of the third pulse for 1 lb. of blasting gelatin[26]. Use was made of the theories of Herring[27], Taylor[28], and Willis[26] to scale these results to the case in hand. The effects of the gauge itself, the surface, and the bottom on the bubble motion have been ignored.

This result confirms the results of other investigators on the effect of the bubble from small charges on targets above the charge but does not invalidate the earlier conclusion that UERL damage gauges mounted at the same level as the charge are normally affected only by the primary shock wave.

(b) Mach effect on diaphragm damage. Damage gauges located in the region of the intersection of two shock waves under conditions such that Mach type interference[29] was expected, showed maximum depressions up to nearly 1.5 times the maximum depression observed when the same total weight was detonated at the position midway between the positions of the two equal charges producing the intersecting waves.

The experimental arrangement is shown schematically in Figure 28.
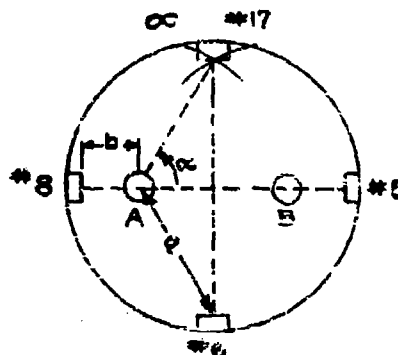
Fig. 28. Arrangement for testing Mach effect.

The charges were arranged so that the line joining their centers and the line between the two opposite gauges, 6 and 17, bisected each other perpendicularly.

Equal lengths of primacord from a No. 8 detonator were used to fire the charges simultaneously. According to Seeger and von Neumann (private communication), the theoretical critical angle α at which the Mach effect first appears for these charge weights and charge-to-gauge distances is 69°. This series covered the range from 62° to 90°. The results are listed in Table XXIII.

26/ H. F. Willis and R. T. Ackroyd, Undex 36
27/ Conyers Herring, NDRC C4 sr20-010, OSRD 236
28/ G. I. Taylor, TMB No. 510
29/ For a discussion of this effect see F. C. keenan and R. J. Seeger, Navy BuOrd Explosives Research Report 15, February 1944.

In the shots at small values of α the greater depressions recorded by gauges 5 and 8 can be attributed to the proximity of each of these gauges to one of the charges. In the 72° and 80° shots the lower damage of gauge 17 may possibly mean that the narrow Mach region missed the gauge.

A graphical representation of the magnitude of this effect, Figure 29, shows the ratio of the maximum depressions recorded by gauges 6 and 17 to the depression produced by a 224 gm. charge at 49-1/2 in. Note that gauges 6 and 17 were 49-1/2 in. from a point midway between the separate 112 gm. charges and hence at distances greater than 49-1/2 in. from the individual charges. The maximum effect was 47%.
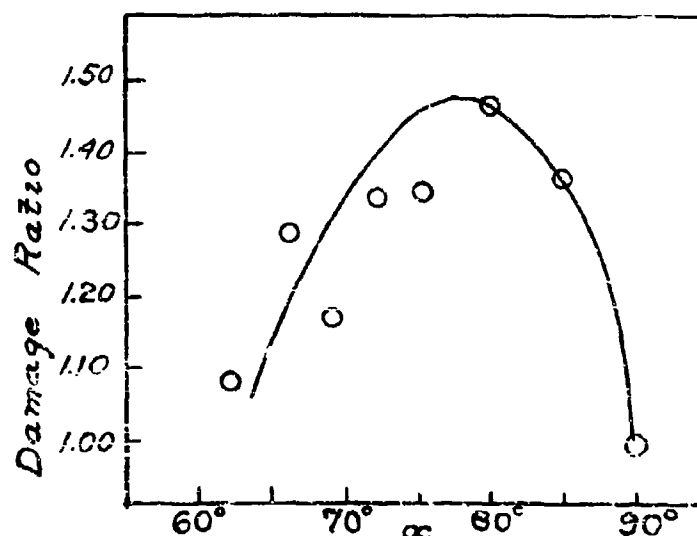
Fig. 29

Mach effect on damage.

(c) Screening one charge by the gas bubble from another. In the experiments reported in the previous section, gauges 5 and 8 were apparently affected only by the nearer of the two charges until the distance between charges was made less than 17-1/2 in. This result can be explained by the shielding effect of the bubble of the nearer charge on the wave from the farther charge. In Figure 30 a plot is made, as a function of the distance "b", of the average damage recorded by gauges 5 and 8, corrected from distance "b" to a charge-to-gauge distance of 49-1/2 in. (A distance exponent of 1.20 was assumed.) From the damage obtained for the 224 gm. charge in the center of the ring, and assuming a weight exponent of 0.59, the damage to be expected from a 112 gm. charge at 49-1/2 in. is 0.158, which is to be compared with 0.17, the average damage along the flat portion of the curve of Figure 30. It might be expected that the screening effect would persist until the charges were placed so close to one another that the gas bubbles coalesced before the effective portion of the shock wave was fully emitted. Table XXIV lists the data.

ded

age

re 29,
7 to

ate
he

, 29

effect
lamage.

ie
par-
ice

s

age
ing

Table XXIV - Screening effect

b	Average Damage for Gauges 5 and 8	Corrected to 49-1/2 in. Assuming Distance Exponent = 1.20
(in.)	(10^{-2} in.)	(10^{-2} in.)
23.5	42.4	17.4
28.0	34.1	17.2
30.7	29.0	16.4
33.5	27.5	17.2
36.3	24.0	16.6
40.9	21.6	17.1
45.0	23.3	20.8
49.5	23.6	23.6
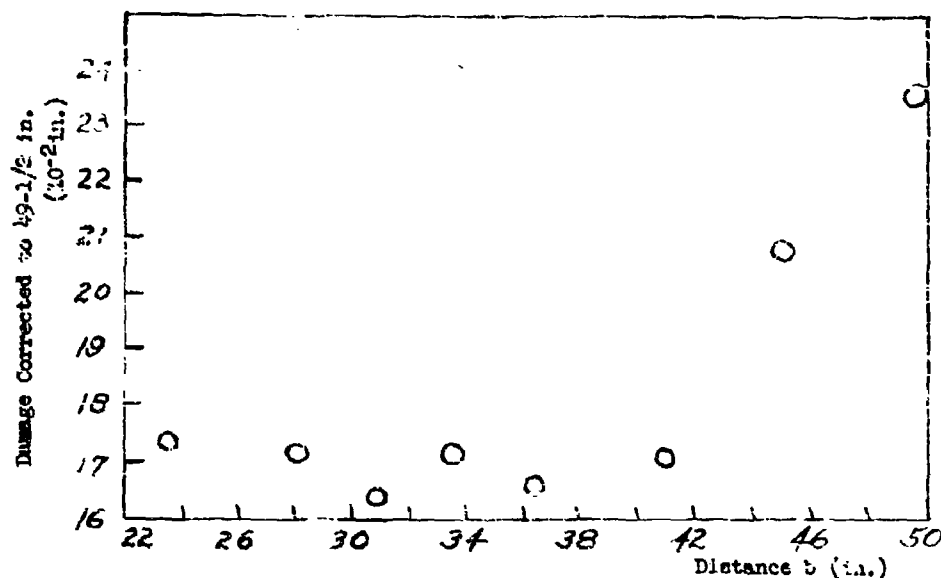
Fig. 30. Effect of screening one charge by the gas bubble from another; a graphical representation of Table XXIV.

(d) A test of Hopkinson's scaling rule. Hopkinson's scaling rule (Section V,3,d) was tested using Lot 5 steel diaphragms in half-scale and full-scale UERL damage gauges and was found to apply, within the precision of measurement, under these conditions.

Two thicknesses of steel diaphragms (average thickness 0.079 and 0.038 in.) were rolled from the same melt of steel so as to have as nearly identical properties as possible. By the manufacturer's test, the ultimate tensile strength was about 68,000 lbs/in² for the thicker and about 63,000 lbs/in² for the thinner diaphragms. The full-scale gauges were regular UERL damage gauges and the half-scale gauges were accurately scaled in all dimensions. The gauges were mounted on steel rings with the charges in the center.

The loose tetryl charges were scaled in their linear dimensions (within 5%) and the weights were in the ratio 8 to 1. Both tin cans and cardboard containers were used and no difference was observed due to container.

The results are given in Table XXV. It will be noted that, on the average, Hopkinson's rule is followed to within 3%.

Table XXV - Results of scaling tests with diaphragm gauges

Charge Weight Loose Tetryl (gm.)	Charge-to-Gauge Distance (in.)	Gauge Size	Maximum Depression Corrected to Plate Thickness of 0.76 in.[b] (full size) or 0.38 in. (half size) (in.)
500	46	Full	0.373 ± 0.004[a]
62.5	24	Half	.192 ± .001[a]
2000	48	Full	.837 ± .007[a]
250	24	Half	.425 ± .010[a]

a/ Standard deviation of the mean.
b/ Corrections based upon Kirkwood's theory (Sec. V,4,a).

(e) Static calibration of steel diaphragms. In an attempt to determine whether or not the variations in the physical properties of the steel diaphragms used in the UERL damage gauges were sufficiently large to cause significant variations in damage, a number of 1 in. diameter steel disks were deformed by static pressure. These disks were cut from the regular diaphragms used in the damage gauges; as many as four could be cut from the area outside the damage portion in the case of a diaphragm which had already been damaged. Otherwise, disks were cut from undamaged diaphragms. The disks were cut to fit into Modugno[30] gauges; they were placed in the gauges and clamped in position as in the customary use of these gauges. Illustrations of a Modugno gauge apart and assembled are given in Figure 31.

30/ Preliminary Design Branch (Ship Protection Group), BuShips Underwater Explosion Report 1942-3, October 1942.

BODY

DISC AFTER FIRING

ASSEMBLED GAUGE

DISC BEFORE FIRING

CAP
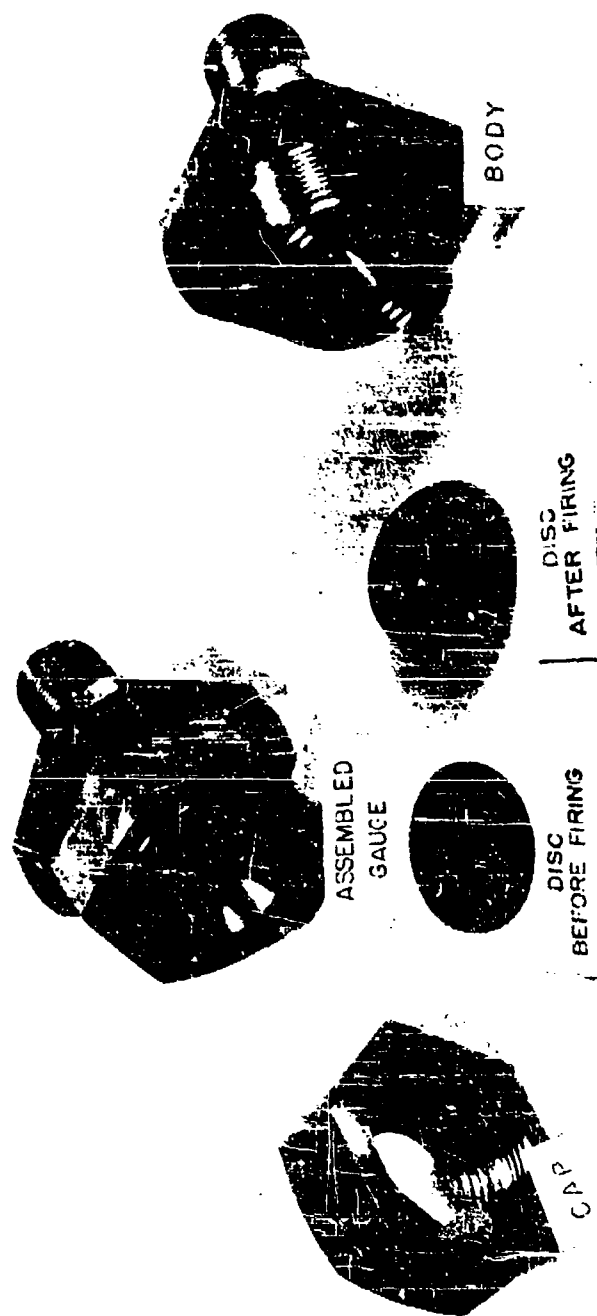
Fig. 31. Modugno gauge.

As many as eight Modugno gauges were placed in a large static pressure chamber and subjected to desired pressures indicated on a Bourdon gauge. Resulting deformations were measured to .001 in. with a micrometer depth gauge. Diaphragm thicknesses were measured before and after deformation to .005 in.

The reproducibility of the experiment was investigated at pressures of 5000 lbs/in.^{2} and 10,000 lbs/in.^{2}. The variation of damage with diaphragm thickness was studied for several pressures. Also, static depressions were used to calculate the tensile strength of the diaphragm.

Typical results of consistency experiments listed in Table XXVI show that damages for disks cut from a single diaphragm of uniform thickness could be reproduced to somewhat better than 2%. (Each set of four was deformed simultaneously.)

Table XXVI - Static deformations

5000 lbs/in^2		10,000 lbs/in^2		10,000 lbs/in^2	
Thickness (in.)	Damage (in.)	Thickness (in.)	Damage (in.)	Thickness (in.)	Damage (in.)
.0782	.087	.0773	0.169	.0773	0.167
.0784	.088	.0786	0.169	.0777	0.167
.0786	.089	.0781	0.167	.0774	0.168
.0782	.085	.0775	0.166	.0773	0.169

In order to get an empirical correction for thickness variations, a number of disks were deformed at pressures of 4600, 5000, 6000, 7000, 8000, and 9000 lbs/in^2. The results are plotted in Figure 32.

The tensile strength of a thin diaphragm may be calculated by means of the theoretically derived formula[31]:

$$\text{T.S.} = \frac{Rp}{2t} = \left(\frac{r^2 + x^2}{4tx}\right) \, p \tag{37}$$

where R is the radius of curvature, p the static pressure, t the thickness of the diaphragm, r the radius of the undamaged diaphragm, and x the maximum deformation.

31/ A. N. Gleyzal, Taylor Model Basin, U. S. Navy Report No. 490. Sept 1942.
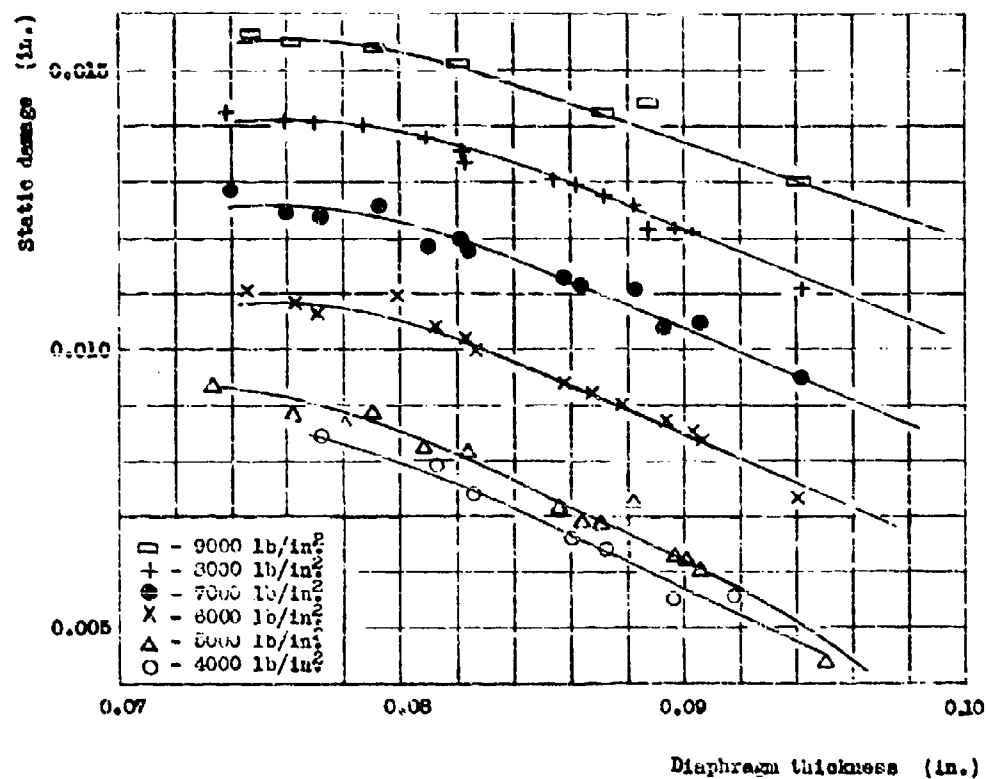
Fig. 32. Static damage vs. diaphragm thickness
(steel diaphragms in Modugno gauges).

This formula takes no account of increase of yield strength with cold working, plastic bending, the decrease in thickness, or the elastic recovery of the diaphragm. We have calculated tensile strength by means of this formula using the diaphragm thickness after deformation. These data for three pressures are plotted in Figure 33. It may be noted that there are large variations outside the experimental error (about 3%) in tensile strength with thickness and pressure. The negative slope for the thinner diaphragms and the shift in the minimum can be qualitatively explained by work hardening. The positive slope which increases with decreasing pressure may be qualitatively explained by elastic recovery.

6. Study of Errors

Mounting the gauges on a steel ring accounted for a reduction in the standard deviation of the damage of one diaphragm from the mean of four diaphragms on a shot from 5% to less than 2%. Correspondingly, the probable error of the damage of one diaphragm from the mean of four diaphragms was reduced from 3.4% to about 1%. (Cf Section V,3,c).

594
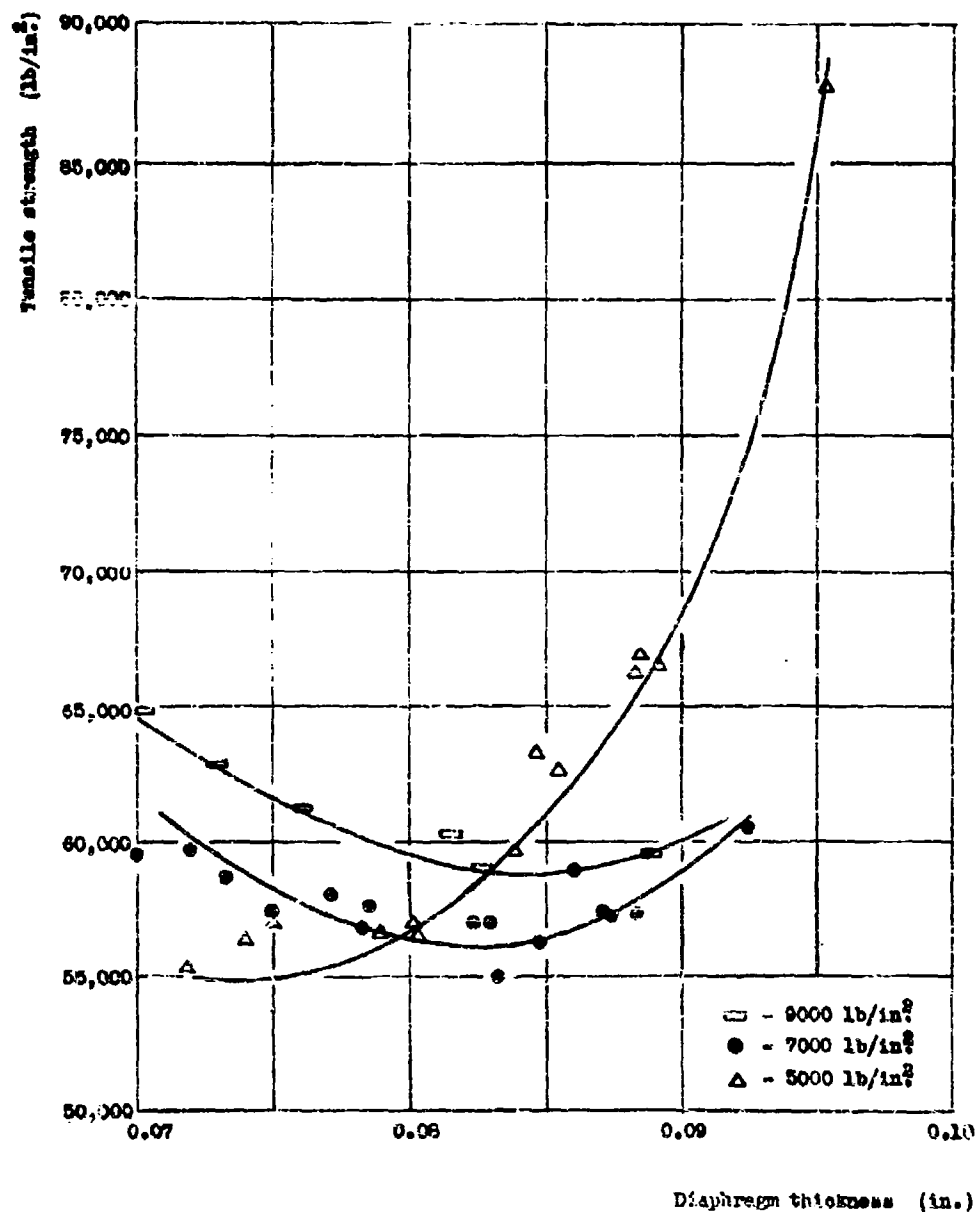
Fig. 33. Change of tensile strength with diaphragm thickness after deformation.

THEORETICAL ANALYSIS OF THE DISHING OF SIX INCH DIAMETER COPPER DIAPHRAGM GAUGES BY UNDERWATER EXPLOSIONS

E. N. Fox and W. T. Rollo
Admiralty Undex Works, Rosyth, Scotland

British Contribution

March 1947

THEORETICAL ANALYSIS OF THE DISHING OF SIX INCH DIAMETER COPPER DIAPHRAGM GAUGES BY UNDERWATER EXPLOSIONS

E. N. Fox and W. T. Bells

Admiralty Undex Works

March 1947

*   *   *   *   *   *   *   *   *

Summary.

An empirical analysis of the results of the dishing of 36 six-inch diameter copper diaphragm gauges is given. From this analysis an empirical formula connecting weight of charge, distance of gauge from charge and the volume of dishing is derived.

A theoretical analysis is undertaken assuming the diaphragm deform plastically into a parabolic shape under the action of the primary pressure pulse behaving as a small amplitude plane wave, the pressure decaying exponentially with time. From the relatively poor agreement between experimental and theoretical volumes of dishing it is concluded that the basic assumptions and/or data must err considerably in one or more respects. Before any further refinements of the basic theoretical analysis are attempted it is recommended that controlled experiments should be carried out to check first whether the discrepancy depends primarily on inaccuracies in the assumed data and form of the incident pressure pulse.

Introduction.

In the past, six inch diameter copper diaphragm gauges have been extensively used, mainly for comparing the underwater damaging efficiencies of various explosives. Little attempt, however, has been made to determine the physical entity measured by the gauge, this latter being regarded as an empirical "damage gauge" from the point of view of comparing explosives. As there is now available a considerable mass of data obtained by the use of these gauges it seemed opportune to attempt a theoretical analysis. The results of this analysis are now presented in this report.

Experimental data and empirical analysis.

The results of the dishing of 36 gauges are given in Table 3, these results having been obtained in numerous trials some of which were carried out primarily to compare the underwater damaging efficiencies of various explosives, others to compare different qualities of steel in box models and others to compare the efficiency of riveted targets with that of welded targets. Only the results of shots in which T.N.T. was used are analysed in this report.

As several empirical formulae of the power-law type, i.e.

$$V = KW^\alpha / D^\beta \tag{1}$$

where

V = volume of dish in cubic inches.

W = weight of charge in lbs.

D = distance of gauge from charge in feet.

K, α and β being constants, have been used in the past, it seemed advisable to obtain an empirical formula of this type from the analysis of as many results as are available at present. Expressed logarithmically equation (1) may be written

$$\log V = \log K + \alpha \log W - \beta \log D \tag{2}$$

and ....

and the experimental data in Table 1 have been fitted to this formula by the method of least squares. In Table 1 it will be seen that there are several groups of repeat shots. In applying the method of least squares the average value of V for each group has been used, being weighted according to the number of shots in the group. No allowance has been made for variations in the thickness of the diaphragms which deviate by 5% at most from the nominal value of 0.1916 inch.

The formula resulting from this analysis is

$$\log V = 1.409 + 0.856 \log W - 0.791 \log D \tag{3}$$

which expressed in power-law form is

$$V = 25.63 \, W^{0.856}/D^{0.791} \tag{4}$$

differing little from that most recently published by S.H.O. viz.

$$V = 27.3 \, W^{0.85}/D^{0.80} \tag{5}$$

The fact that the probable errors in V resulting from the use of formula (4) and (5) are ± 2.5% and ± 2.6% respectively shows that the difference between these two formulae is insignificant.

In figure 1 the experimental data of Table 1 is fitted to the empirical formula (4) and in figure 2 a nomogram is given connecting W, D and V using this formula.

Theoretical analysis.

   (i)   Basic assumptions.

   (a)   For the practical range of distance from charge to gauge in the trials considered in this report, varying from about 25 to 70 charges radii, the opening of the diaphragms is assumed to be caused by the primary pressure pulse behaving as a small amplitude plane wave. The pressure pulse is assumed to decay exponentially with time.

   (b)   The gauge is assumed sufficiently small relative to the effective length of pulse for diffraction to be complete so that the gauge experiences no bodily motion.

   (c)   The diaphragm is assumed to deform into a parabolic shape and to absorb energy plastically. For a given mean deflection the amount of energy is assumed to be the same as that measured statically under uniform lateral pressure. For an amended form of assumption to take into account the effect of dynamic loading see paragraph (iii).

   (ii)   Solution assuming incompressible flow and Wood's formulae.

Neglecting the compressibility of water the equation of motion connecting the mean deflection d of the diaphragm and time t both expressed in non-dimensional units is shown in the Appendix to be

$$\frac{1}{\gamma^2} \frac{d^2 \bar{d}}{d\tau^2} + F(\bar{d}) = \frac{p_0}{p_1} e^{-\tau} \tag{A.37}$$

y being a numerical constant depending upon the effective dimensions of the diaphragm allowing for the increase in inertia due to the layer of water following the motion of the diaphragm whilst $p_1 F(\bar{d})$ is the static pressure required to produce a non-dimensional mean deflection $\bar{d}$.

It was found from the static pressure-volume calibration curve reproduced in figure 3 that a good approximation for the function $F(\bar{d})$ is given by the simple linear expressions

$$F(\bar{d}) = \bar{d} \text{ for } 0 \leq \bar{d} \leq 0.5$$
$$= 2\bar{d} - 0.5 \text{ for } \bar{d} \geq 0.5$$

in .....

In solving the equation of motion the parameters p_0 and n of the pressure-time equation

$$pl = p_0 e^{-nt} \qquad (a.1)$$

as given by Wood's formulae were used viz.

$$p_0 = \frac{11,000 \; W^{0.38}}{D} \; \text{lbs./sq.in} \quad \left.\begin{array}{c} \end{array}\right\} \quad W \text{ in } t.$$

$$n = \frac{9200}{D^{0.77}} \; \text{sec}^{-1} \quad \left.\begin{array}{c} \end{array}\right\} \quad D \text{ in ft.} \qquad (6)$$

giving

$$\frac{p_0}{P_1} = \frac{12 \; W^{0.38}}{D} \quad \left.\begin{array}{c} \end{array}\right\}$$

$$n = \frac{0.453}{W^{0.27}} \qquad (7)$$

The results of solving the equation of motion for the maximum values of d are summarised in Table 2 from which it will be seen that the calculated values are from 20% to 40% in excess of the observed experimental values.

(iii)   Effect of dynamic loading.

Undoubtedly, at least part of this discrepancy between calculated and observed volumes of dishing is due to the assumption that the energy absorbed in deforming the diaphragm is the same as that measured statically under uniform lateral pressure.   To take account of dynamic loading it is simplest to derive a hypothetical dynamic pressure-volume calibration curve from the static calibration curve by increasing the pressure ordinates by a fixed percentage.   In Table 3 are shown the percentage increases required in using the calculated values of volume of dishing to within about 3% of the observed values.   From this table it is seen that the percentage increases required vary from 40% to 60%.

That such large percentage increases really obtain in practice seems unlikely so that we are next led to suspect that the discrepancy between theoretical and experimental volumes of dishing may be at least partly accounted for by errors in the values assigned to the parameters of the pressure-time equation by Wood's formulae.

(iv)   Effect of replacing Wood's formulae by the corresponding American formulae.

To check whether the discrepancy between calculated and observed volumes of dishing in Table 2 is due in part to errors in Wood's formulae for the parameters of the pressure-time equation the calculations were repeated replacing Wood's formulae by those published in American reports (1).

viz.

$$p_0 = \frac{20800 \; W^{0.38}}{D^{1.14}} \; \text{lbs./sq.in.} \quad \left.\begin{array}{c} \end{array}\right\} \quad W \text{ in lbs.}$$

impulse

$$\frac{o}{n} = \frac{1.3 \; W^{2/3}}{D} \; \text{lbs. sec./sq.in.} \qquad (8)$$

whence

$$n = \frac{13600}{W^{0.29} \; D^{0.14}} \; \text{sec}^{-1} \quad \left.\begin{array}{c} \end{array}\right\} \quad D \text{ in ft.}$$

giving

$$\frac{p_0}{P_1} = \frac{0.8 \; W^{0.38}}{D^{1.14}}$$

and

$$n = \frac{14.39}{W^{0.29} \; D^{0.14}} \qquad (9)$$

The results of these calculations which were carried out by Admiralty Computing Service (2) are summarised in Table 4.   On average the values for the calculated volumes of dishing show a reduction of about 9% on the values given by using Wood's formulae.   Despite this improvement, however, the calculated volumes of dishing are still 10% to 30% in excess of the observed values.

(v) .....

— 4 —

(v) Effect of taking into account the compressibility of water.

There still remains another likely source of error to account for the poor agreement between the theoretical and experimental volumes of dishing. So far we have assumed incompressible flow whereas it would be more correct to allow for the compressibility of water.

As shown in the Appendix the equation of motion taking into account the compressibility of water is given by

$$\frac{1}{y^2}\frac{d^2z}{dT^2} + F(z) = \frac{p_0}{p_1}e^{-nT} + x\int_0^1 \phi_3(x)\,d^m(T-x)\,dx \qquad (A.35)$$

x being a numerical constant and ϕ_3 and z rather complicated functions.

Integrating this equation by parts three times gives

$$\left(\frac{1}{y^2} - \frac{6nx}{315}\right)\frac{d^2z}{dT^2} + \frac{\pi x}{6}\frac{dz}{dT} + F(z)$$

$$= \frac{p_0}{p_1}e^{-nT} + x\int_0^1 \phi_3^-(x)\,d(T-x)\,dx$$

$$= \frac{p_0}{p_1}e^{-nT} + x\int_0^1 d(x)\,d(T-x)\,dx \qquad 0 < T < 1 \qquad (A.33)$$

This equation was numerically integrated by Admiralty Computing Service for two extreme cases, viz. 650 lbs. T.N.T. at 16/ foot and 5 lbs. at 10 feet corresponding to charge distances of 88 and 17 charge radii respectively.

The effect of this more refined treatment by allowing for compressibility is very small, the calculated volumes of dishing being thereby reduced by only about 2% as shown in Table 4.

General discussion and conclusions.

The original calculated values and the observed values of dishing are compared in Table 2 and exhibit a large discrepancy ranging from 20% – 40% overestimation by the theory. As possible sources of this discrepancy we have considered

(a) increased energy absorption under dynamic loading as compared with static loading.

(b) use of the American formula (e), based on more modern data than Wood's formula (d), for the parameters of the pressure pulse.

(c) allowance for the compressibility of the water.

Of these the third possibility (c) introduces only a very small correction of order 3% and is only therefore a minor factor in the discrepancy. The second possibility (b) however produces an appreciable improvement in the agreement but still leaves a remaining discrepancy of order 10% – 30%. If this is primarily due to the first possibility (a) we should require an overall increase of order 25% – 35% of resistance to dishing under dynamic as opposed to static loading. This seems unduly high for the annealed copper used in the diaphragms since, so far as is known, there is no evidence to indicate an increase of more than about 15% for copper due to dynamic loading.

There remain, of course, other possible sources of error in the assumptions which we have not examined, on account of their implicit complexity. Thus we have neglected diffraction effects round the gauge and bodily motion but it seems unlikely that such is so important for the present purpose in view of the observed fact that the two diaphragms on opposite sides of the gauge exhibit the same overall variation of dishing with charge weight etc. The assumption that the dish is of parabolic shape throughout is, of course, only an approximation and will certainly not be valid in the early stages of dishing when the deformation will correspond more to a plastic wave travelling inwards from the circumference. It seems unlikely, however, that the difference in

and .....

the mode of dishing leading to the same final shape of dish will make a large difference in the final energy absorbed, always provided that the energy is absorbed in the same way by plastic stretching and thinning of the diaphragm. It is conceivable, though somewhat unlikely, that the plastic wave mechanism involves a large absorption of energy in bending since each element is first bent in one direction and then back again as the wave passes. Such a source of energy absorption is not allowed for in our theory based primarily on plastic stretching which certainly predominates in the case of dishing under static load. Since the energy absorption due to stretching depends on the square of the dished volume we should need a large contribution from any such bending mechanism to account for the discrepancies shown in Table 2.

Finally we have made throughout the customary assumption that the pressure-pulse varies exponentially in time whereas we know that this is not accurately the case in practice, the pulse being rather of an initial exponential form followed by a tail decaying more slowly. In particular we have, in the absence of direct information, derived the formula for n given in equation (8) from the associated maximum pressure and impulse formulae, the latter of which depends somewhat on the tail of the wave. For the initial part of the wave n should be higher than assumed and this would tend to improve agreement, more especially for the intermediate charge weights where the pulse is neither so short that impulse is the deciding factor nor so long that maximum pressure is the main parameter. The fact that the discrepancy in Table 8 is greatest for the intermediate charge weight of 100 lb. suggests that part of the error at least is due to this lack of accurate representation of the pressure-time for the incident pulse. In view of this it seems desirable to carry out controlled experiments in which copper diaphragms and piezo-gauges are both used so that the observed pressure time curve can be used direct in the present theory, i.e. in place of the assumed exponential term on the right-hand side of equation (A.37). Any further refinements of the theory are better deferred pending a better check on the present theory obtained from such experiments.

References.

(1)   Division R, N.D.R.C. Interim Report U.E.10

(2)   Report S.P.E./A.C.S.83 by Admiralty Computing Service.

APPENDIX

1. *Symbols*.

p_i = Incident pressure.

p_o = maximum pressure of pressure pulse.

n = decay constant of pressure pulse p_i $p_o e^{-nt}$

p' = relief pressure due to motion of diaphragm.

a = radius of diaphragm.

h = thickness of diaphragm.

ρ_o = mass density of water.

ρ = mass density of diaphragm.

c = velocity of sound in water.

h_1 = effective thickness of diaphragm due to layer of water following the motion of the diaphragm.

$$= h + \frac{256 \, a \, \rho_o}{105 \, \pi \rho}$$

η = mean deflection of diaphragm.

$$= h_1 \, z$$

t = time.

p_1 = arbitrary pressure unit.

$p_1 \, (z)$ = static pressure required to produce non-dimensional mean deflection z.

$$T = \frac{c}{2a} t$$

$$N = \frac{2a}{c} n$$

$$v = \sqrt{\frac{3 \, p_1 \, a^2}{\rho_1 \, c^2}}$$

$$K = \frac{4 \, \rho_o \, c^2 \, h_1}{\pi \, a \, p_1}$$

Other symbols are defined in the text.

Subscripts to z and ϕ denote integration:-

$$z_n \, (T) = \int_0^T z_{n-1} \, (T) \, dT; \quad \phi_n \, (x) = \int_1^x \phi_{n-1} \, (x) \, dx.$$

2. *Equation of motion of diaphragm*.

The incident pressure pulse is assumed to be

$$p_i = p_o e^{-nt} \tag{1}$$

while the pressure at any point of the diaphragm is

$$p = p_i + p' \tag{2}$$

where .....

where p' is the relief pressure due to the motion of the diaphragm.

The diaphragm is assumed to deform plastically into the parabolic form

$$w = 2\eta \left(1 - \frac{r^2}{a^2}\right) \tag{3}$$

and the energy absorbed in dishing to a mean deflection η is assumed to be $\phi(\eta)$ which is known from static tests.

The kinetic energy of the diaphragm in dishing is

$$\frac{1}{2} \int_0^a \rho h \left(\frac{dw}{dt}\right)^2 2\pi r dr = \frac{2}{3} \pi a^2 \rho h \left(\frac{d\eta}{dt}\right)^2 \tag{4}$$

The rate of increase of the kinetic energy is given by

$$\frac{4}{3} \pi a^2 \rho h \frac{d^2\eta}{dt^2} \frac{d\eta}{dt} \tag{5}$$

while the rate of absorption of energy plastically is

$$\frac{d}{dt} \phi(\eta) = \phi'(\eta) \frac{d\eta}{dt} \tag{6}$$

The rate of work on the diaphragm by the pressure p is

$$\int_0^a p \frac{dw}{dt} 2\pi r dr = 4\pi \frac{d\eta}{dt} \int_0^a p \left(1 - \frac{r^2}{a^2}\right) r dr \tag{7}$$

so that the equation of motion is given in the form

$$\frac{4}{3} \pi a^2 \rho h \frac{d^2\eta}{dt^2} + \phi'(\eta) = 4\pi \int_0^a p \left(1 - \frac{r^2}{a^2}\right) r dr \tag{8}$$

if the pressure in a static test is p_s then

$$\phi(\eta) = \int_0^\eta \pi a^2 p_s(\eta) d\eta \tag{9}$$

whence

$$p_s(\eta) = \frac{\phi'(\eta)}{\pi a^2} \tag{10}$$

so that the equation of motion may be written using (1) and (2) as

$$\frac{4}{3} \rho h \frac{d^2\eta}{dt^2} + p_s(\eta) = p_0 e^{-nt} - \frac{4}{a^2} \int_0^a p' \left(1 - \frac{r^2}{a^2}\right) r dr \tag{11}$$

In this equation p' is a function of r and t and at any point $r = r_1$ is given by

$$(p')_{r_1} = \frac{\rho_0}{2\pi} \int \int_s \frac{1}{R} \left[\frac{d^2 w}{dt^2}\right]_{t - \frac{R}{c}} dS \tag{12}$$

where the integral is taken over the whole diaphragm and R is the distance from the point P (at which p' is being evaluated) to the element dS at the point Q (figure 4). This expression is based on the assumption that diffraction effects due to the finite size of gauge can be neglected. Unfortunately, except in the very early stages for the front diaphragm of a "face on" gauge, the diffraction phenomena are far too complex to take into account.

However, it may be noted that the gauge always has a diaphragm at each end and in practice it is usually found that the front and back diaphragms show about the same amount of dishing. This indicates that the overall effect of diffraction on the dishing is small and suggests our assumption as a reasonable simplification to make the theory tractable.

If Q is at distance r_2 from the centre then

$$\frac{d^2 w}{dt^2} = 2 \frac{d^2 \eta}{dt^2} \left(1 - \frac{r_2^2}{a^2}\right) \tag{13}$$

so that

$$(p'')_{r_1} = \frac{\rho_0}{\pi} \int \int \left\{ \frac{\ddot{\eta}\left(t - \frac{R}{c}\right)}{R} \left(1 - \frac{r_2^2}{a^2}\right) \right\} dS \tag{14}$$

From Figure 4 we have the following relation between R, r_1 and r_2

$$r_2^2 = r_1^2 + R^2 - 2 R r_1 \cos \alpha \tag{15}$$

Before simplifying the integral in (14) and the resulting integral in (11) we shall put the equations in non-dimensional form using the following substitutions:-

$\eta = h_1 \bar{\eta}$		$p' = \frac{p_1 K P'}{16}$	
$t = \frac{2c}{c} T$			
$p_s = p' F(\bar{\eta})$		$r_1 = a x_1$	
$n = \frac{L}{2a} N$	and	$r_2 = a x_2$	
$K = \frac{4 \rho_0 c^2 h_1}{\pi a p_1}$		$R = a X$	
$J^2 = \frac{3 \rho_1 a^2}{\mu n_1^2 c^2}$		$dS = a^2 dS'$	(16)

where

$$\frac{h_1}{r} = 1 + \frac{256 \rho_0 a}{105 \pi r^4}$$

Equation (14) then becomes

$$\frac{p_1 K P'}{16} = \frac{\rho_0 h_1 c^2}{4 \pi a} \int \int \frac{\ddot{\eta}\left(T - \frac{X}{2}\right)(1 - x_2^2)}{X} dS' \tag{17}$$

whence

$$p' = \int \int \frac{\ddot{\eta}\left(T - \frac{X}{2}\right)(1 - x_2^2)}{X} dS' \tag{18}$$

in which $\ddot{\eta}$ is regarded as a function of T and the surface integral is taken over a circle of unit radius (Figure 5). Also from (11) and (16) the equation of motion becomes

$$\frac{h}{J} \frac{h}{h_1} \frac{d^2 \bar{\eta}}{dt^2} + F(\bar{\eta}) = \frac{p_0}{p_1} e^{-aT} - \frac{Kl}{8 \gamma} \tag{19}$$

where

$$l = 2 \pi \int_0^1 p'(x_1, T)(1 - x_1^2) x_1 dx_1 \tag{20}$$

and P' is given by equation (18).

Finally the non-dimensional form of equation (15) is

$$x_2^2 = x_1^2 + X^2 - 2 X x_1 \cos \alpha \tag{21}$$

2...

3.   *Calculation of relief pressure.*

In order to simplify (16) we take polar coordinates X, α with origin P (Figure 5). Then using (21) we obtain

$$\delta S' = X \, dX \, d\alpha \qquad (22)$$

so that after integration by parts with respect to X and use of geometry of Figure 5 we find

$$\sim = \int_0^{\pi} \int_0^{X} z^* \left(T - \frac{x^2}{2}\right)(1 - x_1^2 - x^2 + 2 x x_1 \cos\alpha)\, dx \, d\alpha \qquad (23)$$

$$= 8\pi (1 - x_1^2)\, z'\,(T) - 32\pi z_1\,(T) + 8\int_0^{2\pi} \pi \left(T - \frac{x'}{2}\right)\cos\theta\, d\alpha$$

$$+ 16\int_0^{2\pi} z_1 \left(T - \frac{x'}{2}\right)\, d\sigma \qquad (24)$$

$$= 8\pi(1 - x_1^2)\, z'\,(T) - 32\pi z_1\,(T) + 8 \oint \frac{2 z_1\left(T - \frac{x'}{2}\right)\cos\theta + z\left(T - \frac{x'}{2}\right)\cos^2\theta}{x'}\, d\sigma \qquad (25)$$

the integral being taken round the boundary.

4.   *Contribution of relief pressure to equation of motion.*

From equations (20) and (25) we have

$$I = 8\pi^2 z'(T) \int_0^1 (1 - x_1^2)^2 x_1\, dx_1 - 64\pi^2 z_1\,(T) \int_0^1 (1 - x_1^2)\, x_1\, dx_1$$

$$+ 8 \iint (1 - x_1^2) \oint \frac{z\left(T - \frac{x'}{2}\right)\cos^2\theta + 2 z_1\left(T - \frac{x'}{2}\right)\cos\theta}{x'}\, dS\, d\sigma' \qquad (26)$$

the first two terms giving a contribution

$$I_1 = \frac{4\pi^2}{3} z'\,(T) - 16\pi^2 z_1\,(T) \qquad (27)$$

Interchanging the line and surface integrals and using symmetry the last term of (26) gives a contribution

$$I_2 = 16\pi \iint \frac{z\left(T - \frac{x'}{2}\right)\cos^2\theta + 2 z_1\left(T - \frac{x'}{2}\right)\cos\theta}{x'}(1 - x_1^2)\, dS' \qquad (28)$$

where this integral is to be evaluated for any given element dS of the circumference and will by symmetry be the same for any element on the circumference.

Taking polar coordinates (X', θ) as in Figure 5 then

$$\frac{I_2}{16\pi} = 2\int_{-\pi/2}^{\pi/2} \int_0^{2\cos\theta} \left\{ z\left(T - \frac{x'}{2}\right)\cos^2\theta + 2 z_1\left(T - \frac{x'}{2}\right)\cos\theta \right\}(1 - x_1^2)\, dx' \, d\theta \qquad (29)$$

Using the fact that

$$x_1^2 = x'^2 + 1 - 2 x' \cos\theta \qquad (30)$$

we finally have after some integration by parts and thence using (27)

$$I_2 \ldots\ldots$$

$$I_2 = \ldots m^2 a_1(T) = \epsilon \pi \int_0^1 \phi(x)\, \ddot{a}\,(T - x)\, dx$$

$$I = \epsilon \frac{\pi^2}{3} a'(T) - \epsilon \pi \int_0^1 \phi(x)\, \ddot{a}\,(T - x)\, dx \tag{31}$$

where $\quad x = \cos\theta$

and $\quad \phi(x) = \ldots \theta - \frac{16}{9}\sin 2\theta + \frac{3}{3}\sin 4\theta$ $\tag{32}$

5. *Final forms of equation of motion.*

Substituting from (31) in (19) we have for the equation of motion

$$\frac{h}{\gamma^2 h_1} \cdot \frac{d^2 a}{dT^2} + F(a) = \frac{p_0}{p_1} e^{-kT} - \frac{\pi \lambda}{6}\frac{da}{dT}$$

$$+ \kappa \int_0^1 \phi(x)\, \ddot{a}\,(T - x)\, dx \tag{33}$$

For alternative form we have

$$\int_0^1 \phi(x)\, \ddot{a}\,(T - x)\, dx = \left[\phi_1(x)\, \ddot{a}\,(T - x) + \phi_2(x)\, \dddot{a}\,(T - x) + \phi_3\, \ddot{a}\,(T - x)\right]_0^1$$

$$+ \int_0^1 \phi_3(x)\, \dddot{a}\,(T - x)\, dx$$

$$= \frac{\pi}{6}\, a'(T) - \frac{68}{315}\, a'''(T) \tag{34}$$

$$+ \int_0^1 \phi_3(x)\, \dddot{a}\,(T - x)\, dx$$

so that the equation of motion may also be written as

$$\frac{1}{\gamma^2}\frac{d^2 a}{dT^2} + F(a) = \frac{p_0}{p_1} e^{-kT} + \kappa \int_0^1 \phi_3(x)\, \dddot{a}\,(T - x)\, dx \tag{35}$$

since $\quad \dfrac{h}{\gamma h_1} = \dfrac{1}{\gamma^2} - \dfrac{68\,\kappa}{315} \tag{36}$

form (33) is more suitable in the early stages when T is small while form (35) is more suitable when T is large. The initial conditions are

$$a(T) = a'(T) = 0 \quad T \leqslant 0$$

Since $a''(T)$ is discontinuous at $T = 0$ and $a'''(T)$ is therefore infinite, the form (33) should be used for $0 \leqslant T \leqslant 1$.

6. *Incompressible approximation.*

If the compressibility term, i.e. the integral term in form (35) is small then a first approximation is given by neglecting it, i.e.

$$\frac{1}{\gamma^2}\frac{d^2 a}{dT^2} + F(a) = \frac{p_0}{p_1} e^{-kT} \tag{37}$$

which gives

$$\frac{1}{\gamma^2}\frac{d^2 a}{dT^2} = -\frac{p_0}{p_1} k e^{-kT} - F(a)\frac{da}{dt} \tag{38}$$

Now since p_s and therefore $F(z)$ increases with deflection we have $F'(z) > 0$ and up to time of maximum deflection $\frac{dz}{dt} > 0$ and therefore $\frac{d^2z}{dt^2} < 0$ up to time of maximum deflection.

The compressibility term is $\kappa \displaystyle\int_0^1 \phi_3(x)\, z''\,(T-x)\,dx$

$$= \kappa z''(T-\epsilon) \int_0^1 \phi_3(x)\,dx \qquad\qquad \text{since } \phi_3(x) > 0$$

$$= \frac{\kappa \pi}{64}\, z''\,(T-\epsilon) \qquad\qquad \text{where } 0 < \epsilon < 1 \quad (39)$$

Hence, if compressibility is small we can solve on the assumption that it is negligible and then estimate the error by expression (39). Since $z''(T) < 0$ the error will involve a relief pressure and therefore the calculated deflection on the incompressible approximation will be an over-estimation.

7.   *Properties of the function* $\phi_3(x)$

The following properties of $\phi_3(x)$ defined by

$$\phi_3(x) = \frac{1}{3} y(1-4y^2)(\theta \cos\theta - 1 + \frac{1}{3}y^2 + \frac{1}{15}y^4 + \frac{2}{105}y^4) + \frac{16\,y^6}{315}$$

$$(40)$$

where $x = \cos\theta$

and $y = \sin\theta$

may be noted:-

(a) $\phi_3''(x) = \phi(x)$

$$= 4\theta - \frac{10}{3}\sin 2\theta + \frac{2}{3}\sin 4\theta \qquad\qquad (39)$$

(b) $\phi_3(x) > 0, \quad 0 \leq x \leq 1$ $\qquad\qquad\qquad\qquad (41)$

(c) $\phi_3(x) \to \frac{64}{315}$ as $x \to 0$ $\qquad\qquad\qquad (42)$

(d) $\phi_3(x) \to \frac{32\,y^6}{315}$ as $x \to 1, \quad y \to 0$ $\qquad (43)$

(e) $\displaystyle\int_0^1 \phi_3(x)\,dx = \frac{\pi}{64}$ $\qquad\qquad\qquad\qquad (44)$

TABLE 1. EXPERIMENTAL DATA FOR THE DISHING OF 6 INCH
DIAMETER COPPER DIAPHRAGM GAUGES. T.N.T. CHARGES.

CHARGE			VOLUME of DISH	AVERAGE VOLUME	VOLUME CALCULATED from
Weight	Distance				$V = \dfrac{25.65\ W^{0.456}}{D^{0.791}}$
(lbs.)	(ft)	Charge Radii	(c.ins.)	(c. ins.)	(c.ins.)
5	10	27	8.72		
5	10	27	8.80		
5	10	27	9.03	8.93	8.65
5	10	27	9.15		
5	15	40	6.34		
5	15	40	6.37		
5	15	40	6.42	6.43	6.38
5	15	40	6.60		
5	20	54	4.64		
5	20	54	4.72		
5	20	54	4.81	4.82	5.00
5	20	54	5.10		
100	25	25	15.23		
100	25	25	15.87		
100	25	25	15.87	15.86	16.44
100	25	25	16.15		
100	25	25	16.18		
100	40	39	11.21		
100	40	39	11.25		
100	40	39	11.25	11.28	11.33
100	40	39	11.31		
100	40	39	11.36		
100	50	49	9.02		
100	50	49	9.38		
100	50	49	9.42	9.38	9.50
100	50	49	9.52		
100	50	49	9.56		
300	40	27	19.22	19.22	18.70
300	60	41	13.12		
300	60	41	14.70	13.91	13.57
300	80	55	10.60		
300	80	55	11.30	10.95	10.81
650	83	44	15.30	15.30	14.94
650	117	62	12.00	12.00	11.39
650	133	70	10.20	10.20	10.20
650	167	88	8.65	8.65	8.60

TABLE 2.   COMPARISON OF EXPERIMENTAL AND THEORETICAL
VOLUMES OF DISHING DERIVED BY ASSUMING INCOMPRESSIBLE
FLOW AND WOOD's FORMULAE FOR THE PRESSURE-TIME EQUATION
PARAMETERS.

	CHARGE		OBSERVED VOLUME of DISH (c. ins)	$\frac{P_o}{P_1}$	N	CALCULATED VOLUME of DISH (c. ins)	RATIO Cald.Vol./Obsd.Vol.
Weight (lbs)	Distance (ft.)	Charge Radii					
5	10	27	8.9	2.24	0.416	11.8	1.33
	20	54	4.8	1.11		6.5	1.15
100	25	25	15.9	2.76	0.185	22.3	1.40
	50	49	9.4	1.38		12.8	1.36
300	40	27	19.2	2.62	0.138	24.2	1.26
	80	55	11.0	1.31		13.9	1.26
650	83	44	15.3	1.69	0.112	18.3	1.20
	167	88	8.65	0.841		10.7	1.24

TABLE 3.   SHOWING PERCENTAGE INCREASES IN THE PRESSURE
ORDINATES OF THE STATIC PRESSURE-VOLUME CALIBRATION
CURVE TO TAKE INTO ACCOUNT THE EFFECT OF DYNAMIC LOADING,
THE PERCENTAGE INCREASES BEING CHOSEN TO BRING THE
CALCULATED VOLUMES OF DISHING TO WITHIN ABOUT 5% OF THE
EXPERIMENTAL VALUES.

CHARGE		OBSERVED VOLUME of DISH (c. ins)	% INCREASE IN PRESSURE ORDINATE	CALCULATED VOLUME of DISH (c. ins)	RATIO Cald. Vol./Obsd. Vol.
Weight (lbs.)	Distance (ft.)				
5	10	8.9	60	9.4	1.06
	20	4.8	60	4.9	1.02
100	50	9.4	60	9.8	1.04
300	80	11.0	40	11.4	1.04
650	167	8.65	40	8.73	1.01

TABLE 4. COMPARISON OF EXPERIMENTAL AND THEORETICAL
VOLUMES OF DISHING ASSUMING AMERICAN FORMULAE FOR THE
PRESSURE-TIME EQUATION PARAMETERS.

CHARGE			OBSERVED VOLUME of DISH (c. ins.)	$\frac{P_0}{P_1}$	N	CALCULATED VOLUME of DISH (c. ins.)	RATIO Cald. Vol. Obsd. Vol.
Weight (lbs)	Distance						
	(ft.)	Charge Radii					
5	10	27	8.9	2.72	0.631	10.4 ⎫	1.17
	10	27	8.9	2.72	0.631	10.3⁄ ⎭	1.16
	20	54	4.8	1.24	0.573	5.6	1.17
100	25	25	15.9	2.99	0.233	21.3	1.34
	50	49	9.4	1.36	0.211	11.8	1.26
300	40	27	19.2	2.66	0.159	23.1	1.20
	80	55	11.0	1.21	0.144	12.8	1.16
	83	44	15.3	1.55	0.115	16.9	1.10
650	167	88	8.65	0.70	0.104	9.4 ⎫	1.05
	167	88	8.65	0.70	0.104	9.2⁄ ⎭	1.06

⁄ Values allowing for compressibility of water.
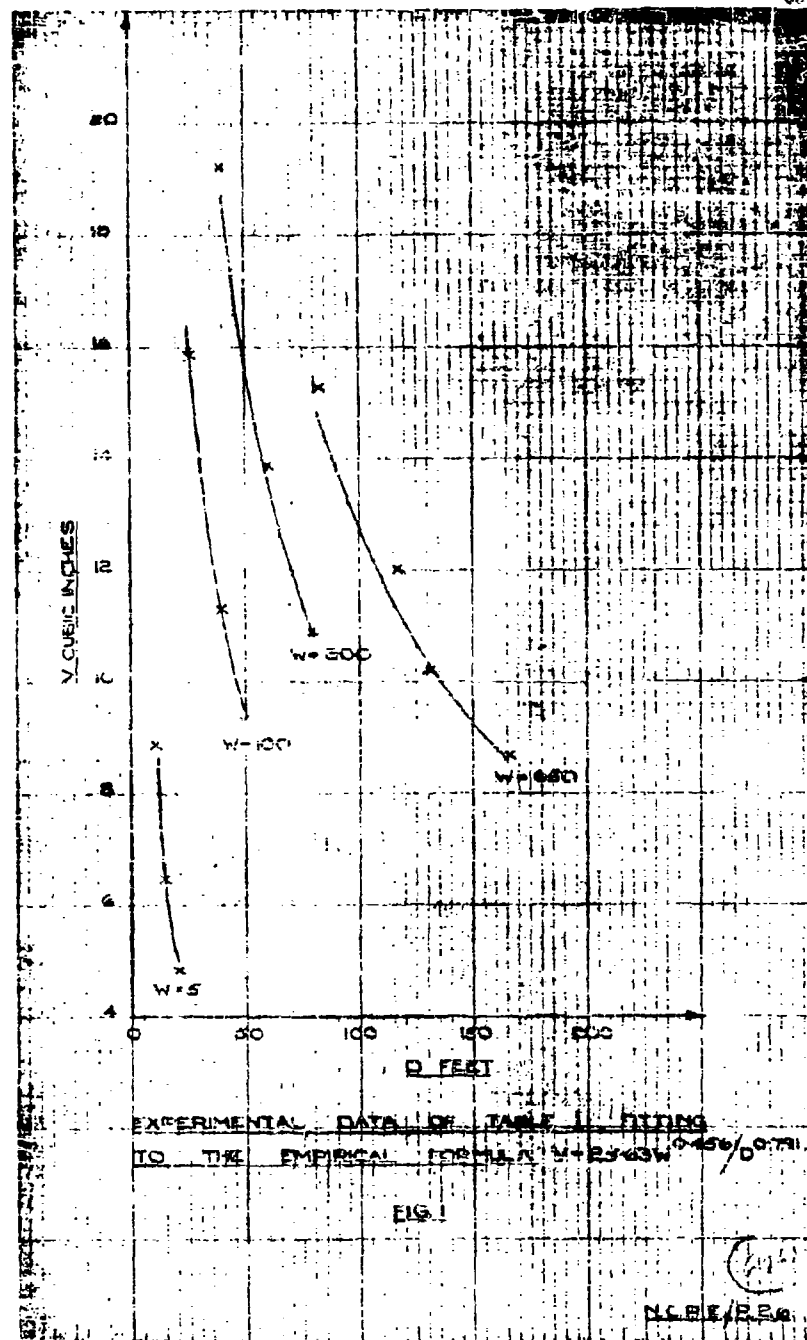
EXPERIMENTAL DATA OF TABLE I FITTING
TO THE EMPIRICAL FORMULA V = 2.543W 0.456/D 0.751

FIG. I

NOMOGRAM FOR THE VOLUME OF DISHING
OF INCH DIAMETER COPPER DIAPHRAGM GAUGES
FOR T.N.T. CHARGES

FIG. II

N.O.R.C./R.W.

FIG. III
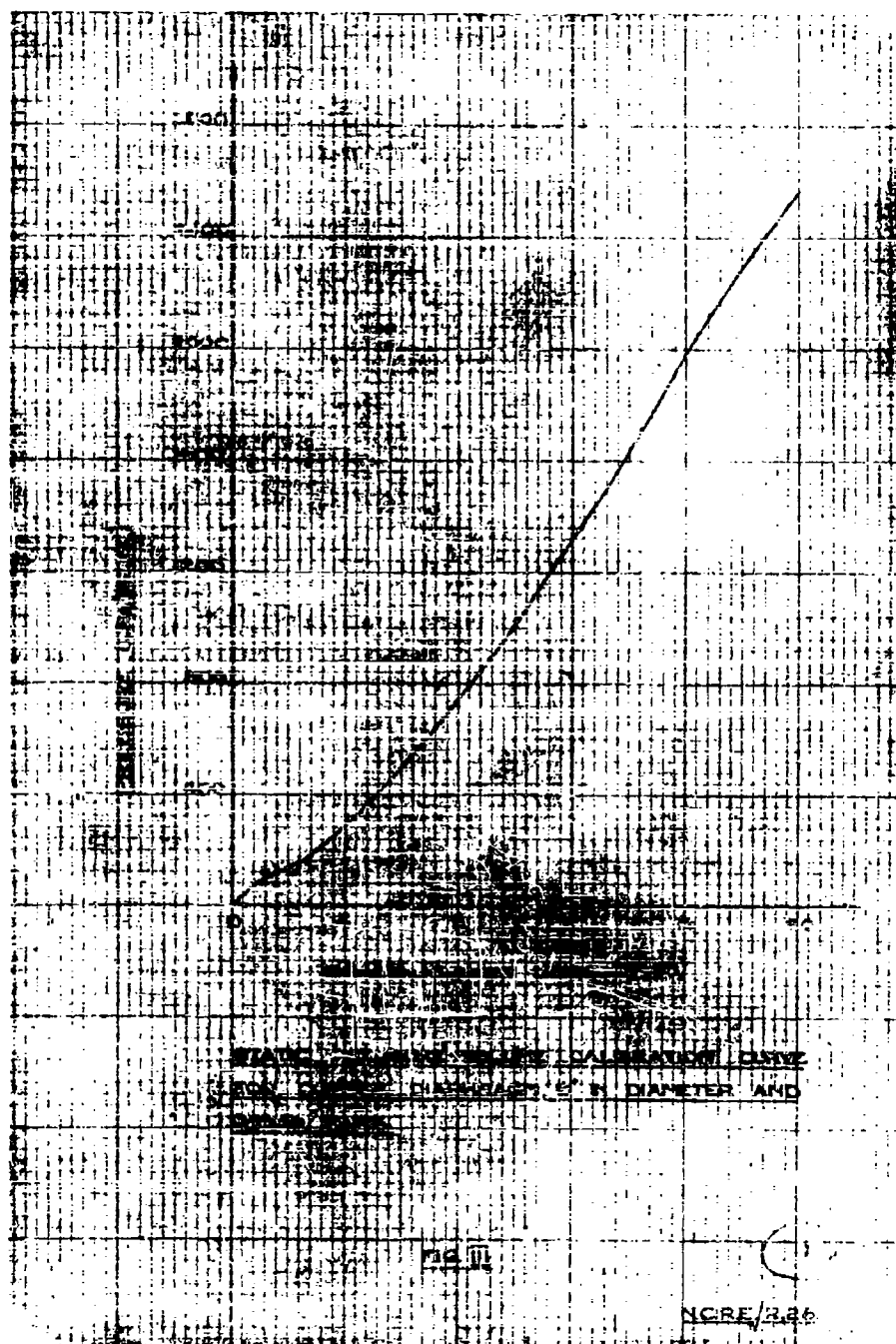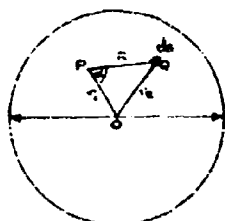
FIG. IV
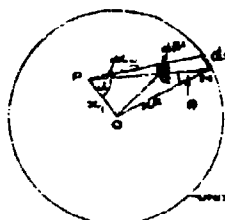
PN = x'
PQ = x
OP = x₁
OQ = x₂
ON = 1
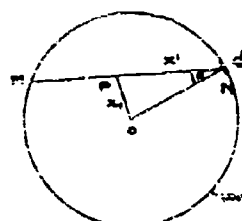
FIG. V

NP = x'
OP = x₁
ON = 1
NM = 2 cos θ

FIG. VI

N.C.11.E/R.26

EXPERIMENTS ON THE PLASTIC FAILURE OF CYLINDRICAL SHELLS

A. J. S. Pippard and L. Chitty
Imperial College of Science and Technology, London

British Contribution

1948

EXCERPT FROM VOLUME 3

OF

"THE CIVIL ENGINEER IN WAR"

"Experiments on the Plastic Failure of Cylindrical Shells."*

By Professor ALFRED JOHN SUTTON PIPPARD, M.B.E., D.Sc., M.I.C.E.,
and LETITIA CHITTY, M.A.

TABLE OF CONTENTS.

INTRODUCTION.

THE work described in this Paper was carried out during the war in the Civil Engineering Laboratories of the Imperial College of Science and Technology for the Director of Scientific Research, Admiralty, to supplement research into the behaviour of submarine hulls subjected to underwater explosions. The explosive work was carried out elsewhere partly on large scale specimens and partly on exactly similar models to those described in this Paper. The object of the investigation was to study the behaviour of cylindrical shells when loaded beyond the plastic range by forces acting on a small area of the surface, and under certain specified conditions of support. These conditions were most satisfactorily represented by bedding the cylinders for half their depth in carefully sifted sand, and with few exceptions the loads were applied through a ball or spherical-ended ram.

The experiments included static tests in a test frame, dynamic tests by means of dropping weights, and a few tests under hydrostatic pressure on a variety of specimens. Some of the results recorded were needed for a specific purpose, but the whole series is presented here as a general account of an experimental investigation which may be of value as a study of the plastic behaviour of cylindrical shells.

Scope of the Experiments

The original object of the investigation was to obtain information about the behaviour of cylinders stiffened in a particular way which will be described later. The manufacture of the test specimens was not easy and was delayed by the usual war-time difficulties in obtaining suitable material, scarcity of labour, and so on. During the waiting period certain makeshifts were adopted which extended the scope of the original tests and provided useful data of a more general character than was originally contemplated. Steel drums normally used for storing cement in the laboratory were found suitable for investigating the efficacy of the test rig and the results of these preliminary experiments led to the manufacture and test of a copper drum of approximately the same size for the purpose of investigating certain peculiarities which the steel drums had revealed.

It then appeared probable that useful results might be obtained from tests on small unstiffened cylinders, an ample supply of which were available in the tins used to pack coffee and household milk. The former were $3\frac{1}{4}$ inches in diameter, 4 inches long and made of 0·010-inch sheet metal; the latter were $3\frac{7}{8}$ inches in diameter, $4\frac{3}{8}$ inches long and of the same thickness. These tins were sufficiently near to the proportions of the standard test specimens in respect of diameter-thickness ratio to justify results. Further, while it would have been very difficult, or even impossible, to make laboratory tests on the standard specimens under impact loading or hydraulic pressure, it was a simple matter to make such tests on the small specimens. The experimental programme was therefore extended to include the following :—

   (1) Preliminary tests on steel and copper drums.
   (2) Tests on small cylinders.
   (3) Tests on large cylinders.

Tests were made on internally stiffened and unstiffened shells and on specimens with end-plates of different degrees of stiffness. Subsidiary tests of the material used and tests on single internal stiffening rings are also described.

Taylor's Hypothesis of Distortion.

Sir Geoffrey Taylor propounded the hypothesis that a thin cylindrical shell would distort without any stretching of the cylinder wall provided that the end plates had no stiffness out of their own plane and served only to maintain the circular form. He observed that when such a shell was subjected to a point load a transverse groove was formed and flats developed. The cross-section of the deformed cylinder through the groove is shown in *Fig. 1*.

If it be assumed that the lines running from the ends of the groove are straight and tangential to the undistorted part of the cross-section and

that no stretching of the shell occurs, it is a matter of simple geometry to obtain the relations

$$\frac{d}{a} = 2 - \frac{\theta \sin \theta}{1 - \cos \theta},$$

$$\frac{b}{2a} = \frac{\sin \theta - \theta \cos \theta}{1 - \cos \theta}.$$

The possibility of such an inextensible distortion was demonstrated by Taylor by a model made from a single sheet of paper which is shown at (a) in *Fig. 2*. It will be shown that that hypothesis was justified by the results of tests, both static and dynamic, made on the small cylinders.

Fig. 1.

SYMBOLS USED IN TAYLOR'S HYPOTHESIS.

TEST APPARATUS.

The apparatus designed for the main tests is shown in *Fig. 3*. The cylinder to be tested, as already stated, was bedded in sifted sand to half its diametral depth, the sand box resting on the heavily reinforced concrete base of a compression machine which was originally built for testing slabs. Loads were applied by an inverted hydraulic jack which was modified to prevent oil leakage

Fig. 3.

ARRANGEMENT OF APPARATUS FOR MAIN TESTS.

Fig. 2.
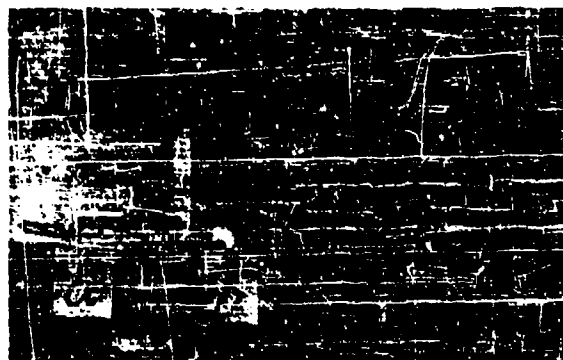
(a) TAYLOR's MODEL.
(b) STATIC TEST ON COFFEE TIN.
(c) DYNAMIC TEST ON MILK TIN.
(d) STATIC TEST ON MILK TIN.

Fig. 5.

CYLINDER WITH END REMOVED.

642
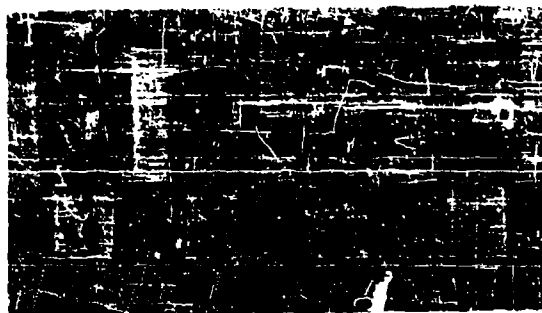
(a) First Tin Showing Form of Dent.
(b) Second Tin Showing Split.
(c) Badly Reinforced Tin which Eventually Split.
(d) Badly Reinforced Tin which Did not Split.

Fig. 19.

(a) Taylor's Second Model.
(c) Result of Hydrostatic Test.
(d) Static Test with Line Loading.

when working in that position, and the loads were assessed by the diametral strains of a calibrated ring placed between the jack and the specimen, the strains being measured by an Ames dial. The ram which applied the load to the specimen was spherically ended, its diameter being 1¾ inch.

Displacements of the ram were observed by a telescope carrying a cross-hair focused on a scale attached to the bottom of the calibrated ring. Rods attached to the bottom of each end of the cylinder also carried scales and the readings of the scales by separate telescopes gave the bodily sinking of the cylinder in the sand and so enabled the true amount of indenting of the specimen to be determined.

Two Ames dials supported from the bottom of the sand box at opposite ends of a horizontal diameter of the cylinder enabled the diametral spread under load to be measured, but those measurements were not found to be of particular importance.

In some tests the longitudinal alterations in length of the cylinders were measured; steel balls were attached near the top of the cylinder at each end and provided bearing points for the ends of a micrometer measuring bar; a sufficiently accurate overall strain measurement was thus obtained.

STANDARD TEST CYLINDERS.

The standard test cylinder is shown in *Figs 4* and *5*. It consisted of a 14-gauge cylindrical shell 2 feet 1½ inch in length and 16½ inches external diameter, internally stiffened by eleven rings made of ¾-inch by ¾-inch by 14-gauge T-section steel. The rings were evenly spaced along the length of the cylinder and the legs of the T's were tack-welded to the shell, the welds having a pitch of approximately 2 inches. That was found by trial to be more satisfactory than continuous welding which introduced a serious danger of damaging the shell by over-heating it.

The end plates were also of 14-gauge steel and were stiffened by ¾-inch by ⁷⁄₁₆ inch T-sections and brackets arranged as shown in *Figs 4*.

The cylinders were made by Messrs. Benham and Company of Wandsworth and in the first place six were completed. An experiment in manufacture, however, provided an additional unfinished specimen which gave useful information on test. It had a central stiffening ring continuously welded to the shell and a ring spot-welded to the shell at 3 inches from either side of the central ring. No end-plates were provided in that cylinder.

At a later date further cylinders were made, three to the original design and three as shown in *Figs 6*. The feature of those was the replacement of the normal end-plates by 1-inch disks to give resistance to bending out of their planes and the discs were connected by four 1¼-inch-diameter steel rods.

PRELIMINARY TESTS ON STEEL AND COPPER DRUMS.

A steel cement drum 20 inches long, 14 inches diameter and 0.029 inch in wall thickness, served for a preliminary check of the test apparatus. The drum was unstiffened except for the supports of the bottom and the cover. The load-displacement curve which was obtained as a result of that test indicated that displacement curve which was obtained as a result of the experiment indicated that displacements had been measured before the

Fig. 4.

LONGITUDINAL SECTION
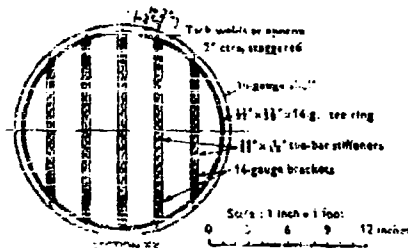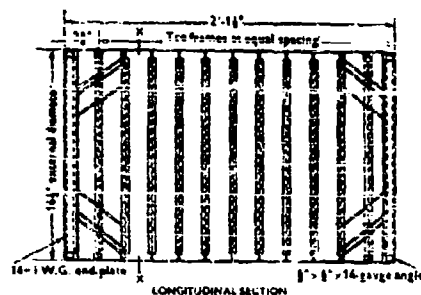
THE EXPERIMENTAL CYLINDER.

strains had fully developed. While the modifications to the rig dictated by that preliminary test were being made, a second drum was tested, but the load was applied by dead weights; that drum was similar to the first but the wall thickness was 0.032 inch. The load displacement curve is shown in *Fig. 7*.

The area under the curve is a measure of the energy absorbed in deforming the cylinder and is 153 inch-lb. In a second test the drum was inverted and a 4-inch-diameter iron ball weighing 7.9 lb. was dropped upon it from a height calculated to give it that amount of energy on impact after

correction for rebound. The amount of restitution was, however, mis-judged and the actual energy absorbed in plastic deformation was only 132 inch-lb. Both the damaged surfaces of the cylinder were contoured as explained later and *Fig. 8* shows a c... ion of the results of static and dynamic loading. The general sha... the contours agree well, but the maximum indentation was less in the dynamic than in the static test being under estimated.

Fig. 6.

LONGITUDINAL SECTION

SECTION XX
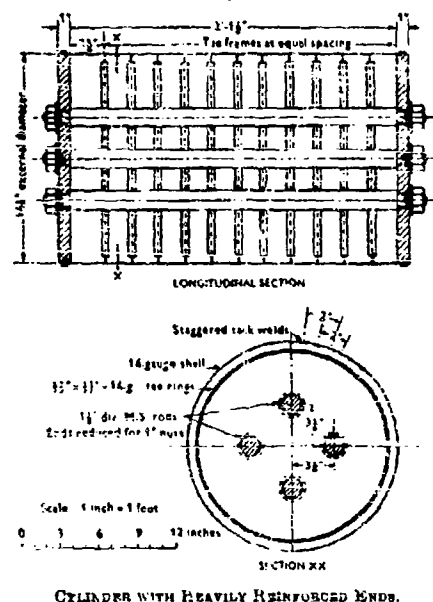
CYLINDER WITH HEAVILY REINFORCED ENDS.

Similar experiments were then made on a drum of soft copper, 24 inches long, 15 inches in diameter and of thickness 0·048 inch. The ends were heavy wooden disks to which the shell was screwed. The static load-displacement curve is shown in *Fig. 9* and a comparison of the contours obtained in the static and dynamic tests in *Fig. 10*. The energy absorbed in the dynamic test was about 10 per cent. greater than in the static test and that is reflected in the contours, which show rather greater indentation.

The close agreement between the results of static and dynamic tests on the copper drum suggests that the rates of loading within those limits

sure unimportant. There were, however, differences between the corresponding tests on the steel drum which indicated that the time factor was of some importance.

Fig. 7.
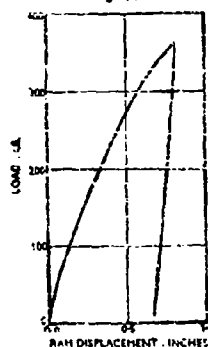
LOAD-DISPLACEMENT CURVE FOR STATIC TEST ON UNSTIFFENED STEEL DRUM.

Fig. 8.
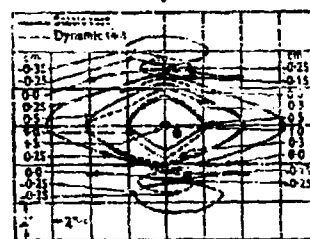
CONTOURS RESULTING FROM STATIC AND DYNAMIC TESTS ON UNSTIFFENED STEEL DRUM.

Fig. 9.
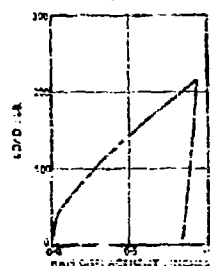
LOAD-DISPLACEMENT CURVE FOR STATIC TEST ON COPPER DRUM.

Fig. 10.
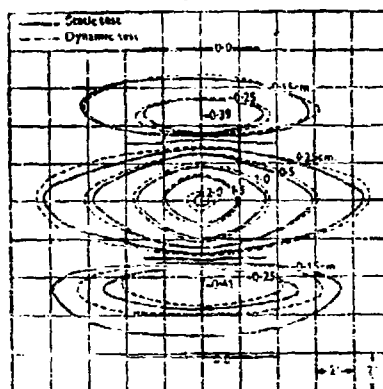
CONTOURS RESULTING FROM STATIC AND DYNAMIC TESTS ON COPPER DRUM.

TESTS ON SMALL CYLINDERS.

Static tests.—A number of coffee and household milk tins, complete with covers, were half embedded in sand in the same way as was proposed for the tests on the standard cylinders and were then loaded through a $\frac{15}{16}$-inch-diameter steel ball at the mid-section. The loads were applied in small increments by dead weights and at different stages in the test the

Fig. 11.

STATIC TEST OF COFFEE TIN.   STATIC TEST ON MILK TIN.
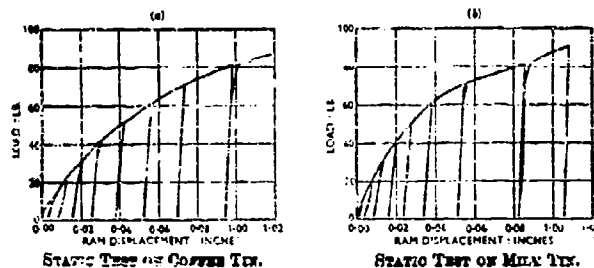
whole load was removed and re-applied. Typical curves obtained from those tests are shown in *Figs. 11*, and it is noticeable that there is practically no looping due to the removal and re-application of the load. That was characteristic of all the tests made in the course of the investigation, irrespective of the size or construction of the cylinders. At (b) and (d) in *Fig. 2* are shown typical specimens after test; they are arranged with Taylor's model for comparison and the similarity is marked.

Fig. 12.   *Fig. 13.*

HEAVILY REINFORCED TIN.   DENT IN HEAVILY REINFORCED TIN.
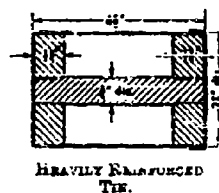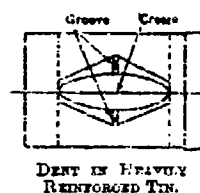
The type of failure illustrated in *Fig. 2* by Taylor's model can only occur if the ends of the cylinder are free to bend out of their own plane; if the ends resist bending, tensions will be induced in the shell and the resulting strained shell cannot be developed into a plane surface.

To examine the effect of end stiffness a series of tests were made on tins in which the normal thin bottom and cover were replaced by steel

disks, $\frac{1}{16}$-inch thick, connected by a central distance-piece of $\frac{3}{4}$-inch diameter as shown in *Fig. 12*. In the first test a point load was applied opposite

Fig. 14.   Fig. 15.
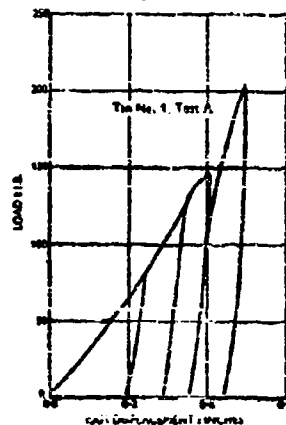
LOAD-DISPLACEMENT CURVE FOR TIN
WITH HEAVILY REINFORCED ENDS.
POINT LOAD ON SEAM.
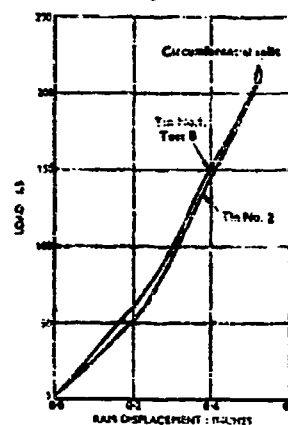
LOAD-DISPLACEMENT CURVES FOR TINS
WITH HEAVILY REINFORCED ENDS.
POINT LOAD AWAY FROM SEAM.

to the longitudinal seam in the tin, the specimen being half bedded in sand as in other tests. The type of failure is shown in *Fig. 13* and the resulting load-displacement curve in *Fig. 14*. For small loads the dent

TABLE I.

Diameter of ball . inches.	Weight of ball : grammes.	Rebound : inches.	Depth of dent, d : inches.	Length of groove, h : inches.	$\dfrac{d}{a}$	$\dfrac{h}{2a}$
$\frac{1}{2}$	8·5	45	0·06	0·8	0·04	0·29
$\frac{5}{8}$	16·0	16	0·16	1·40	0·11	0·50
$\frac{3}{4}$	28	10	0·24	1·75	0·17	0·61
$\frac{7}{8}$	45	4	0·39	2·25	0·27	0·78
1	67	2	0·55	2·7	0·36	0·94
$1\frac{1}{8}$			0·77			
$1\frac{1}{4}$	130	1	0·85	3·3	0·59	1·11
$1\frac{3}{8}$	227	0	1·08	3·6	0·75	1·26

was elliptical, the major axis being a well-defined crease. As the load was increased the edge of the dent was defined by two ellipses on the same major axis, grooves forming along the minor axis between them. The

outer ellipse ultimately developed into a hexagonal figure as shown in *Fig. 13* and at (c) in *Fig. 16* (facing p. 5).

The same tin was then turned in the sand bed and another test made, away from the seam. The test figures are shown in *Fig. 16* (Tin 1, Test B) and failure occurred by the development of a circumferential split at the centre of the cylinder on the minor axis of the smaller ellipse ; that split was significant in the light of results to be described later. After the test

Fig. 17
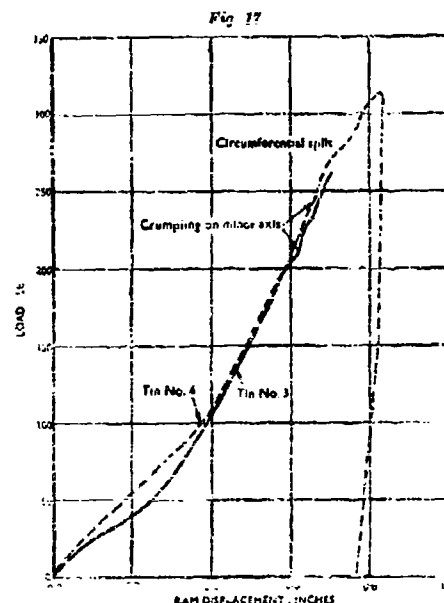
LOAD DISPLACEMENT CURVES FOR MILK
TINS WITH IMPERFECTLY REINFORCED ENDS.

an elliptical dent was found on the previously undamaged under-side of the specimen, opposite to the loading point and is shown on the right of (a) in *Fig. 15* ; the split was on the far side of the cylinder. A check test was made on the second of the stiffened cylinders ; the results were similar and are shown in *Fig. 16* (Tin 2) and at (b) in *Fig. 15* (facing p. 5).

The two remaining reinforced cylinders were deliberately made badly to allow some, but not complete, freedom at the ends.

In one, the specimen eventually split in spite of crumpling along the minor axis of the dent as shown at (c) in *Fig. 15* ; in the other the flexibility

325
11

n in

iade,
st 3)
o this
split
test

of the ends was sufficient to prevent splitting as shown at (d) in *Fig. 16*. The load displacement curves for those specimens are shown in *Fig. 17*.

The results of tests on specially prepared specimens under hydrostatic pressure, which will be described later, led to the production of a second paper model by Sir Geoffrey Taylor which showed that the type of failure obtained could also occur without stretching of the shell. As it seemed likely that similar distortions could be produced by static loading distributed along a line parallel to the axis of the specimen, several experi-

Fig. 18.
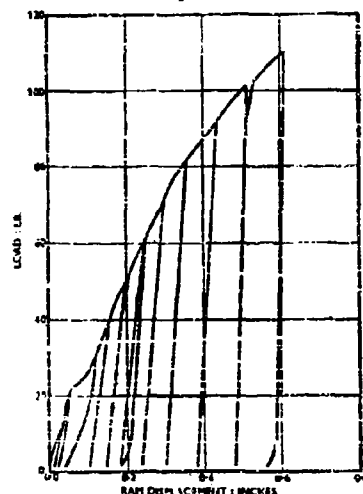
LOAD-DISPLACEMENT CURVE FOR LINE LOAD ON
MILK TIN WITH LID SOLDERED IN POSITION.

ments were made with the load applied through bars of different lengths and diameters, the covers of the tins being soldered into position.

The general result was the same; the best comparison with the model was obtained when a rod 1¼-inch in diameter and 1½-inch long was used, the ends of the rod being rounded to prevent local damage to the thin shell.

The complete load-displacement curve for that case is shown in *Fig. 18* and the deformed specimen at (d) in *Fig. 19* (facing p. 5) which also includes Taylor's second model.

Dynamic tests.—Tins of both types were subjected to dynamic loading. They were half bedded in sand as in previous static tests and steel balls of

different weights were dropped upon them from a height of 23 feet. Each specimen was subjected to one impact only and the results are given in Table I. A typical specimen after test is shown at (c) in *Fig. 2.*

In that series of tests the depth of the dent and the length of groove were measured in each case and the corresponding values of $\frac{d}{a}$ and $\frac{h}{2a}$ (p. 4, *ante*) are plotted in *Figs 20.*

Figs 20.
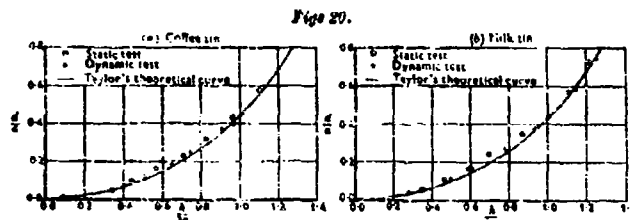
COMPARISON OF TEST RESULTS WITH TAYLOR'S CURVE.

The results from the static tests previously described are shown plotted in the same figures and for comparison the theoretical curve connecting these parameters is also shown. The closeness of agreement between the experimental and theoretical results is remarkable and justifies the acceptance of Taylor's theory of the form of distortion which occurs.

Fig. 21.
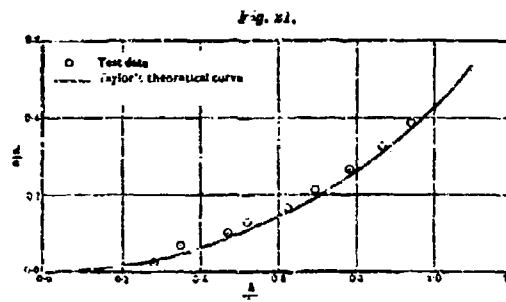
COMPARISON OF TEST RESULTS WITH TAYLOR'S CURVE.

Although Taylor's hypothesis is not strictly applicable to the case previously described in which the load was distributed along a line, it is interesting to note the close agreement between the test figures and his theoretical curve as shown in *Fig. 21.*

Tests under hydrostatic pressure.—Tests were also made on household milk tins under hydrostatic pressure. The test specimens were filled with molten lead up to a diametral plane to stabilize that portion against failure, and the seam and cover were carefully soldered to make the whole shell watertight. They were then immersed in water in a pressure chamber. In the first test, pressure was raised continuously. Collapse occurred suddenly at 50 lb. per square inch, and was, in that respect so unlike the failure observed under steadily increasing static loads that a second specimen was subjected to 5 lb. increments of pressure and was removed for inspection after each increase. Up to 25 lb. per square inch no effect was discernible, but at 27 lb. per square inch a slight flicker of the pressure gauge gave warning of a collapse. On removal from the chamber an elliptical dent with a double margin was found in the shell as shown in *Fig. 22*. That dent extended the whole length of the specimen.

Fig. 22.
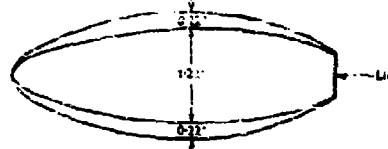
DENT FORMED DURING HYDROSTATIC TEST
ON TIN WITH UNREINFORCED ENDS.

The test was continued and flickers of the gauge were noted at 21 lb. per square inch and 24 lb. per square inch but the specimen was not removed until at 50 lb. per square inch it was found impossible to maintain the pressure. Complete collapse similar to that in the first test had occurred; this is shown at (c) in *Fig. 19* (facing p. 5) which clearly indicates the double margin. Agreement with Taylor's model shown at (c) in *Fig. 19* is again striking.

Specimens with stiff ends as previously described (*Fig. 11*) were next half-filled with lead and subjected to hydrostatic pressure. The pressure was slowly increased to 38·5 lb. per square inch when a flicker of the gauge indicated that collapse had occurred. A small elliptical dent about 2·8 inches long (the free length between reinforcing disks) and 0·95 inch wide had formed. Its position is shown on the developed surface of the specimen at (a) in *Figs 23*. The specimen was replaced and the pressure again raised until the gauge indicated further failure; inspection was then made. That process was repeated and the history of the collapse determined. At 42 lb. per square inch a second slightly unsymmetrical elliptical dent formed adjacent to the first as shown at (b) in *Figs 23*. That was also 2·8 inches long and 1·00 inches wide; the dimensions of the first dent were unchanged. At 46 lb. per square inch a click was heard but

there was no flicker of the gauge until 49 lb. per square inch was reached. A third dent had then formed at ¼ inch from the second ; that was also slightly asymmetrical and, with the second dent, formed a left and right hand pair as shown at (c) in *Figs 23*. The area between those two showed a slight bulge. The next collapse occurred at 62 lb. per square inch when a fourth and much narrower elliptical dent developed ; that was of the

Figs 23.
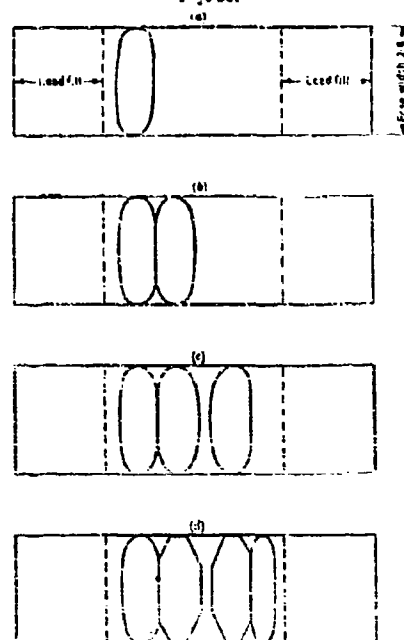
DEVELOPMENT OF FAILURE DURING HYDROSTATIC TEST
ON STIFF-ENDED TUBE, HALF-FILLED WITH LEAD.

same length as the earlier ones but was only 0·6 inch wide. In addition the second and third dents had become hexagonal in outline as shown at (d) *Figs 23*. *Fig. 24* (facing p. 16) shows the final appearance of the specimen.

Those experiments indicated that a cylinder under extreme hydrostatic pressure will fail by the formation of a single dent if the ends are flexible out of their p———— if the ends are rigid, failure occurs by multiple "lobing." If the ends possess a small degree of stiffness it is probable

that failure will start by the development of multiple lobing but that the buckling of the ends subsequently will cause the lobes to merge into a single dent showing the boundary between the initial lobes as a ridge. That effect is shown at (c) in *Fig. 19*, and later evidence obtained from explosive experiments clearly indicates that it does occur.

TESTS ON LARGE CYLINDERS.

As stated in the beginning of this Paper, the original object of the investigation was to determine the behaviour of the cylinders shown in *Figs 4*. The work originally contemplated, however, was extended on account of the results obtained from the small cylindrical tins which have been described in preceding pages. One result of those small-scale tests was to emphasize the importance of the stiffness of the ends and a few cylinders were therefore made with very stiff end disks connected by steel

TABLE II.—SCHEDULE OF TESTS ON LARGE CYLINDERS.

Cylinder No.	Test No.	Description of cylinder.	Test conditions.
0	0A	Shell and three rings only (see page 6).	Point load at central ring.
	0B	Ditto.	Ditto.
1	1A	As in *Figs 4*.	Point load at central ring.
	1B	As in *Figs 4*.	Point load between rings.
2	2	As in *Figs 4*, but with no end plates.	Point load at central ring.
3	3	As in *Figs 4*	Point load between rings.
11	11A	As in *Figs 6*.	Point load between rings.
	11B	As in *Figs 6*.	Point load between rings.

rods as shown in *Figs 6*. Some of those, as well as some of the original design, were used for tests under explosive loads, but one of them was tested statically in the way described earlier.

Table II is a schedule of the cylinders tested as described in this Paper; each one was given a reference number and when it was possible to make two tests on one cylinder they are distinguished by letters after the number.

The method of testing has already been described. Before the cylinders were embedded in the sand, lines dividing the surface into 1-inch squares were carefully scribed upon them. Those lines served as a reference grid for plotting contours of the dents obtained. The contours were actually

Fig. 26.
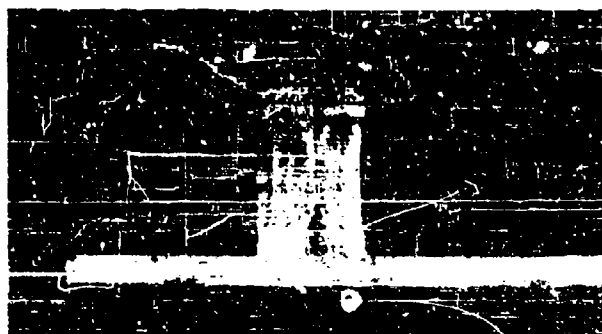
APPEARANCE OF TIN WITH REINFORCED ENDS AFTER HYDROSTATIC TEST.

Fig. 27.
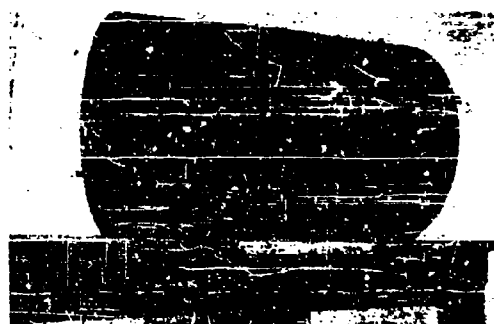
DEFORMATION OF CYLINDER No. O AFTER TEST B.

632

Fig. 38.

(a) Tube 14. Loaded on Rib. Shell Fractured.
(b) Tube 19. Loaded between Ribs.

Fig. 39.

(a) Cylinder No. 2. Open Ends. Loaded over Rib.
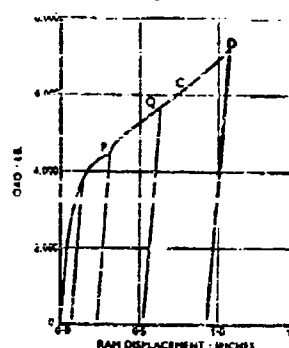(b) Cylinder No. 3. Loaded between ribs. Shell Fractured.

Fig. 41.
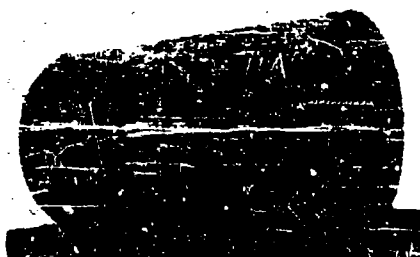
Dent in Cylinder No. 11, with Reinforced Ends, showing fracture in Shell.

plotted on the surface of the cylinder by the following method. A brass straight-edge was carried for the whole length of the cylinder from the end plates, that straight edge coinciding with each of the axial grid lines in turn. A depth gauge set to a definite reading was moved along the straight-edge until its point just touched the distorted cylinder; the point of contact was marked and gave one position on that contour. The contours were finally drawn in white paint and the cylinder was photographed. The grid was then used to plot the contours on the plane development of the surface, and those contours are shown in a number of the figures to follow. The first tests were made on the incomplete specimen O, the ends of which were supported by wooden disks to which the shell was screwed. The load-displacement curve obtained in Test OA is shown in *Fig. 25*. The test data for this curve are contained in Table III. These are given as an example of the records kept for each test, but the remainder are not reproduced.

Fig. 25.

TEST A ON CYLINDER O.

TABLE III.—TEST DATA FOR TEST A ON CYLINDER No. O LOADED OVER RIB.

First loading.		Second loading.		Third loading.		Fourth loading.	
Load : lb.	Ram displacement : inches.	Load : lb.	Ram displacement : inches.	Load : lb.	Ram displacement : inches.	Load : lb.	Ram displacement : inches.
25	0·0	25	0·06	25	0·22	25	0·52
350	0·0	990	0·08	790	0·23	6240	0·51
730	0·01	1870	0·10	1680	0·25	7380	1·0?
1110	0·02	2820	0·11	2330	0·26	25	0·93
1490	0·03	3770	0·13	3600	0·29		
1870	0·04	4150	0·12	4530	0·31		
2350	0·05	4530	0·30	4720	0·32		
2630	0·06	3590	0·22	4930	0·42		
5910	0·07	2630	0·27	5100	0·44		
3590	0·09	1690	0·47	5230	0·50		
8770	0·13	730	0·24	5460	0·56		
1670	0·10	25	0·22	5670	0·63		
25	0·06			4550	0·60		
				3770	0·58		
				2630	0·58		
				1870	0·56		
				790	0·54		
				25	0·52		

W.E.P. III—2

When the load was removed and then replaced as at P, Q, etc., the keeping was negligible. In the region PQ the load was applied in five increments, but the regions QC and CD each represent a single increment. The displacement at D was smaller than was expected and suggested some unaccountable recovery of the cylinder between C and D. To investigate the reason for that, the cylinder was turned over in the sand bed and a second test was made on the undamaged surface. The load-displacement curve for that test (OB) is shown in *Fig. 26*, and it consists of a number of

Fig. 26.

TEST 6 ON CYLINDER O.
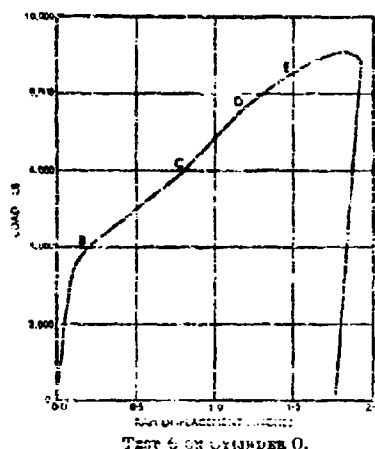
distinct sections. OB was a region of linear load-displacement and the strains were practically elastic. At B there was a marked increase in the rate of displacement with load, but that was followed by another region of linear proportionality, BC. The slope in that region, however, was very much flatter than in OB. At C the slope became steeper again and CD was a third region of comparatively linear proportionality. At D the slope changed once more and for the short length DE it was very nearly the same as for BC. At E, linear proportionality finally broke down. The maximum load carried was just under 9,000 lb. and the depth of the permanent dent was about 1·75 cm.

The explanation of the shape of the curve appears to be as follows. In the region, OB, the central ring and its attached shell resisted the loads without plastic deformation. At B the limit of proportionality of stress was exceeded in the material of the ring and an appreciable dent developed in the shell in the range represented by BC. Load was then transferred

to the two rings adjacent to the central one through the medium of the shell, and plastic deformation of the central ring was accompanied by elastic deformation of those adjacent to it. At D, all three rings were in

the range of plastic deformation and ultimately complete collapse occurred at the load represented by E.

This explanation suggests that in the fully stiffened cylinders the presence of further rings would give more sections of the curve similar to CD and DE. This was borne out by the later test on cylinder No. 2, although the efficacy of the remaining rings was small compared with that of those adjacent to the load point.

The appearance of cylinder No. O after test OB is shown in *Fig. 27* (facing p. 16).

Fig. 26.

Test A on Cylinder No. 1.

Test No. 1A was the first made on a complete cylinder and the results are shown in *Fig. 28*. The maximum load carried was only 5,600 lb. compared with 9,000 lb. by the incomplete cylinder No. O, which had only three stiffening rings and very inadequate end plates compared with those in the standard cylinder. That result was surprising until the load was removed and the surface of the cylinder exposed. It was found that a circumferential split had developed in the shell against the central ring under the loading ram. The split was a characteristic tensile fracture and left no room for doubt that the end plates had restrained the free distortion of the shell sufficiently to produce large tensile stresses in the shell plate. That was consistent with tests already described which were made on small cylinders.

When cylinder No. 1 was turned over in the sand bed and the undamaged surface loaded (Test No. 1B), no split developed; possibly because the split from the previous test gave sufficient flexibility to relieve the longitudinal tensile stresses. The load-displacement curve for Test No. 1B is shown in *Fig. 29* and the two sets of contours of the damaged surfaces in *Figs 30* and 31. *Figs 32* (facing p. 17) show cylinder No. 1 after tests, with the contours painted on it.

During the progress of Test No. 1B, the alteration in overall length of the top generator of the cylinder was measured at intervals; the maximum shortening was about 0·26 inch.

As a result of those tests it was decided that cylinder No. 2 should be modified so that the ends were entirely unstiffened and the end disks were therefore removed. The load-displacement curve is shown in *Fig. 33* and exhibits no new features. Very large distortions were obtained without any sign of cracking in the shell, although one or two of the spot-
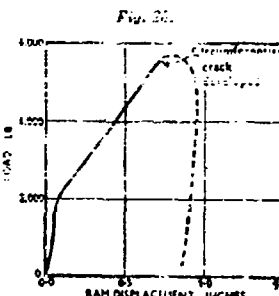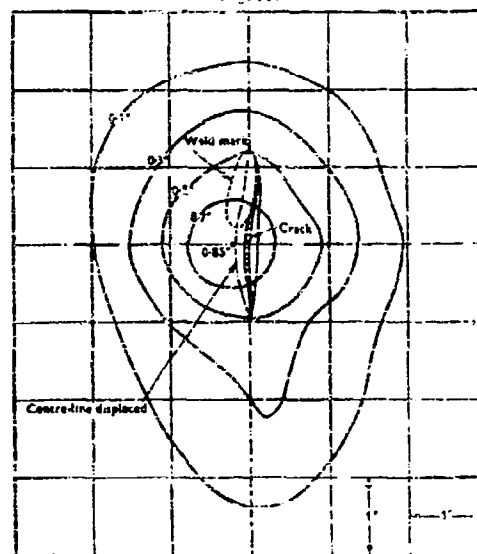
Fig. 29.

TEST B ON CYLINDER No. 1.

Fig. 30.

CONTOURS OF DENTS IN CYLINDER No. 1 AFTER TEST A.

welds connecting the stiffening rings to it failed. Those failures, however, did not appear to affect the load-carrying capacity of the cylinder to any significant extent. The overall shortening of the cylinder was greater than in the earlier tests and *Fig. 34* shows its amount at various stages. The maximum shortening was about 0·3 inch instead of 0·2 inch obtained in Test No. 1B. The contours of the damaged surface are shown in *Fig. 35* and the appearance of the dent at 'a' in *Figs 36* (facing p. 17).

The absence of end plates allowed the cylinder to flatten and the end

Fig. 31.

Fig. 33.

LOAD-DISPLACEMENT CURVE FOR
CYLINDER No. 2.
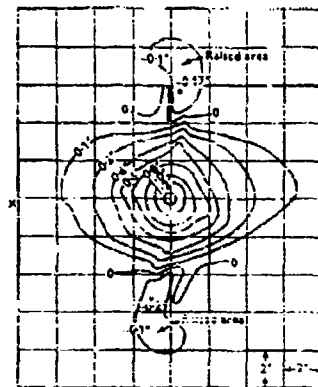
CONTOURS AND SECTION OF DENT IN
CYLINDER No. 1 AFTER TEST B.

sections at the conclusion of the test were ovals having major and minor axes of 17 inches and 16 inches respectively instead of circles of 16½ inches diameter. In view of that distortion a second test on the cylinder would have been of no value. The distortion affects the absolute accuracy of the contours which, as mentioned previously, were based upon the final end plates as datum lines. For obtaining the shape of the sections of the dent along the axis of the cylinder they are reliable; in the case of circumferential sections, however, slight distortion is produced.

Test No. 3 was made on a complete cylinder under the same conditions as Test No. 1B, that is to say, with the load applied mid-way between two rings. In that test the load was steadily increased to the maximum value that it would sustain, there being no removal and re-application of loads

SHEPARD AND SHIPPS ON EXPERIMENTS ON THE
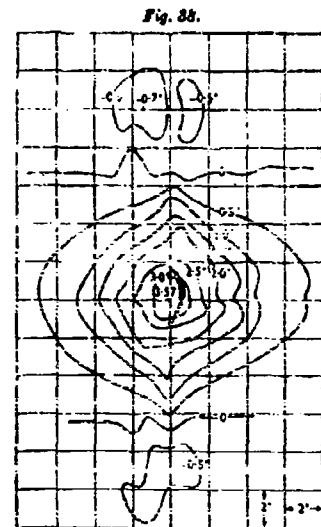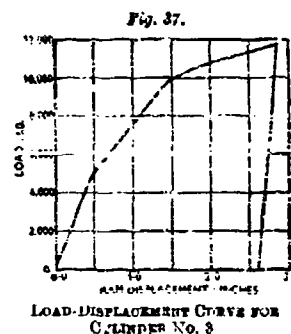
Fig. 34.
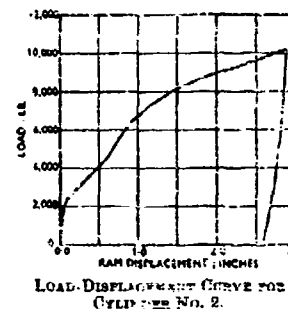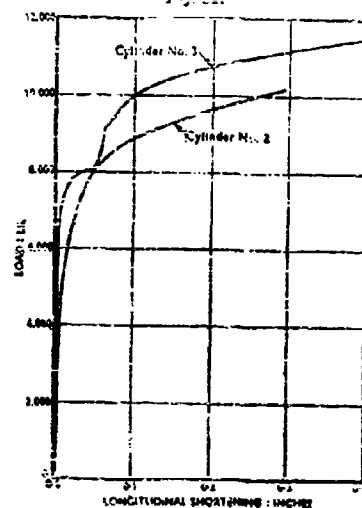
LONGITUDINAL SHORTENING OF CYLINDERS NOS. 2 AND 3.

Fig. 35.
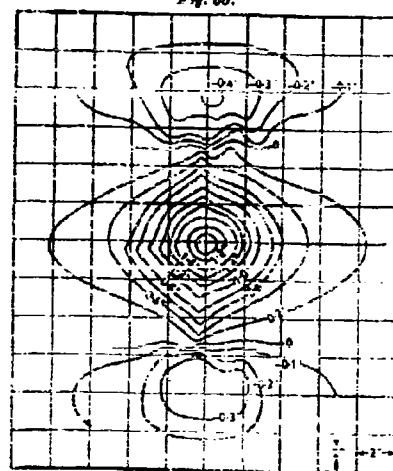


CONTOURS OF DUST IN CYLINDER NO. 2.

as in earlier tests. At 11,750 lb., which appeared to be the maximum which could be reached, the load was removed to ensure that the jack was working properly. Everything was found to be in order and on re-loading the cylinder it was found impossible to increase that load of 11,750 lb. Plastic straining, however, continued for some time and ultimately a split occurred in the shell; the depth of dent was then 5·6 inches. That split is seen at (5) in *Figs 36*, the contours being at intervals of 0·2 inch. The load-deflexion curve, which is shown in *Fig. 37*, calls for no special comment, as it is similar in its features to those obtained in earlier tests. The

Fig. 37.

LOAD-DISPLACEMENT CURVE FOR CYLINDER No. 3.

Fig. 38.

CONTOURS OF DENT IN CYLINDER No. 3.

shortening of the cylinder is shown in *Fig. 34*, and the plotted contours in *Fig. 38*.

Two tests were made on the stiff-ended cylinder No. 11 and the load-displacement curves for these are given in *Fig. 39*. In Test No. 11A the maximum load carried was practically identical with that in Test No. 3 on a cylinder with normal ends, but the depth of dent produced was only 1·5 inch as compared with 3·6 inches. Failure occurred by a tensile fracture of the skin as shown on the contour drawing of the final dent in *Figs 40* and *41* (facing p. 17). At a loading of 11,700 lb. the overall shortening of

cylinder No. 11 was only 0·07 inch as compared with 0·30 inch in cylinder
No. 5 under the same load.

In Test No. 11B a considerably higher load was reached than in

Fig. 39.

Fig. 40.
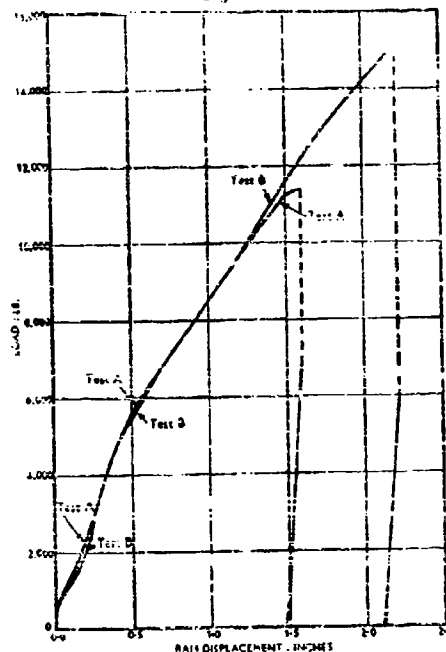
LOAD-DISPLACEMENT CURVES FOR CYLINDER No. 11.

the first with a correspondingly deeper dent (2·1 inches), but the main
characteristics were the same.

## ENERGY ABSORPTION IN PLASTIC DEFORMATION.

The energy absorbed in making the dent is measured by the area under
the load-displacement curve and practically the whole of it is used in
producing plastic deformation. The load-displacement curves for the
static tests on the small cylinders were integrated to obtain the curves of
Fig. 42, which show energy plotted against depth of dent; the smoothness
of the curves indicates a general consistency in the relationship.
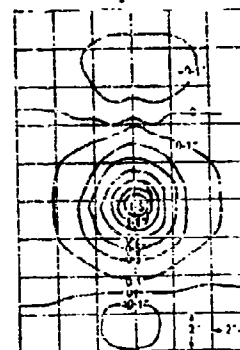
Curves deduced from the dynamic tests on the small cylinders are also shown in *Fig. 42*. Those specimens were deformed by balls of various weights dropped from a height of 20 foot. The height of rebound was deduced from that and the difference gave the effective height of drop which caused denting. These curves are also reasonably smooth, but the

Fig. 42.
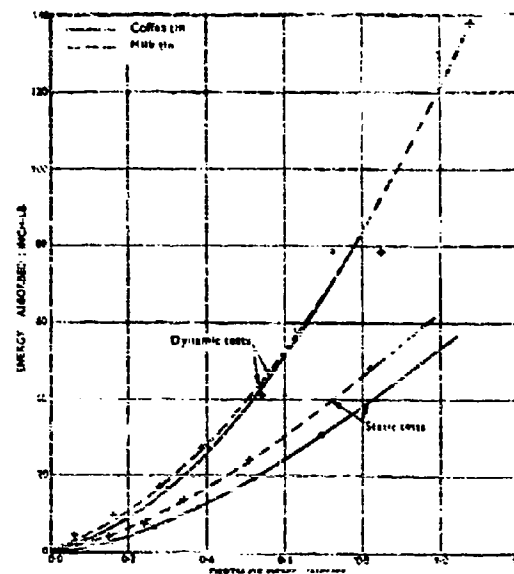
ENERGY ABSORBED IN TESTS ON SMALL CYLINDERS.

energy required to produce a given dent is greater than when the dent is produced by static dead loading in spite of the similarity of the deformations. This is consistent with the results of the tests on the steel cement drum.

Fig. 43 shows results obtained from static tests on the large cylinders. These points also lie very fairly on a smooth curve and explanatory notes on the diagram indicate the main features. The higher point for No. 3 was estimated from the test curve obtained after the load was so applied and plastic strains allowed to develop until a tensile fracture occurred (see p. 23). The energy absorbed when the maximum load was reached and immediately before it was removed is given by the lower point for

No. 3. The curve shows the increase in energy-absorbing capacity of that cylinder compared with the substantially end-stiffened cylinder No. 11.

TESTS ON STIFFENING RINGS.

Tests were made on a single ring used for stiffening the standard cylinders and also on such a ring with a 2-inch-wide strip of the shell

Fig. 43.
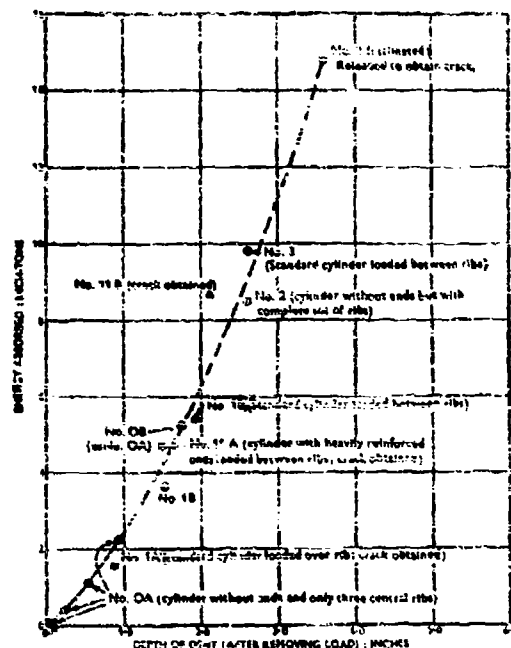
ENERGY ABSORBED IN STATIC TESTS ON LARGE CYLINDERS.

spot-welded in position. The latter was cut from an undamaged section near one end of a cylinder after the main test had been made.

The conditions of test were as nearly those of the cylinders as was practicable. In the case of the single ring, support was given to one-half of it by a three-ply cradle and a similar cradle of heavier construction was used for the ring with its attached shell. These cradles represented the support given by the sand bed.

Point loads were applied to the single ring by dead weights, the speci-
men being supported in a horizontal position on a lathe bed as shown in
Figs 44, Plate 1.

The ring with its 2-inch attached shell was tested vertically in a 10-ton
Buckton testing machine as shown in Figs 45, Plate 2, lateral instability
being prevented by light guides which offered no restraint to movements
in the plane of the ring.
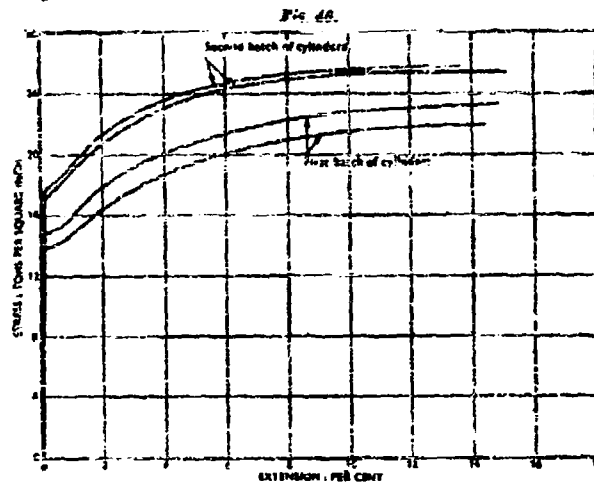
Fig. 46.

TENSILE TESTS OF THE MATERIALS USED FOR THE CYLINDER SHELLS.

At successive loads the contours of the deformed rings were traced
directly on sheets of paper mounted behind the specimens and the results
are given in Figs 44, Plate 1, and Fig. 46, Plate 2.

A feature of both of these tests is the evidence of two well-defined points
in each ring which suffered no radial displacement. These do not coincide
with the theoretically calculated positions of zero radial displacement for
elastic strains, the discrepancy apparently being due to a slight spread of
the horizontal diameter of the test rings which was assumed in the calcu-
lation to be completely restrained. This feature may be important in
simplifying an analytical treatment of the plastic distortion of rings.

CONTROL TESTS ON MATERIAL.

Test specimens of the material used for the shell were provided by the
makers of the cylinders. The curves obtained in tensile tests on specimens
of 1-inch gauge-length are shown in *Fig. 46.*

There was a difference in ultimate strength between the material for the two batches of cylinders (Nos. 0 to 6 and Nos. 7 to 11 respectively). The first batch gave approximately 23 tons per square inch and the second batch approximately 26 tons per square inch.

All specimens gave a value of Young's Modulus of 13,000 tons per square inch, an ultimate extension of 14 to 15 per cent., and a reduction in area at fracture of 40 per cent.

Conclusions.

As indicated earlier the investigation was made primarily to supplement research into the behaviour of submarine shells subjected to underwater explosions, but the following general conclusions upon the plastic failure of cylindrical shells may be drawn from the results of the experiments.

1. The effect of removing the load from a cylinder under test and then reloading it was very slight. There was little or no looping of the load-displacement diagram either in the small cylinders or the large stiffened shells.

2. The stiffness of the end plates had a marked effect on the type of distortion. When those plates had negligible resistance to bending out of their plane the tests strongly supported the hypothesis advanced by Taylor. The resemblance of his models to the actual deformed shells was striking and that visual evidence was confirmed by the quantitative agreement of the experimental results with calculations based on his hypothesis. The agreement held for cylinders deformed either by static or dynamic loading.

3. The stiffness of the end plates also governed the type of distortion resulting from hydrostatic tests on cylinders stabilized against failure over one-half of their depth. When the ends were flexible failure occurred by the development of a single dent, but when they could resist bending out of their original planes, failure was multi-lobed. The lobes developed successively—not simultaneously. There is evidence (supported later by tests under explosive forces), for assuming that if the ends are not completely flexible, but are capable of resisting some degree of bending out of their planes, failure begins by multi-lobed deformation, but subsequent bending of the ends leads to the incipient lobes merging into a single dent showing the boundary between initial lobes as ridges.

4. In cylinders with flexible ends no actual fractures of the shell occurred, but with stiff ends longitudinal stresses were induced sufficient to cause such fractures. They were circumferential and were characteristically tensile.

5. The load-displacement curves for the internally stiffened cylinders showed evidence of the progressive extension of the region of plastic straining from the loaded ring to the adjoining sheet and then to rings
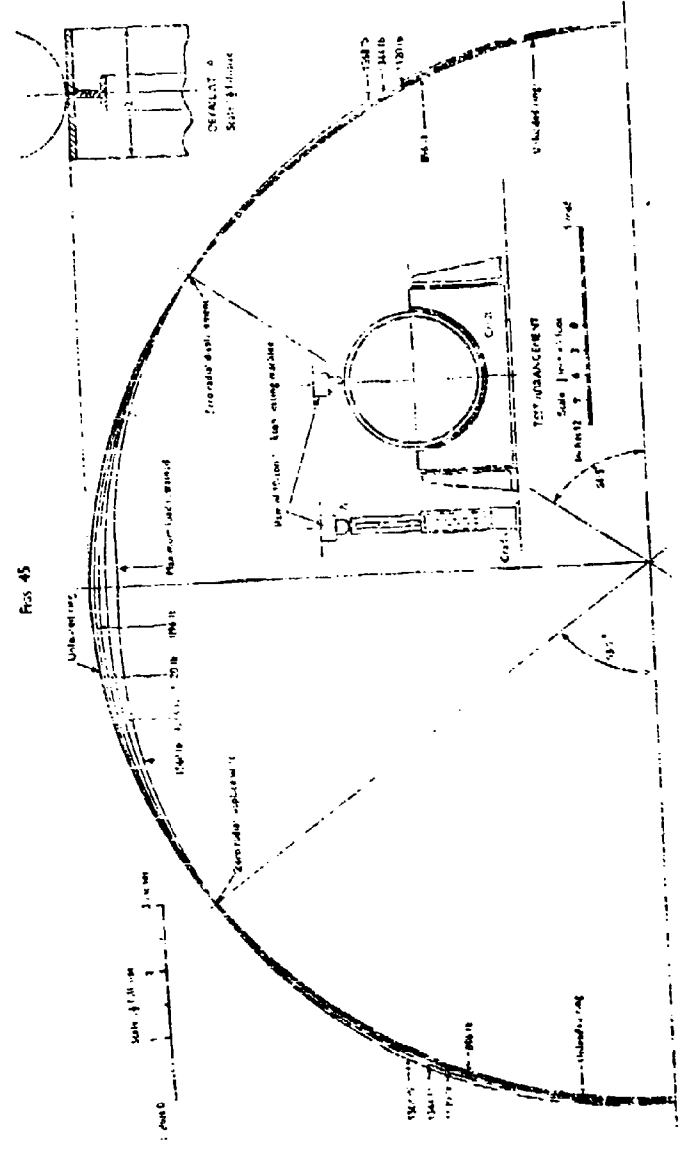
EXPERIMENTS ON THE PLASTIC FAILURE OF CYLINDRICAL SHELLS. PLATE I.

FIG. 44.
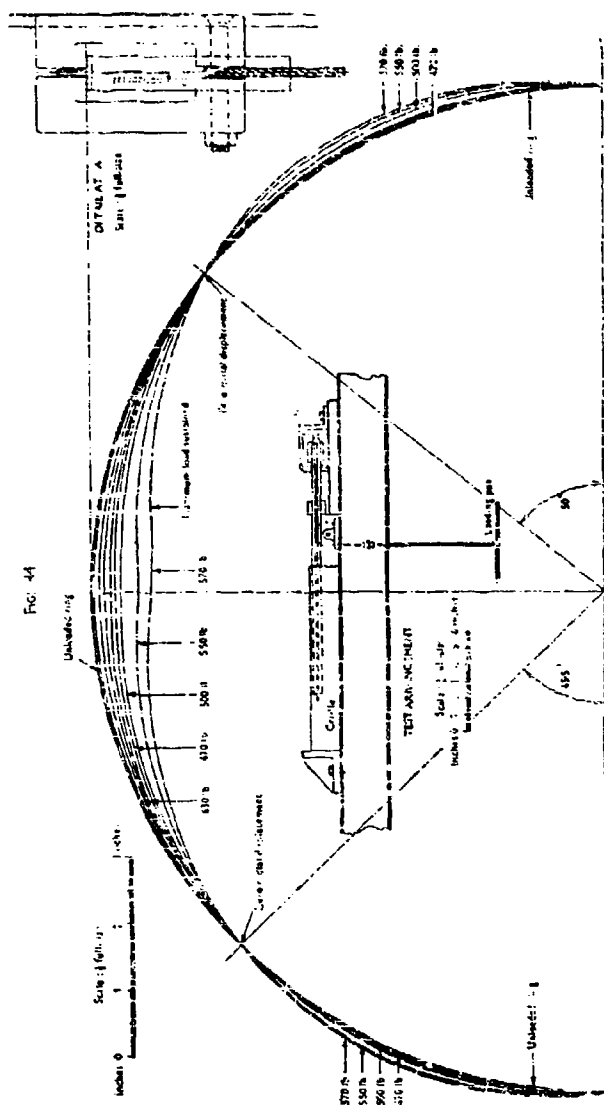
PLASTIC DEFORMATION OF SINGLE RING

645

A. J. S. PIPPARD
and ...

EXPERIMENTS ON THE PLASTIC FAILURE OF CYLINDRICAL SHELLS.

PLATE 2

Fig. 45

PLASTIC DEFORMATION OF SINGLE RING AND 2-INCH ATTACHED SHELL

A. J. S. PIPPARD
and L. CHITTY

further removed from the loaded point. That appears to be the explanation for the succession of comparatively straight sections which make up the curves.

6. A discrepancy between the energy required to deform an unstiffened steel cement drum in static and dynamic tests was not repeated when a copper cylinder was subjected to the same tests. In the latter case the energies were nearly the same and the distorted shapes were practically identical. That suggests that the time factor was of some importance in the case of the steel but not of the copper drum. That view was strengthened by the results of tests on small steel cylinders in which the same amount of energy produced smaller dents when applied dynamically than when applied statically.

7. In tests on single rings two points remained undisplaced whatever the magnitude of the applied load. That may be of importance in a simplified mathematical approach to the treatment of the problem here examined experimentally.

ACKNOWLEDGEMENT.

647
29

auation
up the

tiffened
when a
ase the
otically
ance in
rength-
ie same
lly than

hatever
on in a
em here

nh, Ad-
e results

thirteen
e plates,

NOTE ON THE COPPER DIAPHRAGM GAUGE

J. H. Powell
Construction Research Establishment
Rosyth, Scotland

British Contribution

March 1950

HISTORICAL NOTE ON THE COPPER DIAPHRAGM GAUGE

J. H. Powell

Naval Construction Research Establishment
Rosyth

March 1950

*   *   *   *   *   *   *   *   *   *

Original design.

The 12" gauge.

One of the earliest devices for the measurement of the explosive efficiency of underwater explosions was the Copper Diaphragm Gauge. Its first recorded use was in Mining School, Portsmouth (now Admiralty Mining Establishment, Havant) in 1915 where it was originally designed to indicate if a series of nominally equal charges did in fact develop the same power as estimated by the size of the indentation at any given distance. Experiment, however, showed that the diaphragm were capable of giving approximate absolute measures of certain physical quantities connected with the explosion.

Under static pressure the diaphragm distorts to a spherical form as nearly as can be measured, and a static calibration was made so that the work done in distorting the diaphragm could be expressed as a function either of the volume change, the surface area change or the central depression. Under the influence of explosion pressure the diaphragm distorts to a remarkably smooth form which, however, is not a sphere, but a compromise between a cone and a paraboloid. It was assumed that the work done by the explosion wave in producing a given volumetric distortion is the same as that done by a uniform static pressure in producing an equal volumetric distortion, though it was admitted that this supposition was not strictly correct.

The diaphragm originally consisted of carefully annealed copper plates, 0.04" in thickness. They were clamped within flanges at the end of a circular or cylindrical drum, so that the exposed area of each diaphragm was a circular plate 6" in radius.

Actual experiment soon demonstrated that the relationship

$$w = \text{constant} \times Ed^2$$

held approximately for charges ranging as 1b. and 350 1b. T.N.T. where w = weight of charge; E = energy absorbed by gauge and d = distance of the gauge from the charge. The quantity E was determined by static calibration and it was found that the value based on the volume estimate was more consistent than that determined on an increase in area basis. The volume estimate was therefore, adopted as the basis of measurement. Since the energy is roughly proportional to the square of the depression (Δ), the approximate relation

$$\Delta = \text{constant} \times w^2/d$$

is also applicable.

The original suggestion for this type of gauge was due mainly to Mr. F.R. Shaw (Chief Technical Adviser) and to Mr. F. Pickford of H.M. Mining School, while the elementary mathematical analysis was due to Dr. G.W. Walker (Chief Scientist), from whose reports the foregoing paragraphs are largely quoted.

Standard design.

The 6" Gauge.

Following the death of Dr. Walker in 1921, no further attempt was made to develop the diaphragm gauge as an absolute measure of any particular parameter of the pressure pulse, but it

WSB .....

650

~ 2 ~

was extensively used as an empirical gauge fo
of completeness of detonation and of primer e
considerably modified.

The original 12" diameter gauges, bas
could not be used at ranges less than 75 feet
a diaphragm 0.2" thick and 6" effective diamet
continuous use ever since.

A photograph of the standard gauge is re,
mounting. The body of the gauge or "pot" consi
10" long and with wide flanges 10" diameter. T
circular fillet of hard steel is inserted at eac
provide a bearing ring round the effective circu
slightly to prevent shearing of the diaphragm.

The utmost care was taken to select uniform diaphragms
electrolytic copper. Even with these precautions
with different batches of copper and in all later x. is the c p
Vickers diamond hardness test. It was found that
within the Vickers diamond hardness range 45 to 5
diaphragms with the same hardness numbers were ch

This gauge could be used at ranges close
bursting the diaphragm, but at this range the mea
ranges were preferred.

The static energy and pressure calibration
Similar curves obtained independently after a laps

It was soon established that the volume of
,w⁴/d and as measurements accumulated the relation

It was observed that the depression did not
that oriented directly away from the charge having

In addition to the 6" gauge, smaller gauges
None of these gave such consistent reading as the 6
noticed, however, that the depression tended to vary
charges, suggesting that the small gauge measures a
might be expected from its dimensions relative to the

Until 1945 the gauge had been used entirely
was made to determine the parameter of the pressure

An attempt was then made by Dr. F.H. Fox and
which might be expected in a diaphragm gauge from
on this calculation was issued in the report "Index
out that the larger discrepancy between calculated an
depression, although rendering the gauge of little va
parameters, does not
was originally devised and for which it has proved so
years.

lency of charge
and its design

us objection that they
andardised design with
ich has been in

the method of
steel or cast iron
cylinder is 6" and a
of the flange to
fillet is rounded
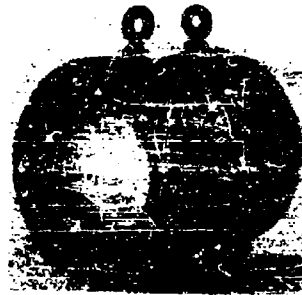
he purest
sometimes used
used by
practically
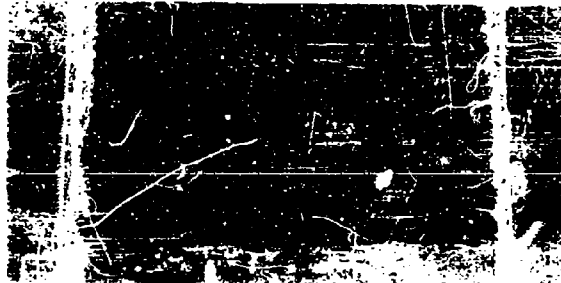es of trials,

charge without
istent and longer

odic in Figure
ly different.

proximately to

a diaphragm
ing
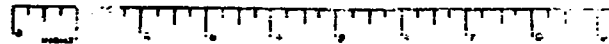
sometimes used.
ely. it was
large

(a) GAUGE ASSEMBLED FOR USE.

(b) GAUGE WITH END PLATE REMOVED, SHOWING P/ 18.

DIAPHRAGM SECTIONED TO SHOW LISHING.

FIGURE 1.

ANDARD 6" COPPER DIAPHRAGM GAUGE.

DEPARTMENT OF THE NAVY
OFFICE OF NAVAL RESEARCH
800 NORTH QUINCY STREET
ARLINGTON. VA 22217-5660

IN REPLY REFER TO
5510/6
Ser 43/655
4 Sep 03

From: Chief of Naval Research
To: Commanding Officer, Naval Research Laboratory (NRL 5996.3)

Subj: PUBLIC RELEASE APPROVAL

Ref: (a) Your e-mail to me of 14 Jul 2003

Encl: (1) Underwater Explosion Research, Volume I - The Shock Wave, 1950 (AD 006 841)
(2) Underwater Explosion Research, Volume II - The Gas Globe, 1950 (AD 037 466)
(3) Underwater Explosion Research, Volume III - The Damage Process, 1950
(AD 037 467)

1. In response to reference (a), enclosures (1), (2) and (3) are approved for public release; distribution is unlimited. They are returned for your use.

2. Questions may be directed to the undersigned on (703) 696-4619.

PEGGY LAMBERT
By direction

Copy to:
DTIC-OCQ (Larry Downing)